Univerzita Karlova v Praze
Přírodovědecká fakulta
Katedra Zoologie

Studijní program: Zoologie
Studijní obor: Zoologie

Srovnání kraniální skeletogeneze a odontogeneze bazálních zástupců paprskoploutvých ryb

Comparative analyses of cranial skeletogenesis and odontogenesis in basal Ray-finned fishes

Mgr. Anna Pospíšilová

Dizertační práce

Vedoucí práce: Mgr. Robert Černý, Ph.D.

Praha
2020

Prohlášení
Prohlašuji, že jsem závěrečnou práci zpracovala samostatně a že jsem uvedla všechny použité informační zdroje a literaturu. Tato práce, ani její podstatná část, nebyla předložena k získání jiného nebo stejného akademického titulu.

V Praze, 1. 9. 2020

.....
podpis

Poděkování

Na tomto místě bych ráda poděkovala všem, bez jejichž pomoci by tato práce bývala byla nikdy nevznikla. Mám na mysli všechny kolegy, kteří po dobu mého působení prošli labem a kteří mi vytvořili náhradní rodinu tady v Praze. Mé nezměrné dík tak patří „Papa Jan und Mutti Jani“ Štundlovým za výtečnou spolupráci během mé intenzivní činnosti v laboratoři i všude jinde. Děkuji Honzovi za zasvěcení do tajů laboratorní práce, o kterých se mi dříve ani nesnilo, počínaje navrhováním primerů přes „high-tech“ píchání crisprů až po klasické histologické techniky. Oběma pak děkuji za legraci nikoli jen po práci, zkrátka za podporu všech stránek mého bytí. Děkuji také všem svým „velkým bráchům“. Laďovi Soukupovi děkuji nejen za zastřešení mého kancelářského stolu i části mého projektu, ale i za rady týkající se experimentů a neutuchající všeobecné povzbuzování. Vojtovi Millerovi patří můj nehynoucí vděk za technickou asistenci a jeho péči o mě i další zvířata, jež jsou v této práci zahrnuta. Jsem však vděčná i dalším bratrům ve zbrani, kteří momentálně působí na jiném bojišti. Děkuji tedy Martinu Minaříkovi, Peterovi Fabianovi a Davidu Jandzikovi za řadu vědeckých podnětů a diskuzí. Nesmím opomenout ani spřízněnou duši Zuzku Karpeckou, která v tom byla už od dob magisterského studia se mnou. Nutno podotknout, že ke všem chovám také obdiv za trpělivost, se kterou snášeli mé kanadské žertíky… Díky!
Děkuji rovněž všem vzdálenějším, ale neméně důležitým „příbuzným“, které jsem pravidelně, alespoň po nějakou dobu, v laborce -Viki & Týna, Štěpánka, Terka, Agáta, Tomáš, Yosuke, Rolf, Simča- či jinde na fakultě -Jirka, Péťa, Karel, Milan, členové labu Pavla Němce- potkávala. Ráda bych také poděkovala Martinu Kráľovičovi za úplně prvotní data, na které předkládaná práce navazuje. Nerada bych opomněla poděkovat kolegům z líhniště ryb ve Vodňanech, Litomyšli a Mexiku, bez jejichž intenzivního množení by to prostě nešlo.
Také nemohu nezmínit, že práce by nevznikla bez pomoci Dr. Briana Metschera ve Vídni, který laskavě skenoval všechno, co jsem si vymyslela, a bez odborných rad Dr. Stephana Handschuha týkajících se kalibrace naskenovaného materiálu. Ráda bych také poděkovala Jindrovi Brejchovi suplujícího mé pokulhávající matematicko-statistické nadání. Děkuji prof. Marcele Buchtové a Marušce Landové Šulcové za ochotu a čas strávený se mnou v jejich laboratoři při zaučování nových histologických technik. Dále chci poděkovat prof. Chrisu Klingenbergovi, který se všemožně snažil najít cestu, jak aplikovat geometrickou morfometriku na tak krásně odlišné lebky a prof. Ann Huysseune za řadu vědecky plodných diskuzí, byť byly nelítostně předčasně uťaty řádícím virem. Mé velké díky taky patří Pavlovi Munclingerovi za motivaci a podporu při mých studijních výjezdech do zahraničí a Radkovi Šandovi za umožnění práce na muzejní binolupě.
Komu však nemůžu zapomenout poděkovat, je můj školitel Robert Černý, který mě uchránil od nejisté budoucnosti kariéry statistického sčitatele hnízdní populace ptáků. Uvedením do krás vývojové biologie a diverzity všech živých organismů mi ukázal možnosti vědy a rozšířil obzory mého poznání. Děkuji, že ještě dále prohloubil poznatky, jak naporcovat slona, které touto prací byly jistě zúročeny.
Mé obrovské dík však patří také mé rodině (nejen) v rodné hroudě, všem mým přátelům (jejichž výčet by se zde nevešel) a v neposlední řadě i příteli za trpělivost, se kterou snášeli všechna má dosavadní studia… a že jich bylo!!

Děkuji!

Finanční podpora

Tato práce byla finančně podpořená následujícími grantovými projekty:
Grantová agentura UK (640616; 640213),
Grantová agentura ČR (16-23836S; 18-04580S; 19-18634S),
Aktion ICM-2016-03562.

Prohlášení o podílu na publikacích

Data přiložená do předkládané dizertační práce Mgr. Anny Pospíšilové byla získána za spolupráce se studenty a pracovníky „*Laboratory for the study of craniofacial evolution & development*“. Podíl řešitelky na jednotlivých publikacích je specifikován níže.

I. **Pospisilova A**, Brejcha J, Miller V, Holcman R, Šanda R & Stundl J (2019) Embryonic and larval development of the Northern pike: a new emerging fish model system for evo-devo research. *Journal of Morphology* 280, 1118–1140.

Podíl řešitelky: barvení a následná obrazová analýza chrupavčitých (Alcian Blue) a osifikovaných (Alizarin Red) tkání; *in vivo* barvení pomocí calceinu (společně s J. Štundlem); odchov a fixace embryonálních a larválních vývojových stádií (společně s J. Štundlem, V. Millerem); příprava obrazových tabulí a tvorba schémat (společně s J. Štundlem); sepisování manuskriptu (společne s J. Štundlem)

Mgr. Robert Černý, Ph.D.

II. **Pospisilova A**, Stundl J, Metscher BD, Brejcha J, Psenicka M & Cerny R (in prep) Comparative cranial skeletogenesis in fishes: towards understanding of developmental strategies of fish craniofacial diversity.

Podíl řešitelky: barvení a následná obrazová analýza chrupavčitých (Alcian Blue) a osifikovaných (Alizarin Red) tkání; *in situ* hybridizace (společně s J. Štundlem); 3D rekonstrukce zhotovených microCT skenů, konverze získaných dat do kódování barevné škály na základě propočtu denzity osifikovaných struktur (společně s B. Metscherem a S. Handschuhem), analýza vývoje denzity osifikovaných struktur lebky (společně s J. Brejchou); příprava obrazových tabulí a schémat manuskriptu; sepisování manuskriptu (společně s R. Černým)

Mgr. Robert Černý, Ph.D

III. Rizzato PP*, **Pospisilova A***, Hilton EJ & Bockmann FA (2020) Ontogeny and homology of cranial bones associated with lateral-line canals of the Senegal Bichir, Polypterus senegalus (Actinopterygii: Cladistii: Polypteriformes), with a discussion on the formation of lateral-line canal bones in fishes. *Journal of Anatomy* 00, 1–29.

* stejný příspěvek autorů

Podíl řešitelky: odchov a fixace larválního materiálu; barvení a následná obrazová analýza osifikovaných tkání (Alizarin Red)

Mgr. Robert Černý, Ph.D

IV. Stundl J, **Pospisilova A**, Jandzik D, Fabian P, Dobiasova B, Minarik M, Metscher BD, Soukup V & Cerny R (2019) Bichir external gills arise via a heterochronic shift that accelerates hyoid arch development. *eLife* 8, e43531.

Podíl řešitelky: farmakologické experimenty; odchov a fixace embryí

Mgr. Robert Černý, Ph.D.

V. Stundl J, **Pospisilova A**, Matějková T, Psenicka M, Bronner ME & Cerny R (2020) Migratory patterns and evolutionary plasticity of cranial neural crest cells in ray-finned fishes. *Developmental Biology* (forthcoming)

Podíl řešitelky: barvení a následná obrazová analýza chrupavčitých tkání (Alcian Blue); *in situ* hybridizace (společně s J. Štundlem); podíl na sepisování manuskriptu

Mgr. Robert Černý, Ph.D.

VI. Soukup V, Tazaki A, Yamazaki Y, **Pospisilova A**, Epperlein H-H, Tanaka EM & Cerny R (in prep) Oral and palatal dentition of axolotl arises from a common tooth-competent zone and co-localizes with the ecto-endoderm boundary.

Podíl řešitelky: barvení a následná obrazová analýza osifikovaných tkání (Alizarin Red)

Mgr. Robert Černý, Ph.D.

VII. **Pospisilova A**, Stundl J, Brejcha J, Metscher BD, Psenicka M, Cerny R & Soukup V (in prep) The dentition is a highly dynamic organ system during the sterlet sturgeon ontogeny (*Acipenser ruthenus*).

Podíl řešitelky: odchov a fixace embryonálních a larválních vývojových stádií; barvení a následná obrazová analýza osifikovaných tkání (Alizarin Red); analýza osteoklastů pomocí TRAP; histologická analýza; *in situ* hybridizace (společně s J. Štundlem); 3D rekonstrukce zhotovených microCT skenů (společně s B. Metscherem); příprava obrazových tabulí a schémat manuskriptu (společně s V. Soukupem a J. Brejchou); sepisování manuskriptu (společně s V. Soukupem)

Mgr. Robert Černý, Ph.D.

Obsah

Seznam obrazových příloh

Seznam použitých zkratek

Do níže uvedeného seznamu zkratek jsou zahrnuty pouze ty, které jsou explicitně použity v textu této práce. Zkratky použité v jednotlivých článcích jsou uvedeny v popiscích obrázků daného článku. Vzhledem k tomu, že termíny zahrnuté v publikacích jsou psány anglicky, je v tomto přehledu uveden i anglický ekvivalent (prostřední sloupek).

an	(angular)	angulare
bb	(basibranchial)	basibranchiale
cb	(ceratobranchial)	ceratobranchiale
ch	(ceratohyal)	ceratohyale
co	(coronoid)	coronoid
de	(dentary)	dentale
dmp	(dermometapterygoid)	dermometapterygoid
dpl	(dermopalatinum)	dermopalatinum
ecp	(ectoperygoid)	ektopterygoid
enp	(entopterygoid)	entopterygoid
hb	(hypobranchial)	hypobranchiale
ipb	(infrapharyngobranchial)	infrafaryngobranchiale
lmx	(lacromo-maxillary)	lacrimo-maxila
mx	(maxila)	maxila
par	(prearticular)	prearticular
pas	(parasphnenoid)	parasphenoid
pmx	(premaxilla)	premaxila
ppt	(palatopterygoid)	palatopterygoid
pre	(prearticular)	prearticulare
vo	(vomer)	vomer

COLII	collagen type II
COLX	collagen type X
Col10a1	collagen type X alpha 1 chain
Shh	Sonic hedgehog
Pitx2	Paired Like Homeodomain 2
TRAP	Tartrate-resistant acid phosphatase

Abstrakt

Skeletální, tzn. chrupavčité, kostěné a zubní tkáně patří ke klíčovým inovacím nás obratlovců. Jednu z druhově nejpočetnějších skupin obratlovců vůbec reprezentují paprskoploutvé ryby (Actinopterygii), což se odráží i v mimořádné diverzitě jejich skeletálních systémů. V této práci se zabývám překvapivě odlišnou kraniální i dentální architekturou zastoupenou již u členů bazálních linií paprskoploutvých ryb. Zatímco bichiři a kostlíni svým masivním exoskeletem hlavy i trupu představují doslova obrněné formy se zuby několika typů pokrývajícími celou orofaryngeální oblast, u jeseterů došlo k rozsáhlé redukci a restrukturalizaci skeletu včetně dentice, takže dospělci jsou bezzubí. Celou analýzu zastřešuje štika, tedy zástupce kostnatých ryb s odlehčenou skeletální architekturou při zhruba srovnatelném počtu kraniálních elementů. Předkládaná práce nabízí první komplexní srovnávací analýzu jejich skeletogeneze a odontogeneze, která nám umožní porozumět tomu, co vývojově zakládá odlišnou kraniální architekturu obratlovců.

Komparativní deskripce růstové dynamiky chrupavčitých a kostěných tkání odhalila distribuci heterochronií na několika úrovních. Rozdílné bylo tedy (i) pořadí (sekvence) formování chrupavčitých i kostěných kraniálních regionů, (ii) relativní načasování počátku samotné chondrogeneze a osteogeneze, stejně jako (iii) doba trvání těchto procesů. Překvapivě odlišná pak byla mezidruhová dynamika vývoje denzity kostí s nečekaným nejprogresivnějším počátkem osifikace u jesetera. Odlišné načasování exprese klíčových skeletálních markerů raných stádií vývoje chrupavky (COLII) a kosti (*Col10a1*) zjevně představuje důležitý faktor regulující následný proces mineralizace. Významná vývojová heterochronie pak byla identifikována během raných stádií diferenciace hlavových tkání se zrychlenou morfogenezí hyoidního proudu hlavové neurální lišty zakládající klíčové hyoidní struktury larválních stádií.

Již základní deskripce odontogeneze unikátních vývojových řad bazálních paprskoploutvých ryb prokázala výraznou variabilitu v distribuci a v raném patternování dentice. Zcela poprvé byla detailně popsána exprese klíčových zubních genů ilustrující proces zakládání zubních polí u těchto linií. Vizualizace mineralizace zubů pak umožnila vysledovat dynamiku jejich nahrazování. Získaná data poukázala na zachovalé ancestrální prvky ve vývoji dentice bichira kontrastující s výjimečně odvozenou denticí jesetera. Zcela poprvé byly popsány aspekty zakládání a vývoje komplexní zubní dentice kostlína.

Klíčová slova: kraniální skeletogeneze, odontogeneze, heterochronie, paprskoploutvé ryby, chrupavka, kost, dentice, neurální lišta

Abstract

Skeletal (cartilaginous, bony, and dental) tissues undoubtedly exemplify the key innovation of vertebrates. Among all recent vertebrates, the most numerous and successful lineage is represented by the Ray-finned fishes that, accordingly, exhibit amazing variety of skeletal architectures and phenotypic adaptations. In order to depict fundamental principles of fish cranial skeletogenesis the developmental formation of skeletal architectures was described, compared and analyzed using members of early branching fish lineages, that exemplify very different strategies of skeletogenesis. While the Senegal bichirs and the Tropical gars are heavily armored forms with massive exoskeleton and hyperossified dental structures covering the whole oropharyngeal region, the European sterlets, on the contrary, possess mostly cartilaginous skeleton and reduce their dental structures during early development. Whole analysis is underpinned by the Northen pike, teleostean species with lightened skeletal architecture with comparable number of cranial elements. The present study represents the first complex comparative analysis of their skeletogenesis and odontogenesis. This allowed to define developmental strategies founding different lineage-specific skeletal architecture of vertebrates.

Comparative description of developmental dynamics of cartilaginous and bony tissues revealed distribution of heterochrony at various levels. We identified differences in (i) sequence of cranial cartilaginous and bony regions development, (ii) relative timing of cartilage and bone formation, and (iii) duration (overal rate of development) of these processes. Quantitative analysis uncovered surprisingly different interspecies dynamic of skull density development with the most progressive beginning of ossification in sterlet. Moreover, different timing of key sketelal markers expression obviously represents an important factor regulating the proccess of ossification. Developmental heterochrony was also identified during early stages of head tissue differentiation with accelerated morphogenesis of hyoid stream of cranial neural crest. This developmental heterochrony is associated with the early formation of hyoid structures during larval development.

Detailed description of odontogenesis based on unique developmental series of basal Ray-finned fishes revealed substantial variation in dental distribution and early patterning of their dentition. Expression of key dental markers depicting early process of dentate field differentiation was thoroughly decribed for the first time. Analysis of dental mineralization patterning allowed to trace dynamics of teeth replacement among studied lineages. These data revealed ancestral state of dentition development in bichir contrasting with exceptionally derived sterlet dentition. Moreover, aspects of teeth formation and development of complex dentition of gar was described in detal for the first time.

Key words: cranial skeletogenesis, odontogenesis, heterochrony, Ray-finned fishes, cartilage, bone, dentition, neural crest

1 Seznam zařazených publikací

Vzhledem k širokému záběru, kterým se tato studie zabývá, je práce pro přehlednost rozdělena do dvou ucelených částí, a to konkrétně do:

I. ČÁST: Srovnání strategií kraniální skeletogeneze

představuje srovnávací analýzu klíčových vývojových procesů zakládající odlišné strategie skeletogeneze napříč skupinou paprskoploutvých ryb.

II. ČÁST: Srovnání patrnosti odontogeneze

deskriptivními přístupy posuzuje vývojovou variabilitu dentice, jež je v liniích ne-kostnatých paprskoploutvých ryb zastoupena.

Předkládaná dizertační práce se opírá o data publikovaná v odborných publikacích (Článek I, III, IV, V), případně o manuskripty v různé fázi připravené k publikování (Článek II, VI, VII). Pořadí číslování článků bylo určeno na základě jejich výskytu v textu. Odkazování na obrazové tabule, zařazené do jednotlivých článků, je uvedeno zkratkou **Fig.** s dodatkem čísla článku, ve kterém se tabule nachází. Zkratka **Obr.** odkazuje na obrázky vyskytující se v samotném textu práce.

I. ČÁST: Srovnání strategií kraniální skeletogeneze

I. **Pospisilova A**, Brejcha J, Miller V, Holcman R, Šanda R & Stundl J (2019) Embryonic and larval development of the Northern pike: a new emerging fish model system for evo-devo research. *Journal of Morphology* 280, 1118–1140.

II. **Pospisilova A**, Stundl J, Metscher BD, Brejcha J, Psenicka M & Cerny R (in prep) Comparative cranial skeletogenesis in fishes: towards understanding of developmental strategies of fish craniofacial diversity.

III. Rizzato PP*, **Pospisilova A***, Hilton EJ & Bockmann FA (2020) Ontogeny and homology of cranial bones associated with lateral-line canals of the Senegal Bichir, Polypterus senegalus (Actinopterygii: Cladistii: Polypteriformes), with a discussion on the formation of lateral-line canal bones in fishes. *Journal of Anatomy* 00, 1–29.

* stejný příspěvek autorů

IV. Stundl J, **Pospisilova A**, Jandzik D, Fabian P, Dobiasova B, Minarik M, Metscher BD, Soukup V & Cerny R (2019) Bichir external gills arise via a heterochronic shift that accelerates hyoid arch development. *eLife* 8, e43531.

V. Stundl J, **Pospisilova A**, Matějková T, Psenicka M, Bronner ME & Cerny R (2020) Migratory patterns and evolutionary plasticity of cranial neural crest cells in ray-finned fishes. *Developmental Biology* (forthcoming)

II. ČÁST: Srovnání patternu odontogeneze

VI. Soukup V, Tazaki A, Yamazaki Y, **Pospisilova A**, Epperlein H-H, Tanaka EM & Cerny R (in prep) Oral and palatal dentition of axolotl arises from a common tooth-competent zone and co-localizes with the ecto-endoderm boundary.

VII. **Pospisilova A**, Stundl J, Brejcha J, Metscher BD, Psenicka M, Cerny R & Soukup V (in prep) The dentition is a highly dynamic organ system during the sterlet sturgeon ontogeny (*Acipenser ruthenus*).

Vzhledem k tomu, že řada skeletálních dat vznikala po delší dobu (již od diplomového projektu) a skeletální část práce je tedy podložená pěti ze 7 článků (viz výše), odpovídá tomu i samotná struktura textu I. a II. části. Zatímco je skeletální část pojatá jako úvod do problematiky s detaily a obrazovými figurami deponovanými do jednotlivých článků, v části zubní jsou, až na jesetera, uvedeny dosud nepublikované výsledky studie s obrazovými tabulemi přiloženými přímo do textu práce. Kompozice kapitol pojednávajících o odontogenezi bichira a kostlína pak odpovídá struktuře jeseteřího zubního manuskriptu (**Článek VII**).

2 Úvod

Skeletální, tedy chrupavčité, kostěné a zubní tkáně jsou považovány ze jednu z klíčových evolučních novinek nás obratlovců (Gans & Northcutt, 1983; Northcutt & Gans, 1983; Northcutt, 2005; Green et al., 2015). Jejich výsledná strukturální diverzifikace se odráží v mohutné evoluční radiaci a fenotypické adaptaci řady obratlovčích linií (Abzhanov et al., 2004; Albertson et al., 2005; Streelman & Albertson, 2006 atd.). Neméně významnou roli v evolučním úspěchu obratlovců sehrála evoluce hlavy (Northcutt & Gans, 1983), jejíž skeletální pokryv chránící mozek a smyslové orgány vystavuje lebku. Přestože se jedná o značně komplexní strukturu, je tvořená relativně jednoduchým a uniformním souborem skeletálních elementů a vykazuje pozoruhodnou diverzitu napříč celou skupinou obratlovců. Již v 19. století si Ernst Haeckel, přední německý evoluční biolog, povšiml nápadných odlišností dospělých lebek u různých skupin obratlovců, která kontrastuje s jejich pozoruhodnou podobností patrnou u základů hlavových struktur v raném vývoji (Haeckel, 1874). Sám Haeckel však tento fenomén nedokázal optikou tehdejší vědy dostatečně vysvětlit, svým výzkumem však podnítil sílící zájem o problematiku vzniku lebky potažmo celé hlavy (Olsson et al., 2005). Tento zájem o studium lebky ještě zintenzivnil po zjištění, že hlavový skeletogenní mezenchym, čili prekurzor skeletálních tkání lebky, může pocházet ze dvou zárodečných vrstev, a to z mezodermu nebo z unikátní populace buněk neurální lišty (kupř. Helms & Schneider, 2003; Santagati & Rijli, 2003; Hall, 2005; Kague et al., 2012; Piekarski et al., 2014; Hirasawa & Kuratani, 2015 atd.).

V posledních letech se ukázalo, že ve srovnání s postkraniálním skeletem, který je z drtivé většiny odvozen z mezodermu, je jedinečným zdrojem hlavového mezenchymu neurální lišta. Stejně jako lebka samotná je i neurální lišta považována za obratlovčí apomorfii a předpokládá se, že její vznik sehrál zásadní roli v evoluci obratlovců (Gans & Northcutt, 1983; Northcutt & Gans, 1983; Northcutt, 2005; Holland et al., 1994; Green et al., 2015). Během vzniku neurální trubice dochází k oddělení buněk neurální lišty, které migrují a následně přispívají k drtivé většině skeletálních tkání hlavy. Přestože je neurální lišta, a zejména migrace buněk neurální lišty, považována za vysoce konzervativní napříč celou skupinou obratlovců, výsledné kraniofaciální skeletální struktury vykazují nebývalou morfologickou diverzitu (srv. kupř. Schneider, 2005; Cerny et al., 2006; Schneider, 2018; Štundl, 2019; **Článek V**). Právě plasticita a evolvabilita buněk neurální lišty a jejich skeletálních derivátů pravděpodobně umožnila schopnost modulovat životní strategie u obratlovců a adaptovat se na nejrůznější prostředí (kupř. Abzhanov et al., 2004; Albertson et al., 2005; Albertson et al., 2010; Powder et al. 2015).

Nebývalou morfologickou diverzitu lze spatřit rovněž u zubů, jejichž vznik je považován za další klíčovou novinku podtrhující evoluční úspěch jejich nositelů. Přestože je evoluční původ zubů dosud předmětem mnoha debat (kupř. Smith, 2003; Fraser et al., 2009; Fraser et al., 2010; Murdock et al., 2013; Donoghue & Rücklin, 2014; Chen et al., 2016; Vaškaninová et al., 2020; Chen et al., 2020), charakter adultní dentice je detailně popsaný u řady obratlovců (shrnuto kupř. v Berkovitz & Shellis, 2017). Množství detailních studií zabývajících se raným vývojem zubů poukázalo na striktně konzervativní proces provázející

samotné zakládání zubních tkání obratlovců, který kontrastuje s jejich finální morfologickou variabilitou. Formování zubních zárodků (stejně jako ostatních ektodermálních orgánů, kupř. chlupy, peří, slinné žlázy, chuťové pohárky) je indukováno interakcí epitelu a přiléhajícího mezenchymu pocházejícího z mezodermu či z buněk neurální lišty (Pispa & Thesleff, 2003; Bloomquist et al., 2015).

Zdaleka nejpočetnější a nejúspěšnější skupinou v rámci současných obratlovců je linie paprskoploutvých ryb (Actinopterygii), která s více než 35 500 doposud popsanými druhy představuje dominantní radiaci obratlovců (Fricke et al., 2020). Vzhledem ke své ohromné morfologické a vývojové variabilitě tak reprezentuje atraktivní systém pro studium vnitrodruhové a mezidruhové proměnlivosti, kterou skelet snad více než kterýkoli jiný systém vykazuje. Právě tato fascinující rozmanitost se dostala do hledáčku řady genetiků a evolučně-vývojových biologů s cílem identifikovat a popsat kandidátní mechanismy, které ji zakládají (Alberch, 1982; Lefebvre & Bhattaram, 2010). Oblast vzniku a vývoje kraniálních skeletálních struktur se tak stala předmětem výzkumu mnoha komparativních studií, ovšem většina z nich zvolila pro posouzení morfogenetických mechanizmů odlišné skeletogeneze fylogeneticky příliš vzdálené druhy (Hanken & Thoroghood, 1993; Mabee & Trendler, 1996).

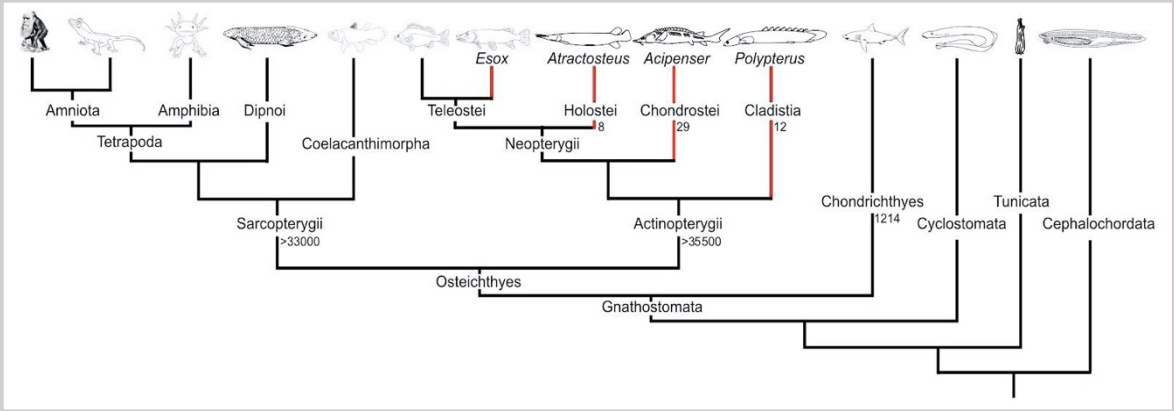

Obr. 1: Schéma fylogeneze recentních skupin strunatců s vyznačenými studovanými liniemi paprskoploutvých ryb (převzato z Štundl, 2019; upraveno).

Předkládaná dizertační práce analyzuje vývoj skeletálních, především tedy hlavových a dentálních, struktur v rámci širší fylogenetické škály a zahrnuje převážně „bazální“[1] linie paprskoploutvých ryb s přesahem k „nejodvozenější“ korunové linii. Jedná se o zástupce zaujímající klíčové postavení v současném fylogenezi paprskoploutvých ryb (Hurley et al., 2007; Obr. 1). V první řadě jde o bichira senegalského (*Polypterus senegalus* Cuvier, 1829) reprezentujícího v rámci paprskoploutvých ryb starobylou, nejraněji se odvětvující linii Cladistia a představuje tedy sesterskou skupinu ke zbylým liniím této analýzy (kupř. Hughes et al., 2018; Betancur-R et al., 2017; Betancur-R et al., 2013; Broughton et al., 2013). Jeseter malý *(Acipenser ruthenus* Linnaeus, 1758), jakožto zástupce Chondrostei, je spolu s veslonosy uznáván jako linie odštěpující se nejblíže skupině Neopterygii seskupující kostlíny, kaprouny

[1] Je známo, že termín bazální (stejně jako odvozený) není zcela vhodný a zpravidla bývá užíván ke zdůraznění, že u těchto linií dochází k zachování řady ancestrálních znaků vyskytujících se u jejich předků. Dále v práci proto používám termínu ne-kostnaté linie.

a kostnaté ryby (Teleostei) (kupř. Near et al., 2012; Broughton et al., 2013; Betancur-R et al., 2017). Právě kostlín mexický (*Atractosteus tropicus* Gill, 1863) reprezentuje spolu se zbylými druhy kostlínů a monotypickým kaprounem poslední „ne-kostnatý" taxon (non-Teleostei, tedy náležející mimo linii kostnatých ryb), který byl molekulárně-fylogenetickými studiemi uznán jako monofyletický a byl pojmenován jako Holostei (kupř. Broughton et al., 2013; Betancur-R. et al., 2013). Celou analýzu zastřešuje štika obecná (*Esox lucius* Linnaeus, 1758) náležející do korunové skupiny kostnatých ryb (Teleostei) (Froese & Pauly, 2019).

Zatímco bichiři a kostlíni představují vysoce osifikované formy s tělem pokrytým mohutnými ganoidními šupinami, s masivním kostěným exokraniem a s množstvím zubů různých tvarů a velikostí v rámci orofáryngu (u kostlína s omezením na struktury branchiálních oblouků v posteriorní části fáryngu, viz dále) (kupř. Bartsch, 1997; Bartsch et al., 1997; Clemen et al., 1998; Jollie, 1984b, Pehrson, 1947; Pehrson, 1958; Grande, 2010; Jollie, 1984a; Scherrer et al., 2017; **Článek III** atd.), u jeseterů došlo k rozsáhlé redukci osifikace a ztrátě ganoidních šupin. Tvorba řady kostí je tak potlačena a ve skeletu dominuje chrupavka. I přesto na lebce pozorujeme mohutnou dorzální dermální osifikaci kryjící chrupavčité chondrokranium i anteriorně protažené rostrum. Čelistní aparát jeseterů prošel v souvislosti s jeho ventrální pozicí výraznou restrukturalizací a redukce osifikace zasáhla i dentici, takže zuby jsou přítomny pouze v raných larválních stádiích a dospělci jsou považováni za bezzubé (kupř. Bemis et al., 1997; Hilton, 2005; Jollie, 1980; Parker, 1882; Pehrson, 1944; Sewertzoff, 1928; Berkovitz & Shellis, 2017; **Článek VII**). To vše kontrastuje s odlehčenou konstrukcí lebky štiky, kdy mezi jednotlivým kostmi je zachována zvýšená mobilita zajištěná jejich překryvy. Již na první pohled nejsou dermální kosti lebky tak mohutné jako u linií popsaných výše. Charakteristické pro tento druh jsou zuby různých tvarů a velikostí, a to zejména na čelistech. V rámci fáryngu dominují zejména na pátém branchiálním oblouku (kupř. Jollie, 1975; Burdi, 2010; **Článek I**), ačkoliv se v juvenilním vývoji objevují na všech obloucích.

Tato práce tedy zahrnuje širokou škálu kraniálních architektur od mohutně osifikované lebky bichira a kostlína přes sekundárně redukovanou osifikaci u jesetera až ke specializované lebce štiky. Přestože řada klasických prací a učebnic popisuje výše uvedené odlišnosti výsledných kraniálních architektur (kupř. de Beer, 1937; Goodrich, 1930; Kent, 1987 atd.), je překvapivé, že se až doposud nikdo nezabýval mechanismy, které tuto disparátnost zakládají. Vzhledem k unikátnímu komparativnímu materiálu, kterým laboratoř školitele disponuje, detailní pochopení těchto mechanismů může být přínosem k nazírání na původ a evoluci kraniální diverzity.

Jednou z hypotéz, která nese zásadní význam pro porozumění potenciálních mechanismů zakládajících evoluční diverzitu v přírodě patrnou, je hypotéza heterochronie v nejširším slova smyslu, tedy změny v načasování různých vývojových procesů (kupř. de Beer, 1951; Alberch et al., 1979; Smith, 2003 atd.). Počátek historie konceptu heterochronie sahá do dob již zmiňovaného Ernsta Haeckla a samotná náplň tohoto pojmu byla v různých dobách výrazně pozměňována v souvislosti s aktuálními potřebami (detaily viz Smith, 2003). V posledních několika desetiletích byla studie heterochronie revitalizována zahrnutím molekulárních přístupů a technik, které odhalily, že většina fenotypické diverzity

je zapříčiněna časoprostorovými změnami probíhajícími již na úrovních genové exprese (kupř. Smith, 2001; Smith, 2003; Albertson et al., 2010; Gunter et al., 2014). Kromě této úrovně dochází k heterochronickým událostem v důsledku diferenciace buněčných populací a ukázalo se, že nositelem plasticity kraniofaciální oblasti, a tedy i hybatelem evoluční diverzifikace, mohou být již zmíněné buňky neurální lišty (kupř. Gans & Northcutt, 1983; Eames & Schneider, 2005; Schneider, 2018).

Tato dizertační práce tak představuje snad vůbec první pokus o identifikaci vývojových strategií kraniálního mezenchymu ovlivňujících disproporční růstovou dynamiku různých typů hlavového skeletu.

3 Cíle práce

Předkládaná dizertační práce úzce navazuje na data získaná v rámci předcházejícího diplomového projektu (Pospíšilová, 2015), ve kterém jsem se zabývala srovnávací analýzou skeletálních a dentálních struktur lebky u bazálních skupin paprskoploutvých ryb, konkrétně u bichira senegalského (*Polypterus senegalus*) a jesetera malého (*Acipenser ruthenus*). Hlavním výstupem této práce pak byla semikvantitativní analýza přirůstání jednotlivých vývojových modulů v rámci lebky definovaných s cílem popsat detaily disproporční růstové dynamiky a identifikovat mechanismy zakládající jejich disparátní skeletální systémy, které zůstávaly nepoznané. Tato studie však byla založená na 2D materiálu s již diferencovanou chrupavkou a kostí. Klíčové informace týkající se mocnosti jednotlivých skeletálních struktur stejně jako charakteristika jejich raných buněčných kondenzací tak zůstaly nerozřešeny. Z tohoto důvodu bylo nutné zaměřit se na časnější vývojová stádia a v navazujícím dizertačním projektu tak analýzu metodicky rozšířit o moderní zobrazovací techniky, čímž by se docílilo hlubšího pochopení vývoje skeletogeneze a odontogeneze u paprskoploutvých ryb. Díky navázání spolupráce s několika institucemi se podařilo získat unikátní embryonální materiál kostlína a štiky a analyzovaná fylogenetická škála se tak obohatila o další linie s rozdílnou kraniální skeletogenezí.

Předkládaná dizertační práce se snaží naplnit následující cíle:

- Detailně charakterizovat kraniální skeletogenezi a odontogenezi za pomocí tzv. „whole-mount“ barvení chrupavčitých a mineralizovaných tkání.

- Popsat raná stádia skeletogeneze a odontogeneze za pomocí genové exprese v mezenchymu studovaných linií.

- Zanalyzovat proces skeletogeneze za využití 3D počítačové mikrotomografie (microCT) umožňující citlivější rozlišení a přesnější detekci přibývání mineralizované tkáně.

- Srovnat dynamiky vývoje kraniálních struktur a stanovených homologických modulů mezi studovanými druhy.

- Získaná data zasadit do kontextu současného poznání skeletogeneze obratlovců.

4 Srovnání strategií kraniální skeletogeneze

4.1 Adultní skeletální architektury studovaných linií vykazují nápadné rozdíly

Morfogeneze (čili „geneze tvaru“) kraniálních skeletálních struktur v rámci rozmanité linie paprskoploutvých ryb přitahovala pozornost řady anatomů a morfologů již po staletí (na tomto místě tedy nelze nezmínit obsáhlé práce autorů jako de Beer, Goodrich, Jarvik, Sewertzoff, Pehrson, Allis atd.). Už v rámci těchto studií bylo poukázáno na překvapivě odlišnou kraniální architekturu u zástupců všech ne-kostnatých radiací ryb ve srovnání s korunovou skupinou ryb kostnatých (Teleostei) (Obr. 2). Nutno podotknout, že vývojovým pozadím zakládajícím tuto diverzitu se však nikdo podrobněji nezabýval.

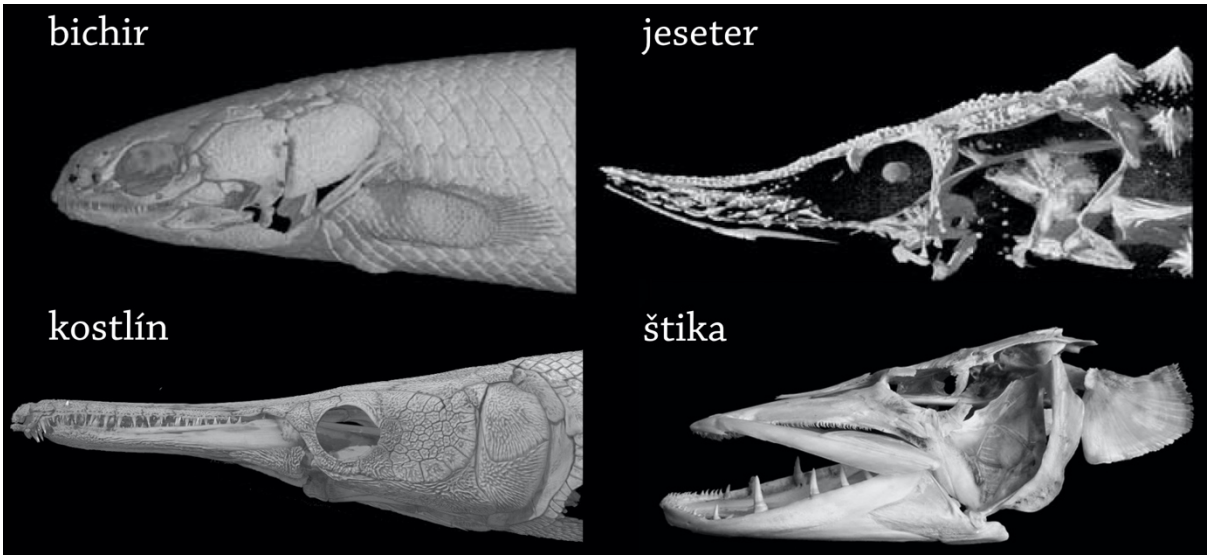

Obr. 2: Odlišnosti výsledné kraniální skeletální architektury bichira (vlevo nahoře), jesetera (vpravo nahoře), kostlína (vlevo dole) a štiky (vpravo dole).
Lebky převzaty z www.digimorpg.org; www.BioLib.cz [navštíveno 28 05 2020]

Vzhledem k tomu, že naše laboratoř již delší dobu disponuje a běžně pracuje se zástupci všech ne-kostnatých radiací ryb (např. Minařík, 2018; Štundl, 2019), studium mechanismů zakládajících diverzitu patrnou u lebek paprskoploutvých ryb zůstávala nasnadě. Pro komparaci se skupinou kostnatých ryb byla zvolená snadno dostupná linie štiky obecné (*Esox lucius*), nicméně její vývoj, a to včetně toho skeletálního, byl doposud popsán spíše sporadicky. Pro srovnání vývoje s takto fylogeneticky vzdálenými druhy, jakými výše uvedené linie jsou, bylo tedy nezbytné identifikovat a popsat zásadní mezníky v průběhu embryonálního a larválního vývoje štiky (**Článek I**). Štika se ukázala být vhodným modelovým organismem, a to hned z několika důvodů. Kromě snadné dostupnosti embryonálního materiálu a obrovského množství velkých jiker (cca 100 tisíc na samici) je bezesporu výhodou usnadněná manipulace s embryonálním materiálem během experimentů.

4.2 Variabilita v pořadí chondrifikace kraniálních struktur u studovaných skupin

Lebka obratlovců vykazuje neobyčejnou strukturální diverzitu kontrastující s uniformními komponentami, jež kraniální skelet vystavují. Tato komplexní struktura sestává

z komponentů chondrokrania[2], viscerokrania a dermatokrania definovaných dle své topografické pozice i zárodečným původem. Dominantní složku během raného vývoje obratlovců představuje chrupavčité chondrokranium a viscerokranium (kupř. Kerr, 1919; Goodrich, 1930; de Beer, 1937; Liem et al., 2001; Kardong, 2019 atd.). Zajímavé je, že podle de Beera (de Beer, 1937) bylo chondrokranium jako specifická komplexní entita vůbec poprvé popsáno v roce 1822 na modelu štiky.

Klíčové pro pochopení formování lebky se ukázalo být pořadí (sekvence) kraniální chondrifikace a osifikace (viz níže) představující jednu z kategorií heterochonie, tzv. „sequence heterochrony" (dále v textu jako sekvenční heterochronie) (Smith, 2001). Informace plynoucí ze studia sekvence zakládání a vývoje kraniálních skeletálních elementů napříč linií obratlovců se ukázaly být užitečným nástrojem pro pochopení evolučních změn a pro identifikování klíčových ontogenetických novinek či heterochronických událostí (Lukas & Olsson, 2020).

Pro rychlé identifikování a pochopení stěžejních proměnných zakládajících rozdíly v procesech kraniální chondrogeneze a pro orientaci v jejím samotném průběhu byla provedena detailní analýza vývoje chondrokrania za pomocí Alcian Blue barvení chrupavčitých tkání. Data prokázala nápadnou variabilitu provázející zakládání jak chondrokrania, tak viscerokrania (Fig. 1, 2; **Článek II**; kompletní deskripce tamtéž). U řady obratlovců jsou parachordália mezi prvními chrupavčitými elementy, které se v rámci chondrokrania zakládají (kupř. de Beer, 1937; Langille & Hall, 1987; Schultze, 1993) jako tomu je u bichira s jeseterem. Je zajímavé, že u těchto linií pozorujeme přednostní chondrifikaci posteriorní části lebky. U kostlína dochází oproti bichirovi či jeseterovi ke zrychlenému zakládání anteriorních trabekul, takže chondrifikace báze chondrokrania probíhá současně. Tato strategie je však odlišná u štiky, u které parachordália chondrifikují až po trabekulách (Fig. 1, 2; **Článek II**). U kostnatých ryb byla tato situace popsána např. u kapra (*Cyprinus carpio*) (Pashine & Marathe, 1977) či bojovnice (*Betta splendens*) (Mabee & Trendler, 1996), u linie Tetrapoda pak pozorujeme přednostní zakládání trabekul v rámci modelového organismu drápatky vodní (*Xenopus laevis*) a u kuňky východní (*Bombina orientalis*) (Lukas & Olsson, 2020). Stejně nekonzistentní je pattern zakládajícího se viscerokrania. Zatímco mandibulární oblouk je u všech linií přítomen ve formě pre-chrupavčitých struktur, pouze u kostlína a štiky se přidávají chrupavky hyoidního oblouku, které, s ohledem k pokročilému stavu chrupavčité diferenciace, vznikly ve srovnání s ostatními strukturami ještě dříve. Rovněž v prvním analyzovaném stádiu kostlína a štiky pozorujeme pre-chrupavčité struktury branchiálních oblouků, které u raných stádií vývoje bichira a jesetera identifikovány nebyly (Fig. 1, 2; **Článek II**). Takový průběh je v rozporu s premisí antero-posteriorního gradientu viscerokraniální chondrifikace u paprskoploutvých ryb (Schultze, 1993). Právě u štiky jsme strukturu hyoidního oblouku (tzv. hyosymplectic)

[2] V literatuře se často setkáváme s pojmem neurokranium v mnoha odlišných způsobech užití, a to buď jako ekvivalent k chondrokraniu, nebo jako pojem zahrnující chondrokranium (chrupavka okolo mozku) spolu s připojenými pouzdry smyslových orgánů, případně jako pojem označující osifikované části chondrokrania (Kardong, 2019). Abych se vyhnula případným nedorozuměním v interpretaci tohoto pojmu, rozhodla jsem se v práci používat pouze pojem chondrokranium.

identifikovali jako vůbec první diferencující se chrupavčitý element v rámci celého chondrokrania (viz **Článek I**; **Článek V**). To se ukázalo být unikátní odchylkou od tradičně uznávaného postupu chondrogeneze, kdy nejdříve dochází k zakládání chrupavčité báze chondrokrania, tj. trabekuly-parachordália a teprve posléze se diferencují struktury viscerokrania (Kerr, 1919; Goodrich, 1930). Obdobný případ byl zatím popsán pouze u tresky (*Gadus merlangus*), u které byla pozorována chondrifikace viscerokrania ještě před založením báze chondrokrania (de Beer, 1937).

4.3 První dermální osifikace lebky odhalila odklon od klasického schématu u štiky

U všech obratlovců s kostní tkání (Osteichthyes) dochází v průběhu vývoje k postupnému zatlačování chondrokrania procesem známým jako endochondrální osifikace. Zastoupení kostí vznikajících tímto procesem, a tedy i míra osifikace chondrokrania, je napříč Osteichthyes dosti variabilní (kupř. Smith & Hall, 1990; Hall, 2005). Již v rámci linií zahrnutých v této studii je podíl endochondrální osifikace lebky značně fragmentární, a to zejména v případě jesetera. U bichira s kostlínem již k endochondrální osifikaci dochází více, avšak převážně v pozdějších vývojových stádiích, ale chondrokranium je stále dobře zachováno i u adultních forem. Podobně tomu je u štiky, u které je zastoupení endochondrálních kostí lebky větší, nicméně narůstá až v pozdějších vývojových stádiích (kupř. Goodrich, 1930; Kent, 1987). Z výše uvedených důvodů se v této studii endochondrální osifikaci blíže nevěnuji, byť je nedílnou součástí lebky obratlovců.

Podstatně více rozšířený je však exoskelet, který, jak již název napovídá, pokrývá výše zmíněný endoskelet, ať už je převážně chrupavčitý či kostěný. Tato struktura vytvářela mohutný hlavohrudní štít zejména u dnes již vymřelých skupin Placodermi a u převážné části Osteostraci. Vedle bazální kompaktní a střední trabekulární kosti nesla rovněž superficiální odontogenní vrstvu složenou z typicky zubních tkání – enameloidu a dentinu (zuboviny), která však byla mnohdy redukována. V průběhu evoluce pak došlo k rozsáhlé redukci hlavohrudního štítu, jež zasáhla i zmíněnou odontogenní vrstvu. Mezi současnými liniemi ryb lze však i nadále nalézt zástupce s lebečními kostmi nesoucími superficiální odontogenní vrstvu (kupř. bichiři, latimérie či sumci) (Hall, 1975; Smith & Hall, 1993; Schultze, 1993; Sire & Hyusseune, 2003; Donoghue & Sansom, 2002; Sansom et al., 2005). V současné době je exoskelet omezen do dermatokrania zahrnujícího všechny kostěné elementy lebky, které vznikají a vyvíjejí se v rámci dermis (tedy bez jakékoli účasti chrupavky) a které vykazují značnou diverzitu morfologickou i histologickou (Smith & Hall, 1993).

Pro rychlé identifikování a pochopení stěžejních proměnných zakládajících rozdíly v procesech kraniální osteogeneze a pro orientaci v jejím samotném průběhu byla provedena detailní analýza vývoje osteokrania za pomocí Alizarin Red barvení kostěných tkání. Data jasně prokázala odlišnosti již v procesu první osifikace. Zatímco u bichira, jesetera a kostlína přednostně osifikují struktury asociované s čelistmi (kdy u bichira s kostlínem dochází k dočasné blokaci osifikace horní čelisti mohutnými cementovými orgány), u štiky se první kosti překvapivě nacházejí v dermální části pletence prsní ploutve, konkrétně jde o strukturu cleithra (Fig. 3; **Článek II**). Obecně panuje domněnka, že pořadí osifikace kostí se odvíjí od funkčních požadavků jejich nositelů a je tedy konzervativní (Mabee & Trendler, 1996;

Adriaens & Verraes, 1998; Schoch, 2006). Vzhledem k tomu, že je u kostnatých ryb popsána korelace první dermální osifikace se strukturami přímo se účastnících příjmu potravy nebo dýchání, se situace identifikovaná u štiky zdá být přinejmenším nestandardní (Schultze, 1993). Mabee & Trendler (1996) však uvádí, že tyto závěry mohou být unáhlené, protože kostěné struktury účastnící se na příjmu potravy a dýchání nepřímo (jako je kupř. cleithrum, hyomandibula, symplectic a urohyal) mohou osifikovat dříve.

4.4 Problematika homologizace dermálních kostí napříč linií paprskoploutvých ryb

V rámci linie Osteichthyes byla identifikována nápadná podobnost co do uspořádání kostí lebky. Až na pár pozoruhodných výjimek (např. vysoce odvozená lebka u bahníků či latimérie) bylo toto rozložení kostí stanoveno jako vysoce konzervativní (kupř. Goodrich, 1930; Kardong, 2019). Vzhledem ke značné morfologické plasticitě osifikovaných struktur dermatokrania odrážející adaptivní požadavky odlišných životních a potravních strategií se však hledání homologie mezi všemi lebečními kostmi ukázalo být mnohdy takřka nemožné (Westneat, 2004). Linie paryb (Chondrichthyes) a vymřelých Acanthodii tento problém vyřešila formováním flexibilního dermálního skeletu vystavěného z malých šupinových jednotek, stav označovaný jako mikromerní (Zhu et al., 2013). Již na sklonku 19. století se užitečným nástrojem pro posuzování homologických struktur v rámci makromerního uspořádání lebečních struktur u ryb ukázal být kanálek postranní čáry, jehož průběh je asociován se specifickými kostmi dermatokrania. To umožňuje komparaci i mezi fylogeneticky vzdálenými taxony, a to včetně těch fosilních (kupř. Allis, 1898; Allis, 1934; Webb, 1989; Webb & Northcutt, 1997). Samotná interakce neuromastů (tj. epidermálních receptorových orgánů sdružených do kanálku postranní čáry) a vznikajících dermálních kostí vzbudila zájem řady vědců s cílem rozklíčovat vzájemnou korelaci těchto dvou entit (více viz **Článek III**). Ukázalo se, že kanálek postranní čáry indukuje okolo sebe kondenzaci mezenchymu, čímž určuje formování dermální kosti (Devillers, 1947).

Přestože byla lebka bichira podrobena zevrubným skeletálním studiím, homologie řady dermálních struktur zůstávala spíše kontroverzní, a to především těch složeného původu (rostral, preoperkulum a sphenotic). Z tohoto důvodu se analýza sekvence přirůstání kraniálních kostí napříč skupinou Osteichthyes omezila pouze na snáze homologizovatelné palatální kosti (viz Schoch, 2006). Ukázalo se, že u řady linií bude potřeba přezkoumat dříve stanovené hypotézy o homologii kostí asociovaných s kanálkem postranní čáry, jak tomu bylo učiněno v případě bichira (**Článek III**). I s ohledem na fylogenetickou pozici se předpokládá, že kraniální skelet bichira inklinuje svou architekturou spíše k velmi raným formám paprskoploutvých ryb (Giles et al., 2017). Avšak další ne-kostnaté linie ryb mají vysoce odvozené lebky, u nichž je řada kostí sekundárně redukována (kupř. jeseteři), proto jsou výše uvedené studie stanovující homologii kraniálních kostí velmi žádoucí.

Vzhledem k tomu, že cílem předkládané práce není srovnání vzniku a přirůstání jednotlivých kraniálních kostí mezi sebou, byly tyto elementy uskupeny do osmi kraniálních regionů (více viz **Článek II**) a časová variabilita v zakládání takových regionů byla následně posuzována na základě těchto regionů (viz níže).

4.5 Variabilita v pořadí osifikace kraniálních struktur u studovaných skupin

Přestože se lebka obratlovců značně liší co do architektury, funkce a patrnosti růstu, ukázalo se, že vývojové mechanismy, které tyto odlišnosti zakládají, mohou být evolučně dosti konzervativní (kupř. Hanken & Hall, 1993; Schoch, 2006). Jak již bylo zmíněno, značný vliv na vývoj lebky bývá přisuzován funkčním požadavkům daných vývojových stádií (např. aktivní lov potravy u raných larválních stádií, potřeba respirace atd.). Obecně tedy platí, že struktury, které zajišťují klíčové fyziologické funkce ve velmi raném vývoji, osifikují přednostně, což bylo potvrzeno např. u ryb (kupř. Mabee & Trendler, 1996; Adriaens & Verraes, 1998), ocasatých obojživelníků (kupř. Germain & Laurin, 2009) či savců (kupř. Sanchez-Villagra et al., 2008). Srovnání pořadí vzniku kraniálních kostěných struktur může rozklíčovat mechanismy sehrávající důležitou roli v diverzifikaci studovaných linií.

Komparace načasování vzniku jednotlivých kraniálních regionů (Fig. 7; **Článek II**) potvrdila rychlou osifikaci všech zubonosných elementů u bichira, jesetera a kostlína, přičemž u bichira dochází k rychlé osifikaci hyoidního oblouku a orbitálního regionu, u jesetera pak k urychlené formaci operkulárního regionu. Tato data jsou v souladu s výše uvedenou hypotézou preferenčního formování struktur zajišťujících životní pochody nezbytných pro přežívání a vývoj. Zároveň data jasně ukazují na přednostní zakládání struktur pletence prsní ploutve u všech linií (zejm. cleithrum), nicméně největší zrychlení je patrné u štiky. U jesetera, jako u jediné linie, pozorujeme osifikaci otického regionu před orbitálním, což odpovídá pozorovanému upřednostnění osifikace postorbitální části lebky (více viz **Článek II**). Vzhledem k vysunovatelnému uspořádání čelistního aparátu se zdá, že účel této posteriorní koncentrace osifikace souvisí s vytvořením pevného rámce pro uložení čelistí a zároveň tím poskytuje čas potřebný k rozvoji a růstu anteriorního rostra, jež je pro hlavu jesetera typické.

Na základě Fig. 7 (**Článek II**) je jasné, že zatímco u bichira dochází k dynamickému zakládání dermatokrania již od počátku osifikace lebky (s raným formováním zubonosných struktur mandibulárního a branchiálního regionu společně s regionem hyoidním, orbitálním a operkulárním), u štiky je tento proces nápadně pozvolnější a posouvá se spíše do pozdějších vývojových stádií s přednostní osifikací regionu pletence prsní ploutve, mandibulárního a operkulárního kraniálního regionu. Nápadně podobný pattern pak vykazuje osifikace lebky jesetera a kostlína s raným zakládáním čelistí a parasphenoidu (mandibulární a orbitální region) u kostlína a čelistí společně se suboperkulem (mandibulární a operkulární) u jesetera.

4.6 První kvantitativní analýza přirůstání kostní tkáně odhalila diametrálně odlišné strategie v dynamice deponování vápníku

Přestože se kost řadí mezi nejprostudovanější kompozitní pojivový materiál velmi dobře dokumentovaný podrobným histologickým barvením napříč obratlovci, mnoho otázek zůstává nevyřešených. Aplikací počítačové tomografie (microCT), případně synchrotronové analýzy, se znalosti prohloubily a ještě naléhavější se ukázala potřeba podrobných 3D vizualizací tak komplexního systému, kterým vývoj skeletu bezpochyby je (Silvent et al., 2017). Velkým přínosem těchto analýz je poměrně přesný propočet hustoty kostní tkáně, který je jinak na základě histologického barvení jen těžko uchopitelný (kupř. Weinhardt et al.,

2018; Hanschuh et al., 2017). Vzhledem k tomu, že 3D vizualizace pomocí microCT nejrůznějších anatomických struktur je již léta zaběhnutou a poměrně dobře dostupnou metodou, je až zarážející, že se doposud nikdo ontogenetické dynamice vývoje hustoty kostí blíže nevěnoval.

Na základě Alizarin Red barvení osifikovaných kostí u studovaných linií je nápadná odlišnost v mocnosti dermálních kraniálních kostí (Obr. 3). Zatímco lebku bichira, jesetera a kostlína vyztužují mohutné kostěné desky, odlehčená architektura štičí lebky charakterizovaná na první pohled tenkými kostmi tomu výrazně kontrastuje. Velmi rychle tedy vyvstala otázka, kdy a jak tato variabilita denzity kraniálních kostí vzniká.

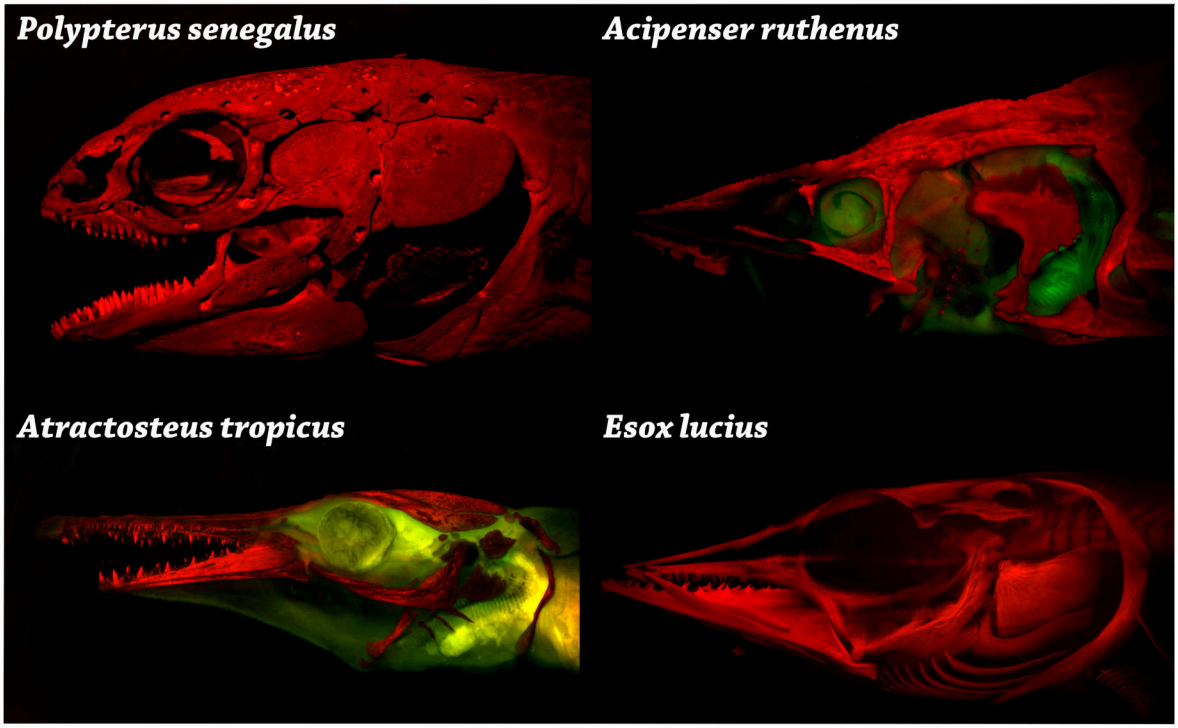

Obr. 3: Odlišnosti v mocnosti kostí sestavujících lebku bichira (vlevo nahoře), jesetera (vpravo nahoře), kostlína (vlevo dole) a štiky (vpravo dole).

Kvantitativní analýza přirůstání kostní tkáně pomocí microCT skenování srovnatelných vývojových stádií odhalila nápadné odlišnosti v dynamice procesu osifikace mezi studovanými liniemi (Fig. 10, 11; **Článek II**). Překvapivě nejrychlejší nástup osifikace překračující prahový limit nutný pro detekci rentgenovým paprskem byl identifikován u jesetera. U kostlína k překročení zmíněné prahové hodnoty rovněž došlo, nicméně na základě barevného kódování je zřejmé, že hustota kostí nedosahuje hodnot u jesetera patrných. U zbylých linií bichira a štiky pak došlo k výraznému zpoždění první osifikace, respektive k pozdnímu navyšování denzity kostí (Fig. 10; **Článek II**). Samotný průběh přirůstání hustoty kostí jasně ukazuje nápadné zrychlení tohoto procesu u kostlína s exponenciálním deponováním vápníku do struktury lebky. Podobný vývoj pak vykazuje lebka bichira, byť kosti lebky nedosahují takové hustoty ani v pozdějších stádiích. Spíše lineární průběh přibývání hustoty kostí je pak patrný u štiky, která zároveň vykazuje nápadné zpoždění v nárůstu hustoty kostí. Vývoj hustoty lebečních kostí u jesetera však vykazuje spíše

nelineární průběh s prudkým nárůstem slabě osifikované kostní tkáně zhruba v polovině studovaného vývoje (Fig. 11; **Článek II**). To je pravděpodobně způsobeno začátkem intenzivní osifikace okrajových částí kosti, jejíž průběh je spíše pozvolný.

U paprskoploutvých ryb se ukázalo, že skeletální vývoj je do značné míry ovlivněn dalšími faktory, jako je životní strategie, konkrétně tedy způsob lokomoce a míra aktivity daného druhu, či lokální adaptací k podmínkám prostředí jako kupř. mechanickému zatížení, vztlaku, ochraně, okolní teplotě atd. (Hall, 1975; Eastman et al., 2014). Redukce vývoje kostí a potažmo celé osifikace je v této linii často se vyskytujícím jevem a míra mineralizace skeletu nemusí tedy přímo souviset s fylogenetickým trendem (kupř. de Beer, 1937; Hall, 1975; Meunier & Huysseune, 1992). U jeseterovitých se zdá být redukce osifikace a rozsáhlý chrupavčitý skelet adaptací k extrémnímu růstu, kterou někteří zástupci vykazují. Právě chrupavka rychlý růst skeletu do extrémních délek umožňuje (viz Hall, 1975). Ztráta řady kraniálních kostí pak souvisí s bentickým způsobem života a s tím spojeným modifikovaným způsobem příjmu potravy za účasti vysunovatelných čelistí. Lebka štiky, podobně jako všech kostnatých ryb, je charakteristická odlehčenou konstrukcí se zvýšenou mobilitou kostěných elementů. Vzhledem ke způsobu lovu s rychlými výpady a schopností pozřít poměrně velké kusy potravy vcelku může být odlehčená architektura lebky jistě výhodou. U bichira s kostlínem předpokládáme, že vysoce osifikovaná lebka je podporou pro rozsáhlou mineralizovanou dentici, kdy minimálně mohutně osifikované čelisti jsou nezbytným předpokladem pro její potřebné ukotvení. Vzhledem k tomu, že lebka představuje vysoce komplexní ucelený systém je sjednocení míry osifikace všech jejich elementů nezbytným požadavkem její funkčnosti (Thomson, 1993).

4.7 Raná dynamika skeletogenního mezenchymu a její podíl na odlišných architekturách ryb

Řada studií zabývajících se zdrojem druhově specifické disparátnosti kraniofaciálních struktur v rámci obratlovců se omezuje pouze na vliv vnějších faktorů (jako kupř. přirozené prostředí, potravní strategie) nesoucích nepochybně zásadní podíl na řízení těchto procesů. Obecně málo se však ví o molekulárních mechanismech, které druhově specifické odlišnosti generují (Fish & Schneider, 2014). Naše výše uvedené analýzy naznačují, že pravděpodobným mechanismem zakládajícím odlišné kraniální architektury bichira, jesetera, kostlína a štiky jsou heterochronie distribuované v procesech chondrifikace a osifikace skeletálních hlavových struktur (pro komparaci heterochronie v samotném načasování vzniku chrupavky a kosti viz Fig. 8; **Článek II**). V posledních letech však byly studie heterochronií rozšířeny o analýzy vývojových procesů na molekulární úrovni, které odhalily, že diverzita fenotypů může být podložena změnami v časoprostorové regulaci exprese konzervovaných genů (např. Smith, 2001; Smith, 2003; Abzhanov et al., 2004; Albertson et al., 2005; Streelman & Albertson, 2006). Dokládá to práce na rodině kolagenů, které jsou nezbytné pro rané formování chrupavek a kostí. Ta prokázala, že zpožděný vývoj kostí v branchiální a kraniální oblasti je podmíněn prodlouženou expresí chondrogenního programu na úkor toho osteogenního, jehož nástup je výrazně opožděn (Albertson et al., 2010).

Ukázalo se tedy, že vývojové události předcházející samotnému formování chrupavek a kostí mohou být klíčovým hybatelem určujícím adultní skeletální morfologii. Pro ověření této hypotézy byla provedena analýza strategií skeletálního mezenchymu v raných larválních vývojových stádiích.

4.7.1 Odlišné načasování aktivity skeletálních genových markerů

Vývojové studie zabývající se kraniální skeletogenezí ukázaly, že formování chrupavky (předznamenávající endchondrální osifikaci) a dermální kosti jsou zakládány identickým shlukováním mezenchymatických buněk (původu mezodermálního či pocházejícího z buněk neurální lišty), které v interakci s epitelem podnítí vznik kondenzací osteo-chondroprogenitorových buněk. Na základě genové exprese následně dochází k jejich diferenciaci směrem k chondrogenním či osteogenním prekurzorům (kupř. Hall & Miyake, 2000; Abzhanov et al., 2007).

V případě chrupavky dochází ke vzniku chondroblastů, tedy prekurzorů chondrocytů, ty následně maturují a skládají se do výsledné chrupavčité struktury (kupř. Hall, 2005). Většina kostí kraniofaciálního skeletu se zakládá procesem tzv. intramembranózní osifikace, jejímž výsledkem jsou dermální kosti lebky (Noden 1983; Hall & Myiake, 1992). Jak již bylo zmíněno, dermální kost vzniká přímo diferenciací mezenchymu bez chrupavčitého základu a oproti endchondrální osifikaci byl tento proces po dlouhou dobu jen velmi málo znám. Vznik dermální kosti předznamenává buněčná kondenzace (viz výše) následně se diferencující do shluku skleroblastů, které dále maturují v osteoblasty. Ty syntetizují a deponují osteoid, kostní matrix procházející mineralizačním procesem (Sire et al., 2009).

Tradičně panovala domněnka, že to, jestli se progenitorová buňka vyvine v chondrocyt či osteoblast, je určené ranou expresí transkripčního faktoru *Sox9* výhradně pro chrupavku či *Runx2* explicitně pro kost (Eames et al., 2003). Recentní studie však prokázaly, že osteoblasty zejména u tzv. „nižších obratlovců“ (ryby a obojživelníci) exprimují molekulární markery běžně asociované s chrupavkou u tzv. „vyšších obratlovců“ (savci a ptáci) (kupř. Eames et al., 2012; Enault et al., 2015). Stejně tak se ukázalo, že *Runx2* je důležitý marker pro diferenciaci raných chondrocytových progenitorů (kupř. Stricker et al., 2002). V průběhu pozdějšího vývoje však začínají být jednotlivé markery vysoce specifické k danému buněčnému typu, takže kupř. *Col2a1* je exprimovaný pouze v rámci diferencovaných chondrocytů, *Col1a1* je charakteristický pro diferenciaci osteoblastů (kupř. Abzhanov et al., 2007; Albertson et al., 2010).

Poměrně velké rozpory se však týkaly aktivity genu *Col10a1*, zpočátku striktně definovaného jako marker zralé hypertrofující chrupavky na prahu endchondrální osifikace u amniot (Zheng et al., 2003). Analýza protilátkového značení COLX později prokázala přítomnost tohoto markeru ve skeletu paryby (Seidel et al., 2017). K velkému překvapení však byla identifikována silná exprese tohoto genu v osteoblastech dánia a kostlína (Eames et al., 2012), stejně jako u drápatky a medaky (pro detaily viz Debiais-Thibaud et al., 2019). Tím se prokázalo, že *Col10a1* nehraje roli pouze při mineralizaci chrupavky, ale je přítomen ve všech typech mineralizované tkáně včetně dentálních struktur. Komparativní analýza

exprese tohoto genu odhalila nápadné odlišnosti v načasování aktivity jeho exprese v rámci studovaných linií ryb (pro detaily viz Fig. 9; **Článek II**).

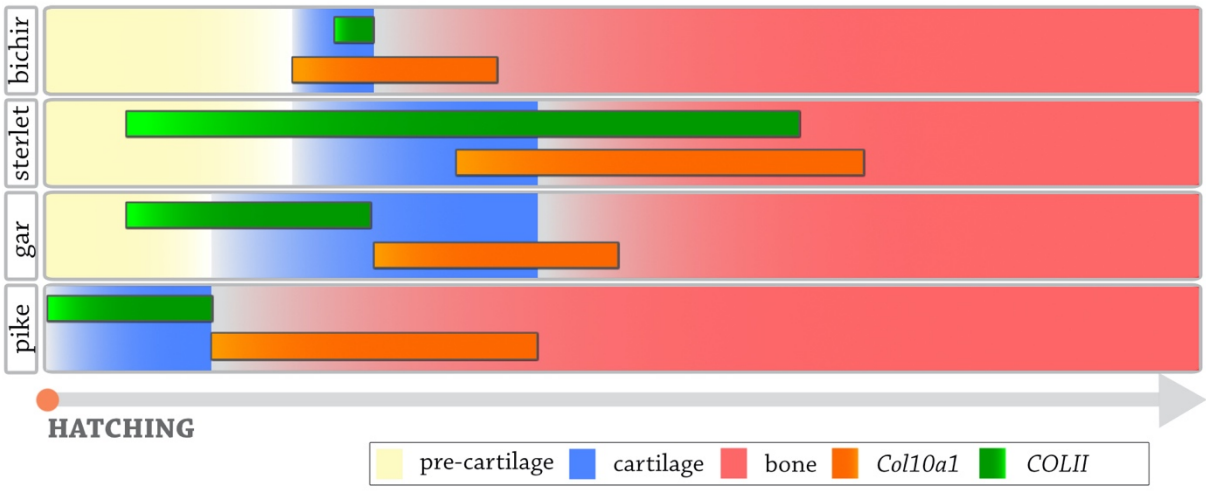

Obr. 4: Časová souvztažnost exprese genu *Col10a1* a chrupavčitého markeru COLII s procesy kraniální skeletogeneze. Chrupavčitá a kostěná perioda byla stanovená na základě Alcian Blue a Alizarin Red barvení skeletálních struktur. Doba exprese genu *Col10a1* byla vysledována pomocí analýzy *in situ* hybridizace, aktivita COLII protilátky byla analyzována imunologickým značením.

Překvapivě variabilní se ukázala být interakce genu *Col10a1* s aktivitou chrupavčitého markeru COLII[3] (Obr. 4). Vůbec nejdelší aktivita COLII proteinu je patrná v kraniálním skeletu jesetera, která začíná dlouho před diferenciací první chrupavky a trvá nejdelší časový úsek po první kraniální osifikaci. Tato data svědčí o delším časovém úseku zakládání chrupavčitých struktur lebky, což pravděpodobně koresponduje popsanému zvýšenému zastoupení chrupavčitých struktur v lebce. Naproti tomu nejkratší COLII protilátkové značení vykazuje skelet bichira vyskytující se pouze ve dvou stádiích krátce za sebou. Pozitivní COLII signál však začíná již v průběhu chondrifikace detekované Alcian Blue barvením a oproti zbývajícím liniím mu předchází exprese *Col10a1* genu. Tato situace odpovídá dynamickému počátku osifikace kraniálních struktur u bichira, jež byla výše popsána. U kostlína se štikou byla pozorována zhruba stejně dlouhá doba přítomnosti COLII. Rozdíl však je patrný v počátku jeho exprese, který byl u štiky detekovaný spolu s prvním barvením diferencovaných chrupavčitých struktur, v případě kostlína však sahá počátek exprese do prechrupavčitých stádií vývoje (Obr. 4). Zhruba stejně dlouhá perioda potom charakterizuje dobu trvání exprese genu *Col10a1* u všech studovaných linií. Rozdíly však vyvstávají v načasování začátku aktivity tohoto genu v rámci celého skeletu. Zatímco u kostlína se štikou nastupuje jeho exprese bezprostředně po ukončení aktivity proteinu COLII (u štiky navíc tato alternace koreluje s dobou první skeletální osifikace), u jesetera dochází ke spuštění exprese v průběhu COLII aktivity. U bichira se pak exprese *Col10a1* posouvá před

[3] Skupina kolagenů se řadí mezi nejhojněji zastoupené proteiny u obratlovců s důležitou strukturální rolí v extracelulární matrix definující mechanické vlastnosti tkání, ve kterých se nachází (různé typy se podílejí na stavbě pokožky, šlach, kostí a zubů, stěn cév atd.). Z tohoto důvodu byla analýza genové exprese *Col2a1* u studovaných skupin náročná a nepřinesla kýžené výsledky. Naproti tomu protilátkové značení fungovalo spolehlivěji, proto je tato analýza tvořená kombinací těchto metodických přístupů.

počátek COLII aktivity a odpovídá počátku první diferenciace chrupavek (Obr. 4). S ohledem na kraniální struktury, ve kterých je *Col10a1* exprimován (viz Fig. 9; **Článek II**) odpovídá tento průběh dynamické osifikaci zubonosných struktur bichira identifikovaný na základě Alizarin Red barvení.

4.7.2 Role buněk neurální lišty ve vývoji lebky

Je známo, že značná část kraniofaciální lebky je utvářená unikátní populací buněk hlavové neurální lišty (Santagati & Rijlli, 2003; Knight & Schilling, 2006; Kague et al., 2012; Pieakarski et al., 2014; Hirasawa & Kuratani, 2015). Dlouhou dobu bylo ventrální viscerokranium zahrnující mandibulární, hyoidní a branchiální oblouky považováno za výhradní derivát buněk neurální lišty (kupř. Cerny et al., 2006), v poslední době se však prokázala účast mezodermu stoupajícího anteroposteriorním gradientem (kupř. Davidian & Malashichev, 2013; Kloučková, 2011). Zárodečný původ dorzálního chondrokrania chránícího mozek a smyslové orgány, stejně jako povrchového dermatokrania, je rovněž zkomplikován účastí mezodermu (Hirasawa & Kuratani, 2015). Výsledky transplantačních experimentů (Couly et al., 1993) stanovily hranici mezi těmito zárodečnými vrstvami, a to v souladu s pozicí notochordu („prechordální kranium" je tvořeno převážně buňkami neurální lišty, struktury umístěné paralelně s notochordem jsou mezodermální). Je nutno zdůraznit, že tato hranice je velmi zjednodušující a tedy pouze orientační. Cílem této studie však není přesné rozhraní u studovaných skupin rozklíčovat, proto je toto pojetí postačující (detaily viz např. Gross & Hanken, 2008; Piekarski et al., 2014 atd.). Pro následnou chondrifikaci chordální části chondrokrania tak nese zásadní význam interakce s notochordem, v případě prechordálního kránia probíhá indukce signály z endodermu (Noden, 1978; Couly et al., 1993; Couly et al., 2002; Kuratani et al., 2013). Z výše uvedeného je tedy zřejmé, že buňky neurální lišty se v hlavě obratlovců podílí na drtivé většině skeletálních tkání a struktur. Právě pochopení detailů migrace a následné morfogeneze této „zárodečné vrstvy" tak může přinést zásadní vhled do mechanizmů zakládajících diverzitu kraniálních struktur jejich nositelů.

U obratlovců je považována diferenciace a následná migrace buněk hlavové neurální lišty za vysoce konzervativní v rámci antero-posteriorní (AP) osy (kupř. Cerny et al., 2004). U bichira však v souvislosti s vývojem vnějších žaber dochází k přednostní diferenciaci hyoidního proudu buněk neurální lišty (**Článek IV**). Tento trend koreloval se zrychlením morfogeneze svalů souvisejících s hyoidní doménou (původu mezodermálního) a s masivní expanzí hlavového endodermu. Jedním z potenciálně důležitých procesů pro vznik kraniální diverzity napříč linií paprskoploutvých ryb se tak ukázala být modulace vysoce konzervativního průběhu migrace buněk neurální lišty v součinnosti s variabilní morfologií endodermu a mezodermu (**Článek V**). Překvapivě zrychlený vývoj hyoidního proudu dříve popsaný u bichira (viz výše) byl následně identifikován rovněž u kostlína a štiky. I zde se ukázalo, že tento trend souvisí s přednostní diferenciací hlavových struktur napojených na hyoidní oblouk (vnější žábry bichira vs. operkulární záhyb s unikátními operkulárními žábrami u kostlína), případně s hyoidním obloukem samotným, jako tomu je u štiky. Hyoidní oblouk je totiž u paprskoploutvých ryb nezbytný pro připojení čelistí k chondrokraniu. Neobvyklá strategie migrace buněk neurální lišty charakterizuje průběh diferenciace hlavy u

jesetera, u kterého dochází ke spojení hyoidního a branchiálního proudu do mohutné hyo-branchiální populace. Teprve ta se v pozdějším vývoji separuje do jednotlivých proudů (pro více detailů viz Štundl, 2019; **Článek V**).

Přestože se výše uvedené odchylky v migraci buněk neurální lišty týkají velmi raného embryonálního vývoje, vzhledem ke skeletogennímu potenciálu buněk neurální lišty tak vytvářejí zdroj variability raných skeletálních kondenzací a potažmo celé adultní lebky.

4.8 Proces skeletogeneze studovaných linií je ve všech aspektech až překvapivě odlišný

Již pilotní deskripce skeletogeneze pomocí vizualizace chrupavčitých a kostěných tkání (**Článek II**; Figs. 1, 4–6) ukázala, že chondrogeneze a osteogeneze kraniálních struktur budou napříč studovanými liniemi značně odlišné. Analýza počátku a celkového načasování těchto procesů (**Článek II**; Fig. 8) pak tuto odlišnost potvrdila a ukázala, že přestože bichir s kostlínem vykazují podobné vysoce osifikované kraniální skeletální architektury dospělců (Obr. 2) načasování prvního vzniku chrupavky a kosti je u těchto linií až překvapivě odlišné (**Článek II**; Fig. 8). Nápadná variabilita panuje i v rámci pořadí chondrifikace a osifikace srovnatelných kraniálních regionů (**Článek II**; Figs. 2, 7). Kvantitativní zhodnocení nárůstu hustoty osifikovaných struktur v průběhu vývoje lebek (**Článek II**; Fig. 10) odhalilo netušený nejrychlejší nárůst hustoty kostí s následným nespojitým průběhem u redukované lebky jesetera (**Článek II**; Fig. 11). I tato analýza však ukázala spíše variabilní patrnost přirůstání denzity kostní tkáně s podobným trendem exponenciálního růstu u kostlína a bichira (**Článek II**; Fig. 11) s vysoce osifikovanou lebkou dospělců. Ranější stádia zakládání chrupavčitých a kostních kondenzací (Obr. 4 a **Článek II**; Fig. 9) byla tak odlišná jako samotný výše popsaný průběh skeletogeneze.

Embryonální vývoj studovaných linií dlouho před samotným vznikem skeletálních kondenzací však poukázal na společnou unikátně zrychlenou morfogenezi buněk hyoidního proudu hlavové neurální lišty (**Článek IV, V**) narušující konzervativní anterio-posteriorní gradient migrace popsaný u obratlovců (Štundl, 2019). Tento průběh odpovídá zrychlenému formování klíčových hyoidních struktur studovaných linií (viz výše) a nepochybně se tedy účastní generování variability kraniálních struktur paprskoploutvých ryb.

5 Srovnání patrnosti odontogeneze

Jak již bylo zmíněno, paprskoploutvé ryby reprezentují nebývalou druhovou diverzitu v rámci obratlovců (viz výše) a osídlují téměř všechny dostupné vodní habitaty, což koreluje s jejich nezbytnou potravní adaptací. Zuby, jakožto ústřední orgán zpracování potravy, se ukázaly být maximálně specializované k potravní strategii jejich nositelů, a tak i diverzita dentice napříč touto linií je ohromující. Zuby se mohou lišit svou velikostí či tvarem (srovnej např. špičák kostlínů s drtícími zuby mořana zlatého *Sparus aurata*), orientací, počtem, strukturou (rozeznáváme např. několik typů dentinu; enamel vs. enameloid), způsobem připojení k zubonosné struktuře (kupř. zuby na čelistech vs. faryngeální desky atd.), lokací (orální vs. faryngeální dentice) a nahrazováním zubů (kupř. polyfyodontní, monofyodontní dentice) (Sire et al., 2002). Podrobné analýzy studující zakládání dentice napříč celou linií obratlovců však identifikovaly iniciaci a raný vývoj dentice jako vysoce stabilní biologický proces regulovaný konzervovaným souborem genů přesně fungujících od žraloka až po člověka (kupř. Jernvall & Thesleff, 2012; Martin et al., 2016; Rasch et al., 2016 atd.). Vývoj zubů obratlovců začíná na rozhraní epitelu a mezenchmu v oblasti odontogenního potenciálu definovaného, alespoň u ryb, jako tzv. odontogenní proužek (angl. odontogenic band). Tato epiteliální zóna je však morfologicky jen těžko rozlišitelná a zpravidla bývá charakterizovaná vizualizací exprese genů *Shh* a *Pitx2* (Fraser et al., 2006; Fraser et al., 2008; Martin et al., 2016; Rasch et al., 2016). U ryb pak tyto signály indukují ztluštění epitelu v místě budoucího zubu a podnítí tak vznik první zubní plakody, která následně invaginuje do mezenchymu za vzniku tzv. zubní lišty (ang. dental lamina) (Smith et al., 2009). Dentice tak představuje zajímavý paradox: zatímco raný vývoj zubu (viz výše) a jeho samotná architektura (zub je podle definice vystavěn z dřeně, tzv. „pulp cavity“ obsahující cévy a nervy; z dentinu neboli zuboviny; z povrchového enamelu neboli skloviny či enameloidu) jsou přísně konzervativní, morfologie výsledné dentice je značně diverzifikovaná, a to dokonce mezi blízce příbuznými druhy, např. cichlidy (Fraser et al., 2008).

I v rámci studovaných skupin ryb lze spatřit značnou diverzitu v uspořádání dentice. U bichira je celá orofaryngeální oblast (s výjimkou struktur hyoidního oblouku) poseta zuby různých tvarů a velikostí (Obr. 5A, B), což pravděpodobně odpovídá situaci typické pro rané Osteichthyes (Nelson, 1969). Podobně je tomu i u kostlína, u kterého je dentice na čelistech a palatálním komplexu (Obr. 5E, G) až na ještě markantnější heterodoncii obdobná stavu u bichira (srovnej Obr. 5A, E). Faryngeální dentice je oproti bichirovi limitována do ventrálního ceratobranchiale V, v pozdějších stádiích vývoje včetně ceratobranchiale IV (Obr. 5H), a do dorzálního infrafaryngobranchiale II, III a epibranchiale IV (Obr. 5F; detaily viz Grande, 2010). To vše kontrastuje se spíše specializovanou denticí jesetera izolovanou do šesti párů zubních polí v rámci orofáryngu, a to pouze během larválních a raných juvenilních stádií vývoje (Obr. 5C, D). Oproti kostlínovi a většině kostnatých ryb se však faryngeální dentice jesetera nachází na anteriorních chrupavčitých strukturách hypobranchiale I a II. Skrze dentální charakteristiku uvedených linií tak projekt srovnává zachovalé ancestrální znaky (bichir a kostlín) stejně jako ty odvozené (jeseter) u bazálních paprskoploutvých ryb, což je

důležitým vodítkem pro pochopení původního/archetypálního stavu dentice v rámci evoluce obratlovců.

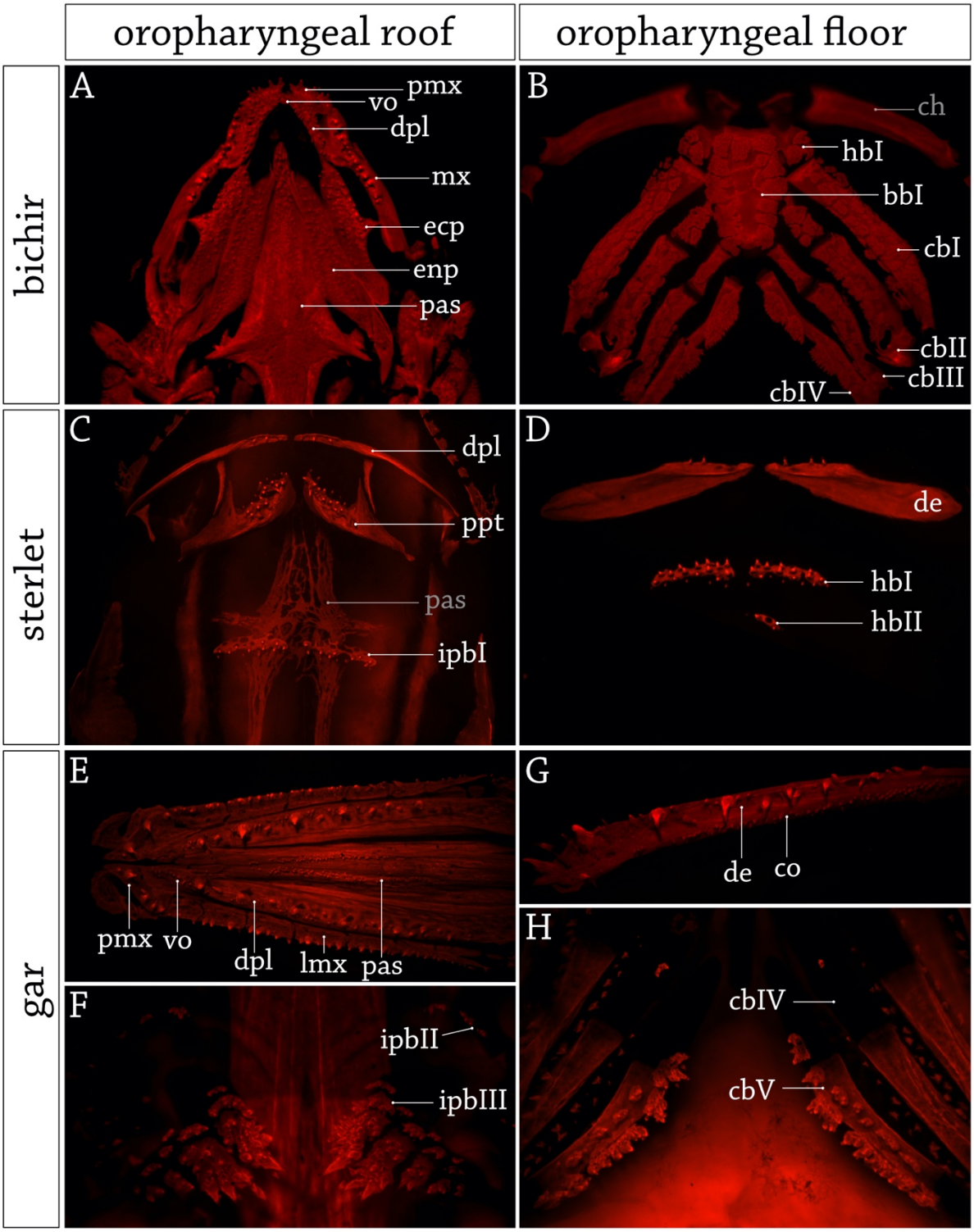

Obr. 5: Uspořádání dentice u bazálních paprskoploutvých ryb. (A, C, E) Pohled na horní čelist a palatální komplex prokazující distribuci zubů na všech strukturách u bichira (A) a kostlína (E) a výraznou redukci zubů potažmo zubních polí v případě jesetera (C). V dorzální části fáryngu kostlína (F) pozorujeme izolovaná zubní pole v rámci infrafaryngobranchiale II, III a epibranchiale IV. (B, D, G, H) Pohled na dolní čelist a ventrální část branchiálních oblouků zobrazující zubní desky pokrývající povrch všech branchiálních oblouků u bichira (B). U jesetera (D) dochází k limitování dentice do izolovaných zubních polí na dentale spodní čelisti a do hypobranchiale I a II. U kostlína zuby pokrývají dentale a koronoidy spodní čelisti (G) a pharyngeální dentice je redukována do zubních polí na ceratobranchiale IV a V.

5.1 Charakteristika dentice bichira

Dentice bichira sestává z komplexního uskupení zubonosných kostí posetých zuby odlišných morfologických charakteristik. Marginální kosti bichira formující čelisti (tj. dentale, premaxila a maxila) jsou charakterizovány zuby uspořádanými do jediné řady (tzv. monostychní uspořádání). Linguální okraje dentale spodní čelisti lemují zubní pole prearticulare a dvou párů coronoidů, které jsou posety drobnými kónickými zoubky polystychního uspořádání, podobně jako tomu je i na kostech palatálního komplexu (Berkovitz & Shellis, 2017; Clemen et al., 1998; Wacker et al., 2001).

Vzhledem ke klíčové fylogenetické pozici, kterou skupina bichirů zaujímá (viz výše), byla jejich dentice podrobená řadě morfologických analýz, nicméně po dlouhou dobu spíše nedostupný embryonální a larvální materiál neumožňoval zahrnutí takových detailních přístupů, jaké by si tato problematika zasloužila. I přesto byly podrobně popsány jednotlivé zubní typy a jejich distribuce v rámci orofaryngeálních zubních polí juvenilního a adultního bichira, sekvence přirůstání kostí asociovaných s denticí a způsoby nahrazování zubů (Clemen et al., 1998; Wacker et al., 2001), stejně jako proces patternování zubů první generace (De Clercq et al., 2014). Rané zakládání dentice, stejně jako pattern vývoje faryngeální detice, však zůstávaly zcela nepopsány. Vzhledem k tomu, že naše laboratoř disponuje tímto vzácným embryonálním materiálem, byly pilotní studie v této oblasti provedeny v rámci diplomových projektů členů skupiny (viz Kráľovič, 2009; Macháčová, 2014). Získaná data jsou však neúplná a v této části dizertace jsem se rozhodla tyto poznatky ještě dále prohloubit.

5.1.1 Některá zubní pole bichira se zakládají rozpadem kontinuálního odontogenního proužku

Znalosti nejranější odontogeneze bichira jsou dosud založené na datech získaných vizualizací mineralizovaných tkání pomocí Alizarin Red barvení, a to u stádia s již pokročile osifikovanými kostmi dentale, maxily, premaxily a ektopterygoidů (Wacker et al., 2001). Abychom tento proces zachytili v samotných počátcích vývoje, navrhli jsme anti-mRNA sondy pro analýzy genové exprese *Pitx2* a *Shh* za účelem detekce oblasti zubní kompetence před samotnou zubní mineralizací. Analýza exprese genu *Shh* však v případě bichira neprokázala signál v oblasti čelistí, přestože pozitivní signál lokalizovaný v mozku potvrdil funkčnost sondy. I přes absenci exprese *Shh* se však pro potřeby popisu rané odontogeneze jako plně funkční ukázal být gen *Pitx2* exprimovaný v odontogenním epitelu.

První exprese genu *Pitx2*, patrná jako pruh v laterálních koutcích úst (Obr. 6A), je lokalizovaná do stádia 29, kdy se poprvé otevírají ústa (Psutková, 2019). Tento zpočátku spíše nezřetelný signál (Obr. 6B, C) se během vývoje ohraničuje a exprese se rozšiřuje mediálně, a to zejména ve spodní čelisti (Obr. 6D, F). V horní čelisti je tento proces blokován mohutnými cementovými orgány (Obr. 6E). V následujícím vývoji dochází ke spojení *Pitx2* exprese v mediáně spodní čelisti (Obr. 6G, I) za setrvávajícího blokování signálu v čelisti horní (Obr. 6H). Teprve v následujícím stádiu vývoje dochází k resorpci cementových orgánů umožňující zrychlené mediální šíření signálu v horní čelisti (Obr. 6J). Zároveň zde pozorujeme separaci signálu do jednotlivých zubních polí na výrazný labiální pruh (Obr. 6K;

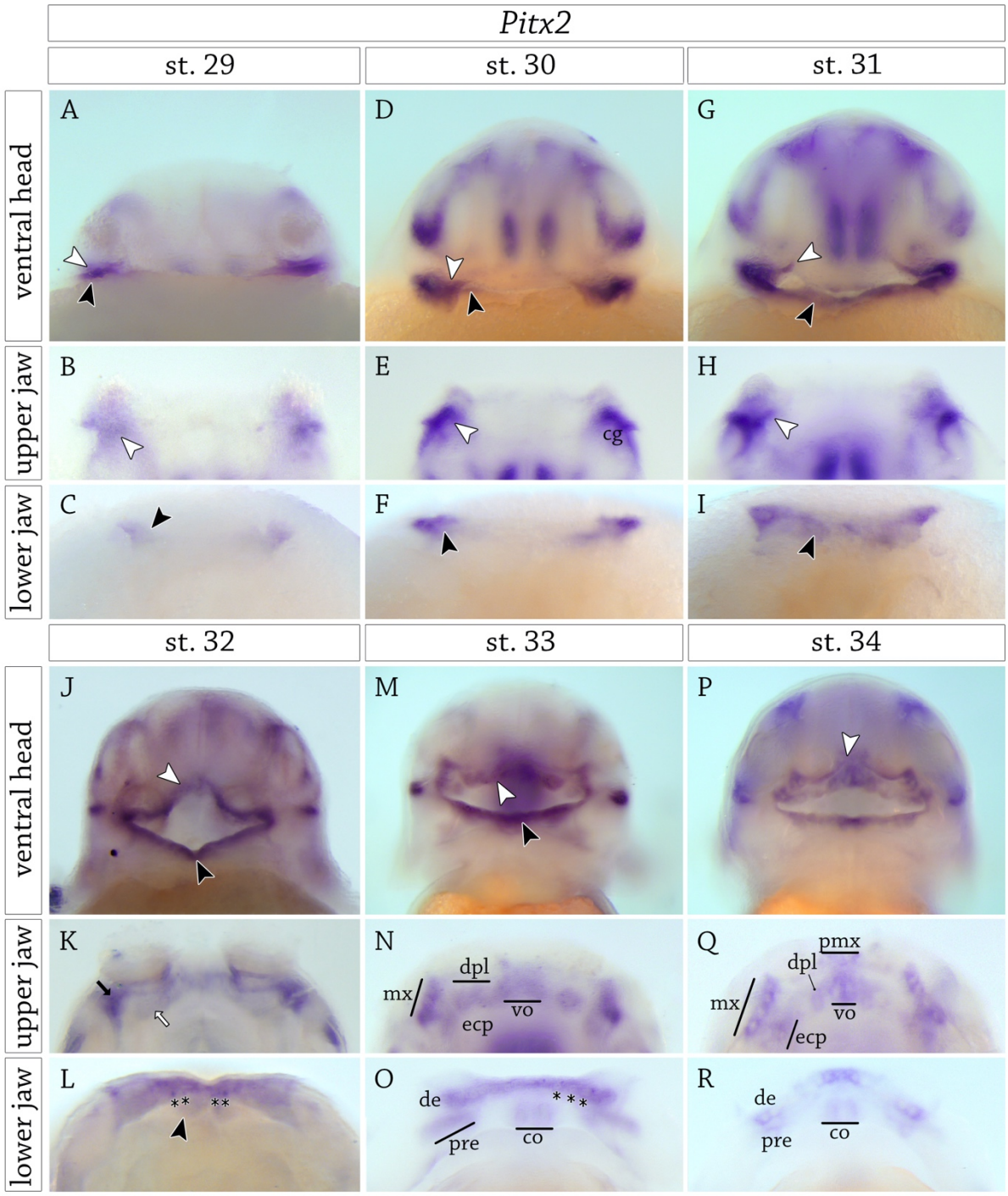

Obr. 6: Exprese genu *Pitx2* během raných stádií odontogeneze bichira. (A, D, G, J, M, P) Ventrální pohled na whole-mount *in situ* hybridizaci zobrazující pozitivní signál v kontextu celé hlavy. (B, E, H, K, N, Q) Palatální pohled zobrazující expresi genu v rámci horní čelisti a palatálního komplexu. (C, F, I, L, O, R) Dorzální pohled na pozitivní *Pitx2* expresi spodní čelisti. bílé hroty šipek poukazují na struktury horní čelisti, černé hroty šipek poukazují na struktury čelisti spodní; bílá a černá šipka značí separaci signálu; hvězdičky značí zubní zárodky.

černá šipka) a slabší pruh linguální (Obr. 6K; bílá šipka). V totožném stádiu vývoje pak ve spodní čelisti přibývá linguální exprese (Obr. 6L; černý hrot šipky) na místě budoucích coronoidů (Obr. 6O). Na dentale spodní čelisti dochází k fokální akumulaci signálu (Obr. 6L; oblast nad hvězdičkami) odpovídající zubním pozicím. Během následujících stádií proces

separace signálu výrazně pokročil (Obr. 6M–O). V rámci horní čelisti je patrná exprese v jednotlivých zubních polích (Obr. 6N), ve spodní čelisti dochází k linguálnímu oddělení prearticulare přičemž signál na dentale a coronoidech výrazně perforují již mineralizované špičky zubů (Obr. 6O, hvězdičky). V posledním studovaném stádiu (Obr. 6P) dochází ke zřetelné diferenciaci zubních pozic jednotlivých zubních polí (Obr. 6Q, R). Zatímco na horní čelisti dochází vlivem ustupujících cementových orgánů ke zpožděnému oddělení premaxiárního zubního pole od vomeru (Obr. 6Q), *Pitx2* exprese uprostřed zubního pole na dentale spodní čelisti slábne a signál je limitován do okrajových anteriorních a posteriorních oblastí (Obr. 6R).

Obecně tedy můžeme shrnout, že v rámci raného vývoje dentice dochází k expresi *Pitx2* signálu v odontogenním epitelu, zpočátku lokalizovaného do koutků otevírajících se úst. Následně se signál šíří mediálně (v horní čelisti je tento proces blokován cementovými orgány), po jehož dovršení nastává separace tohoto uniformního pruhu do jednotlivých zubních polí, v rámci nichž se izolují jednotlivé zubní pozice (viz Obr. 6). Podobný pattern *Pitx2* signalizace byl popsán na příkladu vývoje dentice axolotla (viz **Článek VI**). Rozdílem však jsou raná stádia exprese tohoto genu u axolotla, u kterého nebyla pozorována limitace aktivity *Pitx2* genu do koutků úst a jeho následné dostředivé šíření. U axolotla dochází k expresi coronoidu po jeho separaci ze společného odontogenního pruhu, kdežto u bichira se toto pole zdá být založeno nezávisle na signálu v dentale.

5.1.2 Pořadí nejranější mineralizace zubů a osifikace jednotlivých zubních polí bichira

Přestože byl průběh mineralizace zubů u bichira v minulosti již podroben analýze (viz výše), pořadí vzniku jednotlivých polí se kvůli nedostatečnému stádiování zachytit nepodařilo. Je zjevné, že raná mineralizace jednotlivých zubů odpovídá pořadí diferenciace zubních polí popsaných pomocí analýzy exprese genu *Pitx2* (Obr. 6) a samotný proces se zdá být až překvapivě rychlý (Obr. 7). Ve stádiu 33 (Obr. 6M–O) je zjevná pokročilá diferenciace *Pitx2* signálu na maxile horní čelisti a dentale čelisti spodní, což také odpovídá nejrychlejší mineralizaci těchto zubních polí (Obr. 7A). Již dříve bylo u bichira popsáno, že u řady zubonosných kostí dochází k jejich osifikaci ještě před mineralizací zubů (De Clercq et al., 2014). Stejně tomu je u spodní čelisti v prvním zachyceném stádiu mineralizace zubů, kdy je dentale tvořeno pruhem osifikující kosti, zatímco pozitivní barvení zubu značí pouze jeho špičku. Proces osifikace struktur horní čelisti, a tedy i vývoj zubů, je blokován setrvávajícími cementovými orgány.

Další analyzované stádium vykazuje značný pokrok v počtu mineralizovaných zubů (Obr. 7B). Hlavní kost horní čelisti maxila je na počátku osifikace a je zjevné, že oproti spodní čelisti dochází nejdříve k zubní mineralizaci, která je posléze doprovázená osifikací zubonosné kosti. Po odhalení palatálního komplexu odříznutím spodní čelisti je patrná osifikace struktur vnitřního zubního oblouku a prozatím monostychní uspořádání zubů na dermopalatinu a ektopterygoidu (Obr. 7D). Tomuto rozložení dentice odpovídá i exprese *Pitx2* genu (viz Obr. 6 N,Q), pouze u vomerálního zubního pole ještě nedochází k jeho mineralizaci (Obr. 7D). V rámci spodní čelisti pozorujeme markantní osifikaci zubonosné kosti dentale a s tím související nárůst počtu zubů. Linguálně od dentale vzniklo nové zubní

pole na coronoidech (Obr. 7E; bílý hrot šipky) a v posteriorní části pozorujeme mineralizaci prvního zubu na prearticulare (Obr. 7E; úzká šipka). Nápadný je rozdíl v přirůstání nových zubů na horní a spodní čelisti, kdy na horní čelisti se nové zuby přidávají anteriorně k postupně mineralizující maxile (Obr. 7D; bílá hvězdička), kdežto na čelisti spodní se přirůstající zuby vmezeřují mezi již ukotvené zuby na anteriorní části dentale (Obr. 7E; bílé hvězdičky), posteriorně pak vyplňují volný prostor (Obr. 7E; široká šipka).

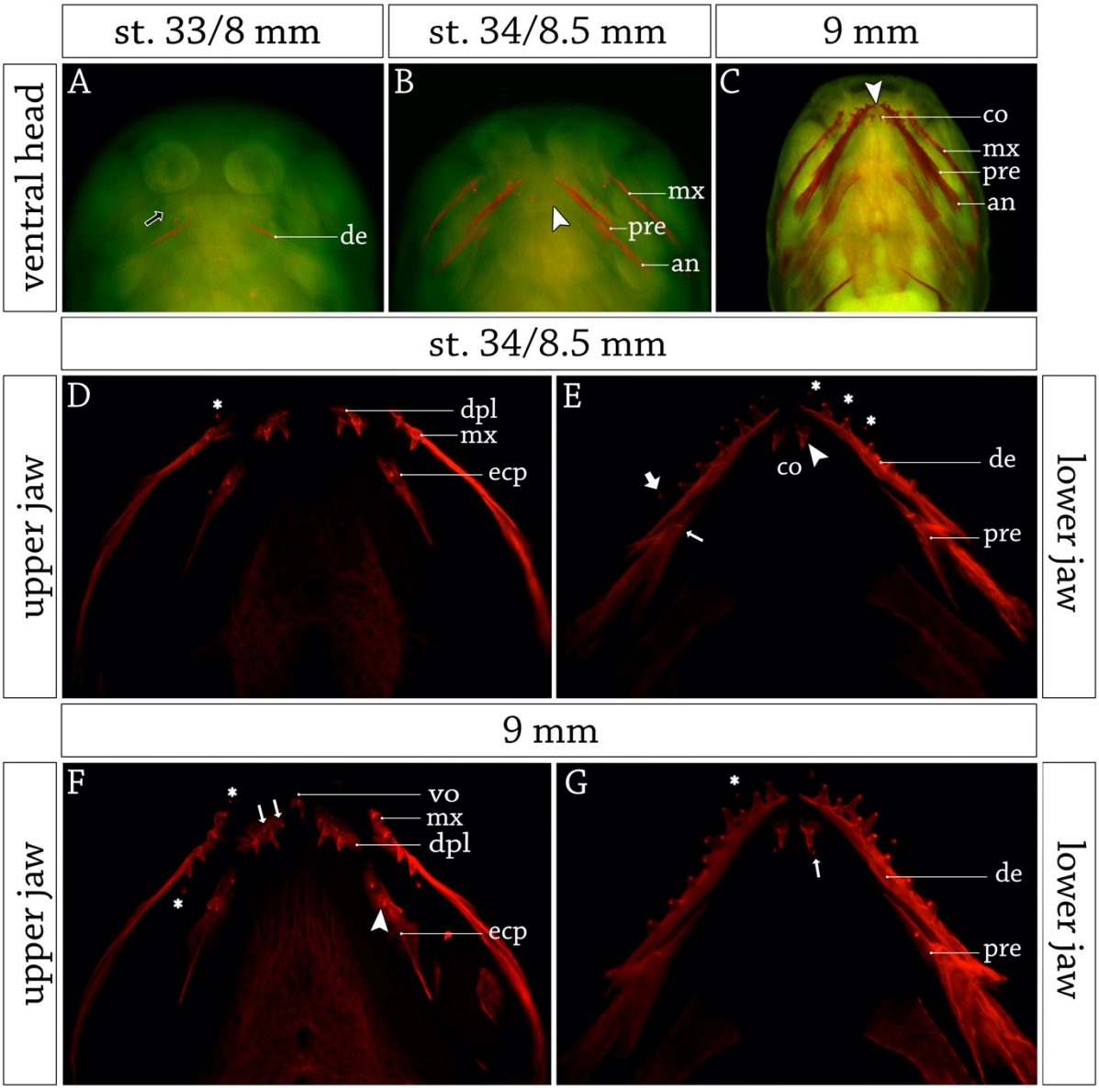

Obr. 7: Časoprostorové zakládání zubních polí bichira. (A-C) Ventrální zobrazení oblasti hlavy s vizualizací osifikovaných a mineralizovaných tkání (červená) v kontextu ostatních tkání (zelená). (D, F) Pohled dovnitř úst na oblast patra odhalující vznikající zubní pole. (E, G) Pohled dovnitř úst zobrazující dentici spodní čelisti. Detailněji viz hlavní text práce.

V rámci následujícího stádia pozorujeme nápadné zmohutnění osifikovaných struktur čelistí a vůbec první mineralizaci zubů na vomeru (Obr. 7C; bílý hrot šipky). Vizualizace palatální dentice po odříznutí spodní čelisti pak potvrdila nárůst počtu zubů všech zubních polí (Obr. 7F, G). Nově se mezi palatální struktury zařazuje nepárový mediálně

umístěný vomer patrný jako izolovaný zub mezi strukturami dermopalatina, na kterých se zakládá polystychní uspořádání (Obr. 7 F; úzké šipky). Podobně tomu je u posteriorně umístěných polí ektopterygoidů, na kterých se k iniciačním zubům (Obr. 7F; bílý hrot šipky) laterálně přidávají nově mineralizující zuby. Na vnějším zubním oblouku maxily je patné přidávání nových zubů jak na anteriorní okraj této kosti tak posteriorně na konec pole (Obr. 7F; hvězdičky). Na spodní čelisti pozorujeme i nadále přidávání nových zubů do alternujících pozic na anteriorní části dentale (Obr. 7G; hvězdička). U zubů lokalizovaných na coronoidech se linguálně zakládá další řada zubů tohoto zubního pole (Obr. 7G; úzká šipka).

5.1.3 Iniciace a vývoj faryngeální dentice u bichira

Zatímco vnitřní zubní oblouk na patře již nabývá polystychního uspořádání (Obr. 7F–G, 8A), branchiální oblouky, které jsou u dospělců hustě pokryty zuby (Obr. 5B), nenesou ani u 10 mm larev známky jediného zubu (Obr. 8B). Počátek formování faryngeální dentice byl již dříve identifikován ve stádiu 11 mm (Pospíšilová, 2015). Ve srovnání s předcházejícím stádiem vývoje je u 10 mm larev zřejmé, že počet zubů na maxile horní čelisti je během raných stádií mineralizace dosti variabilní (srovnej Obr. 7F a Obr. 8A), nicméně souběžné antero-posteriorní přidávání zubů na této struktuře je nápadné (Obr. 8A; hvězdičky). Podobně variabilní se v rámci raného vývoje jeví i počet zubů na vomeru (Obr. 8A, C; bílý hrot šipky). Na spodní čelisti dochází k postupné mineralizaci drobných zubů prearticulare (Obr. 8B; šipka).

V následujícím studovaném stádiu 15 mm se k monostychní struktuře maxily anteriorně přidává premaxila. Mineralizace zubů s touto strukturou asociovaných (Obr. 8C; šipka) probíhá až po spuštění osifikace kosti. Samotná maxila se i nadále prodlužuje (směrem k premaxile), a to anteriorním přidáváním nových zubů (Obr. 8C; hvězdička) a zároveň se mediálně rozšiřuje až k sousedním ektopterygoidům. Na ektopterygoidech pozorujeme počáteční vývoj polystychního uspořádání dentice (Obr. 8C). V rámci spodní čelisti nápadně vzrostl počet zubů na elementech prearticulare lemujících dentale, přičemž na anteriorním okraji této struktury se nově zakládá zubní pole coronoidů 2 (Obr. 8D; bílá šipka). Na prvním branchiálním oblouku pozorujeme první anteriorně zahnuté izolované zuby se širokou bází (Obr. 8D; bílý hrot šipky).

Struktury vnitřního zubního oblouku se v následujícím stádiu 17 mm prodlužují do délky a zvětšují svůj povrch růstem do stran. Tomu odpovídá i proces mineralizace zubů s nimi asociovaných (viz kupř. Obr. 8E; bílé šipky). Na maxile linguálním směrem pozorujeme počáteční vývoj náhradních zubů (Obr. 8E; bílý hrot šipky), což zejména v následujícím stádiu působí dojmem polystychního uspořádání zubního pole (Obr. 8G). V rámci spodní čelisti je patrné intenzivní přibývání zubů na dentale, které se vmezeřují mezi již dříve formované

Na další straně:

Obr. 8: Zakládání a vývoj polystychního uspořádání palatálních zubních polí bichira. (A, C, E, G) Pohled dovnitř úst na oblast patra odhalující formování polystychního uspořádání zubních polí a diferenciaci náhradních zubů. (B, D, F, H) Pohled dovnitř úst zobrazující dentici spodní čelisti a formování zubů na branchiálních obloucích. Detailněji viz hlavní text práce.

zuby (Obr. 8F; hvězdičky), ovšem počet ozubených struktur branchiálních oblouků zůstává v tomto stádiu nezměněn (Obr. 8F).

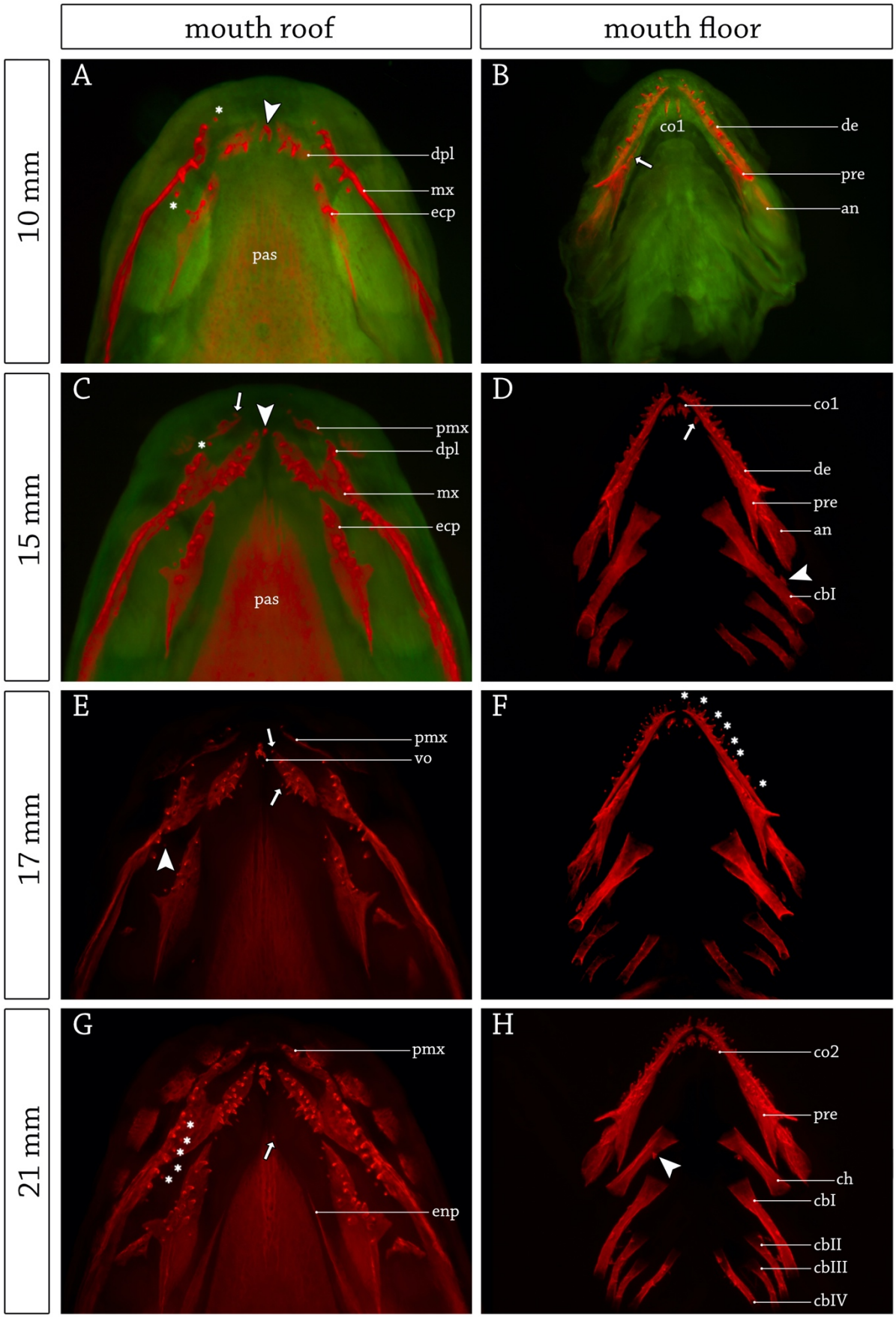

V dalším studovaném stádiu 21 mm je pak nápadné propojení struktur posteriorní premaxily s anteriorní části maxily, nicméně mediálně nespojené premaxily nechávají tento zubní oblouk anteriorně otevřený. V rámci maxily je pak nápadné intenzivní formování náhradních zubů téměř na všech pozicích (Obr. 8G; hvězdičky). Na palatálním komplexu nově osifikuje entopterygoid lokalizovaný po stranách parasphenoidu, na jehož povrchu ještě není patrná známka dentice. První dentální struktura však mineralizuje na špičce parasphenoidu (Obr. 8G; šipka). Nápadný pokrok zubní mineralizace vykazují struktury fáryngu, ve kterém se zuby objevují na hypobranchiale prvního oblouku (Obr. 8H; bílý hrot šipky) a na všech ceratobranchiálních elementech.

5.1.4 Patternování faryngeální dentice bichira je ve srovnání s orální denticí nápadně opožděné

V následujícím vývoji je přirůstání faryngeální dentice dynamičtější, kdežto většina zubních polí čelistí a palatálního komplexu je již dobře diferencována. Ve stádiu 25 mm i nadále pozorujeme vmezeřování nových zubů na maxile (Obr. 9A; hvězdičky), stejně jako mineralizaci dentálních struktur na anteriorním poli parasphenoidu (Obr. 9A; šipky). V rámci faryngeální dentice je nápadné přibývání zubů do dříve založeného zubního pole na hypobranchiale prvního branchiálního oblouku (Obr. 9B; bílý hrot šipky) i formování nových zubů na hypobranchiale II (Obr. 9B; šipka). Přesná identifikace pozice tohoto zubního pole byla posouzena na základě rozložení faryngeální dentice ve stádiu 39 mm (Obr. 9F).

Z následujícího stádia 32 mm je zřejmé, že v rámci zubů na parasphenoidu panuje značná variabilita v procesu zubní mineralizace (Obr. 9C). Labiálně na entopterygoidu dochází k založení dentice (Obr. 9C; šipky) a proces nahrazování zubů na maxile již v tomto stádiu téměř ustal (Obr. 9C; hvězdička). Značný pokrok vykazuje faryngeální dentice, kdy shluk tří zubů na hypobranchiale I předešlého stádia nyní postoupil v zubní desku složenou z malých tupě zakončených zoubků uspořádaných do jedné (pravá strana) nebo dvou (levá strana) zubních desek již nesoucích známky po ztrátě zubů. To kontrastuje s denticí na ceratobranchiale IV vykazující rovněž pravo-levou asymetrii v rozložení zubů, nicméně zuby na této struktuře jsou mnohem větší a ostře zakončené (Obr. 9D). V rámci ostatních ceratobranchií je pak nápadné shlukování zubů do skupin složených z více zubů (Obr. 9D; hrot šipky).

Orální a palatální dentice juvenilního stádia 39 mm vykazuje značný nárůst dentálních struktur hustě pokrývající každé popsané zubní pole, čímž zdrsňuje povrch zubonosných kostí (Obr. 9E). Na ventrálních strukturách fáryngu lze vidět náznak mediálního rozšiřování zubů z ceratobranchiálních a hypobranchiálních struktur na povrch basibranchiale (Obr. 9F). Na ceratobranchiale IV je pak nápadný markantní přírůstek zubů a pokrytí celé její ventrální plochy (Obr. 9F).

Na další straně:

Obr. 9: Pozdní stádia vývoje zubů orální a faryngeální dentice bichira. (A, C, E, G) Pohled dovnitř úst na oblast patra odhalující formování zubů na čelistech a palatálních strukturách. (B, D, F, H) Pohled dovnitř úst a na ventrální část fáryngu zobrazující dentici spodní čelisti a formování zubonosných desek na branchiálních obloucích. Detailněji viz hlavní text práce.

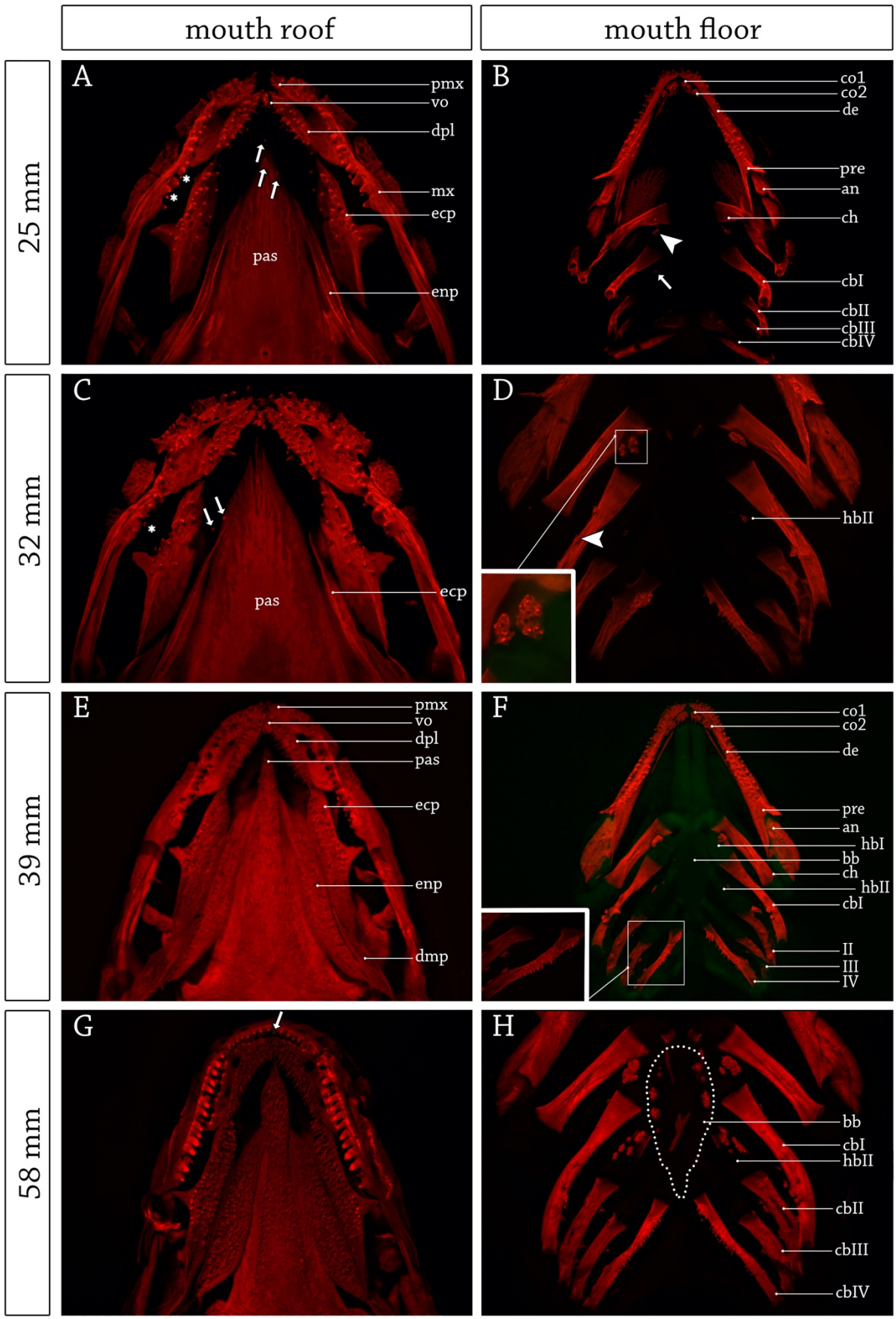
mouth roof
mouth floor
25 mm
32 mm
39 mm
58 mm
A
pmx
vo
dpl
mx
ecp
pas
enp
B
co1
co2
de
pre
an
ch
cbI
cbII
cbIII
cbIV
C
pas
ecp
D
hbII
E
pmx
vo
dpl
pas
ecp
enp
dmp
F
co1
co2
de
pre
an
hbI
bb
ch
hbII
cbI
II
III
IV
G
H
bb
cbI
hbII
cbII
cbIII
cbIV

Poslední studované stádium 58 mm charakterizuje značná velikostní diferenciace dentice. Marginální struktura maxily horní čelisti je lemována zuby výrazně větší velikosti než tomu je na zbývajících palatálních elementech (Obr. 9G). Na symfyzeálním zubu premaxily je patrný proces mineralizace náhradního zubu (Obr. 9G; šipka). Zubní desky ventrální faryngeální dentice v tomto stádiu pokrývají okraje anteriorního basibranchiale stejně jako značnou část hypobranchiale I a II (Obr. 9H).

5.1.5 Na procesu nahrazování zubů se u bichira nepodílí zubní lišta

Drtivou většinu paprskoploutvých ryb (ale i paryb) charakterizuje polyfyodontní dentice umožňující náhradu zubů v průběhu celého života, ale i změnu dentální morfologie mezi zubními generacemi (kupř. Sire et al., 2002; Fraser et al., 2008; Huysseune & Witten, 2006; Thiery et al., 2017). Navíc je polyfyodontní uspořádání pleziomorfním znakem v rámci Chondrichthyes a Osteichthyes a má se za to, že představuje ancestrální stav dentice obratlovců. Schopnost produkovat mnoho zubních generací tak byla pravděpodobně vlastní i raným čelistnatým obratlovcům (Vaškaninová et al., 2020; Maisey et al., 2014; Rücklin et al., 2012).

Klíčovým a jedinečným orgánem umožňujícím kontinuálně nahrazovat dentici byla po dlouhou dobu považována epiteliální struktura tzv. zubní lišta (angl. dental lamina), ve které byly identifikovány epiteliální kmenové buňky účastnící se zakládání nového zubu (kupř. Martin et al., 2016; Thiery et al., 2017; Vandenplas et al., 2016). Překvapením proto bylo zjištění, že u lososa obecného (*Salmo salar*) a u bichira senegalského (*Polypterus senegalus*) s jednoznačným nahrazováním zubů není tato struktura přítomná a autoři navrhli její funkční nahrazení středním dentálním epitelem (angl. middle dental epithelium) lokalizovaným mezi funkčním a náhradním zubem (Hyusseune & Witten, 2008; Vandenplas et al., 2014). Další analýzy tuto hypotézu však nepodpořily a potvrdily, že náhradní zuby se vyvíjejí přímo z vnějšího dentálního epitelu, byť je střední dentální epitel u těchto linií přítomný (Vandenplas et al., 2016).

5.2 Charakteristika dentice jesetera

U některých druhů ryb zuby přítomné u juvenilních forem nejsou dále nahrazovány a dospělci jsou bezzubí, jako tomu je kupř. u sumečků *Corydoras* spp. a *Hoplosternum littorale* (Huysseune & Sire, 1997) či u jeseterů (Hilton et al., 2011).

Přestože byl jeseter podroben celkem podrobné morfologicko-anatomické skeletální analýze, komplexní studie týkající se zakládání a vývoje zubů zůstávaly spíše limitované. Snad vůbec prvním počinem byl detailní popis dentice blízce příbuzného veslonosa (*Polyodon spathula*) (Smith et al., 2015).

Dentice jeseterů přitom vykazuje komplexní systém morfologicky uniformních zubů zahrnující zubní pole monofyodontního i polyfyodontního uspořádání, ovšem ukázalo se, že výměna zubů probíhá pouze na polích polyfyodontních (viz **Článek VII**). Jejich dentice se konkrétně člení do marginální (okrajové) dentice na vzájemně okludující horní (dermopalatinum) a dolní (dentale) čelisti, která je limitována pouze do jedné generace zubů, zatímco palatální (palatopterygoid) a faryngeální zubní pole (tzn. infrafaryngobranchiale a

hypobranchiale I & II) vykazují dynamický, různě dlouhý proces cyklizace dentice, kdy je ztráta zubů kompenzována jejich kontinuálním nahrazováním na protější straně pole. V momentě, kdy je proces formování nových zubů značně zpomalen a zastaven, dochází k redukci uvedených polí. Detailní deskripce zakládání těchto zubních polí a včetně charakterizace jejich dynamického vývoje je předmětem přiloženého článku **Článku VII** a nebude jí zde proto věnováno větší pozornosti.

5.3 Charakteristika dentice kostlína

Kostlíni představují jednu z ne-kostnatých větví paprskoploutvých ryb, jejichž sladkovodní, výhradně piscivorní, zástupci jsou charakterističtí dlouhými úzkými čelistmi posetými řadou zubů nejrůznějších tvarů a velikostí. Během posledních 30 let se podařilo nashromáždit enormní množství fixovaného materiálu, a to hned celé vývojové série kostlína obecného (*Lepisosteus osseus*) a kostlína obrovského (*Atractosteus spatula*), a vzniklo obsáhlé kompendium pojednávající o skeletální morfologii a anatomii všech zástupců recentních i fosilních druhů kostlínů (viz Grande, 2010). Je až zarážející, že je dentální oblast u kostlínů pole zcela neprobádané a jakákoli komplexní studie věnující se aspektu vzniku a formování zubů, včetně patrnosti dentice, chybí. V této kapitole se po vzoru předcházejících analýz odontogeneze bichira a jesetera blíže zaměřuji na popis mineralizační sekvence a morfologie zubů, stejně jako na raná stádia zubního vývoje.

5.3.1 Časoprostorová exprese genů *Pitx2* a *Shh* v průběhu rané odontogeneze kostlína

Řada odontologických studií současné doby se zaměřuje na identifikaci odontogenního proužku (viz výše) jako na strukturu charakterizující nejranější odontogenezi. Také v případě kostlína se nám podařilo navrhnout anti-mRNA sondy pro analýzy genové exprese *Pitx2* a *Shh* za účelem detekce oblasti zubní kompetence před samotnou zubní mineralizací (Obr. 10).

Podobně jako tomu je u bichira (Obr. 6) a jesetera (Fig. 2; **Článek VII**), i u kostlína pozorujeme první expresi genu *Pitx2* v oblastech marginální dentice (Obr. 10A). Tento signál v raných stádiích patrný jako pruh je však lokalizován pouze do spodní čelisti (Obr. 10A, C), v horní čelisti exprese přítomná není (Obr. 10B). Tento průběh signalizace nápadně kontrastuje s expresí na obou čelistech u bichira a jesetera a setrvává i během následujícího stádia (Obr. 10D–F), nicméně signál na spodní čelisti je širší a více ohraničený (Obr. 10F). V dalším vývoji pak dochází k expresi *Pitx2* i na horní čelisti (Obr. 10G), a to hned ve dvou oblastech. V první řadě jde o oblast marginální dentice (Obr. 10H; bílý hrot šipky), linguálně je pak exprese lokalizovaná do zubního zárodku na budoucím vomeru (Obr. 10H; hvězdička). Pozitivní signál na spodní čelisti i nadále setrvává a zdá se být více povrchový a koncentrovaný do okraje čelisti (Obr. 10I). V následujícím stádiu pak dochází ke zřetelné diferenciaci signálu do zubních zárodků na obou čelistech (Obr. 10J). V rámci horní čelisti pozorujeme rozpad marginálního signálu premaxily se zřetelnou iniciační pozicí uprostřed (Obr. 10K; bílá šipka) a nově vznikají zárodky laterálně od dříve založeného vomeru odpovídající pozici zubů na budoucí dermopalatinu (Obr. 10K; hvězdička). Podobně tomu je na čelisti spodní v místě budoucího dentale s patrnou iniciační pozicí uprostřed pole

(Obr. 10L; černá šipka) a labiálními zubními zárodky na budoucím coronoidu 1 (Obr. 10L; hvězdička).

Odlišný je však průběh exprese *Shh*, kdy u kostlína přítomnost exprese tohoto genu v nejranějších analyzovaných stádiích chybí (Obr. 10M–O). *Shh* signál se objevuje až ve stádiu, kdy už se *Pitx2* exprese separuje do jednotlivých zubních zárodků (Obr. 10 J–L a Obr. 10P–R). Exprese *Shh* pak koreluje s výše popsanou expresí *Pitx2*. Místo nejsilnější exprese *Shh* označuje přítomnost prvního zubu v rámci horní (Obr. 10Q; bílá šipka) i spodní (Obr. 10R; černá šipka) čelisti. U dříve založeného zubního zárodku vomeru přibývá laterálně zárodek další (Obr. 10Q; hvězdička).

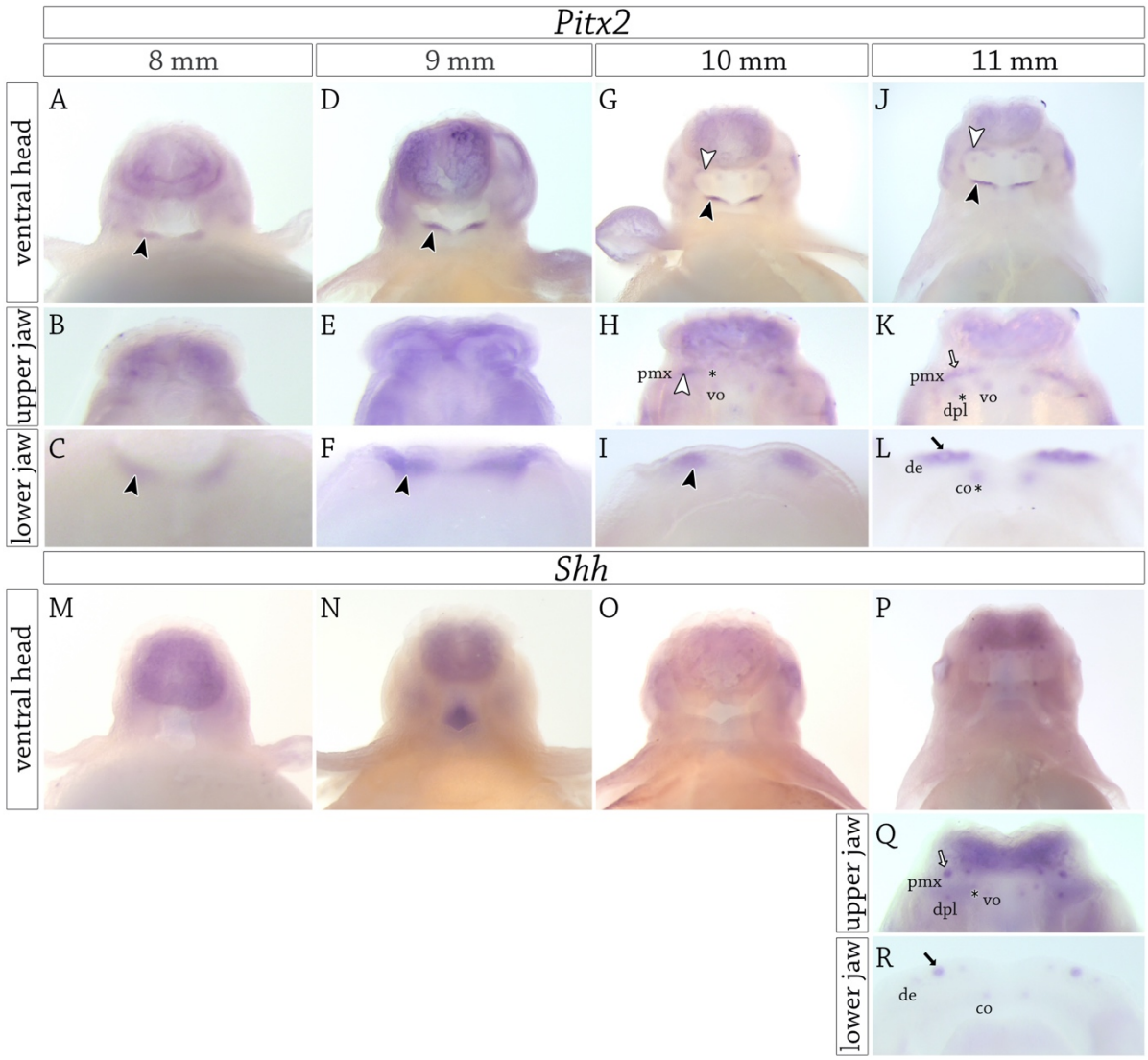

Obr. 10: Exprese genů *Pitx2* a *Shh* během raných stádií odontogeneze kostína. (A-L) Vizualizace exprese genu *Pitx2* a (M-R) genu *Shh* v nejranějších stádiích zubního vývoje v kontextu celé hlavy (A, D, G, J; M-P), na horní čelisti a patře (B, E, H, K, Q) a na čelisti spodní (C, F, I, L, R) po odseparování čelistí. bílé hroty šipek poukazují na struktury horní čelisti, černé hroty šipek poukazují na struktury čelisti spodní; bílá šipka značí zubní zárodek na horní čelisti, černá šipka značí zubní zárodek na čelisti spodní. Detailněji viz hlavní text práce.

5.3.2 Časoprostorová exprese genů *Pitx2* a *Shh* až po mineralizaci všech zubních polí kostlína

V následujícím vývoji pozorujeme kromě genové exprese korelující s pokračující diferenciací orální a palatální dentice posun exprese posteriorně do faryngeální oblasti (Obr. 11). *Pitx2* exprese na horním patře (až na nově se diferencující zárodek budoucího vomeru (Obr. 11A; hvězdička)) vykazuje stejnou patrnost jako ve stádiu předešlém. Na spodní čelisti pak jsou patrné tři stejně diferencované zubní pozice na dentale spolu s linguálními zárodky na coronoidu (Obr. 11A‘). Silná exprese *Pitx2* genu je pak lokalizovaná do dorzálního fáryngu (Obr. 11B). Exprese v tomto zubním poli je výrazná zejm. v prostřední části se třemi zubními zárodky (Obr. 11B; černý hrot šipky), další zubní zárodky jsou pak umístěny anteriorně a posteriorně (Obr. 11B). U stejného jedince pak nebyla lokalizovaná exprese na protilehlém zubním poli ve ventrální části fáryngu (Obr. 11B‘). To však kontrastuje s expresí *Shh* v této oblasti u srovnatelného stádia, u kterého byla exprese lokalizována ve ventrálním fáryngu, nikoli v dorzálním (Obr. 11H, H‘). Jasně rozeznatelný svou velikostí je pak iniciační zubní zárodek tohoto pole (Obr. 11H‘; černá šipka). Je nutné však dodat, že vzhledem k nedostatku jedinců studovaného stádia nebylo možné tuto nestandardní situaci, tj. současnou přítomnost exprese *Shh* a absenci exprese *Pitx2*, ověřit. Distribuce exprese *Shh* na čelistech pak odpovídala expresi *Pitx2* s nápadným velikostním rozlišením iniciačních zubních pozic (Obr. 11G, G‘; šipky).

V následujícím stádiu se rozložení zubních pozic na horní čelisti nemění (Obr. 11C), na čelisti spodní pak pozorujeme posun *Pitx2* exprese na bázi zubu (srovnej Obr. 11A’ a Obr. 11C‘). Totéž je pak patrné i v rámci dorzálního faryngeálního zubního pole (Obr. 11D). Na ventrálním faryngeálním zubním poli se objevuje první exprese *Pitx2* ve třech zubních zárodcích (Obr. 11D‘). Podle exprese *Shh* je zřejmé, že iniciační zub této dentice se nachází ve středu pole (Obr. 11J‘; šipka). Exprese tohoto genu vykazuje na horní čelisti rozložení obdobné předcházejícímu stádiu (Obr. 11I), nicméně velikostní rozdíly zubních základů se v tomto stádiu na čelisti spodní ztrácejí (Obr. 11I‘). Na dorzálním fáryngu, kde se signál objevuje poprvé, jsou nápadně velké zubní zárodky umístěné mediálně v prostřední a dolní řadě (Obr. 11J; šipky), laterálně umístěné signály jsou menší a ohraničenější (Obr. 11J; hvězdičky). Obdobně tomu je i v následujícím studovaném stádiu (Obr. 11L; šipky a hvězdičky). Zda větší exprese genů odpovídá pokročilejšímu zubu by mohla ozřejmit analýza mineralizace faryngeální dentice.

Exprese *Shh* v dalším analyzovaném stádiu ukazuje novou adici zubních zárodků na okrajích dříve založených pozic na premaxile (Obr. 11K; šipky), a nově se formující zubní zárodky na dermopalatinu (Obr. 11K; hvězdičky). Na dentale čelisti spodní naopak pozorujeme vmezeřování nových zárodků mezi dříve formované pozice (Obr. 11K‘; šipky). Je nutné však podotknout, že levo-pravá asymterie v patternu přibývání zubů je u studovaných jedinců často přítomným jevem a stejně tomu je i u diferenciace zubních zárodků ventrálního fáryngu. Na tuto skutečnost bylo již dříve poukázáno u blízce příbuzného kaprouna (*Amia calva*) (Miller & Radnor, 1973). Iniciace nových zubů ventrálního fáryngu se objevuje v alternujících pozicích, jako tomu je na dentale (Obr. 11L‘; šipky).

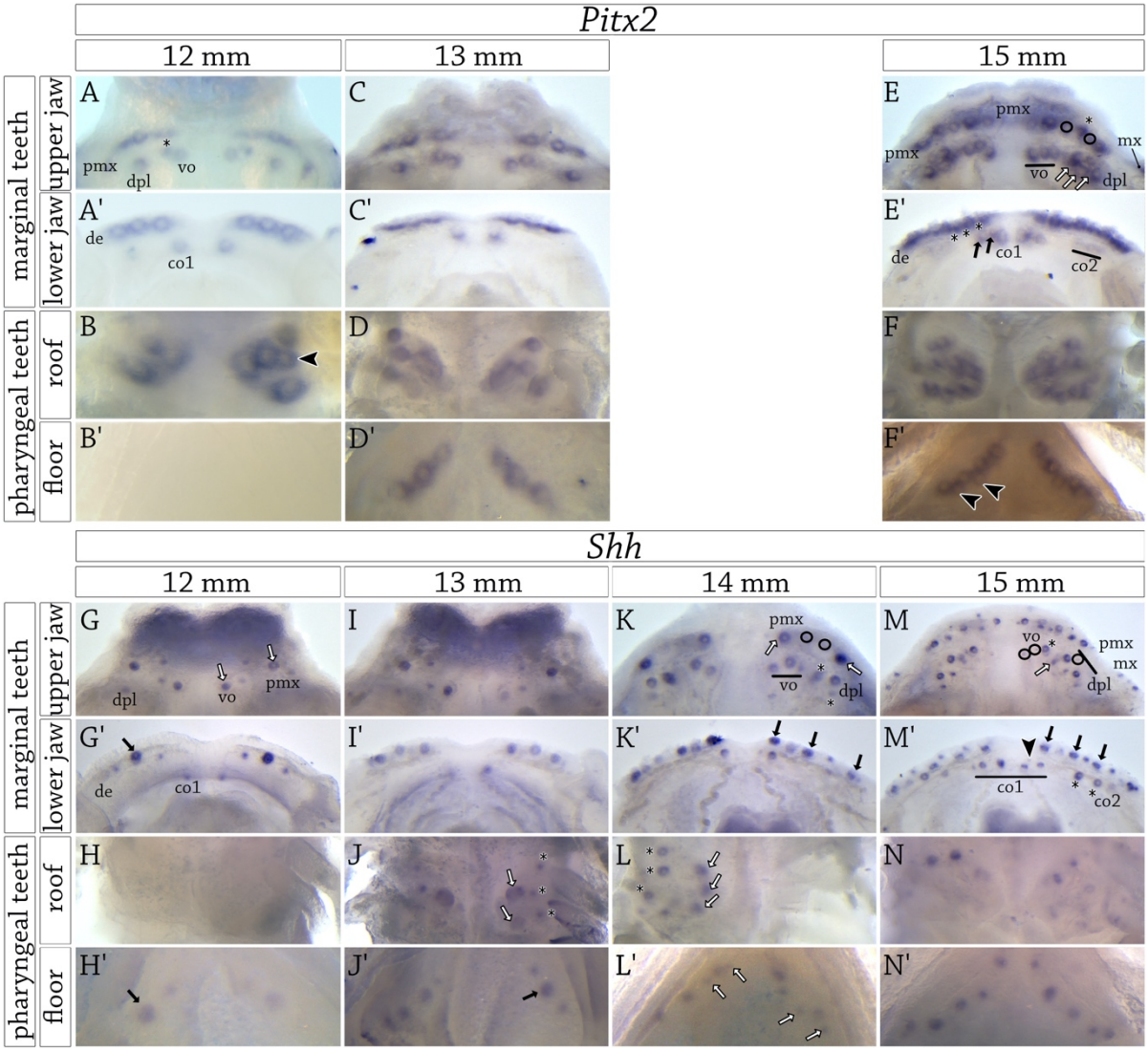

Obr. 11: Exprese genů *Pitx2* a *Shh* během pozdějších stádií odontogeneze kostlína až po mineralizaci všech polí orofaryngu. (A-F') Vizualizace exprese genu *Pitx2* a (G-N') genu *Shh* na horní čelisti a patře (A, C, E; G, I, K, M), na čelisti spodní (A‘, C‘, E’; G‘, I‘, K‘, M‘), v dorzální části fáryngu (B, D, F; G, J, L, N) a na ventrální části fáryngu (B‘, D‘, F’; H‘, J‘, L‘, N‘) po odseparování čelistí. Více detailů v textu.

Následná distribuce signálu *Pitx2* na premaxile dokládá vmezeření nového zárodku mezi dva již dříve formované zuby (Obr. 11E; hvězdička). Posteriorně jsou zřejmé první známky exprese ve vznikající dentici na maxile (Obr. 11E). Linguálně sledujeme topografické rozdělení zubů vnitřního oblouku na mediální vomery a laterální dermopalatina s uskupením zubů do shluků (Obr. 11E; šipky). Tomuto rozvržení také odpovídá rozložení exprese *Shh* (Obr. 11M–N‘). Nápadně alternující signál je zřetelný na premaxile, nové zubní zárodky se tvoří na vomeru (Obr. 11M; hvězdička) a maxile, na dermopalatinu se pak zubní zárodky uskupují do shluků (Obr. 11M; šipka). Na tomto zubním poli se zdá, že nejstarší zub je umístěn labiálně (Obr. 11M, kroužek) zatímco nově se diferencující zárodek vzniká na protější linguální straně (Obr. 11M; šipka). V rámci *Pitx2* exprese spodní čelisti však podobná distribuce není. Signál se však jeví jako střídavé proužky tmavého a světlého pole (Obr. 11E‘). Nové dva laterální zubní zárodky jsou zřetelné na coronoidech 1 (Obr. E‘; šipky), laterálně je slabý signál lemující dentale, místo budoucích coronoidů 2. *Shh* exprese zřejmě o něco málo

staršího stádia pak zřetelně ukazuje na vmezeřování nových zubních pozic mezi dříve formované zárodky na dentale (Obr. 11M‘; šipky), rozšíření coronoidů 1 vmezeřením zubů mezi ty již mineralizované (Obr. 11M‘; černý hrot šipky) a nové formování zubního pole coronoidů 2 (Obr. 11M‘; hvězdičky). Exprese genu na zubním poli dorzálního fáryngu je charakterizována plošnou aktivitou *Pitx2*, na jejímž základě nelze rozlišit pozice nově vznikajících zubů od pozic již utvořených zubů (Obr. 11F). Stejně tomu je i na protějším ventrálním faryngeálním poli. Ve srovnání s předešlým stádiem je však zřejmé, že adice zubních zárodků probíhá na tomto poli na alternativních pozicích (srovnej Obr. 11D’, F‘; černé hroty šipek). Tento proces je však jen stěží vysledovatelný pomocí *Shh* (Obr. 11N‘). Exprese tohoto genu na protějším zubním poli je koncentrována na anteriorní okraj, což je v kontrastu s kontinuální aktivitou *Pitx2* na celém tomto poli (srovnej Obr. 11N a F).

5.3.3 Pořadí mineralizace zubů a osifikace jednotlivých zubních polí kostlína

Obrazová data získaná pomocí barvení mineralizovaných a osifikovaných struktur na podrobné vývojové škále kostlína mexického (*Atractosteus tropicus*) dokládají postup zakládání jednotlivých zubních polí v celém orofáryngu. První mineralizace zubů u kostlína je patrná ve stádiu 14 mm viditelná jako izolované body pozitivního signálu na budoucí premaxile (Obr. 12 A2; krátká šipka) a vomeru (Obr. 12 A2; hrot šipky). Na spodní čelisti pozorujeme izolovaný zub asociovaný s dentale (Obr. 12 A3), zub na pravé straně byl během separace čelistí ztracen. Grande (2010) ve své práci uvádí, že zuby jsou první mineralizující struktury. Na čelisti horní je to bezesporu pravda (Obr. 12 A2), na čelisti spodní se však dle mých dat zdá, že nejdříve dochází k osifikaci dentale a teprve posléze mineralizují zuby s touto strukturou asociované (Obr. 12 A3)

V následujícím stádiu 15 mm je již signál více zřetelný ve větším počtu zubů včetně těch faryngeálních (Obr. 12 B1, B2). V oblasti marginální dentice premaxily mineralizuje nový zub (Obr. 12 B3; hvězdička) a laterálně k iniciačnímu zubu se objevuje nový zub i na vomerech (Obr. 12 B3; krátká šipka). Posterolaterálním směrem se formuje budoucí pole dermopalatina s izolovaným iniciačním zubem (Obr. 12 B3). Tento pattern mineralizace koresponduje s výše uvedenou expresí genů *Pitx2* a *Shh* (Obr. 10–11). U zubního pole umístěného na dorzálních branchiálních obloucích lze spatřit první osifikaci tzv. připojovací kosti (angl. bone of attachment) (Obr. 12 B4; hrot šipky), tedy kosti spojující báze zubů do celistvé zubní desky (viz níže). Zároveň lze jasně vidět rozvrstvení zubního pole do jednotlivých řad, přičemž zubní řada s uvedenou osifikací připojovací kosti představuje nejstarší zubní řadu, pod kterou je umístěna zubní řada č. 2 se dvěma mineralizujícími zuby a zároveň již dochází k zakládání anteriorní řady č. 3 s jedinou špičkou zubu (Obr. 12 B4; hvězdička). Tato data tedy potvrdila domněnku z genových expresních analýz, že nejvíce laterální zuby tohoto pole odpovídají těm nejnověji formovaným zárodkům. V rámci čelisti spodní nové zuby mineralizovaly po obou stranách dříve založeného zárodku (Obr. 12 B5; dlouhá šipka) a nové zubní pole se diferencuje linguálně od dentale. Jedná se o budoucí zubní pole coronoidu 1 (Obr. 12 B5). V posteriorním fáryngu lze spatřit první pár zubů řadící se k ventrální části branchiálních oblouků (Obr. 12 B6; hrot šipky).

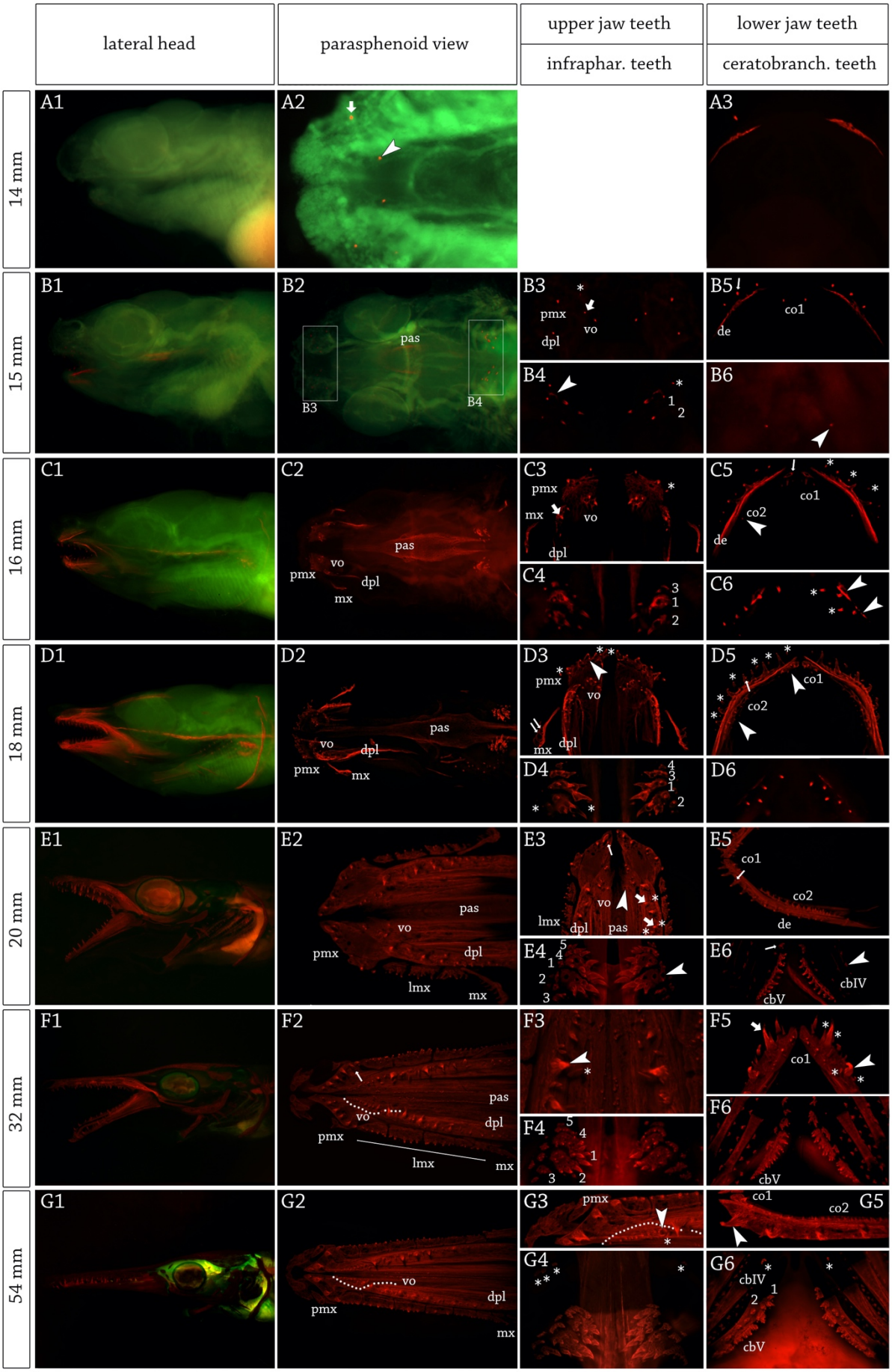
lateral head
parasphenoid view
upper jaw teeth
infraphar. teeth
lower jaw teeth
ceratobranch. teeth
14 mm
15 mm
16 mm
18 mm
20 mm
32 mm
54 mm
A1
A2
A3
B1
B2
B3
B4
B5
B6
C1
C2
C3
C4
C5
C6
D1
D2
D3
D4
D5
D6
E1
E2
E3
E4
E5
E6
F1
F2
F3
F4
F5
F6
G1
G2
G3
G4
G5
G6
pas
pmx
vo
dpl
mx
lmx
co1
co2
de
cbIV
cbV

Na předešlé straně:
Obr. 12: Časoprostorové utváření zubních polí kostlína. (A1-G1) Laterální pohled na celou hlavu ilustrující poměr čelistí k celé lebce kostlína, (A2-G2) pohled dovnitř úst na čelisti a palatální komplex, B3-G3 detail vybraných struktur palatálního komplexu, (B4-G4) vývoj dentice na dorzálních branchiálních obloucích, (B5-G5) pohled na dentici spodní čelisti po odseparování čelistí, (B6-G6) vývoj dentice na ventrálních branchiálních obloucích. Detailněji viz hlavní text práce.

Ve stádiu 16 mm dochází k nárůstu osifikovaných struktur čelistního aparátu (Obr. 12 C1) a zuby v předešlém stádiu přítomné jako mineralizované špičky se tak napojují k příslušné zubonosné kosti premaxily, vomeru a dermopalatina (Obr. 12 C2). Na premaxile dochází k formování zubu na pozici 3 (Obr. 12 C3; hvězdička), na vomeru se rovněž počet zubů zvyšuje o jeden (vpravo). V případě dermopalatina se zdá, že iniciační zub z předešlého stádia se nachází uprostřed tohoto zubního pole (Obr. 12 C3; krátká šipka) a po obou stranách je obklopen nově vzniklými zuby. Dále se k těmto strukturám přidává maxila, jejíž počátek osifikace koreluje s počátkem mineralizace zubů na této kosti (Obr. 12 C3). Posteriorně na zubním poli dorzálních branchiálních oblouků dochází k nárůstu počtu zubů a zároveň k rozšiřování kosti spojující jednotlivé zuby (Obr. 12 C4). Na spodní čelisti se nové zuby vmezeřují mezi ty již k dentale připojené (Obr. 12 C5; hvězdičky) a v posteriorní části se pak zuby řadí za sebe, čímž vyplňují volný prostor. Iniciační zuby coronoidu 1 na své bázi secernují připojovací kost (Obr. 12 C5; dlouhá šipka) a laterálně jsou již patrné špičky nově vznikajících zubů tohoto pole. V tomto stádiu rovněž pozorujeme první diferenciaci zubu náležejícího ke coronoidu 2 (Obr. 12 C5; hrot šipky). V rámci ventrálních branchiálních oblouků pak oproti předešlému stádiu vidíme nárůst počtu zubů vmezeřováním mezi dříve založené zuby (Obr. 12 C6; hvězdičky) a u některých z nich je zřejmý počátek formování připojovací kosti (Obr. 12 C6; hroty šipek).

Následující analyzované stádium 18 mm je charakterizované nápadným prodloužením čelistí (Obr. 12 D1) korelující s růstem jednotlivých kostí čelistního aparátu (Obr. 12 D2). Na vnějším zubním oblouku premaxily je zjevný nárůst počtu zubů napojených k této struktuře a zdá se, že zde dochází ke vmezeřování nových zubů mezi ty již ukotvené, jako tomu je na čelisti spodní (Obr. 12 D3; hvězdičky). Zároveň na tomto poli sledujeme první evidenci formování náhradních zubů, které se formují linguálně v těsné blízkosti zubu nahrazovaného (Obr. 12 D3; hrot šipky). Na vomeru sledujeme rovněž nárůst počtu zubních struktur, nicméně jejich přibývání se zdá být spíše nahodilé a jen těžko lze vysledovat na základě barvení mineralizovaných tkání nějakou patrnost (Obr. 12 D3). Na dermopalatinu je ve srovnání s předešlým stádiem nápadné formování polystychního uspořádání pole s novými zuby přidávajícími se převážně linguálním směrem (Obr. 12 D3). Zajímavá je pak morfologie zubů na maxile, které se vydiferencovaly ve výrazně zahnuté tesáky“ (angl. fangs). I na tomto zubním poli dochází ke vmezeřování nových zubů mezi ty již ukotvené (Obr. 12 D3; dlouhé šipky). Ve srovnání s bichirem představuje maxila u kostlína značně redukovanou kost, která je v průběhu růstu čelistí posunována posteriorně (srovnej Obr. 12 D2 a Obr. 12 F2). Zubní pole na dorzálních branchiálních obloucích vykazuje zmohutnění kosti spojujících jednotlivé zuby a nápadné zvětšení mediálních zubů tvořících velké tesáky. Laterálním a anteriorním směrem pak sledujeme výraznou redukci velikosti zubů (Obr. 12 D4). I nadále je toto zubní pole rozvrstveno do pomyslných zubních řad,

přičemž anteriorně dochází k založení čtvrté řady. Zuby na tomto poli přibývají oběma směry, tj. mediálně i laterálně (Obr. 12 D4; hvězdičky). Markantní nárůst počtu zubů však pozorujeme na spodní čelisti, přičemž se nové zuby i nadále vmezeřují do prostorů mezi ty již ukotvené (Obr. 12 D5; hvězdičky). I v případě této dentice dochází k zakládání náhradních zubů umístěných linguálně v těsné blízkosti zubů z první generace (Obr. 12 D5; dlouhá šipka). Zubní pole coronoidů 1 & 2 již vytváří zubní desky lemující dentale (Obr. 12 D5; hroty šipek). Dentice na ventrální straně branchiálních oblouků se ukazuje být nejpomaleji se formující pole, v tomto stádiu je stále ve formě mineralizovaných špiček zubů s počáteční osifikací připojovací kosti (Obr. 12 D6).

Během následujícího vývoje dochází ve stádiu 23 mm k dalšímu prodlužování čelistí (Obr. 12 E1) stejně jako k markantní osifikaci všech zubonosných kostí (viz kupř. Obr. 12 E2). V rámci palatálního komplexu horní čelisti dosahuje mediálně umístěný parasphenoid úrovně vomerů, mezi něž vrůstá (Obr. 12 E2). Laterálně lemuje okraje čelistí nově se formující série lacrimo-maxilárních kůstek nesoucí uvnitř kanálek postranní čáry hlavy. Jejich palatální plocha je hustě poseta kuželovitými zuby (Obr. 12 E3). Posteriorně tato série ústí ve výše zmíněnou maxilu (Obr. 12 E2). Na premaxile je oproti předešlému stádiu nápadné velikostní rozvrstvení zubů formujících nespojitou zubní řadu, což svědčí o aktivním procesu jejich vypadávání. Formování náhradních zubů i nadále probíhá na linguální straně zubu nahrazovaného (Obr. 12 E3; dlouhá šipka). Počet zubů na vomerech se redukoval a v kosti jsou patrné stopy jejich vypadávání (Obr. 12 E3; hrot šipky). Na dermopalatinech je situaci odlišná. Zuby zde jsou různých velikostí a vyskytují se izolovaně nebo se shlukují do skupin obsahující zub původní (Obr. 12 E3; krátké šipky) společně s jedním nebo dvěma zuby náhradními (Obr. 12 E3; hvězdičky). V rámci zubního pole na dorzálních branchiálních oblucích dochází k vypadávání zubů v centrální části zanechávající za sebou otvory v kosti (Obr. 12 E4; hrot šipky). Zuby se tedy mediálně shlukují do velkých zahnutých špičáků, zatímco zuby umístěné na laterálním okraji mají podobu spíše nevýrazného nízkého kuželu (Obr. 12 E4). Anteriorně se formuje další zubní řada č. 5 (Obr. 12 E4). Ve spodní čelisti je oproti předešlému stádiu proces vmezeřování nových zubů zastaven, nicméně formování náhradních zubů na linguální straně zubu předcházejícího je nadále aktivní (Obr. 12 E5; dlouhá šipka). Nápadný je rozdíl morfologie zubů na dentale tvořící vysoké zahnuté tesáky a na coronoidech s nízkými kuželovitými zuby (Obr. 12 E5). Značný pokrok pak vykazuje dentice ve ventrálním fáryngu, kde úzké mírně zahnuté zuby lemují celou vnitřní plochu ceratobranchiale V s anteriorním nespojitým shlukem třech zubů na obou stranách (Obr. 12 E6; dlouhá šipka). Okraje zbylých ceratobranchií lemují izolované struktury tzv. žaberní tyčinky (angl. gill rakers) (Obr. 12 E6; hrot šipky).

Protože jsou všechna zubní pole již založena a kromě výměny zubů (tedy vypadávání doprovázené novým formováním zubů) se na nich výraznější změny nedějí, je mezi následujícími dvěma stádii větší časová prodleva než tomu je v předchozí deskripci. Ve stádiu 32 mm juvenilního jedince i nadále pozorujeme prodlužování čelistí (Obr. 12 F1) korelující s prodlužováním všech zubonosných kostí čelistí a palatálního komplexu (Obr. 12 F2). Zuby na premaxile jsou mírně zahnuty dovnitř čelisti, jsou uspořádány do jedné řady (tj. monostychní) v pravidelném rozmístění na okraji kosti (Obr. 12 F2). Náhradní zuby se i

nadále vytvářejí v těsné linguální blízkosti zubu nahrazovaného (Obr. 12 F2; úzká šipka). Na tuto řadu plynule navazují zuby lemující okraj lacrimo-maxilárních kůstek, které však jsou poněkud menší než je tomu na premaxile. V rámci vnitřního zubního oblouku je nápadný rozdíl morfologie zubů na vomerech vs. dermopalatinech. Zatímco zuby na vomeru jsou malé kónické a působící spíše dojmem, že jejich funkce spočívá ve zdrsnění kosti, zuby na dermopalatinu vykazují širokou škálu zubních tvarů a velikostí (Obr. 12 F2, F3). A to od zahnutých špičáků se širokou bází po shlukující se úzké kuželovité zuby. Za povšimnutí stojí zvrásnění báze některých zubů tohoto zubního pole (Obr. 12 F3; hrot šipky, podrobněji viz níže) v jehož těsné blízkosti se nachází mineralizovaný kužel náhradního zubu (Obr. 12 F3; hvězdička). V rámci zubního pole lokalizovaného na dorzálních strukturách branchiálních oblouků je již pořadí přibývání jednotlivých fragmentů tohoto pole spíše nahodilé, velmi často pravo-levě asymetrické (Obr. 12 F4). Obecně však platí, že větší zuby jsou lokalizované na mediálním okraji tohoto pole, zatímco laterálně se nacházejí spíše malé kuželovité zuby. Na spodní čelisti je nápadná velikostní a tvarová variabilita zubů. Zatímco anteriorní okraj dentale v oblasti symfýzy je poset rovnými velkými zuby (Obr. 12 F5; krátká šipka), posteriorně se nacházejí silně zahnuté zuby s rozšířeným hrotem enameloidu (Obr. 12 F5; hrot šipky). Jak je patrné, náhradní zuby se mohou vytvářet jak linguálně tak labiálně k původnímu zubu (Obr. 12 F5; hvězdičky). Naproti tomu zuby na coronoidech si zachovávají malé rozměry (Obr. 12 F5). Dentice na ventrální části branchiálních oblouků je i nadále lokalizovaná do ceratobranchiale V, nicméně anteriorní rozložení těchto zubů je patrné jako několik nespojitých desek. Nápadné je rovněž rozvrstvení těchto zubních desek do dvou řad (Obr. 12 F6).

Poslední analyzované stádium 54 mm dlouhého juvenila je i nadále charakterizované prodlužováním čelistí (Obr. 12 G1). Oproti předcházejícímu stádiu se snižuje počet zubů na marginální premaxile (Obr. 12 G2), nicméně samotná velikost těchto zubů se zvětšuje a jejich báze se zvrásňuje (Obr. 12 G3). V rámci vomeru jsou patrné stopy po ztrátě zubu ve formě zbytku zubní báze (Obr. 12 G3; hrot šipky), v těsné blízkosti již však roste zub náhradní (Obr. 12 G3; hvězdička). Zatímco velikost zubů na tomto poli směrem posteriorním evidentně narůstá, gradient velikostí zubů na dermopalatinech se posteriorně snižuje (Obr. 12 G2). Zubní desky lokalizované na dorzálních branchiálních obloucích se plošně zvětšují (Obr. 12 G4), takže působí kompaktnějším dojmem než v předcházejících stádiích. Anteriorně od tohoto zubního pole se nachází izolované zuby, jejich pozice je na základě starších stádií identifikována do infrafaryngobranchiale II (Obr. 12 G4; hvězdičky). Na dentale spodní čelisti nabývají i nejvíce anteriorní zuby morfologii velkých zahnutých tesáků s výrazným hrotem enameloidu a se zvrásněnou bází (Obr. 12 G5; hrot šipky). V rámci zubního pole lokalizovaného do ventrálního fáryngu je nápadné uspořádání zubních desek do dvou paralelních řad na ceratobranchiale V, přičemž vývojově mladší řada je ta blíže struktuře ceratobranchiale IV (Obr. 12 G6). Na anteriorním ceratobranchiale IV se nově nacházejí izolované špičky zubů funkčně rozšiřující zubní pole z ceratobranchiale V (Obr. 12 G6; hvězdičky).

5.3.4 Dentice kostlína sestává z komplexu morfologicky různých typů zubů

Z výše uvedeného je patrné, že dentice juvenilních stádií kostlína je složená hned z několika morfologicky rozdílných zubních typů. Nejvýraznějšími jsou již uvedené tesáky (angl. fangs), které se u studovaných jedinců liší mezi dolní (Obr. 13A) a horní (Obr. 13B) čelistí. Na obou čelistech jsou tyto zuby ostré, kónické a mírně zahnuté, nicméně zatímco se na premaxile horní čelisti plynule zužují do špičky, na dentale čelisti spodní jsou zakončeny rozšířeným hrotem enameloidu (Obr. 13A; bílé hroty šipek). Tato struktura byla popsána jako tzv. acrodinová čepička (Richter & Smith, 1995). Podobný typ zubů byl popsán kupř. u atlantické ryby *Trichiurus lepturus* (Bemis et al., 2019). Báze těchto zubů je pak charakteristická výrazným zprohýbáním dentinu (Obr. 13 A, B; šipky). Taková morfologie byla popsána jako plicidentinová organizace zubů kostlína (kupř. Grande, 2010; Meunier & Brito, 2017). Mimo uvedené marginální kosti čelistí premaxily a dentale se tento typ zubů nachází rovněž na dermopalatinu (viz bílá šipka na Obr. 13D), oproti výše uvedeným tesákům je tento zub přímý, tedy bez prohnutí. V rámci dentice kostlína byly zastoupeny zuby obou typů ve všech výše uvedených zubních oblastech. Je nutné však podotknout, že během raného vývoje jsou tyto zuby hladké (Obr. 12A–E). Ke zprohýbání bází tedy dochází později. Otázka však zůstává, zda-li se tak děje v průběhu vývoje zubů první generace či až po jejich obměně. Vzhledem k tomu, že řada zubů na premaxile a dentale má během dřívějších vývojových stádií špičky náhradních zubů připravené na linguální straně zubu předcházejícího (kupř. Obr. 12 D3 a D5), s největší pravděpodobností se uvedeným způsobem zprohýbá až dentin pozdějších zubních generací.

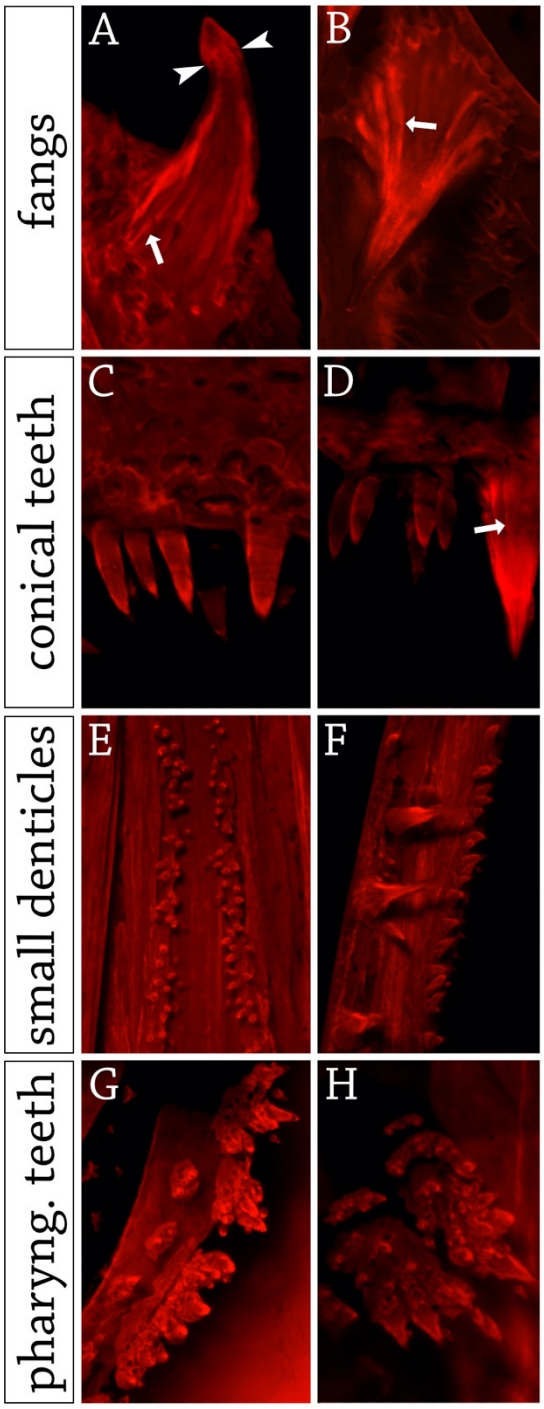

Obr. 13: Přehled typů zubů přítomných v dentici juvenilních kostlínů. (A, B) Špičaté prohnuté „tesáky" na spodní (A) a horní (čelisti). (C, D) Středně velké kónické zuby na lacrimo-maxilare (C) a obklopující tesáky na dermopalatinech (D). Okrouhlé drobné zoubky na vomerech (E) a coronoidech (F). (G, H) Zuby sdružující se do zubních desek lokalizovaných do ventrálního (G) a dorzálního (H) fáryngu. Bílé hroty šipek značí rozhraní zubu a čepičky acrodinu; šipky značí záhyby dentinu.

Dalším typem zubů, který byl v rámci dentice kostlína identifikován, jsou přímé kónické zuby typicky lemující okraj lacrimo-maxilárních kůstek (Obr. 13C). Poměrně často jsou pak patrné na strukturách dermopalatina, kde zpravidla ve skupinách několika stejných zubů vedle sebe obklopují výše uvedené tesáky (Obr. 13D). Jejich velikost je ve srovnání s lacrimo-maxilárními zuby menší. Podobně tomu je i na dentale, nicméně jejich zastoupení je oproti dermopalatinu výrazně nižší.

Poměrně častým zubním typem jsou malé spíše zaoblené zoubky se širokou bází vyskytující se na neokrajových palatálních strukturách vomeru a v pozdějších vývojových stádiích rovněž parasphenoidu (Obr. 13E). Na coronoidech spodní čelisti (zejm. na těch lemujících linguální stranu dentale) pak vytvářejí souvislý pokryv složený výhradně z těchto zubů (Obr. 13F). Vzhledem k jejich velikosti nepředpokládáme, že by tyto zuby představovaly hlavní kousací struktury dentice. Jejich funkce bude spíše spočívat ve zdrsnění povrchu kostí.

Samostatnou entitu potom představují zuby faryngeální dentice, které se ve srovnání se zuby čelistí a palatálního komplexu zdají být morfologicky jedinečné. Mohutné báze těchto velikostně značně variabilních zubů srůstají ve shluky pokrývající plochu ceratobranchiale V orientovanou dovnitř fáryngu (Obr. 13G), v rámci dorzálního fáryngu pak vytvářejí mohutné kompartmentalizované zubní desky na epibranchiáliích (Obr. 13H).

5.3.5 Diferenciace plicidentinu podtrhuje predační potravní strategii kostlína, ale i bichira

Morfologická deskripce zubních typů kostlína (viz výše) identifikovala zprohýbání dentinu na velkých zubech dentice. Na tuto skutečnost poukázal již Grande (2010) ve své rozsáhlé komparativní anatomicko-morfologické studii skeletu kostlínů, kde uvádí, že se tato struktura, známá jako plicidentin, nachází na bázi tesáků. V minulosti byl plicidentin nejlépe prostudován především u fosilních svaloploutvých (Sarcopterygii) a u řady fosilních a recentních amniot. V rámci paprskoploutvých ryb se však plicidentin vyskytuje spíše okrajově (kupř. Peyer, 1968; Meunier et al., 2015b; Doealand et al., 2019). V posledních letech se ukazuje, že jeho zastoupení u kostnatých ryb je možná vlivem nedostatečných metodických přístupů podhodnocováno a na základě microCT vizualizace byl plicidentin identifikován u arapaimy velké (*Arapaima gigas*), tahira cayenenského (*Hoplias aimara*) a ďasa mořského (*Lophius piscatorius*) (Germain et al., 2016). Častější výskyt byl však popsán u ne-kostnatých linií paprskoploutvých ryb. Vedle již zmíněných kostlínů byla totiž struktura plicidentinu identifikována u kaprouna a dospělců bichira senegalského (Germain & Meunier, 2017).

Detailní Alizarin Red barvení mineralizovaných tkání ukázalo, že první vertikální prohýbání dentinu probíhá v juvenilním stádiu zhruba 30 mm (Obr. 14A–C) a je zjevné, že diferenciace plicidentinu neprobíhá na všech polí identicky. První záhyby dentinu jsou nápadné zejm. na zubech lokalizovaných na dermopalatinech a dentale (Obr. 14B, C; šipky), na premaxile jsou však zuby na povrchu hladké (Obr. 14A). První prohýbání dentinu na tomto zubním poli je bezpečně rozeznatelné od velikosti 40 mm (Obr. 14D; šipky) dále. U zubů na dermopalatinech takto velkých juvenilních jedinců se plicidentin rozšiřuje až k samotné bázi zubu (Obr. 14E; šipky). Podobně tomu je rovněž u zubů na dentale spodní čelisti (Obr. 14F), nicméně záhyby dentinu nejsou tak výrazné. O 15 mm větší juvenil již vykazuje nápadné vertikální záhyby plicidentinu od báze zubu (tedy od rozhraní zub-připojovací kost)

(Obr. 14G–H; šipky) zhruba do 2/3 výšky zubu, a to na všech polích. Transverzální řezy zubem (Obr. 14J–L) jasně prokázaly prohýbání povrchového dentinu dovnitř zubu.

Schultze (1970) podle hloubky a stupně záhybů dentinu definoval tři morfologické typy plicidentinu, na jejímž základě byla u kostlína identifikována přítomnost plicidentinu tzv. „polyplocodontního typu“ (Grande, 2010; Meunier & Brito, 2017; Peyer, 1968). Později byla na základě poměrně mělkého prohýbání dentinu (ve srovnání s fosilními zástupci obojživelníků a plazů) určená čtvrtá kategorie tzv. „simplexodontního plicidentinu“ (Germain et al., 2015; Meunier at al., 2015a) popsaná mj. u latimérie (Meunier et al., 2015b), kaprouna a námi studovaného bichira (Germain & Meunier, 2017). Je nutné dodat, že všechny výše uvedené obratlovce spojuje predační strategie příjmu potravy a přítomnost plicidentinu v jejich dentici byla interpretována jako specializace stabilizující a upevňující ukotvení zubů do kosti zvětšením povrchu úponové plochy zubu (Peyer, 1968; Meunier et al., 2015b). Samotný průběh formování plicidentinu na základě podrobných histologických analýz byl doposud studován spíše sporadicky a do budoucna by si jistě zasloužil pozornost detailních analýz (Berkovitz & Shellis, 2017).

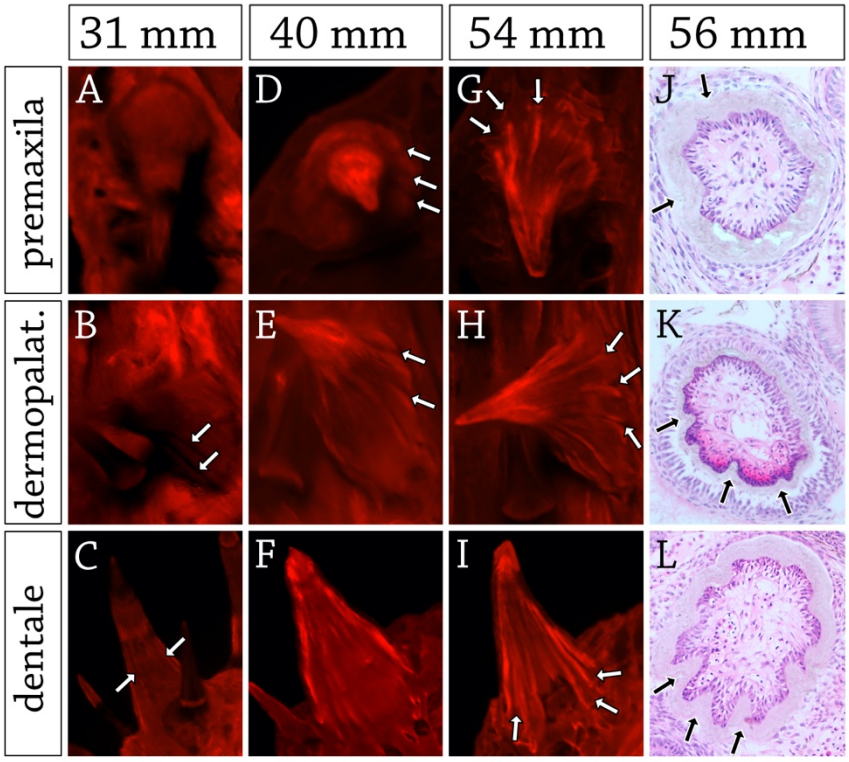

Obr. 14: Diferenciace a vývoj plicidentinu v dentici kostlína. (A–I) Alizarin Red barvení mineralizovaných zubů na premaxile (A, D, G), dermopalatinu (B, E, H) a dentale (C, F, I) prokazující přítomnost záhybů dentinu typických pro plicidentin (bílé šipky). (J–L) Transverzální řez zubem na premaxile (J), dermopalatinu (K) a dentale (L) barvený pomocí Mayer's Hematoxylin & Eosin a ilustrující prohýbání dentinu (černé šipky) do zubu.

5.3.6 Výměna zubů kostlína se zdá být dynamickým procesem probíhajícím bez účasti dentální laminy

Na základě barvení mineralizovaných struktur (viz Obr. 12) se ukázalo, že dentice kostlína představuje komplexní systém obsahující několik zubních typů (Obr. 13) přítomných na řadě struktur orální i faryngeální dentice. Alizarin Red barvení umožnilo sledování i nově se formujících náhradních zubů, čímž se zřetelně ukázalo, že proces nahrazování opotřebovaných zubů je aktivní už v raných stádiích vývoje (všimni si kupř. nově mineralizujících špiček zubů po stranách formovaného tesáku na

Obr. 14C). Analýza resorpce mineralizovaných tkání prostřednictvím vizualizace aktivity osteoklastů (tzv. metodika TRAP, viz **Článek VII**) u juvenila o velikosti 46 mm poukazuje na paralelně probíhající proces ztráty zubů (Obr. 15). Soudě podle všudypřítomného signálu je zřejmé, že proces resorpce a nahrazování zubů bude alespoň v průběhu juvenilního vývoje velmi dynamický (známky resorpce zubu jsou patrné i na bázi tesáku na Obr. 14I).

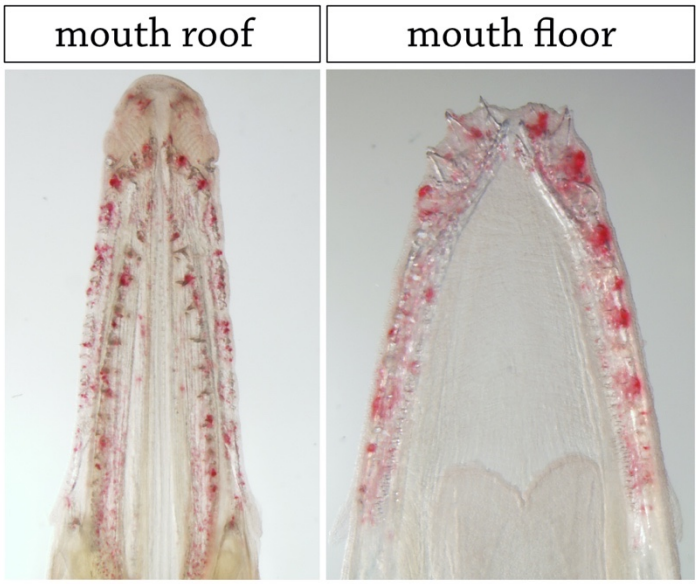

Obr. 15: Resorpce mineralizovaných tkání během procesu vypadávání zubů kostlína. Vizualizace aktivity osteoklastů prostřednictvím TRAP na horní čelisti a palatálním komplexu (vlevo) a na čelisti spodní (vpravo) u jedince o velikosti 46 mm.

Stejně jako bichir, i kostlín se prokazatelně řadí mezi paprskoploutvé ryby kontinuálně nahrazující zuby po celou dobu své existence. Bylo popsáno, že navzdory jejich extrémně osifikovaným kraniálním strukturám dochází u nich k tzv. „extraosseos tooth replacement“ (Trapani, 2001). To znamená, že se náhradní zuby zakládají na povrchu kosti za účasti permanentí či přechodné (non-permanent) dentální laminy lokalizované linguálně k funkčnímu zubu (Huysseune & Witten, 2006; Huysseune & Thesleff, 2004; Trapani, 2001). Tento způsob náhrady zubů je považován za pleziomorfní a zdá se být výhradně přítomen u ne-kostnatých ryb (Trapani, 2001). Na tomto místě je však nutné připomenout, že u bichira (ale i řady dalších ryb) byl popsán totožný způsob náhrady zubů (tzn. etraosseos tooth replacement), ale bez účasti dentální laminy (viz výše). Situace u kostlína je však v tomto směru doposud neznámá.

Předchozí data ukázala, že náhradní zuby (ať už za účasti zubní lišty či bez ní) se zpravidla zakládají v těsné blízkosti zubů funkčních, jehož báze podstupuje resorpci a následně vypadává. U náhradního zubu následně dochází k erupci a jeho ukotvení do zubní pozice či řady (Berkovitz & Shellis, 2017). Proces vzniku a výměny zubů u kostlína je dle mého pozorování obdobný cyklu popsaného u pstruha duhového (*Salmo gairdneri;* v současnosti známého spíš jako *Oncorhynchus mykiss*) procesem ilustrovaným na Obr. 16A (Berkovitz, 1977). Zubní zárodek vzniká diferenciací povrchového epitelu (formování dentální laminy nebylo pozorováno) interagujícího s kondenzujícím mezenchymem (Obr. 16B; hvězdička). Epitel tedy mezenchym proliferací obklopí za vzniku tzv. stádia čepičky (angl. cap stage) (Obr. 16B). Oblast kondenzujícího mezenchymu dá v pozdějším vývoji vzniknout dřeňové dutině, která se stává zdrojem odontoblastů formujících dentin. Epiteliální komponent v této fázi vývoje se označuje jako tzv. dentální epitel a již zde lze rozlišit jeho komponenty vnitřního a vnějšího dentálního epitelu (angl. inner & outer dental epithelium), které jsou zřetelnější v dalším vývoji (Obr. 16C). Následnou diferenciací vnitřního dentálního epitelu (inner dental epithelium, IDE) vznikají ameloblasty produkující enameloid, na povrchu dentální papily se formují odontoblasty secernující dentin (Obr. 16C, D) a zub se připojuje ke kosti (Obr. 16D). V následujícím vývoji se objevuje zárodek zubu náhradního (Obr. 16E; šipka), zřetelný jako mezenchymatická kondenzace (Obr. 16E; hvězdička)

obklopená dentálním epitelem. V dřeňové oblasti zubu původního ubývá zastoupení buněk a na bázi je patrné zeslabené místo dentinu (Obr. 16F; hrot šipky). Náhradní zub se zvětšuje a roste směrem k bázi zubu předcházejícího (Obr. 16F). Míra resorpce báze zubu funkčního se nadále zvyšuje a probíhá na několika místech zubu současně (Obr. 16G; hroty šipek) a zub náhradní se růstem dolů dostává do jeho těsné blízkosti (Obr. 16G). Zároveň je u tohoto zubu patrná aktivní formace enameloidu (Obr. 16G).

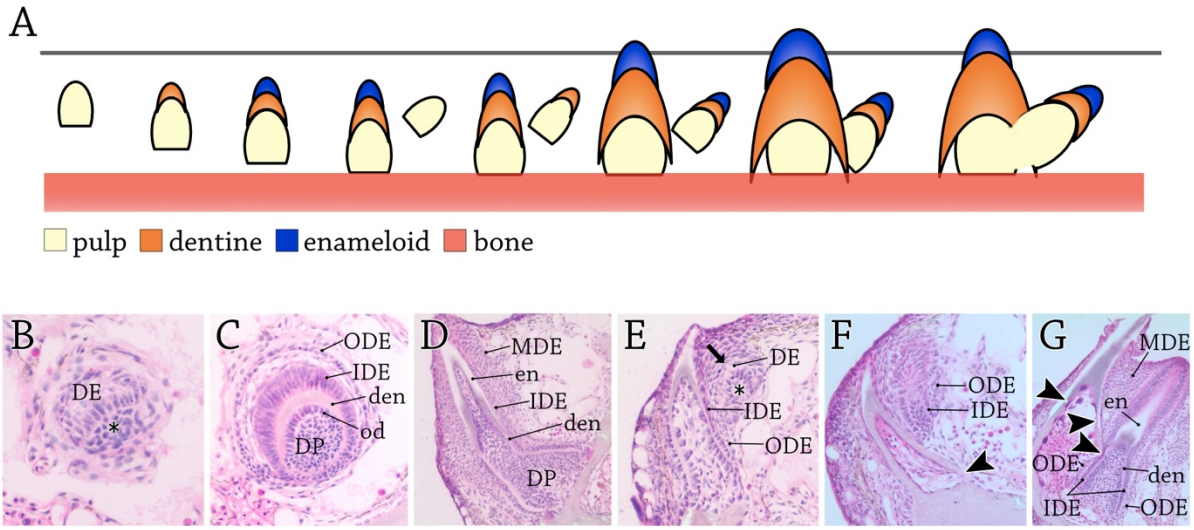

Obr. 16: Formování zubů první generace stejně jako náhradních zubů prochází u kostlína stejnými vývojovými fázemi. (A) Schematická ilustrace zakládání a vývoje zubu funkčního a následného formování zubu náhradního u kostlína (modifikováno podle Berkovitz, 1977). (B-G) Sagitální řezy skrz dentale ilustrující fáze zakládání zubu funkčního a na něj vývojově napojeného zubu náhradního. Barveno pomocí Mayer's Hematoxylin & Eosin. Hvězdička značí kondenzující mezenchym zubního zárodku; šipka značí nový zubní zárodek, hroty šipek poukazují na oblast resorpce funkčního zubu. DE, dental epithelium; den, dentin; DP, dental papila; en, enameloid; IDE, inner dental epithelium; MDE, middle dental epithelium; od, odontoblasty; ODE, outer dental epithelium.

Data uvedená výše (Obr. 16) nám mimo průběh formování náhradních zubů rovněž odhalila struktury s tímto procesem úzce související. Zejména z obrázků Obr. 16G a Obr. 17 je zjevné, že je náhradní zub napojen prostřednictvím vnějšího zubního epitelu na zub funkční. Tato struktura plynule přechází do vnitřního zubního epitelu zubu náhradního s ameloblasty následně formujícími enameloid. Prostor mezi vnitřním zubním epitelem zubu náhradního a samotným zubem funkčním vyplňuje kapsa s buňkami topograficky náležejícími k tzv. střednímu dentálnímu epitelu (Obr. 17). V průběhu procesu náhrady zubů se nepodařilo identifikovat žádnou epiteliální strukturu,

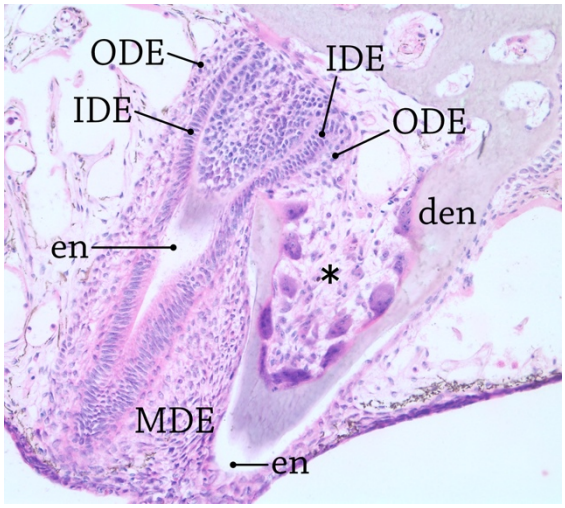

Obr. 17: Histologický řez ilustrující proces náhrady zubů kostlínů. Sagitální řez zubů na dermopalatinu zobrazující zub funkční (hvězdička) a zub náhradní propojené strukturou vnějšího zubního epitelu. Barveno pomocí Mayer's Hematoxylin & Eosin. Vysvětlení zkratek viz Obr. 16.

která by se mohla považovat za dentální laminu a je tedy zjevné, že se procesu výměny zubů u kostlína dentální lamina neúčastní.

5.4 Proces odontogeneze u studovaných skupin je ve všech ohledech značně odlišný

Jak již bylo v této práci několikrát zmíněno, dentice studovaných bazálně fylogeneticky umístěných nekostnatých paprskoploutvých ryb představuje svým rozložením a vnější morfologií odlišné entity. Na základě výše uvedených výsledků se ukázalo, že tyto odlišnosti mohou být podloženy variabilitou mnoha aspektů dentálního vývoje, které nebyly doposud úplně popsány a pochopeny. Na druhou stranu je třeba zmínit, že mezi studovanými liniemi je rovněž řada znaků společných. Následující část zasazuje všechny detailní výsledky kapitoly 5 Srovnání patrnosti odontogeneze do komparativního čtecího rámce.

5.4.1 Raná exprese vývojově konzervovaných zubních markerů vykazuje nápadné odchylky

Již raná stádia zubního vývoje vykazují nápadně odlišnou patrnost zakládání zubů, která se projevuje již u samotné exprese základních genových markerů. Exprese genu *Pitx2* u jesetera vykazuje během raného zubního vývoje poměrně uniformní signál lokalizovaný do marginální dentice horní i spodní čelisti současně (Fig. 2 & Fig. S1; **Článek VII**), u bichira s kostlínem pak pozorujeme nápadné zpoždění exprese v čelisti horní (Obr. 6 & Obr. 10) zapříčiněné vývojem cementových orgánů. U bichira a jesetera dochází k první expresi *Pitx2* v koutcích úst a k následnému mediálnímu šíření signálu, který se později uprostřed čelisti sbíhá (Obr. 6 a Fig. S1; **Článek VII**). Podobně i u kostlína sledujeme expresi genu lemující okraj budoucí spodní čelisti levé a pravé strany odděleně, nicméně tyto signály se nikdy mediálně nepropojí (Obr. 10). U jesetera s kostlínem vzniká *Pitx2* exprese v každém zubním poli zvlášť, čili nebyl pozorován rozpad širokého pruhu *Pitx2* signálu do několika zubních polí, jako tomu je v případě dentice axolotla (**Článek VI**). Zajímavé je, že v případě jesetera se každé zubní pole zakládá jako kontinuální pruh či oblast a ty se v pozdějším vývoji separují do jednotlivých zubních zárodků (Fig. 2; **Článek VII**). U kostlína se tímto způsobem zakládá jen okrajová dentice na dentale a zkráceně na premaxile (Obr. 10), exprese v ostatních zubních polích je od svého počátku lokalizovaná do izolovaných zubních zárodků, a to včetně faryngeální dentice (Obr. 11). U bichira je situace odlišná a nápadně připomíná již zmíněného axolotla (**Článek VI**), a to procesem separace kontinuálního signálu na horní i spodní čelisti zároveň (Obr. 6K), přičemž na čelisti spodní trvá déle.

Nápadnou variabilitu vykazovala rovněž exprese genu *Shh*. Zatímco u bichira se mi žádná exprese zachytit nepodařila, u jesetera jsem identifikovala signál velmi raných stádií ve formě pruhu, který se v průběhu pozdějšího vývoje separoval do jednotlivých zubních pozic (viz Fig. S1; **Článek VII**). Naopak u kostlína jakýkoli signál v raných stádiích chybí (Obr. 10M–O) a objevuje se až v pozdějším vývoji již izolovaný do jednotlivých zubních zárodků (Obr. 10P). Zajímavá se u kostlína rovněž ukázala být první exprese *Shh* ve fárynguve srovnání s expresí *Pitx2*. Zatímco nejranější expresi genu *Pitx2* vidíme na dorzálních branchiálních obloucích bez protilehlé ventrální exprese (Obr. 11B, B'), u *Shh* je tomu přesně naopak (Obr. 11H, H'). Protože však z důvodu nedostatku materiálu nebylo možné tuto skutečnost ověřit, může se jednat pouze o vývojovou odchylku.

Vzhledem k nápadné variabilitě v patternech exprese *Pitx2* a *Shh* (tj. dvou základních vývojově konzervovaných zubních markerů) u mnou studovaných druhů se nabízí otázka, zda tato variabilita nemůže být zodpovědná za variabilitu dentic patrnou u studovaných zástupců ne-kostnatých ryb. Hypotéza tzv. „periodic pattern generator for diversity" navrhuje, že přítomnost a odchylky ve vzájemném působení několika faktorů (zahrnujících *bmp2*, *bmp4*, *eda*, *edar*, *fgf8*, *pax9*, *pitx2*, *runx2*, *shh* a *wnt7b*) mohou být zodpovědné za variabilitu orálních dentic u blízce příbuzných druhů cichlid (Fraser et al., 2008). Samotná kombinace *Shh* a *Pitx2* je nezbytná pro diferenciaci iniciační zubní kompetentní zóny, podle jejíž šířky lze minimálně usuzovat na velikost budoucího pole (Fraser et al., 2008; Stock et al., 2006). Avšak vzhledem k tomu, že tyto faktory reprezentují pouze dva epiteliální zubní markery, jakékoli další závěry vztahované k variabilitě dentic by byly unáhlené a v budoucnu bude jistě nezbytné rozšířit škálu studovaných genů.

5.4.2 Značná variabilita panuje i v průběhu mineralizace dentice

Zatímco u jesetera jsou zuby na všech polích morfologicky uniformní (**Článek VII**), v dentici bichira bylo identifikováno několik odlišných typů zubů osidlujících odlišná zubní pole (Clemen et al., 1998). Podobně i naše vizualizace mineralizovaných dentálních struktur odhalila na základě odlišné vnější morfologie i v případě kostlína čtyři rozdílné typy zubů (Obr. 13). U kostlína jsem navíc identifikovala výrazné zprohýbání dentinu na největších zubech dentice (Obr. 14), které u bichira pozorováno nebylo, nicméně je rovněž známo především z pozdějších vývojových stádií (viz výše). Ve srovnání s jeseterem představuje tedy dentice bichira s kostlínem mnohem komplexnější systém (Obr. 7–9 a Obr. 12) . Nápadný rozdíl pak představuje faryngeální dentice. Zatímco u bichira nesou všechny struktury mimo hyoidní oblouk zuby, u kostlína jsou zubní desky lokalizovány pouze do posledního branchiálního oblouku (i když se v pozdějším vývoji izolované zubní desky rozšiřují na struktury předcházejících oblouků). Přestože představuje fárynx bichira nejvíce ozubenou doménu mezi studovanými druhy (Obr. 5), vývoj zubů zde je značně opožděn a probíhá až po založení většiny polí orální dentice (Obr. 8). Naproti tomu formování prvních faryngeálních zubů u kostlína probíhá záhy po první mineralizaci dentice na čelistech (Obr. 12), což odpovídá i průběhu zakládání faryngeálních zubních zubních polí jesetera (**Článek VII**).

Nápadné byly rovněž rozdíly v patrnosti mineralizované dentice. Zcela unikátní se ukázala být výrazně redukovaná dentice jesetera s faryngeální denticí posunutou na anteriorní elementy branchiálních oblouků. Na všech zubonosných strukturách dochází k poměrně rychlému založení zubů, přičemž na marginální dentici horní a spodní čelisti nedochází k výměně zubů a tato zubní pole jsou tedy brzy redukována. Zbývající zubní pole jsou pak i přes probíhající resorpci zubů po dlouhou dobu udržována funkční díky kontinuální zubní adici na protilehlé straně. V pozdějších vývojových stádiích pak pozorujeme výraznou restrukturalizaci dentice na všech zubních polí (viz **Článek VII**).

Raná mineralizace orální dentice je u bichira s kostlínem obdobná, nicméně u kostlína pozorujeme brzké formování prvních vomerálních zubů z vnitřního zubního oblouku společně se zrychlenou mineralizací zubů napojených na premaxilu. Zatímco je maxila bichira dominantní ozubenou strukturou horní čelisti, u kostlína je její vývoj zpožděn a samotná struktura je značně redukována a posunuta posteriorně ke koutkům úst. Právě na maxile bichira pozorujeme unikátně synchronizovaný proces nahrazování většiny zubů v juvenilním stádiu cca 20 mm (Obr. 8A). Orální

dentice bichira je v pozdějších stádiích vystavěna z proporčně větších kuželovitých zubů uskupených do řady blízko sebe na okrajových strukturách horní i dolní čelisti a z obrovského množství malých zoubků na vnitřním zubním oblouku, které hustě pokrývají i zbývající struktury palatálního komplexu (Obr. 9). Naproti tomu orální dentice juvenilních kostlínů je charakterizována velkými tesáky nepravidelně rozmístěnými převážně v anteriorní části horní a dolní čelisti. Okraje horní čelisti jsou pak posety středně velkými kuželovitými zuby rozmístěnými blízko sebe. Vnitřek palatálního komplexu i spodní čelisti je pak pokryt drobnými zoubky (Obr. 12G). Oproti bichirovi se však dentice, alespoň v rámci studovaných stádií, jeví býti méně ozubená (srovnej Obr. 9G a Obr. 12G).

5.4.3 Proces nahrazování zubů je u bichira a kostlína založen na stejném principu

Společným znakem dentic studovaných skupin je nepochybně nápadná dynamika nahrazování zubů. Právě proces nahrazování zubů je základním předpokladem funkčnosti polyfyodontní dentice, jež je pro paprskoploutvé ryby typická (Huysseune & Witten, 2006). Dlouhotrvající předpoklad, že formování zubů náhradních je podloženo přítomností dentální laminy byl však u této linie zkomplikován zakládáním nových zubů z dentálního epitelu zubu funkčního (shrnuto kupř. Tucker & Fraser, 2014). Zatímco u jesetera nahrazování zubů neprobíhá na všech identifikovaných zubních polích (viz výše), u bichira s kostlínem je tento proces všudypřítomný. U bichira bylo na dentale spodní čelisti již dříve explicitně popsáno že formování náhradních zubů probíhá bez účasti jakéhokoli typu dentální laminy (Vandenplas et al., 2014), u kostlína tato data dlouhodobě chyběla. Naše analýza i v případě kostlína žádnou dentální laminu nepotvrdila a ukázalo se, že proces nahrazování jejich zubů na všech zubních polích je identický tomu u bichira (Obr. 16 a Obr. 17). Vzhledem k jejich fylogenetické pozici se tedy zdá, že přímý vývoj zubů náhradních z epiteliální populace buněk zubu funkčního (tj. nahrazovaného) bez účasti dentální laminy reprezentuje ancestrální způsob nahrazování zubů dentice u skupiny paprskoploutvých ryb. Ani u jesetera naše předběžné výzkumy dentální laminu neprokázaly a tato oblast je stále předmětem probíhající studie. Právě dentice jesetera vykazující jak monofyodontní tak polyfyodontní uspořádání tak nabízí výjimečnou příležitost k identifikování faktorů zodpovědných za ztrátu kontinuálního zubního nahrazování.

6 Závěrečné shrnutí

Záběr předkládané dizertační práce je rozložen do dvou oblastí. Stěžejní část představuje srovnávací analýza vývoje skeletálních hlavových tkání a struktur napříč linií paprskoploutvých ryb s odlišnou adultní morfologií lebek s cílem popsat zásadní mechanismy, které tyto odlišnosti zakládají. Cílem druhé části zaměřující se na odontogenezi bazálních paprskoploutvých ryb je popsat patrnost a dynamiku zakládání a následného vývoje dentice, jež je doposud u těchto linií pouze sporadicky studována, a posoudit tak vývojovou variabilitu dentálních struktur u těchto linií.

Vzhledem k tomu, že se výzkumné skupině školitele podařilo získat unikátní, avšak v různé míře dostupný, embryonální materiál bichira, jesetera, kostlína a štiky, na který se podařilo optimalizovat jejich odchov a již zavedené laboratorní postupy (Minařík, 2018; Štundl, 2019; **Článek I**; **Článek V**), vznikla tak jedinečná příležitost etablovat tyto linie jako nové modelové organismy. Tím se podařilo rozšířit zavedený modelový systém evo-devo výzkumů, na kterém jsem se podílela charakterizací vývoje štiky (**Článek I**). Právě studium širší fylogenetické škály je klíčové pro pochopení evolučního původu morfologických struktur a různých vývojových fenoménů.

Až doposud se nikdo nezabýval identifikací klíčových mechanismů sehrávajících zásadní roli v zakládání diverzity skeletálních a dentálních struktur na tak fylogeneticky unikátní škále organismů. Výsledky naší analýzy identifikovaly, že vývoj skeletálních tkání je již od prvopočátku mezi studovanými liniemi značně odlišný (**Článek II**). Jako hlavní mechanismus byla identifikována distribuce heterochronií na několika vývojových úrovních. V první řadě byly zřetelné rozdíly v sekvenci formování kraniálních regionů, ať už těch chrupavčitých či posléze osifikovaných. Výrazné pak byly rozdíly v koncentraci morfogeneze do odlišných hlavových lokalit. Zatímco u jesetera přednostně osifikují struktury posteriorní části hlavy formující pevný rámec pro vysunovatelné čelisti, u kostlína byla identifikována přednostní osifikace anteriorní části hlavy, tedy výrazně ozubených čelistí. U bichira došlo k dynamickému založení zubonosných kostí čelistí a branchiálních oblouků. Nejpomalejší byl potom vývoj kraniálních kostěných struktur štiky. Rozdíly byly rovněž nápadné v načasování vzniku chrupavek a kostí, a to včetně nejranějších stádií vývoje. Zcela zrychlené bylo zakládání první chrupavky štiky korelující s časem líhnutí, čili bez zjevné pre-chrupavčité fáze vývoje, což odpovídá i nejrychlejšímu nástupu osifikace. U zbývajících linií bylo formování chrupavky vzhledem k době líhnutí zpožděno, zanechávající nejdelší pre-chrupavčitou dobu vývoje u bichira a jesetera stejně dlouhou. S ohledem na načasování počátku chondrogeneze nastupuje proces první osifikace nejrychleji u bichira, nejpomaleji však u kostlína. Tomu odpovídá i delší doba potřebná pro resorpci cementového orgánu u kostlína déle blokující osifikaci horní čelisti. Kvantitativní analýza vývoje hustoty kostí ukázala, že přestože byla identifikována nejrychlejší kraniální osifikace vzhledem k době líhnutí u štiky, proces vývoje denzity kostí je u této linie velmi pomalý. Překvapivě nejdynamičtější nárůst hustoty kostí během nejranějších stádií byl odhalen u „řídkokostého" jesetera, nicméně záhy dochází k překonání této úrovně hustoty kostí kostlínem. Z výše uvedeného je patrné že v rámci zakládání a následného vývoje kraniálních skeletálních struktur panuje napříč studovanými liniemi velká a do značné míry neprediktabilní variabilita.

To se však netýká ranějších stádií vývoje, u nichž teprve probíhá diferenciace tkání jednotlivých hlavových struktur. U bichirů s výraznými vnějšími žábry, které jsou pro ně typické, dochází k přednostní diferenciaci hyoidního (druhého) proudu buněk neurální lišty (**Článek IV**) a tedy

k narušení antero-posteriorního gradientu. Totéž bylo identifikováno i u kostlína se štikou (**Článek V**) s následnou zrychlenou formací operkulárního záhybu a hyoidního oblouku samotného. Takové vychýlení patrnosti migrace buněk hlavové neurální lišty je mezi dosud studovanými liniemi obratlovců unikátní (viz Štundl, 2019).

Podobné rozdíly byly pozorovány i během vývoje dentice. Detailní deskripce průběhu mineralizace zubů jednotlivých zubních polí byla nejdříve provedena na jeseterovi se značně redukovanou denticí (**Článek VII**) a posloužila jako předloha pro charakterizaci odontogeneze u bichira se zachovanými ancestrálními znaky dentice i kostlína s výrazně redukovanými zubními poli v rámci fáryngu (viz Kapitola 5). Už nejranější stádia diferenciace zubních zárodků analyzovaná pomocí exprese genů *Shh* a *Pitx2* vykázala nápadné rozdíly mezi studovanými liniemi. Zároveň se touto analýzou ukázalo, že proces separace odontogenního proužku do jednotlivých zubních polí, který je přítomný na několika místech dentice bichira, nápadně připomíná pattern popsaný u axolotla. Přestože se tato studie zabývá zakládáním a vývojem dentice u ne-kostnatách paprskoploutvých ryb, v průběhu doktorátu se mi naskytla příležitost podílet se na studii odontogeneze u axolotla náležejícího mezi linii Tetrapoda (**Článek VI**). Srovnání získaných dat s touto linií však nabízí rozšíření fylogenetické škály, což je jeden z předpokladů jasnější interpretace evolučního původu morfologických struktur či vývojových fenoménů. Vzhledem k pozici bichira poblíž dichotomie čelistnatců s kostní tkání (Osteognathostomata) do linií paprskoploutvých a svaloploutvých ryb se zdá, že je rozpad odontogenního proužku do zubních polí znakem ancestrálním. U kostlína ani jesetera již tento rozpad pozorován nebyl a předpokládáme tedy, že byl v průběhu evoluce paprskoploutvých ryb ztracen. Sdíleným znakem dentic bichira a kostlína pak je náhrada zubů, na které se nepodílí struktura dentální laminy a zub je založen z epiteliálního orgánu zubu nahrazovaného.

V průběhu řešení tohoto dizertačního projektu jsem se rovněž podílela na pilotních „up-to-date" experimentech mutageneze prostřednictvím CRISPR/Cas9 systému či detekce pomalu cyklujících buněk za pomoci EdU za účelem vizualizace zubních kmenových buněk. Vygenerovaná anatomicko-morfologická data předložené práce převážně deskriptivního charakteru, jež byla dosud v rámci studovaných linií spíše neznámá, tak vytvářejí výchozí platformu, na kterou lze v budoucnu aplikovat moderní přístupy vývojové biologie.

7 Použitá literatura

Abzhanov A, Protas M, Grant BR, Grant PR & Tabin CJ (2004) Bmp4 and morphological variation of beaks in Darwin's finches. *Science* 305, 1462–1465.

Abzhanov A, Rodda SJ, McMahon AP & Tabin CJ (2007) Regulation of skeletogenic differentiation in cranial dermal bone. *Development* 134, 3133–3144.

Adriaens D & Verraes W (1998) Ontogeny of the osteocranium in the African catfish, *Clarias gariepinus* Burchell (1822) (Siluriformes: Clariidae): ossification sequence as a response to functional demands. *Journal of Morphology* 235, 183–237.

Alberch P, Gould SJ, Oster FG & Wake DB (1979) Size and shape in ontogeny and phylogeny. *Paleobiology* 5, 296–317.

Alberch P (1982) Developmental constraints in evolutionary processes. *In*: Bonner JT (Ed) *Development in evolution*. Berlin and New York: Springer. pp. 313–332.

Albertson CR, Streelman TJ, Kocher TD & Yelick PC (2005) Integration and evolution of the cichlid mandible: The molecular basis of alternate feeding strategies. *PNAS* 102(45), 16287–16292.

Albertson RC, Yan Y-L, Titus TA, Pisano E, Vacchi M, Yelick PM, Detrich W & Postlethwait JH (2010) Molecular pedomorphism underlies craniofacial skeletal evolution in Artartic notothenoid fishes. *BMC Evolutionary Biology* 10(4), 1–12.

Allis EP (1898) On the morphology of certain of the bones of the cheek and snout of Amia calva. *Journal of Morphology* 6(3), 425–466.

Allis EP (1934) Concerning the course of the latero-sensory canals in recent fishes, pre-fishes and Necturus. *Journal of Anatomy* 68(3), 361–415.

Bartsch P (1997) Aspects of craniogenesis and evolutionary biology in polypteriform fishes. *Nertelands Journal of Zoology* 47(4), 365–381.

Bartsch P, Gemballa S & Piotrowski T (1997) The Embryonic and Larval Development of *Polypterus senegalus* Cuvier, 1829: its Staging with Reference to External and Skeletal Features, Behaviour and Locomotory Habits. *Acta Zoologica* 78(4), 309–328.

de Beer GR (1937) *The development of the vertebrate skull*. Oxford University Press, Oxford.

de Beer GR (1951) *Embryos and Ancestors*. Oxford University Press, London.

Bemis WE, Findeis EK & Grande L (1997) An overview of Acipenseriformes. *Environmental Biology of Fishes* 48, 25–71.

Bemis KE, Burke SM, St. John CA, Hilton EJ & Bemis WE (2019) Tooth development and replacement in the Atlantic Cutlassfish, *Trichiurus lepturus*, with comparisons to other Scombroidei. *Journal of Morphology* 280, 78–94.

Berkovitz BKB (1977). The order of tooth development and eruption in the rainbow trout (Salmo gairdneri). *Journal of Experimental Zoology* 201(2), 221–225.

Berkovitz B & Shellis P (2017). *The Teeth of Non-Mammalian Vertebrates*. Academic Press.

Betancur-R R, Broughton RE, Wiley EO, Carpenter K, López JA, Li C, Holcroft NI, Arcila D, Sanciangco M, Ii JCC, Zhang F, Campbell MA, Ballesteros JA, Roavaron A, Willis S, Borden WC, Hough DJ & Lu G (2013) The Tree of Life and a New Classification of Bony Fishes. *PLOS Currents Tree of Life* 732988, 1–45.

Betancur-R R, Wiley EO, Arratia G, Acero A, Bailly N, Miya M, Lecointre G & Ortí G (2017) Phylogenetic classification of bony fishes. *BMC Evolutionary Biology* 17, 1–45.

Bloomquist RF, Parnell NF, Phillips KA, Fowler TE, Yu TY, Sharpe PT & Streelman JT (2015) Coevolutionary patterning of teeth and taste buds. *PNAS* 112(44), E5954-E5962.

Broughton RE, Betancur-R R, Li C, Arratia G & Ortí G (2013) Multi-locus phylogenetic analysis reveals the pattern and tempo of bony fish evolution. *PLoS Currents Tree of Life*.

Burdi AM (2010*) Morphological Development of the Axial Skeletons of Esox Lucius and Esox Masquinongy (Euteleostei: Esociforms), with Comparisons in Developmental and Mineralization Rates*. MSc Chicago: Loyola University. pp 91.

Cerny R, Meulemans D, Berger J, Wilsch-Bräuninger M, Kurth T, Bronner-Fraser M & Epperlein H-H (2004) Combined intrinsic and extrinsic influences pattern cranial neural crest migration and pharyngeal arch morphogenesis in axolotl. *Developmental Biology* 266, 252–269.

Cerny R, Horáček I & Olsson L (2006) The Trabecula cranii: development and homology of an enigmatic vertebrate head structure. *Animal Biology* 56(4), 503–518.

Chen D, Blom H, Sanchez S, Tafforeau P & Ahlberg PE (2016) The stem osteichthyan Andreolepis and the origin of tooth replacement. *Nature* 539, 237–241.

Chen D, Blom H, Sanchez S, Tafforeau P, Märss T & Ahlberg PE (2020) Dental ontogeny in the most primitive bony fish Lophosteus reveals the developmental relationship between teeth and dermal odontodes. *bioRxiv* 2020.07.14.202234.

Clemen G, Bartsch P & Wacker K (1998) Dentition and dentigerous bones in juveniles and adults of *Polypterus senegalus* (Cladistia, Actinopterygii). *Annals of Anatomy* 180, 211–221.

Couly GF, Coltey PM & Le Douarin NM (1993) The triple origin of skull in higher vertebrates: A study in quail-chick chimeras. *Development* 117, 409–429

Couly GF, Creuzet S, Bennaceur S, Vincent C & Le Douarin NM (2002) Interactions between Hox-negative cephalic neural crest cells and the foregut endoderm in patterning the facial skeleton in the vertebrate head. *Development* 129(4), 1061–1073.

Davidian A & Malashichev Y (2013) Dual embryonic origin of the hyobranchial apparatus in the Mexican axolotl (*Ambystoma mexicanum*). *The International Journal of Developmental Biology* 51, 821–828.

Debiais-Thibaud M, Simion P, Ventéo S, Muñoz D, Marcellini S, Mazan S & Haitina T (2019) Skeletal Mineralization in Association with Type X Collagen Expression Is an Ancestral Feature for Jawed Vertebrates. *Molecular Biology and Evolution* 36(10), 2265–2276.

De Clercq A, Vandenplas S & Huysseune A (2014) A comparison of the larval and juvenile dentition in *Polypterus senegalus*. *Journal of Apllied Ichthyology* 30, 790–795.

Devillers C (1947) Recherches sur le crane dermique des Téléostéens. *Annales de Paléontologie* 33, 1–94.

Doeland M, Couzens AMC, Donoghue PCJ & Rücklin M (2019) Tooth replacement in early sarcopterygians. *Royal Society Open Science* 6: 191173.

Donoghue PCJ & Rücklin M (2014) The ins and outs of the evolutionary origin of teeth. *Evolution & development* 18(1), 19–30.

Donoghue PCJ & Sansom IJ (2002). Origin and early evolution of vertebrate skeletonization. *Microscopy Research and Technique* 59, 352–372.

Eames BF, de la Fuente L & Helms JA (2003) Molecular Ontogeny of the Skeleton. *Birth Defects Research (Part C)* 69, 93–101.

Eames BF & Schneider RA (2005) Quail-duck chimeras reveal spatiotemporal plasticity in molecular and histogenic programs of cranial feather development. *Development* 132, 1499–1509.

Eames BF, Amores A, Yan YL & Postlethwait JH (2012) Evolution of the osteoblast: skeletogenesis in gar and zebrafish. *BMC Evolutionary Biology* 12(27), 1–13.

Eastman JT, Witmer LM, Ridgely RC & Kuhn KL (2014) Divergence in Skeletal Mass and Bone Morphology in Antarctic Notothenioid Fishes. *Journal of Morphology* 275, 841–861.

Enault S, Muñoz DN, Silva WT, Borday-Birraux V, Bonade M, Oulion S, Ventéo S, Marcellini S & Debiais-Thibaud M (2015) Molecular footprinting of skeletal tissues in the catshark Scyliorhinus canicula and the clawed frog Xenopus tropicalis identifies conserved and derived features of vertebrate calcification. *Frontiers in Genetics* 6(283), 1–14.

Fish JL & Schneider RA (2014) Chapter 6. Neural crest-mediated tissue interactions during craniofacial development: the origin of species-specific pattern. *In*: Trainor PA (Ed.) *Neural Crest Cells*. Academis Press, Boston, 101–124.

Fraser GJ, Graham A & Smith MM (2006) Developmental and evolutionary origins of the vertebrate dentition: molecular controls for spatiotemporal organisation of tooth sites in osteichthyans. *Journal of experimental zoology. Part B, Molecular and developmental evolution* 306B, 183–203.

Fraser GJ, Bloomquist RF & Streelman JT (2008) A periodic pattern generator for dental diversity. *BMC Biology* 6(32), 1–15.

Fraser GJ, Hulsey CD, Bloomquist RF, Uyesugi K, Manley NR & Streelman JT (2009) An Ancient Gene Network Is Co-opted for Teeth on Old and New Jaws. *PLOS Biology* 7(2): e1000031.

Fraser GJ, Cerny R, Soukup V, Bronner-Fraser M & Streelman JT (2010) The odontode explosion: The origin of tooth-like structures in vertebrates. *BioEssays*, 32(9), 808–817.

Fricke R, Eschmeyer WN & Van der Laan R (eds.) 2020. Eschmeyer‘s catalog of fishes: genera, species, references.
(http://researcharchive.calacademy.org/research/ichthyology/catalog/fishcatmain.asp).
Electronic version accessed 03 06 2020.

Froese R & Pauly D (eds.) 2019. FishBase. World Wide Web electronic publication.www.fishbase.org, version (12/2019). Electronic version accessed 03 06 2020.

Gans C & Northcutt RG (1983) Neural crest and the origin of vertebrates – a new head. *Science* 220, 268–274.

Germain D & Laurin M (2009) Evolution of ossification sequences in salamanders and urodeles origins assessed through event-pairing and new methods. *Evolution & Development* 11, 170–190.

Germain D, Mondéjar-Fernández J & Meunier FJ (2016) The detection of weakly developed plicidentine in teleost teeth using 3D tomography. *Cybium* 40(1), 75–82.

Germain D & Meunier F (2017) Teeth of extant Polypteridae and Amiidae have plicidentine organization. *Acta Zoologica*, 1–7.

Giles S, Xu G-H, Near TJ & Friedman M (2017) Early members of ‘living fossil’ lineage imply later origin of modern ray-finned fishes. *Nature* 549, 265–268.

Goodrich SE (1930) *Studies on the structure and development of vertebrates*. Macmillan and Co, London.

Grande L (2010) An empirical synthetic pattern study of gars (Lepisosteiformes) and closely related species, based mostly on skeletal anatomy. The ressurection of Holostei. *Copeia* 2010(2A), 1–871.

Green SA, Simoes-Costa M & Bronner ME (2015) Evolution of vertebrates as viewed from the crest. *Nature* 520, 474–482.

Gross JB & Hanken J (2008) Review of fate-mapping studies of osteogenic cranial neural crest in vertebrates. *Developmental Biology* 317(2), 389–400.

Gunter HM, Koppermann C & Meyer A (2014) Revisiting de Beer's textbook example of heterochrony and jaw elongation in fish: calmodulin expression reflects heterochronic growth, and underlies morphological innovation in the jaws of belonoid fishes. *EvoDevo* 5(8), 1–13.

Haeckel E (1874) *Antropogenie oder Entwickelungsgeschichte des Menschen*. W. Engelmann, Leipzig.

Hall BK (1975) Evolutionary consequences of skeletal differentiation. *American Zoologist* 15(2), 329–350.

Hall BK & Miyake T (1992) The membranous skeleton: the role of cell condensations in vertebrate skeletogenesis. *Anatomy and Embryology* 186(2), 107–124.

Hall BK & Miyake T (2000) All for one and one for all for one and one for all: Condensations and the initiation of skeletal development. *Bio-Essays* 1878, 138–147.

Hall BK (2005) *Bones and cartilage: developmental and evolutionary skeletal biology*. Elsevier Academic Press, London.

Handschuh S, Beisser CJ, Ruthensteines B & Metscher BD (2017) Microscopic dual-energy CT (microDECT): a flexible tool for multichannel ex vivo 3D imaging of biological specimens. *Journal of Miscroscopy* 267, 3–26.

Hanken J & Hall BK (1993) Mechanisms of skull diversity and evolution. *In:* Hanken J & Hall BK (eds.) *The Skull*. Vol. 3, Functional and Evolutionary Mechanisms. Chicago: University of Chicago Press, pp. 1–36.

Hanken J & Thorogood P (1993) Evolution and Development of the Vertebrate Skull: The Role of Pattern Formation. *Trends in Ecology and Evolution* 8, 9–15.

Helms JA & Schneider RA (2003) Cranial skeletal biology. *Nature* 423, 326–331.

Hilton EJ (2005) Observations of the skulls of stuergeons (Acipenseridae): shared similartities of Pseudoscaphirhynchus kaufmanni and juvenile specimens of Acipenser stellatus. *Environmental Biology of Fishes* 72, 135–144.

Hilton EJ, Grande L & Bemis WE (2011). Skeletal Anatomy of the Shortnose Sturgeon, Acipenser Brevirostrum Lesueur, 1818, and the Systematics of Sturgeons (Acipenseriformes, Acipenseridae). *Fieldiana Life and Earth Sciences* 3, 1–168.

Hirasawa T & Kuratani S (2015) Evolution of the vertebrate skeleton: morphology, embryology, and development, *Zoological Letters* 1(2), 1–17.

Holland PWH, Garcia-Fernàndez J, Williams NA & Sidow A (1994) Gene duplications and the origins of vertebrate development. *Development* 1994, 125–133.

Hughes LC, Ortí G, Huang Y, Sun Y, Baldwin CC, Thompson AW, Arcila D, Betancur-R R, Li C, Becker L, Bellora N, Zhao X, Li X, Wang M, Fang C, Xie B, Zhou Z, Huang H, Chen S, Venkatesh B & Shi Q (2018) Comprehensive phylogeny of ray-finned fishes (Actinopterygii) based on transcriptomic and genomic data. *PNAS* 115, 6249–6254.

Hurley IA, Mueller RL, Dunn KA, Schmidt EJ, Friedman M, Ho RK, Prince VE, Yang Z, Thomas MG & Coates MI (2007) A new time-scale for ray-finned fish evolution. Proceedings. *Biological sciences* 274(1609), 489–498.

Huysseune A & Sire J-Y (1997) Structure and Development of Teeth in Three Armoured Catfish, *Corydoras aeneus*, *C. arcuatus* and *Hoplosternum littorale* (Siluriformes, Callichthyidae). *Acta Zoologica* 78, 69–84.

Huysseune A & Thesleff I (2004) Continuous tooth replacement: the possible involvement of epithelial stem cells. *BioEssays* 26, 665–671.

Huysseune A (2006) Formation of a successional dental lamina in the zebrafish (Danio rerio): support for a local control of replacement tooth initiation. *The International journal of developmental biology* 50, 637–643.

Huysseune A & Witten PE (2006) Developmental mechanisms underlying tooth patterning in continuously replacing osteichthyan dentitions. *Journal of experimental zoology. Part B, Molecular and developmental evolution* 306B, 204–215.

Huysseune A & Witten PE (2008) An evolutionary view on tooth development and replacement in wild Atlantic salmon (*Salmo salar* L.). *Evolution & Development* 10, 6–14.

Jernvall J & Thesleff I (2012) Tooth shape formation and tooth renewal: Evolving with the same signals. *Development* 139, 3487–3497.

Jollie M (1975) Development of the Head Skeleton and Pectoral Girdle in Esox. *Journal of Morphology* 147, 61–88.

Jollie M (1980) Development of Head and Pectoral Girdle Skeleton and Scales in Acipenser. *Copeia* 2, 226–249.

Jollie M (1984a) Development of Cranial and Pectoral Girdle Bones of Lepisosteus with a Note on Scales. *Copeia* 2, 476–502.

Jollie M (1984b) Development of the head and pectoral skeleton of Polypterus with a note on scales (Pisces: Actinopterygii). *Journal of Zoology* 204, 469–507.

Kague E, Gallagher M, Burke S, Parsons M, Franz-Odendaal T & Fisher S (2012) Skeletogenic fate of zebrafish cranial and trunk neural crest. *PLoS One* 7: e47394.

Kardong KV (2019) *Vertebrates. Comparative Anatomy, Function, Evolution*. 8th ed., McGraw-Hill Education, New York.

Kent GC (1987) *Comparative anatomy of vertebrates*. 7th ed., Wm. C. Brown Publishers, Dubuque, Melbourne, Oxford.

Kerr JG (1919) *Text-book of Embryology*. Volume 2. Macmillan and Co, London.

Kloučková L (2011) *Developmental Origin of Cartilage Skull Elements in axolotl*. MSc. Prague: Charles University, pp. 63.

Knight RD & Schilling TF (2006) Cranial neurocrest and the development of the head skeleton. In: Saint-Jeannet JP (Ed.). Neural Crest Induction and Differentiation. *Advances in Experimental Medicine and Biology* 589, 120–133.

Kráľovič M (2009) *Early craniofacial and dental morphogenesis in bichir, P. senegalus*. MSc. Prague: Charles University, pp. 76.

Kuratani S, Adachi N, Wada N, Oisi Y & Sugahara F (2013) Developmental and evolutionary significance of the mandibular arch and prechordal/premandibular cranium in vertebrates: revising the heterotopy scenario of gnathostome jaw evolution. *Journal of Anatomy* 222, 41–55.

Langille RM & Hall BK (1987) Development of the head skeleton of the Japanese medaka, Oryzias latipes (Teleostei). *Journal of Morphology* 193, 135–158.

Lefebvre V & Bhattaram P (2010) Vertebrate skeletogenesis. *Current Topics in Developmental Biology* 90, 291–317.

Liem KF, Bemis W, Walker WF & Grande L (2001) *Functional anatomy of vertebrates: an evolutionary perspective*. Harcourt College Publishers, Fort Worth, 703 pp.

Lukas P & Olsson L (2020) Sequence of chondrocranial development in the oriental fire bellied toad *Bombina orientalis*. *Journal of Morphology* 281, 688–701.

Mabee PM & Trendler TA (1996) Development of the Cranium and Paired Fins in *Betta splendens* (Teleostei: Percomorpha): Intraspecific Variation and interspecific Comparisons. *Journal of Morphology*, 249–287.

Macháčová S (2014) *Dlx genes in odontogenesis and craniofacial morphogenesis in bichir*. MSc. Prague: Charles University, pp. 90.

Maisey JG, S. TurnerS, Naylor GJP & Miller RF (2014) Dental patterning in the earliest sharks: Implications for tooth evolution. *Journal of Morphology* 275, 586–596.

Martin KJ, Rasch LJ, Cooper RL, Metscher BD, Johanson Z & Fraser GJ (2016) Sox2+ progenitors in sharks link taste development with the evolution of regenerative teeth from denticles. *PNAS* 113, 14769–14774.

Meunier FJ & Huysseune A (1992) The concept of bone tissue in Osteichthyes. *Netherlands Journal of Zoology* 42, 445–458.

Meunier FJ, De Mayrinck D & Brito PM (2015a) Presence of plicidentine in the labial teeth of *Hoplias aimara* (Erythrinidae; Ostariophysi; Teleostei). *Acta Zoologica* 96, 174–180.

Meunier FJ, Mondéjar-Fernández J, Goussard F, Clément G & Herbin M (2015b) Presence of plicidentine in the oral teeth of *Latimeria chalumnae* (Sarcopterygii; Actinistia; Coelacanthidae). *Journal of Structural Biology* 190(1), 31–37.

Meunier FJ & Brito PM (2017) Histological characteristics of lower jaw bones and oral teeth of the short nose gar, *Lepisosteus platostomus* Rafinesque, 1820 (Lepisosteidae). *Cybium* 41(3), 279–286.

Miller WA & Radnor CJP (1973) Tooth replacement in the bowfin (*Amia calva* – Holostei). *Journal of Morphology*, 140(4), 381–395.

Minařík M (2018) *Ontogeny, evolution & homology of cement glands and attachment organs in lower vertebrates*. PhD. Prague: Charles University, pp. 65.

Murdock D, Dong X, Repetski J, Marone F, Stampanoni M & Donoghue PCJ (2013) The origin of conodonts and of vertebrate mineralized skeletons. *Nature* 502, 546–549.

Nelson GJ (1969) Gill arches and the phylogeny of fishes, with notes on the classification of vertebrates. *Bulletin of the American Museum of Natural History* 141, 479–552.

Near TJ, Eytan RI, Dornberg A, Kuhn KL, Moore JA, Davis MP, Wainwright PC, Friedman M & Smith WL (2012) Resolution of ray-finned fish phylogeny and timing of diversification. *Proceedings of the National Academy of Sciences of the United States of America* 109, 13698–13703.

Noden DM (1978) The control of avian cephalic neural crestcytodifferentiation. I. Skeletal and connective tissues. *Developmental Biology* 67, 296–312.

Noden DM (1983) The role of the neural crest in patterning of avian cranial skeletal, connective and muscle tissues. *Developmental Biology* 96, 144–165.

Northcutt RG & Gans C (1983) The genesis of neural crest and epidermal placodes: a reinterpretation of vertebrate origins. *Quarterly Review of Biology* 58, 1–28.

Northcutt RG (2005) The New Head Hypothesis Revisited. *Journal of experimental zoology. Part B, Molecular and developmental evolution* 304B, 274–297.

Olsson L, Ericsson R & Cerny R (2005) Vertebrate head development: Segmentation, novelties, and homology. *Theory in Biosciences* 124, 146–163.

Parker WK (1882) On the Structure and Development of the Skull in Sturgeons (Acipenser ruthenus and A.sturio). *Philosophical Transactions of the Royal Society of London* 173, 139–185.

Pashine RG & Marathe VB (1977) The development of the chondrocranium of *Cyprinus carpio* Linn. *Proceedings of the Indian Academy of Science* 85, 351–363.

Pehrson T (1944) Some observations on the development and morphology of the dermal bones in the skull of Acipenser and Polyodon. *Acta Zoologica* 25, 27–48.

Pehrson T (1947) Some new interpretations of the skull in Polypterus. *Acta Zoologica* 28, 399–455.

Pehrson T (1958) The early ontogeny of the sesory lines and the dermal skull in Polypterus. *Acta Zoologica* 39, 241–257.

Peyer B (1968) Osteichthyes. In: Zangerl R (Ed.) *Comparative Odontology*. University Chicago Press, Chicago, 80–110.

Piekarski N, Gross JB & Hanken J (2014) Evolutionary innovation and conservationin the embryonic derivation of the vertebrate skull. *Nature Communications* 5, 1–9.

Pispa J & Thesleff I (2003) Mechanisms of ectodermal organogenesis. *Developmental Biology* 262, 95–205.

Pospíšilová A (2015) *Characterization of cranial skeletogenesis and odontogenesis in basal ray-finned fishes*. MSc. Prague: Charles University, pp. 102.

Powder KE, Milch K, Asselin G & Albertson RC (2015) Constraint and diversification of developmental trajectories in cichlid facial morphologies. *EvoDevo* 6(25), 1–14.

Psutková V (2019) *Primary mouth formation in basal fishes*. MSc. Prague: Charles University, pp. 91.

Rasch LJ, Martin KJ, Cooper RL, Metscher BD, Underwood CJ & Fraser GJ (2016) An ancient dental gene set governs development and continuous regeneration of teeth in sharks. *Developmental Biology* 415, 347–370.

Richter M & Smith M (1995) A microstructural study of the ganoine tissue of selected lower vertebrates. *Zoological Journal of the Linnean Society* 114, 173–212.

Rücklin M, Donoghue PCJ, Johanson Z, Trinajstic K, Marone F & Stampanoni M (2012) Development of teeth and jaws in the earliest jawed vertebrates. *Nature* 491, 748–751.

Sanchez-Villagra MR, Goswami A, Weisbecker V, Mock O & Kuratani S (2008) Conserved relative timing of cranial ossification patterns in early mammalian evolution. *Evolution and Development* 10(5), 519–530.

Sansom IJ, Donoghue PCJ & Albanes G (2005) Histology and affinity of the earliest armoured vertebrate. Biology Letters 1, 446–449.

Santagati F & Rijli FM (2003). Cranial neural crest and the building of the vertebrate head. *Nature reviews. Neuroscience* 4, 806–818.

Scherrer R, Hurtado A, Garcia EM & Debiais-Thibaud M (2017) MicroCT survey of larval skeletal mineralization in the Cuban gar *Atractosteus tristoechus* (Actinopterygii; Lepisosteiformes). *MorphoMuseuM* 3(3), 1–15.

Schneider RA (2005) Developmental mechanisms facilitating the evolution of bills and quills. *Journal Anatomy* 207(5), 563-573.

Schneider RA (2018) Neural crest and the origin of species-specific pattern. *Genesis* 56(6-7), e23219.

Schoch RR (2006) Skull ontogeny: developmental patterns of fishes conserved across major tetrapod clades. *Evolution & Development* 8(6), 524–536.

Schultze H-P (1970) Folded teeth and the monophyletic origin of Tetrapodes. *American Museum novitates* 2408, 1–10.

Schultze H-P (1993) Patterns of diversity in the skull of jawed fishes. *In:* Hanken J & Hall BK (eds.) *The skull*. Vol. 2, Patterns of Structural and Systematic Diversity. Chicago: University of Chicago Press, pp. 189–254.

Seidel R, Blumer M, Pechriggl E-J, Lyons K, Hall BK, Fratzl P, Weaver JC & Dean MN (2017) Calcified cartilage or bone? Collagens in the tessellated endoskeletons of cartilaginous fish (sharks and rays). *Journal of structural biology* 200(1):54–71.

Sewertzoff AN (1928) The head skeleton and muscles of *Acipenser ruthenus*. *Acta Zoologica* 9, 193–127.

Silvent J, Akiva A, Brumfeld V, Reznikov N, Rechav K, Yaniv K, Addadi L & Weiner S (2017) Zebrafish skeleton development: High resolution micro-CT and FIB-SEM block surface serial imaging for phenotype identification. *PLoS ONE* 12(12), e0177731.

Sire J-Y, Davit-Beal T, Delgado S, Van Der Heyden C & Huysseune A (2002) First-generation teeth in nonmammalian lineages: Evidence for a conserved ancestral character?. *Microscopy Research and Technique* 59, 408–434.

Sire J-Y & Huysseune A (2003) Formation of dermal skeletal and dental tissues in fish: a comparative and evolutionary approach. *Biological Reviews* 78, 219–249.

Sire J-Y, Donoghue PCJ & Vickaryous MK (2009) Origin and evolution of the integumentary skeleton in non-tetrapod vertebrates. *Journal of Anatomy* 214, 409–440.

Smith KK (2001) Heterochrony revisited: the evolution of developmental sequences. *Biological Journal of the Linnean Society* 73, 169–186.

Smith KK (2003) Time's arrow: heterochrony and the evolution of development. *The International journal of developmental biology* 47, 613–621.

Smith MM & Hall BK (1993) A developmental model for evolution of the vertebrate exoskeleton and teeth: the role of cranial and trunk neural crest. *Evolutionary Biology* 27, 387–448.

Smith MM (2003) Vertebrate dentitions at the origin of jaws: when and how pattern evolved. *Evolution & Development* 5(4), 394–413.

Smith MM, Johanson Z, Butts T, Ericsson R, Modrell M, Tulenko FJ, Davis MC & Fraser GJ (2015) Making teeth to order: conserved genes reveal an ancient molecular pattern in paddlefish (Actinopterygii). *Proceedings of Royal Society B* 282: 20142700.

Stock DV, Jackman WR & Trapani J (2006) Developmental genetic mechanisms of evolutionary tooth loss in cypriniform fishes. *Development* 133, 3127–3137.

Streelman JT & Albertson RC (2006) Evolution of novelty in the cichlid dentition. *Journal of experimental zoology. Part B, Molecular and developmental evolution* 306B, 216–226.

Stricker S, Fundele R, Vortkamp A & Mundlos S (2002) Role of Runx genes in chondrocyte differentiation. *Developmental Biology* 245, 95–108.

Štundl J (2019) *Migration and morphogenesis of neural crest cells in the context of craniofacial development of selected ray-finned fishes*. PhD. Prague: Charles University, pp. 78.

Thiery AP, Shono T, Kurokawa D, Britz R, Johanson Z & Fraser GJ (2017) Spatially restricted dental regeneration drives pufferfish beak development. *PNAS* 114, 4425–4434.

Thomson KS (1993) Segmentation, the adult skull, and the problem of homology. *In:* Hanken J & Hall BK (eds.) *The skull*. Vol. 2, Patterns of Structural and Systematic Diversity. Chicago: University of Chicago Press, pp. 36–68.

Trapani J (2001) Position of Developing Replacement Teeth in Teleosts. *Copeia* 1, 35–51.

Tucker AS & Fraser GJ (2014) Evolution and developmental diversity of tooth regeneration. *Seminars in Cell & Developmental Biology* 25–26, 71–80.

Vandenplas S, De Clercq A & Huysseune A (2014) Tooth replacement without a dental lamina: The search for epithelial stem cells in *Polypterus senegalus*. *Journal of Experimental Zoology Part B: Molecular and Developmental Evolution* 322(5), 281–293.

Vandenplas S, Willems M, Witten PE, Hansen T, Fjelldal PG & Huysseune A (2016) Epithelial Label-Retaining Cells Are Absent during Tooth Cycling in *Salmo salar* and *Polypterus senegalus*. *PLoS ONE* 11(4): e0152870.

Vaškaninová V, Chen D, Tafforeau P, Johanson Z, Ekrt B, Blom H & Ahlberg PE (2020) Marginal dentition and multiple dermal jawbones as the ancestral condition of jawed vertebrates. *Science* 369, 211–216.

Wacker K, Bartsch P & Clemen G (2001) The development of the tooth pattern and dentigerous bones in *Polypterus senegalus* (Cladistia, Actinopterygii). *Annals of Anatomy* 183, 37–52.

Webb JF (1989) Gross morphology and evolution of the mechanosensory lateral line system in teleost fishes. *Brain, Behavior and Evolution* 33, 34–53.

Webb JF & Northcutt RG (1997) Morphology and distribution of pit organs and canal neuromasts in non-teleost bony fishes. *Brain, Behavior and Evolution* 50, 139–151.

Weinhardt V, Shkarin R, Wernet T, Wittbrodt J, Baumbach T & Loosl F (2018) Quantitative morphometric analysis of adult teleost fish by X-ray computed tomography. *Scientific Reports* 8, 16531.

Westneat MW (2004) Evolution of levers and linkages in the feeding mechanism of fishes. *Integrative and comparative biology* 44(5), 378–389.

Zheng Q, Zhou G, Morello R, Chen Y, Garcia-Rojas X & Lee B (2003) Type X collagen gene regulation by Runx2 contributes directly to its hypertrophic chondrocyte-specific expression in vivo. *The Journal of cell biology* 162(5), 833–842.

Zhu M, Yu, X, Ahlberg PA, Choo B, Lu J, Qiao T, Qu Q, Zhao W, Jia L, Blom H. & Zhu Y (2013) A Silurian placoderm with osteichthyan-like marginal jaw bones. *Nature* 502, 188–193.

Zdroje použitých obrázků:

DigiMorph Staff (2004) "*Acipenser fulvescens*" (On-line), Digital Morphology. Accessed 28 05 2020 at http://digimorph.org/specimens/Acipenser_fulvescens/.

Humphries J (2003) "*Polypterus senegalus*" (On-line), Digital Morphology. Accessed August 28 05 2020 at http://digimorph.org/specimens/Polypterus_senegalus/head/.

Long J (2015) "*Atractosteus spatula*" (On-line), Digital Morphology. Accessed 28 05 2020 at http://digimorph.org/specimens/Atractosteus_spatula/.

Zuber P (2008) „*Esox lucius*“ (On-line), Biological Library. Accessed 28 05 2020 at https://www.biolib.cz/en/image/id71817/.

8 Publikace do dizertační práce zahrnuté

I. **Pospisilova A**, Brejcha J, Miller V, Holcman R, Šanda R & Stundl J (2019) Embryonic and larval development of the Northern pike: a new emerging fish model system for evo-devo research. *Journal of Morphology* 280, 1118–1140.

IF (2019) = 1,563

Received: 12 November 2018 | Revised: 9 April 2019 | Accepted: 10 May 2019

DOI: 10.1002/jmor.21005

RESEARCH ARTICLE

Journal of morphology WILEY

Embryonic and larval development of the northern pike: An emerging fish model system for evo-devo research

Anna Pospisilova[1] | Jindřich Brejcha[2,3] | Vojtech Miller[1] | Radek Holcman[4] | Radek Šanda[2] | Jan Stundl[1,2]

[1]Department of Zoology, Faculty of Science, Charles University, Prague, Czech Republic

[2]Department of Zoology, National Museum, Prague, Czech Republic

[3]Department of Philosophy and History of Science, Charles University, Prague, Czech Republic

[4]Rybarstvi Litomysl s.r.o., Litomysl, Czech Republic

Correspondence
Jan Stundl, Department of Zoology, Faculty of Science, Charles University, Prague, Czech Republic.
Email: jan.stundl@natur.cuni.cz

Funding information
Grantová Agentura, Univerzita Karlova, Grant/Award Numbers: 1448514, 640616; Ministry of Culture of the Czech Republic, Grant/Award Number: DRKVO 2019-2023/6.V.a,00023272; National Museum, Prague, Grant/Award Number: NM-P15/01IG-ŠT; Univerzita Karlova v Praze, Grant/Award Number: SVV 260434/2019

Abstract

The northern pike, *Esox lucius*, is one of the largest temperate freshwater apex predators with a characteristic morphology: an elongated body with pelvic, dorsal, and anal fins located at the rear as a functional feature to sprint predation. However, the typical pike character is its head, which is characterized by a long, flattened snout, a well-armed mouth with numerous teeth, and large eyes characteristic of shallow water visual predators. Although the northern pike is becoming increasingly popular as a model system for ecology and evolutionary research, a detailed staging table has not yet been reported. In this study, we report the first comprehensive staging table for the northern pike, spanning from the one-cell stage to the freely-swimming juvenile stage. In addition to classical embryological descriptions, we use a DAPI staining to distinguish individual cells and embryonic structures during the early development. This dataset, in combination with the genomic and transcriptomic resources already available, serves as a foundation for in-depth mechanistic studies dealing with development using this species.

KEYWORDS
embryology, ray-finned fishes, staging, chondrogenesis, skeletogenesis

1 | INTRODUCTION

The northern pike (*Esox lucius* Linnaeus, 1758; Figure 1a) is a well-known freshwater apex predator with a circumpolar distribution across a broad range of aquatic environments (Craig, 2008; Crossman, 1996). It belongs to the family Esocidae (Grande, Laten, & Lopez, 2004), whose members are characterized by duck-billed snouts, well-armed mouths with numerous teeth, and elongated bodies. Pikes and mudminnows (order Esociformes) are the sister group of salmon and trouts (order Salmoniformes). There is a single genus of pike, *Esox* (Froese & Pauly, 2018), with seven extant species that are of considerable economic interest to commercial and recreational fishing industries (Mann, 1996; Raat, 1988). Consequently, the reproductive biology of the northern pike is both relatively well-described (e.g., Billard, 1996; Bondarenko, Drozd, & Policar, 2015; Kucska et al., 2005) and foundational for European aquacultures and commercial fisheries.

Pike spawn in the wild when water temperatures reach 6 °C, typically between February and June depending on geographical region (Raat, 1988). Embryonic development can proceed over a broad range of non-lethal temperatures spanning from ~4 to ~23 °C (Hassler, 1982), but appears to be most efficient between 6 and 10 °C (Bondarenko et al., 2015). The development of the northern pike was first described by Lindroth (1946) and Gihr (1957); however, these studies encompass only a few stages and lack detailed descriptions. Later studies investigate only the general developmental pattern with emphasis on several selected developmental stages (Kotlyarevskaya, 1969; Toner & Lawler, 1969). A number of other studies have examined skeletal anatomy and morphology of the northern pike. For example, Besrukow (1928) described the

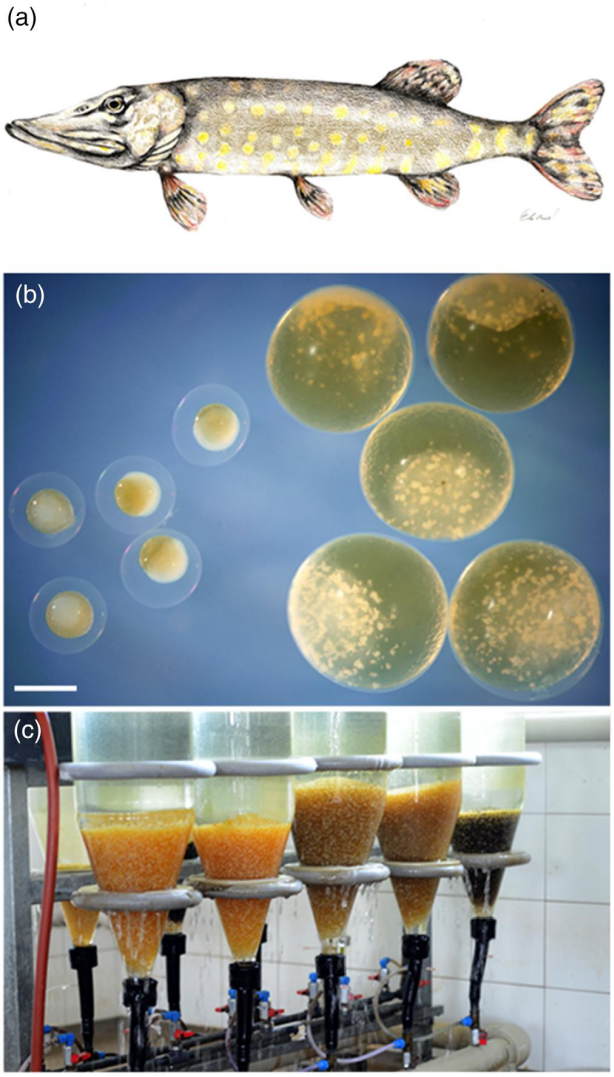

FIGURE 1 The northern pike. (a) Illustration of an adult northern pike. (b) Comparison of zebrafish (left) and pike (right) eggs. Scale bar = 1 mm. (c) Embryos in Zug jars

development of the chondrocranium; Pehrson (1944) examined the formation of the lateral line canal and its relationship to the skull development; Jollie (1975) studied the development of the head skeleton; and Burdi and Grande (2010) analyzed the skull and axial skeleton development. In the recent work, Sadeghinezhad et al. (2014) described the morphology of the northern pike tongue. Although the northern pike has teeth that are present at multiple sites in the oropharyngeal region, odontogenesis of the pike has been investigated only at the ultrastructural level (Herold, 1974). Thus, despite numerous studies documenting different aspects of pike development, a comprehensive staging table with a detailed description of embryonic and larval development has not yet been presented. With the recent development of high-quality genome and reference transcriptome assemblies (Rondeau et al., 2014; Zerbino et al., 2018) the northern pike is rapidly emerging as a new fish model for evo-devo research (Braasch et al., 2014), but progress has been hindered by the absence of staging table. Therefore, such a resource would be of considerable value to the growing pike research community.

Thanks to its morphological features and commercial availability, the northern pike is emerging as powerful experimental model system, particularly for developmental biology and evolutionary studies (Forsman et al., 2015; Nilsson, Skov, & Farrell, 2008). Although its natural breeding season is limited to spring, it has several advantages over the conventional fish model organism, the zebrafish (*Danio rerio*), including a large number of eggs (up to 100,000 eggs per female) which are large and therefore more experimentally accessible than those of zebrafish (Figure 1b), numerous teeth throughout the whole oropharyngeal region that should be the basal condition for early vertebrates (Donoghue, 2002), and a characteristic ambush predator body plan.

This study aims to highlight the important features of each developmental stage from fertilization to free-living juvenile with the first dermal bones. Collectively, the presented staging table of the northern pike represents a foundational resource for evo-devo research and a tool for commercial hatcheries.

2 | MATERIALS AND METHODS

2.1 | Husbandry and sample collection

Clutches of fertilized eggs were obtained from four different females housed at the hatchery (Rybarstvi Litomysl s.r.o., Czech Republic) in March–April 2015 and 2016. Fish were experimentally manipulated in accordance with institutional and international guidelines for the protection of animal welfare (Directive 2010/63/EU) in the animal facility at the Department of Zoology, Charles University in Prague. For developmental staging, embryos were maintained at an optimized temperature of 12 ± 0.5 °C (aeration: 9 mg L^{-1}; water flow rate: 10 m^3 hr^{-1}; photoperiodicity: 10 hr light and 14 hr total darkness) in incubation jars (Zug jars) at the hatchery (Figure 1c). Development of embryos was monitored every 2–4 hr until end of the first day. In the following days, the development was monitored every 3–8 hr until the hatching occurred. Posthatching development was monitored once a day. The staging series is based on sampling made during these monitoring sessions. Each developmental stage was determined as the time point when the most embryos in the sample reached the identical developmental point. Live embryos were anesthetized with MS-222 (tricaine methanesulfonate) prior to microscopic observations or fixation.

2.2 | Developmental staging, microscopic observation, and scanning electron microscopy

Description of individual developmental stages was based on published resource for the most frequently used fish model systems,

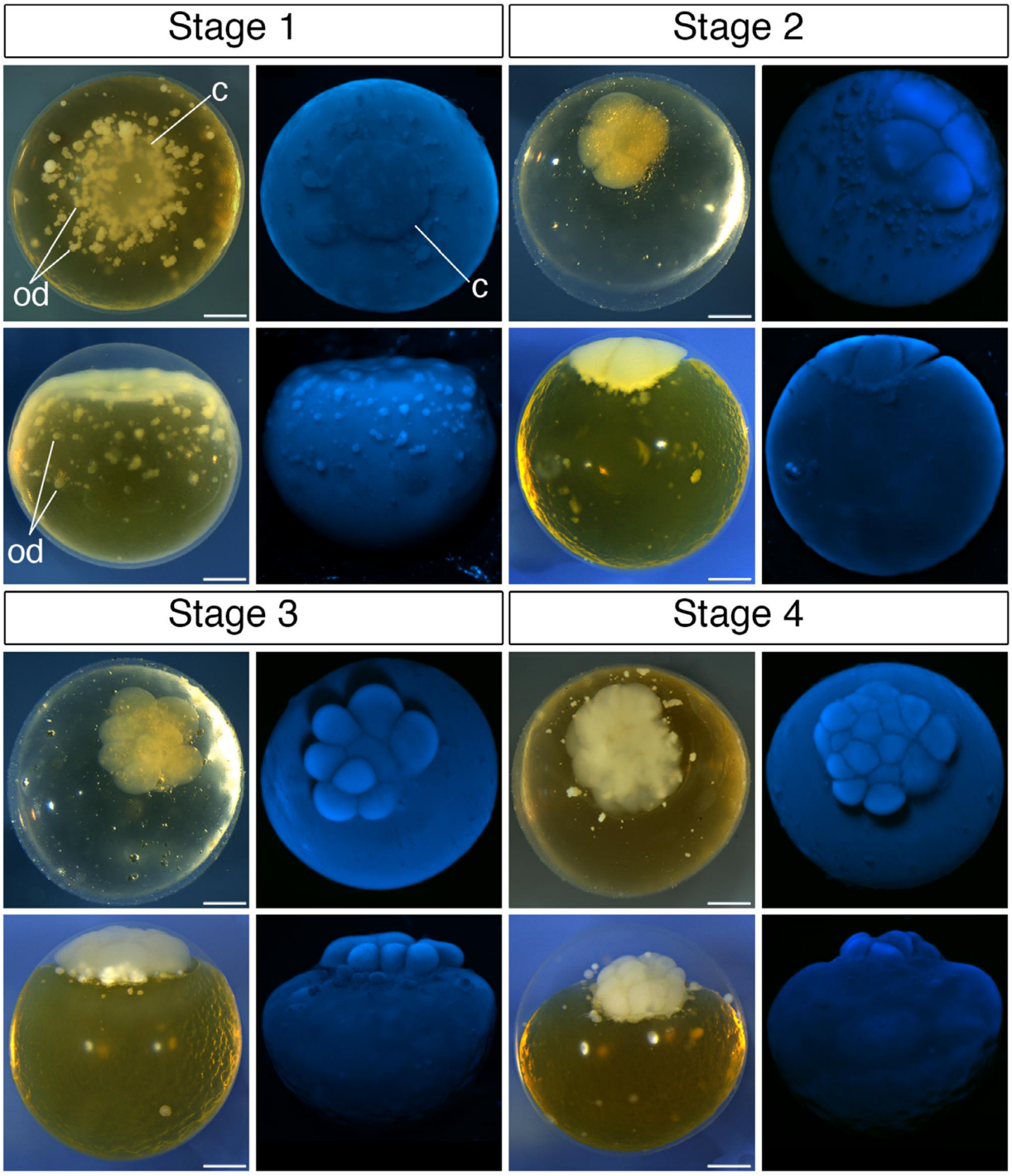

FIGURE 2 Cleavage, blastula, and gastrula period. Northern pike developmental stages to the end of gastrulation. Each stage contains a dorsal or animal pole view of the embryo at the top and a lateral view of the embryo at the bottom. Each brightfield photograph is paired with DAPI staining to highlight detailed morphology. See the text for detailed description of each stage. Scale bars are 0.5 mm. White arrowhead marks the anterior tip of the embryonic shield at stage 12–15. c, cell; es, embryonic shield; gr, germ ring; h, head; np, neural plate; od, oil droplets; yp, yolk plug; ysl, yolk syncytial layer

zebrafish (*Danio rerio*; Kimmel et al., 1995) and medaka (*Oryzias latipes*; Iwamatsu, 2004). Illustrations were created in Inkscape 0.92.3 (Inkscape Team, 2018) based on photographs. All embryos and hatched larvae were mounted on Petri dishes containing agarose for live imaging and photographed using a dissection microscope SZX12 (Olympus). For better visualization of individual cells,

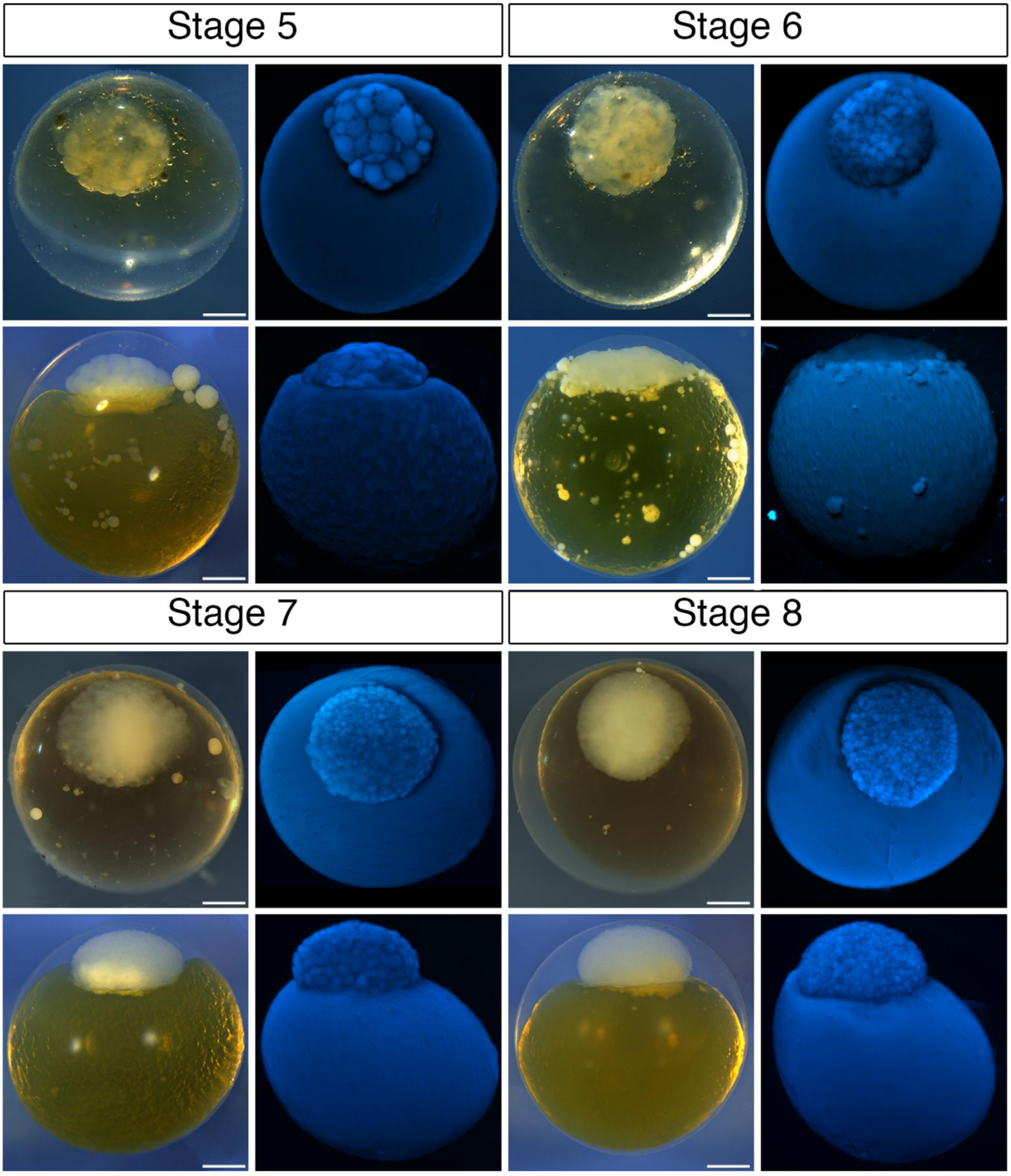

FIGURE 2 Continued

embryos were dechorionated, stained with DAPI and observed using a SteREO Lumar V12 fluorescent stereomicroscope (Zeiss, Germany). Samples for scanning electron microscopy (SEM) were fixed at least overnight in modified Karnovsky's fixative (Mitgutsch et al., 2008). After washing in PBS, samples were dehydrated through a graded series of ethanol, dried in a critical point dryer, mounted in resin, and coated with gold. SEM images were acquired with a JSM-6380LV scanning electron microscope (JEOL, Japan).

2.3 | Cartilage and bone staining

Larvae were fixed in 4% PFA in PBS overnight, washed with PBS, and transferred into 80% ethanol. Cartilage and bone staining was

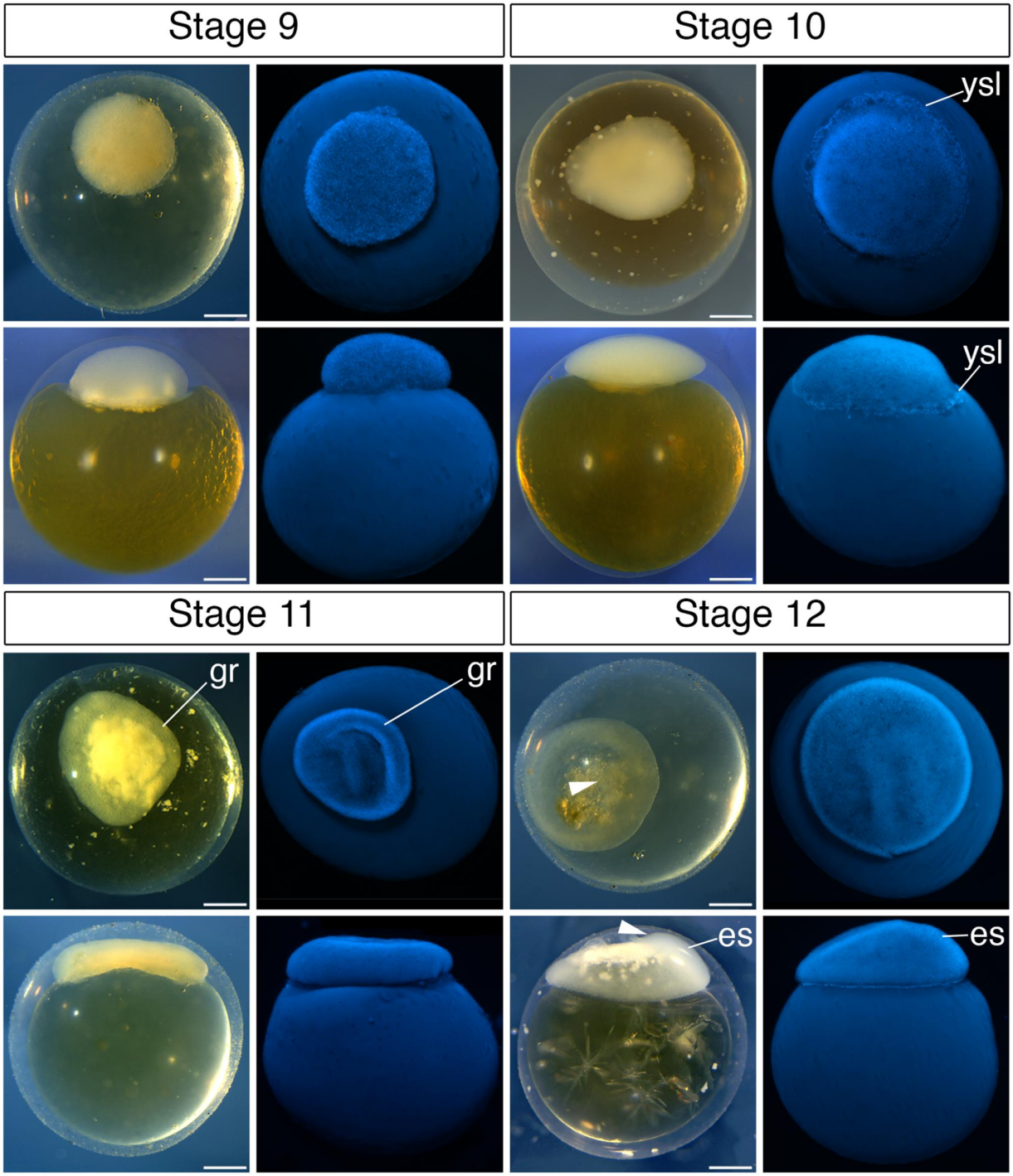

FIGURE 2 Continued

carried with Alcian Blue and Alizarin Red as described by Taylor and Van Dyke (1985). To trace the onset of cartilage and bone development we stained larvae 8–19 mm in length. For visualizing bone structures, we also used calcein in vivo staining (Du et al., 2001). Live fish larvae were incubated in freshly-made staining solution (2 g calcein in 1 L water, pH ~7) in the dark for 3 min, anesthetized, and observed under a fluorescent stereomicroscope as described above.

2.4 | Histology

Embryos were anesthetized, fixed in 4% PFA in PBS overnight, washed, and dehydrated as described above and then embedded in

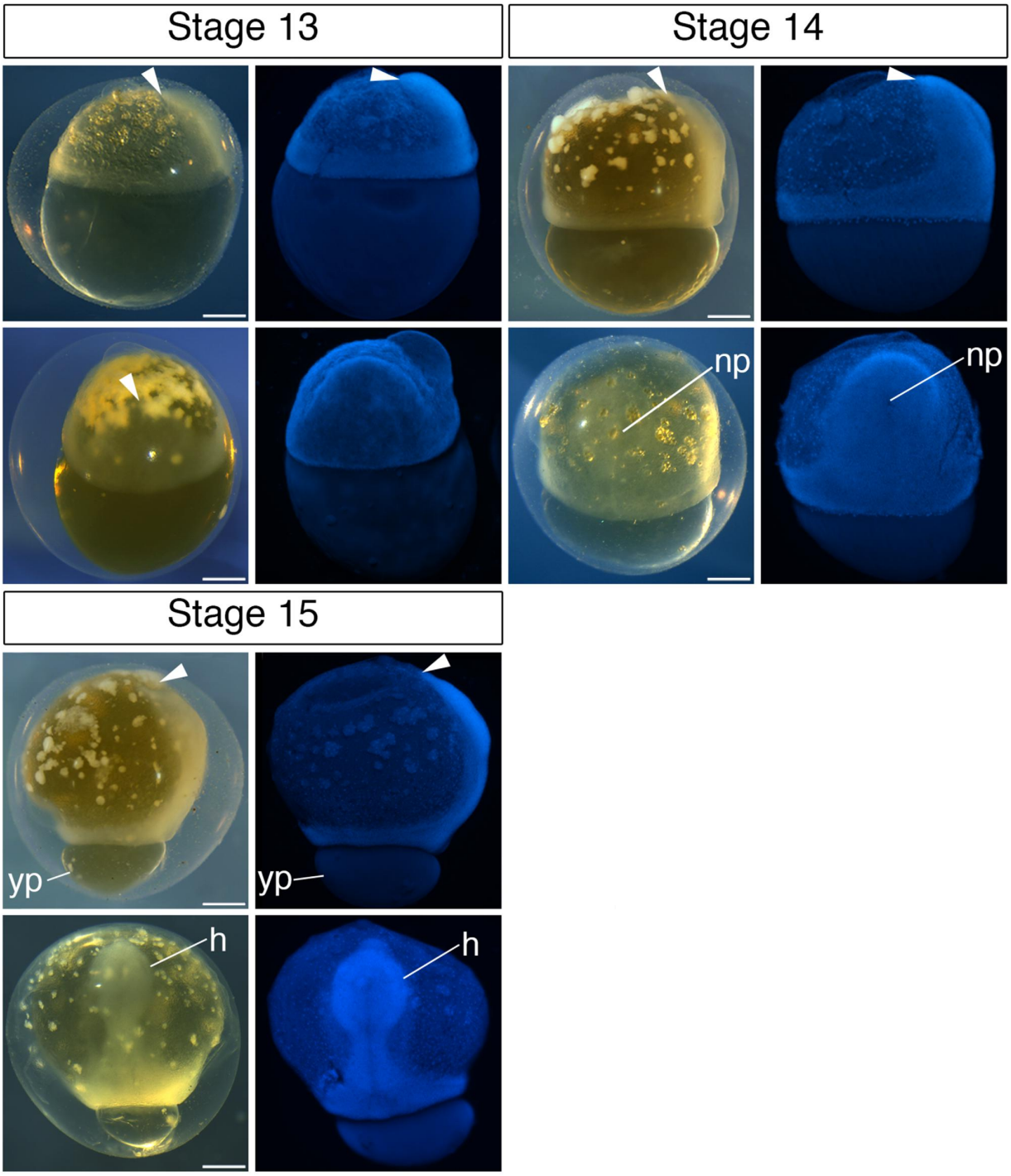

FIGURE 2 Continued

JB4 resin (Polysciences) according to the manufacturer's instructions. Embedded embryos were sectioned on an RM 2155 microtome (Leica), stained with Azure B-Eosin (SERVA) and mounted in DePeX (SERVA). For selective staining of the cement gland epithelium, a Periodic-acid Schiff (PAS) kit (Sigma) was used according to the manufacturer's instructions.

2.5 | Analysis of the influence of temperature on developmental timing

As the timing of development depends on water temperature, we systematically tested the influence of this variable on northern pike development. For this, we maintained comparable cohorts of embryos

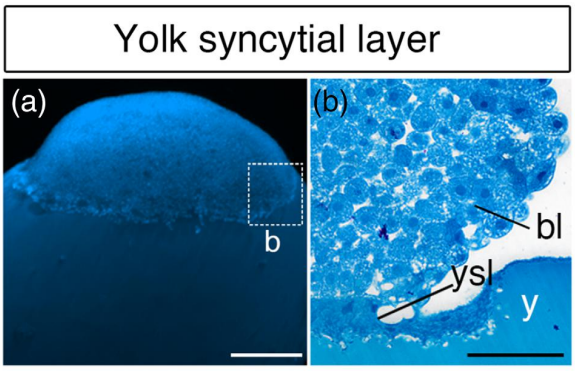

FIGURE 3 Yolk syncytial layer. (a) Side view of stage 10 stained with DAPI. (b) Transversal histological section of stage 10. bl, blastoderm; y, yolk; ysl, yolk syncytial layer. Scale bars = 0.3 mm in (a), 100 μm in (b)

under six constant temperature regimes (9–14 °C). Ten individuals were randomly selected twice a day from each cohort for developmental staging and inspection for developmental abnormalities, until hatching occurred in 80% of examined individuals. On the basis of these data, the average heat needed to reach each developmental stage was calculated and expressed as "day-degrees," i.e., the average temperature in degrees of Celsius above the pike's known lower developmental threshold (3.3 °C) per day (Bondarenko et al., 2015). To visualize the effect of different temperature regimes we fitted locally estimated scatterplot smoothing (loess; α = 0.75) curve to the measured data using loess function in R 3.3.2 (R Core Team, 2017).

3 | RESULTS

3.1 | Cell cleavage, blastula, and gastrula period

3.1.1 | Stage 1 (1-cell stage)

Newly-fertilized pike eggs are typically spherical and surrounded by a chorion with a perivitelline space of between 0.1 and 0.3 mm permitting egg rotation despite the presence of the chorion. Fertilized eggs are approximately 2.4 mm in diameter, that is, three times larger than those of zebrafish (Figure 1b). A single blastomere is present at the animal pole. Oil droplets are concentrated at the periphery of the blastomere (Figure 2). The yolk is pale amber in color prior to fixation and pale yellow thereafter.

3.1.2 | Stage 2 (4-cell stage)

Four blastomeres arise from the second cleavage at a right angle to the first cleavage furrow. The shape of the blastodisc is ellipsoidal, and blastodermal cells are of equal size.

3.1.3 | Stage 3 (8-cell stage)

The blastomeres do not form two symmetrical rows as in zebrafish or medaka. From this stage onwards, blastomeres gradually become more irregular in size and shape. Division asynchrony is more pronounced for the small blastomeres that protrude from the lateral accumulation of larger blastomeres.

3.1.4 | Stage 4 (16-cell stage)

Blastomeres form one sheet of 16 cells differing in shape and size.

3.1.5 | Stage 5 (32-cell stage)

The arrangement of blastomeres is variable and forms a solid blastoderm.

3.1.6 | Stage 6 (128-cell stage)

The blastomeres become smaller at this stage. The solid blastoderm is formed by six clear layers of cells.

3.1.7 | Stage 7 (256-cell stage)

The blastoderm rearranges into 8–9 layers of cells.

3.1.8 | Stage 8 (512-cell stage)

The blastoderm forms a solid ball with 10 cell layers.

3.1.9 | Stage 9 (1000-cell stage)

Cells around the edge of the blastoderm and adjacent to the yolk ball start to create the yolk syncytial layer (YSL).

3.1.10 | Stage 10 (high stage)

The boundary between the blastoderm and yolk is evident due to the presence of the YSL. The individual YSL nuclei are visible at the periphery of the blastoderm (Figures 2 and 3a). From this stage onwards, the blastodisc gradually becomes more flattened.

3.1.11 | Stage 11 (germ ring)

The edge of the blastodisc is characterized by a distinctly thickened brim, the germ ring. The appearance of the germ ring marks the onset of gastrulation, whereby cells at the ring periphery give rise to the hypoblast, and remaining cells form the epiblast.

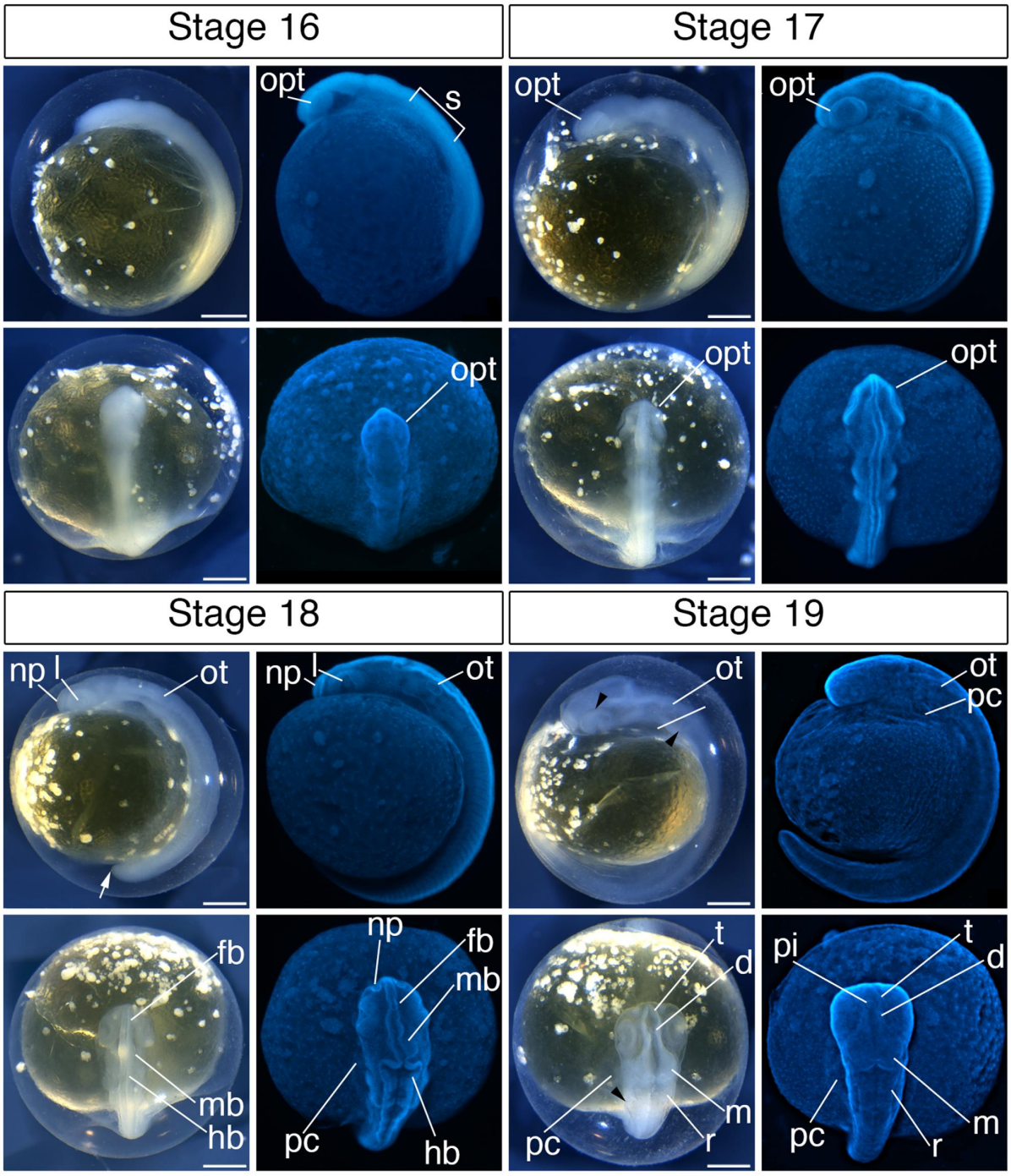

FIGURE 4 Organogenesis period. Each stage contains a dorsal or animal pole view of the embryo at the top and a lateral view of the embryo at the bottom. Each brightfield photograph is paired with DAPI staining to highlight detailed morphology. See the text for detailed description of each stage. Scale bars are 0.5 mm. White arrow marks tip of the tail. Black arrowhead marks first pigmentation. cg, cement gland; d, diencephalon; fb, forebrain; h, heart; hb, hindbrain; l, lens; m, mesencephalon; mb, midbrain; np, nasal pit; opt, optic vesicle; ot, otic vesicle; pb, pectoral fin bud; pc, pericardial cavity; pi, pineal gland; r, rhombencephalon; s, somites; t, telencephalon

3.1.12 | Stage 12 (embryonic shield)

The embryonic shield, visible as a thick cell mass, forms on one side of the blastodisc and extends over the surface of the yolk sphere. The blastodisc thins during shield formation and epiboly is at 10%.

3.1.13 | Stage 13 (25% epiboly)

Epiboly progressively advances and is at 25%. The embryonic shield extends laterally and anteriorly. The blastoderm covers about one quarter of the yolk sphere.

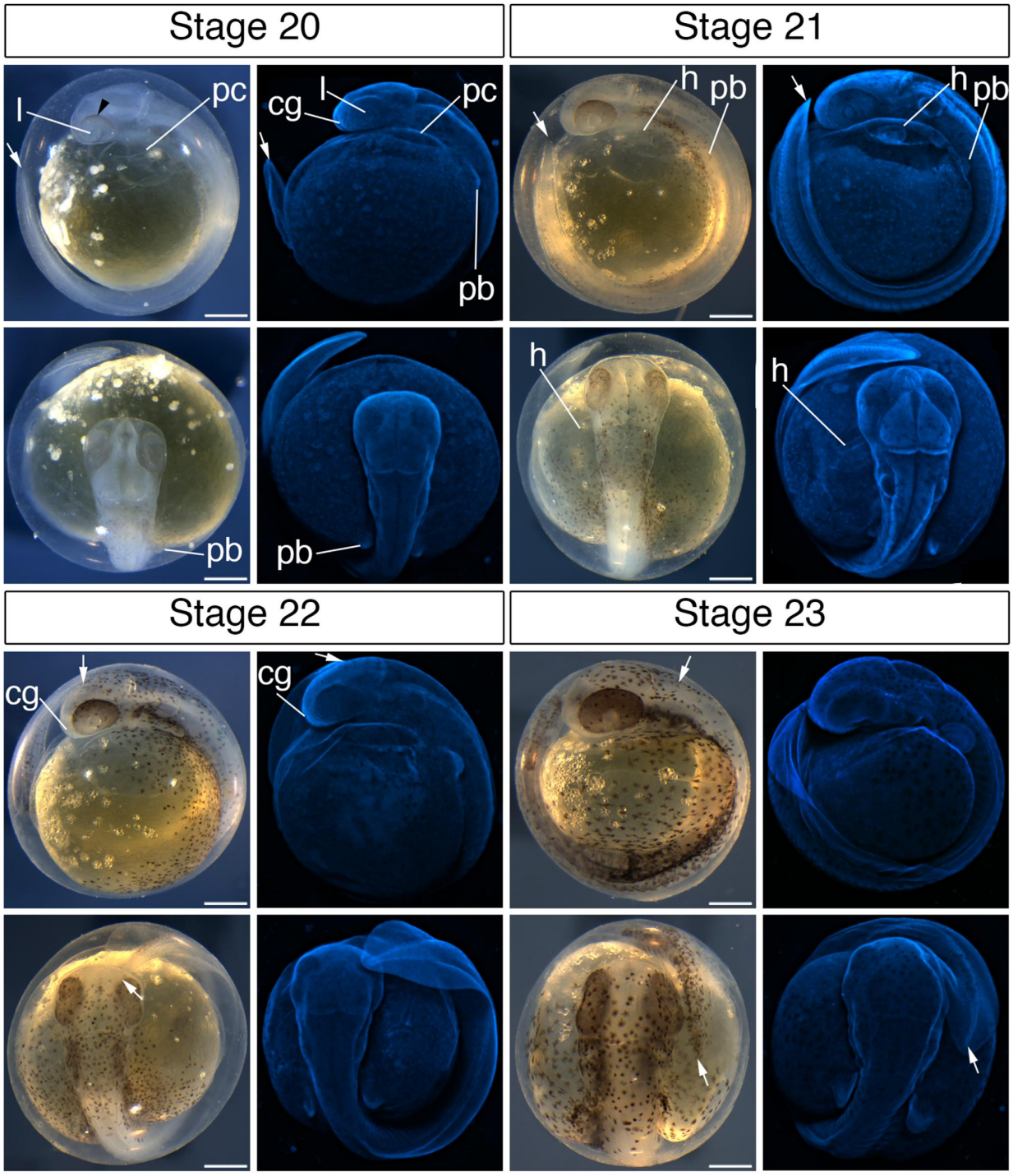

FIGURE 4 Continued

3.1.14 | Stage 14 (neural plate)

The blastoderm envelops half of the yolk sphere and epiboly is at 50–60%. The forming neural plate is visible at the midline of the embryonic shield.

3.1.15 | Stage 15 (85% epiboly)

The embryonic shield begins to narrow laterally and continues to grow anteriorly. The future head starts to become evident as a noticeable thickening in the anterior part of the embryonic shield.

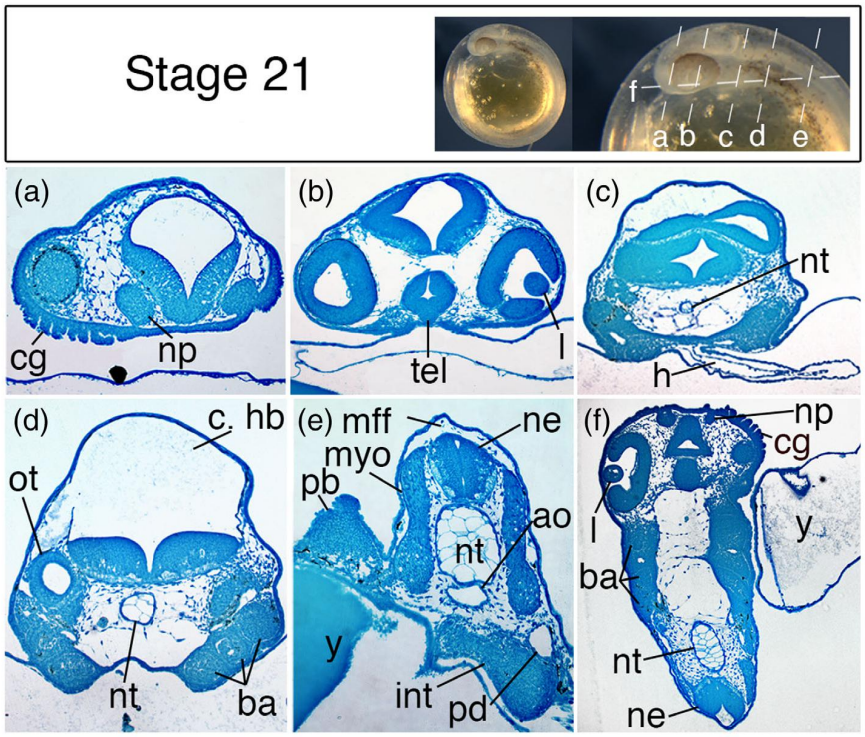

FIGURE 5 Histological sections of early pharyngula stage. The dashed lines represent orientations of histological sections. (a–f) all images represent transverse sections, with the exception of image (f) (horizontal section). ao, dorsal aorta; ba, branchial arches; c. hb, cavity of hindbrain; cg, cement gland; h, heart; int, intestine; l, lens; mff, median fin fold; myo, myotome; ne, neural tube; np, nasal pit; nt, notochord; ot, otic vesicle; pd, pronephric duct; pb, pectoral fin bud; tel, telencephalon; y, yolk

The blastoderm covers almost the entire extent of the yolk and the yolk sphere remains as the yolk plug at the site of blastopore closure. Involution continues until the blastoderm completely closes the yolk plug.

3.2 | Organogenesis period

3.2.1 | Stage 16 (bud)

The rudimentary optic vesicles appear lateral to the anteriormost part of the neural tube (Figure 4). The first 5–10 pairs of somites emerge during this stage, but the precise number is hard to discern by eye. The blastopore is entirely closed.

3.2.2 | Stage 17 (optic vesicle formation)

The optic vesicles are well-defined, but the lenses are not yet present. The dorsal neural furrow is noticeably distinguished. There are 24–28 pairs of somites.

3.2.3 | Stage 18 (lens formation)

The lenses and the otic vesicles begin to form. The neural tube begins to differentiate into distinct forebrain, midbrain, and hindbrain domains. The nasal pits are visible in the anteriormost part of the forming telencephalon. The forming pericardial cavity is visible ventral to the head region. The tip of the tail is free from the surface of the yolk.

3.2.4 | Stage 19 (pigmented eye)

The first melanocytes are present on the dorsal surface of the optic cups, and first several melanocytes occupy the lateral wall of rhombencephalon, especially around the otic vesicles. The otic vesicle and pineal gland are easily visible. The neural tube is subdivided into the telencephalon, diencephalon, mesencephalon, and rhombencephalon. The mesencephalon is particularly widened laterally. The heart in the pericardial cavity exhibits regular contractions. The embryo elongates, primarily, in the caudal region. At least 40 pairs of somites, including 10 at the postcloacal level, are present.

3.2.5 | Stage 20 (body pigment)

The embryo covers approximately three quarters of the yolk sphere. The lens placodes are pronounced, and the eyes exhibit darker pigmentation in the dorsal optic cup. The brain continues to grow and differentiate. The primordium of the future cement glands is visible anterior to the eyes. Melanocytes sparsely occupy the medial trunk region. The anlage of the pectoral fin bud begins to form. Twitching of the trunk muscles is apparent at this stage.

3.2.6 | Stage 21 (full overgrowth)

The embryo covers the entire yolk sphere, and the tip of the tail extends to the anteriormost part of the developing head. The head becomes free of yolk (Figure 5a). The anlage of the tubular heart is visible ventral to the head at the level of the mid-hindbrain boundary

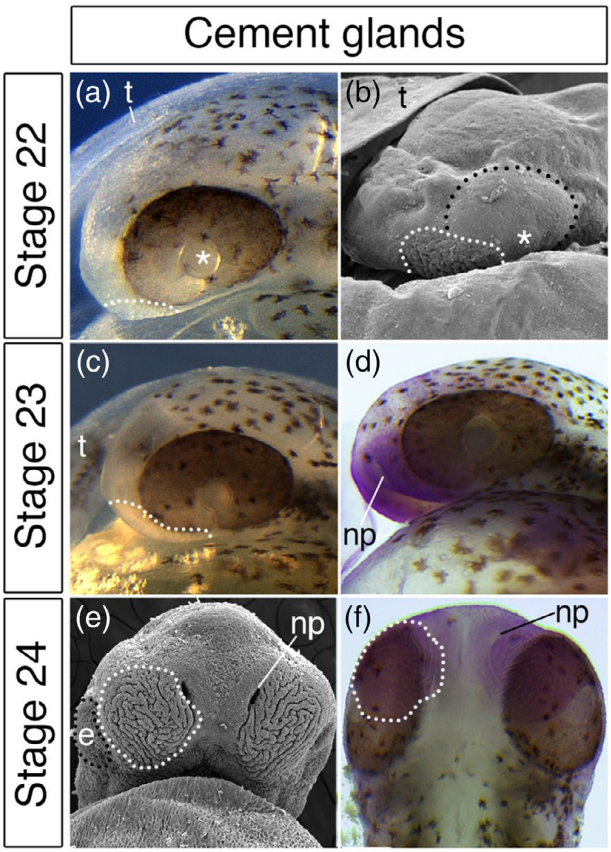

FIGURE 6 The cement glands of the northern pike. (a) Magnified view of the head region at stage 22. (b) SEM image of the head region at stage 22. Black dotted line marks eye primordium. (c) Magnified view of the head region at stage 23. (d and f) Mucus-secreting cells detected via PAS staining (pink color). (d) Lateral view. (f) Ventral view. (e) SEM image of cement glands at stage 24 (ventral view). White dotted line mark cement glands. Asterisks mark lens. e, eye primordium; np, nasal pits; t, tail

(Figure 5c). Melanocytes cover the posterior three-quarters of the embryo and pigment cells cover two-thirds of the eyecups. Pectoral fin buds are easily visible lateral to the fourth or fifth pair of somites and are filled with mesenchymal cells (Figure 5e) that will form the girdle cartilages (Figure 8). Histological examination confirms the presence of a pair of nasal cement glands (Figure 5a). The notochord is vacuolized (Figure 5d) and branchial arches are well distinguished at the histological level (Figure 5d,f). The median fin fold can be recognized in the trunk region (Figure 5e).

3.2.7 | Stage 22 (early prehatching)

Melanocytes cover the entire embryo, including the tail. The coloration of the eyes is darker than at the previous stage. The tip of the tail extends over the head to the mid of the eye. The cement glands are evident anteroventral to the eye (Figure 6a,b).

3.2.8 | Stage 23 (late prehatching)

Melanocytes increase in density and size to cover almost the entire yolk sphere. The tip of the tail extends over the head to the posterior of the eyes. The cement glands become wider (Figure 6c) and mucus-secreting cells start to secrete mucus (Figure 6d).

3.3 | Hatching and posthatching period

3.3.1 | Stage 24 (hatching)

Most of the larvae have hatched by this stage (Figure 7). The yolk is still oblong. The standard length (SL) of hatching larvae is approximately 8.3 mm (Table 1). Most larvae hatch head first, but some hatch tail first. The pair of cement glands occupies the ventral head (Figure 6e), and their mucus-secreting cells are fully functional (Figure 6f). The first well-developed cartilage is associated with the pectoral girdle. At the same time, the first viscerocranial element, the hyosymplectic, begins to emerge anterior to the notochord but it is not yet well-defined (Figure 8). The mouth is still not open (Figure 9b–d). In the eyes, it is possible to distinguish retinal pigment epithelium and the outer nuclear layer (Figure 9a,b). The fin fold is formed primarily by epithelial cells (Figure 9e,f). The pronephric ducts are located dorsolateral to the intestine, in the mid-trunk region (Figure 9f).

3.3.2 | Stage 25 (the opening of the mouth)

The mouth is open in most larvae (Figure 10c,d) and their SL is approximately 8.6 mm (Table 1). Cement glands are still fully functional (Figure 10a). Trabecular condensations (Figure 10c) and branchial arches (Figure 10f) are noticeable only at the histological level. Meckel's cartilage and the quadrate appear in the viscerocranium, and the cleithrum is present as thin cartilage (Figure 8). Two additional layers in the eyes, the ganglion cell layer and the inner plexiform layer, start to emerge (Figure 10b). The swim bladder, situated posterior to the end of the pectoral fins, is visible in horizontal sections (Figure 10e). The first otoliths are present (Figure 10e).

3.3.3 | Stage 26 (protruding mouth)

The mouth protrudes anteriorly, and the lower jaw extends (Figure 7). The yolk ball is reduced in size compared to the previous stage. The tubular heart is located in the pericardial cavity at the anterior aspect of the yolk (Figure 7). The eyes are fully pigmented. Individual melanophores occupy the dorsal part of the body but not the ventral part, where the pigmented lateral stripe forms (Figure 7). The SL is approximately 9.7 mm (Table 1). The development of the neurocranium starts with the *trabeculae cranii* and the otic capsules (Figure 8). The branchial arches appear in the posterior part of the viscerocranium (Figure 8).

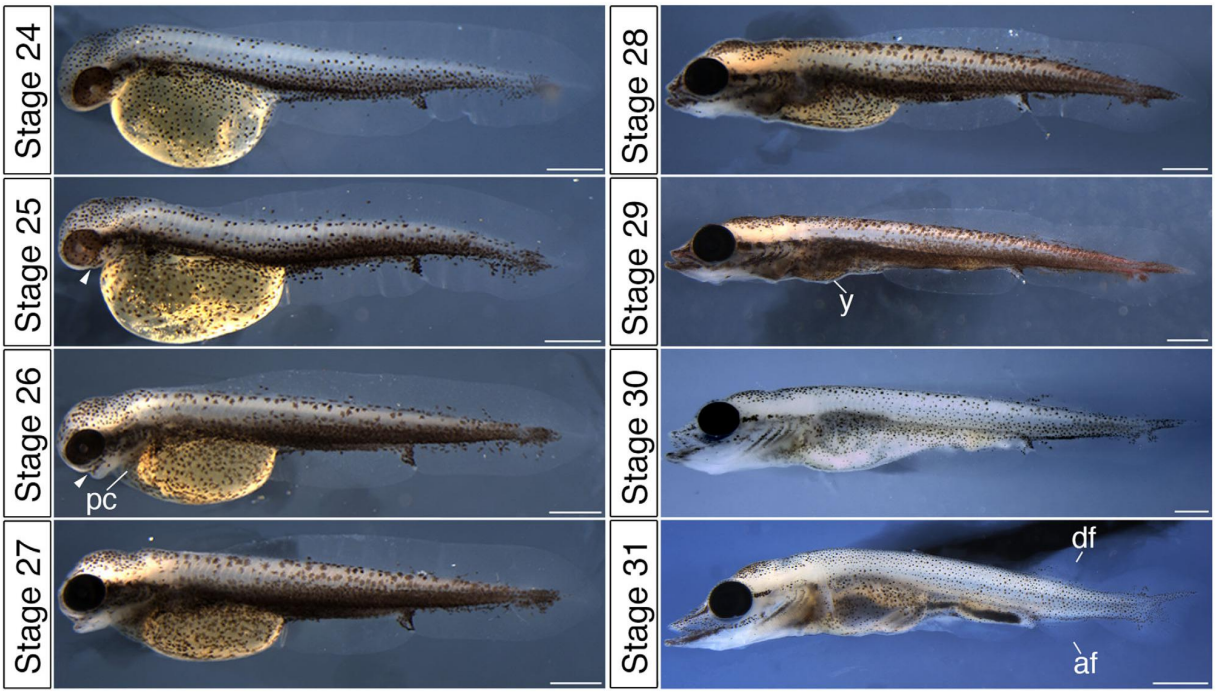

FIGURE 7 Hatching and posthatching period. Each stage represents the lateral view. Note the development of the larval pigmentation pattern. Scale bars are 1 mm and 2 mm (stage 31). White arrowhead marks mouth position. af, anal fin; df, dorsal fin; pc, pericardial cavity; y, yolk

TABLE 1 Standard length (SL) of northern pike larvae

Stage	SL (mm)	*SD*
24	8.3	0.17
25	8.6	0.25
26	9.7	0.21
27	10.3	0.10
28	12.0	0.29
29	13.7	0.47
30	15.0	0.20
31	18.9	0.28

3.3.4 | Stage 27 (first bone)

The SL is approximately 10.3 mm (Table 1). The head becomes straight, and the jaws have almost extended to their final position (Figure 7). The development of the neurocranium continues with the formation of the ethmoid plate (Figure 8). The preformed nasal capsules are evident in the rostral area (Figure 8). Ceratohyal cartilage appears in the lower jaw and the ceratobranchial components of gill arches 1–4 form obliquely in relation to the anteroposterior axis (Figure 8). The cleithrum is the first ossified structure in the developing embryo (Figure 11).

3.3.5 | Stage 28 (first teeth)

The SL is approximately 12.0 mm (Table 1). Yolk abundance is further reduced. The jaws have reached their terminal position, coincident with active oral feeding. The snout takes on its characteristic duck-billed appearance (Figure 7). The hyomandibula and pterygoid process of quadrate are present as cartilaginous elements (Figure 8). Also present at this stage are the interhyale and first epibranchial elements (Figure 8). A single basibranchial cartilage in the ventral midline is encircled by hypobranchials 1–3 (Figure 8). Ceratobranchial 5 is not yet pronounced but can be detected by Alcian Blue staining (Figure 8). The parasphenoid and maxilla begin to ossify (Figure 11). The oral teeth extend from the dentary, palatines and vomers (Figure 11). The pharyngeal teeth are visible as tooth plates anterior to the forming operculum (Figure 11). An aggregation of chondrocytes is present in the forming caudal fin, where the hypural cartilage will form at a later stage (Figure 8).

3.3.6 | Stage 29 (caudal fin cartilages)

The SL is approximately 13.7 mm (Table 1) and the yolk is almost absorbed (Figure 7). The hyomandibula, ceratohyal, and ceratobranchial elements begin to ossify (Figure 11). In the lower jaw, the small coronoid process is recognizable as a widened element of Meckel's cartilage (Figure 8). The hypohyal is a small paired element located at the anterior edge of the basibranchial (Figure 8). A single, small branchiostegal is present ventral to the operculum (Figure 11). The post-temporal appears as a thin elongate element dorsal to the operculum (Figure 11). Two hypurals and parhypural plate cartilages appear in the forming caudal fin (Figure 8).

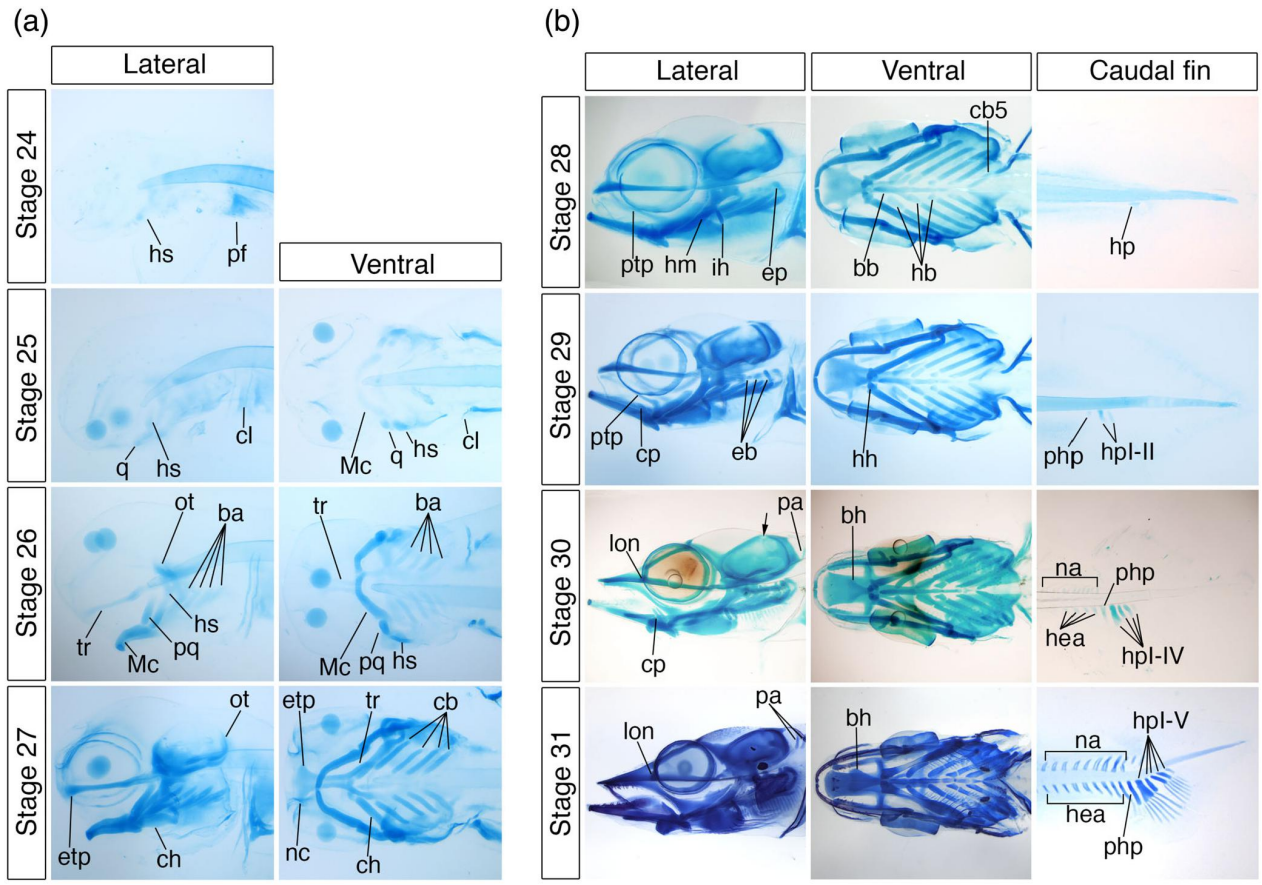

FIGURE 8 Chondrogenesis of craniofacial cartilages and caudal complex cartilages revealed by Alcian Blue staining. Lateral and ventral views of the skull, and lateral view of the caudal fin are shown. Note that the first detectable cartilaginous element in the head is hyosymplectic. Caudal fin develops rather later during the development. Black arrow marks almost enclosed auditory capsule. ba, branchial arches; bb, basibranchial; bh, basihyal; cb, ceratobranchials; ch, ceratohyal; cl, cleithrum; cp, coronoid process; ep, epibranchial; etp, ethmoid plate; hh, hypohyal; hm, hyomandibula; hb, hypobranchial; hea, hemal vertebral arch; hp, hypural; hs, hyosymplectic; ih, interhyal; lon, *lamina orbitonasalis*; Mc, Meckel's cartilage; na, neural vertebral arch; nc, nasal capsule; ot, otic capsule; pa, parapophyses; pf, pectoral fin; php, parhypural; pq, palatoquadrate; ptp, pterygoid process of quadrate; q, quadrate; tr, *trabeculae cranii*

3.3.7 | Stage 30 (yolk absorbed)

The SL is approximately 15.0 mm (Table 1), and the yolk is completely absorbed. Larvae exhibit a typical ambush predator body plan (Figure 7). The coronoid process of the Meckel's cartilage is well-formed (Figure 8). The sides of the ethmoid plate are raised to the *lamina orbitonasalis*, which represents the border between nasal and orbital regions (Figure 8). The basihyal appears as an hourglass-shaped element anteriorly to the basibranchial in the gill arch skeleton (Figure 8). The auditory capsule is almost enclosed. The parapophyses appear dorsal to the notochord and posterior to the head (Figure 8). The caudal fin has four hypurals I-IV and one parahypural (Figure 8). Furthermore, the neural and hemal vertebral arches become visible in the caudal part of the axial skeleton (Figure 8).

3.3.8 | Stage 31 (larva)

The SL is at least 18.9 mm (Table 1). The non-paired anal and dorsal fins are almost fully formed, and the rest of the fin fold is progressively regress (Figure 7). The caudal fin has a three-lobed shape (Figure 7). The skull elements are considerably more ossified than at the previous stage. The angulare, mesethmoid, palatine, ceratohyal, interopercle, subopercle, and preopercle are clearly stained with Alizarin Red and calcein (Figure 11). The first dermatocranial elements, the frontal and lacrimal elements, appear (Figure 11).

3.4 | Developmental timing under different temperature regimes

The effects of different temperatures on developmental timing in the northern pike are summarized in Figure 12. The estimated average heat necessary to reach developmental stage (in "day-degrees") is for: 1-cell, 0.54; 4-cell, 1.72; 8-cell, 1.92; 32-cell, 3.55; 128-cell, 6.38; 512-cell, 6.65; 1,000-cell, 10; germ ring, 14.52; embryonic shield, 20.52; 50–60% epiboly, 23.05; 85% epiboly, 30.62; optic vesicle, 31.76; lens, 39.23; body pigment, 41.30; full overgrowth, 50.15; early prehatching, 56.18; late prehatching,

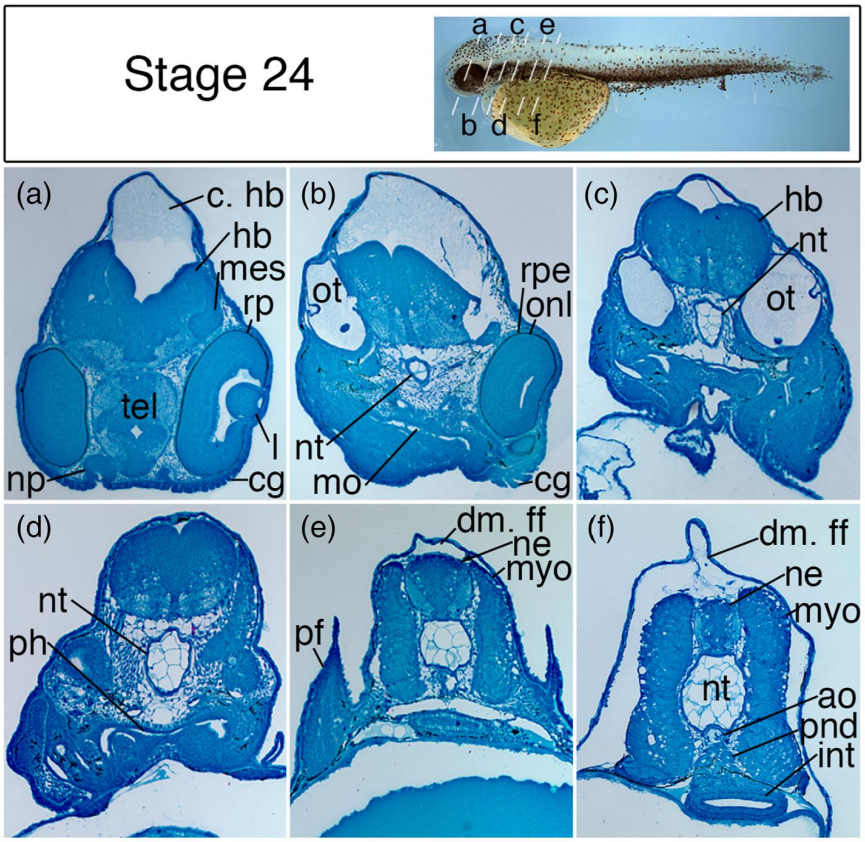

FIGURE 9 Histological sections of the hatching larva stage. The dashed lines represent locations of histological sections. (a–f) All images represent transversal sections. ao, dorsal aorta; c. hb, the cavity of hindbrain; cg, cement gland; dm. ff, dorsal median fin fold; hb, hindbrain; int, intestine; l, lens; mes, mesencephalon; mo, mouth; myo, myotome; ne, neural tube; np, nasal pit; nt, notochord; onl, outer nuclear layer; ot, otic vesicle; pnd, pronephric duct; pf, pectoral fin; ph, pharynx; rpe, retinal pigment epithelium; tel, telencephalon

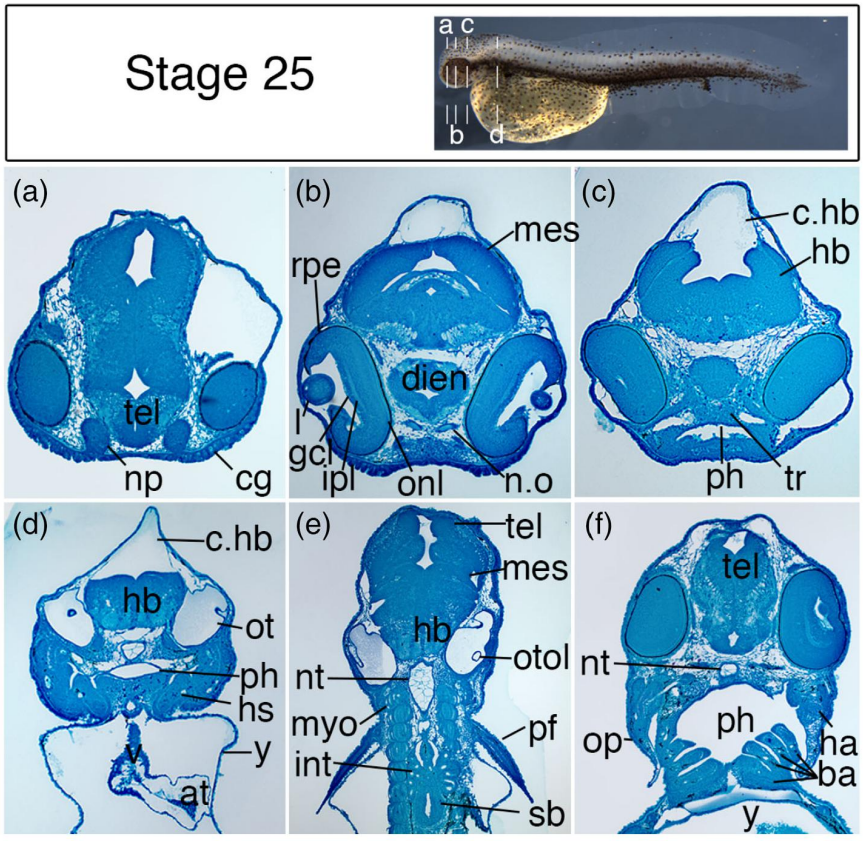

FIGURE 10 Histological sections of hatching larva with an open mouth. The dashed lines represent locations of histological sections. (a–d) Images represent transversal sections. (e–f) Images represent horizontal sections. at, atrium; ba, branchial arch; c. hb, the cavity of hindbrain; cg, cement gland; dien, diencephalon; gcl, ganglion cell layer; ha, hyoid arch; hb, hindbrain; hs, hyosymplectic; ipl, inner plexiform layer; int, intestine; l, lens; mes, mesencephalon; myo, myotome; n. opt, nervus opticus; np, nasal pits; nt, notochord; onl, outer nuclear layer; op, opercle; ot, otic vesicle; otol, otolith; pf, pectoral fin; ph, pharynx; rpe, retinal pigment epithelium; sb, swim bladder; tel, telencephalon; tr, trabecula; v, ventricle; y, yolk

56.94; hatching, 67.46. Incubation at higher temperatures results in accelerated development, compared to lower temperatures within the examined range (9–14 °C). The data also show that decreasing/increasing the incubation temperature allows for fine-tuning of the timing of various developmental stages. For example, the 2.5 "day-degrees" required for the transition to 50–60% epiboly from the Embryonic shield stage can be reached in 5.5 hr at 14 °C or 10.5 hr at 9 °C. It should be noted that temperature within 9–14 °C range did not have any obvious effect on the incidence of developmental abnormalities.

4 | DISCUSSION

The northern pike is a fish species of considerable interest to aquaculture and fisheries across the northern hemisphere (Nilsson et al., 2008), but also emerging as an experimentally-tractable model system for addressing questions of ecology and evolution (Forsman et al., 2015). However, the notable absence of a comprehensive developmental staging table has limited the use of the northern pike. Here, we provide a description of embryonic and larval stages that, together with the already available genomic and transcriptomic resources

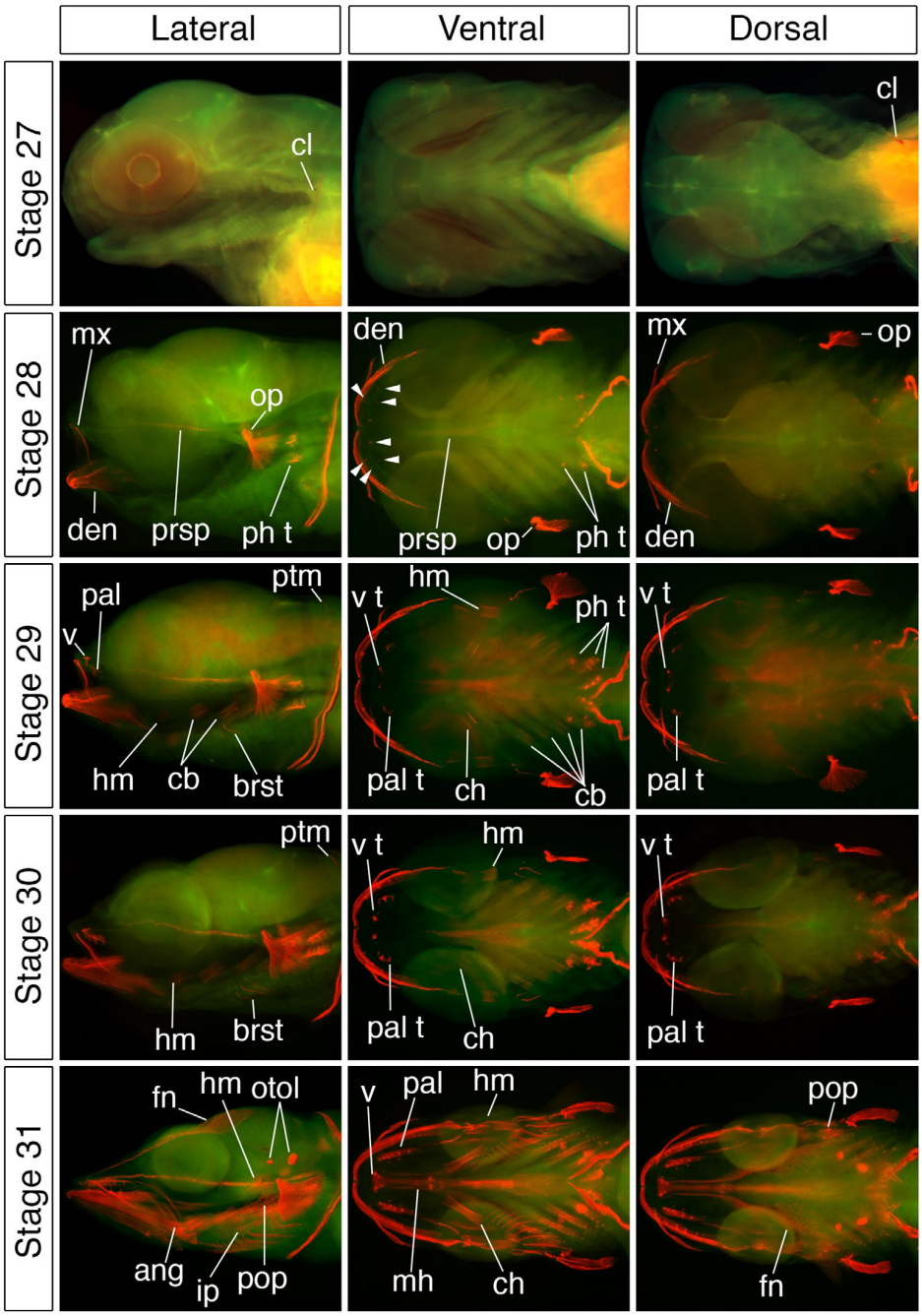

FIGURE 11 Ossification progress of craniofacial skeleton revealed by Alizarin Red and calcein staining. Each stage is shown as lateral, ventral and dorsal views. Note the complementarity of these two staining methods. White arrowheads mark the first teeth. ang, angular; bb, basibranchial; brst, branchiostegal; cb, ceratobranchial; ch, ceratohyal; cl, cleithrum; den, dentary; fn, frontal; hm, hyomandibula; ip, interopercle; lac, lacrimale; mx, maxilla; mh, mesethmoid; op, opercle; otol, otoliths; pal, palatine; pal t, palatal teeth; ph t, pharyngeal teeth; pop, preopercle; prsp, parasphenoid; ptm, post-temporal; v, vomer; v t, vomer teeth

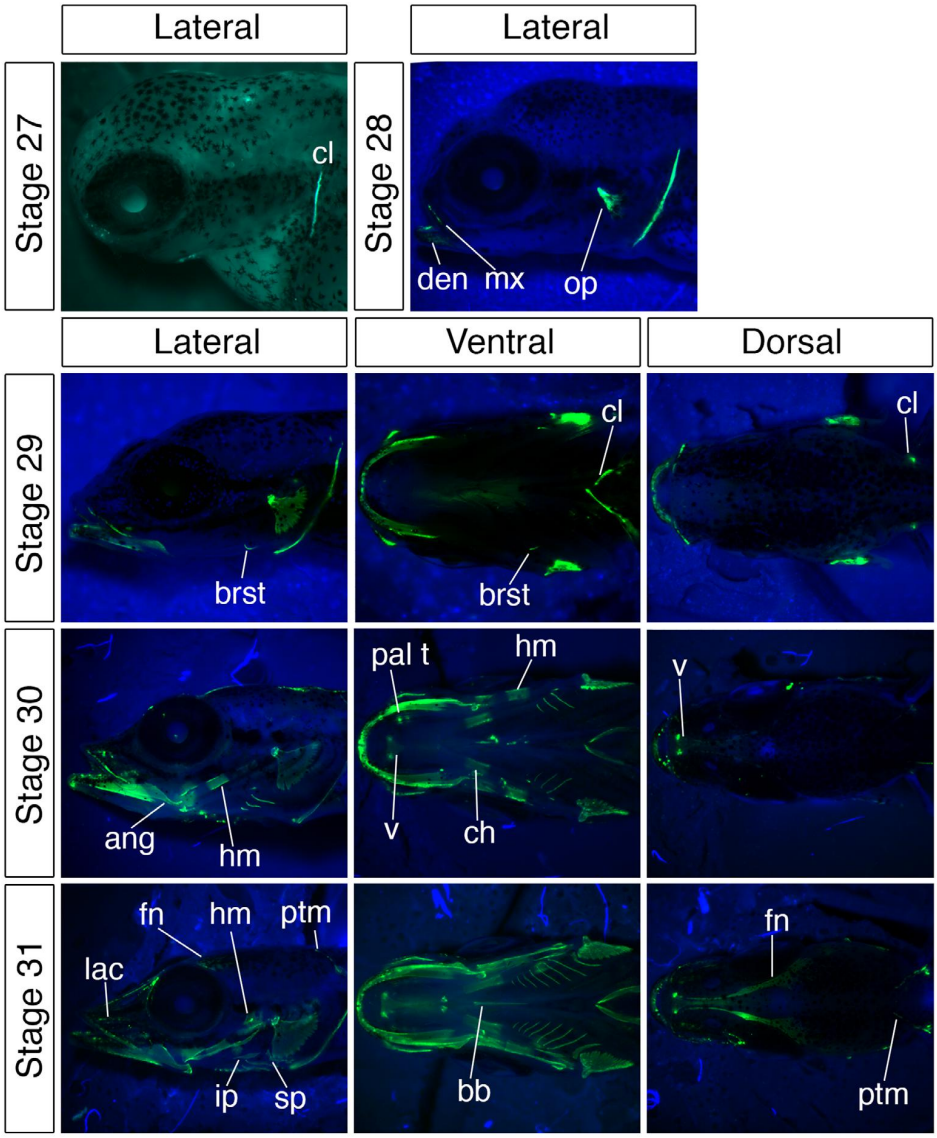

FIGURE 11 Continued

(Rondeau et al., 2014; Sanger & Rajakumar, 2018), lays a strong foundation for the wider adoption of this powerful research organism. The present study provides the first reliable staging table of the northern pike, from the one-cell stage to the first dermal bones of free-swimming juveniles, supplemented with histological details of embryonic tissues (summarized in Table 2, Figures 13 and 14).

The northern pike differs from conventional model teleosts (medaka and zebrafish) with respect to several embryonic traits, including cell cleavage, melanophore pattern, prominent cement glands, chondrification pattern, and tooth development. The first noticeable difference between model teleosts and pike is in a third cleavage that is irregular in size and shape (stage 3) and does not form two proper rows of blastomeres (Iwamatsu, 2004; Kimmel et al., 1995). However, a similar pattern of unequal blastomere cleavage was described in the sister species muskellunge (*E. masquinongy*; Galat, 1973) and the Atlantic wolffish (*Anarchichas lupus*) during the formation of the first two blastomeres (Pavlov, Dzerzhinsky, & Radzikhovskaya, 1992). In general, asymmetrical cleavage of the first blastomeres is usually associated with decreased egg viability, and thus many embryos terminate prematurely (Valdebenito et al., 2012; von Westernhagen, 1988). Even though pike eggs and embryos were kept in optimal conditions in this study, irregular blastomeres were still observed in all embryos. Moreover, embryos displayed high survival and hatching rates. Thus, the unequal blastomeres from the third cleavage onwards appear to be a bona fide feature of pike development.

The pigmented pattern of the northern pike is different from model teleosts such as zebrafish (Kimmel et al., 1995). Specifically, the prominent dorsal and ventral pigmented stripes typical of zebrafish are absent in pike. The first pigmentation becomes evident along the dorsal part of the eye primordia. The first detectable melanophores of

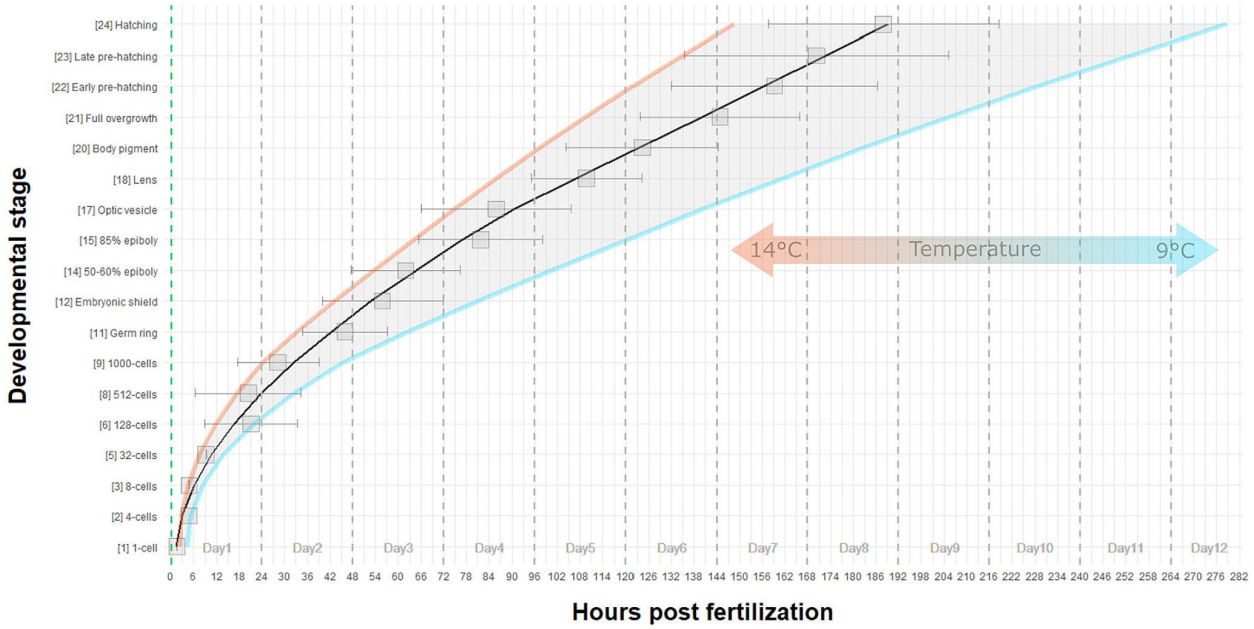

FIGURE 12 Developmental timing of the northern pike. The plot shows average timing (gray squares; whiskers denote ± *SD*) of stages of development on basis of incubation in six temperature regimes (9–14 °C). Consensus line was fitted by locally estimated scatterplot smoothing and corresponds to developmental timing approximately at 12 °C

TABLE 2 Stages of embryonic and larval development of the northern pike

Period	Approximate dpf/hpf (12 °C)		Stage ID	Name	Description
Cell cleavage, blastula, and gastrulation	1 dpf	1.5 hpf	1	1-cell stage	A single clear blastomere at the animal pole
		3 hpf	2	4-cell stage	The four blastomeres developed by the second cleavage
		7 hpf	3	8-cell stage	The blastomeres do not form two symmetrical rows
		9 hpf	4	16-cell stage	Blastomeres form 1 sheet of 16 cells
		14 hpf	5	32-cell stage	The arrangement of blastomeres is variable and forms a solid blastoderm
		21 hpf	6	128-cell stage	The blastoderm is formed by 6 layers of cells
		23 hpf	7	256-cell stage	The blastoderm is formed by 8–9 layers of cells
	2 dpf	27 hpf	8	512-cell stage	The blastoderm is formed by 10 cell layers
		33 hpf	9	1,000-cell stage	Marginal cells of blastoderm create the yolk syncytial layer (YSL)
		40 hpf	10	High stage	Over than 1,000 cells in the blastoderm; individual YSL nuclei visible at the periphery
		45 hpf	11	Germ ring	Germ ring visible; hypoblast and epiblast visible
	3dpf	57 hpf	12	Embryonic shield	10% epiboly; embryonic shield visible
		60 hpf	13	25% epiboly	Embryonic shield extends laterally and anteriorly
		67 hpf	14	Neural plate	50–60% epiboly; the blastoderm envelops half of the yolk sphere; neural plate visible at the midline of embryonic shield
	4 dpf	74 hpf	15	85% epiboly	The head region in the anterior part of the embryonic shield; blastopore closure; yolk plug
Organogenesis		85 hpf	16	Bud	Optic vesicles are discernible; at the end of stage the first 5–10 pairs of somites developed; blastopore is entirely closed

(Continues)

TABLE 2 (Continued)

Period	Approximate dpf/hpf (12 °C)		Stage ID	Name	Description
		93 hpf	17	Optic vesicle	The optic vesicles are well-defined, but the lenses are not yet present; 24–28 pairs of somites
	5 dpf	96 hpf	18	Lens	The lenses and the otic vesicles formation; differentiation of fore-, mid-, and hindbrain; pericardial cavity visible; nasal pits; free tail
		117 hpf	19	Pigmented eye	The first melanocytes formation; beating heart; the neural tube partition into the telen-, dien-, mesen-, and rhombencephalon; more than 40 somites
	6 dpf	123 hpf	20	Body pigment	The lens placodes visible; contractions of trunk muscles; anlage of the pectoral fin bud
		138 hpf	21	Full overgrowth	The head becomes free of yolk; anlage of the tubular heart is visible; the rudiment of the median fin fold
	7 dpf	156 hpf	22	Early prehatching	The tip of the tail extends to the mid of the eye; the cement glands are visible
	8 dpf	174 hpf	23	Late prehatching	The tip of the tail extends to the posterior of the eye; mucus-secreting cells are active
Hatching and posthatching	8–9 dpf		24	Hatching	The first cartilage in the pectoral girdle and hyosymplectic cartilage; the mouth still closed
	10 dpf		25	Opening mouth	The mouth is open; cartilaginous Meckel's cartilage, quadrate and cleithrum; first otoliths
	10–11 dpf		26	Protruding mouth	The eyes are fully pigmented; cartilage formation of *trabeculae cranii*, the otic capsules, and the branchial arches
	12 dpf		27	First bone	The jaws almost in the final position; formation of cartilage of ethmoid plate, nasal capsules, ceratohyal and ceratobranchial; the first ossification of cleithrum
	17 dpf		28	First teeth	Active oral feeding; the first teeth on dentary, palatines, vomers and pharyngobranchials; cartilaginous hyomandibula, pterygoid process of quadrate and epibranchials, hypural precartilage in tail; ossification of maxilla and parasphenoid
	24 dpf		29	Caudal fin cartilage	The yolk almost absorbed; ossification of hyomandibula, ceratohyal and ceratobranchials; cartilages in caudal fin: two hypurals and parhypural
	30 dpf		30	Yolk absorbed	Yolk is completely absorbed; *Lamina orbitonasalis* formation; closing of auditory capsule; neural and hemal arches of vertebrae in the caudal part of the axial skeleton
	38 dpf		31	Larva	The anal and the dorsal fin almost formed; the caudal fin has a 3-lobed shape; the first dermatocranial elements of frontals and lacrimals

the body occupy the lateral part of the rhombencephalon around the otic capsule, and some melanophores begin to cluster on the yolk sphere as in medaka (Iwamatsu, 2004). The first forming stripe is noticeable ventral to the well-developed otic capsule and grows until the larval period. Thus, pike has only one pigmented stripe that occupies the ventral part of the body. At hatching, melanophores cover over 80% of the pike's yolk sac and are more pigmented than in the muskellunge (Cooper, 2016).

Immediately after hatching, pike larvae attach in a vertical position to variable substrates using their adhesive organs, the cement glands. These larval organs are chiefly well-known from amphibians (Nokhbatolfoghahai & Downie, 2008) and lungfishes (Kerr, 1900), but, they are also present in many actinopterygians, for example, bichirs (*Polypterus senegalus*; Budgett, 1907), mexican tetra (*Astyanax mexicanus*; Pottin, Hyacinthe, & Retaux, 2010), tilapia (*Tilapia mariae*; Arnold, Kriesten, & Peters, 1968), and African pike (*Hepsetus odoe*;

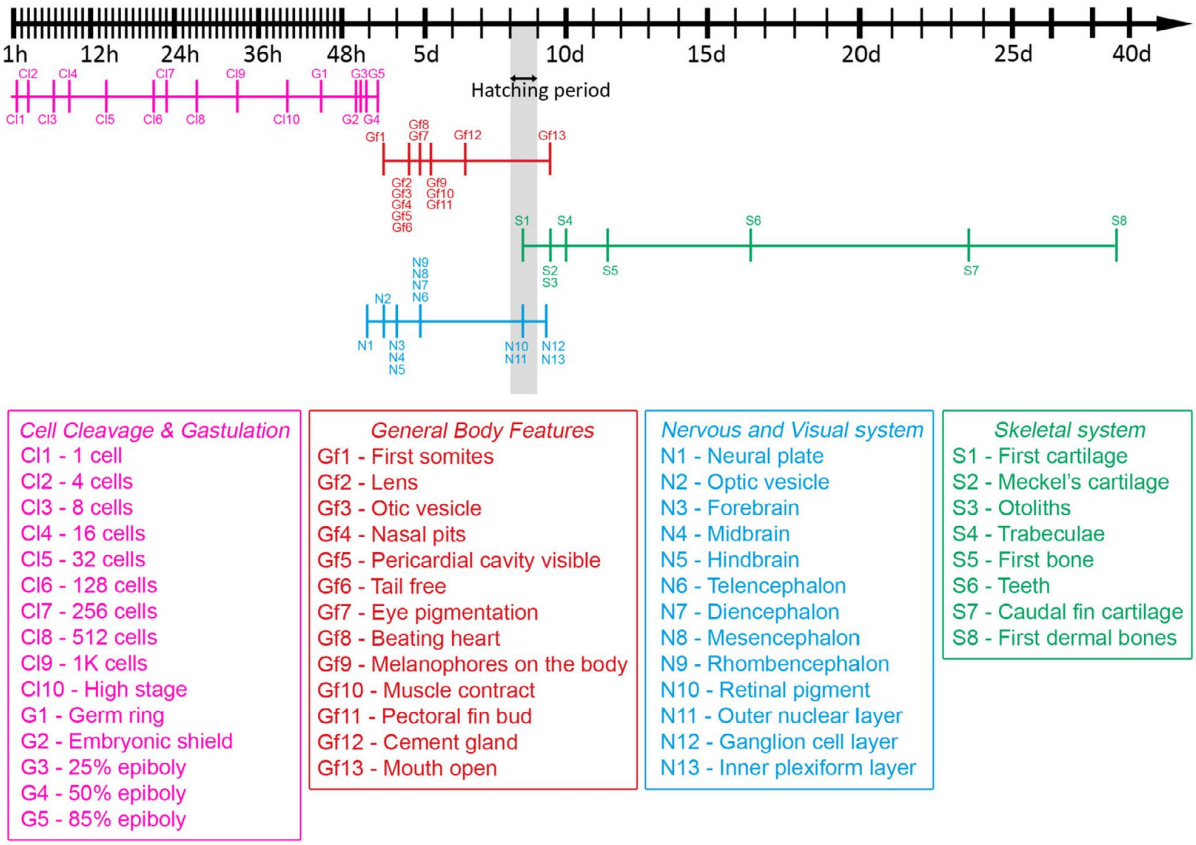

FIGURE 13 Developmental table of the northern pike. Summary of the most important steps of the embryonic and larval development at 12 °C. The timescale is given in hours (h) and days (d)

Merron, Holden, & Bruton, 1990). The cement glands of teleostean larvae vary in pattern, numbers, size, and developmental origin (Arnold et al., 1968; Minarik et al., 2017; Pottin et al., 2010). The northern pike has paired cement glands that form dorsal to the mouth opening in the rostronasal region and have a markedly sculptured surface of epidermal grooves and folds that contain adhesive cells secreting sticky mucus (Braum, Peters, & Stolz, 1996). However, these larval organs are not observed in zebrafish and medaka. Thus, the northern pike could represent another ideal model for investigating origins of adhesive organs.

In all vertebrates, the process of chondrification first becomes apparent around the notochord (Goodrich, 1931). The first cartilaginous element, the pectoral girdle, starts to form immediately after hatching in pike and not at the time of chondrification as in other fish species (e.g., de Beer, 1937, Podrabsky et al., 2017). Unlike most teleosts, the trabeculae and parachordals begin to chondrify in pike after the visceral arch skeleton (Meckel's cartilage, quadrate, cartilaginous elements of the hyoid arch). Such a pattern of chondrification has thus far only been described in the whiting (*Merlangius merlangus*; de Beer, 1937). According to Cooper (2016), the mouth opening coincides with the formation of two large teeth at the edge of the vomer. However, we did not identify any such structures at mouth opening stage (stage 25). At stage 28, the first oral teeth are evident on the dentary, palatines and vomers and the first pharyngeal teeth are visible on the pharyngeal arches. Adult dentition of pikes is characterized by many teeth of various sizes and shapes present throughout the entire oropharyngeal region, in contrast to the teeth of zebrafish, which are restricted to the fifth branchial arch (e.g., Berkovitz & Shellis, 2017). Therefore, the pike also represents a powerful model system for studying tooth development.

Traditional "model organisms" represent only a small fraction of the Earth's biodiversity, and, yet, our understanding of how the world works is largely based on them. Nevertheless, insights arising from their use in research constitute the core of our biological knowledge. In recent years, a wide range of non-traditional organisms have been developed as model systems for evo-devo research (Braasch et al., 2014). These animals provide novel and important evolutionary insights when used in the appropriate comparative context (Sanger & Rajakumar, 2018). One such organism, the northern pike, has several distinct advantages associated with it, for example, a large number of eggs that are three times larger than those of zebrafish and therefore amenable to experimental manipulations (e.g., fate-mapping or transplantation of small groups of cells), controlled spawning, a broad range of suitable incubation temperatures, numerous teeth around the whole oropharyngeal region, and an ambush predator body plan. Additionally, for all of these reasons, we assume that the staging table presented here, together with the high-quality genome

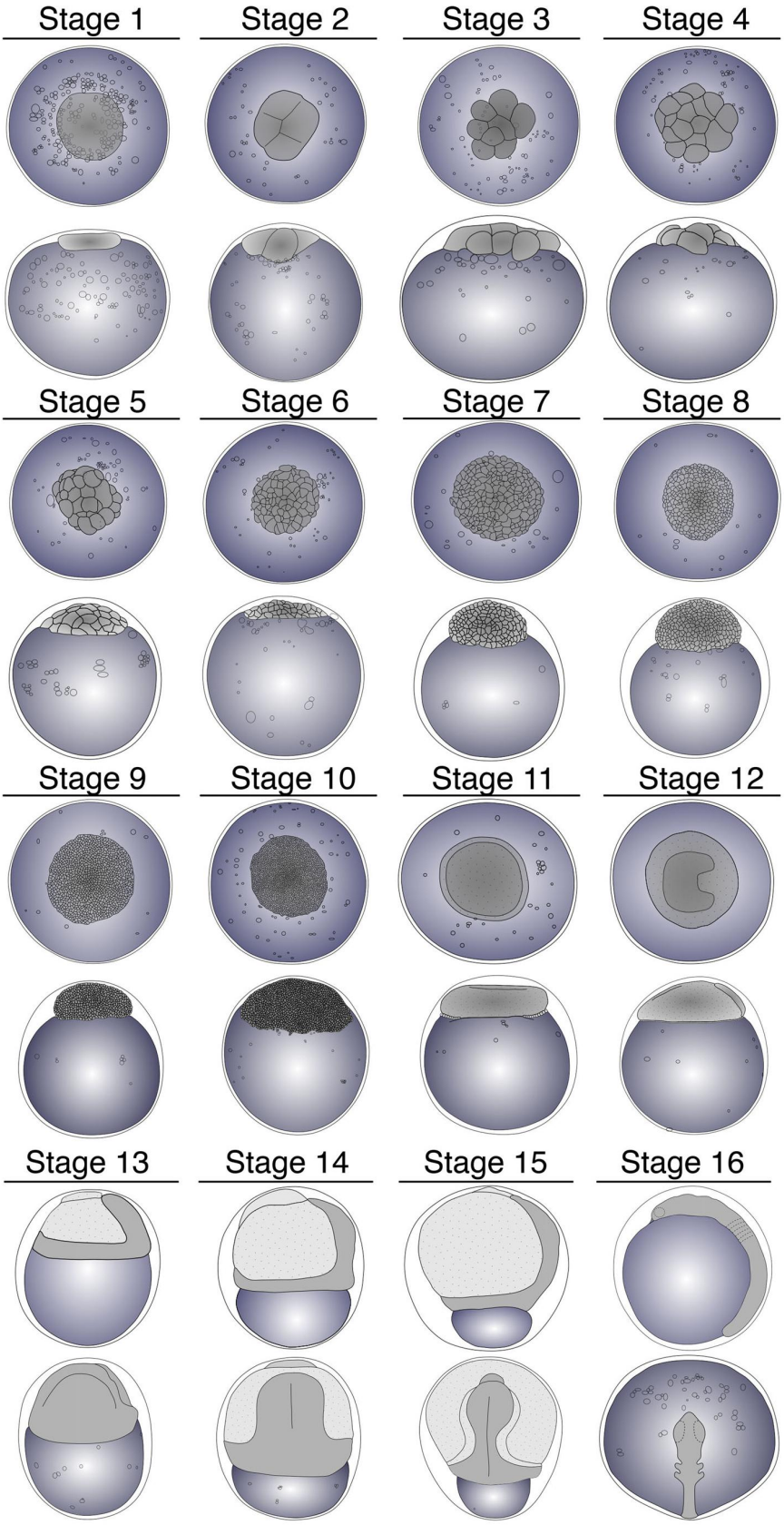

FIGURE 14 Line drawings of described stages in the development of the northern pike. Each prehatching stage contains a dorsal or animal pole view of the embryo at the top and a lateral view of the embryo at the bottom. Posthaching stages are shown from the lateral view

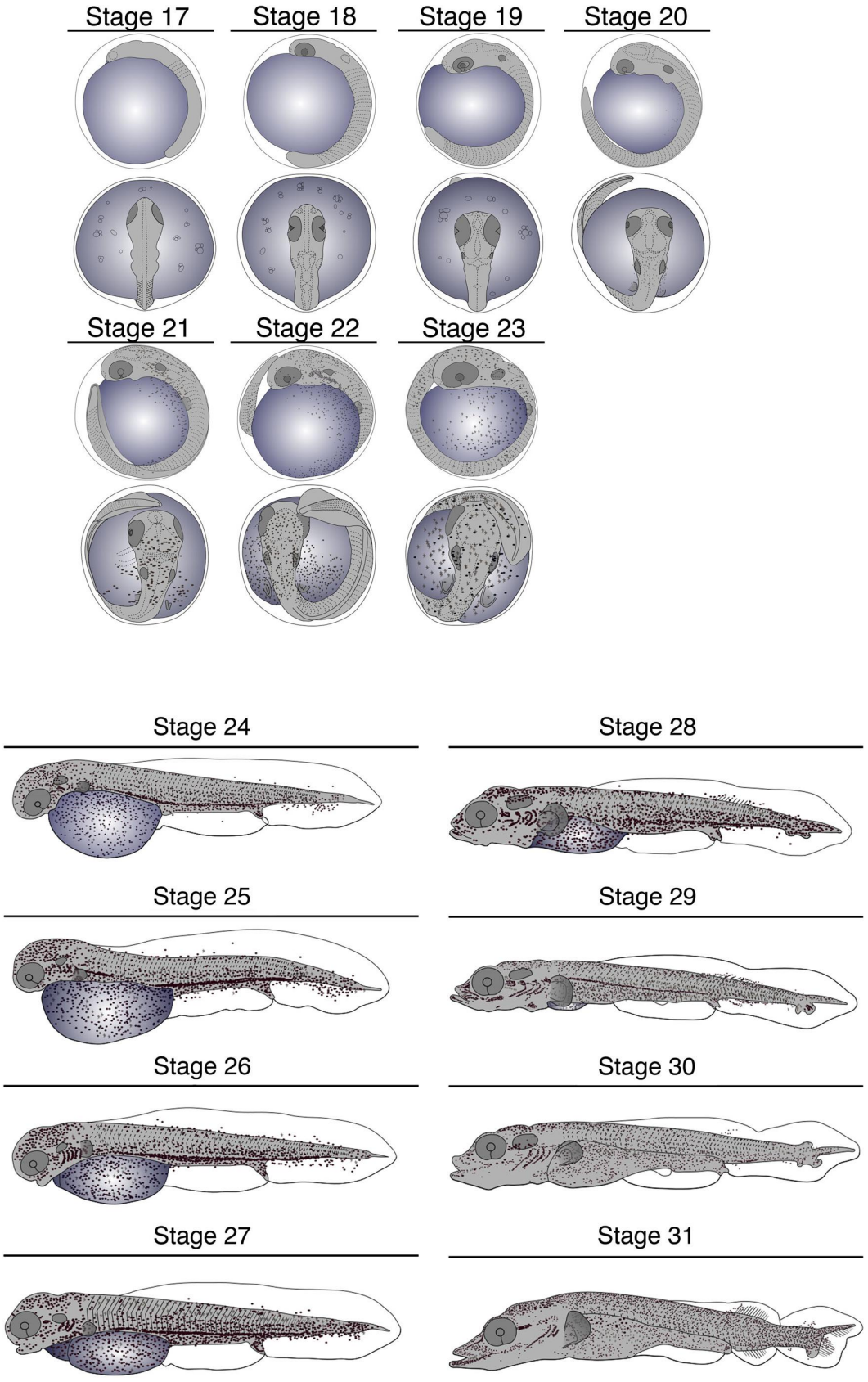

FIGURE 14 Continued

and transcriptome assemblies recently made available to the research community (Rondeau et al., 2014; Zerbino et al., 2018), will establish the northern pike as powerful new model system for evo-devo research.

ACKNOWLEDGMENTS

We thank Vladimir Soukup and Jana Stundlova for critical reading of earlier versions of the manuscript and also for their helpful comments. Special thanks are due to James Cleland for reviewing the English of the manuscript. We would like to thank Kristyna Eliasova for a beautiful drawing of the northern pike, Martin Minarik for a technical assistance with PAS staining, and Robert Cerny for an essential help in various aspects of the research. The work of J.B., R.S., and J.S. was financially supported by the Ministry of Culture of the Czech Republic (DKRVO 2019–2023/6.V.a, 00023272). The work of J.S. was financially supported by the Internal grant of the National Museum (NM-P15/01IG-ŠT). The work of A.P., J.B., V.M., and J.S. was financially supported by the Charles University grant SVV 260434/2019, and Charles University GAUK projects 640616 (A.P.) and 1448514 (J.S.).

CONFLICT OF INTEREST

The authors declare no competing interest.

AUTHOR CONTRIBUTIONS

A.P., J.B., R.S., and J.S. conceived and designed the experiments; A.P., J.B., V.M., and J.S. performed the experiments; A.P., J.B., and J.S. analyzed the data; R.H. provided the northern pike embryonic material; A.P., J.B., and J.S. wrote the manuscript; all authors read and approved the final version of the manuscript.

ORCID

Jan Stundl https://orcid.org/0000-0002-3740-3378

REFERENCES

Arnold, M., Kriesten, K., & Peters, H. M. (1968). Cement glands of larval *Tilapia mariae* (Cichlidae, Teleostei). *Cell and Tissue Research*, *91*, 248–260.

Berkovitz, B., & Shellis, P. (2017). Osteichthyes. In B. Berkovitz (Ed.), *The teeth of non-mammalian vertebrates*. London: Academic Press.

Besrukow, E. A. (1928). Die Entwicklung des Chondrocraniums bei *Esox lucius*, L. *Revue Zoologique Russe*, *8*, 89–111.

Billard, R. (1996). Reproduction of pike: Gametogenesis, gamete biology and early development. In J. F. Craig (Ed.), *Pike: Biology and exploitation*. London: Chapman & Hall.

Bondarenko, V., Drozd, B., & Policar, T. (2015). Effect of water temperature on egg incubation time and quality of newly hatched larvae of northern pike (*Esox lucius* L., 1758). *Journal of Applied Ichthyology*, *31*, 45–50.

Braasch, I., Peterson, S. M., Desvignes, T., McCluskey, B. M., Batzel, P., & Postlethwait, J. H. (2014). A new model army: Emerging fish models to study the genomics of vertebrate evo-devo. *Journal of Experimental Zoology B*, *324*, 316–341.

Braum, E., Peters, N., & Stolz, M. (1996). The adhesive organ of larval pike *Esox lucius* L., (Pisces). *Internationale Revue der Gesamten Hydrobiologie*, *81*, 101–108.

Budgett, J. S. (1907). Chapter XII. The development of *Polypterus senegalus* Cuv. In J. G. Kerr (Ed.), *The work of John Samuel Budgett*. Cambridge, UK: Cambridge University Press.

Burdi, A., & Grande, T. (2010). Morphological development of the axial skeleton of *Esox lucius* and *Esox masquinongy* (Euteleostei: Esociformes), with comparisons in developmental and mineralization rates. In J. S. Nelson, H.-P. Schultze, & M. V. H. Wilson (Eds.), *Origin an phylogenetic interrelationships of teleosts: Honouring Gloria Arratia*. München, Germany: Dr. Friedrich Pfeil.

Cooper, J. E. (2016). *Development, growth, and food of early life stages of northern pike (*Esox lucius*) and muskellunge (*Esox masquinongy*) in the upper St. Lawrence River*. Available at http://cooperenvironmentalresearch.com

Craig, J. F. (2008). A short review of pike ecology. *Hydrobiologia*, *601*, 5–16.

Crossman, E. J. (1996). Taxonomy and distribution. In J. F. Craig (Ed.), *Pike: Biology and exploitation*. London: Chapman & Hall.

de Beer, G. R. (1937). *The development of the vertebrate skull*. London: Oxford University Press.

Donoghue, P. C. J. (2002). Evolution of development of vertebrate teeth and scales: Unravelling concepts, regulatory theories and homologies. *Paleobiology*, *28*, 474–507.

Du, S. J., Frenkel, V., Kindschi, G., & Zohar, Y. (2001). Visualizing normal and defective bone development in zebrafish embryos using the fluorescent chromophore calcein. *Developmental Biology*, *238*, 239–246.

Forsman, A., Tibblin, P., Berggren, H., Nordahl, O., Koch-Schmidt, P., & Larsson, P. (2015). Pike *Esox lucius*: An emerging model organism for studies in ecology and evolutionary biology—A review. *Journal of Fish Biology*, *87*, 472–479.

Froese, R., & Pauly, D. (Eds.). (2018). *Fishbase*. Available at http://www.fishbase.org, version (06/2018).

Galat, D. L. (1973). Normal embryonic development of the muskellunge (*Esox masquinongy*). *Transactions of the American Fisheries Society*, *102*, 384–391.

Gihr, M. (1957). Zur Entwicklung des Hechtes. *Revue Suisse de Zoologie*, *64*, 355–474.

Goodrich, E. S. (1931). *Studies on the structure and development of vertebrates*. London: Macmillan.

Grande, T., Laten, H., & Lopez, J. A. (2004). Phylogenetic relationships of extant esocid species (Teleostei: Salmoniformes) based on morphological and molecular characters. *Copeia*, *4*, 743–757.

Hassler, T. J. (1982). Effect of temperature on survival of northern pike embryos and yolk-sac larvae. *The Progressive Fish-Culturist*, *4*, 174–178.

Herold, R. C. B. (1974). Ultrastructure of odontogenesis in the pike (*Esox lucius*). Role of dental epithelium and formation of enameloid layer. *Journal of Ultrastructure Research*, *48*, 435–454.

Inkscape Team. (2018). *Inkscape: A vector drawing tool*. Available at http://www.inkscape.org

Iwamatsu, T. (2004). Stages of normal development in the medaka *Oryzias latipes*. *Mechanisms of Development*, *121*, 605–618.

Jollie, M. (1975). Development of the head skeleton and pectoral girdle in *Esox*. *Journal of Morphology*, *147*, 61–88.

Kerr, J. G. (1900). The external features in the development of *Lepidosiren paradoxa*, Fitz. *Philosophical Transactions of the Royal Society B: Biological Sciences*, *192*, 299–330.

Kimmel, C. B., Ballard, W. W., Kimmel, S. R., Ullman, B., & Schilling, T. (1995). Stages of embryonic development of the zebrafish. *Developmental Dynamics*, *203*, 253–310.

Kotlyarevskaya, N. V. (1969). The hatching process in the pike (*Esox lucius*, L.). *Problems of Ichthyology*, *9*, 85–95.

Kucska, B., Müller, T., Sári, J., Bódis, M., & Bercsényi, M. (2005). Successful growth of pike fingerlings (*Esox lucius*, L.) on pellet at artificial condition. *Aquaculture*, *246*, 227–230.

Lindroth, A. (1946). Zur Biologie der Befruchtung und Entwicklung beim Hecht. *Report: Institute of Fresh-Water Research, Drottningholm*, *24*, 1–173.

Mann, R. H. K. (1996). Fisheries and economics. In J. F. Craig (Ed.), *Pike: Biology and exploitation*. London: Chapman & Hall.

Merron, G. S., Holden, K. A., & Bruton, M. N. (1990). The reproductive biology and early development of the African pike, *Hepsetus odoe*, in the Okavango Delta, Botswana. *Environmental Biology of Fishes*, *28*, 215–235.

Minarik, M., Stundl, J., Fabian, P., Jandzik, D., Metscher, B. D., Psenicka, M., … Cerny, R. (2017). Pre-oral gut contributes to facial structures in non-teleost fishes. *Nature*, *547*, 209–212.

Mitgutsch, C., Piekarski, N., Olsson, L., & Haas, A. (2008). Heterochronic shifts during early cranial neural crest cells migration in two ranid frogs. *Acta Zoologica Stockholm*, *89*, 69–78.

Nilsson, P. A., Skov, C., & Farrell, J. (2008). Current and future directions for pike ecology and management: A summary and synthesis. *Hydrobiologia*, *601*, 137–141.

Nokhbatolfoghahai, M., & Downie, J. (2008). The external gills of anuran amphibians: Comparative morphology and ultrastructure. *Journal of Morphology*, *269*, 1197–1213.

Pavlov, D., Dzerzhinsky, K., & Radzikhovskaya, E. (1992). Assessing the quality of roe from White Sea wolf fish (*Anarhichas lupus marisalhi* L.), obtained under experimental conditions. *Journal of Ichthyology*, *32*, 88–104.

Pehrson, T. (1944). The development of latero-sensory canal bones in the skull of *Esox lucius*. *Acta Zoologica*, *25*, 135–157.

Podrabsky, J. E., Riggs, C. L., Romney, A. L., Woll, S. C., Wagner, J. T., Culpepper, K. M., & Cleaver, T. G. (2017). Embryonic development of the annual killifish *Austrofundulus limnaeus*: An emerging model for ecological and evolutionary developmental biology research and instruction. *Developmental Dynamics*, *246*, 779–801.

Pottin, K., Hyacinthe, C., & Retaux, S. (2010). Conservation, development, and function of a cement gland-like structure in the fish *Astyanax mexicanus*. *Proceedings of the National Academy of Sciences of the United States of America*, *107*, 17256–17261.

R Core Team. (2017). *R: A language and environment for statistical computing*. Available at http://www.R-project.org

Raat, A. J. P. (1988). Synopsis of the biological data on the northern pike, *Esox lucius* L. 1758. *FAO Fisheries Synopsis*, *30*(Rev. 2), 1–178.

Rondeau, E. B., Minkley, D. R., Leong, J. S., Messmer, A. M., Jantzen, J. R., von Schalburg, K. R., … Koop, B. F. (2014). The genome and linkage map of the northern pike (*Esox lucius*): Conserved synteny revealed between the salmonid sister group and the Neoteleostei. *PLoS One*, *9*, e102089.

Sadeghinezhad, J., Rahmati-Holasoo, H., Fayyaz, S., & Zargar, A. (2014). Morphological study of the northern pike (*Esox lucius*) tongue. *Anatomical Science International*, *90*, 235–239.

Sanger, T. J., & Rajakumar, R. (2018). How a growing organismal perspective is adding new depth to integrative studies of morphological evolution. *Biological Reviews*, *94*, 184–198.

Taylor, W. R., & Van Dyke, G. C. (1985). Revised procedures for staging and clearing small fishes and other vertebrates for bone and cartilage study. *Cybium*, *9*, 107–119.

Toner, E. D., & Lawler, G. H. (1969). Synopsis of biological data on the pike *Esox lucius*. *FAO Fisheries Synopsis*, *30*(Rev. 1), 39.

Valdebenito, I. I., Sánchez, R. R., Effer, B. R., & Ubilla, A. M. (2012). Morphometric characterization of the first blastomeres of rainbow trout (*Oncorhynchus mykiss*). *Zygote*, *20*, 327–331.

von Westernhagen, H. (1988). Sublethal effects of pollutants on fish. In W. S. Hoar & D. J. Randall (Eds.), *Fish physiology*. San Diego, CA: Academic Press.

Zerbino, D. R., Achuthan, P., Akanni, W., Amode, M. R., Barrell, D., Bhai, J., …, Flicek, P. (2018). *Ensembl*. Available at http://www.ensembl.org, version 94 (10/2018).

How to cite this article: Pospisilova A, Brejcha J, Miller V, Holcman R, Šanda R, Stundl J. Embryonic and larval development of the northern pike: An emerging fish model system for evo-devo research. *Journal of Morphology*. 2019; 1–23. https://doi.org/10.1002/jmor.21005

II. **Pospisilova A**, Stundl J, Metscher BD, Brejcha J, Psenicka M & Cerny R (in prep) Comparative cranial skeletogenesis in fishes: towards understanding of developmental strategies of fish craniofacial diversity.

Comparative cranial skeletogenesis in fishes: towards understanding of developmental strategies of fish craniofacial diversity

Anna Pospisilova[1], Jan Stundl[1,2], Brian D. Metscher[3], Jindrich Brejcha[4], Martin Psenicka[5] & Robert Cerny[1]*

(1) Department of Zoology, Charles University in Prague, Czech Republic;
(2) Division of Biology and Biological Engineering, California Institute of Technology, Pasadena, CA, USA;
(3) Department of Theoretical Biology, University of Vienna, Vienna, Austria;
(4) Department of Philosophy and History of Science, Charles University in Prague, Czech Republic;
(5) Research Institute of Fish Culture and Hydrobiology in Vodnany, University of South Bohemia in Ceske Budejovice, Czech Republic.

* autor correspondence: robert.cerny@natur.cuni.cz

key words:

Abstract:

Introduction

Skeletal tissues (bone, cartilage, dentine and enamel) are widely considered as crucial innovations that have facilitated evolutionary radiation and phenotypic adaptation of vertebrates (Gans & Northcutt, 1983; Northutt & Gans, 1983; Northcutt, 2005; Green et al., 2015). Probably the most complex skeletal structure within a vertebrate body comprises the head skeleton with its remarkable morphological plasticity and phylogenetic diversity. Incredible morphological variation of the skull elements reflects the varied life history strategies of vertebrates, and so provides a unique opportunity for examining the role of developmental proces in evolutionary changes (Abzhanov et al., 2004; Albertson et al., 2005; Streelman & Albertson, 2006 etc.). Although an understanding of the developmental and evolutionary origins of the skeletal tissues and especially the cranium have long been a major task in comparative morphology and evolutionary developmental biology (i.e. Goodrich, 1930; de Beer, 1937; Hanken & Thoroghood, 1993; Schilling & Thoroghood, 2000), developmental factors enabling extensive morphological and functional diversification of the skull remains rather limited.

Among all recent vertebrates, the ray-finned fishes (Actinopterygii) represent the most numeous and successful lineage. With >35,500 known extant species it constitutes the dominant radiation of vertebrates and it's an attractive clade in which to investigate the topic because fishes exhibit endless morphological and developmental variations (Fricke et al., 2020). This morphological diversity is mirrored in amazing diversity of their skeletal architectures, classically determining the major division within the bony fishes into 3 phylogenetic levels: (i) a Chondrostei (cartilage bone) grouping sturgeons (*Acipenseriformes*) and paddlefish (*Polyodontiformes*) is characterized by reduction of ossification, the condition is thought to be derived; (ii) a Holostei (whole bone) containing gars (*Lepisosteiformes*), bichirs (*Polypteriformes*) and eventually bowfins (*Amia*) with well-developed bony skeleton; (iii) a Teleostei (perfect bone) referring to their evolutionary position as the modern ray-finned fishes (Müller,1844; Müller, 1846).

The Senegal bichirs (*Polypterus senegalus* Cuvier, 1829) and the Tropical gars (*Atractosteus tropicus* Gill, 1863) are heavily armored forms with a massive exoskeleton, upper jaws bones incorporated into the skull and hyperossified dental structures (Bartsch, 1997; Bartsch et al., 1997; Clemen et al., 1998; Jollie, 1984b; Pehrson, 1947; 1958; Grande, 2010; Jollie, 1984a; Scherrer et al., 2017; Rizzato et al., 2020), European sterlets (*Acipenser ruthenus* Linnaeus, 1758), on the contrary, have reduced especially their endochondral ossification and possess mostly cartilaginous skeleton. However, numerous overlying dermal bones hide the cartilaginous neurocranium. Their jaws apparatus underwent significant restructuralization and the reduction intervened their dental structures also, so they posses teeth only during early development (Bemis et al., 1997; Hilton, 2005; Hilton et al., 2011; Jollie, 1980; Parker, 1882; Pehrson, 1944; Sewertzoff, 1928). All this contrasts with lightened skull of Northern pike (*Esox lucius*) with increased mobility of elements, the jaws and palate are more independently maneuverable and dermal bones of the skull are more thinner (Jollie, 1975; Burdi, 2010; Pospisilova et al., 2019). Our analysis thus ranges in cranial architecture from heavily ossified skulls of bichir and gar through a secondary reduced ossification of sterlet up to a highly specialized skull of pike.

In vertebrates, it has been shown that heterochrony (variation in relative developmental growth rates and timing), can play an important role in origin and evolutionary diversification of complex skeletal phenotypes (Gould, 1977; Alberch et al., 1979). Mainly changes in the order of developmental events (sequence heterochrony) in a variety of vertebrates proved to be crucial for an understanding of evolutionary changes and for an

explaining phenotypic diversity in craniofacial skeleton, especially because of independency of sequence from developmental stages, the size of the embryos and any variation in rate of development (Smith 2001; 2002; 2003).

To better understand fundamental principles of fish cranial skeletogenesis, developmental formation of skeletal architectures was described, compared and analyzed among fish species in context of a well defined phylogeny. In order to analyze distribution and effect of heterochrony on fish cranial skeletogenesis we compare these main aspects: (i) sequence (interspecific variation in temporal arrangement of cranial regions formation; (ii) relative timing (onset and offset of skeletal developmental process with respect to specific developmental events); and (iii) duration (overall rate of skeletal development). Finally, we applied quantitative investigations of mineral tissue development to characterize interspecific and ontogenetic differences in skeletal tissue density.

Material & methods

Embryo collection and rearing

All fish were maintained and exploited according to institutional and international guidelines for the protection of animal welfare (Directive 2010/63/EU) in the animal facility of the Department of Zoology, Charles University, Prague. The analyzed material comprises developmental series of (i) the Senegal bichir (*Polypterus senegalus* Cuvier, 1829) from the Department of Zoology of the Charles University, Prague; (ii) the European sterlet (*Acipenser ruthenus* Linnaeus, 1758) from the hatcheries of the Research Institute of Fish Culture and Hydrobiology in Vodnany, at the University of South Bohemia in Ceske Budejovice; (iii) the Tropical gar (*Atractosteus tropicus* T. N. Gill, 1863) from the hatcheries of the División Académica de Ciencias Biológicas, Universidad Juárez Autónoma de Tabasco in Villahermosa, Tabasco, Mexico and (iv) the European pike (*Esox lucius* Linnaeus, 1758) from the Hatchery of Litomysl (Czech Republic). These fishes were obtained, reared and staged as previously described (Minarik et al., 2017; Pospisilova et al., 2019).

The specimens were anaesthetized by an overdose of MS-222 (Serva), fixed in 4% PFA and stored at 4 °C for 24 hours. Specimens for in situ hybridization were fixed in 4% PFA overnight and stored in 100% methanol at −20 °C until further processed.

Although a number of comprehensive developmental staging tables for bichir (Bartsch et al., 1997), sturgeon (Dettlaff et al., 1993), gar (Long & Ballard, 2001) and pike (Pospisilova et al., 2019) was already published, they are focused on limited embryonic and early larval period with rather insufficient staging during later development. To cope with difficult interspecific standardization of larval staging and to make comparison between species reliable, we staged all specimens according to their total length [mm TL] measured after the PFA fixation (see above). Normalizing developmental stages is based on a particular developmental event (such as the first pre-cartilaginous condensation, the first ossification etc.) specified at the beginning of each results section.

Skeletal clearing and staining

Staining of early cartilaginous elements was performed using a modified Alcian Blue protocol based on Taylor and Van Dyke (1985) in which the last step of bone staining has been skipped. To avoid the problem of decalcification when using acetic acid during Alcian Blue staining, most stages, especially the smaller one, were stained separately with Alizarin Red (for the protocol see Rizzato et al., 2020). Due to lack of several stages especially in rather rare embryonal material of bichir double staining of cartilage and bone was performed following the protocol of Taylor and Van Dyke (1985).

Cartilaginous skulls were photographed using SZX12 (Olympus) and images were stacked with the software AxioVision 4.0. The osteocranium was observed under a fluorescent stereomicroscope (Zeiss Lumar.V12) using the fluorescent filter Alexa 568 (for mineralized tissue) and GFP (for surrounding tissue). Images were stacked with the software AxioVision 4.0.

Probe synthesis and in situ hybridization

Primers for PCR amplifications were designed based on sequences from de novo assembled transcriptomes of non-teleost fishes, and on predicted gene sequences in the northern pike genome assembly (Roundeau et al., 2014). Partial clones for col10a1 of examined species, were isolated by direct amplification from cDNA libraries (primers: col10a1_Ps forward: 5'-TACCAYGTSCACGBHAAAGG-3'; reverse: ; col10a1_Ar forward: 5'-

CAAGTGGCTCCCATATCTGC-3'; reverse: 5'-CCAATCAGGAATCCAGAGAA-3' col10a1_At forward: 5'-CGGGATMSCCYATVMAGTTC-3'; reverse: 5-'CCAATCAGGAATCCAGAGAA-3'; col10a1_El forward: 5'-CAGCGGGATCACCTATTCAG-3'; reverse: 5'-AATCCAGAGAAAGAGCAGTG-3'), cloned into pGEM-T Easy Vector (Promega), and sequenced. The digoxigenin-labeled in situ probes were prepared by standard protocols. In situ hybridizations (ISH) were carried out as described previously (Minarik et al., 2017; Stundl, et al., 2020), with few modifications. Proteinase K treatment was adjusted to 6 ug/ml for 30 min for bichir and sterlet, 60-90 min for gar and 45 min pike larvae.

Micro-CT imaging, image processing and data analysis

For microCT analysis, selected PFA-fixed specimens were rinsed in PBS and mounted in 1% low melt agarose into 200 µl, 1000 µl pipette tips, or into 5 ml plastic tube, according to the specimen's size. Subsequently, samples were scanned using MicroXCT (Xradia) at the Department of Theoretical Biology, University of Vienna, Austria.

For comparable quantitative imaging of skulls (Fig. 7), material attenuation properties from glass and agarose were measured as the reference components that were always scanned simultaneously with the analysed skull. As such, the reference material was captured with exactly the same scan parameters as for samples, i.e. identical source settings (kVp), geometry (source distance, detector distance and cone angle), x-ray filter and camera settings (exposure time and detector binning). Commonly used objective magnification was 4x except the oldest sturgeon (Tab. 1). When the skull exceeded the size appropriate for this magnification, we stitched an oversized image from several overlapping scans to visualize the whole cranium. In order to reduce noise in reconstructed image volumes, we used a glass filter during scanning in selected specimens (see Tab. 1).

After image acquisition, tomographic slices were reconstructed by Xradia's supplied software and reconstructed volumes were stored as 16-bit format. To reconstruct image volumes, we had to convert image intensities to Hounsfield units (as described by Handschuh et al., 2017). We measured the X-ray absorption coefficients of glass and agarose using regions of interest and HU conversion was done using the Arithmetic tool of the commercial 3D software package Amira 6.1. (FEI Visualization Sciences Group, Mérignac Cédex, France). After this algorithmic material decomposition, the plasma colormap coding provided by Amira software was applied on obtained data.

species	bichir			sterlet			gar			pike		
staining	AB	AB & AR	AR	AB	AB & AR	AR	AB	AB & AR	AR	AB	AB & AR	AR
total length [mm]	7	22	7	11	20	11	10	18	13.5	9	19	10
	8	25	8	12	21	12	11	20	14	10	21	11
	10	29	9	13	22	13	12	23	15	11	24	12
	11	32	10	14	23	13.5	13	24	16	13	25	13
	14	33	11	15	24	14	14	25	17	15	26	15
	16	34	12	16	25	15	16	26	18	18	28	18
	18	40	13	17	28	16	18	28	19		31	20
			16	18	33	16.5		31	20		34	25
			17	19	36	17		34	23		37	28
			18			18		37	25		40	31
			19			19		39	29		105	36
			21			20		40	31			38
			61			21		44	35			43
						22		54	50.5			46
						23		68				51
						24						56
						25						
						26						
						27						
						28						
						29						
						30						
						31						
						32						
						33						
						34						
						35						
						37						
						38						
						43						
						50						
						77						
Total	7	7	13	9	9	32	7	15	14	6	11	16

Results

Comparative analysis of chondrocranium element formation

In order to visualize the first cartilaginous condensation and to analyse sequence of the chondrocranium formation, cleared and Alcian Blue stained specimens were used (bichir: 7–10 mm TL, sterlet: 11–14 mm TL, gar: 10–13 mm TL, pike: 8–11 mm TL; Tab. 1). To make interspecific comparisons equivalent, all studied species were aligned into 4 stages according to their total length, with the initial stage (Stage 1; for details see Fig. 2, left box) defined by the first presence of a pre-cartilaginous condensation within a neurocranium (i.e. pre-chordals or parachordals). For the sake of easy and straightforward comparison all specimens are presented in the ventral views (Fig. 1).

In bichir, chondrocranium formation begins with two independent pairs of pre-cartilaginous condensations: the parachordals, situated lateral to the notochord, and the Meckel's cartilages of the mandibular arch (Stage 1; Fig. 1A). At Stage 2, the parachordals are already chondrified, and they laterally project to the otic capsules. In a prechordal part of the head, the trabeculae (*trabeculae cranii)* form anterior to the parachordals, reaching roughly the lower jaw level. The Meckel's cartilages are already well developed on both sides, but are not yet fused anteriorly. At the same time, the hyoid arch and first two branchial arches are formed (Stage 2; Fig. 1B). At Stage 3, the trabeculae are still lengthening, and beginning of the *lamina orbitonasalis* formation can be observed (Fig. 1C; black arrowhead). The Meckel's cartilages are already fused at the symphysis. The hyoid and branchial arches are well developed, and two more branchial arches are forming. Their ceratobranchial cartilages are connected to cartilaginous condensation of future basibranchial cartilage (Fig. 1C). At the final stage (Stage 4), anterior tips of trabeculae are fused into trabecula communis which expands into an ethmoid plate outlined by lateral prominent structure of lamina orbitonasalis. The orbital cartilages appear as independent longitudinal bars parallel with the trabecula (Fig. 1D; tm, taenia marginales) and the otic capsule is well chondrified. Cartilaginous condensation of the fourth branchial arch is forming and a broad median cartilage representing basibranchial is well developed.

In a sum, bichir chondrocranium initially starts from parachordals and the lower jaw cartilages, but it is soon rapidly completed with a noticeable preferential cartilage formation at the posterior part of the head, and with a forward neurocranium expansion only at the very end of development.

In sterlet, the earliest signs of chondrocranium formation appear as a bulky pre-cartilaginous condensation surrounding the anterior notochord (Fig. 1E; black arrowhead), forming the base of prospective neurocranium (Stage 1; Fig. 1E). At the same time (Stage 1), the Meckel's cartilage together with the palatoquadrate cartilage of the mandibular arch appear (Fig. 1E). Noticeable is the ventral position of the palatoquadrate and Meckel's cartilage. At the next stage, parachordals extend along the side of the notochord, and further in a prechordal part of the head, separate pre-cartilaginous condensations of trabeculae are present (Stage 2; Fig. 1F). Advanced cartilaginous differentiation of the jaw elements is seen by stronger Alcian Blue staining. At the same time, the first chondrified elements of the hyoid arch and separate rudiments of the otic capsules are present (Fig. 1F). At Stage 3, the trabeculae and parachordal plate are joined (Fig. 1G; black arrowhead) forming the base of the neurocranium. The hyomandibula of the hyoid arch is well differentiated, similar to the relatively advanced formation of the otic capsules with already visible side walls. At the same time, the ceratobranchial cartilage of the first two branchial arches is present (Stage 3; Fig. 1G). The final stage of chondrocranium formation in sterlet is characterized by a massive hypertrophy of base of neurocranium composed of trabeculae and parachordals (Stage 4; Fig.

1H). Both otic capsules are well developed and attached to the parachordal, and they are also well connected to the hyoid arch. Several cartilages have appeared among pharyngeal arches. Ventrally located median basibranchial copula connects newly formed paired hypohyals and hypobranchials of 3 branchial arches. The 4th hypo- and ceratobranchial are forming.

In a sum, sterlet chondrocranium formation is characterized by rather a slow progression early, but with a great advance in development during the final stage; also, parachordal cartilage surrounding the anterior tip of the notochord is leaving the hypophyseal fenestra disproportionately smaller as compared to bichir and gar. The anterior tip of the notochord is surrounded by parachordal cartilage (Fig. 1E; black arrowhead) and the process of chondrification is concentrated into the posterior part of the head (Fig. 1E-G). This pattern apparently corresponds to formation of an interface between the dorsal neurocranium and a ventral oropharyngeal chamber supporting fully retracted jaws.

In gar, the first stage of chondrocranium formation is represented by simultaneous appearance of the pre-chordal (trabeculae) and parachordal pre-cartilages, together with the Meckel's cartilage, structures of the hyoid and branchial arches, and elements of the otic capsule (Stage 1; Fig. 1I). During the next stage (Stage 2; Fig. 1J), all these elements undergo further enlargement and differentiation. Pre-chordal and parachordal cartilages fuse together, and anterior trabeculae become interconnected at their rostral ends (Fig. 1J; black arrowhead), enclosing the hypophyseal and basicranial fenestrae that are widely confluent yet (Fig. 1J). The palatoquadrate cartilage newly appears as a longitudinal bar parallel with the trabecula. The palatoquadrate is not yet articulated with Meckel's cartilages, that are still separated in the midline. The cartilages of the hyoid arch are well developed and attained to the otic capsule. Ceratobranchial cartilages are now well developed (Fig. 1J). At Stage 3, the anterior fusion of trabeculae has advanced into the trabecular plate which subsequently develops into an ethmoid plate. The Meckel's cartilages fuse together at the symphysis. In branchial arches, the 4th ceratobranchial cartilage form, together with a median basibranchial copula that corresponds to the first two ceratobranchial elements at the floor of the pharynx (Stage 3; Fig. 1K). At the final stage (Stage 4), the anterior chondrocranium formation is apparently blocked by persisting cement glands (Stage 4; Fig. 1L; arrowhead) and the trabecular plate extends laterally instead. Ceratobranchial cartilages of branchial arches are more developed and extended laterally (Fig. 1L).

In a sum, gar chondrocranium formation is characterized by early and simultaneous appearance of a number of structures with subsequent rapid chondrification. Also, development of the anterior neurocranium is significantly delayed due to the presence of cement glands forming prominent craniofacial structures during embryonic development.

In pike, the first pre-cartilaginous element to form at the base of neurocranium is a paired trabecula visible as two medially aligned thin bars between eyes (Stage 1; Fig. 1M). At the same stage of chondrocranium formation the pre-cartilaginous Meckel's cartilages appear, similar as structures of the hyoid arch that are more advanced in cartilage differentiation than the otic capsules. At the first stage, all branchial arches are already formed (Stage 1; Fig. 1M). At the next stage of development, anterior trabeculae fuse to form trabecula communis while their posterior ends attach to the parachordals. Note that outlines of parachordals and lateral otic capsules are obvious, even though their Alcian Blue staining is rather vague (Stage 2; Fig. 1N). New element of ceratohyal is forming and cartilaginous structures of ceratobranchial are well differentiated (Fig. 1N). During the next stage (Stage 3; Fig. 1O), trabecula communis is anteriorly extending into the ethmoid plate, and scleral cartilage ringing the eye appears. At

the same time, cartilaginous condensation of hypohyal element forms at the ventral pharynx which is followed by median basibranchial copula and hypobranchial 1 (Stage 4; Fig. 1P).

In a sum, the pattern of early chondrocranium formation in pike is similar to that seen in gar, with delayed formation of parachordal cartilages. Also, fusion of trabeculae cranii is closer to the anterior tip of notochord when compared to bichir and gar.

Comparative developmental analysis of chondrocranium regions

Previous comparative analysis revealed rather modified sequences and a specific pattern of chondrocranium element formation. In order to better facilitate interspecific comparisons among studied fishes, disparate chondrocranium elements were in the next analysis sorted according to their segmental and topographic position into five regions: prechordal (i) and parachordal (ii) within the neurocranium, and mandibular (iii), hyoid (iv) and branchial (v) within the viscerocranium.

Comparative analysis of such regional development of chondrocranium revealed a variable position of the first cartilage element within both the neurocranium and viscerocranium in studied fishes (Fig. 2, left box). In bichir and sterlet, the first neurocranial structure forms in the parachordal region at the posterior head. In gar, a fully formed base of neurocranium comprises both parachordal and prechordal regions. In pike, on the contrary, the first structure to appear within the neurocranium is an element in a rostral (prechordal) region (Fig. 2; left box). Similar variability in the first cartilage position appears in viscerocranium of studied fishes as well. While in bichir and sterlet, the Meckel's cartilage of the mandibular region clearly appears as the first viscerocranium element, in gar and pike, a number of elements of both the mandibular and hyoid regions appears concurrently during the Stage 1 (Fig. 2; left box). According to cartilage maturation (dark blue) these regions show early and accelerated differentiation of the jaw with its suspensory apparatus in pike running prior the Stage 1, similar as the structure of the hyoid region in gar. At the same time point of early viscerocranium development, bichir and sterlet lack elements of branchial regions. In contrast, branchial and hyoid regions in gar and pike form early and concomitantly with several other viscerocranium regions (Fig. 2; left box).

Comparative developmental analysis also revealed a variable temporal sequence of appearance of respective chondrocranium regions in studied fishes (Fig. 2, right box). Whereas in gar, formation of all chondrocranium regions begins early and concurrently already during Stage 1 (except accelerated development of the hyoid region) in bichir, sterlet or pike, sequence of appearance of chondrocranium regions is detached and more gradual (Fig. 2; right box). In pike, nearly all regions appear early and concurrently with only the parachordal region forming in the next stage (Fig. 2; right box). Chondrocranium regions in bichir and sterlet appear more gradually, with especially delayed branchial arches formation in sterlet (Stage 3), and more rapid appearance of several bichir chondrocranium modules already within Stage 2 (Fig. 2; right box).

The rate at which maturation of a pre-cartilage (light blue) proceed to already differentiated cartilage (dark blue) significantly varies among species. The most accelerated process of cartilage differentiation characterizes development of neurocranium in pike and gar with conspicuous delayed formation of the branchial region in gar (Fig. 2; right box). In bichir, the parachordal, mandibular, and hyoid regions show accelerated cartilaginous maturation as compared to the prechordal and branchial regions. The slowest cranial regions differentiation defines chondrocranium of sterlet (Fig. 2; right box).

We conclude that the pattern of the appearance of chondrocranium regions is surprisingly different among studied fishes. Whereas gar chondrocranium is characterized by

rapid and complex early formation (at Stage 1) with hyoid region appearing even earlier (Stage 0), sterlet chondrocranium is early rather incomplete with only slow and gradual formation (Stages 1-4). In contrast to this, bichir and pike chondrocranium formation is characterized by rather rapid and concurrent appearance of several regions during Stage 2 and 3. Surprisingly, two of five regions in pike (mandibular and hyoid) are differentiating during Stage 0, long before the first pre-cartilaginous structure formation in the neurocranium.

Variation in the first skeletal ossification

After analysing patterns of chondrocranium formation in studied fishes we moved our attention to the pattern of their early cranial ossification. Alizarin Red was used to identify the first ossification (Fig. 3) which time point was later also used to align comparative developmental series of studied fishes in order to analyse pattern and sequence of osteocranium formation (Fig. 4-6).

The first cranial ossification in both bichir and gar was found within the dentary, a tooth bearing bone of the lower jaw (Fig. 3A, A', C, C'). In sterlet, the first ossification in dentary is accompanied by its counterpart in the dermopalatine, an upper jaw bone (Fig. 3B, B'). In both bichir and gar, development of the upper jaw ossification seems limited by the presence of prominent cement glands (Fig. 3A,C; asterisk), similarly as it is the case with chondrocranium formation (Fig. 1A, B, L). This blocking in ossification lasts till a resorption of this organ and it takes a longer period of time in gar (see Fig. 4). In sterlet, hatching glands are more superficial structures (Minarik et al., 2017) which do not limit ossification and both upper and lower jaw ossifications appear simultaneously (Fig. 3B, B'; arrowheads).

Whereas tooth bearing structures of the jaw are the first bones to appear in bichir, sterlet, and gar, the pattern of the first ossification is considerably different in pike (compare Fig. 3A–D). The first bone to ossify represents cleithrum (Fig. 3D, D'; arrowheads) located in a postorbital part of the head which belongs to dermal elements of the pectoral girdle. In pike, the first cranial structure to ossify is opercle together with dermal components of upper and lower jaws (see Fig. 4).

Variation in pattern and sequence of osteocranium formation

Having identified the first cranial ossification, we next sought to describe and compare developmental patterns of ossification during osteocranium formation in bichir, sterlet, gar, and pike. Detailed post-hatching growth series focusing on cranial bone development was collected and utilized, comprising 20 developmental series of bichir (7–61 mm), 41 series of sterlet (11–77 mm), 29 series of gar (13.5–68 mm), and 26 series of pike (10–105 mm) (see Tab. 1). This comprehensive developmental series was classified according to ossification into an early, middle and late time period, which were compared separately. The early time period includes stages after the first bone formation and the end is classified as a one stage before the beginning of dorsal scutes ossification in sterlet. The middle time period corresponds to the first dorsal scute ossification in sterlet up to stage of the first ossification of spiracular ossicle series in bichir. This bony series supports air breathing in juveniles and belongs to one of the last bony ossifications filling the dermal skull bones. Then, for the sake of easy comparison only some key specimens were selected and presented in the lateral views (Fig. 4–6).

Variation in pattern and sequence of osteocranium formation during early time period

In bichir, among the first bones to ossify are especially those that bear teeth (maxilla and dentary forming upper and lower jaw, palatal complex and branchial arches) as well as jaw supporting hyoid arch, and cleithrum belonging into a pectoral girdle (Fig. 4A). New bony structures formation is restricted into posterior branchial arch ossification (Fig. 4B) and to the laminar flange of posteriorly expanding preopercle (Fig. 4C) during all the rest of early time period.

The first ossification of a marginal dentigerous bone in sterlet (see Fig. 3B, B') is followed by completion of upper jaw palatal complex to which tooth bearing palatopterygoid is incorporated. At the same time, we observed the first evidence of subopercle ossification (Fig. 4D) getting its typical plate-like appearance during the following development (Fig. 4E). Together with branchiostegals (Fig. 4F) it constitutes reduced opercular series in sturgeons. The very first evidence of skull roof ossification is visible dorsally as a tiny stripe of bony condensation associated with the supratemporal sensory canal (Fig. 4E; black arrowhead). Posteriorly located precursors of the pectoral girdle series, i.e. posttemporal and supracleithrum (Fig. 4E) are subsequently overlaid and newly formed cleithrum is incorporated into this series (Fig. 4F). New structure of parietal is appearing as a longitudinal dermal ossification parallel with a newly appeared parasphenoid which forms the ventral surface of the neurocranium inside the head (Fig. 4F). Note preferential ossification proceeding in postorbital part of the head during early time period, so tiny ossicles associated with extended infraorbital lateral line canal are the only anteriorly located structure (Fig. 4E, F; white arrowheads). We assume that it's because a still growing rostrum on the anterior part of the head inhibits preorbital ossification during early time period.

In gar, we detected relatively long blocking of upper jaw ossification by massive cement gland during early time period, so even two consecutive developmental stages show ossified dentary of the lower jaw without any bone in the opposite upper jaw (Fig. 3C and Fig. 4G). The first evidence of parasphenoid, probably the largest bone supporting much of the ventral surface of the neurocranium, is appearing right in the middle of the head (Fig. 4G). Next developmental stage is characterized by the allocation of ossification process into fast extending preorbital part of the head, as it is obvious from ossification of 3 structures in upper jaw: premaxilla, maxilla and dermopalatine. Posteriorly, perichondral ossification begins to form first bone around ceratohyal cartilage (Fig. 4H; white arrowhead) and dermal elements of pectoral girdle (supracleithrum, cleithrum) are appearing (Fig. 4H). The last stage of this period is characterized by an extensive jaw lengthening affecting especially jaw dentigerous bone. The premaxilla extends posteriorly to the close proximity of newly formed frontals but these bones are still separated. A tiny aggregation of ossified tissue in the otic region represents the first evidence of dermopterotic bone (Fig. 4I; black arrowhead) belonging to dermal bones covering the dorsal surface of the head. The first ossification of ceratohyal structure and two branchiostegals are appearing on the ventral part of the head Fig. 4I).

In pike, next structures added to the first ossified cleithrum are tooth bearing dentary of the lower jaw, edentulous maxilla on the opposite jaw and opercle located in the postorbital part of the head (Fig. 4J). Light Alizarin Red staining of these structures shows rather low mineral density during the whole early time period. Later development corresponds to gentle expansion of these structures (Fig. 4K) followed by unpaired parasphenoid ossification located at the base of the neurocranium (Fig. 4L). At the same time, dermal structure of supracleithrum is incorporated into a pectoral girdle and we observed the first appearance of branchiostegal rays (Fig. 4L).

Variation in pattern and sequence of osteocranium formation during middle time period
Compared to the previous time period, the number of new bones is growing remarkably during a middle time period in bichir (Fig. 5A–C). We observed advanced ossification of perichondral ceratohyal bone as well as quadrate which is formed by endochondral ossification of cartilaginous precursor (Fig. 5A). Furthermore, new bony condensation clearly visible as a tiny cluster of ossified tissue is opercle (Fig. 5A) which is in direct connection with the hyoid arch. Additional small aggregations of calcified tissue are appearing in connection with a lateral line canal above (supraorbital, Fig. 5A; black arrowhead) and below (infraorbital, Fig. 5A; white arrowhead) the eye. Subsequently, the number of these ossification centers is rapidly growing (Fig. 5B) in connection with supraorbital (black arrowheads) and infraorbital (white arrowheads) lateral line canal on the head. New tubular ossification is associated with otic canal (black arrow; for more detail see Rizzato et al., 2020). Previously founded ossification above the eye gave rise to a frontal bone that expands and represents the beginning of cranial vault formation. On the opposite side, an early condensation of paired gulars are appearing (Fig. 5B). A great advance has been made in cranial bone development during the following stage. All of calcified structures have undergone bone expansion (compare e.g. dermopterotic, Fig. 5B and 5C) and we observed incorporation of many tubular ossification into the set of cranial bones (Fig. 5C). A small aggregations of bony tissue around supraorbital line on a dorsal surface of rostrum (black arrowheads) correspond to future series of nasals with the anteriormost element belonging to infraorbital line (white arrowhead) forming rostral bone respectively (for more detail see Rizzato et al., 2020). Due to postorbital and dermosphenotic bone ossification the infraorbital series is fully developed now. The posteriormost part of the dorsal skull is supplemented by series of tubular ossification around the supratemporal line associated with future extrascapulars. Note a pair of gular bones that cover the throat region ventrally (Fig. 5C).

In sturgeon, we observed a shifting of ossification process into a preorbital part of the head during a middle time period. Newly formed frontals represent the biggest bony structure located in this region and together with dermosphenotic are fully incorporated into the anterior skull roof. Structures located on the postorbital dorsal skull roof are showing surface expansion. At the same time, we observed a conspicuous chain of small ossicles which constitutes a series of rostral canal bones surrounding an infraorbital lateral line of the head. The posteriormost bone terminating this series (jugal) belongs to postorbital bones (Fig. 5D). During the following development, we observed rather small tubular ossicles ossifying around the supraorbital canal (Fig. 5E, F; white arrowheads). At the last stage of this middle time period, we observed formation of supraorbitals which together with dorsal rostral bones belong to irregularly shaped and positioned anamestic bones. On the opposite side, there is a series of rostral bones associated with the ventral surface of the chondrocranium (ventral rostral bones, Fig. 5F) crossing the midline of the rostrum. At the same time, tubular postorbital bone is one of the last forming structure completing the infraorbital series (Fig. 5F).

In gar, frontals representing the largest bones of the dorsal skull roof overlap the posterior region of premaxillae positioned anteriorly (Fig. 5G, white arrow points to solid dermal roof structure). This is happening despite the fact that the process of jaw lengthening is still significant over the whole middle time period (see Fig. 5G-I). The series of tooth bearing lacrimomaxillary bones around the infraorbital canal of lateral line is appearing alongside the upper jaw with function as the main part of the upper jaw margin. The dermal bones of the skull roof now include newly formed nasals, located at the anteriormost tip of the snout, parietals and dermopterotics on the postorbital part of the head. Ventrally, we observed ossification of preopercle which is connected to the hyoid arch posteriorly and to the

quadratojugal anteriorly. At the same time, we observed the first perichondral ossification of ceratobranchial 1 (Fig. 5G). The number of ossified ceratobranchial is growing and new ossicles are integrated into branchiostegal series (Fig. 5H). The last stage of this time period is characterized by remarkable surface expansion of previously formed bony structures and opercular series development. Opercle and subopercle are appearing to cover the branchial chamber laterally (Fig. 5I). At the same time, the anteriormost bone of the snout is appearing. This median rostral ossicle is located anterior to the previously formed nasals.

In pike, the bone thickness as well as a number of ossified structures is growing during the middle time period. Tooth bearing structures of the palatal complex continue to ossify while the process of new bone formation is concentrated especially to the postorbital part of the head, where we observed new ossification of hyoid and branchial arches (Fig. 5J). At the same time, new weakly stained bony condensations of future subopercle and interopercle are appearing. New ossicles are integrated into the branchiostegal series of bones and the posttemporal dermal component of the pectoral girdle develops. Frontals forming the largest portion of the dorsal skull roof begin to form (Fig. 5J). All the structures described above slowly develop during the following stage and preopercle is being incorporated into the opercular series (Fig. 5K). A great advance has been made in the following stage. Previously formed bones show remarkable expansion of their surface (Fig. 5L) and new bony structures around the lateral line (dermosphenotic and dersmopterotic) are completing the dermal skull roof at the posterior part of the head. On the opposite side, a new accessory toothless jaw bone (supramaxilla) parallel to maxilla is forming.

Variation in pattern and sequence of osteocranium formation during late time period

The first stage of the late time period in bichir is characterized by the beginning of spiracular ossicle series formation (Fig. 5A; black arrowhead). These small bones are fully integrated into the cranial set of bones during the following development and span along dorsal margins of preopercle and opercle (Fig. 5B; white arrowheads). The dorsal surface of the skull roof is completed by dermal nasals and rostral bone anteriorly as well as posttemporal and extrascapulars posteriorly. Subopercle is the last bone to form within the opercular series, that is visible as a small triangular bone wedged between opercle and preopercle (Fig. 5B). We observed a significant expansion of bony surface and increase of bone density during the transition between the last two analyzed stages resulting in compact/solid/firm skull architecture in juveniles (Fig. 5B).

In sturgeon, the speed of new cranial bone formation is slowed down as compared to the middle time period, so rather than an increase of a bone number we observed the expansion of bony surface during the late time period of skeletal development (Fig. 5C). At the last stage of development, the lateral side of the snout starts to be armored by anamestic border rostral bones and striking development of bone density is obvious within the whole juvenile skull (Fig. 5D).

We observed only insignificant increase of bony structures in gar during the late time period. Tiny aggregation of calcified tissue marks the sphenotic formation located on the underside of dermopterotic (Fig. 5E). The last analyzed stage is characterised by the appearance of many small ossicles in the proximity of the eye. Right above the eye, two clusters of mineralized tissue mark a future suborbital bony element. Anteriorly, there is a series of bony aggregation reaching a level of the jaw that is penetrated by the infraorbital line of the head. We call them lacrimals and compared to previously described lacrimomaxillae, these elements do not bear teeth (Fig. 5F). As can be seen, the jaws of gar are still lengthening even during a late time period.

A significant expansion of bony surface as well as increase of bone density are dominant processes during a late time period in pike. At the same time, new structures are observed to complete the dermal skull roof at the posterior part of head. Relatively small parietals (positioned posterior to the frontals) together with epiotic and exoccipitals form posterior dorsal portion of the skull (Fig. 5G). Anteriorly, we observed lacrimal and ceratohyal bone as new relatively late ossified structures. The last developmental stage is characterized by jaws lengthening and by surface expansion of dermal pectoral girdle bones so the skull gets its compact design (Fig. 5H).

Comparative analysis reveals modified sequence of osteocranium formation

Our detailed dataset of cranial bone formation providing accurate information of every single bone development (for selection of crucial stages see Fig. 4-6) offers a valuable source for assessing/analysis of sequential osteocranium transformation during development among species. In order to facilitate interspecific evaluation and to circumvent problems regarding bone homology, its development was described according to their topographic position within each of the eight regions. These are: (i) olfactory, (ii) orbital, (iii) otic, (iv) mandibular arch, (v) hyoid arch, (vi) branchial arches, (vii) opercular series, and (viii) pectoral fin (Tab. 2). This regional approach was elaborated in Mabee & Trendler (1996). As it is mentioned in this study, there is inconsistency in a way of sorting bones into regions among authors. Given the loss of a number cranial bones especially those endochondral ossifying or their relatively late formation, the design of regions was adjusted to suit the condition of our non-teleost species which allows more efficient comparison of their development. For example we reduced the complex of jaw bones into a single mandibular arch according to pharyngeal arch topography (like we used in this regional approach of chondrocranium formation, see above). Based on the presence of teeth on vomer we placed this bone between the palatal complex of the mandibular region (Tab. 2). This region comprises dermopalatine, palatopterygoid and dentary in sterlet due to radical restructuring of jaw apparatus.

Such analysis clearly revealed surprising diversity in ossification sequence among studied lineages. In bichir, the first structures to ossify are dentigerous bones within the mandibular region followed by accelerated ossification of jaw supporting hyoid arch and parasphenoid which belongs into the orbital region. Other bones that ossify soon after are tooth bearing branchial arches and structures of pectoral fin girdle appearing right at the beginning of early time period identically. The process of region formation is decelerated up to the last third of the early time period when the opercular region is established and remaining cranial regions including dermal roof bones of otic and olfactory regions are formed during the middle time period (Fig. 7).

Osteocranium development in sterlet shows slower ossification especially at the very beginning. The first formed region is the mandibular represented by marginal jaws followed by opercular region that ossifies at the beginning of the early time period. Next development is characterized by accelerated formation of olfactory, otic and pectoral fin regions appearing in synchrony within the second third of the early time period. Note preferential ossification at the postorbital part of the head (except olfactory region that is represented by isolated tiny ossicles at the anterior tip of the rostrum throughout early time period, see Fig. 4E, F; white arrowheads). Hyoid arch supporting previously formed opercle region is mineralizing immediately afterwards followed by structures in the orbital region represented by parasphenoid at first and further accompanied by frontal and dermosphenotic. This is an evidence of anterior expansion of the process of ossification. By this, almost all cranial regions

are established except very delayed perichondral ossification of branchial arches that proceeds during late juvenile development (Fig. 7).

Also in gar, the first ossifying structures are dentigerous bones belonging into the mandibular arch that are soon followed by parasphenoid belonging to the orbital region. However, the dynamic pattern of region formation succeeds especially during the last two thirds of the early time period in which five out of eight cranial regions appear. Firstly, bones associated with hyoid and pectoral fin girdle regions are appearing simultaneously followed by stepwise formation of branchial, otic and opercular regions. Note that ossification of opercular series is delayed in gar and represents the last region to form during early time period. The osteocranium is completed by an olfactory region which is established at the very beginning of the middle time period (Fig 7).

The sequence of cranial region formation is considerably modified in pike. While structures of pectoral fin girdle are first forming bones within their skull, the process of dentigerous bones ossification is delayed as compared to bichir, sterlet, and gar and is accompanied by opercular region differentiation. Further region formation is rather gradual during the early time period characterized by ossification of parasphenoid belonging to the orbital region and structures within the hyoid region. The middle time period is initiated by perichondral ossification of branchial arches. The last forming otic and olfactory cranial regions are delayed within the middle time period (Fig. 7).

Based on the dataset above we conclude that in bichir the most dynamic progress of ossification is apparent especially during early osteocranium development with five consecutive regions forming soon after each other. In sterlet and gar, there is a longer initial period of stasis followed by sudden appearance of battery of cranial regions proceeding in synchrony in sterlet but in a rather gradual pattern in gar. In pike, the process of region formation is delayed as compared to bichir, sterlet and gar (Fig. 7). While we observed preferential formation and subsequent concentration of ossification into a dentigerous bones (jaw bones, branchial arches) in bichir, sterlet, and gar, there is prominently accelerated ossification of dermal pectoral girdle and opercular series in pike (Fig. 7). Interestingly, the process of osteocranium ossification is concentrated into postorbital cranial region which is in contrast with preferential ossification allocated into preorbital bony structures in gar.

region	bones
OLFACTORY	nasal
	rostral
ORBITAL	frontal
	infraorbital
	parasphenoid
	supraorbital
OTIC	epiotic
	jugal
	parietal
	postorbital
	posttemporal
	pterotic
	dermo-sphenotic
MANDIBULAR ARCH*	angular
	articular
	coronoids
	dentary
	maxilla
	preacticular
	premaxilla
	vomer
	bones of palatal complex
HYOID ARCH	branchiostegals rays
	ceratohyal
	symplectic
	hyomandibula
BRANCHIAL ARCHES	ceratobranchials
OPERCULAR SERIES	interopercle
	opercle
	preopercle
	subopercle
PECTORAL FINS	cleithrum
	postcleithrum
	posttemporal
	clavicle
	supracleithrum

Tab. 2 * in sterlet instead: dentary, dermopalatine, palatopterygoid

Interspecific variation in timing of chondrocranium and osteocranium formation

Having detailed description of developmental dynamics of chondrocranium (Fig. 1, 2) and osteocranium (Fig. 3, 4, 5, 6, 7) during cranial development, we sought to compare timing of chondrocranium and osteocranium formation among studied species. To do this we focused on plotting of previously described patterns of the first cranial cartilage and bone differentiation. Time of hatching is considered as a reference point, in order to standardize developmental stages of this analysis among species (Fig. 8).

The results showed that cartilage differentiation in pike is tightly connected with hatching so their skeletal development lacks any pre-cartilaginous stages (characterized as a time period between hatching and the first cranial cartilage appearance) as compared to bichir, sterlet, and gar. Consequently, the process of ossification in pike is most accelerated based on hatching time (Fig. 8). On the contrary, the pattern of chondrocranium formation is remarkably delayed in bichir, sterlet, and gar. Considering the time of hatching, the beginning of chondrocranium formation shows the same delay in bichir and sterlet, but the process of the first mineralization in bichir is considerably accelerated based on the first cartilage formation (Fig. 8). We observed prolonged time of chondrocranium differentiation in gar although the first ossification of osteocranium is coincided with the sterlet (Fig. 8).

We conclude that cartilage and bone formation is considerably accelerated in pike based on time of hatching. Despite the same timing of cartilaginous skull formation in bichir and sterler, the process of bone ossification is accelerated in bichir (as compared to situation in sterlet and gar). Surprisingly, the most extended process of cartilaginous development before the first bone formation is obvious during skeletogenesis in gar (Fig. 8). To investigate this process in earlier developmental stages we examined the developmental *col10a1* expression.

Altered patterns of *col10a1* gene expression shows differences in development of early skeletal mineralization

To trace and to compare the timing of *col10a1* expression, a crucial factor of skeletal mineralization in amniotes, whole-mount in situ hybridization was performed on a detailed developmental series of all studied lineages (Fig. 9). The pattern of developmental expression was plotted together with the data of the first cartilage and bone formation (see Fig. 8). In order to standardize developmental stages and to make reliable interspecific comparison, time of hatching is considered as a reference point.

We observed accelerated *col10a1* expression relative to time of hatching in pike. This gene expression lasts quite a long time period (Fig. 9A). Gene expression was variously delayed relative to the time of hatching in comparatively staged bichir, sterlet, and gar. The most delayed onset of *col10a1* expression is in sterlet, but they exhibit prolonged expression of this marker through extended periods of larval development. In contrast, we identified a substantially truncated developmental expression in bichir (Fig. 9A).

Using a normalization of development according to emerging skeletal structures (first cartilage or bone formation, see above), the timing of *col10a1* gene expression is radically different (Fig. 9A). In all species examined, expression of *col10a1* is variably united with the process of cartilage development (Fig. 9A). While beginning of gene expression run concurrently with a formation of the first cartilage in bichir, we observed pattern of delayed developmental expression in sterlet, gar, and pike (Fig. 9A). The onset of the gene expression is shifted until the first ossification in pike. This could be caused by an absence of pre-cartilaginous stage in pike (i.e. time of the first cartilage formation corresponds with the process of hatching). While we detected cessation of *col10a1* expression soon after the first

bone formation in gar, the prolonged developmental expression over extended periods of bone development is obvious in sterlet and pike (Fig. 9A).

Location of *col10a1* expression is also completely different among studied species. The first gene expression in bichir is localized into structures of maxillary with the posterior elongated element (Fig. 9B; black arrowhead) and dentary together with posteriorly formed cleithrum (Fig. 9B). Subsequently, signal spreads into the hyoid and branchial arch (data not shown). The positive signal is fading over time so relatively short gene expression terminates as a weak gene expression in maxillary and at a contact zone of already ossified dentary with teeth (Fig. 9B; white arrowhead), as well as in a hyoid arch with the first ceratobranchial and cleithrum.

In sterlet, the first *col10a1* positive signal is expressed in dermopalatine of upper jaw and dentary of lower jaw (Fig. 9D). This expression takes a relatively long time. The signal then moves into the preopercle and supracleithrum during the late development (Fig. 9E) where it suddenly disappears.

The first evidence of *col10a1* expression is limited to the dentary of the lower jaw in gar (Fig. 9F). The gene expression culminates in a massive expansion of signal to the dentigerous bones (such as premaxillary, maxillary, vomers, dermopalatine of the upper jaw and dentary of the lower jaw), to the perichondrium surrounding the ceratohyal cartilage and to the pectoral girdle (Fig. 9G). We observed a sudden loss of positive signal in all structures during the following development.

The first gene expression in pike corresponds to maxillary and dentary of the jaw and posteriorly placed cleithrum belonging to structures of pectoral girdle (Fig. 9H). Over time, the signal spreads to the opercle (data not shown). The last stage of gene expression is characterized by an overall reduction of previously positive *col10a1* signal in maxillary, margin of dentary, opercle and pectoral girdle (Fig. 9I).

Developmental variation in skeletal tissue density development

During *description of ossification strategy* we noticed a conspicuous variability in the mass of bone among studied lineages (see Fig. 4, 5, 6). To comparatively describe developmental dynamics of skeletal tissue density we performed micro-CT scans across all studied lineages. In Figure 10 and Figure 11, volumes are rendered in a false-color spectrum ranging from less dense (cooler colors) to more dense (warm color). In order to standardize developmental stages and to make reliable comparison between studied species, we normalized developmental series based on addition of 4 mm interval to the stage of the first skeletal ossification (Fig. 3; i.e. bichir: 8 mm, sterlet: 14 mm, gar: 14 mm, pike: 10 mm). The following development was determined according to the total length. Thus, analyzed developmental series comprises stages 12–35 mm TL in bichir, 18–35 mm TL in sterlet and gar, 14–36 mm TL in pike. In sterlet and gar we had to left out the analysis of the last stage because of the enormous amount of data that was impossible to calibrate (see Material and methods).

The detection of the first mineralized tissue is delayed in bichir. During the second skeletal developmental stage, there is clear evidence of tooth bearing bones ossification together with medially placed parasphenoid and structures of pectoral girdle. Rather limited occurrence of yellow color thus indicates lower bone density with the densest area on the posterior part of dentary and at the contact zone of dentigerous bones with teeth (Fig. 10B). Micro-CT scanning of the following stage detected prevailing orange-yellow color of skeletal cranial structures demonstrating a steep increase in bone density (Fig. 10C). A reddish or bluish bone edge indicates the active process of bony ossification. The volume of mineral tissue deposited into skeletal structures is decreasing and the subsequent pattern of bone

density development in bichir is rather gradual (Fig. 10C–E). Considering the contribution of orange or red signals in the skull during the last analyzed stage, the final bone density doesn't reach the maximum (Fig. 10F).

The pattern of bone density development is rather gradual in sterlet. While the first stage of analysis represents the most advanced condition among studied lineages, next development is characterized by a linear increase in number and volume of bony structures (Fig. 10G–K). During the first three analysed stages, we observed noticeable concentration of bone deposition into a postorbital part of the head. Based on a warm colors mostly represented by orange and yellow, substantially ossified structures are those involved in feeding (dentigerous bones) as well as breathing (subopercle) (Fig. 10G–I). We detected remarkable accumulation of yellow color into a postorbital part of the head even in later stages of development characterized by anterior spreading of ossification into a rostral part of the skull (Fig. 10J, K).

The most intensive increase of bony mass is obvious in skulls of gar. While the volume of ossification within the first analyzed stage is hard to recognize (Fig. 10L; white arrowhead), micro-CT scanning of the following stage detected a steep increase of bone density which is predominantly concentrated into the preorbital part of the head (Fig. 10M). The pattern of ossification is extending caudally during following development and bright yellow color (compare to bichir, Fig. 10F) is prevailing within the whole skull (Fig. 10N–P).

Micro-CT scanning reveals a very slow increase of bone mass in pikes. Whereas the first two stages don't even reach a threshold for calibration (Fig. 10Q, R), the first detected ossification is restricted into the jaws (Fig. 10S). Based on purple signal proving lower density, there is relatively little bone with denser area located at the contact zone of dentigerous bones with teeth. We observed the same pattern in two following stages (Fig. 10T, U) with no modification. The last analyzed stage is characterized by an increase of bone mass within jaws and other bones of the skull (Fig. 10V).

Surprisingly, our data revealed the well-ossified skeletal tissue of dentigerous bones and subopercle in sterlet during the first analysed stage (Fig. 10G). The Micro-CT scanning of comparable stage in gar detected positive blue signal in upper and lower jaw (check magnification of Fig. 10L; white arrowhead) pointing to very low mineral tissue density. The dynamics of mineral deposition is most accelerated in gar

Comparative analysis of mineral tissue development

Having overall characterization of tissue density development we sought to describe and analyse the dynamics of volume density expansion in developing skulls.

Whereas the density of ossified tissue during early development is too low to reach the threshold for calibration in bichir and pike, surprisingly the densest bones of skull were revealed in sterlet at comparable Stage 1 (note the proportion between the warm and cold color; Fig. 11). Based on the slope of the trajectory, the pattern of density development appears to be rather unstable with linear density increase during later stages in sterlet. In gar, despite the low bone density at Stage 1, the process of mineralization is rising sharply very soon (Fig. 11). Thus, the proportion of high bone density grows exponentially during skull development. Similar developmental trajectory characterizes volume density development of the skull in bichir, but the process of ossification is significantly delayed as compared to gar. Moreover, the proportion of the densest bony tissue doesn't reach as high values as in gar (Fig. 11). The dynamics of bone density development is significantly different in pike. In addition to remarkable delay with achievement of calibration threshold at the beginning of skull

development, the trajectory characterizing skull density development is linear (Fig. 11) thus indicating gradual increase of bone density.

Alberch, P., Gould, S. J., Oster, G. F. & Wake, D. B. (1979). Size and shape in ontogeny and phylogeny. *Paleobiology* 5: 296–317.

Bartch, P. (1997). Aspects of craniogenesis and evolutionary biology in polypteriform fishes. *Nertelands Journal of Zoology* 47(4): 365–381.

Bartsch, P., Gemballa, S. & Piotrowski, T. (1997). The Embryonic and Larval Development of Polypterus senegalus Cuvier, 1829: its Staging with Reference to External and Skeletal Features, Behaviour and Locomotory Habits. *Acta Zoologica* 78(4): 309–328.

de Beer, G. R. (1937). *The development of the vertebrate skull*. Oxford University Press, Oxford.

Bemis, W.E., Findeis, E.K. & Grande, L. (1997). An overview of Acipenseriformes. *Environmental Biology of Fishes* 48, 25–71.

Burdi, A. M. (2010*) Morphological Development of the Axial Skeletons of Esox Lucius and Esox Masquinongy (Euteleostei: Esociforms), with Comparisons in Developmental and Mineralization Rates*. MSc Chicago: Loyola University. pp 91.

Clemen, G., Bartsch, P. & Wacker, K. (1998). Dentition and dentigerous bones in juveniles and adults of *Polypterus senegalus* (Cladistia, Actinopterygii). *Annals of Anatomy* 180, 211–221.

Dettlaff, T. A., Ginsburg, A. S. & Schmalhausen, O. J. (1993). *Sturgeon Fishes.Developmental Biology and Aquaculture*. Berlin; New York: Springer-Verlag Berlin Heidelberg.

Fricke R, Eschmeyer WN & Van der Laan R (eds.) (2020). Eschmeyer‘s catalog of fishes: genera, species, references. (http://researcharchive.calacademy.org/research/ichthyology/catalog/fishcatmain.asp). Electronic version accessed 03 06 2020.

Gans, C. & Northcutt, R. G. (1983). Neural crest and the origin of vertebrates – a new head. *Science* 220, pp. 268–274.

Goodrich, S. E. (1930). *Studies on the structure and development of vertebrates*. Macmillan and Co, London.

Gould, S.J. (1977). *Ontogeny and Phylogeny*. Cambridge, Mass: Belknap Press of Harvard University Press.

Grande, L. (2010). An empirical synthetic pattern study of gars (Lepisosteiformes) and closely related species, based mostly on skeletal anatomy. The resurrection of Holoste. *Copeia*, 1–871.

Green, S.A., Simoes-Costa, M. & Bronner, M. E. (2015) Evolution of vertebrates as viewed from the crest. *Nature* 520, 474–482.

Handschuh, S., Beisser, C. J., Ruthensteiner, B. & Metscher, B. D. (2017). Microscopic dual-energy CT (microDECT): a flexible tool for multichannel *ex vivo* 3D imaging of biological specimens. *Journal of Microscopy*, 1–24.

Hanken, J. & Thorogood, P. (1993). Evolution and Development of the Vertebrate Skull: The Role of Pattern Formation. *Trends in Ecology and Evolution* 8: 9–15.

Hilton, E.J. (2005). Observations of the skulls of sturgeons (Acipenseridae): shared similarities of Pseudoscaphirhynchus kaufmanni and juvenile specimens of Acipenser stellatus. *Environmental Biology of Fishes* 72, 135–144.

Hilton, E.J., Grande, L. & Bemis, W.E. (2011). Skeletal Anatomy of the Shortnose Sturgeon, Acipenser brevirostrum Lesueur, 1818, and the Systematics of Sturgeons (Acipenseriformes, Acipenseridae*). Fieldiana Life and Earth Sciences* 3, 1–168.

Jollie, M. (1975). Development of the Head Skeleton and Pectoral Girdle in Esox. *Journal of Morphology* 147, 61–88.

Jollie, M. (1980). Development of Head and Pectoral Girdle Skeleton and Scales in Acipenser. *Copeia* 2, 226–249.

Jollie, M. (1984a). Development of Cranial and Pectoral Girdle Bones of Lepisosteus with a Note on Scales. *Copeia* 2, 476–502.

Jollie, M. (1984b). Development of the head and pectoral skeleton of Polypterus with a note on scales (Pisces: Actinopterygii). *Journal of Zoology* 204, 469–507.

Long, W. L. & Ballard, W. W. (2001). Normal embryonic stages of the Longnose Gar, Lepisosteus osseus. *BMC Developmental Biology* 1(6).

Mabee, P. M. & Trendler, T. A. (1996). Development of the Cranium and Paired Fins in *Betta splendens* (Teleostei: Percomorpha): Intraspecific Variation and interspecific Comparisons. *Journal of Morphology*, 249–287.

Minarik, M., Stundl, J., Fabian, P., Jandzik, D., Metscher, B. D., Psenicka, M., Gela, D., Osorio-Pérez, A., Arias-Rodriguez, L., Horácek, I. & Cerny, R. (2017). Pre-oral gut contributes to facial structures in non-teleost fishes. *Nature* 547, 209–212.

Müller, J. (1844). Über den Bau and die Grenzen der Ganoiden und über das natürliche System der Fische. Physikalisch-Mathematische Abhandlungen der Koniglichen Akademie dei Wissenschaften zu Berlin 1845, 117–216.

Müller, J. (1846). Über den Bau und die Grenzen der Ganoiden und über das natürliche System der Fische. Abhandlungen der Deutschen Akademie der Wissenschaften zu Berlin 1844, 119–216.

Northcutt, R. G. (2005) The New Head Hypothesis Revisited. *Journal of experimental zoology. Part B, Molecular and developmental evolution* 304B, 274–297.

Northcutt, R. G. & Gans, C. (1983). The genesis of neural crest and epidermal placodes: a reinterpretation of vertebrate origins. *Quarterly Review of Biology* 58, 1–28.

Parker, W.K. (1882). On the Structure and Development of the Skull in Sturgeons (Acipenser ruthenus and A.sturio). *Philosophical Transactions of the Royal Society of London* 173, 139–185.

Pehrson, T. (1944). Some observations on the development and morphology of the dermal bones in the skull of Acipenser and Polyodon. *Acta Zoologica* 25, 27–48.

Pehrson, T. (1947). Some new interpretations of the skull in Polypterus. *Acta Zoologica* 28, 399–455.

Pehrson, T. (1958). The early ontogeny of the sensory lines and the dermal skull in *Polypterus*. *Acta Zoologica* 39, 241–257.

Rizzato, P. P., Pospisilova, A., Hilton, E. J. & Bockmann, F. A. (2020). Ontogeny and homology of cranial bones associated with lateral-line canals of the Senegal Bichir, *Polypterus senegalus* (Actinopterygii: Cladistii: Polypteriformes), with a discussion on the formation of lateral-line canal bones in fishes. *Journal of Anatomy*, 1–29.

Pospisilova, A., Brejcha, J., Miller, V., Holcman, R., Šanda, R. & Stundl, J. (2019). Embryonic and larval development of the northern pike: An emerging fish model system for evo-devo research. *Journal of Morphology*, 1–23.

Scherrer, R., Hurtado, A., Garcia, E. M. & Debiais-Thibaud, M. (2017) MicroCT survey of larval skeletal mineralization in the Cuban gar Atractosteus tristoechus (Actinopterygii; Lepisosteiformes). MorphoMuseuM 3(3), 1–15.

Schilling, T.F & Thorogood, P. V. (2000). Development and evolution of the vertebrate skull. In: O'Higgins, P., Cohn, M. (eds). *Development, Growth and Evolution: Implications for the Study of the Hominid Skeleton.* London: Linnean Society of London, Academic Press.

Sewertzoff, A.N. (1928). The head skeleton and muscles of Acipenser ruthenus. *Acta Zoologica* 9, 193–127.

Smith, K. K. (2001). Heterochrony revisited: the evolution of developmental sequences. *Biological Journal of the Linnean Society* 73, 169–186.

Smith, K.K. (2002). Sequence heterochrony and the evolution of development. *Journal of. Morphology* 252, 82–97.

Smith, K. K. (2003). Time's arrow: heterochrony and the evolution of development. *Int. J. Dev. Biol.* 47, 613-621.

Stundl, J., Pospisilova, A., Matějková, T., Psenicka, M., Bronner, M. E. & Cerny, R. (2020) Migratory patterns and evolutionary plasticity of cranial neural crest cells in ray-finned fishes. Developmental Biology (forthcoming)

Taylor, W. R. & Van Dyke, G. C. (1985). Revised procedures for staining and clearing small fishes and other vertebrates for bone and cartilage study. *Cybium*, 9, 107–119.

Figure legends:

Figure 1: Comparative development of chondrocranium among studied specimens.
Cleared and Alcian Blue stained skeletal preparations of (A-D) bichir, (E-H) sterlet, (I-L) gar, and (M-P) pike in ventral views. Stages are matched based on the first pre-cartilaginous structure formation within the neurocranium. There is preferential cartilaginous formation in the posterior part of the chondrocranium in bichir and sterlet as compared to progressed architecture of chondrocranium in gar and pike. Note prominent cement gland in gar (asterisk) temporarily blocking anterior development of chondrocranium. Abbreviations: bbc, basibranchial copula; bf, basicranial fenestra; cb, ceratobranchial; ch, ceratohyal; ect, lamina orbitonasalis; ep, ethmoid plate; hb, hypobranchial; hf, hypophyseal fenestra; hh, hypohyal; hm, hyomandibula; hs, hyosymplectic; ihy, interhyal; Mc, Meckel's cartilage; nt, notochord; oc, otic capsule; pch, parachordal; pq; palatoquadrate; qu, quadrate; sc; scleral cartilage; tc, trabecula cranii; tcom, trabecula communis; tm, taenia marginales; tpl, trabecular plate.

Figure 2: Regional comparison of sequential chondrocranium formation.
Scheme of chondrocranium element distribution within a neurocranium and viscerocranium during the Stage 1 identified on a base of the presence of pre-cartilaginous structure in the neurocranium (left box). Temporal sequence of cartilaginous region formation during development (right box). Stage 0 illustrates our suggestion of earlier development. Note different slope of trajectories characterizing pattern of chondrocranium formation with different representation of pre-cartilaginous (light blue) and cartilaginous (dark blue) regions during development. Dashed line marks prechordal-parachordal region boundary. Abbreviations: HY, hyoid arch region; MA, mandibular arch region; I-V; region of branchial arches.

Figure 3: Variation in a pattern formation of the first ossification.
Fluorescence microscopy images of cleared and Alizarin Red stained skeletal preparations of (A, A') bichir, (B, B') sterlet, (C, C') gar, and (D, D') pike. (A-D) Left lateral views of the head with detailed visualization of the first ossification in ventral (A', B') and lateral (C',D') orientation. Arrowheads point to the very first cranial ossification. Asterisks mark cement glands positioned at the anterior part of the head.

Figure 4: Comparative skeletal development during an early time period.
Fluorescence microscopy images of cleared and Alizarin Red stained skeletal preparations of (A-C) bichir, (D-F) sterlet, (G-I) gar, and (J-L) pike visualized in lateral orientation. White arrowheads point to the early aggregation of skeletal tissue connected to infraorbital lateral line on the head; black arrowheads point to the early aggregation of skeletal tissue connected to supratemporal lateral line on the head. Abbreviations: an; angular; br, branchiostegals; brr, branchiostegal rays; cb, ceratobranchial; cb5 ttp, tooth plate on ceratobranchial 5; ch, ceratohyal; cl, cleithrum; de, dentary; dpl, dermopalatine; dpt, dermopterotic; eb5 ttp, tooth plate on epibranchial 5; ecp, ectopterygoid; fr, frontal; hb1 ttp, tooth plate on hypobranchial 1; hm, hyomandibula; ifr ttp, infrapharyngobranchial toothplate; mx, maxillary; op, opercle; pa, parietal; par, prearticular; pas, parasphenoid; pm, posterior process of maxillary; pmx, premaxillary; ppt, palatopterygoid; prp, preopercle; pt, posttemporal; scl, supracleithrum; sop, subopercle.

Figure 5: Comparative skeletal development during a middle time period.
Fluorescence microscopy images of cleared and Alizarin Red stained skeletal preparations of (A-C) bichir, (D-F) sterlet, (G-I) gar, and (J-L) pike visualized in lateral orientation. White arrowheads point to the early aggregation of skeletal tissue connected to infraorbital lateral line on the head; black arrowheads point to the early aggregation of skeletal tissue connected to supraorbital lateral line on the head; black arrow points to the early aggregation of skeletal tissue connected to otic lateral line on the head; white arrow points to transition between frontal and premaxilla bone. Abbreviations: ba, branchial arch; brr, branchiostegal rays; cb, ceratobranchial; ch, ceratohyal; clv, clavicle; dpt, dermopterotic; drb, dorsal rostral bones; dsp, dermosphenotic; ect, ectopterygoid; fr, frontal; gu, gular; hb2 ttp, tooth plate on hypobranchial 2; hm, hyomandibula; ip, interopercle; j, jugal; lmx, lacrimo-maxillary; n, nasal; op, opercle; pa, parietal; pal, palatine; po, postorbital; pop, preopercle; pt, posttemporal; q, quadrate; qj, quadratojugal; rcb, rostral canal bones; ro, rostral; smx, supramaxilla; so, supraorbital; sop, subopercle; sym, symplectic; t escp, tubular extrascapular; vrb, ventral rostral bones.

Figure 6: Comparative skeletal development during a late time period.
Fluorescence microscopy images of cleared and Alizarin Red stained skeletal preparations of (A, B) bichir, (C, D) sterlet, (E, F) gar, and (G, H) pike visualized in lateral orientation. White arrowheads point to edges of spiracular bone series; black arrowhead points to the first ossifying structure of spiracular bone series. Abbreviations: brr, branchiostegal rays; brb, border rostral bones; ch, ceratohyal; ep, epiotic; escp, extrascapular; fr, frontal; lac, lacrimal; na, nasal; pa, parietal; ro, rostral; pt, posttemporal; sio, subinfraorbital; sop, subopercle; spo, sphenotic.

Figure 7: Regional comparison of sequential osteocranium formation.
The panel summarizes variation of developmental timing of cranial region ossification. Ossification sequence of 8 defined cranial regions among bichir, sterlet, gar, and pike is plotted against early, middle, and late time period.

Figure 8: Comparison of timing of cranial chondrification and ossification.
The timing of pre-cartilaginous (grey), cartilaginous (blue), and bony (red) developmental period varies among species. Normalizing developmental stages is based on hatching. Note that there is no pre-cartilaginous period of development in pike (the first cartilage appears in a time of hatching).

Figure. 9: Altered patterns of *Col10a1* gene expression among studied lineages.
(A) Panel summarizes relative pattern of *Col10a1* expression during larval skeletogenesis in correlation with chondrocranium (blue line) and osteocranium (red line) development. Normalizing developmental stages is based on hatching. (B–I) Whole-mount *in situ* hybridization mapping onset and offset of *Col10a1* gene expression in (B, C) bichir, (D, E) sterlet, (F, G) gar, and (H, I) pike visualized in (B, E, G, H, I) lateral and ventral (C, D, F, G) orientation. Abbreviations: cb, ceratobranchial; ch, ceratohyal; cl, cleithrum; de, dentary; dpl, dermopalatine; mx, maxilla; op, opercle; pmx, premaxilla; scl, supracleithrum; sop, subopercle; vo, vomer.

Figure 10: Comparative visualization of tissue density development.
The lateral view on skulls of (A–F) bichir, (G–K) sterlet, (L–P) gar, and (Q–V) pike with an illustration of density of bony tissue. Stages are matched based on the first cranial bone ossification. Tissue density is mapped in a false color on a spectrum ranging from less dense (cool colors) to more dense (warm color). White arrowhead points to the first identified cranial structures in gar visible in magnification.

Figure 11: Quantitative analysis of bone density development during skull ossification.
Comparison of growth trajectories based on micro-CT scanning revealed differences in proportion of cranial bone density during development. Tissue density is mapped in a false color on a spectrum ranging from less dense (cool colors) to more dense (warm color). Grey colors mark predicted pattern according to mathematical calculation.

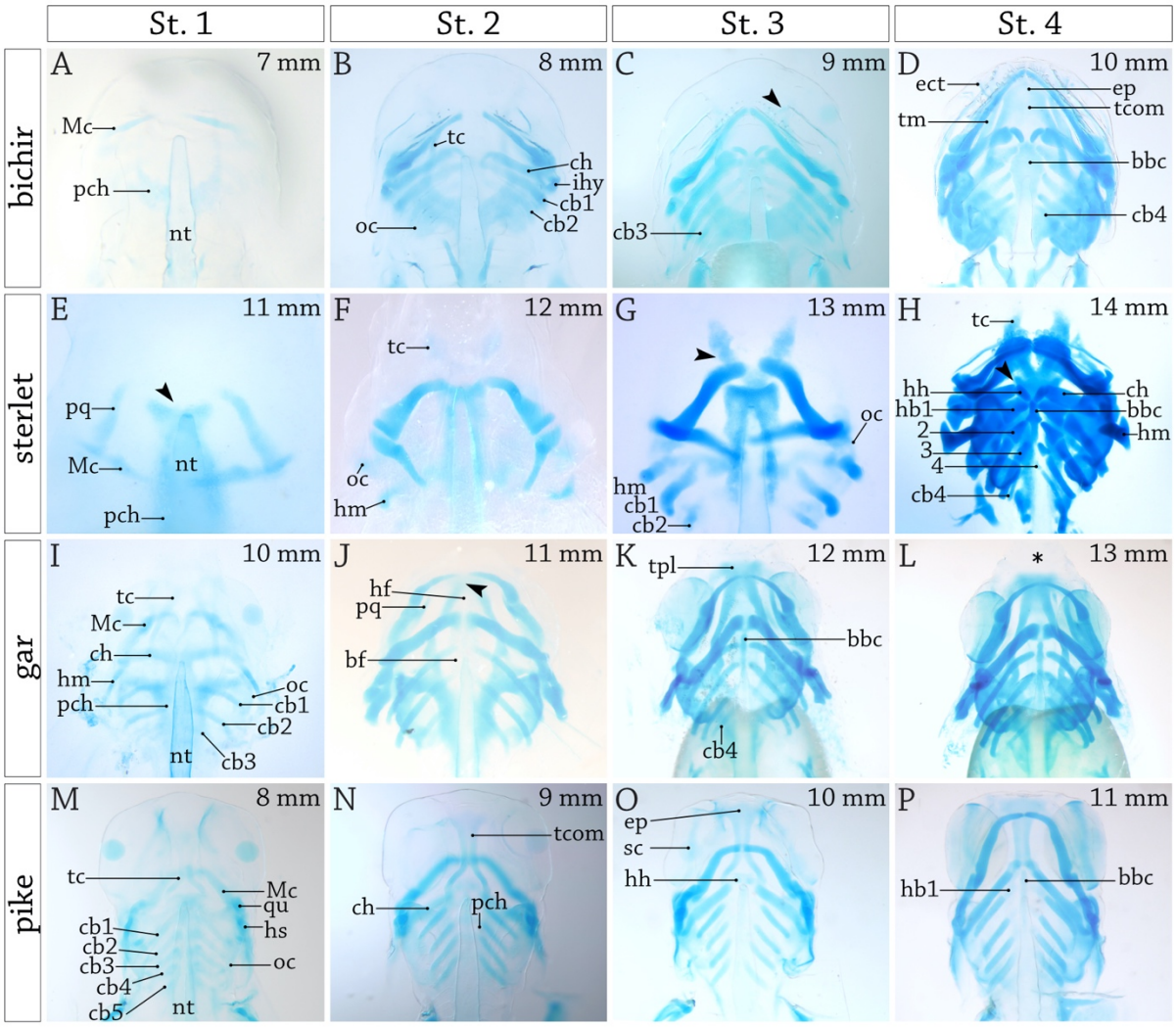
St. 1
St. 2
St. 3
St. 4
bichir
sterlet
gar
pike
A 7 mm
Mc
pch
nt
B 8 mm
tc
ch
ihy
cb1
cb2
oc
C 9 mm
cb3
D 10 mm
ect
ep
tcom
tm
bbc
cb4
E 11 mm
pq
Mc
nt
pch
F 12 mm
tc
oc
hm
G 13 mm
oc
hm
cb1
cb2
H 14 mm
tc
hh
ch
hb1
bbc
2
hm
3
4
cb4
I 10 mm
tc
Mc
ch
hm
pch
oc
cb1
cb2
nt
cb3
J 11 mm
hf
pq
bf
K 12 mm
tpl
bbc
cb4
L 13 mm
*
M 8 mm
tc
Mc
qu
cb1
hs
cb2
cb3
oc
cb4
cb5
nt
N 9 mm
tcom
ch
pch
O 10 mm
ep
sc
hh
P 11 mm
hb1
bbc

Fig. 1

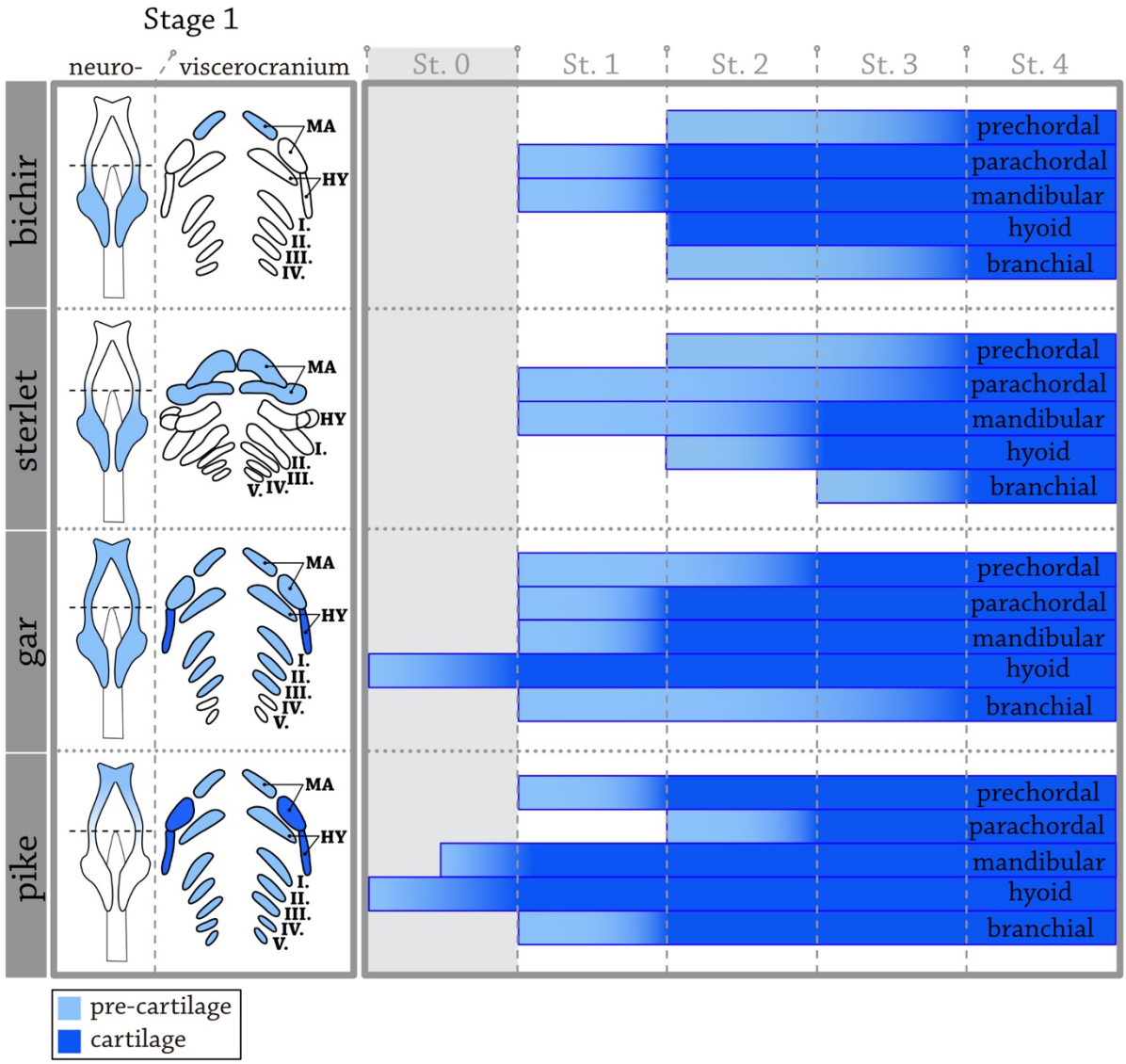
Stage 1
neuro-
viscerocranium
St. 0
St. 1
St. 2
St. 3
St. 4
bichir
sterlet
gar
pike
MA
HY
I.
II.
III.
IV.
V.
prechordal
parachordal
mandibular
hyoid
branchial
pre-cartilage
cartilage

Fig. 2

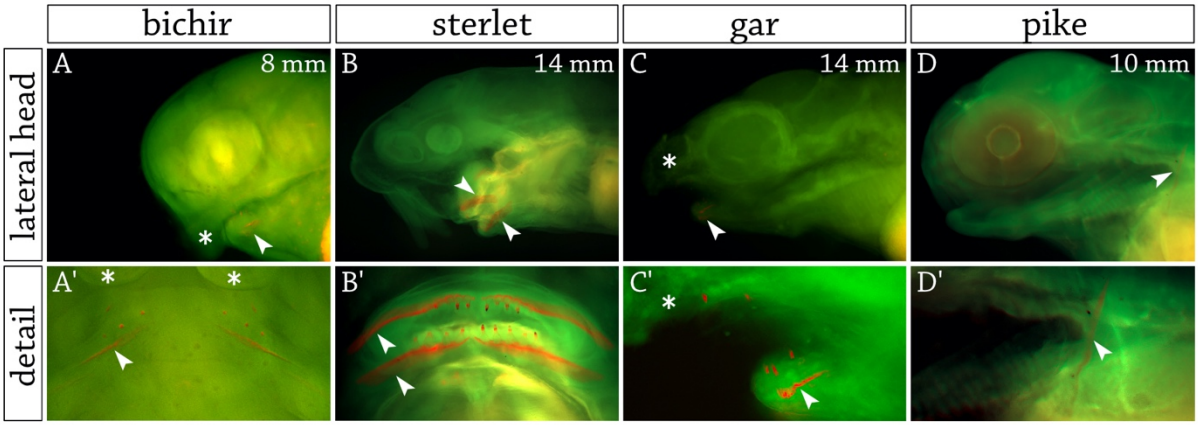
bichir
sterlet
gar
pike
lateral head
detail
A
8 mm
B
14 mm
C
14 mm
D
10 mm
A'
B'
C'
D'

Fig. 3

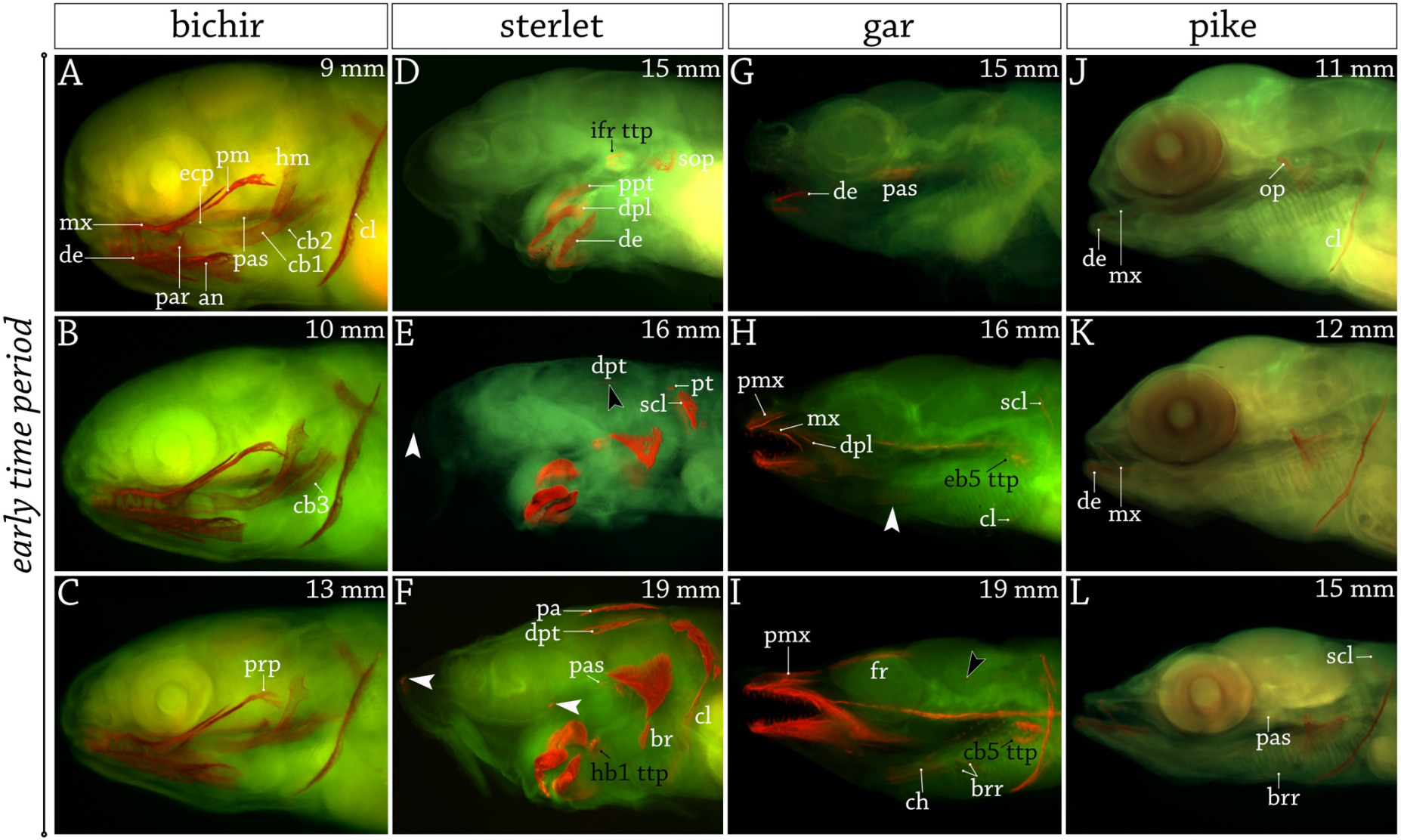
bichir
sterlet
gar
pike
early time period
A
9 mm
ecp
pm
hm
mx
de
par
an
pas
cb2
cb1
cl
D
15 mm
ifr ttp
sop
ppt
dpl
de
G
15 mm
de
pas
J
11 mm
op
cl
de
mx
B
10 mm
cb3
E
16 mm
dpt
pt
scl
H
16 mm
pmx
mx
dpl
scl
eb5 ttp
cl
K
12 mm
de
mx
C
13 mm
prp
F
19 mm
pa
dpt
pas
cl
br
hb1 ttp
I
19 mm
pmx
fr
cb5 ttp
brr
ch
L
15 mm
scl
pas
brr

Fig. 4

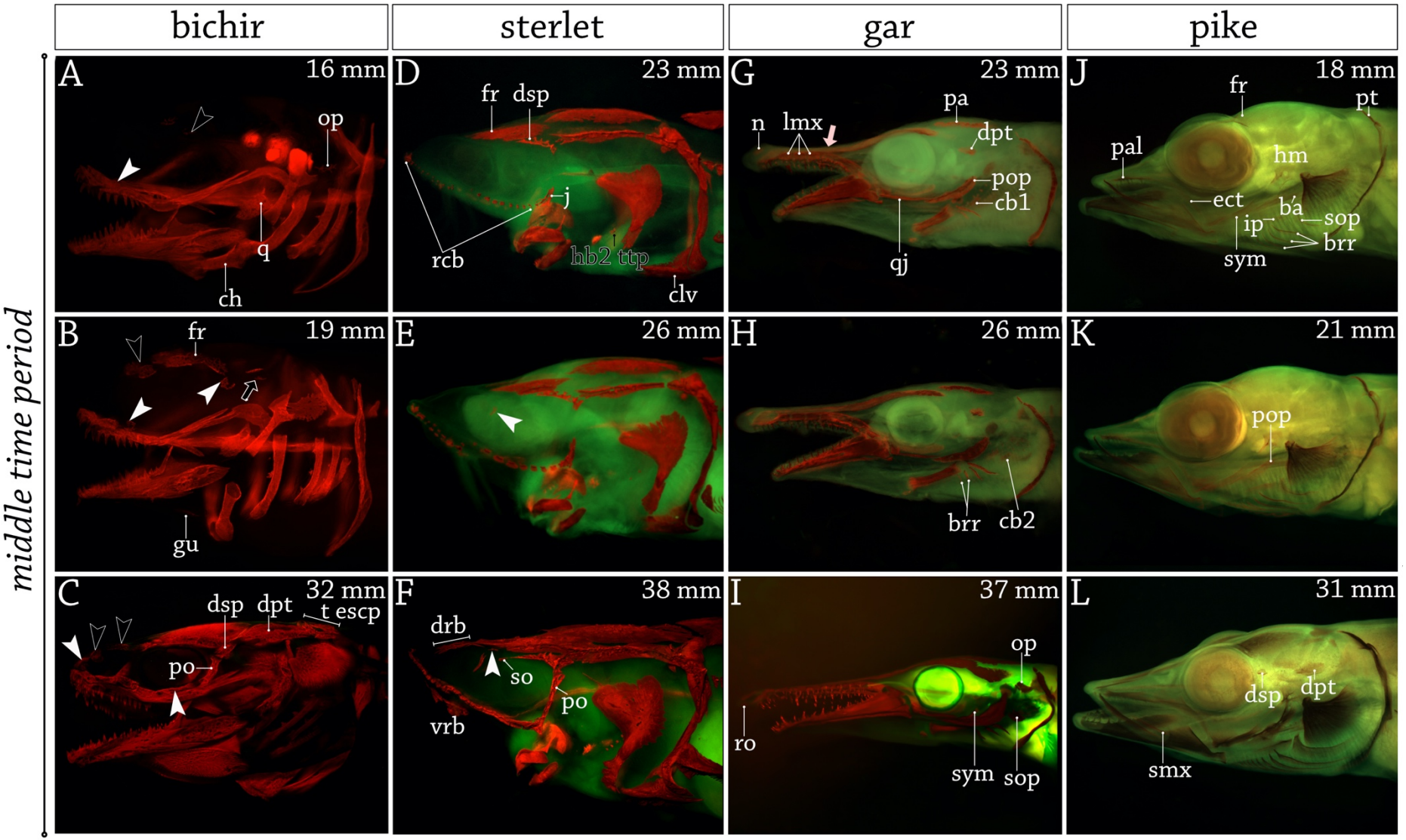
bichir
sterlet
gar
pike
middle time period
A
16 mm
op
q
ch
D
23 mm
fr
dsp
j
rcb
hb2
ttp
clv
G
23 mm
n
lmx
pa
dpt
pop
cb1
qj
J
18 mm
fr
pt
pal
hm
ect
ba
ip
sop
brr
sym
B
19 mm
fr
gu
E
26 mm
H
26 mm
brr
cb2
K
21 mm
pop
C
32 mm
dsp
dpt
t escp
po
F
38 mm
drb
so
po
vrb
I
37 mm
op
ro
sym
sop
L
31 mm
dsp
dpt
smx

Fig. 5

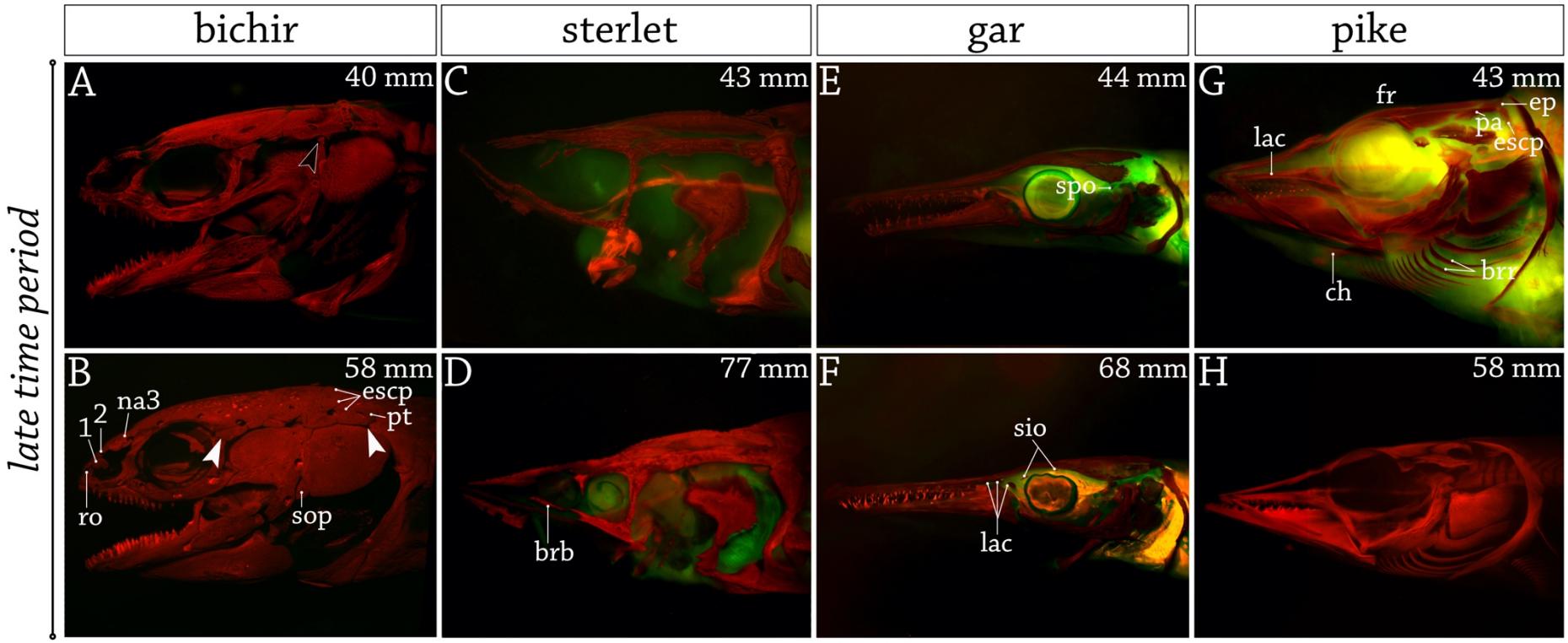
bichir
sterlet
gar
pike
late time period
A
40 mm
C
43 mm
E
44 mm
G
43 mm
fr
ep
pa
escp
lac
spo
brr
ch
B
58 mm
escp
pt
na3
1
2
ro
sop
D
77 mm
brb
F
68 mm
sio
lac
H
58 mm

Fig. 6

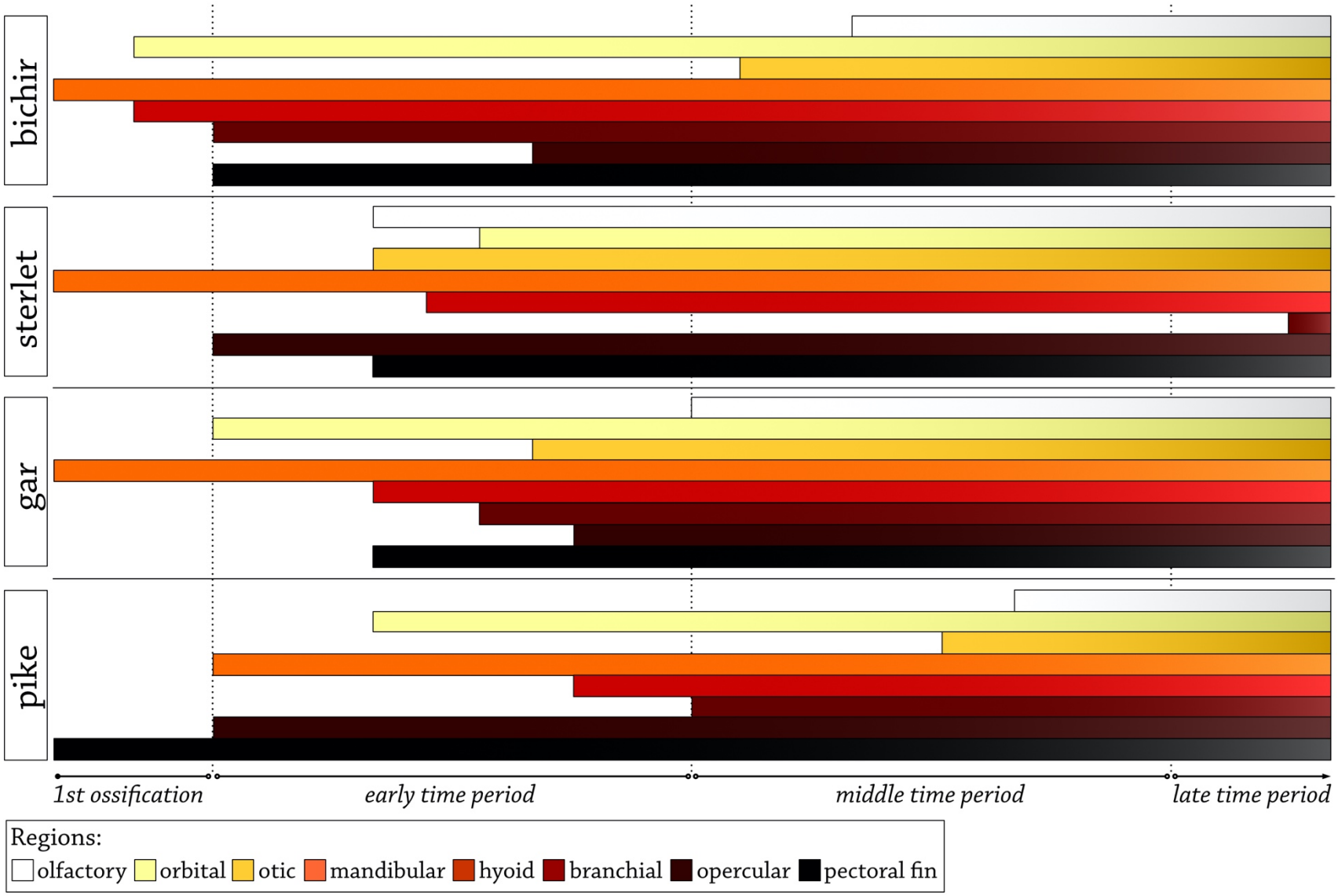
bichir
sterlet
gar
pike
1st ossification
early time period
middle time period
late time period
Regions:
olfactory
orbital
otic
mandibular
hyoid
branchial
opercular
pectoral fin

Fig. 7


pre-cartilage
cartilage
bone
bichir
sterlet
gar
pike
HATCHING

Fig. 8

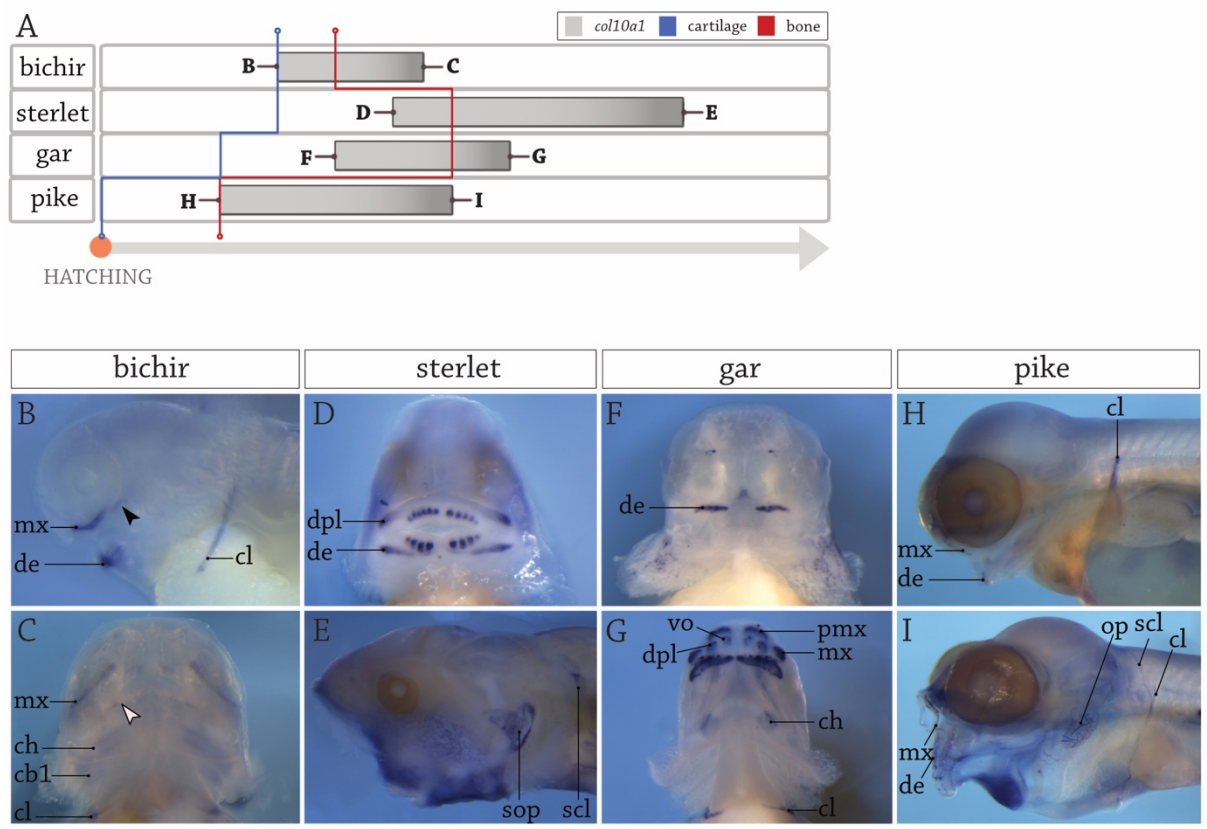
A
col10a1
cartilage
bone
bichir
sterlet
gar
pike
B
C
D
E
F
G
H
I
HATCHING
bichir
sterlet
gar
pike
mx
de
cl
dpl
de
de
cl
mx
de
mx
ch
cb1
cl
sop
scl
vo
dpl
pmx
mx
ch
cl
op
scl
cl
mx
de

Fig. 9

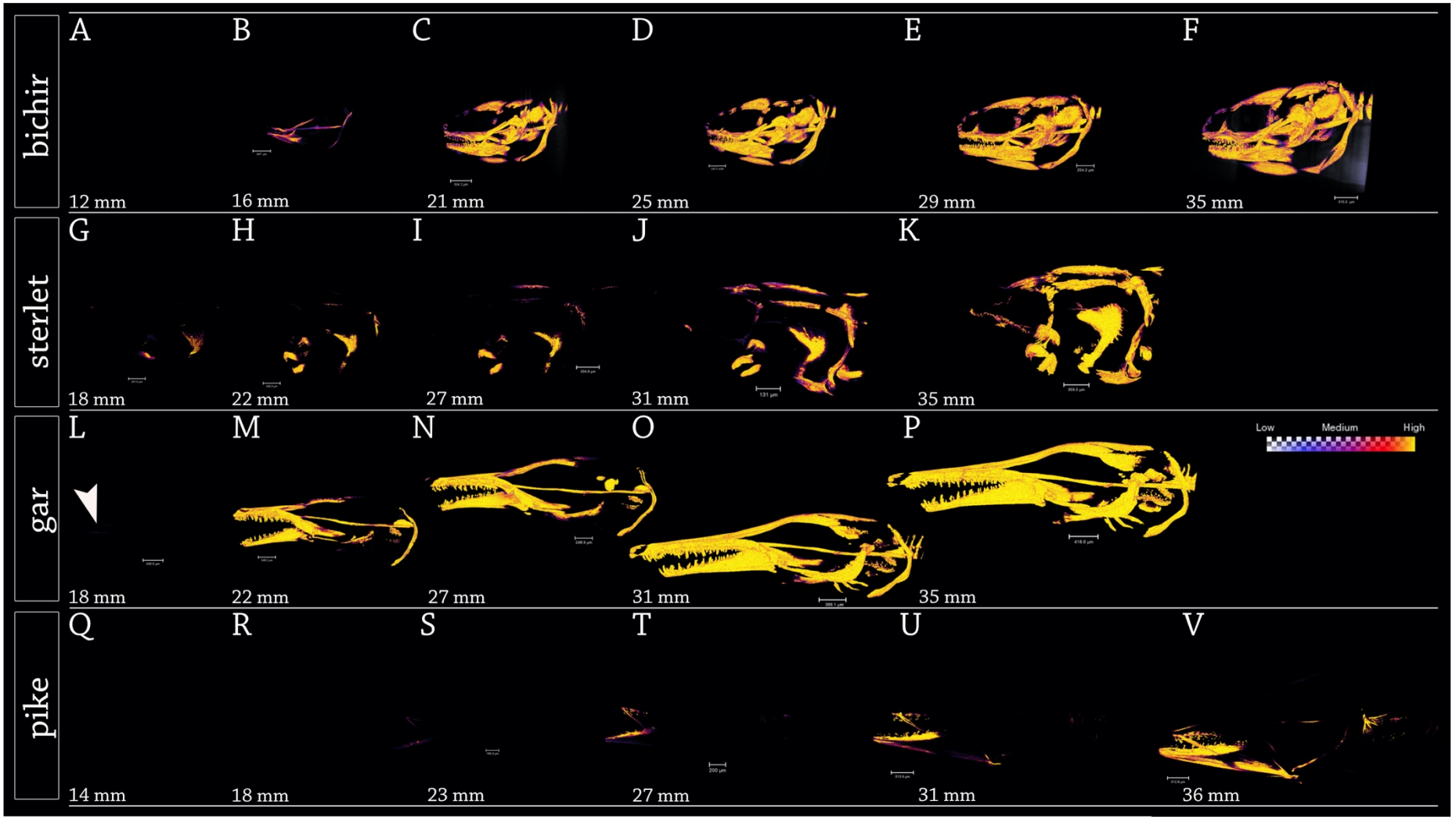
bichir
A
B
C
D
E
F
12 mm
16 mm
21 mm
25 mm
29 mm
35 mm
sterlet
G
H
I
J
K
18 mm
22 mm
27 mm
31 mm
35 mm
gar
L
M
N
O
P
Low
Medium
High
18 mm
22 mm
27 mm
31 mm
35 mm
pike
Q
R
S
T
U
V
14 mm
18 mm
23 mm
27 mm
31 mm
36 mm

Fig. 10

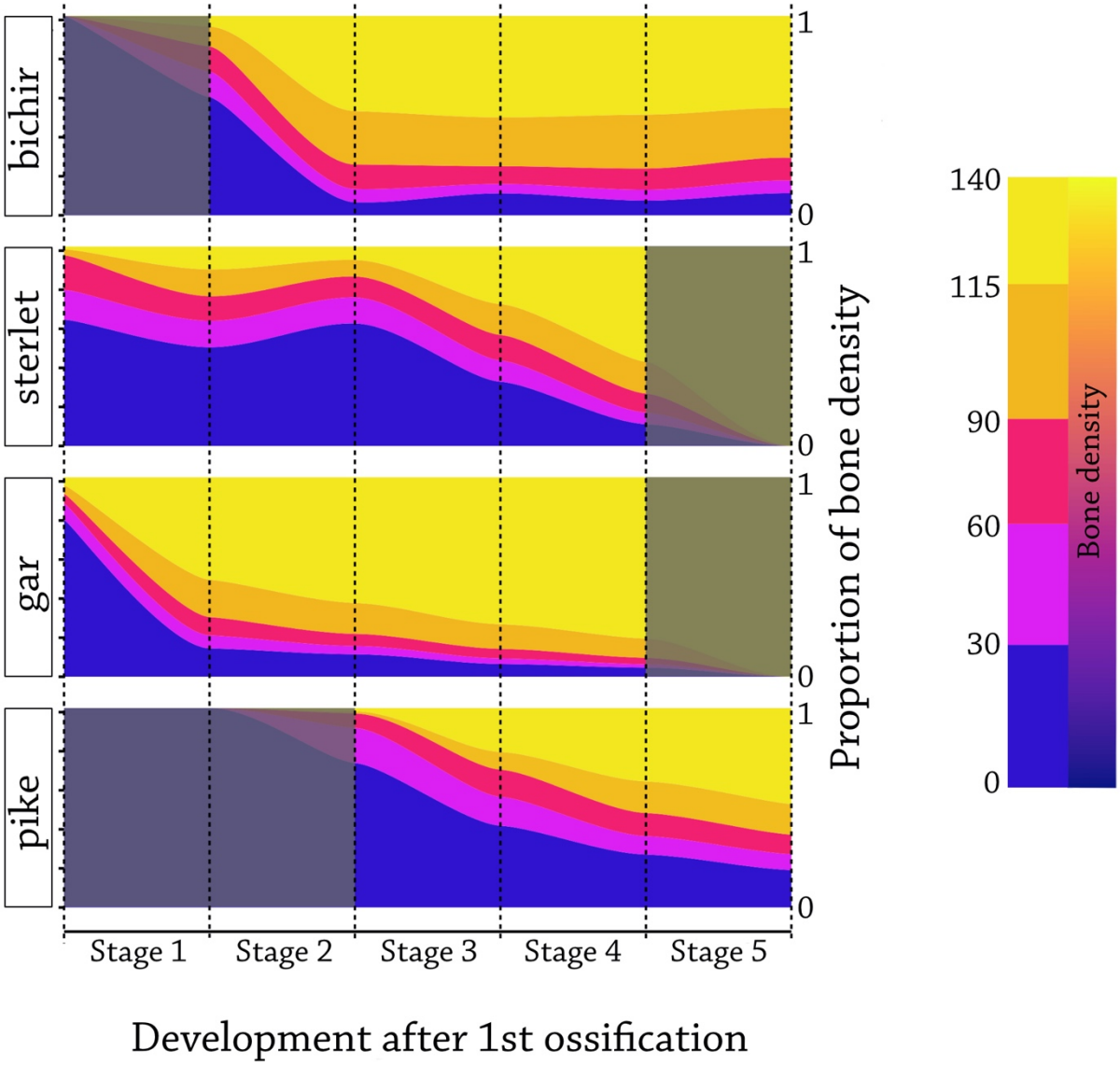
bichir
sterlet
gar
pike
1
0
Proportion of bone density
140
115
90
60
30
0
Bone density
Stage 1
Stage 2
Stage 3
Stage 4
Stage 5
Development after 1st ossification

Fig. 11

III. Rizzato PP*, **Pospisilova A***, Hilton EJ & Bockmann FA (2020) Ontogeny and homology of cranial bones associated with lateral-line canals of the Senegal Bichir, Polypterus senegalus (Actinopterygii: Cladistii: Polypteriformes), with a discussion on the formation of lateral-line canal bones in fishes. *Journal of Anatomy* 00, 1–29.

* stejný příspěvek autorů

IF (2019) = 2,013

Received: 23 March 2019 | Revised: 13 March 2020 | Accepted: 19 March 2020

DOI: 10.1111/joa.13202

ORIGINAL ARTICLE

ANATOMICAL SOCIETY Journal of Anatomy WILEY

Ontogeny and homology of cranial bones associated with lateral-line canals of the Senegal Bichir, *Polypterus senegalus* (Actinopterygii: Cladistii: Polypteriformes), with a discussion on the formation of lateral-line canal bones in fishes

Pedro P. Rizzato[1,2*] | **Anna Pospisilova**[3*] | **Eric J. Hilton**[4] | **Flávio A. Bockmann**[1,2]

[1]Laboratório de Ictiologia de Ribeirão Preto (LIRP), Departamento de Biologia, FFCLRP, Universidade de São Paulo, Ribeirão Preto, Brazil

[2]Programa de Pós-Graduação em Biologia Comparada, FFCLRP, Universidade de São Paulo, Ribeirão Preto, Brazil

[3]Department of Zoology, Charles University, Prague, Czech Republic

[4]Department of Fisheries Science, Virginia Institute of Marine Sciences, William & Mary, Gloucester Point, VA, USA

Correspondence
Pedro P. Rizzato, Laboratório de Ictiologia de Ribeirão Preto, Departamento de Biologia, Faculdade de Filosofia, Ciências e Letras de Ribeirão Preto, Universidade de São Paulo, Avenida Bandeirantes, 3900, Bairro Monte Alegre, Ribeirão Preto, São Paulo 14040-901, Brazil .
Email: rizzatopp@gmail.com

Funding information
Coordenação de Aperfeiçoamento de Pessoal de Nível Superior, Grant/Award Number: 001; Grantová Agentura, Univerzita Karlova, Grant/Award Number: 1448514 and 640016; Fundação de Amparo à Pesquisa do Estado de São Paulo, Grant/Award Number: 2014/10849-6 and 2016/06677-0

Abstract

The association between lateral-line canals and skull bones in fishes has been the subject of several studies and raised a series of controversies, particularly with regard to the hypothesized role of lateral-line organs (i.e. neuromasts) in osteogenesis and the consequences for hypotheses of homology of the bones associated with lateral-line canals. Polypteridae, a group of freshwater fishes that occupies a key phylogenetic position as the most basal extant lineage of ray-finned fishes (Actinopterygii), provides an interesting model for the study of the relationships between lateral-line canals and skull bones. We describe the development of bones associated with lateral-line canals in the Senegal Bichir, *Polypterus senegalus*, and use these data to re-address previous hypotheses of homology of skull bones of polypterids. We demonstrate that the lateral-line canals constitute a separate component of the dermatocranium that may interact with a membranodermal component, thereby forming compound bones in the adult. Differences in the interactions between these components determine the characteristics of the development of each independent bone in the skull of adult *P. senegalus*. Our results shed light on long-standing controversies about the identity of skull bones such as the rostral, preopercle, and sphenotic in Polypteridae, and suggest the presence of an ancestral two-component pattern of formation of bones associated with lateral-line canals in bony fishes. These findings reveal the need to re-address previous hypotheses of homology of bones associated with lateral-line canals in different groups of bony fishes, especially fossil taxa.

KEYWORDS

Calamoichthys, development, *Erpetoichthys*, laterosensory system, neuromast

1 | INTRODUCTION

> *'I desire to mention, at this point, that hitherto the relation of the mucous canals to the bones of the cranium have hardly been given a thought, and yet they deserve a closer study, as these relations are very constant, and in questionable cases they can be used to determine doubtful homologies.'*
>
> R. W. Shufeldt (1847: p. 6)

The laterosensory or lateral-line system is a mechanosensory system present in all major lineages of craniates, including agnathans,

*These authors contributed equally to this work.

chondrichthyans, actinopterygians, non-tetrapod sarcopterygians, and larval and aquatic adult lissamphibians (Coombs et al., 1988; Northcutt, 1989; Webb, 1989; 2014). The system is composed of small epidermal receptor organs called neuromasts. These are innervated by a specific set of lateral-line nerves and respond to mechanical stimuli produced by flows in the water (Northcutt, 1989; Puzdrowski, 1989; Northcutt and Bemis, 1993; Piotrowski and Northcutt, 1996; Northcutt et al., 2000). These receptor organs are of two basic types, superficial and canal neuromasts, which define two distinct sensory submodalities characterized by different morphological, topographical and functional characteristics (Chagnaud and Coombs, 2014; McHenry and Liao, 2014; van Netten and McHenry, 2014; Webb, 2014). As the name suggests, superficial neuromasts (SNs) are distributed on the surface of the head and body, and are the only type of neuromast present in jawless fishes and in larval and aquatic adult amphibians (Webb, 2014). Canal neuromasts (CNs), in turn, are located in the epithelium lying on the bottom of canals formed when neuromasts are enclosed in a stereotyped process (Tarby and Webb, 2003; Webb and Shirey, 2003; Bird and Webb, 2014; Wada et al., 2014; Webb, 2014; Pastana et al., 2019). Lateral-line canals are distributed in a consistent fashion on the body and especially on the head of fishes, which allows comparisons across even distantly related taxa, including fossils (Garman, 1888; Allis, 1934; Stensiö, 1947; Webb, 1989; Webb and Northcutt, 1997; Rizzato and Bichuette, 2017; Pastana et al., 2019).

In bony fishes, lateral-line canals are usually associated with dermatocranial bones on the head and scales on the body (Tarby and Webb, 2003; Webb and Shirey, 2003; Wada et al., 2014; Webb, 2014). In the skull, the canals are usually associated with specific bones, in a generally conserved association that was noticed in early studies on comparative fish anatomy (e.g. Shufeldt, 1847; Vrolik, 1873; Walther, 1882; Sagemehl, 1884; Allis, 1889; 1898, Collinge, 1894). Some authors, such as Shufeldt (1847) and Sagemehl (1884), suggested that the association between lateral-line canals and skull bones might be useful as a basis for addressing hypotheses of bone homologies across taxa. The proposal was more formally presented by Allis (1898: 430), who stated: 'it is highly probable, though certainly not as yet established, that a bone or a part of a bone developed in any particular fish in relation to a particular part of the lateral-line system is always the homologue of the bone, or part of a bone, developed in relation to the same part of the lateral-line system in any other fish or animal'. Since that time, the relationship between lateral-line canals and skull bones has been the subject of several studies and has raised many controversies, especially regarding the role of lateral-line organs in osteogenesis (discussed in Tarby and Webb, 2003 and Pastana, 2014). Some authors (e.g. Pehrson, 1922) suggested that the neuromasts might have a causal relationship in the formation of some of the skull bones, whereas others disagreed (e.g. De Beer, 1937, Moy-Thomas, 1941). A somewhat compromising proposal was presented by Graham-Smith (1978) who stated that the lateral line could act only to determine the precise positions and influence the timing of the intramembranous ossifications of the dermatocranial bones, which would nevertheless develop even in the absence of neuromasts. In recent years, descriptive developmental studies and the use of new imaging technologies and methodologies (e.g. Tarby and Webb, 2003; Webb and Shirey, 2003; Nakae et al., 2012; Wada et al., 2014; Becker et al., 2016; Edgley and Genner, 2019) have improved the study of the lateral-line system and added new information that can be incorporated in the investigation of the relationships between lateral-line canals and skull bones.

Polypteridae (Cladistii: Polypteriformes) is a group of freshwater and brackish water fishes that includes 14 valid species (Eschmeyer et al., 2019; Moritz and Britz, 2019) in two genera, *Calamoichthys* Smith 1866 (the name *Erpetoichthys* Smith 1866, commonly used in recent years, is a junior synonym of *Calamoichthys*, see Rizzato and Bockmann, 2017) and *Polypterus* La Cepède 1803. *Calamoichthys* is monotypic, represented only by the African Reedfish, *Calamoichthys calabaricus* Smith 1866, whereas *Polypterus* includes 13 extant species (Eschmeyer et al., 2019; Moritz and Britz, 2019). Modern polypterids are distributed exclusively in tropical rivers and estuaries of Africa, although some fossils attributed to the group are known from isolated fin spines and scales from the Maastrichtian (Late Cretaceous) of Bolivia and Brazil (Gayet and Meunier, 1991; 1992). A few more complete specimens are known from the Late Cretaceous (Cenomanian) and Late Miocene of Africa (Dutheil, 1999; Gayet et al., 2003; Otero et al., 2006). Polypteridae is considered to be the sister group of the clade formed by all the remaining extant actinopterygians (Patterson, 1982; Giles et al., 2017). Because of this key phylogenetic position, and because of the generally primitive nature of their skull, the group has attracted the attention of some of the most renowned fish anatomists, including those interested in the interrelationship between lateral-line canals and bones (e.g. Allis, 1900; 1904; 1922; 1934; Pehrson, 1947; 1958; Jollie, 1984a). The development of lateral-line placodes in the head of the Senegal Bichir, *Polypterus senegalus* Cuvier 1829, was described by Thomopoulos (1969; 1970), and the development of the CNs and SNs in this species was described by Pehrson (1958), Jollie (1984a) and Diedhiou and Bartsch (2009). Pehrson (1947; 1958) and Jollie (1984a), relying on rare developmental series of polypterids, also provided descriptions of the development of dermatocranial and endochondral bones in polypterids in order to analyze the relationships between the lateral-line canals and the head skeleton. Despite this long history of study, some controversies remained, especially on the nature and homology of bones regarded to be of compound origin, such as the rostral, preopercle, and sphenotic. A new developmental series resulting from captive-bred *P. senegalus*, as well as new information about the development and innervation of the lateral-line system in this species (Piotrowski and Northcutt, 1996; Diedhiou and Bartsch, 2009), provided the opportunity to revisit these questions. The main objectives of the present work are to describe the development of bones associated with lateral-line canals in the skull of *P. senegalus*, and to use these data to comment on the formation of these bones and the consequences for advancing hypotheses of bone homologies for polypterids and across bony fishes.

2 | MATERIALS AND METHODS

2.1 | Specimen sources and rearing

The material analyzed (see list below and Table 1) includes a developmental series of *P. senegalus* produced at the Department of Zoology of the Charles University in Prague and deposited at the Natural History Museum in Prague (JNMP). The developmental series was supplemented by larger juvenile and adult specimens deposited in the Nunnally Ichthyology Collection at the Virginia Institute of Marine Sciences (VIMS), in the Laboratório de Ictiologia de Ribeirão Preto, Universidade de São Paulo (LIRP), and in the Division of Fishes, National Museum of Natural History, Smithsonian Institution (USNM).

The rearing and staining procedures followed the guidelines of the institutional animal care and use committee of the Charles University in Prague for the use of embryonic material, following Pospisilova (2015). The spawning took place at the Department of Zoology, Charles University in Prague, following water stimulation during the breeding season, from October to April. Fertilized eggs were collected and kept at 28°C until the animals reached the size required for analysis. Larval specimens at appropriate sizes were anesthetized by an overdose of MS-222 (Serva), fixed in 4% paraformaldehyde, and stored at 4°C. The total body size (total length, Table 1) was measured in fixed fish as the distance from the tip of the head to the tip of the caudal fin.

TABLE 1 Developmental material of *Polypterus senegalus* analyzed (JNMP P6d 15/2019)

Total length (mm)	Vial catalog number	Alcian Blue	Alizarin Red
8	P6d 15/2019_1	–	X
8.5	P6d 15/2019_1	–	X
8.8	P6d 15/2019_1	–	X
9	P6d 15/2019_2	–	X
10	P6d 15/2019_3	–	X
11	P6d 15/2019_4	–	X
12	P6d 15/2019_5	–	X
13	P6d 15/2019_6	–	X
14	P6d 15/2019_7	–	X
15	P6d 15/2019_8	–	X
16	P6d 15/2019_9	–	X
17	P6d 15/2019_10	–	X
18	P6d 15/2019_11	–	X
19	P6d 15/2019_12	–	X
21	P6d 15/2019_13	–	X
22	P6d 15/2019_14	X	X
23	P6d 15/2019_15	–	X
25	P6d 15/2019_16	X	X
29	P6d 15/2019_17	X	X
32	P6d 15/2019_18	X	X
33	P6d 15/2019_19	X	X
34	P6d 15/2019_20	X	X
39	P6d 15/2019_21	X	X
40	P6d 15/2019_22	X	X
58	P6d 15/2019_23	X	X
61	P6d 15/2019_24	X	X

2.2 | Preparation and imaging

To avoid decalcification by acetic acid, most stages, especially the smaller ones, were stained only with Alizarin Red. The specimens were bleached in a 2% potassium hydroxide, 3% hydrogen peroxide (1:1) solution under a lamp to accelerate the process. Bones were stained overnight in a solution of 8 ml 0.5% potassium hydroxide with 1 ml of stock solution of Alizarin Red (0.7 g Alizarin Red S [Sigma] in 380 ml 96% ethanol). The specimens were rinsed several times in 0.5–2% potassium hydroxide (according to size), and the soft tissue was cleared in increasing concentrations of glycerol. Samples were stored in 100% glycerol at 4°C. Larger specimens were cleared and double-stained with Alcian Blue and Alizarin Red according to the procedures described by Taylor and Van Dyke (1985). The skulls were observed under a fluorescent stereomicroscope (Zeiss Lumar.V12) using the fluorescent filter Alexa 568 (mineralized tissue) and GFP (surrounding tissue). Images were stacked with the software AxioVision 4.0, and diagrammatic illustrations were prepared based on the images to help clarify the anatomical descriptions and interpretations.

The position of SNs and canal pores on the skin was analyzed using juvenile and adult specimens not belonging to the developmental series; these specimens were previously fixed in 10% formalin and preserved in 70% ethanol. Double-stained (ds) and cleared and double-stained (c&s) juvenile and adult specimens of *P. senegalus* in addition to those in the developmental series were used to analyze the anatomy of the bones and canals in later stages of ontogeny. The specimens were prepared following the procedures described by Datovo and Bockmann (2010) and Taylor and Van Dyke (1985), respectively. One three-dimensional reconstruction of µCT data of the skull of an adult specimen of *P. senegalus* (LIRP 10236, 190.7 mm SL) was used for a more detailed analysis of the course of the canals and their association with dermal bones of the skull (Figure 1). The model was generated using GE Phoenix v|tome|x m equipment at the GE Brazil Technology Center (Rio de Janeiro, RJ, Brazil), analyzed with the software Amira, at VIMS, and VGStudio 3.0, at the Center for Documentation of Biodiversity of the Department of Biology, Faculdade de Filosofia, Ciências e Letras de Ribeirão Preto (CDB, FFCLRP-USP).

2.3 | Terminology

A standardized terminology for polypterid skull bones incorporating new hypotheses of homology, including the ones advanced in

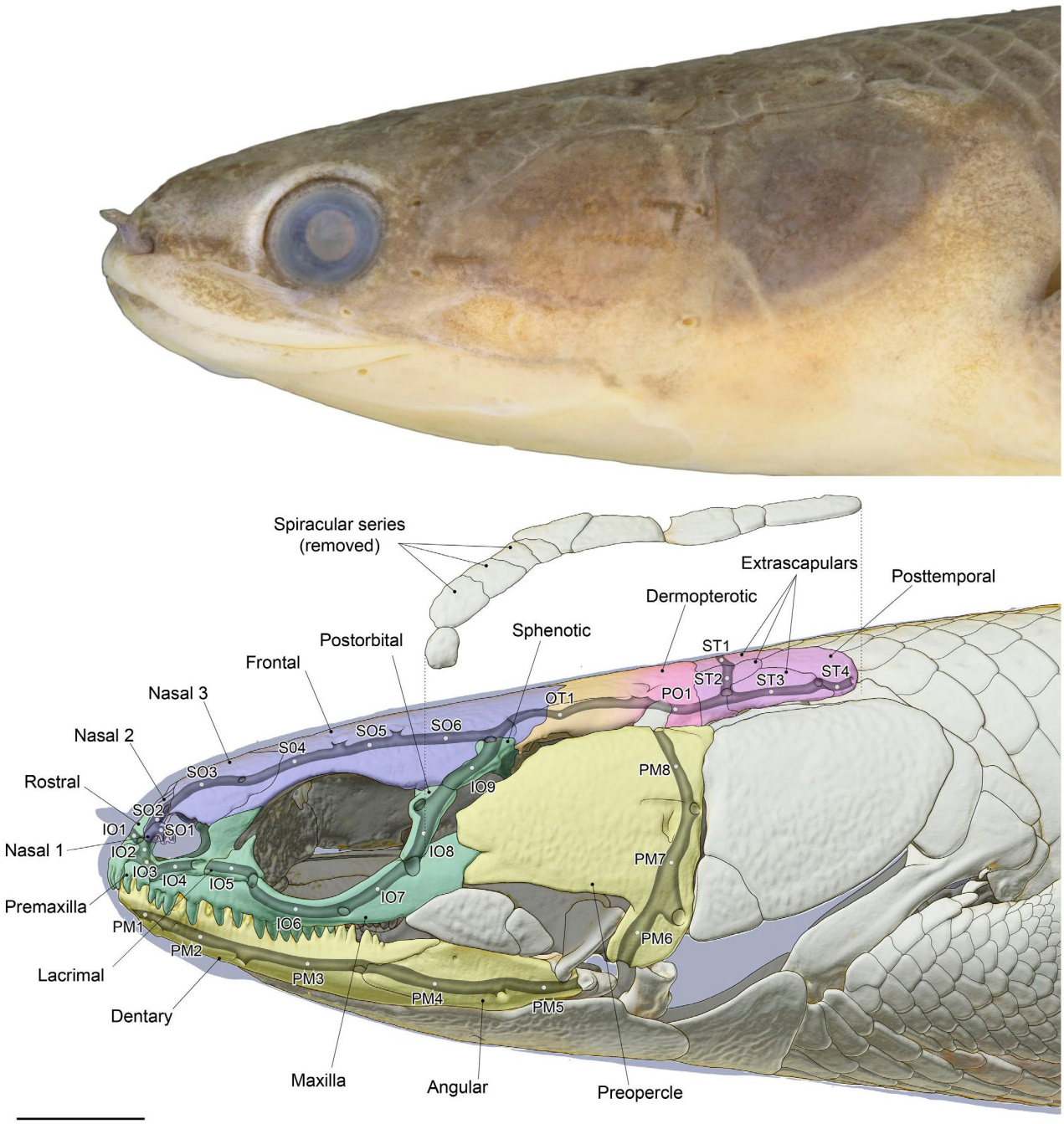

FIGURE 1 Lateral view of a 3D-reconstructed model of the head of an adult specimen of *Polypterus senegalus*, LIRP 10236, 190.7 mm SL, showing the course of the lateral-line canals and the approximate position of the canal neuromasts (white dots). Bones are colored according to the lateral-line canals to which they are associated: blue = supraorbital; green = infraorbital; yellow = preoperculomandibular; orange = otic; pink = postotic; purple = supratemporal. IO1-9 = infraorbital CNs 1–9. OT1 = otic CN. PM1–8 = preoperculomandibular CNs 1–8. PO1 = postotic CN. SO1–6 = supraorbital CNs 1–6. ST1–4 = supratemporal CNs 1–4. Scale bar: 5 mm

the present work, is being prepared and will be published in another work (Rizzato et al., in prep.). In the present work, we follow the terminology presented by Claeson et al. (2007; see Figure 1), except for the intertemporo-supratemporal, here named dermopterotic following the terminology used for other non-teleostean actinopterygians (e.g. Patterson, 1973; 1975; Grande and Bemis, 1991; 1998; Grande, 2010; Hilton et al., 2011), and the dermosphenotic, here named sphenotic (see Discussion). The canals were identified according to the innervation of the associated CNs. Information about number, position, innervation, and development of CNs and SNs in polypterids was obtained from direct observation of specimens and from the literature (Allis, 1900; 1904; 1922;

1934; Stensiö, 1947; Pehrson, 1947; 1958; Jollie, 1984a; Piotrowski and Northcutt, 1996; Diedhiou and Bartsch, 2009).

In the text and figures, the CNs are identified with uppercase abbreviations referring to the respective line of CNs (SO = supraorbital; IO = infraorbital; PM = preoperculomandibular; OT = otic; PO = postotic; ST = supratemporal), and numbered sequentially in an antero-posterior direction (SO1, SO2, SO3, etc.). The membranodermal bones with which the tubular lateral-line ossifications are associated are referred to as the name of the bone in the adult followed by the expression *sensu stricto* (abbreviated as *s.s.*). For example, the dentary in the adult is formed by a membranodermal bone, the dentary *sensu stricto* (or dentary *s.s.*), plus the tubular ossifications formed in association with the three most anterior preoperculomandibular CNs, PM1, PM2, and PM3 (see Discussion).

2.4 | Specimens examined

Polypterus senegalus: JNMP P6d 15/2019 (for catalog numbers of individual vials see Table 1), *n* = 26, 8–61 mm TL, c&s, developmental series, hatchery specimens (Department of Zoology, Charles University in Prague). VIMS 35599, *n* = 1, 61.4 mm SL, aquarium specimen. LIRP 10236, *n* = 1, 190.7 mm SL, Federal Democratic Republic of Ethiopia, Gambela Hizboch Kilil, Alwero River at Abobo, 3 Oct 2008, Friel, J., Lavoué, S., Sullivan J., Tesfaye. LIRP 13550, *n* = 1, 115 mm SL, aquarium specimen, 8 May 2016. USNM 224817, *n* = 2 (1 ds), 224–232 mm SL, Mali, Mopti, Niger River, 15 Sep 1980, Carberry, W. L. USNM 395402, *n* = 3 (1 ds), 170.5–214 mm SL, aquarium specimens.

3 | RESULTS

The development of the bones associated with each line of CNs is described in separate sections. At the end of the description of each sensory canal, we present a review of the different names applied for each bone by previous authors. A more detailed appraisal of the previous hypotheses of homologies, compared with those advanced in this work, is presented in the Discussion.

3.1 | Supraorbital line of CNs

The first evidence of ossification associated with the supraorbital line of CNs is seen in the 16-mm specimen, in which a very small aggregation of calcified tissue is present near the CN SO5. This is the only ossification observed in the dorsal surface of the head in this specimen (Figures 2 and 3). In the 18-mm specimen, bony tissue is also present around the CNs SO4 and SO6, but the more advanced degree of development of the ossification around SO5 provides further evidence that this is the first portion of the supraorbital line of CNs to ossify (Figures 2 and 3). The ossifications around SO4 and SO5 seem to have developed faster than the one around SO6 in the 18- and 19-mm specimens, as they represent the growing canal walls (appearing as a half-pipe) in association with these two neuromasts. In the 21-mm specimen, the ossifications around SO4, SO5, and SO6 are almost completely tubular, each enclosing its corresponding neuromast (Figures 2and 3).

In the 18-mm specimen, the ossifications around SO5 and SO6 are fused to each other by a posterior lamellar bridge extending from the posterior portion of the ossification around SO5, whereas the ossification around SO4 is still separated from them by a large gap (Figures 2 and 3). The fused ossification around SO5 and SO6 then develops a lamellar extension that gradually expands, mostly medially, until it contacts its contralateral bone at the dorsal midline of the skull (Figures 2–5). This medial bony expansion is already present in the 19-mm specimen (Figures 2 and 3) and, as it expands, it gradually grows toward the ossification around SO4, which is still a separate, tubular element until at least 29 mm. In the 32-mm specimen, the medial lamellar extension is fused to the ossification around SO4. In the 33- and 34-mm specimens, the bilateral ossifications involving the CNs SO4, SO5, and SO6 are in contact with each other, mostly along their middle portions, and the medial lamellar expansion extends both anteriorly and posteriorly (Figures 4 and 5). In the 40-mm specimen, the bilateral ossifications contact each other almost completely, and in the 58-mm specimen they are completely connected medially, forming the main portion of the dorsal roof of the skull (Figures 4 and 5). In the latter specimen, the posterior margin of these ossifications covers dorsally the anterior margins of the adjacent, posteriorly located dermopterotic.

The ossification formed in association with the CNs SO4, SO5, and SO6 in polypterids have been named frontal (Agassiz, 1833-44; Müller, 1846; Huxley, 1861; Traquair, 1870; Allis, 1922; Gregory, 1933; Pehrson, 1947; 1958; Daget, 1950; Jollie, 1984a; Claeson et al., 2007; Grande, 2010). Although named as such in accordance with the standard terminology used for Actinopterygii, this bone of ray-finned fishes is actually homologous to the parietal of more advanced sarcopterygians (Westoll, 1936; 1937; 1938; 1943; Schultze, 2008).

In the nasal portion of the supraorbital line of CNs, the ossifications in association with the CNs SO1, SO2, and SO3 start to develop considerably later than those associated with the remaining supraorbital CNs (SO4, SO5, and SO6). The first evidence of ossification in this region appears as a small aggregation of bony tissue around SO3 in the 19-mm specimen (Figures 2 and 3). In the 22-mm specimen, a small ossification is already present around SO2, and in the 25-mm specimen the ossification associated with SO3 is already tubular in form. In the 29-mm specimen, the ossifications associated with SO2 and SO3 are tubular ossifications, and the ossification around SO1 is starting to form. These three ossifications are separated from each other until at least 40 mm, at which time the left and right frontals meet each other almost completely along the dorsal midline of the skull (Figures 4 and 5). In the 58-mm specimen, the ossification around SO3 has noticeable lateral and medial lamellar outgrowths (which are more developed medially), giving the bone its plate-like appearance as in adults (Figures 4 and 5). At this stage, however, the bilateral plate-like ossifications in association with SO3 do not contact each other at the dorsal midline of the nasal region of the skull, but rather

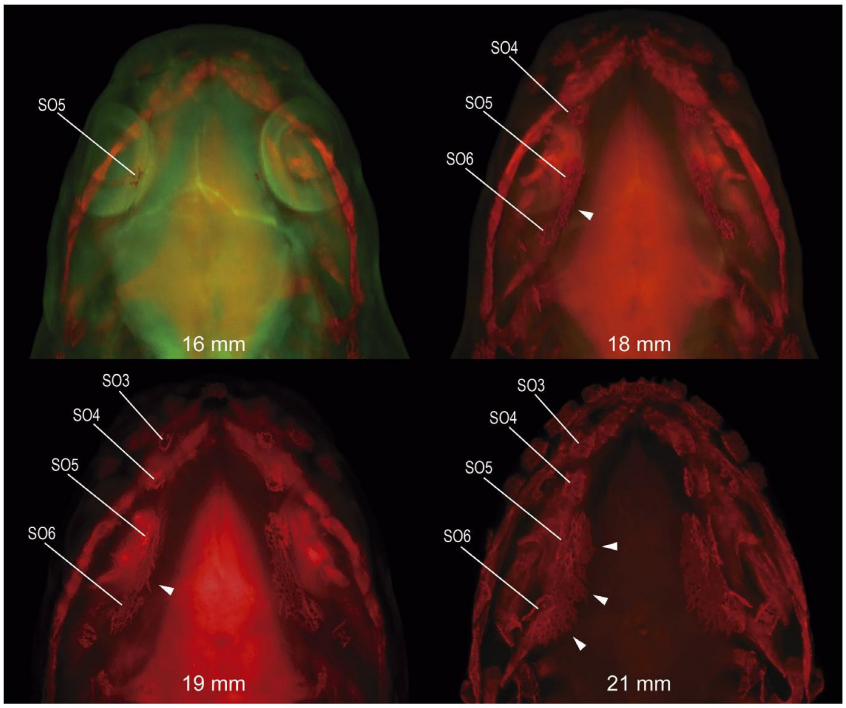

FIGURE 2 Fluorescence microscopy images of early developmental stages of formation of bones associated with the supraorbital line of CNs in *Polypterus senegalus*. Dorsal views of anterior region of the head. Arrowheads point to the lamellar expansion forming in association with neuromasts SO5 and SO6. SO3–SO6 = ossifications associated with supraorbital CNs 3–6

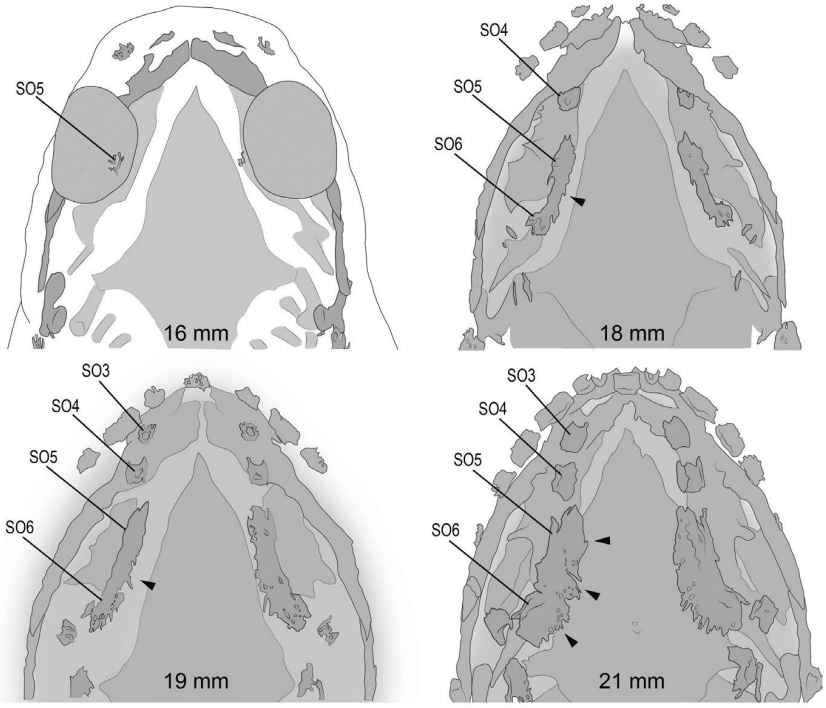

FIGURE 3 Diagrammatic representation based on Figure 2

remain separated by the posterodorsal portion of the rostral bone (see below) and by anterior extensions of the two frontals. In the 64-mm specimen, the contralateral plate-like ossifications associated with SO3 contact each other at the dorsal midline in the nasal region, although in some specimens of other species of *Polypterus* (e.g. *P. ansorgii*, *P. congicus*, *P. lapradei*, *P. ornatipinnis*, and *P. teugelsi*) these ossifications may remain separated until later in development. The ossifications associated with SO1 and SO2 are tubular in form even in very large adult specimens, especially the ossification around SO1, which is located between the anterior and posterior nares.

The three ossifications of the nasal region of the skull that are associated with the CNs SO1–SO3 of the supraorbital line remain separate from each other even in very large adult specimens and have been assigned many names in the literature. The ossification around SO1 has

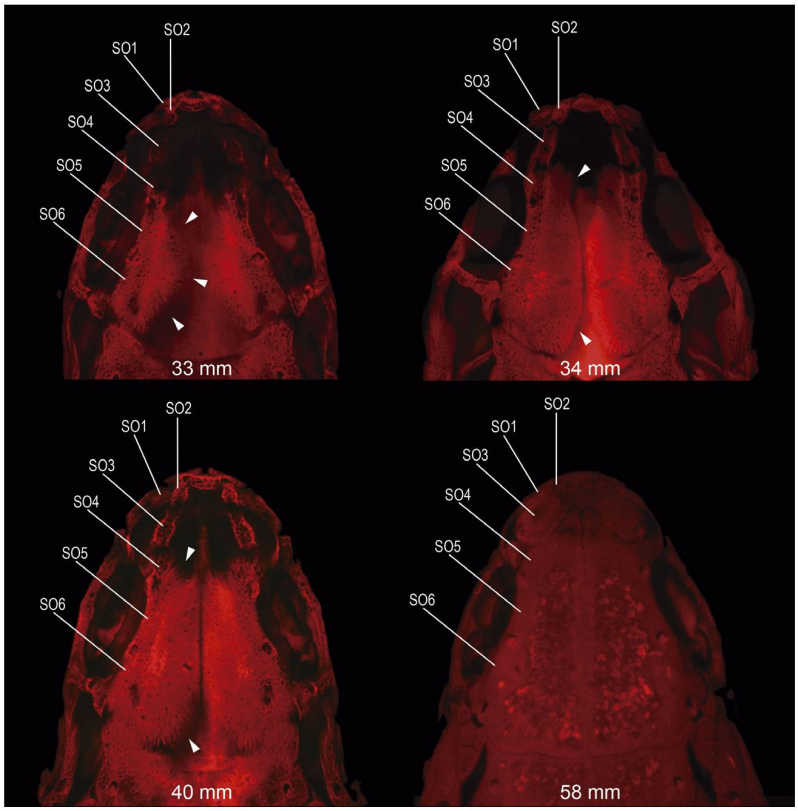

FIGURE 4 Fluorescence microscopy images of late developmental stages of formation of bones associated with the supraorbital line of CNs in *Polypterus senegalus*. Dorsal views of anterior region of the head. Arrowheads point to the lamellar expansion forming in association with neuromasts SO5 and SO6. SO1–SO6 = ossifications associated with supraorbital CNs 1–6

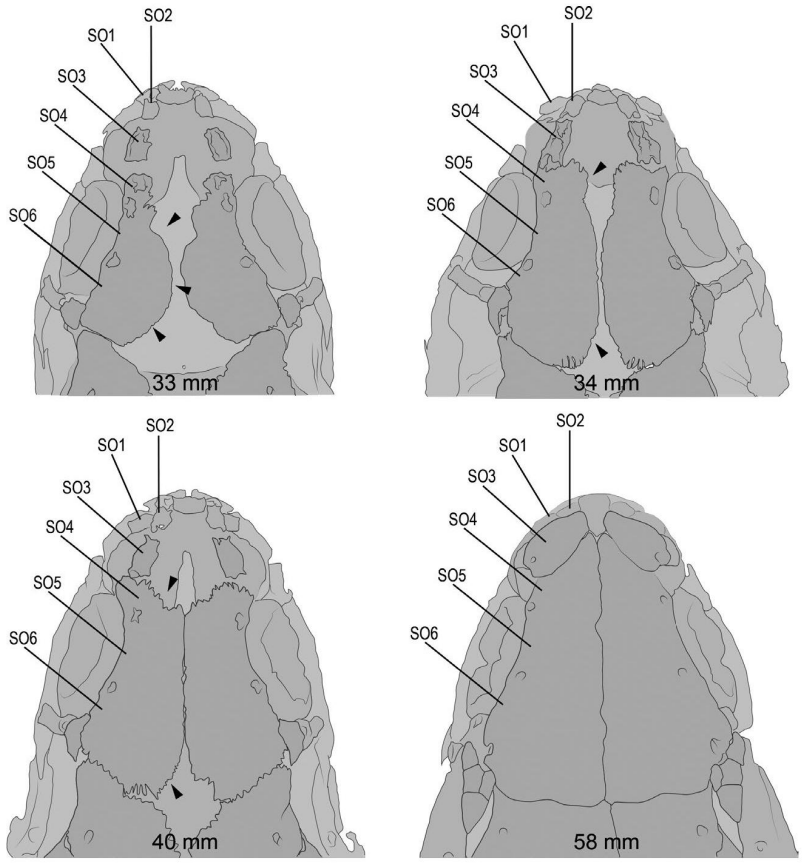

FIGURE 5 Diagrammatic representation based on Figure 4

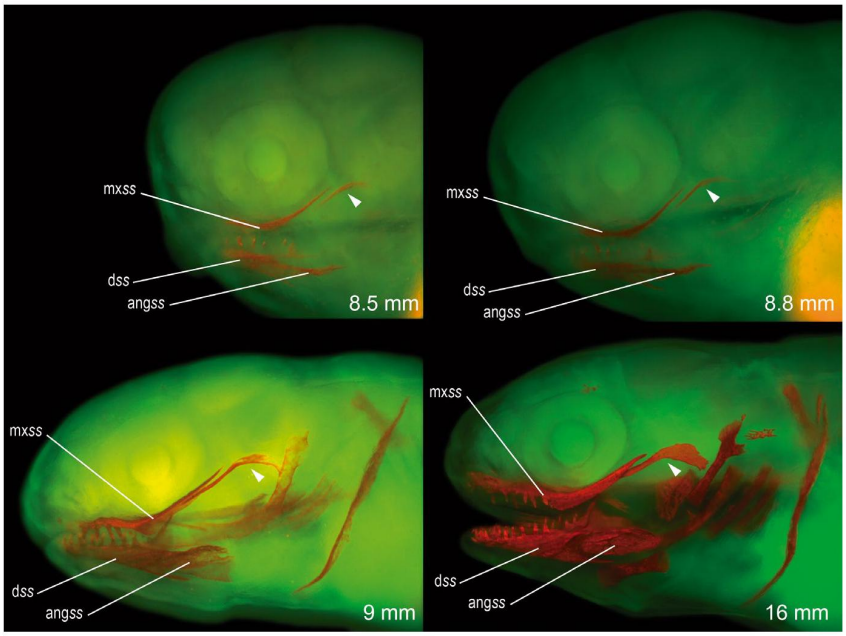

FIGURE 6 Fluorescence microscopy images of developmental stages of formation of bones associated with the infraorbital line of CNs in *Polypterus senegalus*. Left lateral views of the head. Arrowheads point to the elongated element posterior to the maxilla that later associates with the preoperculomandibular neuromasts PM6–PM8 and becomes incorporated in the bone identified as the preopercle. angss, angular *sensu stricto*; dss, dentary *sensu stricto*; mxss, maxilla *sensu stricto*

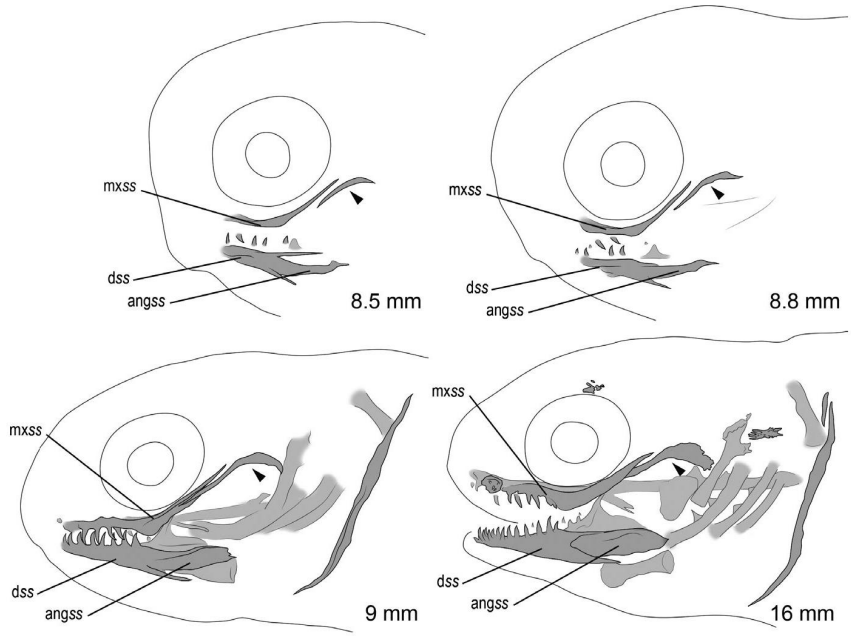

FIGURE 7 Diagrammatic representation based on Figure 6

been named the terminal bone (Traquair, 1870; Allis, 1922; De Beer, 1937; Jollie, 1984a), nasal 1 (Pehrson, 1947; 1958; Claeson et al., 2007), first nasal (Daget, 1950), accessory nasal (Pehrson, 1958), and anterior nasal (Jollie, 1984a). The first nasal was overlooked by some authors (e.g. Gregory, 1933; Grande, 2010). This may be due to the fact that this small tubular bone is located on the delicate flap of tissue that covers the nasal opening of the skull and is easily lost during dry skeleton preparation because is not attached to other bones or cartilages. The ossification around SO2 has been named the accessory nasal (Traquair, 1870; Allis, 1922), adnasal (Gregory, 1933; De Beer, 1937), nasal 2 (Pehrson, 1947; 1958; Claeson et al., 2007), and second nasal (Daget, 1950; Jollie, 1984a). The plate-like ossification around SO3 has been named the ethmoid (Agassiz, 1833-44), nasal (Traquair, 1870; Allis, 1922; De Beer, 1937; Grande, 2010), nasal 3 (Pehrson, 1947; 1958; Claeson et al., 2007), third nasal (Daget, 1950; Jollie, 1984a), and posterior nasal (Jollie, 1984a).

3.2 | Infraorbital line of CNs

The first evidence of ossification associated with the infraorbital line is observed in the 8.5-mm specimen. At this stage, a thin,

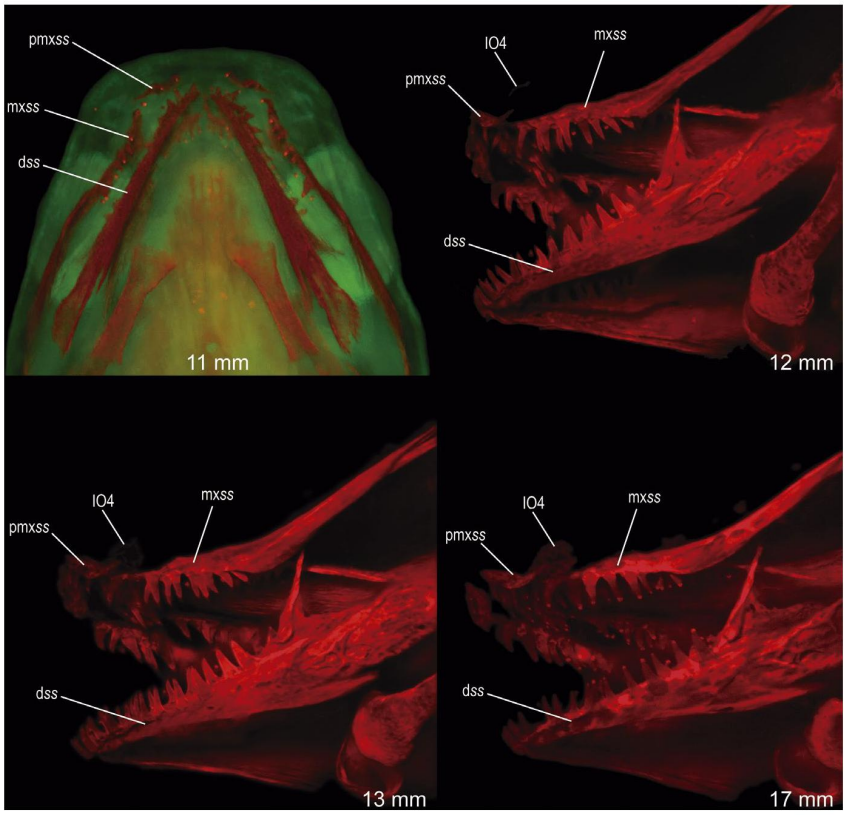

FIGURE 8 Fluorescence microscopy images of early developmental stages of formation of bones associated with the infraorbital line of CNs in *Polypterus senegalus*. Top left: ventral view of anterior region of the head. Top right and bottom: oblique left ventrolateral view of the anterior region of the head. IO4 = ossification associated with infraorbital CN 4. d*ss*, dentary *sensu stricto*; mx*ss*, maxilla *sensu stricto*; pmx*ss* = premaxilla *sensu stricto*

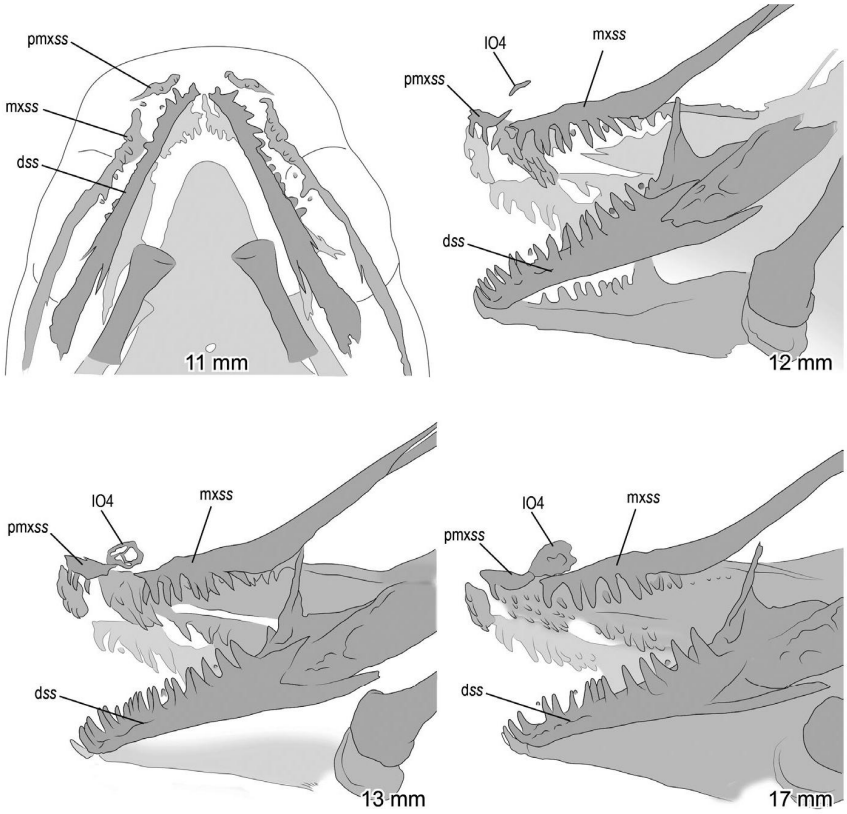

FIGURE 9 Diagrammatic representation based on Figure 8

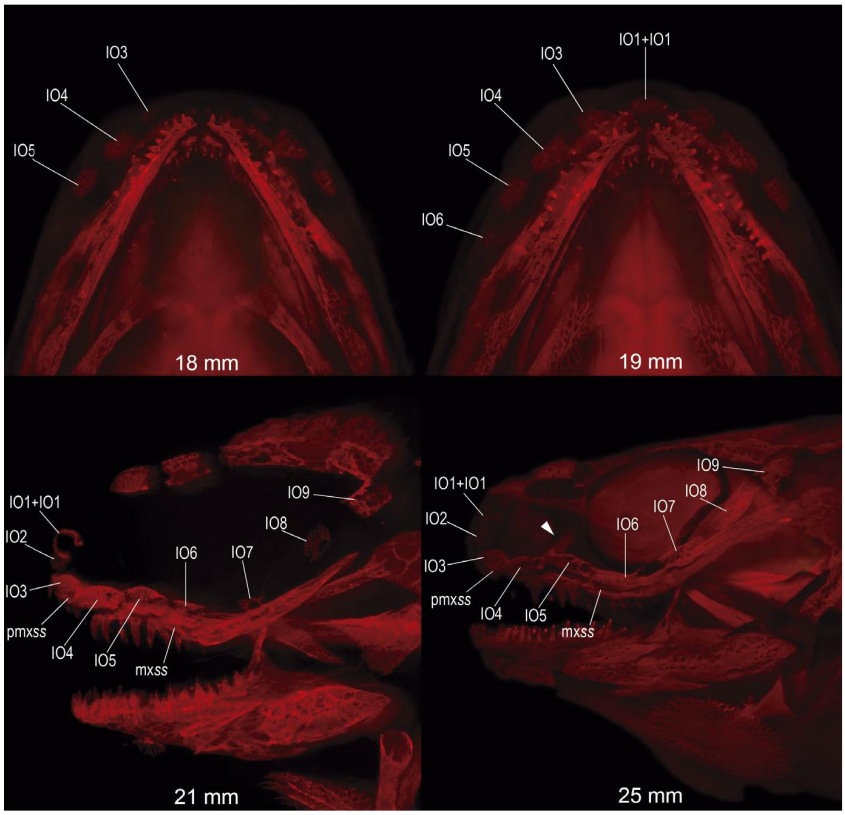

FIGURE 10 Fluorescence microscopy images of late developmental stages of formation of bones associated with the infraorbital line of CNs in *Polypterus senegalus*. Top: ventral views of anterior region of the head. Bottom: left lateral views of anterior region of the head. Arrowhead points to the posterolateral process of the premaxilla. IO1 + IO1 = single ossification formed by the fusion between the ossifications associated with the contralateral infraorbital CNs 1. IO2–IO9 = ossifications associated with infraorbital CNs 2–9. mx*ss*, maxilla *sensu stricto*; pmx*ss*, premaxilla *sensu stricto*

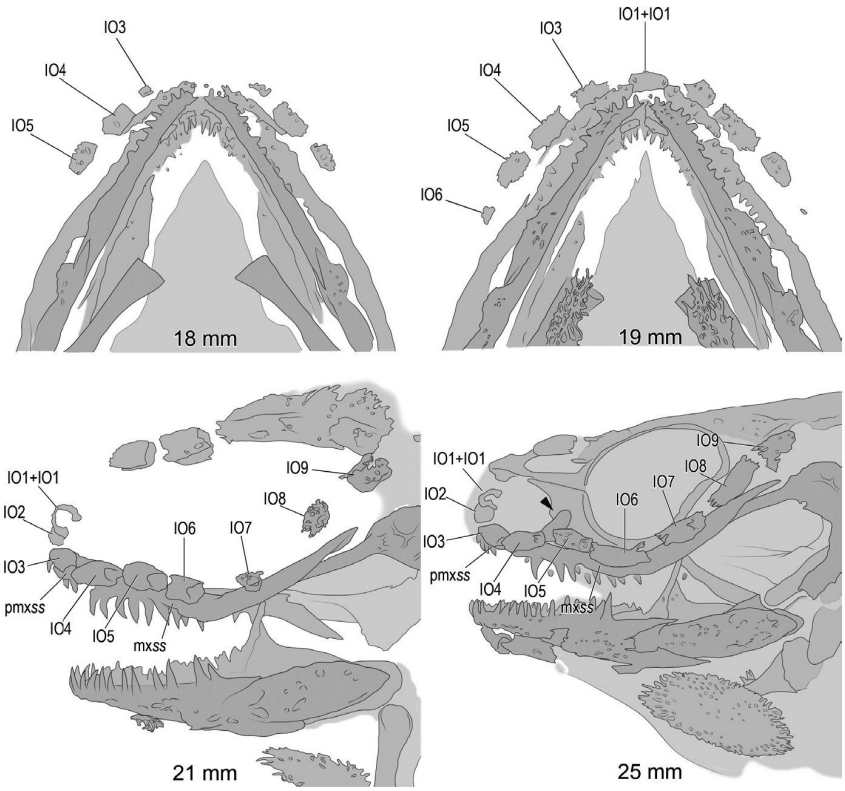

FIGURE 11 Diagrammatic representation based on Figure 10

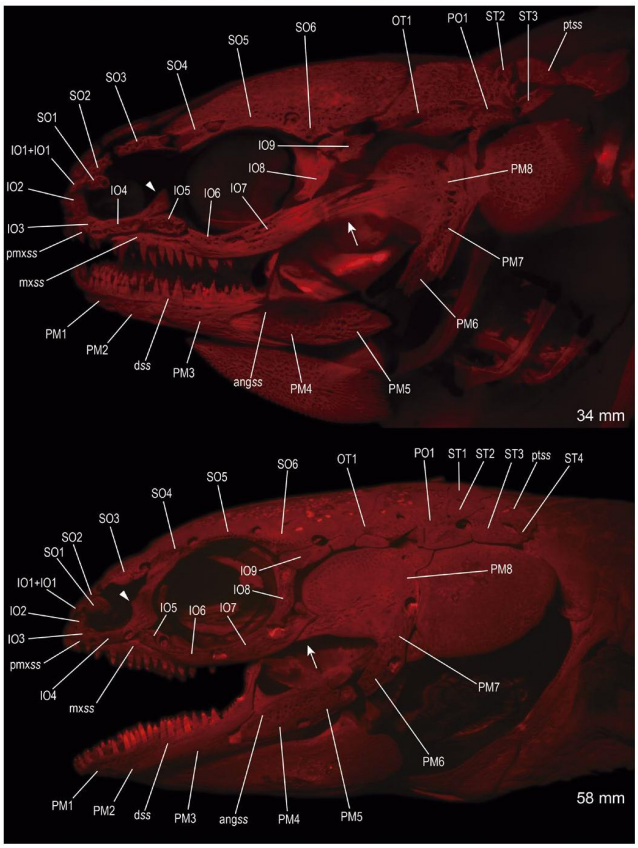

FIGURE 12 Fluorescence microscopy images of late developmental stages of formation of bones associated with laterosensory lines in *Polypterus senegalus*. Left lateral views of the head. Arrowheads point to the posterolateral process of the premaxilla. Arrows point to the interdigitating processes at the posterior portion of the maxilla and the anterior margin of the preopercle. IO1 + IO1 = single ossification formed by the fusion between the ossifications associated with the contralateral infraorbital CNs 1. IO2–IO9 = ossifications associated with infraorbital CNs 2 to 9. OT1 = ossification associated with otic CN. PM1–8 = ossifications associated with preoperculomandibular CNs 1–8. PO1 = ossification associated with postotic CN. SO1–6 = ossifications associated with supraorbital CNs 1–6. ST1–4 = ossifications associated with supratemporal CNs 1–4. ang*ss*, angular *sensu stricto*; d*ss*, dentary *sensu stricto*; mx*ss*, maxilla *sensu stricto*; pmx*ss*, premaxilla *sensu stricto*; pt*ss*, posttemporal *sensu stricto*

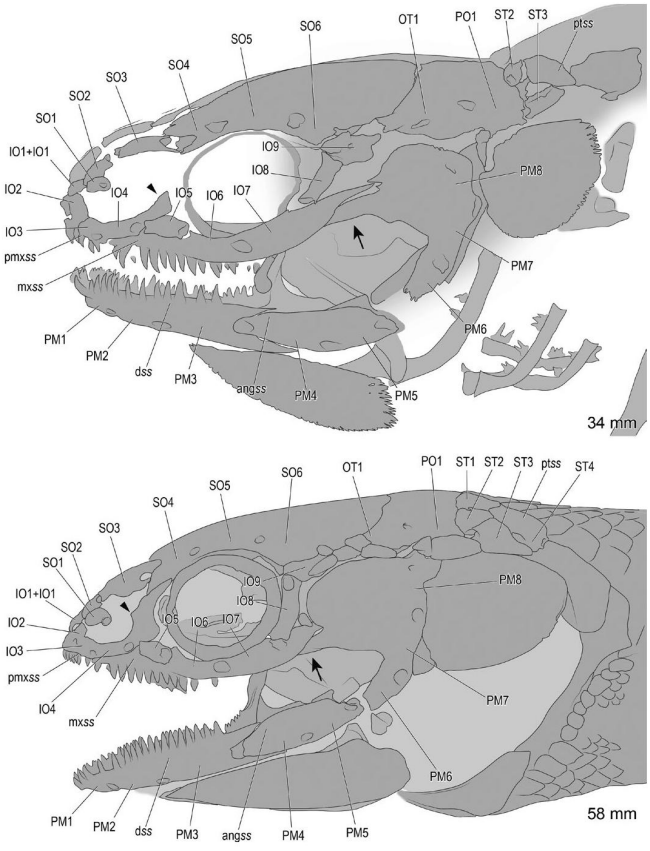

FIGURE 13 Diagrammatic representation based on Figure 12

elongate element bearing teeth is present ventral to the eye (Figures 6 and 7). Initially, it bears teeth only at its anterior tip (e.g. 8.8-mm specimen, Figures 6 and 7), but as it grows, more teeth are added posteriorly. This bone is here identified as the maxilla *s.s.* Posterior to the maxilla *s.s.* there is another thin, elongate element that is similar to the maxilla *s.s.* but differs in that it lacks teeth (Figures 6 and 7). These two elements become intimately associated during development (the development of the posterior element will be described in greater detail below, since it becomes associated with the preoperculomandibular line of CNs). In the 9-mm specimen, a lamellar bony extension develops ventrally from the longitudinal midpoint of the maxilla *s.s.* and tapers gradually at its posterior tip. This lamella surrounds the anterior tip of the posterior elongate element, only medially in small specimens, and then dorsally and laterally in specimens 16 mm and larger (Figures 6 and 7). The close association between the maxilla *s.s.* and the posterior element remains consistent through ontogeny and in adults appears as the interdigitating processes at the posterior portion of the adult maxilla (a compound bone including the maxilla *s.s.*) and the anterior margin the adult preopercle (also a compound bone, of which this posterior elongated element is part, see below).

In the 11-mm specimen, another bone associated with the infraorbital line starts to develop. This bone, herein identified as the premaxilla *s.s.*, is located anterior to the maxilla *s.s.*; it also bears teeth (Figures 8 and 9). Initially, there is a medial gap between the premaxillas *s.s.* on the left and right sides, but this gap is filled as the two bones develop. In the 12-mm specimen, a very faint ossification is present around CN IO4 and is located dorsal to the site of contact between the premaxilla *s.s.* and the maxilla *s.s.* (Figures 8 and 9). In the 16- and 17-mm specimens, this ossification is already developed as a half-pipe as the canal walls form after the CN IO4 sinks into the skin (Figures 8 and 9).

In the 18-mm specimens, two other tubular ossifications are added, one anterior and one posterior to IO4, which are associated with IO3 and IO5, respectively (Figures 10 and 11). In the 19-mm specimen, the ossification associated with IO1 is already present and is fused to the contralateral ossification to form a single bone (Figures 10 and 11). A faint ossification associated with IO6 is already present, but there is no trace of any ossification associated with IO2. This may indicate that the formation of the infraorbital canal occurs independently in at least two portions: one starting in the region between the nasal and orbital regions and another starting at the tip of the snout. In the 21-mm specimen, the ossifications associated with the remaining CNs of the infraorbital line—IO2, IO7, IO8 and IO9—are present, so that all the nine tubular bones associated with CNs of the infraorbital line are already developed, each forming a single, independent, tubular ossification (Figures 10 and 11). Of these bones, the ones associated with IO7 and IO8 are the least developed, whereas the one associated with IO9 is already developed as a half-pipe. This may indicate that the ossification associated with IO9 also develops independently from the remaining portions of the infraorbital canal. Interestingly, the CN IO9 is innervated by a nerve that arises almost immediately anterior to the origin of the superficial ophthalmic and the buccal rami of the ADLLN, according to Piotrowski and Northcutt (1996), and appears to be an independent branch instead of part of the buccal ramus. Indeed, Pehrson (1947: Figure 7, 'dso') represented this branch as emerging independently from the buccal ramus. The degree of development of the remaining ossifications reflects the sequence in which they are formed: the ossification associated with IO4 is the more well-developed, appearing as a tube, followed by the ossifications associated with IO1, IO3, and IO5. All the tubular ossifications associated with the infraorbital CNs are still separated from their underlying lamellar ossifications, when present.

In the 22-mm specimen, the posterolateral process of the premaxilla starts to develop medially to the point of contact between the tubular ossifications enclosing the CNs IO4 and IO5. In the 25-mm specimen, the process is conspicuous, and the tubular ossifications associated with IO6 and IO7 remain separated from the maxilla *s.s.*, whereas all the remaining ossifications of the infraorbital line (IO1 + IO1 to IO5, IO8, and IO9) remain essentially tubular (Figures 10 and 11). The tubular ossification enclosing the IO9 fuses to an endochondral ossification, the autosphenotic (see Discussion below), developing medially at the posteroventral corner of it. In the 29-mm specimen, the ossifications associated with IO2, IO3, and IO4 are fused to the premaxilla *s.s.*, whereas those associated with IO6 and IO7 are fused to the maxilla *s.s.* The ossifications associated with IO1, IO5, and IO8 remain independent and bear tubular shapes. The ossification associated with IO9 is completely fused to the autosphenotic, and its laterodorsal portion is in contact with the lateral portion of the frontal, posterolateral to the concavity of the frontal that forms the dorsal margin of the orbit. The ossification associated with the left and right CNs IO1 (Figures 10–13) retains a tubular shape until the fish reaches 40 mm. In the 58-mm specimen, this tubular ossification has developed a plate-like shape through the development of a posterodorsal lamella that fills the gap between the left and right nasals (Figures 4 and 5). The posterolateral process of the premaxilla has grown dorsally and contacts the anteroventral portion of the frontal in the 40-mm specimen. In the 50- and 58-mm specimens, the posterolateral process of the premaxilla is intimately associated with the frontal, filling the space between the opening of the nasal capsule and the anterior margin of the orbit (Figures 12 and 13). In the 40-mm specimen, the ossification that is associated with IO9 and fused to the autosphenotic is tightly connected to the ventral face of the postorbital process of the frontal. A tubular pore is located at the posterodorsal margin of this ossification at the point where the supraorbital, infraorbital, and otic canals meet. In the 58-mm specimen, this ossification is covered laterally by the anteriormost of the multiple spiracular bones that are present in specimens of this size (Figures 12 and 13).

In adult polypterids, the plate-like ossification associated with the left and right CNs IO1 + IO1 has been named the ethmoid (Huxley, 1861; Traquair, 1870), median ethmoid (Supino, 1914; Allis, 1922), rostral (Holmgren and Stensiö, 1936; Pehrson, 1958;

Patterson, 1975; Claeson et al., 2007), supraethmoid (De Beer, 1937; Daget, 1950), medial rostral (Jarvik, 1942; Pehrson, 1947), rostro-postrostral (Jarvik, 1947; Poplin and Lund, 1995), and medial rostral-internasal (Jollie, 1984a; Grande, 2010). The ossifications associated with IO2, IO3, and IO4 have, in combination with the premaxilla *s.s.*, been named the intermaxillaries (Agassiz, 1833-44), premaxillary (Traquair, 1870; Allis, 1922; Westoll, 1936; Pehrson, 1947; 1958; Claeson et al., 2007), premaxillo-antorbital or antorbito-premaxilar (Holmgren and Stensiö, 1936; Daget, 1950), tecto-rostro-prémaxillary (Jarvik, 1942), and premaxilla-rostral (Jollie, 1984a; Grande, 2010). The ossification associated with IO5 has been named the anterior suborbital (Traquair, 1870), anterior infraorbital (Allis, 1922), and lacrimal (Pehrson, 1947; 1958; Daget, 1950; Jollie, 1984a; Claeson et al., 2007; Grande, 2010). The ossifications associated with IO6 and IO7 in conjunction with the maxilla *s.s.* have been named the superior maxillary (Agassiz, 1833-44), maxillary (Traquair, 1870; Allis, 1922; Pehrson, 1947; 1958; Claeson et al., 2007), maxilla-infraorbitals (Jollie, 1984a), and maxilla-subinfraorbitals (Grande, 2010). The ossification associated with IO8 has been identified as the posterior suborbital (Traquair, 1870), postorbital (Allis, 1922; Pehrson, 1947; 1958; Daget, 1950; Jollie, 1984a; Claeson et al., 2007), and postinfraorbital (Grande, 2010). The ossification associated with IO9 has been identified as the posterior frontal (Agassiz, 1833-44), sphenotic (Bridge, 1888; Pollard, 1892), postfrontal (Traquair, 1870), postfronto-sphenotic (Allis, 1922), dermosphenotic + autosphenotic (Pehrson, 1947; Daget, 1950), and dermosphenotic + sphenotic (Jollie, 1984a; Claeson et al., 2007; Grande, 2010).

3.3 | Preoperculomandibular line of CNs

The first evidence of ossification associated with the preoperculomandibular neuromast line is observed in the smallest specimen analyzed (8 mm), in which a very thin and long ossified element is present in the lower jaw. This element is accompanied by small, conical ossifications that represent the beginning of mineralization of the teeth. In an 8.5-mm specimen, the thin ossification has developed considerably and is a relatively large membranous bone with which a few teeth are associated dorsally (Figures 6 and 7). This tooth-bearing ossification represents the membranodermal component of the dentary, here identified as the dentary *s.s.* Posterior to it, there is another thin, membranous ossification, which is the membranodermal component of the angular, here identified as the angular *s.s.* (Figures 6 and 7). The latter two ossifications cover Meckel's cartilage laterally, while medially the Meckel's cartilage is covered by another membranodermal ossification, the prearticular. In the same specimen, there are also two thin, elongate ossifications present at the lateral portion of the upper jaw, ventral to the orbit. The anterior one is the maxilla *s. s.*, previously described (see section on ''Infraorbital line of CNs' above), and the posterior one is a thin, elongated, curved ossification that is about one-third the size of the maxilla *s.s.* and is located posteroventral to it (Figures 6 and 7). As mentioned above, this ossification remains intimately associated with the maxilla *s.s.* during the entire development. This element, here identified as the jugal, will be discussed later in this work (see Discussion).

During the next developmental stages, the dentary *s.s.*, the angular *s.s.*, and the element posterior to the maxilla *s.s.* develop further. In the 9-mm specimen, the element posterior to the maxilla *s.s.* bears an enlarged posterior portion that is slightly curved ventrally (Figures 6 and 7). The dentary *s.s.* bears strong, well-developed conical teeth, and posterodorsal and posteroventral processes extending dorsal and ventral to the angular *s.s.* In the 10-mm specimen, the anterior portion of the posterior element is enclosed medially and dorsally by the posterior laminar flange of the maxilla *s.s.*, whereas the enlarged portion of the posterior element is strongly curved ventrally, and positioned close to the hyomandibula, at about the level of the posterior process for the articulation with the opercle.

In the next developmental stages, the angular *s.s.* develops irregular bony ridges that represent the beginning of the ossification of the angular portion of the preoperculomandibular canal. In the 16-mm specimen, the enlarged posterior portion of the posterior element starts to expand, and in the same specimen the opercle has started to ossify as a plate-like bone associated with the posterior process of the hyomandibula (Figures 6 and 7). In the 19-mm specimen, half-pipe-like ridges associated with CNs PM3, PM4, and PM5 form along the posterior portion of the dentary *s.s.* and in the angular *s.s.* (Figures 14 and 15). The ridges associated with PM3 and PM4 are a little more developed than those of the PM5, and a very small ossification associated with PM2 is located ventral to the middle portion of the dentary *s.s.* (Figures 14 and 15). At the distal tip of the enlarged portion of the posterior element, a nerve foramen marks the point in which PM7 is located (Figures 14 and 15).

In the 21-mm specimen, the ossification associated with PM2 develops further and acquires a half-pipe-like shape, although it still remains separate from the dentary *s.s.* (Figures 14 and 15). The enlarged portion of the posterior element has expanded and acquired ornamentations, and half-pipe-like ridges formed around the foramen for the nerve associated with PM7. In the 22-mm specimen, another tubular ossification is forming around PM1 and located ventral to the dentary *s.s.*, similar to the one associated with the PM2. In the 25-mm specimen, the enlarged portion of the posterior element has a half-pipe-like ventral extension associated with PM6 (Figures 14 and 15). CN PM3 in the dentary *s.s.* and the CNs PM4 and PM5 in the angular *s.s.* are already enclosed in tubular canals, while the tubular ossifications associated with PM1 and PM2 remain separated from the dentary *s.s.* (Figures 14 and 15). In the 29-mm specimen, ossifications associated with the CNs PM1 and PM2 fuse to the dentary *s.s.*, and the mandibular portion of the preoperculomandibular canal becomes entirely enclosed in tubular canals embedded within the dentary and the angular bones (Figures 14 and 15). Thus, the dentary and the angular each represent the fusion between a membranodermal component, the dentary *s.s.* and the angular *s.s.*, respectively, with tubular components representing the preoperculomandibular canal. These tubular components form as independent ossifications (in the case of the canal segments associated with PM1 and PM2) or

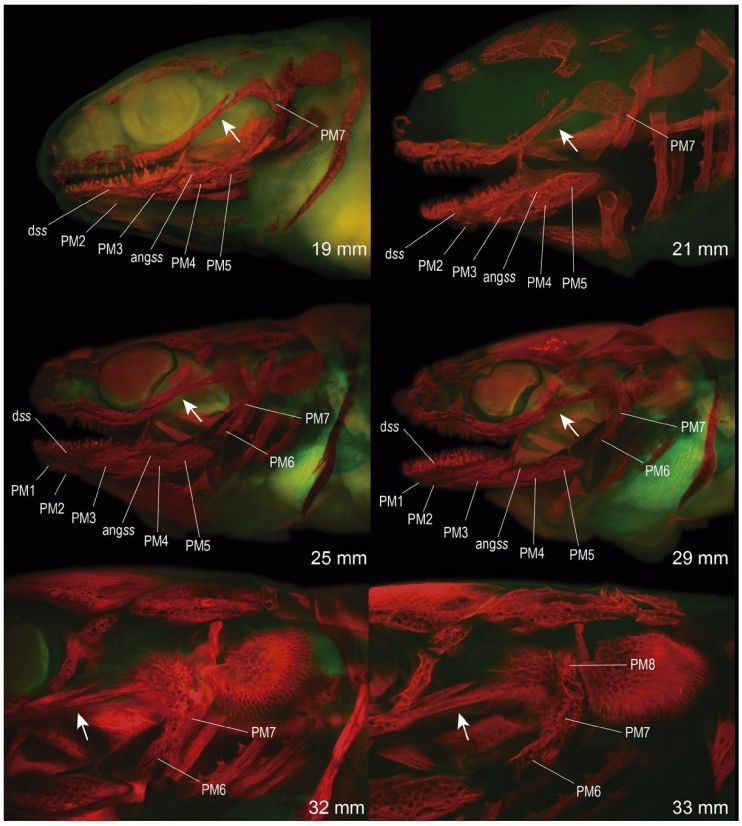

FIGURE 14 Fluorescence microscopy images of developmental stages of formation of bones associated with the preoperculomandibular line of CNs in *Polypterus senegalus*. Top left: left ventrolateral view of the anterior region of the head. Top right and middle: left lateral views of the head. Bottom: left lateral view of the cheek region. Arrows point to the interdigitating processes at the posterior portion of the maxilla and the anterior margin of the preopercle. PM1–8 = ossifications associated with preoperculomandibular CNs 1–8. angss, angular *sensu stricto*; dss, dentary *sensu stricto*

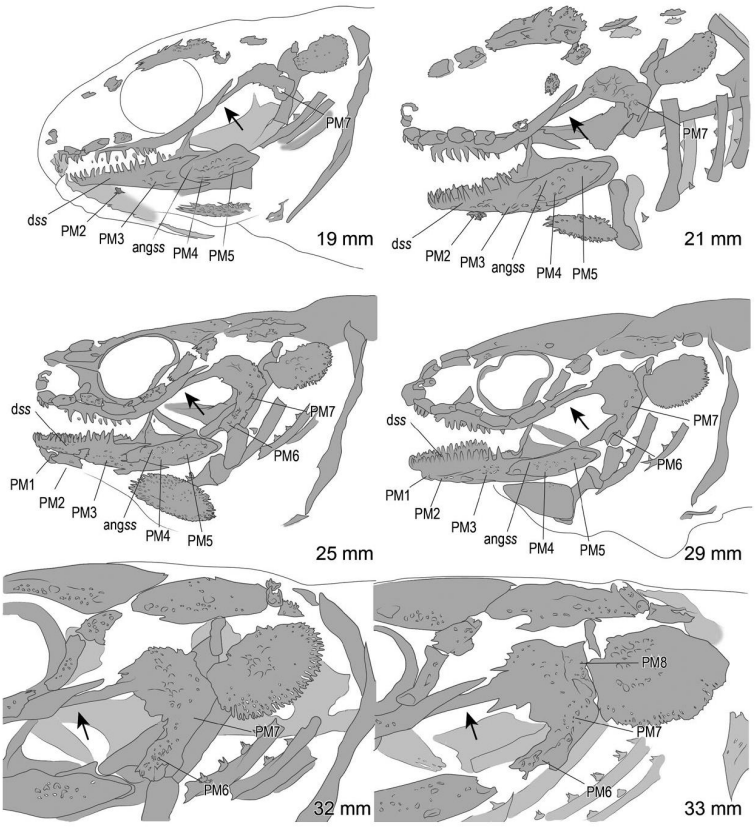

FIGURE 15 Diagrammatic representation based on Figure 14

as ossifications embedded in the membranodermal component of the bone (the canal segments associated with PM3, PM4, and PM5).

In the 32-mm specimen, the element posterior to the maxilla bears a well-developed and ornamented enlarged portion posteriorly, which bears a long ventral process associated with CN PM6 (Figures 14 and 15). In the 33-mm specimen, the enlarged portion is expanded dorsally, forming half-pipe-like ridges on either side of CN PM8 (Figures 14 and 15), and in the 34-mm specimen the preopercular portion of the preoperculomandibular canal is completely tubular in form (Figures 12 and 13). In the next stages, the enlarged portion of the posterior element expands anterodorsally, forming an ovoid plate that reaches the postorbital and the sphenotic. In the 58-mm specimen, this ovoid plate is covered dorsally by the prespiracular and spiracular ossicles that are already formed (Figures 12 and 13). The definitive ossification, the preopercle, is thus formed by the membranodermal element posterior to the maxilla, plus the tubular component that represents the preopercular portion of the preoperculomandibular canal that is associated with the CNs PM7, PM8, and PM9.

The ossifications associated with the CNs PM1 to PM3 have been named the dentary (Agassiz, 1833-44; Traquair, 1870; Allis, 1922; Claeson et al., 2007; Grande, 2010), dentary-splenial (Holmgren and Stensiö, 1936; Pehrson, 1947; 1958; Daget, 1950; Jollie, 1984a), and dentary-infradentary (Jarvik, 1947). The ossification associated with the CNs PM4 and PM5 have been named the angular (Agassiz, 1833-44; Traquair, 1870; Holmgren and Stensiö, 1936; Jollie, 1984a; Claeson et al., 2007; Grande, 2010), dermarticular (Van Whije, 1882; Allis, 1900; 1922), surangulo-angular (Stensiö, 1947), infradentary 4 + 5 (Jarvik, 1947), angulo-splenial (Pehrson, 1947; Daget, 1950), and angular-surangular-splenial (Pehrson, 1958). Finally, the ossification associated with the CNs PM6 to PM8 have been named the preopercle (Agassiz, 1833-44; Müller, 1846; Pollard, 1892; Allis, 1900; Holmgren and Stensiö, 1936; Pehrson, 1947; Jollie, 1984a; Claeson et al., 2007; Grande, 2010), supratemporal + hyomandibula (Huxley, 1861), cheek dermal bone (Traquair, 1870), squamoso-preopercular (Allis, 1922; Jarvik, 1947), and preoperculo-supramaxillary (Pehrson, 1958).

3.4 | Otic and postotic lines of CNs

The earliest evidence of ossification associated with the otic and postotic lines of CNs was observed in the 18-mm specimen. At this stage, a small ossification is associated with the otic neuromast (OT1), whereas there is no evidence of ossification associated with the postotic neuromast (PO1; Figures 16 and 17). In the 21-mm specimen, a small ossification is associated with PO1, and the ossification associated with OT1 is already developing a tubular form, but these ossifications remain separated from each other by a large gap (Figures 16 and 17). In the 25-mm specimen, both of the ossifications associated with OT1 and PO1 have developed considerably. They are already fused to each other, forming a continuous tube with a single pore between them (Figures 16 and 17). The ossification formed by the fusion of the tubular ossifications of the otic and postotic CNs, the dermopterotic, bears lateral and medial flanges, giving the bone a plate-like aspect. The plate-like bone is traversed by the canal and covers the otic capsule dorsally. The bone grows medially, as well as slightly anteriorly and posteriorly. In the 33-mm specimen, its anterior margin contacts the posterior margin of the frontal, and in the 34-mm specimen the bilateral ossifications meet each other at the dorsal midline (Figures 16 and 17). In the 58-mm specimen, the dermopterotic bone is already fully developed as a rectangular plate covering dorsally the posteriormost region of the neurocranium (Figures 4, 5, 12, and 13). The dermopterotic is overlapped anteriorly by the posterior margin of the frontal, and posteriorly by the anterior margins of the extrascapulars. Along the midline of the skull, the left and right dermopterotic bones contact each other in an almost straight line, and laterally they bear a ventral expansion that forms the medial border of the spiracular opening.

The single bone formed by the fusion of the ossifications associated with the otic and postotic neuromasts was initially identified as the parietal by Agassiz (1833-44), Müller (1846), Huxley (1861), Traquair (1870), and Gregory (1933). According to Allis (1922), this bone was named the squamoso-parietal by Van Whije (1882), Collinge (1893), and Allis (1900) because it was assumed to be a fusion between the so-called squamosal (= dermopterotic) and the parietal of teleosts. Accordingly, Allis named this bone the parieto-dermosquamosal (Allis, 1904) or parieto-dermopterotic (Allis, 1922). Holmgren and Stensiö (1936) and Jarvik (1947) used other terminology for the dermopterotic and named this bone the parieto-supratemporo-intertemporal, therefore agreeing that the bone includes a parietal element. Pehrson (1947) suggested, however, that the parietal does not contribute to this ossification in *Polypterus*, and called it the intertemporo-supratemporal. Pehrson (1947) referred to a vestigial, transient parietal during the ontogeny of *Polypterus*, but we were unable to identify such an element in our material. However, since Pehrson (1947) published his work, most authors have called this bone the intertemporo-supratemporal (Perhson, 1958; Jollie, 1984a; Claeson et al., 2007) or the dermopterotic (Daget, 1950; Grande, 2010).

3.5 | Supratemporal line of CNs

The ossifications associated with the supratemporal line of CNs are the last of the ossifications associated with lateral-line canals to form in *P. senegalus*. The earliest evidence of ossification associated with the supratemporal canal is observed in the 29-mm specimen. Two half-pipe ossifications are present at the posterolateral corner of the neurocranium, posterior to the otic capsule and to the posterodorsal corner of the dermopterotic (Figures 18 and 19). The anterior ossification is associated with CN ST2, lies over the posterior margin of the dermopterotic, and is oriented transversely to the longitudinal axis of the head, representing the lateral portion of the supratemporal commissure. The posterior ossification is associated with CN ST3, is aligned parallel to the longitudinal axis of the head, and represents the anterior part of the temporal portion

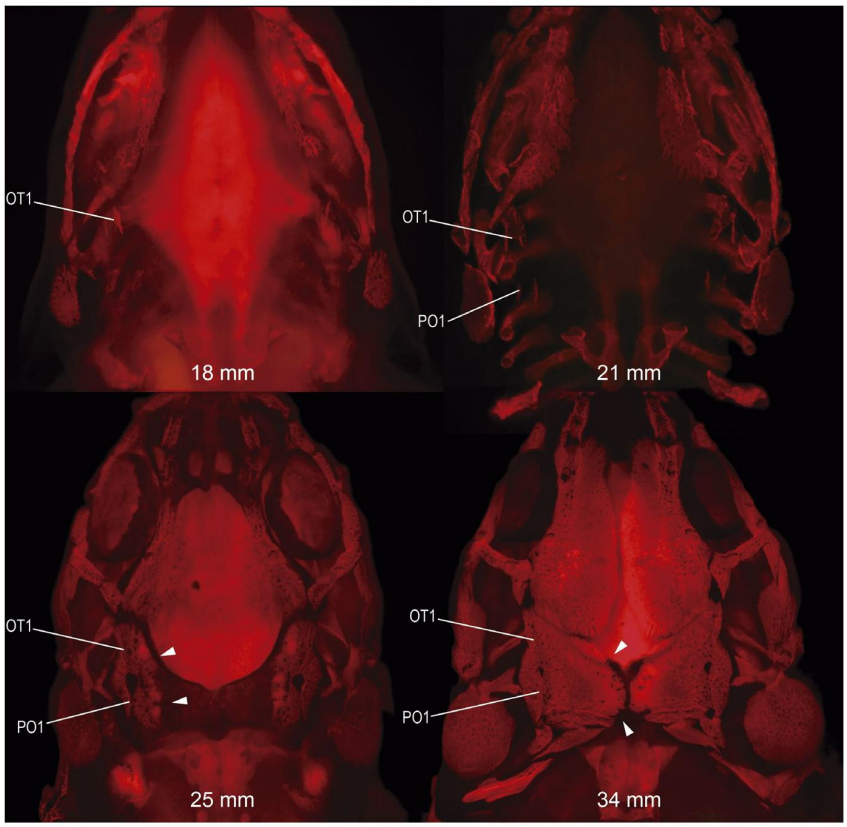

FIGURE 16 Fluorescence microscopy images of developmental stages of formation of bones associated with the otic and postotic lines of CNs in *Polypterus senegalus*. Dorsal view of the head. Arrowheads point to the lamellar expansion forming in association with CNs OT1 and PO1. OT1 = ossifications associated with otic CN. PO1 = ossifications associated with postotic CN

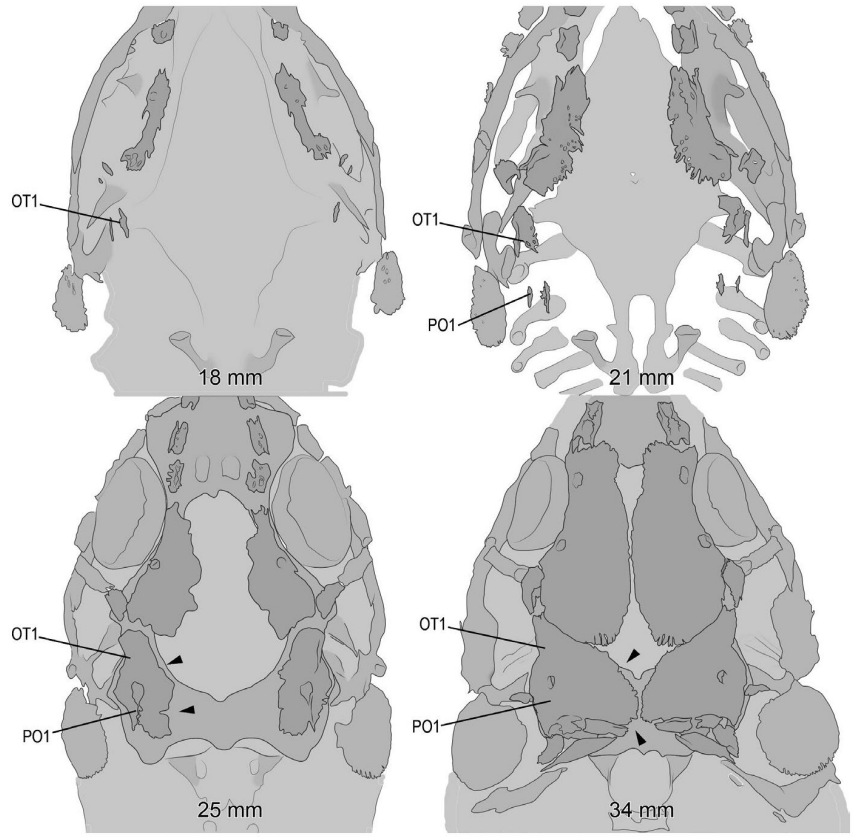

FIGURE 17 Diagrammatic representation based on Figure 16

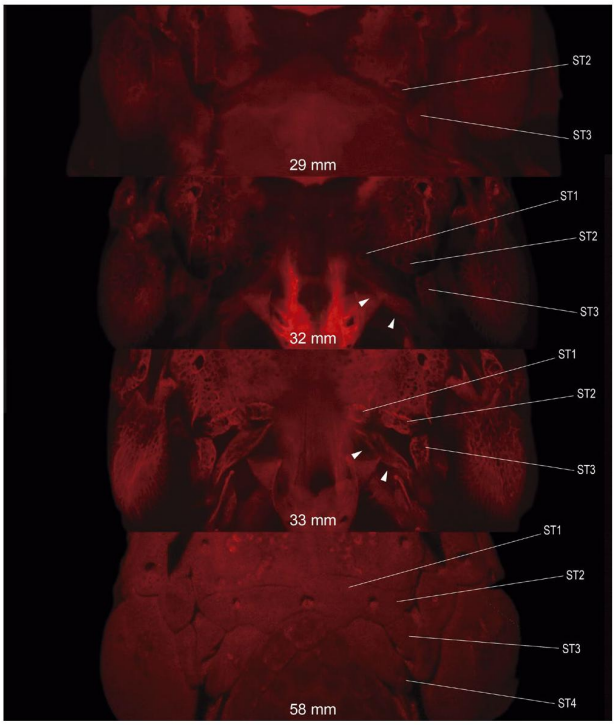

FIGURE 18 Fluorescence microscopy images of developmental stages of formation of bones associated with the supratemporal line of CNs in *Polypterus senegalus*. Dorsal view of posterior region of the head. Arrowheads point to the lamellar ossification forming in association with neuromasts ST4 (posttemporal *sensu stricto*). ST1–4 = ossifications associated with supratemporal CNs 1–4

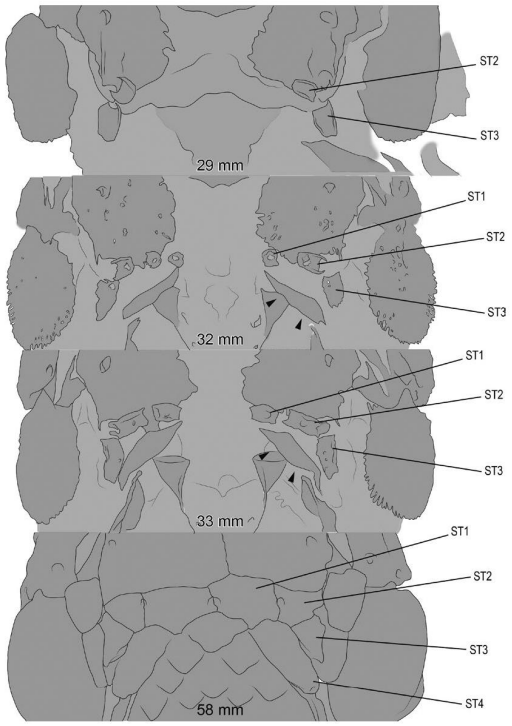

FIGURE 19 Diagrammatic representation based on Figure 18

of the supratemporal canal. The bone, which represents one of the extrascapulars, is located in the gap between the postotic canal running anteriorly in the posterior portion of the dermopterotic and the anterodorsal tip of the supracleithrum posteriorly.

In the 32-mm specimen, the ossifications associated with the CNs ST2 and ST3 are slightly more developed, although still in the form of a half-pipe (Figures 18 and 19). In addition, a medial ossification associated with CN ST1 is also transversely oriented relative to the longitudinal axis of the head, and is less developed than the one associated with ST2. The medial, plate-like portion of the posttemporal is already ossified anterodorsal to the supracleithrum. However, there is no trace of an ossification associated with ST4, which is associated with the posttemporal later in development. In the 33-mm specimen, the three ossifications associated with CNs ST1, ST2 and ST3 are well-developed, as is the medial plate-like portion of the posttemporal, which forms a bridge connecting the supracleithrum to the posterodorsal margin of the skull (Figures 18 and 19). The ossifications associated with the left and right CNs ST1 remain separated from each other by a large gap, and the posttemporal is still a plate-like ossification (posttemporal s.s.) that first associates with the laterosensory canal in the 40-mm specimen. In the 58-mm specimen, the left and right supratemporal canals contact each other at the dorsal midline of the skull forming a complete supratemporal commissure (Figures 18 and 19). The ossifications associated with the CNs ST1, ST2, and ST3 are present as plate-like ossifications, similar in form to the scales on the dorsal surface of the body, located just posterior to the skull. At this stage, the posttemporal bone is traversed on its lateroventral portion by a short tube representing the portion of the supratemporal canal associated with ST4.

The ossifications associated with CNs ST1, ST2, and ST3 have been named supratemporals (Traquair, 1870; Allis, 1900; 1922) and extrascapulars (Pehrson, 1947; 1958; Daget, 1950; Jollie, 1984a; Claeson et al., 2007; Grande, 2010). The ossification associated with ST4 has been named suprascapular (Agassiz, 1833-44) and posttemporal (Traquair, 1870; Allis, 1922; Pehrson, 1947; Daget, 1950; Jollie, 1984a; Claeson et al., 2007; Grande, 2010). The ventral face of the posttemporal bears an anteroventrally directed process continuous with a ligament that attaches on the intercalar process of the epioccipital (Grande, 2010), and a long, posteriorly directed process that is associated with the occipital tendon, as usually observed in the posttemporals of other fishes (Allis, 1922; Jollie, 1984a; Gemballa and Röder, 2004).

4 | DISCUSSION

4.1 | Developmental patterns of canal bones

In *P. senegalus*, a tubular ossification is associated with each CN and is independent from the tubular ossifications associated with other CNs, even if they are in the same line of CNs (e.g. tubular ossifications associated with infraorbital CNs). These tubular bones

represent the ossification of the walls of the lateral-line canal segment that starts in the vicinity of a neuromast and forms first a half-pipe structure and then a fully enclosed tube with ossification of the canal roof over the CN. This developmental sequence generally agrees with the process of enclosure of CNs and formation of lateral-line canals described by several authors (Allis, 1889; Pehrson, 1922; Tarby and Webb, 2003; Webb and Shirey, 2003; Bird and Webb, 2014; Pastana et al., 2019). However, during development these tubular ossifications may also interact with other adjacent ossifications not associated with neuromasts or, in some cases, may develop lamellar expansions or flanges, such that the development of each bone associated with lateral-line canals in *P. senegalus* follows one of four distinct ontogenetic pathways.

- The tubular ossification associated with a CN develops and remains as a distinct tubular bony element even in very large adult specimens. This is the case for the nasals 1 and 2, the lacrimal, and the postorbital (Figure 1).
- The tubular ossification formed by a CN seems to develop lateral lamellar flanges that expand, thereby forming a plate-like ossification traversed by a tubular bony canal in which the CN is located. This is the case for the nasal 3, rostral, dermopterotic, extrascapulars, and the posterior region of the frontal associated with CNs SO5 and SO6 (Figure 1).
- The tubular ossification formed in association with a CN develops from a previously formed, underlying plate-like ossification. In this case, the tubular ossification first appears as ridges (canal walls on either side of a CN) that form in the plate-like bone. The ridges grow over and enclose each CN. This is the case for the posttemporal, preopercle, angular, and the posterior portion of the dentary associated with CN PM3 (Figure 1).
- The tubular ossification associated with the CN develops independently from an underlying or adjacent ossification, such that this fully formed, tubular bone later becomes fused to a plate-like bone forming below it or adjacent to it. This is the case for the premaxilla, maxilla, anterior portion of the dentary associated with the CNs PM1 and PM2, and the anterior region of the frontal, associated with CN PM4 (Figure 1).

These four different developmental trajectories indicate the existence of two distinct and independent components of ossification that interact in different ways in the formation of cranial bones associated with lateral-line canals in *P. senegalus*. One of the components is more superficial and represents the lateral-line canal formed by the invagination of the CNs and subsequent ossification of the canal walls by bony tissue forming in the vicinity of the neuromast. The second component, found beneath the first, is composed of a lamellar, membranodermal element that forms in the dermal layer of the skin. This component usually forms from a plate- or sheath-like ossification that may have ornamentation (e.g. frontal, angular, dermopterotic) or teeth (e.g. premaxilla, maxilla, dentary). These two bony components may or may not interact with each other. The characteristics of the interaction vary in some important details, which will determine the characteristics of the bone that results from this process.

The tubular (laterosensory) and membranodermal (lamellar) components may not interact with each other. When the formation of the bone only involves the tubular component, the resulting ossification constitutes an essentially cylindrical element representing the ossification of a segment of a lateral-line canal associated with one CN. On the other hand, if only the membranodermal component is involved in the formation of a bone, it takes the form of a plate, which may or may not bear ornamentation or teeth. Any dermal bone in the head not associated with lateral-line canals is an example of this type of bone. In *P. senegalus*, this includes the bones of the operculo-gular (except for the preopercle, see below) and spiracular series, quadratojugals, the dermohyal, parasphenoid, vomer, dermopalatine, ectopterygoid, endopterygoid, coronoids, and the prearticular. This type of bone corresponds to those that Westoll (1936, 1941) called anamestic bones (e.g. the rostral bones in acipenserids), interpreted by him as 'space-fillers' located between other, more developed dermal bones associated or not with lateral-line canals. Stensiö (1947) redefined anamestic bones as all of those formed independently from bone primordia associated with the laterosensory system. Hilton and Bemis (1999) considered anamestic bones to be dermal elements formed independently of the lateral-line canal system, and they emphasize the distinction between anamestic and canal bones, the latter being dermal bones that form in more-or-less immediate association with lateral-line canals (the authors also discussed issues related to establishing the homology of anamestic bones, which display remarkably high levels of intraspecific variation in sturgeons).

When the two components interact in the formation of a given bone, the result is the formation of a compound bone that represents the fusion between a tubular ossification (the lateral-line component) and a membrane- or plate-like ossification (the membranodermal component). In this case, the exact way in which the two components interact during their development seems to be influenced by three main factors: the relative position between the two components, the relative depth of each component in the dermis, and the relative timing of the ossification of each component. In *P. senegalus*, there are examples showing how each of these three factors influence the development of compound bones.

The influence of topographic relationships may be exemplified by the development of the frontal bone, with which the supraorbital CNs SO4, SO5, and SO6 are associated. In this case, the onset of ossification of the membranodermal component of the bone occurs in the vicinity of the CNs SO5 and SO6, but topographically distant from the site of formation of the tubular ossification associated with SO4. As a result, whereas the tubular ossifications associated with SO5 and SO6 are attached to the membranodermal component of the bone almost from their origins, the tubular ossification associated with SO4 remains separate, being incorporated into the final bone of the adult relatively late in ontogeny. As result, the bone in the adult is a compound bone formed by a membranodermal component (frontal *s.s.*) plus three tubular components associated with the supraorbital CNs SO4, SO5, and SO6.

The influence of the relative depth of each component in the skin layer may be exemplified by the development of the bones associated with the preoperculomandibular CNs PM1, PM2, and PM3 (the dentary), and PM4 and PM5 (the angular). There is a difference in the depth of the tubular ossifications associated with PM3, PM4, and PM5, and those associated with PM1 and PM2 relative to their underlying membranodermal components. The neuromasts of the former group are located more deeply in relation to the membranodermal components, so that the tubular ossifications form already embedded in them. The latter two tubular ossifications (in association with PM1 and PM2), however, are located at a more superficial position to the underlying membranodermal component (the dentary *s.s.*), so that they originate separate from it and only later become incorporated into the membranodermal component forming a compound bone.

Finally, the influence of the timing of development of each bony component is demonstrated by the fact that, in some cases, development starts with the formation of a tubular ossification, which develops lateral flanges that later expand, forming a plate-like element traversed by the lateral-line canal (e.g. nasal 3). In other cases, the ossification of the membranodermal component forms first and the tubular component then ossifies with the formation of ridges on the surface of the membranodermal component, which grow and enclose the CN (e.g. angular).

The observations above support the view that the CNs, by producing tubular ossifications that represent the ossification of the walls of the canal surrounding the neuromast, constitute an independent layer of dermatocranial ossifications that may or may not interact with the underlying lamellar membranodermal layer. In at least one case, the sphenotic of polypterids, the tubular component of ossifications may interact with the endochondral layer as well (see below). Consequently, some of the bones in the skull of polypterids must be interpreted as consisting exclusively of tubular, laterosensory-associated ossifications, others exclusively of membranodermal ossifications (e.g. the so-called anamestic bones), and finally, others as compound bones formed by the fusion between a tubular and a membranodermal component. The details of how each bone forms, with respect to the interaction of the two bony components, will be determined by the interplay between the factors described above, which explains the diversity in the way in which bones associated with lateral-line canals develop in *P. senegalus*.

Many authors who have studied the anatomy of polypterids have identified and recognized the compound nature of at least some of the bones associated with lateral-line canals, especially the dentary, maxilla, and premaxilla, based either on the development of these bones or by comparison with those of closely related groups (e.g. Allis, 1900; 1922; Pehrson, 1947; 1958; Jollie, 1984a). Allis (1900: p. 257), for example, described the premaxilla of *Polypterus* as being 'formed by the fusion of two components, one developed in relation to the teeth of the animal, and the other in relation to the main infraorbital lateral canal'. Pehrson (1958: p. 256) suggested that there is a 'tendency to form complex bones by means of fusion of anamestic bones and laterosensory elements' in polypterids. He even presents a table showing the correspondence between the ossifications associated with the laterosensory canal organs (i.e. neuromasts), the 'separately developing canal bones' (i.e. the tubular ossifications associated with CNs), and the definite bones of the adult. In his interpretation, the following bones are considered to be compound bones that are formed by the fusion of a tubular and a membranodermal component: premaxilla (his 'premaxillary'), maxilla (his 'maxillary'), dentary, angular, and preopercle (his 'preopercular'). Interestingly, Pehrson (1958) did not mention the fourth supratemporal neuromast (ST4), which is associated with the posttemporal.

Based on the current study, however, the list of compound bones in polypterids should include more bones than just those cited by Pehrson (1958). In addition to the premaxilla, maxilla, dentary, angular, preopercle, and posttemporal, we also found evidence that the following bones are also compound bones, which form as a result of the fusion between laterosensory-derived tubular ossifications and a membranodermal ossification: the nasal 3, frontal, rostral, dermopterotic, and extrascapular. These bones are formed initially as exclusively tubular ossifications that later develop lateral, membrane-like expansions or flanges giving the bone its final plate-like form. Because of this, it is not possible to identify the interaction between the two independent components during development, but the interaction is suggested based on other kinds of evidence. For example, in the frontal, there is a difference between the ossification associated with the CN SO4, which originates independently of the remainder of the bone and only later becomes incorporated in the plate-like bone, and the ossifications associated with the CNs SO5 and SO6, which develop in association with the lamellar expansion that represents the membranodermal component of the bone. This contrast strongly suggests that the ossifications associated with SO5 and SO6 become intermingled with the membranodermal component very early in development, so that it is not possible to identify independent elements associated with each component during the ontogeny. This is mostly due to the fact that the location of the membranodermal component coincides topographically with the regions of origin of the tubular ossifications associated with SO5 and SO6, but not with the location of the origin of the tubular ossification associated with SO4.

The extrascapulars provide another interesting example to consider. There is a striking similarity between the extrascapular bones in polypterids and the rhomboidal ganoid scales of the trunk. Agassiz (1833-44) remarked that the only difference between the extrascapulars of polypterids and the body scales is the presence of the laterosensory canals. In fact, the extrascapulars develop initially as exclusively tubular ossifications and develop flange-like expansions only later in development at about the same time that the body scales are forming. This suggests that the final aspect of each extrascapular, as a plate-like bone traversed by the lateral-line canal, is due to the fusion of the tubular, laterosensory-derived ossifications associated with the canal neuromasts, with scale-derived ossifications forming at the occipital region of the body. In this sense, the extrascapulars of polypterids should be interpreted as compound bones formed by

the fusion of laterosensory-derived components of ossifications with scale-derived elements forming at the dermal layer of the skin.

4.2 | Homology of cranial bones in Polypteridae

Based on our analysis of the development of bones associated with lateral-line canals in *P. senegalus*, the hypothesis of the presence of a superficial layer of laterosensory-derived ossifications interacting with the membranodermal layer of ossifications in the formation of compound bones in the skull of polypterids is supported. Our work sheds light on long-standing controversies regarding the homology of the dermatocranial bones of polypterids, especially those considered to be of compound origin. These are discussed below.

4.3 | Nasals

Polypterids are unique among extant actinopterygians in having three independent ossifications at the dorsal surface of the nasal region associated with the anteriormost portion of the supraorbital canal. The two anteriormost elements are essentially tubular ossifications enclosing the CNs SO1 and SO2, and the third is a plate trespassed by the portion of the supraorbital canal associated with CN SO3. The third element is located very close to the surface of the skin and bears ornamentation on its dorsal face, whereas the two anterior elements are more deeply embedded in the skin and lack ornamentation.

Allis (1900; 1904; 1922) considered the three nasal bony elements of polypterids to 'quite certainly represent the single nasal bone of *Amia* [...] and hence also that of *Lepisosteus*' (Allis, 1922: p. 203), because of the 'striking similarity' of the canals of these fishes (Allis, 1900: p. 442). He highlighted the similarity between polypterids and *Amia calva* in the number of CNs present in this region, in the position of the pores, and in the presence of the posterolateral bend in the canal as result of the position of the CN SO1. According to him, 'the agreement is so exact that it clearly establishes the homology of the three bones in one fish [polypterids] with the single bone in the other [*A. calva*]' (Allis, 1900: p. 442). However, he did not discuss whether the condition of polypterids should be interpreted as plesiomorphic or apomorphic.

Pehrson (1922; 1947) considered the correspondence (i.e. homology) between the three nasal elements of polypterids and the single nasal of *Amia calva* and other actinopterygians to be 'firmly established' (Pehrson, 1947: p. 428). He describes how, in *A. calva*, the single nasal bone originates from three bony primordia, one associated with each CN of the supraorbital line (Pehrson, 1922, 1940), and considered this developmental data to corroborate Allis' (1900, 1904, 1922) hypothesis. Daget (1950) agreed that the three nasals of polypterids should be considered equivalent to the single nasal bone of *A. calva* and other actinopterygians on the basis of the ontogenetic evidence presented by Pehrson (1922; 1947). In his opinion, the condition of polypterids results from the three bony primordia (each associated with one CN) failing to fuse during development to originate a single element. Daget (1950) regarded the condition of polypterids as secondary (i.e. apomorphic), and the presence of a single pair of nasal bones as a 'general' (i.e. plesiomorphic) condition for Actinopterygii. Jollie (1984a: p. 478) agreed with Allis (1900; 1922; 1934), Pehrson (1922; 1947), and Daget (1950) that the three nasals of polypterids and the single nasal of *Amia* are homologous, and described the three independent nasals of polypterids as 'a fragmentation product of such a bone, as seen in *Amia* (where there are three neuromasts) or in *Lepisosteus* (where there are even more neuromasts)'. The author, however, highlighted that the condition of polypterids resembles that in some sarcopterygians (e.g. rhipidistians), which may have three or more independent nasal elements (e.g. †*Osteolepis macrolepidotus* may have four to seven independent nasal ossifications, according to Westoll, 1936).

Our results, however, provide a new interpretation for the homology of the nasal elements of polypterids. Our observations have shown that the two anteriormost nasal bones of *P. senegalus* develop as essentially tubular bones representing the ossification of the portion of the lateral-line canal associated with the CNs SO1 and SO2. The so-called third nasal, however, is a compound bone formed by the fusion between the tubular ossification associated with the CN SO3, and an ornamented, plate-like ossification developing just anterior to the frontal. The plate-like component of the third nasal develops relatively later in development, whereas the tubular components of the three nasal elements develop at about the same time, earlier than the onset of formation of the plate-like component. Therefore, in polypterids, the dorsal surface of the nasal region is formed by a series of three tubular ossifications, each associated with one CN in the nasal portion of the supraorbital canal, the posteriormost of which is fused with a plate-like nasal *s.s.* forming a compound bone.

A similar condition is present in all extant species of Acipenseridae (Hilton et al., 2011). In these species, the nasal portion of the supraorbital canal is represented by a thin (sometimes irregularly fragmented) tubular bone located between the anterior and posterior nares, and by an ornamented plate-like bone just anterior to the frontal and trespassed by the supraorbital canal, which is continuous with the tubular bone (Allis, 1904; Jollie, 1980; Hilton et al., 2011; Warth et al., 2017). The plate-like bone is usually identified as the nasal (e.g. Jollie, 1980, Hilton et al., 2011; Warth et al., 2017), whereas the tubular bone anterior to it has been identified as tubular nasal (Jollie, 1980; Warth et al., 2017), tubular bone anterior to the nasal (Hilton et al., 2011) or merely a 'bar separating the anterior olfactory opening from the posterior one' (Sewertzoff, 1926). Hilton et al. (2011) described how the plate-like nasal of the Shortnose Sturgeon, *Acipenser brevirostrum*, would be difficult to distinguish from the bones of the rostral series of anamestic bones if the sensory canal was not present. Allis (1904) and Hilton et al. (2011) considered the tubular ossicles and the plate-like bone of sturgeons to be distinct parts of the nasal. Jollie (1980), on the other hand, considered the tubular and plate-like elements of sturgeons to be different units, and described the tubular nasal ossicle of *Acipenser ruthenus* as

a tubular bone that remains as such in adults, whereas the plate-like nasal bone is described as 'an irregular bony plate with a canal-associated growth center' (Jollie, 1980: p. 234). Jollie (1980) noticed that the plate-like nasal bone develops later than the formation of the tubular nasal bones in *A. ruthenus*, as was found in *P. senegalus*. The same pattern is reported in *Acipenser baerii* and *Acipenser gueldenstaedtii*, in which the plate-like nasal develops at about the same time as the dorsal rostral anamestic bones (Warth et al., 2017). These examples, together with the ontogeny of these elements in *P. senegalus*, provide further evidence that the tubular and plate-like components of ossification associated with the nasal portion of the supraorbital canal are independent. Another line of evidence is provided by the other extant representatives of Acipenseriformes, the paddlefishes, *Polyodon spathula* and *Psephurus gladius*, both of which are characterized by reductions on the dermatocranial skeleton. In these taxa, the tubular bones representing the nasal portion of the supraorbital canal are present, whereas the plate-like bone associated with them is absent (Allis, 1903b; 1904; Grande and Bemis, 1991).

Taking these facts into consideration, a new interpretation about the correspondence between the three nasals of polypterids and the single nasal of neopterygians is necessary. In both groups, as well as in acipenserids (and thus plesiomorphically in Actinopterygii), the only plate-like ossification associated with the dorsal nasal region is the nasal *s.s.* This ossification is just anterior to the frontal, may bear ornamentation and, when present in neopterygians, usually encompasses the entire nasal portion of the supraorbital canal, such that there is only one plate-like nasal ossification trespassed by the anterior portion of the supraorbital canal. This plate-like ossification of neopterygians interacts with the tubular components of ossification associated with the supraorbital canal, forming a compound bone. In many representatives of Neopterygii, however, this plate-like ossification (i.e. the nasal *s.s.*) is absent, so that there is only a tubular ossification at the dorsal nasal region that represents the tubular component of the ossifications associated with the supraorbital canal: e.g. Hiodontidae—Li and Wilson, 1994; 1996; 1999; Hilton, 2002a; Hilton and Grande, 2008; many characiforms and siluriforms: Ostariophysi—Arratia and Huaquin, 1995; Arratia, 2003, Pastana et al., 2019. There are also cases in which both the tubular and plate-like components of the nasal are absent even though the nasal portion of the supraorbital canal is still present, so that the canal exists as an unossified tubular canal composed only of soft tissue. This is the case in many representatives of Trichomycteridae (Ostariophysi: Siluriformes, e.g. *Ituglanis*), in which the nasal portion of the supraorbital canal is present but not enclosed in any ossification (Arratia and Huaquin, 1995; Rizzato and Bichuette, 2017). However, in the sister group of Trichomycteridae, the Nematogenyidae (Ostariophysi: Siluriformes), and in most siluriforms (including diplomystids, the sister group of the clade formed by all remaining siluriforms) the nasal portion of the supraorbital canal is enclosed by a tubular ossification (Arratia and Huaquin, 1995; Rizzato and Bichuette, 2017).

In polypterids and acipenserids, the plate-like nasal *s.s.* is present but only interacts with the posterior portion of the nasal portion of the supraorbital canal, whereas the anterior portion extends anteriorly and is enclosed only by tubular ossifications associated with the lateral-line canal. In polypterids, two tubular bones are formed in association with the SO1 and SO2 CNs of the supraorbital canal. In acipenserids, a very thin tubular ossification may be fragmented in several pieces and associated with the anteriormost CNs of the supraorbital canal. In contrast, in polyodontids, the nasal *s.s.* is absent, and only the tubular component of ossifications associated with the nasal portion of the supraorbital canal is present forming a thin, osseous tube running at the dorsal region of the nasal capsule.

In sum, the presence of a single, plate-like nasal (i.e. the membranodermal nasal, or nasal *s.s.*) is plesiomorphic for Actinopterygii. The absence of this membranodermal element in polyodontids and in many teleosts is a derived condition within Actinopterygii. When the membranodermal, plate-like nasal is absent, the tubular component of the nasal, i.e. the ossification of the nasal portion of the supraorbital canal, may still be present (e.g. hiodontids, some characiforms, and most siluriforms), and when it is, the tubular bone thus formed is usually identified as the nasal. Both the plate-like and tubular ossifications are absent in some neopterygians, even though the nasal portion of the supraorbital canal is still present as an unossified canal (e.g. many trichomycterids such as *Ituglanis*). In polypterids and acipenserids, both the membranodermal and tubular ossifications are present, but the nasal portion of the supraorbital canal extends anteriorly to the membranodermal nasal, forming tubular ossifications associated with the anteriormost CNs of the supraorbital canal that are located anterior to the membranodermal, plate-like nasal. In Neopterygii, when both the membranodermal, plate-like nasal and the tubular component of the nasal are present, the plate-like nasal usually encompasses the entire nasal portion of the supraorbital canal, encompassing therefore all the tubular ossifications of the nasal portion of the supraorbital canal (e.g. *Amia*). In the light of these new findings, a thorough reevaluation of the elements identified as 'nasals' in the different groups of bony fishes, i.e. distinguishing the plate-like, membranodermal nasal (nasal *s.s.*) and the tubular, lateral-line derived ossification of the nasal portion of the supraorbital canal, would be most valuable and may clarify the evolution of these elements across the bony fishes and especially within Teleostei.

4.4 | Rostral

Müller (1846), Huxley (1861), and Traquair (1870) identified the anteriormost bone of the infraorbital canal in *Polypterus* as the ethmoid. Traquair (1870) remarked that the same bone was called the nasal by Owen (1866) and others, and considered it to be a median perichondral ossification on the rostral region of the neurocranium. He also mentioned the presence of a posterior process of the bone located between the left and right nasal bones. Pollard (1892: p. 400), however, concluded that 'there is no endochondral ossification in front of the nasal septum', and that the ethmoid is a dermal ossification. Allis (1922: p. 203) agreed with Pollard (1892) that the ethmoid is a dermal ossification, 'lying everywhere external to the

cartilage and separated from it by a layer of connective tissue'. Allis (1922: p. 204) mentioned the presence of a 'thickened anterior end of the bone' containing the anteriormost infraorbital CNs of each side of the head, which represents the connection between the left and right contralateral infraorbital canals (i.e. the ethmoid commissure), and compared this bone to the middle portion of the rostral of *Amia calva*. Gregory (1933) agreed with Pollard (1892) and Allis (1922) that in polypterids this bone is of dermal origin and named it the dermethmoid.

Holmgren and Stensiö (1936), Jarvik (1942), Pehrson (1947; 1958), and Claeson et al. (2007) used the term (median) rostral, whereas De Beer (1937) proposed the name supraethmoid 'for the median intramembranous bone resulting from the fusion of two symmetrical laminar bones, which sometimes fuses also with the ethmoid' (Rojo, 1991). Daget (1950) used the name supraethmoid following De Beer (1937), but remarked that there is no indication of a paired (i.e. bilateral) origin of this bone. Interestingly, Daget (1950) mentioned the presence in some palaeoniscoids of a median dermal bone located between the left and right nasals but not trespassed by lateral-line canals that should be named the postrostral. Jarvik (1947) named the rostral bone in polypterids as rostro-postrostral, a name followed by Poplin and Lund (1995). Poplin and Lund (1995) define the postrostral as a median anamestic bone located between the frontals, rostrals, and nasals, whereas the rostrals are defined as paired bones bearing the ethmoid commissure. Following this definition, they considered this bone in polypterids to be the result of the fusion between the postrostral and the rostral elements, which, according to them, are distinct from each other in early developmental stages in *Polypterus* (Poplin and Lund, 1995). According to these authors, in adult polypterids the rostral and postrostral are 'fused as a single median, rostro-postrostral which separates the pair of nasals and bears along its anterior margin the ethmoid commissure' (Poplin and Lund, 1995: p. 226). Jollie (1984a: p. 475), following a similar rationale, named the bone the medial rostral-internasal, remarking that the internasal (i.e. postrostral) portion, 'when exposed, may show signs of partial separation or may be completely separated into (two) separate plates'.

The nature of the rostral bone in polypterids can be easily understood as the result of a fusion between laterosensory and membranodermal bony components. The laterosensory, tubular component corresponds to the rostral bone of other non-teleost actinopterygians such as holosteans, and in polypterids, it contains the left and right anteriormost infraorbital CNs (IO1 + IO1). The membranodermal component, in turn, corresponds to the so-called postrostral in other actinopterygian fishes, and is represented by the posterodorsal process of the bone that is located between the left and right third nasals. The presence of a postrostral element in polypterids must be considered a plesiomorphic character, which occurs only in other non-neopterygian actinopterygians (Poplin and Lund, 1995). The rostral, in turn, is also present in non-teleost neopterygians (e.g. the holosteans, Grande and Bemis, 1998; Grande, 2010), but it was apparently lost in most teleosts (exceptions include basal teleosts such as *Elops*).

4.5 | Sphenotic

Traquair (1870: p. 169) was the first author to notice that the sphenotic of polypterids was a bone formed by two components, including 'a posterior, yellowish and spongy-looking [bone], placed like a little vertical plate projecting down from the posterior external angle of frontal bone; and an anterior part, white and compact, flattened horizontally, and closely applied to the lower surface of the frontal, along its external margin behind the orbit'. Traquair (1870) and Pollard (1892) distinguished two bones in this region, namely, a canal-bearing, dermal ossification (their 'postfrontal'), and an endochondral ossification, the autosphenotic (their 'sphenotic'). Allis (1922: p. 221), however, recognized a single bone formed by the fusion of the elements identified by the former authors, naming it 'postfronto-sphenotic'; according to him, the two components are 'apparently completely fused with each other from their very inception, and not simply anchylosed in later stages of development'. Pehrson (1947: p. 404) also highlighted the fact that the autosphenotic and the canal ossification fuse together very early in development, but remarked that the former originates after the latter and then fuses to it. He described the canal ossification as developing 'as a normal tube-like canal bone lodging the infraorbital neuromast No. 9', and then fusing 'with a perichondral ossification on the lateral edge of the *taenia marginalis*', the autosphenotic (his 'sphenotic') (Pehrson, 1947: p. 438). A compound sphenotic in polypterids was also recognized by later authors (e.g. Daget, 1950; Jollie, 1984a; Claeson et al., 2007; Grande, 2010).

The compound nature of the sphenotic in polypterids can also be easily understood by recognizing the laterosensory, tubular component of ossifications as an independent layer that may or may not interact with the other layers of ossification. The peculiarity in this case is that the tubular component does not interact with a membranodermal bone, as is generally the case, but rather with an endochondral bone. Although apparently rare, the fact that this fusion resulting in a compound bone occurs in the sphenotic of polypterids, demonstrates that this kind of interaction (i.e. with an endochondral instead of a membranodermal component of ossifications) is possible (see also Patterson, 1977 for discussion of homologizing bones of mixed histogenesis).

4.6 | Antorbital

An independent antorbital bone is absent in polypterids, both in adults and young specimens. However, many authors (e.g. Allis, 1922; Holmgren and Stensiö, 1936; Pehrson, 1947; 1958; Daget, 1950) maintained that an antorbital is present as part of the adult premaxilla, forming a compound premaxilla-antorbital bone. Exactly which part of the premaxilla would represent the antorbital element is unclear. Allis (1922) considered the antorbital portion of the premaxilla to be the posterolateral process of the antorbital, located 'lateral and posterior to the *fenestra nasalis* [...] lying against the lateral surface of the nasal capsule and giving support, on its dorsal end, to the lateral edge of the nasal and the antero-lateral

corner of the frontal'. Thus, the antorbital portion of the premaxilla in polypterids does not involve any of the laterosensory-derived tubular ossifications associated with the premaxilla according to Allis (1922). Pehrson (1947), however, considered the antorbital to be represented by the two posteriormost of the three tubular ossifications that become fused to the premaxilla *s.s.* during development. Regarding the posterodorsal process of the premaxilla, Pehrson (1947) concluded that there is no embryological evidence for interpreting it as homologous to the antorbital or to the dorsal part of the antorbital of *Amia*.

In Acipenseridae, the antorbital is composed only of a bilateral, triradiate canal bone termed a lateral rostral bone by Hilton (2002b); see discussion of its homology by Warth et al. (2017). In adult *Amia*, the antorbital is an independent bone formed by a canal portion including four CNs (IO3–IO6), plus a plate-like bone located more posteriorly, just lateroventral to the lacrimal. That element in *Amia* develops initially as a Y-shaped tubular bone, similar to that found in acipenserids, but later develops a posterior plate-like flange (Grande and Bemis, 1998: figures 11 and 17), suggesting that it is formed by the fusion of a tubular and a membranodermal component. Thus, we suggest that the bone identified as the 'antorbital' in *Amia* is actually formed by the fusion of four tubular ossifications associated with infraorbital CNs plus a plate-like component representing the antorbital *s.s.* In support of this view, there are examples of fishes that have antorbital bones consisting solely of plate-like ossifications, without associated lateral-line canals, e.g. many representatives of Characiformes and a few siluriforms (Bockmann, 1998; Pastana et al., 2019). In these fishes, the bone in question represents the antorbital *s.s.*, without associated tubular laterosensory-derived ossifications. Other ostariophysans (e.g. most siluriforms, Gymnotiformes) and a single, basal group of Characiformes (Erythrinidae), however, have antorbitals with associated lateral-line canals (Pastana et al., 2019). This provides support for the view that the element associated with laterosensory canals identified as the 'antorbital' in many groups, including *Amia*, is actually a compound bone formed by the fusion between a tubular laterosensory component plus a membranodermal component, that is, the antorbital *s.s.*

Thus, these examples would agree more with Allis' (1922) interpretation of the posterolateral process of the premaxilla as representing the antorbital (*sensu stricto*) element of the bone than with Pehrson's (1947) interpretation that the antorbital is represented by the two posteriormost tubular ossifications associated with the premaxilla. These two posteriormost tubular ossifications correspond to the four tubular ossifications that in *Amia* fuse to the antorbital *s.s.* In *P. senegalus*, however, it was not possible to identify any fusion between an independent antorbital element and the premaxilla. Our observations show that the posterolateral process of the premaxilla develops as a posterodorsal projection of the bone over the lateral wall of the nasal capsule (Figures 10–13) and not as an independent ossification that becomes fused to the posterolateral margin of the premaxilla. Therefore, we agree with Pehrson (1947) that there is no ontogenetic evidence for considering the posterolateral process of the premaxilla in polypterids as the homologue of the antorbital *s.s.* of other fishes.

If the antorbital is indeed absent in polypterids, it is replaced in these fishes by the posterodorsal expansion of the premaxilla that covers the lateral wall of the nasal capsule. It is interesting to note that in *Hiodon* (Teleostei: Hiodontiformes), the lateral ethmoid has a membranous lateral extension that, similar to the posterodorsal process of the premaxilla in polypterids, covers the lateral wall of the nasal capsule (Hilton, 2002a). This lateral extension was also considered by some authors (e.g. Patterson, 1977; Taverne, 1977; Li and Wilson, 1994) to represent an antorbital element, so that the entire lateral ethmoid of *Hiodon* was interpreted as a fusion between an endochondral (the lateral ethmoid) and a dermal (the antorbital) component. Hilton (2002a), however, interpreted this bone as simply the lateral ethmoid because he did not observe any evidence of fusion between independent elements during the ontogeny of *Hiodon*. This is the same rationale followed here regarding the premaxilla of *P. senegalus*.

4.7 | Preopercle

The nature of the polypterid preopercle (Figure 1) has been historically controversial. Agassiz (1833-44: p. 40) commented that the topological relationships of this bone are 'strange', especially due to its close association with the maxilla anteriorly by means of interdigitating processes (Figures 1, 6, 7, 12, 13, 14, and 15). He regarded this bone as a fusion between the 'true' preopercle, which he identified as the part of the bone not covered by ganoine, and an undetermined number of ossicles that he considered homologous to the bony cheek elements of lepisosteids (suborbitals of Grande, 2010), forming the ganoine-covered portion of the bone. Huxley (1861) raised doubts about the presence of a 'true' preopercle in all crossopterygians, a group proposed by him that included *Polypterus* and many fossil sarcopterygians. Traquair (1870: p. 179) considered the presence of anything corresponding to the preopercle in polypterids to be 'somewhat doubtful', and referred to this bone as an unidentified dermal bone of the cheek. Collinge (1893) considered this bone to be a fusion of the preopercle with elements homologous to the infraorbital bones of *Lepisosteus*, whereas Pollard (1892) considered it a fusion between the preopercle and elements homologous to the postorbitals of *Amia calva*. Allis (1922: p. 238) agreed that the preopercle of polypterids seems to have been formed by the fusion of two distinct components, 'a large plate-like superficial one, and a deeper one which lies along the mesial surface of the hind edge of the superficial component and projects ventrally beyond it as a stout flat process'. He considered the superficial component to be homologous not to the postorbitals of *A. calva* but to the so-called squamosal of sarcopterygians such as †*Glyptopomus* and †*Osteolepis* (Sarcopterygii: Osteolepiformes). The deeper component is, according to him, homologous to the preopercle of *A. calva* and teleosts.

Pehrson (1922; 1947; 1958) was the first to use developmental data to address the question of the homology of the preopercle of

polypterids. At first, he was convinced that this bone was a fusion between a squamoso-preopercular dorsally and a quadrato-jugal-preopercular ventrally (Pehrson, 1922). In another work, he agreed that this bone might consist of a dorsal and a ventral portion, but highlighted that, in his view, 'there is nothing that indicates that these two parts have formed independently of each other' (Pehrson, 1947: p. 445). In his interpretation, the anterior portion of the bone, which reaches the maxilla anteriorly, 'is anything but a process of the preopercular' that broadens during development and becomes the robust cheek plate of adult polypterids. He considered this anterior process of the preopercle of polypterids to correspond partially to the rostral portion of the long preopercle of some †palaeoniscids. In this work, Pehrson (1947) described the development of the preopercle in polypterids as beginning with the ossification of the canal portion associated with CN PM8, which, according to him, develops a long anterior process that reaches and associates with the posterior end of the maxilla. This description, however, was an interpretation based on the smallest specimen available for him at that point, a 24-mm specimen in which the preopercle was already fused to the tubular bones representing the preoperculomandibular canal.

In a later work, however, having analyzed specimens representing earlier developmental stages of *Polypterus*, Pehrson (1958) proposed a new interpretation of the identity of the preopercle of polypterids. That author identified the presence of a thin bony element posterior to the maxilla *s.s.* in a 8-mm specimen. He attributed a decisive importance to the fact that 'it is apparently not connected with any sensory line' (Pehrson, 1958: p. 248), which ruled out the possibility of this bone being an ossification associated with the lateral-line system. The alternative, therefore, was that this bone is of anamestic origin (i.e. a membranodermal ossification). Pehrson (1958: p. 249) then accepted the suggestion of Stensiö (1947) that this element represents 'an ontogenetically independent portion of the maxillary proper', and defended the idea that the bony element posterior to the maxilla plus the plate-like, anamestic ossifications posteroventral to it (bone Y' of Traquair, 1870) represent the broad posterior portion of the maxilla of †palaeoniscids. In polypterids, these three elements of the maxilla would develop independently. He named one of them the supramaxillary, which fuses to the tubular ossifications associated with the CNs PM6, PM7, and PM8 to form a compound preopercle. He then compared the compound nature of the preopercle, formed by the fusion between laterosensory elements and an anamestic bone, to the premaxilla, maxilla, dentary, and angular, in which a similar situation occurs.

Jollie (1984a) rejected the hypothesis of Pehrson (1958) that the element posterior to the maxilla, which fuses to the tubular ossifications representing the preoperculomandibular canal to form the preopercle, is the supramaxilla. He argued that 'functional incorporation of such a bone into the preopercle seems most unlikely' (Jollie, 1984a: p. 481), and that the supramaxilla is a bone present in more derived actinopterygians. Jollie (1984a) disagreed with Pehrson (1958) who said that this bone develops from four different centers of ossification, the supramaxilla and three tubular ossifications, one associated with each of the three CNs PM6, PM7 and PM8. He argued that the preopercle of polypterids arises 'as a coordinated unit, even though one centre, associated with the ventral neuromast, appears separately', and that it is therefore a single element, 'unique in form and origin within actinopterygians' (Jollie, 1984a: pp. 481–482).

Bartsch (1997) described the early ontogeny of the head skeleton in *P. senegalus* with special consideration of the functional implications of development, especially for feeding, breathing, and locomotion. He described the formation of the interdigitation between the posterior process of the maxilla and the so-called 'squamosal part of the preopercular' (Bartsch, 1997: p. 370), noting that the arch supports the lateral portion of the jaw adductor musculature. He also remarked that the element in *P. senegalus* originates separately from the canal-bearing portion of the preopercle, which appears much later in development and fuses to the element in the same way as the 'infraorbitals' fuse to the 'dentigerous maxillary bone' (i.e. the maxilla *s.s.*). Bartsch (1997) considers the element to represent the 'squamosal cheek plate', or squamosal, of sarcopterygians, concluding that this bone is not exclusive of the latter, its presence in early ontogeny representing the 'basic pattern' of actinopterygians (Bartsch, 1997: p. 377). Finally, he remarked that the preopercle of actinopterygians is a compound bone.

Our analysis of the development of *P. senegalus* (Figures 6, 7, 12, 13, 14, and 15) clearly shows that the bone identified as the preopercle in polypterids has a compound origin derived from at least two independent elements. One of the elements is indisputably homologous to the preopercle of other fishes. It is formed by the fusion of three tubular ossifications associated with the CNs PM6–PM8 and corresponds to the posterior portion of the bone, located at the posterior region of the cheek. In other fishes, such as holosteans, the preopercle forms in association with a higher number of CNs in the preopercular portion of the preoperculomandibular canal (e.g. 9–11 in *Lepisosteus osseus*, Song and Northcutt, 1991; 6 in *Amia calva*, Allis, 1889), but it also develops as an essentially tubular ossification at the posterior region of the cheek. The medial face of the preopercular portion of the compound preopercle of polypterids serves as one of the origins of the *m. adductor mandibulae*, as well as in all actinopterygians (except for the acipenseriforms, in which the preopercle is greatly reduced; Hilton et al., 2011; Datovo and Rizzato, 2018), providing additional support for the hypothesis that the posterior portion of the bone includes a preopercular element, homologous to the preopercle of other actinopterygians.

The other component of the preopercle is of anamestic origin and corresponds to the anterior portion of the bone. In *P. senegalus*, it is one of the first membranodermal ossifications to form, together with the maxilla *s.s.*, dentary *s.s.*, angular *s.s.*, and prearticular. From its inception, this element is located posterior to the maxilla *s.s.*, evidently as a separate element; this precludes the interpretation of this bone as a posterior portion of the maxilla. However, early in the ontogeny, the posterior portion of the maxilla becomes intimately associated with the anterior portion of this bone by means of well-developed interdigitating processes that persist through

development. The posterior portion of this bony element fuses to the tubular component of ossifications representing the preoperculomandibular canal (i.e. to the true preopercle) and expands, forming the compound preopercle seen in adults.

Considering the characteristics listed above, especially the early association with the maxilla by means of well-developed interdigitations, this bony element resembles the jugal bone of other vertebrates. The jugal is also called zygomatic, but the latter name is restricted to mammals to avoid the inference that a zygomatic arch is present in nom-mammalian vertebrates (Jollie, 1962; in humans, it may also be called malar). The jugal bone can be easily recognized in tetrapods (including fossils) by its topological relationships with other bones, especially because it is usually involved in the margin of the orbit, and for this reason is considered part of the circumorbital series of bones (Schoch, 2006; Gai et al., 2017). Because of this, the jugal has been tentatively homologized with one of the infraorbital bones of actinopterygians (e.g. infraorbital 3 or the lower postorbital of *Amia*, Schultze, 2008; Gai et al., 2017; suborbital 2 of *Notropis* and other teleosts, Gregory, 1933; Harrington, 1955). Hilton et al. (2011) used the term jugal for a bone of the infraorbital sensory canal positioned posteroventral to the orbit. However, the circumorbitals are bones with associated lateral-line canals, whereas the jugal, when present, is an anamestic ossification. Of greater importance is the close relationship of the jugal with the maxilla, resulting in these bones being firmly attached to each other by means of interdigitating processes or sutures. As in larval stages of *P. senegalus*, this association usually appears very early in the development of many different groups of vertebrates, such as diapsids and mammals (Jollie, 1962; Schoch, 2006; Ollonen et al., 2018), including humans (Mall, 1906). In lissamphibians, the development of the circumorbital bones was found to be postdisplaced, resulting in the absence of the jugal as well as of other elements such as the postfrontal and postorbital (Schoch, 2006). It is important to notice that the squamosal of sarcopterygians, when present, does not develop such an intimate association to the maxilla, precluding the interpretation of this element in polypterids as the squamosal. Additional evidence in support of this view is that the jugal is involved, together with the maxilla anteriorly and the quadratojugal posteriorly, in the formation of the lateral margin of the adductor fossa (including, as mentioned above, in the formation of the zygomatic arch of mammals). This is precisely the case of the compound preopercle of adult polypterids, to which the jugal element is fused (Datovo and Rizzato, 2018: figure 11). The characteristics listed above, therefore, suggest that the membranodermal element that interdigitates with the maxilla early in development and expands posteriorly, fusing to the preopercular element and forming the compound preopercle of adult polypterids, is the jugal.

Based on our analysis of the development of *P. senegalus*, we propose that the preopercle of polypterids is a compound bone formed by at least two independent elements, the jugal anteriorly (a membranodermal ossification) and the preopercle posteriorly (a laterosensory-derived tubular ossification). The presence of a jugal element in polypterids is unusual among actinopterygians and is more parsimoniously interpreted as a plesiomorphic condition of the family, since the jugal bone is elsewhere found, among extant bony fishes, only in sarcopterygians. The re-evaluation of the homology of the jugal of Acipenseriformes (e.g. Hilton et al., 2011) is warranted, but a reevaluation and reinterpretation of the phylogenetic distribution of the jugal in osteognathostomes, including fossils, will be necessary to clarify the evolution of this element across the bony fishes.

5 | CONCLUSION

The present study provides a new perspective on our understanding of the relationships between lateral-line canals and skull bones in fishes. Our results demonstrate that the lateral-line canal system in *P. senegalus* contributes with an independent layer of ossifications that may or may not interact with the underlying layer of membranodermal ossifications in the formation of the dermatocranial skull bones. Previous discussions focused on the question of whether the canal neuromasts of the lateral-line system play a causal role in the formation of the lateral-line canals or the dermal bones with which they are associated (e.g. Pehrson, 1922; De Beer, 1937; Westoll, 1941; Moy-Thomas, 1941; Lekander, 1949; Graham-Smith, 1978; Tarby and Webb, 2003; Pastana, 2014). However, the development of bones associated with lateral-line canals in *P. senegalus* illustrates four ontogenetic pathways by which this interaction may occur, which differ with respect to the nature of the spatial and temporal interaction between the two components that form compound bones.

There has been a discussion in the literature about the existence of two distinct patterns of development of bones associated with lateral-line canals: a one-component pattern and a two-component pattern (Lekander, 1949; Tarby and Webb, 2003; Pastana, 2014). In the two-component pattern, the lateral-line canal system comprises an independent layer of ossifications that interacts with an underlying layer of membranodermal ossifications. This is precisely the pattern observed in *P. senegalus*, and documented in other actinopterygians such as holosteans (*Amia calva*, Allis, 1889; Pehrson, 1922; 1940; *Lepisosteus*, De Beer, 1937; Aumonier, 1941) and basal teleosts including elopomorphs (Allis, 1903a; De Beer, 1937), esocids (Pehrson, 1944), ostariophysans (Kindred, 1919; Lekander, 1949; Reno, 1966; Kapoor, 1970), and salmonids (Pehrson, 1922; De Beer, 1937; Jollie, 1984b). In the one-component pattern, the canal ossification is represented by ridges developing from the underlying membranodermal component so that the lateral-line component is not observed to be an independent bony component. A one-component pattern has been reported only for perciform fishes (Mabee, 1993; Tarby and Webb, 2003; Webb and Shirey, 2003). Tarby and Webb (2003) described a one-component pattern of development of bones associated with lateral-line canals in the perciform *Archocentrus nigrofasciatus* (Cichlidae). They argued that the formation of bones associated with lateral-line canals in this species 'does not appear to follow a two-component pattern of development

because two distinct bony elements (a tubular laterosensory element and a flat underlying lamellar element) could not be distinguished at early stages of lateral-line bone development' (Tarby and Webb, 2003: p. 54).

Interestingly, our results related to the development of the dermatocranial bones in *P. senegalus* demonstrate the co-existence of one-component and two-component patterns of bone formation. A one-component pattern occurs when the interaction between the lateral-line and membranodermal components of ossification is such that the onset of formation of the tubular ossification begins after the onset of formation of the membranodermal ossification associated. Therefore, the so-called one-component pattern of formation of lateral-line bones represents only a specific case of interaction between the laterosensory-derived and the membranodermal components of ossification. However, as Tarby and Webb (2003) correctly highlighted, a phylogenetic signal may explain the presence of a clear two-component or a one-component pattern of lateral-line bone formation in different taxa. This may be due, as suggested by Kapoor (1970: p. 93), to the fact that in more advanced teleosts the dermatocranial bones (including membranodermal and laterosensory-derived tubular bones) have a 'tendency to "retreat" deeper into the softer tissues and away from the epithelium', favoring a one-component-like pattern of ontogenetic development of bones associated with lateral-line canals. Clearly, a broad-scale comparison of the patterns of formation of bones associated with lateral-line canals among representatives of different lineages of actinopterygians is needed to evaluate this hypothesis. Such a study would also help to clarify controversies about the homology of bones across numerous taxa, which may have important implications for our understanding of phylogenetic relationships among groups of bony fishes.

ACKNOWLEDGEMENTS

We thank Robert Cerny (Department of Zoology, Charles University in Prague) for supporting and supplying of embryonic material of *P. senegalus*, Martin Kralovic for helping to complete missing developmental stages of the developmental series, and Radek Šanda from the National Museum in Prague for helping in cataloguing the material. We thank André Esguícero from LIRP, Sarah Huber from the Nunnally Ichthyological Collection of the VIMS, and David Johnson, Sandra Raredon, Jeff Williams, Jeff Clayton, Kris Murphy, Erika Wilbur, and Ai Nonaka from USNM for helping with the loans and visits to collections. We thank Ivan Britto from GE Brazil Technology Center for generating the 3D model of the specimen, and Diego Vaz from VIMS and Daniel Cavallari from CBD-FFCLRP-USP for helping with the analysis of the CT-scan data. We also thank Murilo Pastana, Diego Vaz, and David Johnson for discussions about fish anatomy and the lateral-line system. This study was funded by the São Paulo Research Foundation (FAPESP) and Coordenação de Aperfeiçoamento de Pessoal de Nível Superior – Brasil (CAPES) – Finance Code 001 including a PhD scholarship (Pedro P. Rizzato, contract grant number 2014/10849-6) and an International Research Internship (Pedro P. Rizzato, contract grant number 2016/06677-0). This study was also supported by the Charles University Grant Agency GAUK 640616 (Anna Pospisilova) and Conselho Nacional de Desenvolvimento Científico e Tecnológico (CNPq), Brazilian Federal Government (Flávio Bockmann, contract grant number 312687/2018-4). The authors gratefully acknowledge support from the Center for Documentation of Biodiversity (Centro para Documentação da Biodiversidade - CDB), Department of Biology, FFCLRP, University of São Paulo, Brazil. This article constitutes part of the project 'Core-facility for the conservation of scientific documentation: biological collections and high technology research in comparative morphology' (CT-INFRA 01/2013), financed by the Funding Authority for Studies and Projects (FINEP), Ministry of Science, Technology, Innovation and Communication, Brazilian Federal Government. The authors declare that there are no conflicts of interest involved in the publication of this work. This is contribution number 3893 of the Virginia Institute of Marine Science, William & Mary.

AUTHOR CONTRIBUTIONS

PPR and FAB prepared the CT-scanning images of adult specimens. AP prepared the developmental series and the fluorescence photographs analyzed in the present work. PPR, FAB, and EJH discussed the results and interpretations of the data.

DATA AVAILABILITY STATEMENT

The data that support the findings of this study are available from the corresponding author upon reasonable request.

ORCID

Pedro P. Rizzato https://orcid.org/0000-0002-6010-5686
Anna Pospisilova https://orcid.org/0000-0002-8252-0709
Eric J. Hilton https://orcid.org/0000-0003-1742-3467
Flávio A. Bockmann https://orcid.org/0000-0002-1200-1487

REFERENCES

Agassiz, L. (1833–44) *Recherches sur les Poissons Fossiles*. Tome II. Neuchâtel: Imprimerie de Petitpierre, p. 338.
Allis, E.P. (1889) The anatomy and development of the lateral line system in *Amia calva*. *Journal of Morphology*, 2(3), 463–566.
Allis, E.P. (1898) On the morphology of certain of the bones of the cheek and snout of *Amia calva*. *Journal of Morphology*, 6(3), 425–466.
Allis, E.P. (1900) The lateral sensory canals of *Polypterus bichir*. *Anatomischer Anzeiger*, 17(23), 433–451.
Allis, E.P. (1903a) The lateral sensory system in the Muraenidae. *Internationale Monatsschrift für Anatomie und Physiologie*, 20, 125–170.
Allis, E.P. (1903b) On certain features of the lateral canals and cranial bones of *Polyodon folium*. *Zoologische Jahrbücher. Abteilung für Anatomie und Ontogenie der Tiere*, 17, 659–678.
Allis, E.P. (1904) The latero-sensory canals and related bones in fishes. *Internationale Monatsschrift für Anatomie und Physiologie*, 21, 401–503.
Allis, E.P. (1922) The cranial anatomy of *Polypterus*, with special reference to *Polypterus bichir*. *Journal of Anatomy*, 56(3–4), 189–294.
Allis, E.P. (1934) Concerning the course of the latero-sensory canals in recent fishes, pre-fishes and *Necturus*. *Journal of Anatomy*, 68(3), 361–415.

Arratia, G. (2003) Catfish head skeleton—an overview. In: Arratia, G., Kapoor, B.G., Chardon, M. and Diogo, R. (Eds.) *Catfishes*, 1st edition. Enfield: Science Publishers, pp. 3–46.

Arratia, G. and Huaquin, L. (1995) Morphology of the lateral line system and of the skin of diplomystid and certain primitive loricarioid catfishes and systematic and ecological considerations. *Bonner zoologische Monographien*, 36, 1–110.

Aumonier, J.F. (1941) Development of the dermal bones in the skull of *Lepidosteus osseus*. *Journal of Cell Science*, 2(329), 1–33.

Bartsch, P. (1997) Aspects of craniogenesis and evolutionary biology in polypteriform fishes. *Netherlands Journal of Zoology*, 47(4), 365–381.

Becker, E.A., Bird, N.C. and Webb, J.F. (2016) Post-embryonic development of canal and superficial neuromasts and the generation of two cranial lateral line phenotypes. *Journal of Morphology*, 277(10), 1273–1291.

Bird, N.C. and Webb, J.F. (2014) Heterochrony, modularity, and the functional evolution of the mechanosensory lateral line canal system of fishes. *EvoDevo*, 5(21), 1–22.

Bockmann, F.A. (1998) *Análise filogenética da família Heptapteridae (Teleostei: Ostariophysi: Siluriformes) e redefinição de seus gêneros*. PhD. Universidade de São Paulo.

Bridge, T.W. (1888) Some points in the cranial anatomy of *Polypterus*. *Proceedings of the Birmingham Philosophical Society*, 6, 118–130.

Chagnaud, B.P. and Coombs, S. (2014) Information encoding and processing by the peripheral lateral line system. In: Coombs, S., Bleckmann, H., Fay, R.R. and Popper, A.N. (Eds.) *The Lateral Line System*, 1st edition. New York: Springer, pp. 151–251.

Claeson, K.M., Bemis, W.E. and Hagadorn, J.W. (2007) New interpretations of the skull of a primitive bony fish *Erpetoichthys calabaricus* (Actinopterygii: Cladistia). *Journal of Morphology*, 268(11), 1021–1039.

Collinge, W.E. (1893) Note on the lateral canal system of *Polypterus*. *Proceedings of the Birmingham Philosophical Society*, 8(2), 255–262.

Collinge, W.E. (1894) The sensory canal system of fishes. Part I – Ganoidei. *Quarterly Journal of Microscopical Science*, 36(4), 499–537.

Coombs, S., Janssen, J. and Webb, J.F. (1988) Diversity of lateral line systems: phylogenetic and functional considerations. In: Atema, J., Fay, R.R., Popper, A.N. and Tavolga, W.N. (Eds.) *Evolutionary Biology of Hearing*. New York: Springer-Verlag, pp. 553–593.

Daget, J. (1950) Révision des affinités phylogénétiques des polyptéridés. *Mémoirs de l'Institut français d'Afrique Noire*, 11, 1–180.

Datovo, A. and Bockmann, F.A. (2010) Dorsolateral head muscles of the catfish families Nematogenyidae and Trichomycteridae (Siluriformes: Loricarioidei): comparative anatomy and phylogenetic analysis. *Neotropical Ichthyology*, 8(2), 193–246.

Datovo, A. and Rizzato, P.P. (2018) Evolution of the facial musculature in basal ray-finned fishes. *Frontiers in Zoology*, 15(40), 1–29.

De Beer, G.R. (1937) *The Development of Vertebrate Skull*. New York: Oxford University Press, p. 760.

Diedhiou, S. and Bartsch, P. (2009) Staging of the early development of *Polypterus* (Cladistia: Actinopterygii). In: Kunz, Y.W., Luer, C.A. and Kapoor, B.G. (Eds.) *Development of Non-Teleost Fishes*, 1st edition. Enfield: Science Publishers, pp. 104–169.

Dutheil, D.B. (1999) The first articulated fossil cladistian: *Serenoichthys kemkemensis*, gen. et sp. nov., from the Cretaceous of Morocco. *Journal of Vertebrate Paleontology*, 19(2), 243–246.

Edgley, D.E. and Genner, M.J. (2019) Adaptive diversification of the lateral line system during cichlid fish radiation. *iScience*, 16, 1–11.

Eschmeyer, W.N., Fricke, R. and van der Laan, R. (2019) *Genera, species, references*. [online] Catalog of Fishes. Available at: http://researcharchive.calacademy.org/research/ichthyology/catalog/fishcatmain.asp [Accessed 11 October 2019].

Gai, Z., Yu, X. and Zhu, M. (2017) The evolution of the zygomatic bone from Agnatha to Tetrapoda. *Anatomical Record*, 300, 16–29.

Garman, S. (1888) On the lateral canal system of the Selachia and Holocephala. *Bulletin of the Museum of Comparative Zoology*, 17(2), 57–119.

Gayet, M. and Meunier, F.J. (1991) First discovery of Polypteridae (Pisces, Cladistia, Polypteriformes) outside of Africa. *Geobios*, 24(4), 463–466.

Gayet, M. and Meunier, F.J. (1992) Polyptériformes (Pisces, Cladistia) du maastrichtien et du paléocène de Bolivie. *Geobios*, 25, 159–168.

Gayet, M., Meunier, F.J. and Werner, C. (2003) Diversification in Polypteriformes and special comparison with the Lepisosteiformes. *Paleontology*, 45(2), 361–376.

Gemballa, S. and Röder, K. (2004) From head to tail: the myoseptal system in basal actinopterygians. *Journal of Morphology*, 259, 155–171.

Giles, S., Xu, G.-H., Near, T.J. and Friedman, M. (2017) Early members of 'living fossil' lineage imply later origin of modern ray-finned fishes. *Nature*, 549, 265–268.

Graham-Smith, W. (1978) On the lateral lines and dermal bones in the parietal region of some Crossopterygian and Dipnoan fishes. *Philosophical Transactions of the Royal Society of London B: Biological Sciences*, 282, 41–105.

Grande, L. (2010) An empirical synthetic pattern study of gars (Lepisosteiformes) and closely related species, based mostly on skeletal anatomy. The resurrection of Holostei. *Copeia*, 10(2A), x+1–871.

Grande, L. and Bemis, W.E. (1991) Origin and phylogenetic relationships of fossil and recent paddlefishes (Polyodontidae) with comments on the relationships of Acipenseriformes. *Journal of Vertebrate Paleontology*, 11(S1), 1–121.

Grande, L. and Bemis, W.E. (1998) A comprehensive phylogenetic study of amiid fishes (Amiidae) based on comparative skeletal anatomy. An empirical search for interconnected patterns of natural history. *Journal of Vertebrate Paleontology*, 18(S1), x+1–696.

Gregory, W.K. (1933) Fish skulls: a study of the evolution of natural mechanisms. *Transactions of the American Philosophical Society, New series*, 23, 1–55.

Harrington, R.W. (1955) The osteocranium of the American cyprinid fish, *Notropis bifrenatus*, with an annotated synonymy of teleost skull bones. *Copeia*, 1955(4), 267–290.

Hilton, E.J. (2002a) Osteology of the extant North American fishes of the genus *Hiodon*. Lesueur 1818 (Teleostei: Osteoglossomorpha: Hiodontiformes). *Fieldiana (Zoology), New Series*, 100, 1–142.

Hilton, E.J. (2002b) Observations on rostral canal bones of two species of *Acipenser* (Actinopterygii, Acipenseriformes). *Copeia*, 2002(1), 213–219.

Hilton, E.J. and Bemis, W.E. (1999) Skeletal variation in shortnose sturgeon (*Acipenser brevirostrum*) from the Connecticut River: implications for comparative osteological studies of fossil and living fishes. In: Arratia, G. and Schultze, H.-P. (Eds.) *Mesozoic Fishes 2 – Systematics and Fossil Record*, 1st edition. Munich: Verlag Dr. Friedrich Pfeil, pp. 69–94.

Hilton, E.J. and Grande, L. (2008) Fossil mooneyes (Teleostei, Hiodontiformes, Hiodontidae) from the Eocene of western North America, with a reassessment of their taxonomy. In Cavin, L., Longbottom, A. and Richter, M. (Eds.) *Fishes and the Break-Up of Pangea*. Special Publication 295. London: Geological Society of London, pp. 221–251.

Hilton, E.J., Grande, L. and Bemis, W.E. (2011) Skeletal anatomy of the shortnose sturgeon, *Acipenser brevirostrum* Lesueur, 1818, and the systematics of sturgeons (Acipenseriformes: Acipenseridae). *Fieldiana, Life and Earth Sciences*, 3, 1–168.

Holmgren, N. and Stensiö, E.A. (1936) Kranium und visceralskelet der Akranier, Cyclostomen und Fische. In: Bolk, L., Göppert, E., Kallius, E. and Lubosch, H. (Eds.) *Handbuch der vergleichenden Anatomie der Wirbeltiere*, 1st edition. Berlin: Urban & Schwarzenberg, pp. 203–500.

Huxley, T.H. (1861) Preliminary essay upon the systematic arrangement of the fishes of the Devonian Epoch. *Memoirs of the Geological Survey of Great Britain, Decade* 10. London: HMSO, 1–40.

Jarvik, E. (1942) On the structure of the snout of crossopterygians and lower gnathostomes in general. *Zoologiska Bidrag fran Uppsala*, 21, 235–675.

Jarvik, E. (1947) Notes on the pit-lines and dermal bones of the head in *Polypterus*. *Zoologiska Bidrag fran Uppsala*, 25, 60–78.

Jollie, M. (1962) *Chordate Morphology*. London: Chapman & Hall Ltd., p. 478.

Jollie, M. (1980) Development of head and pectoral girdle skeleton and scales in *Acipenser*. *Copeia*, 1980(2), 226–249.

Jollie, M. (1984a) Development of the head and pectoral skeleton of *Polypterus* with a note on scales (Pisces: Actinopterygii). *Journal of Zoology*, 204(4), 469–507.

Jollie, M. (1984b) Development of the head skeleton and pectoral girdle of salmons, with a note on the scales. *Canadian Journal of Zoology*, 62, 1757–1778.

Kapoor, A.S. (1970) Development of dermal bones related to sensory canals of the head in the fishes *Ophicephalus punctatus* Bloch (Ophicephalidae) and *Wallago attu* Bl. Schn. (Siluridae). *Zoological Journal of the Linnean Society*, 49, 69–97.

Kindred, J.E. (1919) *The Skull of Amiurus*. PhD: University of Illinois.

Lekander, B. (1949) *The Sensory Line System and the Canal Bones in the Head of some Ostariophysi*. Stockholm: Alb. Bonniers Boktryckeri, p. 131.

Li, G.-Q. and Wilson, M.V.H. (1994) An Eocene species of *Hiodon* from Montana, its phylogenetic relationships, and the evolution of the postcranial skeleton in the Hiodontidae (Teleostei). *Journal of Vertebrate Paleontology*, 14, 153–167.

Li, G.-Q. and Wilson, M.V.H. (1996) Phylogeny of the Osteoglossomorpha. In: Stiassny, M.L.J., Parenti, L.R. and Johnson, G.D. (Eds.) *Interrelationships of Fishes*, 1st edition. San Diego, CA: Academic Press, pp. 163–174.

Li, G.-Q. and Wilson, M.V.H. (1999) Early divergence of Hiodontiformes *sensu stricto* in East Asia and phylogeny of some Late Mesozoic teleosts from China. In: Arratia, G. and Schultze, H.-P. (Eds.) *Mesozoic Fishes. 2. Systematics and Fossil Record*, 1st edition. Munich: Verlag Pfeil, pp. 369–384.

Mabee, P.M. (1993) Phylogenetic interpretation of ontogenetic change: sorting out the actual and artefactual in an empirical case study of centrarchid fishes. *Zoological Journal of the Linnean Society*, 107, 175–291.

Mall, F.P. (1906) On ossifications centers in human embryos less than one hundred days old. *American Journal of Anatomy*, 5(4), 433–458.

McHenry, M.J. and Liao, J.C. (2014) The hydrodynamics of flow stimuli. In: Coombs, S., Bleckmann, H., Fay, R.R. and Popper, A.N. (Eds.) *The Lateral Line System*, 1st edition. New York: Springer, pp. 73–98.

Moritz, T. and Britz, R. (2019) Revision of the extant Polypteridae (Actinopterygii: Cladistia). *Ichthyological Exploration of Freshwaters*, 1094, 1–96.

Moy-Thomas, J.A. (1941) Development of the frontal bones of the rainbow trout. *Nature*, 147, 681–682.

Müller, J. (1846) *Über den Bau und die Grenzen der Ganoiden und über das natürliche System der Fische*, Berlin: Gedruckt in der Druckerei der Königlichen Akademie der Wissenschaften, pp. 117–216+6 pl.

Nakae, M., Asaoka, R., Hironori, W. and Sasaki, K. (2012) Fluorescent dye staining of neuromasts in live fishes: an aid to systematic studies. *Ichthyological Research*, 59(3), 286–290.

Northcutt, R.G. (1989) The phylogenetic distribution and innervation of craniate mechanoreceptive lateral lines. In: Coombs, S., Görner, P. and Münz, H. (Eds.) *The Mechanosensory Lateral Line: Neurobiology and Evolution*, 1st edition. New York: Springer-Verlag, pp. 17–78.

Northcutt, R.G. and Bemis, W.E. (1993) Cranial nerves of the coelacanth, *Latimeria chalumnae* (Osteichthyes: Sarcopterygii: Actinistia), and comparisons with other Craniata. *Brain Behavior and Evolution*, 42(S1), 1–76.

Northcutt, R.G., Holmes, P.H. and Albert, J.S. (2000) Distribution and innervation of lateral line organs in the Channel Catfish. *Journal of Comparative Neurology*, 421, 570–592.

Ollonen, J., Da Silva, F.O., Mahlow, K. and Di-Poï, N. (2018) Skull development, ossification pattern, and adult shape in the emerging lizard model organism *Pogona vitticeps*: a comparative analysis with other squamates. *Frontiers in Physiology*, 9, 1–26.

Otero, O., Likius, A., Vignaud, P. and Brunet, M. (2006) A new polypterid fish: *Polypterus faraou* sp. nov. (Cladistia, Polypteridae) from the Late Miocene, Toros-Menalla, Chad. *Zoological Journal of the Linnean Society*, 146, 227–237.

Owen, R. (1866) *On the Anatomy of Vertebrates. Vol. 1 (Fishes and Reptiles)*. London: Longmans, Green and Co., p. 650.

Pastana, M.N.L. (2014) *Canais e Poros do Sistema Látero-sensorial Cefálico de Characiformes (Ostariophysi): Anatomia e seu Significado Filogenético*. MSc. Universidade de São Paulo.

Pastana, M.N.L., Bockmann, F.A. and Datovo, A. (2019) The cephalic lateral-line system of Characiformes (Teleostei: Ostariophysi): anatomy and phylogenetic implications. *Zoological Journal of the Linnean Society*, 1–46.

Patterson, C. (1973) Interrelationships of holosteans. In: Greenwood, P.H., Miles, R.S. and Patterson, C. (Eds.) *Interrelationships of Fishes*, 1st edition. London: Academic Press, pp. 233–305.

Patterson, C. (1975) The braincase of pholidophorid and leptolepid fishes, with a review of the actinopterygian braincase. *Philosophical Transactions of the Royal Society of London, B: Biological Sciences*, 269, 275–579.

Patterson, C. (1977) Cartilage bones, dermal bones, and membrane bones, or the exoskeleton versus the endoskeleton. In: Andrews, S.M., Miles, R.S. and Walker, A.D. (Eds.) *Problems in Vertebrate Evolution*, 1st edition. London: Academic Press, pp. 77–121.

Patterson, C. (1982) Morphology and interrelationships of primitive actinopterygian fishes. *American Zoologist*, 22(2), 241–259.

Pehrson, T. (1922) Some points in the cranial development of teleostomian fishes. *Acta Zoologica*, 2, 1–63.

Pehrson, T. (1940) The development of dermal bones in the skull of *Amia calva*. *Acta Zoologica*, 21, 1–50.

Pehrson, T. (1944) Some observations on the development and morphology of the dermal bones in the skull of *Acipenser* and *Polyodon*. *Acta Zoologica*, 25, 27–48.

Pehrson, T. (1947) Some new interpretations of the skull in *Polypterus*. *Acta Zoologica*, 28(2–3), 399–455.

Pehrson, T. (1958) The early ontogeny of the sensory lines and the dermal skull in *Polypterus*. *Acta Zoologica*, 39, 241–258.

Piotrowski, T. and Northcutt, R.G. (1996) The cranial nerves of the Senegal Bichir, *Polypterus senegalus* (Osteichthyes: Actinopterygii: Cladistia). *Brain, Behavior and Evolution*, 47, 55–102.

Pollard, H.B. (1892) On the anatomy and phylogenetic position of *Polypterus*. *Zoologische Jahrbücher*, 5, 387–428.

Poplin, C. and Lund, R. (1995) Fates of the rostral, postrostral and premaxillary in the early history of actinopterygians. *Geobios*, 19, 225–230.

Pospisilova, A. (2015) *Characterization of cranial skeletogenesis and odontogenesis in basal ray-finned fishes*. MSc. Prague: Charles University, p. 102.

Puzdrowski, R.L. (1989) Peripheral distribution and central projections of lateral-line nerves in goldfish, *Carassius auratus*. *Brain, Behavior and Evolution*, 34, 110–131.

Reno, H.W. (1966) The infraorbital canal, its lateral-line ossicles and neuromasts, in the minnows *Notropis volucellus* and *N. buchanani*. *Copeia*, 1966, 403–413.

Rizzato, P.P. and Bichuette, M.A. (2017) The laterosensory canal system in epigean and subterranean *Ituglanis* (Siuriformes: Trichomycteridae), with comments about troglomorphism and the phylogeny of the genus. *Journal of Morphology*, 278, 4–28.

Rizzato, P.P. and Bockmann, F.A. (2017) Unraveling a 150 years old controversy: *Calamoichthys* Smith, 1866 is the valid name for the African Reedfish (Cladistii: Polypteriformes), with comments about the availability of involuntarily proposed zoological names. *Bionomina*, 11, 62–78.

Rojo, A.L. (1991) *Dictionary of Evolutionary Fish Osteology*. Boca Raton: CRC Press, p. 273.

Sagemehl, M. (1884) Beiträge zur vergleichenden Anatomie der Fische. III. Das Cranium der Characiniden nebst allgemeinen Bemerkungen über die mit einem Weber'schen Apparat versehenen Physostomenfamilien. *Morphologisches Jahrbuch*, 10, 1–118+2 pl.

Schoch, R.R. (2006) Skull ontogeny: developmental patterns of fishes conserved across major tetrapod clades. *Evolution & Development*, 8(6), 524–536.

Schultze, H.P. (2008) Nomenclature and homologization of cranial bones in actinopterygians. In: Arratia, G., Schultze, H.-P. and Wilson, M.V.H. (Eds.) *Mesozoic Fishes 4 – Homology and Phylogeny*, 1st edition. Munich: Verlag Dr. Friedrich Pfeil, pp. 23–48.

Sewertzoff, A.N. (1926) Studies on the bony fishes. I. Structure and development of the bony skull of *Acipenser ruthenus*. *Quarterly Journal of Microscopical Science*, 11, 451–540.

Shufeldt, R.W. (1847) The osteology of Amia calva: including certain special references to the skeleton of teleosteans. *Report of the United States Fish Commission for 1883*, vol. XI, 747–878.

Song, J. and Northcutt, R.G. (1991) Morphology, distribution and innervation of the lateral-line receptors of the Florida Gar, *Lepisosteus platyrhinchus*. *Brain, Behavior and Evolution*, 37, 10–37.

Stensiö, E.A. (1947) The sensory lines and dermal bones of the cheek in fishes and amphibians. *Kungliga Svenska Vetenskapsakademiens Handlingar*, 24(3), 1–195.

Supino, F. (1914) Morphologia del cranio del *Calamoichthys calabaricus*. *Atti della Società Italiana di Scienze Naturali*, 53, 179–188.

Tarby, M.L. and Webb, J.F. (2003) Development of the supraorbital and mandibular lateral line canals in the cichlid, *Archocentrus nigrofasciatus*. *Journal of Morphology*, 255, 44–57.

Taverne, L. (1977) Ostéologie, phylogénèse et systématique des Téléostéens fossiles et actuels du superordre der ostéoglossomorphes. Première partie. Ostéologie des genres *Hiodon*, *Eohiodon*, *Lycoptera*, *Osteoglossum*, *Scleropages*, *Heterotis* et *Arapaima*. *Mémoires de la Classe des Sciences, Académie Royale de Belgique*, 42, 1–235.

Taylor, W.R. and Van Dyke, G.C. (1985) Revised procedures for staining and clearing small fishes and other vertebrates for bone and cartilage study. *Cybium*, 9(2), 107–119.

Thomopoulos, A. (1969) Les premières ébauches du système latéral sensorial chez *Polypterus senegalus* – Poisson – Brachiopterygien. *Bulletin de la Société zoologique de France*, 94, 306–307.

Thomopoulos, A. (1970) Sur le système lateral de *Polypterus senegalus* Cuv. (Poisson-Brachioptérygien). I. Les premières ébauches du système latéral céphalique et troncal. *Zeitschrift für Anatomie und Entwicklungsgeschichte*, 130(4), 316–329.

Traquair, R.H. (1870) On the cranial osteology of *Polypterus*. *Journal of Anatomy and Physiology*, 5(1), 166–183.

Van Netten, S.M. and McHenry, M.J. (2014) The biophysics of the fish lateral line. In: Coombs, S., Bleckmann, H., Fay, R.R. and Popper, A.N. (Eds.) *The Lateral Line System*, 1st edition. New York: Springer, pp. 99–119.

Van Whije, J.W. (1882) Ueber das Visceralskelett und die nerven des Kopfes der Ganoiden und von *Ceratodus*. *Niederländisches Archiv für Zoologie*, 5, 207–320.

Vrolik, A.J. (1873) Studien über die Verknöcherung und die Knochen des Schädels der Teleostier. *Niederländisches Archiv für Zoologie*, 1, 219–318.

Wada, H., Iwasaki, M. and Kawakami, K. (2014) Development of the lateral line canal system through a bone remodeling process in zebrafish. *Developmental Biology*, 392, 1–14.

Walther, J. (1882) Die Entwicklung der Deckknochen am kopfskelett des Heches (*Esox Lucius*). *Jenaische Zeitschrift für Naturwissenschaft*, 16, 59–84.

Warth, P., Hilton, E.J., Naumann, B., Olsson, L. and Konstantinidis, P. (2017) Development of the skull and pectoral girdle in Siberian Sturgeon, *Acipenser baeri*, and Russian Sturgeon, *Acipenser gueldenstaedtii* (Acipenseriformes, Acipenseridae). *Journal of Morphology*, 278(3), 418–442.

Webb, J.F. (1989) Gross morphology and evolution of the mechanosensory lateral line system in teleost fishes. *Brain, Behavior and Evolution*, 33, 34–53.

Webb, J.F. (2014) Morphological diversity, development, and evolution of the mechanosensory lateral line system. In: Coombs, S., Bleckmann, H., Fay, R.R. and Popper, A.N. (Eds.) *The Lateral Line System*, 1st edition. New York: Springer, pp. 99–119.

Webb, J.F. and Northcutt, R.G. (1997) Morphology and distribution of pit organs and canal neuromasts in non-teleost bony fishes. *Brain, Behavior and Evolution*, 50, 139–151.

Webb, J.F. and Shirey, J.E. (2003) Postembryonic development of the cranial lateral line canals and neuromasts in zebrafish. *Developmental Dynamics*, 228, 370–385.

Westoll, T.S. (1936) On the structure of the dermal ethmoid shield of *Osteolepis*. *Geological Magazine*, 73(862), 157–171.

Westoll, T.S. (1937) The old red sandstone fishes of the North of Scotland, particularly of Orkney and Shetland. *Proceedings of the Geologists Association*, 48, 13–45.

Westoll, T.S. (1938) Ancestry of the tetrapods. *Nature*, 3559, 127–128.

Westoll, T.S. (1941) Latero-sensory canals and dermal bones. *Nature*, 148, 168–169.

Westoll, T.S. (1943) The origin of the tetrapods. *Biological Reviews*, 18(2), 78–98.

How to cite this article: Rizzato PP, Pospisilova A, Hilton EJ, Bockmann FA. Ontogeny and homology of cranial bones associated with lateral-line canals of the Senegal Bichir, *Polypterus senegalus* (Actinopterygii: Cladistii: Polypteriformes), with a discussion on the formation of lateral-line canal bones in fishes. *J. Anat.*. 2020;00:1–29. https://doi.org/10.1111/joa.13202

IV. Stundl J, **Pospisilova A**, Jandzik D, Fabian P, Dobiasova B, Minarik M, Metscher BD, Soukup V & Cerny R (2019) Bichir external gills arise via a heterochronic shift that accelerates hyoid arch development. *eLife* 8, e43531.

IF (2019) = 7,080

eLIFE elifesciences.org

RESEARCH ARTICLE

Bichir external gills arise via heterochronic shift that accelerates hyoid arch development

Jan Stundl[1,2], Anna Pospisilova[1], David Jandzik[1,3], Peter Fabian[1†], Barbora Dobiasova[1‡], Martin Minarik[1§], Brian D Metscher[4], Vladimir Soukup[1*], Robert Cerny[1*]

[1]Department of Zoology, Faculty of Science, Charles University in Prague, Prague, Czech Republic; [2]National Museum, Prague, Czech Republic; [3]Department of Zoology, Faculty of Natural Sciences, Comenius University in Bratislava, Bratislava, Slovakia; [4]Department of Theoretical Biology, University of Vienna, Vienna, Austria

***For correspondence:** vladimir.soukup@natur.cuni.cz (VS); robert.cerny@natur.cuni.cz (RC)

Present address: †Eli and Edythe Broad CIRM Center for Regenerative Medicine and Stem Cell Research, University of Southern California, Los Angeles, United States; ‡The Prague Zoological Garden, Prague, Czech Republic; §Department of Physiology, Development and Neuroscience, University of Cambridge, Cambridge, United Kingdom

Competing interests: The authors declare that no competing interests exist.

Funding: See page 10

Received: 09 November 2018
Accepted: 15 March 2019
Published: 26 March 2019

Reviewing editor: Tanya T Whitfield, University of Sheffield, United Kingdom

Abstract In most vertebrates, pharyngeal arches form in a stereotypic anterior-to-posterior progression. To gain insight into the mechanisms underlying evolutionary changes in pharyngeal arch development, here we investigate embryos and larvae of bichirs. Bichirs represent the earliest diverged living group of ray-finned fishes, and possess intriguing traits otherwise typical for lobe-finned fishes such as ventral paired lungs and larval external gills. In bichir embryos, we find that the anteroposterior way of formation of cranial segments is modified by the unique acceleration of the entire hyoid arch segment, with earlier and orchestrated development of the endodermal, mesodermal, and neural crest tissues. This major heterochronic shift in the anteroposterior developmental sequence enables early appearance of the external gills that represent key breathing organs of bichir free-living embryos and early larvae. Bichirs thus stay as unique models for understanding developmental mechanisms facilitating increased breathing capacity.
DOI: https://doi.org/10.7554/eLife.43531.001

Introduction

The vertebrate pharynx is composed of a series of repeated embryonic structures called pharyngeal arches (***Graham, 2008***; ***Grevellec and Tucker, 2010***). In the majority of jawed vertebrates, the first, or mandibular arch contributes to the jaws; the second, or hyoid arch serves as the jaw support, and the more posterior branchial arches typically bear internal pharyngeal gills. Pharyngeal arches form in a highly stereotyped sequence from anterior to posterior, where the contacts between endodermal pouches and surface ectoderm physically separate the mesoderm- and neural crest-derived arch tissues (***Graham and Smith, 2001***; ***Shone and Graham, 2014***; ***Choe and Crump, 2015***). The progressive development of the pharynx has deep deuterostome origins, as it is characteristic of both cephalochordates and hemichordates (***Willey, 1891***; ***Gillis et al., 2012***; ***Koop et al., 2014***). In vertebrates, sequential formation of pharyngeal segments represents a fundamental aspect of the metameric organization of the head and face (***Piotrowski and Nüsslein-Volhard, 2000***; ***Couly et al., 2002***; ***Choe and Crump, 2015***). Any modifications of this well-established anteroposterior differentiation scheme would represent a radical alteration in development of the stereotypic chordate bauplan (***Square et al., 2017***).

Polypterid bichirs represent the earliest diverged living group of ray-finned (Actinopterygian) fishes (***Hughes et al., 2018***) and they are often referred to as the most relevant species for studying character states at the dichotomy of ray- and lobe-finned fishes (e.g., ***Standen et al., 2014***). This places bichirs in a unique phylogenetic position among vertebrates, which can be exploited for

evolutionary and developmental comparative studies (e.g., **Takeuchi et al., 2009**; **Standen et al., 2014**; **Minarik et al., 2017**). Adult bichirs possess several intriguing characteristics that have been associated with air-breathing during the transition from water to land, such as ventral paired lungs or spiracular openings on the head (**Clack, 2007**; **Coates and Clack, 1991**; **Graham et al., 2014**; **Tatsumi et al., 2016**). Moreover, bichirs also share several key larval features with lungfishes or amphibians, such as cranial adhesive organs, and larval external gills (**Kerr, 1907**; **Diedhiou and Bartsch, 2009**).

The external gills of bichirs represent prominent adaptive structures, and constitute major breathing organs of their free-living embryos and early larvae (**Figure 1A**) (**Kerr, 1907**; **Diedhiou and Bartsch, 2009**). Strikingly, while external gills of amphibians and lungfishes derive from branchial arches as a rule (**Duellman and Trueb, 1994**; **Witzmann, 2004**; **Nokhbatolfoghahai and Downie, 2008**; **Schoch and Witzmann, 2011**), those of bichirs have historically been considered as unique hyoid arch derivatives due to their blood supply from the hyoid aortic arch (**Kerr, 1907**; **Goodrich, 1909**). Importantly, the external gills of bichir embryos represent the first cranial structures to appear, emerging before the eyes or mouth are evident (**Figure 1B**) (**Minarik et al., 2017**).

Here, we take advantage of an exceptionally complete embryonic series of the Senegal bichir (*Polypterus senegalus*) to explore the developmental underpinnings of the early formation of their external gills and test their segmental origin. Our results reveal that bichir external gills are definitively derived from the hyoid arch and develop by orchestrated acceleration of tissues of all germ layers of the hyoid segment. Thus, in bichir embryos, the standard anteroposterior differentiation scheme of cranial segments is modified by the unique heterochronic development of the hyoid metamere, allowing early and enhanced development of their external gills.

Results and discussion

External gills of the Senegal bichir are developmentally associated with the hyoid segment

In order to examine the origin of bichir external gills, we first followed the morphological development of this structure from the earliest stages of embryogenesis onwards. The first sign of external gill development is a pair of outgrowths situated lateral to the closing neural folds (**Figure 1C**). The hyoid origin of these outgrowths is suggested by the expression pattern of the *Hoxa2* (**Figure 1D**), a selector gene characteristic of hyoid identity in other vertebrates (**Rijli et al., 1993**; **Hunter and Prince, 2002**; **Baltzinger et al., 2005**). Later, at early pharyngula stages, the hyoid outgrowths produce protuberant bulges situated in the pre-otic region on each side of the embryo (**Figure 1E–H**), that rapidly increase in size (**Figure 1I**), and finally, differentiate into many secondary branches (**Figure 1J–L**). This suggests that the prominent external gills of bichir larva (**Figure 1A**) initially arise from striking accelerated development of the epidermal outgrowths (**Figure 1B**) that are of hyoid segmental origin (**Figure 1F**).

Accelerated and predominant hyoid neural crest stream supplies bichir external gills

To gain insights into the accelerated development of the hyoid segment, we focused on the cranial neural crest that arises from the closing neural folds. Cranial neural crest cells emerge in a characteristic pattern and split into mandibular, hyoid, and branchial streams, which in most vertebrates arise in a sequential anteroposterior order of appearance. As a marker for migrating neural crest cells, we used expression of *Sox9*, a transcription factor critical for their emergence, migration, and differentiation (**Cheung and Briscoe, 2003**; **Mori-Akiyama et al., 2003**; **Theveneau and Mayor, 2012**). In bichir embryos, *Sox9* expression pattern reveals that the hyoid neural crest segment is developmentally advanced, as it forms concurrently with the mandibular neural crest segment (**Figure 2A**). Sections through the neural folds, however, demonstrate that mandibular neural crest cells still reside within the neuroepithelium (**Figure 2B**), while the hyoid neural crest cells have already emigrated from the neural folds (**Figure 2C**). This premature emigration of the hyoid neural crest stream correlates with the previously observed external outgrowths of the hyoid area (**Figure 1C**). Later in migration, the hyoid neural crest stream remains predominant (**Figure 2D**), as it is much larger when compared to the mandibular neural crest stream (**Figure 2E,F**). The hyoid neural crest stream still

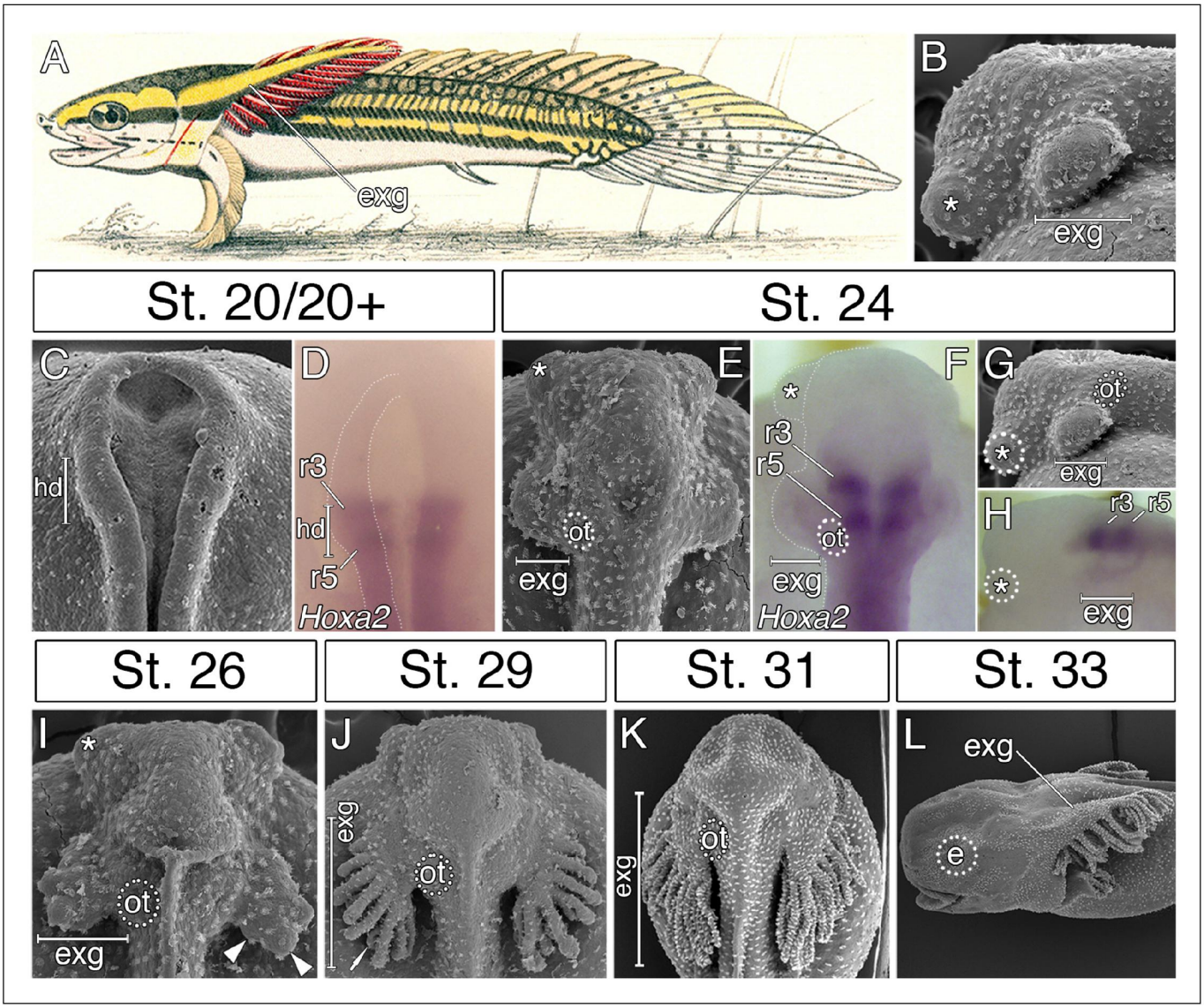

Figure 1. External gills of the Senegal bichir derive from the accelerated epidermal outgrowth of the hyoid segmental origin. (**A**) Budgett's illustration (***Kerr, 1907***) of a 3 cm long bichir larva with prominent external gills (exg). (**B**) Lateral view of an early pharyngula stage, SEM image showing external gills and cement glands (asterisk) as the first forming cranial structures. (**C**) SEM image of an early neurula stage with emerging bulge within the hyoid domain (hd). (**D**) *Hoxa2* expression in the neural tube at the level of the presumptive hyoid arch. (**E, G**) SEM images of a tailbud embryo with external gills anlage. (**F, H**) *Hoxa2* expression pattern in a tailbud stage, with highlighted position of external gills. (**I–L**) SEM images showing developmental morphogenesis of external gills. (**C–F, I–K**) Dorsal view. (**G–H, L**) Lateral view. e, eye primordium; ot, otic vesicle; r3, rhombomere 3; r5, rhombomere 5.
DOI: https://doi.org/10.7554/eLife.43531.002

progresses at later stages (***Figure 2G***), and as such, the majority of the mesenchyme in the early bichir head appears to arise from this source (***Figure 2H***). The Sox9 immunoreactivity further shows that cells of the leading edge of the hyoid stream delaminate from the neural folds prior to the emigration of the mandibular stream (***Figure 2I***), and illustrates the voluminous (***Figure 2J***) and extended (***Figure 2K***) mesenchymal production of the hyoid neural crest segment.

We directly tested whether the hyoid neural crest cell stream contributes to the external gills by performing focal CM-DiI injections into rhombomere 4 (***Figure 2L*** inset), the source of the prospective hyoid neural crest stream in other vertebrates (***Lumsden et al., 1991***; ***Köntges and Lumsden, 1996***; ***Minoux and Rijli, 2010***; ***Theveneau and Mayor, 2012***). One day after neurulation, the CM-

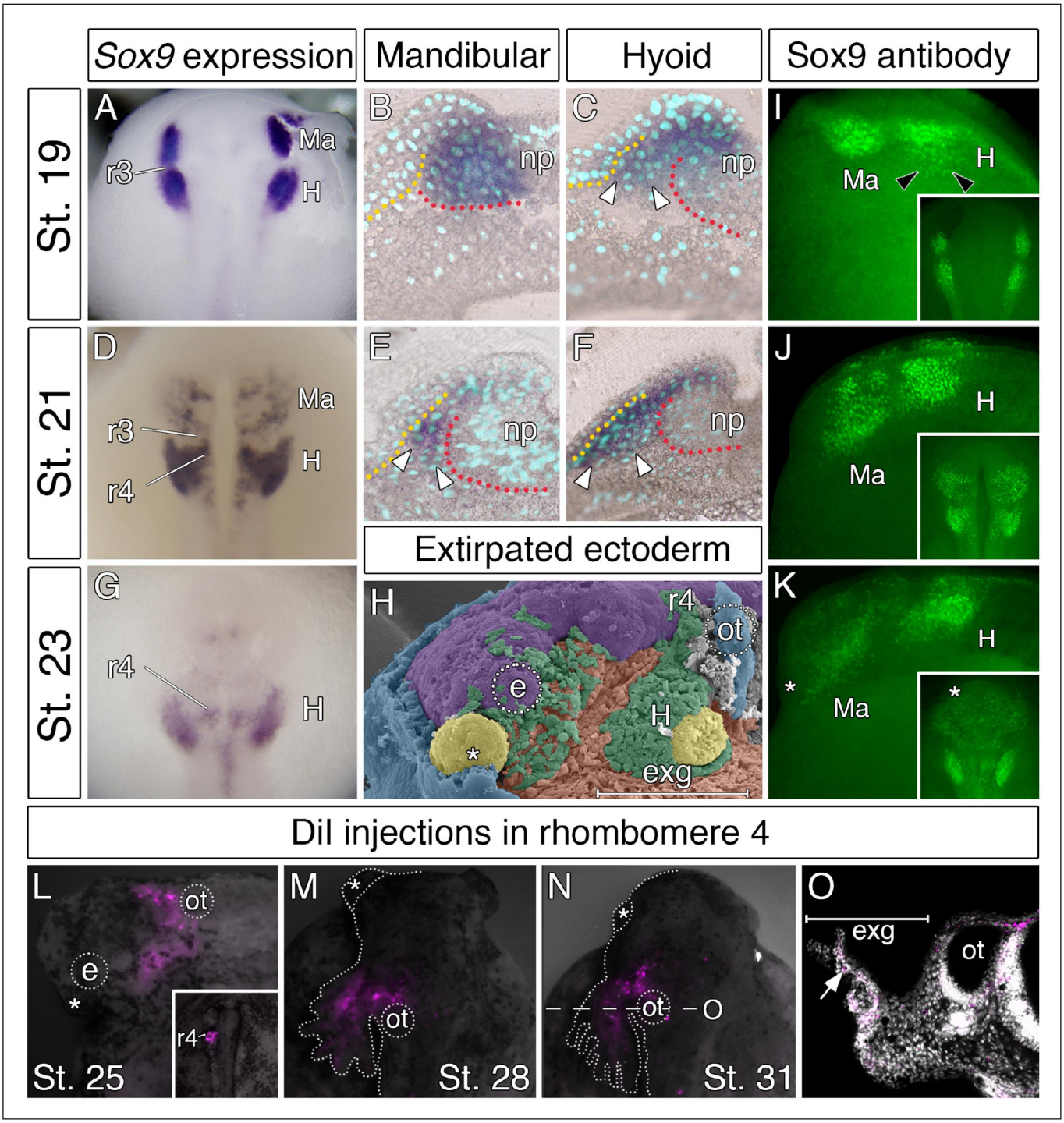

Figure 2. Accelerated formation and heterochronic development of the hyoid neural crest cells supply mesenchyme for the bichir external gills. (**A, D, G**) *Sox9* expression pattern in NC cells, from neurulation until early tailbud stages, dorsal views. Notice that the population of hyoid NC cells (marks as H) forms very early, and it later represents the most prominent cranial NC stream. (**B–C, E–F**) *Sox9* expression pattern in the mandibular and the hyoid domain, respectively, transversal sections. White arrowheads mark the ventral position of the NC cells. Dotted lines represent boundaries of neural- (red) and non-neural (yellow) ectoderm. DAPI (blue) shows cell nuclei. (**H**) Pseudocolored SEM image, lateral view on an embryo with the partially removed surface ectoderm (blue). NC cells are green, notice the amount of hyoid NC cells. Mesodermal mesenchyme is reddish, endodermal pouches are yellow, and the neural tube is violet. (**I–K**) Sox9 antibody visualizes individual neural crest cells. Lateral views, with small insets representing dorsal

Figure 2 continued on next page

Figure 2 continued

views. Black arrowheads in I show the advanced position of the hyoid NC cells. (**L–O**) Hyoid NC cell fate mapping (DiI red). Superimposed fluorescent and dark-field images at successive stages of development. (**L**) Lateral view, stage 25 embryo showing the hyoid NC stream. Small inset (dorsal view) represents an embryo at stage 20 immediately after the focal DiI injection into the rhombomere 4 (**r4**). (**M–N**) DiI signal at developing external gills, dorsal views. (**O**) Transversal section through the external gill (exg) at the level indicated in O. White arrow shows DiI signal in the primary branch of the external gill. Asterisk, cement gland; e, eye primordium; H, hyoid NC stream; Ma, mandibular NC stream; np, neural plate; ot, otic vesicle; r3, rhombomere 3; r4, rhombomere 4.

DOI: https://doi.org/10.7554/eLife.43531.003

Dil-positive hyoid neural crest cells are observed all along the proximodistal axis of the external gill primordium (***Figure 2L***). Two days later, they occupy the primary branches of the external gills (16/21, ***Figure 2M***). After hatching, the CM-DiI-positive cells populate the fully developed and functional external gills (***Figure 2N,O***). Thus, our fate mapping experiment confirms that bichir external gills are, indeed, populated by the cells of the hyoid neural crest stream and, implicitly, that they represent hyoid arch derivatives.

The first cranial muscles of bichir embryos support their external gills and are of hyoid segmental origin

In vertebrates, cranial neural crest cells are the primary source of craniofacial mesenchyme, but also have a major influence on the differentiation and morphogenesis of the cranial myogenic mesoderm (***Ericsson et al., 2004***; ***Tokita and Schneider, 2009***). We, therefore, hypothesized that the pattern of cranial muscle differentiation in bichir embryos may be affected by acceleration of the hyoid neural crest segment (***Figure 2***). Whole-mount antibody staining against skeletal muscle marker 12/101 revealed that the first muscles differentiate stereotypically from the post-otic somites in the trunk region, as in other vertebrates (***Figure 3A***). However, within the cranial region of bichir embryos, the earliest developing muscles form within the hyoid arch and are associated with the external gills (***Figure 3B,C***). This first muscle complex (*levator and depressor branchiarum*, ***Noda et al., 2017***) is situated lateral to the otic vesicle and connects filaments of the external gills to the gill stem (***Figure 3B–D***). The premature differentiation of the external gill-associated muscles is further supported by their innervation from the hyo-opercular ramus of the facial nerve, allowing voluntary movement of external gills from the earliest larval stages (***Figure 3E,F***). Other cranial muscles fully differentiate only at later larval stages when the external gill muscle complex becomes supplemented by other muscles of hyoid and mandibular origins (***Figure 3G***). Thus, bichir embryos display unique heterochrony in the differentiation of the hyoid over the mandibular arch mesoderm, providing muscular supports for their external gills.

Early expansion of the hyoid endoderm triggers the formation of bichir external gills

Interestingly, the accelerated development of the external gill rudiments is also reinforced by the morphogenesis of the hyoid pharyngeal segment (***Figure 4A–J***). Reconstruction of the endodermal epithelium of the bichir pharynx using micro-CT imaging (***Minarik et al., 2017***) reveals that the pharyngeal endoderm forms two pairs of early outpocketings (***Figure 4B***). Whereas the rostral pair represents the embryonic precursor of the cement glands (***Figure 4A–D,F–I***) (***Minarik et al., 2017***), the posterior paired outpocketings constitute primordia of the external gills (***Figure 4A–D***). These posterior outpocketings belong to the hyoid segment, as the first pharyngeal pouch (mandibulo-hyoid, or spiracular) is situated rostrally (***Figure 4C,D***, white arrowhead) and the second pharyngeal pouch (hyoid-branchial) more caudally (***Figure 4H***, black arrowhead). Transverse sections confirm that these hyoid endodermal outpocketings constitute a substantial proportion of the external gill primordium (***Figure 4E***). At later stages, these outpocketings further transform into pocket-like structures (***Figure 4G,H,J***) that become supplemented with mesenchymal cells of the hyoid neural crest stream (***Figure 2L–N***). Thus, while ectoderm covers the entire external gill primordium, the endodermal outpocketing constitutes a considerable portion of the developing external gill (***Figure 4E***).

We sought to explore a possible role of the hyoid endodermal outpocketings in controlling development and morphogenesis of the bichir external gills. Morphogenesis of the pharyngeal pouches is critically regulated by factors from many signaling pathways (***Graham and Smith, 2001***;

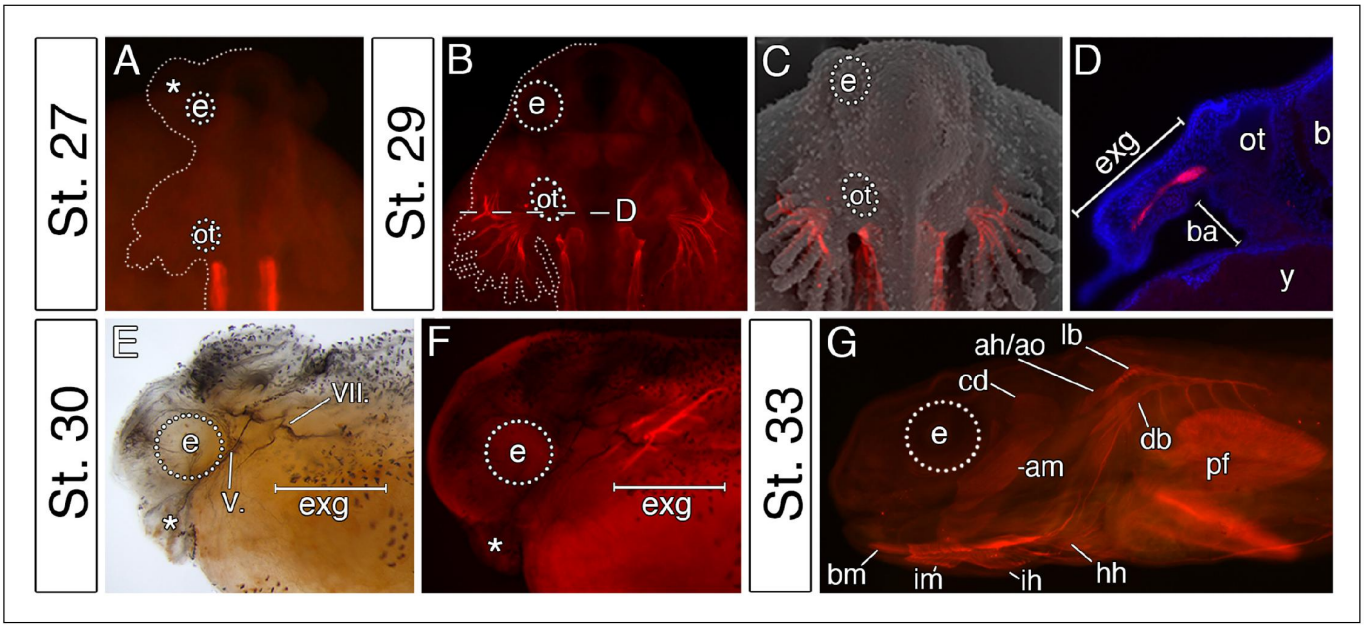

Figure 3. The premature differentiation of the external gill-associated cranial muscle complex in the Senegal bichir larva. (**A–C**) Dorsal view on bichir embryos, developing skeletal muscles are revealed by 12/101 antibody (red). The red signal in A (st. 27) refers to the post-otic somites. The first cranial muscle is associated with the external gills (B, stage 29). (**C**) Superimposed fluorescent and SEM image showing the context of the external gill muscles. (**D**) Transversal section through the external gills at the level indicated in B. DAPI (blue) stains cell nuclei. (**E, F**) Stage 30 bichir embryo, lateral view with (**E**) cranial nerves fibres labeled with anti-acetylated tubulin, and with (**F**) cranial muscles stained with 12/101 antibody (red). (**G**) Stage 33 bichir embryo, lateral view, with developed cranial muscles stained with 12/101 antibody (red). Asterisk, cement gland; am, adductor mandibulae; ah/ao, complex of adductor hyomandibulae and adductor operculi; b, brain; ba, branchial arches; bm, branchiomandibularis; cd,constrictor dorsalis; cement gland; e, eye primordium; lb/db, complex of levator branchiarum and depressor branchiarum; hh, hyohyoideus; ih, interhyoideus; im, intermandibularis; ot, otic vesicle; pf, pectoral fin; y, yolk; V., nervus trigeminus; VII., nervus facialis.

DOI: https://doi.org/10.7554/eLife.43531.004

Graham, 2008), among which alterations in Fibroblast growth factor (Fgf) signaling lead to defects in proper endodermal pouch development and pharyngeal segmentation (***Jandzik et al., 2014***; ***Abu-Issa et al., 2002***; ***Crump et al., 2004***; ***Walshe and Mason, 2003***). To assess the possible role of Fgf signaling during bichir external gill development, we scored expression of the *Fgf8* ligand and the readouts of Fgf signaling activity. *Fgf8* expression is present in endodermal outpocketings and becomes confined to their lateral portions (***Figure 4—figure supplement 1***). These portions of endoderm in fact constitute the outgrowing tips of the prospective external gill (***Figure 4K***). Expression of *Dusp6* and *Pea3* (the Fgf signaling pathway readouts) and antibody localization for activated MAPK (marker of active Fgf signaling) are present in the external gill mesenchyme adjacent to the outgrowing endodermal tips or both in the mesenchyme and the endodermal tips (***Figure 4L–N***; ***Figure 4—figure supplement 2***). The topographical relation of endodermal outpocketings and the direction of Fgf signaling within the external gill primordium thus suggest that the endodermal epithelium signals to the adjacent mesenchyme through Fgf signaling to regulate outgrowth of the external gill (***Figure 4O***).

To test the possible role of signaling events, we treated bichir embryos with SU5402, a collective Fgf and Egf signaling inhibitor, at early neurulation and scored the phenotypes at later pharyngula stages. In contrast to control embryos displaying well-developed hyoid endodermal outpocketings and external gill primordia (18/18, ***Figure 4P–Q***), disrupting Fgf signaling perturbs morphogenesis of the hyoid endodermal outpocketings and leads to the loss of the external gill primordia (14/15, ***Figure 4R–S***) possibly due to the loss of expression of downstream genes (***Figure 4T–U***). These results support a central role of the pharyngeal endoderm in triggering early development of bichir external gills. The pharyngeal origin of the external gill primordia is surprising given that the external gills are commonly considered as outer surface structures composed of ectoderm (***Takeuchi et al.,***

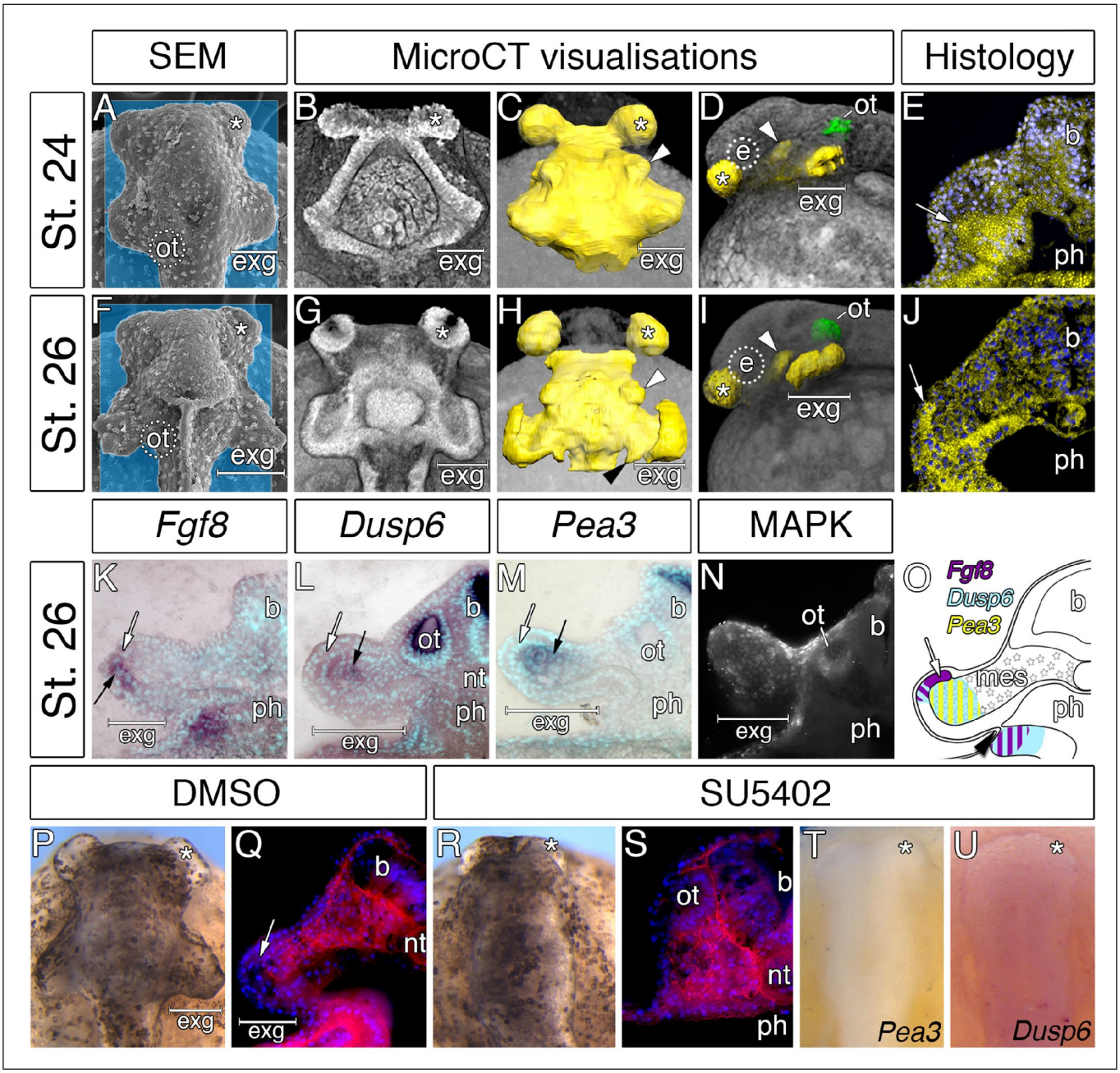

Figure 4. Considerable expansion of the hyoid pharyngeal endoderm contributes to the development of external gills in the Senegal bichir. (**A, F**) SEM images, dorsal view of bichir embryos with developing external gills (exg), showing the level of virtual sections in B and G. Notice the correspondence of the hyoid pharyngeal endoderm (**B, G**) and the external gills (**A, F**). (**B–D, G–H**) 3D models of pharyngeal endoderm (yellow) from dorsal (**C, H**), and lateral (**D, I**) view, respectively. (**E, J**) Transversal sections show prominent lateral expansion of hyoid pharyngeal endoderm (white arrow). (**K–M**) Transversal sections show wild-type expression of *Fgf8*, *Pea3*, and *Dusp6* (black arrow) in the external gills primordium. (**N**) Immunostaining of anti-activated MAP kinase antibody on transversal section of the external gills primordium. (**O**) Scheme summarizing *Fgf8*, *Dusp6*, and *Pea3* (**K–M**) expression patterns in the external gills formation at stage 26. Violet indicates *Fgf8* expression; blue marks *Dusp6* expression in the endoderm and adjacent mesenchyme of the external gills; yellow depicts expression of *Pea3* in the mesechyme of the external gills. (**P–U**) Inhibition of pouch-like endodermal outpocketings (**P, R, T–U**), dorsal view. (**P–Q**) Control larvae treated with DMSO develop normal pouch-like endodermal outgrowths (white arrow). (**R**) Larvae exposed to SU5402 from stage 20 till stage 26. (**S**) Transversal section shows loss of external gill anlagen. (**T–U**) SU5402 treated larvae fixed at stage 26 and probed for *Pea3* (**T**) and *Dusp6* (**U**). Nuclei are stained with DAPI (blue), basal laminae with anti-fibronectin (red). White

Figure 4 continued on next page

Figure 4 continued

arrowheads mark spiraculum (hyomandibular cleft) and black arrowhead marks hyo-branchial pouch. Asterisk, cement gland; b, brain; green, otic vesicle; e, eye primordium; nt, notochord; ot, otic vesicle; ph, pharynx.

DOI: https://doi.org/10.7554/eLife.43531.005

The following figure supplements are available for figure 4:

Figure supplement 1. Fgf8 expression during the course of bichir hyoid arch and external gill development.

DOI: https://doi.org/10.7554/eLife.43531.006

Figure supplement 2. Expression patterns of bichir Fgf8 *and transcriptional readouts of Fgf signaling,* Dusp6 *and* Pea3.

DOI: https://doi.org/10.7554/eLife.43531.007

2009; ***Diedhiou and Bartsch, 2009***). However, our finding of an endodermal component in the early formation of bichir external gills reveals an unanticipated similarity with the true, internal gills of vertebrates, which typically form as pharyngeal endodermal structures (***Warga and Nüsslein-Volhard, 1999***; ***Gillis and Tidswell, 2017***). Pharyngeal morphogenesis might thus represent a central developmental component of vertebrate gill breathing organs irrespective of their actual topographic position.

Conclusions

The sequential formation of pharyngeal segments during embryonic development has deep deuterostome origins (***Willey, 1891***; ***Koop et al., 2014***; ***Gillis et al., 2012***) and it is well conserved among vertebrates, where all the embryonic cranial segments typically follow the sequential anteroposterior order during development (***Quinlan et al., 2004***; ***Grevellec and Tucker, 2010***; ***Schilling, 2008***; ***Santagati and Rijli, 2003***). Bichir embryos diverge from this common scheme by the profoundly accelerated development of the second, hyoid segment, with earlier and orchestrated formation of the endodermal, mesodermal, and neural crest tissues (***Figure 5***). This unique heterochronic shift in the anteroposterior sequence constitutes a developmental basis for the early appearance of external gills that represent key breathing organs of bichir free-living embryos and early larvae.

Bichir external gills significantly differ from the external gills of amphibian and lungfish larvae that characteristically supplement the post-hyoid, branchial arches (***Duellman and Trueb, 1994***; ***Witzmann, 2004***; ***Nokhbatolfoghahai and Downie, 2008***; ***Schoch and Witzmann, 2011***). The hyoid segmental origin represents a major developmental dissimilarity and suggests an independent evolution of bichir external gills. Developmentally, bichir external gills likely correspond to opercular structures that in ray-finned fishes typically form as caudal expansions of the hyoid arch to cover the gill-bearing branchial arches, and that persist in amniotes as early embryonic opercular flaps (***Richardson et al., 2012***). In bichirs, the opercular flap forms directly from the base of their external gills, and it progressively expands during early larval stages while external gills become reduced (***Diedhiou and Bartsch, 2009***). Interestingly, the hyoid arch-derived external gills and opercular flaps are both engaged in breathing and gill ventilation in bichir larvae. Moreover, in adult bichirs, the hyoid domain also contributes to air-breathing by forming paired spiracular chamber with openings located on the dorsal surface of the skull (***Graham et al., 2014***). Bichirs thus seem unique across recent vertebrates in enhancing breathing capacity through the development of several structures associated with the hyoid cranial segment.

Materials and methods

Embryo collection

Fish were manipulated in accordance with the institutional guidelines for the use of embryonic material and international animal welfare guidelines (Directive 2010/63/EU). Senegal bichir (*Polypterus senegalus* Cuvier, 1829) embryos were obtained, reared and staged as previously described (***Minarik et al., 2017***; ***Diedhiou and Bartsch, 2009***). Embryos were dechorionated manually, fixed in 4% PFA in 0.1 M PBS at 4°C overnight, and then gradually dehydrated through a series of PBS/methanol mixtures and finally stored in 100% methanol.

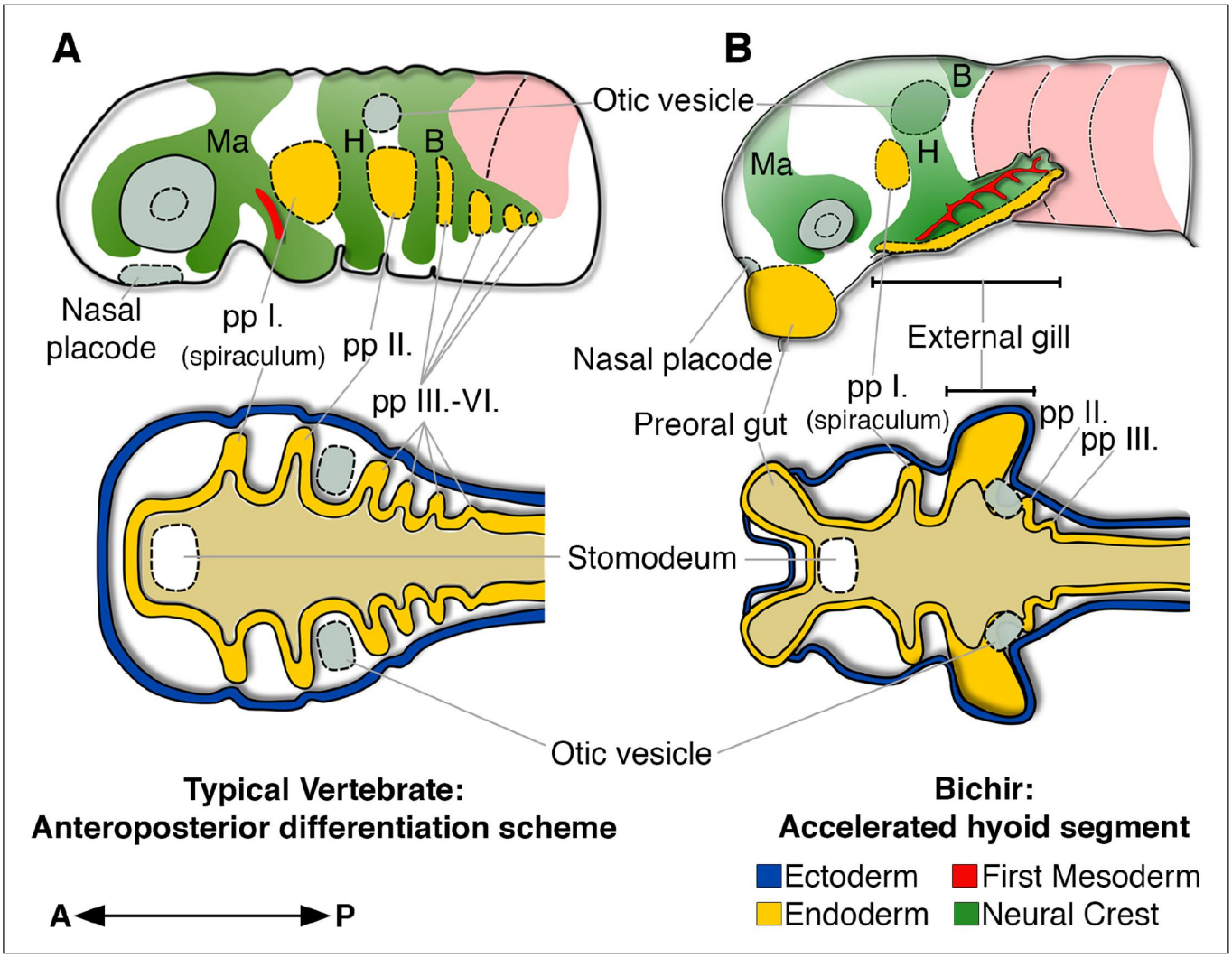

Figure 5. Bichir embryos diverge from the common anteroposterior differentiation scheme by accelerated development of the entire hyoid segment. (**A, B**) A cartoon of cranial neural crest migration (green), the first mesoderm (red), and pharyngeal pouches (yellow) in a typical vertebrate (**A**) and a bichir (**B**). Top are left lateral views, below are left horizontal sections. (**A**) In vertebrates, the sequential anteroposterior formation of cranial segments is well conserved, including pharyngeal pouches and cranial neural crest streams. (**B**) In bichirs, the entire hyoid segment is accelerated with earlier formation of the endodermal, mesodermal, and neural crest tissues, what constitutes a developmental basis for the appearance their external gills. Surface ectoderm in horizontal sections is shown in blue and primitive gut in ochre; B, branchial NC stream; H, hyoid NC stream; Ma, mandibular NC stream; pp I.-pp VI., pharyngeal pouches.

DOI: https://doi.org/10.7554/eLife.43531.008

In situ hybridization and fate mapping

Whole-mount in situ hybridization with probes against *Hoxa2* (GenBank accession number: MK630352), *Sox9* (GenBank accession number: MK630350), *Fgf8* (GenBank accession number: MK630353), *Pea3* (GenBank accession number: MK630351), and *Dusp6* (GenBank accession number: MK630349) was performed as described (***Minarik et al., 2017***). Selected specimens were embedded in gelatine/albumin solution with glutaraldehyde, sectioned and counterstained with DAPI. Fate mapping experiments were carried out as described (***Minarik et al., 2017***). CM-DiI was injected into the neural fold of the prospective rhombomere 4 (***Figure 2L***). To confirm correct localisation of the tracking dye, some embryos were fixed immediately after injection, sectioned, and observed under

the fluorescent stereomicroscope in order to confirm proper localization of the cell tracking dye. The rest of the specimens were incubated until the desired stage and then fixed in 4% PFA in 0.1 M PBS.

Scanning electron microscopy (SEM) and MicroCT imaging

Samples for SEM were fixed in modified Karnovsky's fixative (**Mitgutsch et al., 2008**). For direct visualization of cranial neural crest streams, the epidermis was removed using tungsten needles as described (**Cerny et al., 2004**). Specimens for MicroCT analysis were treated with phosphotungstic acid following the protocol developed by **Metscher (2009)** and scanned with a MicroXCT (X-radia) at the Department of Theoretical Biology, University of Vienna. Images were reconstructed in XMReconstructor (X-Radia), and virtual sections were analyzed in Amira (FEI Software).

Antibody staining

Specimens for antibody staining were fixed in Dent's fixative. Muscles were labeled with 12/101 antibody (AB531892; Developmental Studies Hybridoma Bank), neural crest cells were labeled with Sox9 antibody (AB5535; Merck Millipore), basal lamina was labeled with anti-fibronectin (A0245; DAKO) and MAPK activity was assessed using anti-activated MAP kinase antibody (M8159; Sigma). Primary antibodies were detected by Alexa Fluor 488 and 594 (Invitrogen, Thermo Fisher Scientific Inc.). Visualisation of nerve fibres was performed using anti-acetylated tubulin antibody (T6793; Sigma) and EnzMet Enzyme Metallography kit (Nanoprobes).

Pharmacological treatments

For inhibition of pharyngeal outpocketing morphogenesis, embryos were treated with 50 µM SU5402 in DMSO (Sigma Aldrich) from stage 20 until stage 26. Treatments were performed in E2 medium (**Brand et al., 2002**). Controls were reared in E2 medium with the equivalent DMSO concentrations.

Acknowledgments

We thank Wojta Miller and Karel Kodejs for bichir colony care; James P. Cleland, Tatjana Haitina, Dan Medeiros, Rolf Ericsson and Jana Stundlova for critical reading of earlier versions of the manuscript; Martin Kralovic for initial work on this topic, Viktoria Psutkova and Kristyna Markova for technical assistance. This study was supported by the Charles University Grant Agency GAUK 1448514 (to JS), GAUK 640016 (to AP), GAUK 220213 and GAUK 726516 (to MM), the Charles University grant SVV 260434/2019 (to JS, AP, VS, DJ and RC), the Charles University Research Centre program No. 204069 (to VS), the grant of the Scientific Grant Agency of Slovak Republic VEGA 1/0415/17 and the European Union's Horizon 2020 research and innovation program under the Marie Skłodowska-Curie grant agreement No 751066 (to DJ), and the Czech Science Foundation GACR 16–23836S (to RC). Computational resources were supplied by the Ministry of Education, Youth and Sports of the Czech Republic under the Projects CESNET (Project No. LM2015042) and CERIT-Scientific Cloud (Project No. LM2015085) provided within the program Projects of Large Research, Development and Innovations Infrastructures.

Additional information

Funding

Funder	Grant reference number	Author
Charles University Grant Agency	1448514	Jan Stundl
Charles University Grant Agency	640016	Anna Pospisilova
Charles University Grant Agency	220213	Martin Minarik
Czech Science Foundation	16-23836S	Robert Cerny

Charles University Grant Agency	726516	Martin Minarik
Charles University	Grant SVV 260434/2019	Jan Stundl Anna Pospisilova David Jandzik Vladimir Soukup Robert Cerny
Charles University	Research Centre program 204069	Vladimir Soukup
Vedecká Grantová Agentúra MŠVaŠ SR a SAV	1/0415/17	David Jandzik
H2020 Marie Skłodowska-Curie Actions	751066	David Jandzik

The funders had no role in study design, data collection and interpretation, or the decision to submit the work for publication.

Author contributions

Jan Stundl, Conceptualization, Data curation, Investigation, Writing—original draft, Writing—review and editing; Anna Pospisilova, Martin Minarik, Data curation, Formal analysis, Investigation; David Jandzik, Validation, Investigation, Methodology; Peter Fabian, Formal analysis, Investigation, Methodology; Barbora Dobiasova, Brian D Metscher, Data curation, Formal analysis; Vladimir Soukup, Methodology, Writing—original draft, Writing—review and editing; Robert Cerny, Conceptualization, Funding acquisition, Writing—original draft, Writing—review and editing

Author ORCIDs

Jan Stundl http://orcid.org/0000-0002-3740-3378
Anna Pospisilova http://orcid.org/0000-0002-8252-0709
Peter Fabian http://orcid.org/0000-0002-1096-6875
Martin Minarik https://orcid.org/0000-0001-6660-0031
Brian D Metscher http://orcid.org/0000-0002-6514-4406
Vladimir Soukup http://orcid.org/0000-0002-1914-283X
Robert Cerny http://orcid.org/0000-0002-0022-0199

Decision letter and Author response

Decision letter https://doi.org/10.7554/eLife.43531.011
Author response https://doi.org/10.7554/eLife.43531.012

Additional files

Supplementary files

- Transparent reporting form

DOI: https://doi.org/10.7554/eLife.43531.009

Data availability

All data generated and analysed during this study are included in the manuscript and providing files. All sources are cited in the Methods chapter.

References

Abu-Issa R, Smyth G, Smoak I, Yamamura K, Meyers EN. 2002. Fgf8 is required for pharyngeal arch and cardiovascular development in the mouse. *Development* **129**:4613–4625. DOI: https://doi.org/10.1242/dev.02408, PMID: 12223417

Baltzinger M, Ori M, Pasqualetti M, Nardi I, Rijli FM. 2005. *Hoxa2* knockdown in *xenopus* results in hyoid to mandibular homeosis. *Developmental Dynamics : An Official Publication of the American Association of Anatomists* **234**:858–867. DOI: https://doi.org/10.1002/dvdy.20567, PMID: 16222714

Brand M, Granato M, Nusslein-Volhard C. 2002. Keeping and raising zebrafish. In: Nusslein-Volhard C, Dahm R (Eds). *In Zebrafish: A Practical Approach*. Oxford University Press. p. 7–37.
Cerny R, Meulemans D, Berger J, Wilsch-Bräuninger M, Kurth T, Bronner-Fraser M, Epperlein HH. 2004. Combined intrinsic and extrinsic influences pattern cranial neural crest migration and pharyngeal arch morphogenesis in axolotl. *Developmental Biology* **266**:252–269. DOI: https://doi.org/10.1016/j.ydbio.2003.09.039, PMID: 14738875
Cheung M, Briscoe J. 2003. Neural crest development is regulated by the transcription factor Sox9. *Development* **130**:5681–5693. DOI: https://doi.org/10.1242/dev.00808, PMID: 14522876
Choe CP, Crump JG. 2015. Dynamic epithelia of the developing vertebrate face. *Current Opinion in Genetics & Development* **32**:66–72. DOI: https://doi.org/10.1016/j.gde.2015.02.003, PMID: 25748249
Clack JA. 2007. Devonian climate change, breathing, and the origin of the tetrapod stem group. *Integrative and Comparative Biology* **47**:510–523. DOI: https://doi.org/10.1093/icb/icm055, PMID: 21672860
Coates MI, Clack JA. 1991. Fish-like gills and breathing in the earliest known tetrapod. *Nature* **352**:234–236. DOI: https://doi.org/10.1038/352234a0
Couly G, Creuzet S, Bennaceur S, Vincent C, Le Douarin NM. 2002. Interactions between Hox-negative cephalic neural crest cells and the foregut endoderm in patterning the facial skeleton in the vertebrate head. *Development* **129**:1061–1073. PMID: 11861488
Crump JG, Maves L, Lawson ND, Weinstein BM, Kimmel CB. 2004. An essential role for Fgfs in endodermal pouch formation influences later craniofacial skeletal patterning. *Development* **131**:5703–5716. DOI: https://doi.org/10.1242/dev.01444, PMID: 15509770
Diedhiou S, Bartsch P. 2009. Staging of the early development of *Polypterus* (Cladistia: Actinopterygii). In: Kunz-Ramsay Y. W, Luer C. A, Kapoor B. G (Eds). *Development of Non-Teleost Fishes*. Enfield: Science Publishers. p. 104–109. DOI: https://doi.org/10.1201/b10184-3
Duellman WE, Trueb L. 1994. *Biology of Amphibians*. New York: McGraw-Hill.
Ericsson R, Cerny R, Falck P, Olsson L. 2004. Role of cranial neural crest cells in visceral arch muscle positioning and morphogenesis in the mexican axolotl, ambystoma mexicanum. *Developmental Dynamics* **231**:237–247. DOI: https://doi.org/10.1002/dvdy.20127, PMID: 15366001
Giles S, Xu GH, Near TJ, Friedman M. 2017. Early members of 'living fossil' lineage imply later origin of modern ray-finned fishes. *Nature* **549**:265–268. DOI: https://doi.org/10.1038/nature23654, PMID: 28854173
Gillis JA, Fritzenwanker JH, Lowe CJ. 2012. A stem-deuterostome origin of the vertebrate pharyngeal transcriptional network. *Proceedings of the Royal Society B: Biological Sciences* **279**:237–246. DOI: https://doi.org/10.1098/rspb.2011.0599
Gillis JA, Tidswell OR. 2017. The origin of vertebrate gills. *Current Biology* **27**:729–732. DOI: https://doi.org/10.1016/j.cub.2017.01.022, PMID: 28190727
Goodrich ES. 1909. Vertebrata Craniata (first fascicle: cyclostomes and fishes). In: Lankester R (Ed). *Treatise on Zoology. Part 9*. London: Adam and Charles Black.
Graham A. 2008. Deconstructing the pharyngeal metamere. *Journal of Experimental Zoology Part B: Molecular and Developmental Evolution* **310**:336–344. DOI: https://doi.org/10.1002/jez.b.21182
Graham JB, Wegner NC, Miller LA, Jew CJ, Lai NC, Berquist RM, Frank LR, Long JA. 2014. Spiracular air breathing in polypterid fishes and its implications for aerial respiration in stem tetrapods. *Nature Communications* **5**:3022. DOI: https://doi.org/10.1038/ncomms4022, PMID: 24451680
Graham A, Smith A. 2001. Patterning the pharyngeal arches. *BioEssays* **23**:54–61. DOI: https://doi.org/10.1002/1521-1878(200101)23:1<54::AID-BIES1007>3.0.CO;2-5, PMID: 11135309
Grevellec A, Tucker AS. 2010. The pharyngeal pouches and clefts: development, evolution, structure and derivatives. *Seminars in Cell & Developmental Biology* **21**:325–332. DOI: https://doi.org/10.1016/j.semcdb.2010.01.022, PMID: 20144910
Hughes LC, Ortí G, Huang Y, Sun Y, Baldwin CC, Thompson AW, Arcila D, Betancur-R R, Li C, Becker L, Bellora N, Zhao X, Li X, Wang M, Fang C, Xie B, Zhou Z, Huang H, Chen S, Venkatesh B, et al. 2018. Comprehensive phylogeny of ray-finned fishes (Actinopterygii) based on transcriptomic and genomic data. *PNAS* **115**:6249–6254. DOI: https://doi.org/10.1073/pnas.1719358115, PMID: 29760103
Hunter MP, Prince VE. 2002. Zebrafish hox paralogue group 2 genes function redundantly as selector genes to pattern the second pharyngeal arch. *Developmental Biology* **247**:367–389. DOI: https://doi.org/10.1006/dbio.2002.0701, PMID: 12086473
Jandzik D, Hawkins MB, Cattell MV, Cerny R, Square TA, Medeiros DM. 2014. Roles for FGF in lamprey pharyngeal pouch formation and skeletogenesis highlight ancestral functions in the vertebrate head. *Development* **141**:629–638. DOI: https://doi.org/10.1242/dev.097261, PMID: 24449839
Kerr JG. 1907. The development of *Polypterus senegalus* Cuvier. In: Kerr J. G (Ed). *Budget Memorial Volume*. Cambridge: Cambridge University Press.
Köntges G, Lumsden A. 1996. Rhombencephalic neural crest segmentation is preserved throughout craniofacial ontogeny. *Development* **122**:3229–3242. PMID: 8898235
Koop D, Chen J, Theodosiou M, Carvalho JE, Alvarez S, de Lera AR, Holland LZ, Schubert M. 2014. Roles of retinoic acid and Tbx1/10 in pharyngeal segmentation: amphioxus and the ancestral chordate condition. *EvoDevo* **5**:36. DOI: https://doi.org/10.1186/2041-9139-5-36, PMID: 25664163
Lumsden A, Sprawson N, Graham A. 1991. Segmental origin and migration of neural crest cells in the hindbrain region of the chick embryo. *Development* **113**:1281–1291. PMID: 1811942

Metscher BD. 2009. MicroCT for developmental biology: a versatile tool for high-contrast 3D imaging at histological resolutions. *Developmental Dynamics* **238**:632–640. DOI: https://doi.org/10.1002/dvdy.21857, PMID: 19235724

Minarik M, Stundl J, Fabian P, Jandzik D, Metscher BD, Psenicka M, Gela D, Osorio-Pérez A, Arias-Rodriguez L, Horácek I, Cerny R. 2017. Pre-oral gut contributes to facial structures in non-teleost fishes. *Nature* **547**:209–212. DOI: https://doi.org/10.1038/nature23008, PMID: 28678781

Minoux M, Rijli FM. 2010. Molecular mechanisms of cranial neural crest cell migration and patterning in craniofacial development. *Development* **137**:2605–2621. DOI: https://doi.org/10.1242/dev.040048, PMID: 20663816

Mitgutsch C, Piekarski N, Olsson L, Haas A. 2008. Heterochronic shifts during early cranial neural crest cell migration in two ranid frogs. *Acta Zoologica* **89**:69–78. DOI: https://doi.org/10.1111/j.1463-6395.2007.00295.x

Mori-Akiyama Y, Akiyama H, Rowitch DH, de Crombrugghe B. 2003. Sox9 is required for determination of the chondrogenic cell lineage in the cranial neural crest. *PNAS* **100**:9360–9365. DOI: https://doi.org/10.1073/pnas.1631288100, PMID: 12878728

Noda M, Miyake T, Okabe M. 2017. Development of cranial muscles in the actinopterygian fish Senegal bichir, *Polypterus senegalus* Cuvier, 1829. *Journal of Morphology* **278**:450–463. DOI: https://doi.org/10.1002/jmor.20636, PMID: 28182295

Nokhbatolfoghahai M, Downie JR. 2008. The external gills of anuran amphibians: comparative morphology and ultrastructure. *Journal of Morphology* **269**:1197–1213. DOI: https://doi.org/10.1002/jmor.10655, PMID: 18626919

Piotrowski T, Nüsslein-Volhard C. 2000. The endoderm plays an important role in patterning the segmented pharyngeal region in zebrafish (Danio rerio). *Developmental Biology* **225**:339–356. DOI: https://doi.org/10.1006/dbio.2000.9842, PMID: 10985854

Quinlan R, Martin P, Graham A. 2004. The role of actin cables in directing the morphogenesis of the pharyngeal pouches. *Development* **131**:593–599. DOI: https://doi.org/10.1242/dev.00950, PMID: 14711875

Richardson J, Shono T, Okabe M, Graham A. 2012. The presence of an embryonic opercular flap in amniotes. *Proceedings of the Royal Society B: Biological Sciences* **279**:224–229. DOI: https://doi.org/10.1098/rspb.2011.0740

Rijli FM, Mark M, Lakkaraju S, Dierich A, Dollé P, Chambon P. 1993. A homeotic transformation is generated in the rostral branchial region of the head by disruption of Hoxa-2, which acts as a selector gene. *Cell* **75**:1333–1349. DOI: https://doi.org/10.1016/0092-8674(93)90620-6, PMID: 7903601

Santagati F, Rijli FM. 2003. Cranial neural crest and the building of the vertebrate head. *Nature Reviews Neuroscience* **4**:806–818. DOI: https://doi.org/10.1038/nrn1221, PMID: 14523380

Schilling TF. 2008. Anterior-posterior patterning and segmentation of the vertebrate head. *Integrative and Comparative Biology* **48**:658–667. DOI: https://doi.org/10.1093/icb/icn081, PMID: 21669823

Schoch RR, Witzmann F. 2011. Bystrow's Paradox - gills, fossils, and the fish-to-tetrapod transition. *Acta Zoologica* **92**:251–265. DOI: https://doi.org/10.1111/j.1463-6395.2010.00456.x

Shone V, Graham A. 2014. Endodermal/ectodermal interfaces during pharyngeal segmentation in vertebrates. *Journal of Anatomy* **225**:479–491. DOI: https://doi.org/10.1111/joa.12234, PMID: 25201771

Square T, Jandzik D, Romášek M, Cerny R, Medeiros DM. 2017. The origin and diversification of the developmental mechanisms that pattern the vertebrate head skeleton. *Developmental Biology* **427**:219–229. DOI: https://doi.org/10.1016/j.ydbio.2016.11.014, PMID: 27884657

Standen EM, Du TY, Larsson HC. 2014. Developmental plasticity and the origin of tetrapods. *Nature* **513**:54–58. DOI: https://doi.org/10.1038/nature13708, PMID: 25162530

Takeuchi M, Okabe M, Aizawa S. 2009. The genus polypterus (Bichirs): A fish group diverged at the stem of Ray-Finned fishes (Actinopterygii). *Cold Spring Harbor Protocols* **2009**:emo117. DOI: https://doi.org/10.1101/pdb.emo117

Tatsumi N, Kobayashi R, Yano T, Noda M, Fujimura K, Okada N, Okabe M. 2016. Molecular developmental mechanism in polypterid fish provides insight into the origin of vertebrate lungs. *Scientific Reports* **6**:30580. DOI: https://doi.org/10.1038/srep30580, PMID: 27466206

Theveneau E, Mayor R. 2012. Neural crest delamination and migration: from epithelium-to-mesenchyme transition to collective cell migration. *Developmental Biology* **366**:34–54. DOI: https://doi.org/10.1016/j.ydbio.2011.12.041, PMID: 22261150

Tokita M, Schneider RA. 2009. Developmental origins of species-specific muscle pattern. *Developmental Biology* **331**:311–325. DOI: https://doi.org/10.1016/j.ydbio.2009.05.548, PMID: 19450573

Walshe J, Mason I. 2003. Fgf signalling is required for formation of cartilage in the head. *Developmental Biology* **264**:522–536. DOI: https://doi.org/10.1016/j.ydbio.2003.08.010, PMID: 14651935

Warga RM, Nüsslein-Volhard C. 1999. Origin and development of the zebrafish endoderm. *Development* **126**:827–838. PMID: 9895329

Willey A. 1891. The later larval development of amphioxus. *The Quarterly Journal of Microscopical Science* **32**:183–234.

Witzmann F. 2004. The external gills of paleozoic amphibians. *Neues Jahrbuch Für Geologie Und Paläontologie Abhandlungen* **232**:375–401.

V. Stundl J, **Pospisilova A**, Matějková T, Psenicka M, Bronner ME & Cerny R (2020) Migratory patterns and evolutionary plasticity of cranial neural crest cells in ray-finned fishes. *Developmental Biology* (forthcoming)

IF (2019) = 2,895

Developmental Biology xxx (xxxx) xxx-xxx

Contents lists available at ScienceDirect

Developmental Biology

journal homepage: http://ees.elsevier.com

Migratory patterns and evolutionary plasticity of cranial neural crest cells in ray-finned fishes

Jan Stundl [a,bc,*], Anna Pospisilova [a], Tereza Matějková [a], Martin Psenicka [c], Marianne E. Bronner [b], Robert Cerny [a,**]

[a] Department of Zoology, Faculty of Science, Charles University in Prague, Prague, Czech Republic
[b] Division of Biology and Biological Engineering, California Institute of Technology, Pasadena, CA, USA
[c] South Bohemian Research Center of Aquaculture and Biodiversity of Hydrocenoses, Faculty of Fisheries and Protection of Waters, University of South Bohemia in Ceske Budejovice, Vodnany, Czech Republic

ARTICLE INFO

Keywords
Neural crest
Vertebrates
Craniofacial
Evolution
Neurulation

ABSTRACT

The cranial neural crest (CNC) arises within the developing central nervous system, but then migrates away from the neural tube in three consecutive streams termed mandibular, hyoid and branchial, respectively, according to the order along the anteroposterior axis. While the process of neural crest emigration generally follows a conserved anterior to posterior sequence across vertebrates, we find that ray-finned fishes (bichir, sterlet, gar, and pike) exhibit several heterochronies in the timing and order of CNC emergence that influences their subsequent migratory patterns. First, emigration of the cranial neural crest in these fishes occurs prematurely compared to other vertebrates, already initiating during early neurulation and well before neural tube closure. Second, delamination of the hyoid stream occurs prior to the more anterior mandibular stream; this is associated with early morphogenesis of key hyoid structures like external gills (bichir), a large opercular flap (gar) or first forming cartilage (pike). In sterlet, the hyoid and branchial CNC cells form a single hyobranchial sheet, which later segregates in concert with second pharyngeal pouch morphogenesis. Taken together, the results show that despite generally conserved migratory patterns, heterochronic alterations in the timing of emigration and pattern of migration of CNC cells accompanies morphological diversity of ray-finned fishes.

1. Introduction

Evolution of vertebrates is intimately connected with the advent of the neural crest (Gans and Northcutt, 1983; Northcutt and Gans, 1983; Northcutt, 2005; Green et al., 2015). This embryonic cell population arises within the forming neural tube but then migrates into the periphery to contribute to a remarkable range of structures and cell types such as odontoblasts, facial bone and cartilage, pigment cells, glial cells of the peripheral nervous system, components of heart, etc. (Bronner and Ledouarin, 2012; Simões-Costa and Bronner, 2015; Hall, 2009; Le Douarin and Dupin, 2014). Given its contribution to a plethora of cell types, acquisition of this vertebrate-specific cell types was a key milestone in the evolutionary success of vertebrates on Earth (Gans and Northcutt, 1983; Forey and Janvier, 1994; Donoghue and Keating, 2014; Square et al., 2017).

The vertebrate neural crest is characterized by three key features: (i) multipotency, (ii) origin from the neural plate border, and (iii) ability to migrate long-distance in a directed fashion to diverse locations throughout the embryo (Theveneau and Mayor, 2012; Meulemans Medeiros, 2013; Green et al., 2015). Induction of the neural crest initiates already during gastrulation (Basch et al., 2006; Patthey et al., 2008; Betters et al., 2018). Following neurulation, individual neural crest (NC) cells begin to emigrate from the neural tube via an epithelial to mesenchymal transition controlled by interactions between transcriptional regulators, receptors, and signaling molecules (Sauka-Spengler and Bronner-Fraser, 2008; Simões-Costa et al., 2014; Hockman et al., 2019). While NC cells arise all along the anteroposterior axis of the embryo, they follow different migratory pathways and form different derivatives depending upon their axial level of origin (Kuo and Erickson, 2010; Simoes-Costa and Bronner, 2013; Simões-Costa and Bronner, 2015; Gouignard et al., 2018; Rothstein et al., 2018).

The most anterior and diverse neural crest population is the cranial neural crest (CNC), which migrates in three wide streams called the mandibular, hyoid and branchial, each separated by neural crest-free zones adjacent to rhombomere 3 and 5 (Kulesa et al., 2010; Theve-

* Corresponding author. Department of Zoology, Faculty of Science, Charles University in Prague, Prague, Czech Republic.
** Corresponding author.
E-mail addresses: jstundl@caltech.edu (J. Stundl); robert.cerny@natur.cuni.cz (R. Cerny)

https://doi.org/10.1016/j.ydbio.2020.08.007
Received 27 April 2020; Received in revised form 13 August 2020; Accepted 14 August 2020
Available online xxx
0012-1606/

neau and Mayor, 2012; Szabó and Mayor, 2018). This migratory pattern of CNC cells appears to be mostly conserved across all vertebrates (Falck et al., 2002; Minoux and Rijli, 2010; Theveneau and Mayor, 2012; Rocha et al., 2019).

During migration, CNC cells interact not only with each other within individual streams but also with surrounding tissues (Carmona-Fontaine et al., 2008; Kulesa et al., 2010; Szabó and Mayor, 2018). One key interacting tissue is the head endoderm of the pharyngeal pouches (Graham, 2008; Grevellec and Tucker, 2010). In the final phase of migration, the endoderm influences CNC differentiation into cartilage precursors (Piotrowski and Nüsslein-Volhard, 2000; David et al., 2002; Crump et al., 2004). Thus, modulations of the head endoderm, and heterochronic and heterotopic alterations of CNC migratory patterns might represent a key source of craniofacial diversity in vertebrates (Schneider, 2018).

To better understand the diversity in patterns of CNC migration, it is essential to compare diverse species. To this end, here we investigate CNC cells in representatives of each phylogenetic lineage of non-teleost ray-finned fishes: bichir, sterlet, and gar (Betancur-R et al., 2017; Hughes et al., 2018; Kunz et al., 2009). All these species reflect evolutionarily informative lineages of ray-finned fishes. These species were chosen because they possess characteristics that either resemble lungfishes, amphibians or are transitional between amphibian-like and teleost-like (Cooper and Virta, 2007; Soukup et al., 2013; Minarik et al., 2017; Stundl et al., 2019). For comparison, we also investigate CNC cells of the northern pike as a representative of teleosts. Close examination of early CNC development in these species holds the promise of shedding light on craniofacial evolution of vertebrates, since all these ray-finned fishes possess distinct craniofacial characteristics, such as a massive exoskeleton in bichir, a distinct rostrum in sterlet, and significantly elongated jaws in gar and pike. The results reveal surprising alterations in CNC migration in all species and demonstrate that the migratory patterns of CNC cells are not as stereotypic as generally assumed. This highlights the plasticity of CNC, which apparently contributes to remarkable craniofacial diversity across vertebrates.

2. Materials and methods

2.1. Fish embryo collections and histology

This study was performed by analysis of detailed developmental series of the Senegal bichir (*Polypterus senegalus* Cuvier, 1829), the sterlet sturgeon (*Acipenser ruthenus* Linnaeus, 1758), the tropical gar (*Atractosteus tropicus* T. N. Gill, 1863) and the northern pike (*Esox lucius* Linnaeus, 1758). Husbandry and collection of embryos were performed as previously described (Minarik et al., 2017; Pospisilova et al., 2019), with embryos being staged as previously described (Dettlaff et al., 1993; Long and Ballard, 2001; Diedhiou and Bartsch, 2009; Pospisilova et al., 2019), fixed in 4% paraformaldehyde (PFA) in 0.1 M PBS at 4 °C overnight, and dehydrated in 100% methanol for storage at −20 °C. This study was conducted by following institutional guidelines for the use of embryonic material and international animal welfare guidelines (Directive, 2010/63/EU) in the animal facility of the Department of Zoology, Charles University in Prague. As the use of standard staging tables is unsuitable for direct interspecies comparison, we instead utilize four developmental stages: specification, emigration, early and late migration (Figs. 3–6). To this end, we first analyzed each described developmental stage relevant to the neural crest migration (from late gastrula until pharyngula stage) and based on the obtained data we designated individual stages as follows: specification – first detected expression of neural crest markers; emigration - the developmental stage when one of the neural crest streams begins emigration from the prospective neural tube; early migration - post-neurula stage or early pharyngula stage containing migratory CNC cells; late migration - pharyngula stage with fully developed pharyngeal pouches.

Embryos for histological analyses were embedded in JB4 resin (Polysciences) according to the manufacturer's instructions, sectioned on RM2155 microtome (Leica, Germany) to 4 μm-thick sections, stained with Azure B-Eosin (SERVA), mounted in DePeX (SERVA), and photographed using microscope BX51 (Olympus, Japan). Cartilage staining was performed with Alcian Blue as described previously (Taylor and Van Dyke, 1985), and photographed using a dissection microscope SZX12 (Olympus, Japan).

2.2. Scanning electron microscopy and micro-CT imaging and analysis

Specimens for scanning electron microscopy (SEM) and micro-CT were fixed in 4% PFA in 0.1 M PBS and transferred into modified Karnovsky fixative (Mitgutsch et al., 2008) at least overnight. Samples for SEM were washed in PBS, dehydrated through a graded series of ethanol, transferred into dehydrating capsules with 30 μm pores (SPI Supplies, Germany), and dried in a critical point dryer CPD 030 (BAL-TEC, Liechtenstein). Dried samples were mounted on a steel disc covered by Tempfix resin (SPI Supplies, Germany), and coated with gold in SCD 050 sputter coater (BAL-TEC, Liechtenstein). SEM images were obtained using a JSM-6380LV scanning electron microscope (JEOL, Japan). Specimens for micro-CT visualization were prepared as described previously (Metscher, 2009; Minarik et al., 2017) and scanned with a MicroXCT-200 (Zeiss/Xradia, Germany) at the Department of Theoretical Biology, University of Vienna and with a Sky-Scan 1172 (Bruker, USA) at the Paleontological Department of the National Museum, Prague. Tomographic sections were reconstructed in XMReconstructor (Zeiss/Xradia, Germany), and final visualizations were accomplished in AMIRA 6.0.1 (Thermo Fisher Scientific, USA). The original microCT scans were uploaded to the Morphobank (http://morphobank.org/permalink/?P3784).

2.3. Probes synthesis and in situ hybridization

Primers for PCR amplification were designed based on sequences from *de novo* assembled transcriptomes of non-teleost fishes and on predicted gene sequences in the northern pike genome assembly (Rondeau et al., 2014). Probe templates were isolated by direct amplification from cDNA libraries using specific primers (Table 1), cloned into pGEM-T Easy Vector (Promega), and sequenced.

Digoxygenin-labeled probes were prepared by standard protocols. Whole mount in situ hybridization was performed as described previously (Minarik et al., 2017). Selected embryos were washed in 0.1 M PBS, transferred into the embedding medium (gelatin, albumin, and glutaraldehyde), and sectioned on VT1200S vibratome (Leica, Germany) at 50 μm-thickness. For better visualization of tissue context, the sections were counterstained with Fluoroshield with DAPI (Sigma), and photographed using a BX51 (Olympus, Japan) fluorescent microscope.

2.4. Antibody staining and fate-mapping analysis

Embryos for antibody staining were transferred from 100% methanol into Dent's fixative (80% methanol and 20% DMSO) for 6 h, washed three times in PBST (0.1 M PBS and 0.4% Triton X-100), and then incubated in Antibody diluent buffer (DAKO) for 1 h. Subsequently, primary antibody was applied overnight at room temperature in a damp box. After incubation, the embryos were washed three times in PBST, transferred in Antibody diluent buffer, and incubated with the secondary antibody in a damp box at room temperature for 5–6 h. After labeling, the specimens were washed in 0.1 M PBS and transferred to clearing solution (benzyl alcohol/benzyl benzoate; 2:1). Neural crest cells were labeled with Sox9 antibody (AB5535; Merck Millipore), and primary antibody was detected by Alexa Fluor 594 (Invitrogen, Thermo Fisher Scientific Inc.). For the fate-mapping analysis, individual em-

Table 1
List of primer sequences used for probe synthesis.

Gene	Forward primer	Reverse primer
Hand2_At	5′-ATHAGCCAYCCAGAGATGTC-3′	5′- TTTGAATTCCGCTTTGAAGG -3′
Hand2_El	5′- CTTACCTYATGGACATTCTG -3′	5′- CAAATATCCAMTSTCCGTAG -3′
Hand2_Ps	5′- CAGGACTCAGAGCATCAACAG -3′	5′- CTTTRGTTTTGTCRTTGCTGC -3′
FoxD3_Ar	5′- GAYGTGGAYATCGAYGTGGT -3′	5′- CTSARRAARCTVCCGTTGTC -3′
FoxD3_At	5′- ARYAAGCCHAAAAACAGCCT -3′	5′- TCGAACATRTCTTCDGACTG -3′
FoxD3_El	5′- GAYGTGGAYATCCGAYGTGGT -3′	5′- CTSARRAARCTVCCGTTGTC -3′
Hoxa2_Ps	5′- CTGTCGGTGATDCATTTCAAAG -3′	5′- ARCTYTGGGAHTCDCYATTG -3′
Krox20_Ar	5′- CAGACTTTCACCTACATGGG -3′	5′- ATRTGBGTGGTRAGGTGGTC -3′
Krox20_At	5′- CAGACTTTCACCTACATGGG -3′	5′- ATRTGBGTGGTRAGGTGGTC -3′
Krox20_El	5′- TTTCCCATCATCCCGGACTA -3′	5′- ATGTGTCTGGTTAGCTCGTC -3′
Krox20_Ps	5′- ATGGTCAATGTGGATATGAG -3′	5′- AGGGCATGGAAAGGGCTTGC -3′
Snail1/2_Ps	5′- TACAGCGAACTGGAAAGCCA -3′	5′- GAGCGGATGTGCATYTTCAG -3′
Sox9_Ar	5′- GGCAGAACGAAGCTGAAGAC -3′	5′- CATACTGGGAGCGTGTGATG -3′
Sox9_At	5′- CCAGTACCCTCACCTTCACA -3′	5′- ATGACATCGCTGCTCAGCTC -3′
Sox9_El	5′- TTCAAGCTTTTCCACGTGCG -3′	5′- ATCGTAGCCCTTCAGGACCT -3′
Sox9_Ps	5′- CTCMGCTGCTCCGTYTTDATSTG -3′	5′-TGGWSYYTGGTGCCBATGCCNGT -3′
Sox10_Ar	5′- GAKTACAAGTACCAGCCCNCG -3′	5′- GGNAGGTACTGGTCRAAYTC -3′
Sox10_At	5′- CTGTGGAGGCTTCTGAACGGA -3′	5′- GTGCAKGCTCTTGTAGTGCG -3′
Sox10_El	5′- TACAAGTACCAGCCACGYMG -3′	5′- GGNAGGTACTGGTCRAAYTC -3′
Twist1_Ar	5′- GAAAWGWTGCARGANGAATC -3′	5′- TGVGATGYRGACATGGCCA -3′

bryos were decapsulated and mounted into a Petri dish with plasticine, which helped to orient the embryo before injection. CM-DiI cell tracking dye (Thermo Fisher Scientific Inc.) was prepared for injection as described (Minarik et al., 2017). CM-DiI was injected through the inner egg membrane into the region of prospective CNC. All injected embryos were allowed to develop until the desired stage when the embryos were euthanized with an overdose of MS-222 (Sigma) and fixed in 4% PFA in 0.1 M PBS. For visualization of early neurula stages of pike, embryos were dechorionated and stained with DAPI. Images were taken using Lumar V.12 (Zeiss, Germany).

3. Results

3.1. Transitional patterns of neurulation

The central nervous system of all vertebrates arises during neurulation which occurs by two distinct mechanisms depending on species: (i) invagination of the neural plate until the neural folds meet to form the neural tube (primary neurulation best studied in amniotes) or (ii) cavitation of the neural keel (best studied in teleosts) (Baker and Bronner-Fraser, 1997; Lowery and Sive, 2004; Harrington et al., 2009). We first analyzed the external morphology of cranial neurulation in individual non-teleost fish lineages. SEM images reveal variation in the mechanism of cranial neurulation across species examined here (Fig. 1). Bichir and sterlet embryos undergo primary neurulation with lateral regions of the neural plate forming neural folds, which then roll up and bend into a neural tube with a central lumen (Fig. 1A–H). Nevertheless, both species exhibit remarkable differences in neurulation. In bichir, the entire morphogenetic process occurs above the yolk ball (Fig. 1A–D). In contrast, in sterlet, formation of the neural tube takes place within the yolk ball (Fig. 1E–H), and the developing neural tube is not as elevated as in bichir (cf. Fig. 1D, H). Gar embryos undergo neurulation in a manner that is similar that described for teleosts including pike (Schmitz et al., 1993; Lowery and Sive, 2004; Pospisilova et al., 2019) with the neuroectoderm forming a solid neural keel that only later develops a central lumen of the neural tube by means of cavitation (Fig. 1I-L).

Taken together, non-teleost fish embryos seem to manifest transitional patterns from primary neurulation to neurulation via cavitation, depending on the species. Interestingly, such transitional patterns are also apparent in gastrulation of non-teleost fishes (Takeuchi et al., 2009).

3.2. Accelerated emigration of cranial neural crest cells

In vertebrates, CNC cells typically begin their migration around the time of or after neural tube closure (Tan and Morris-Kay, 1986; Noden, 1988; Horigome et al., 1999; Smith, 2001; Falck et al., 2002; Mitgutsch et al., 2008; Diaz et al., 2019). To characterize the onset of CNC cells emigration, we screened for spatiotemporal expression of *Sox9*, a member of the SoxE transcription factor family, which is expressed in premigratory and migratory neural crest cells and later is associated with chondrogenesis (Cheung and Briscoe, 2003; Mori-Akiyama et al., 2003; Martik and Bronner, 2017). Embryos were examined at two stages: onset of migration and mid-migratory phase (Fig. 2).

In all studied fish species, the first migrating CNC cells are already detectable during the first phase of neurulation. In bichir and sterlet, this occurs before neural tube closure, whereas in gar and pike before lumen formation (Fig. 2). In bichir, *Sox9* expression is apparent in both the mandibular and hyoid regions, even when the neural tube is still widely open (Fig. 2A). However, histological sections reveal that there is a difference between the mandibular and hyoid regions (Fig. 2B-C'; Stundl et al., 2019); whereas *Sox9* is detected in premigratory cells in the mandibular region (Fig. 2B-B′), it is strongly expressed in already emigrating cells of the hyoid stream (Fig. 2C-C′). At a later stage, when the neural tube is still open, *Sox9* transcripts are more abundant in the hyoid region than in the mandibular region (Fig. 2D), and the hyoid neural crest stream is predominant (Fig. 2D-F′). In sterlet, the mandibular region has strong *Sox9* expression compared to the hyoid region (Fig. 2G). Transverse sections reveal *Sox9* transcripts in emigrating cells of the mandibular neural crest stream (Fig. 2H-H′) and presumptive CNC cells of the hyoid stream (Fig. 2I–I'). At later stages of neurulation, *Sox9* transcripts are seen in migrating cells of the mandibular stream and in emigrating cells of the hyoid stream (Fig. 2J-L′). As neurulation begins in gar, *Sox9* is detected only in presumptive CNC in the mandibular region (Fig. 2M–O′). Interestingly, at later stages, *Sox9* expression is detected in the emigrating hyoid NC cells contrasting with the mandibular NC cells, which still reside within

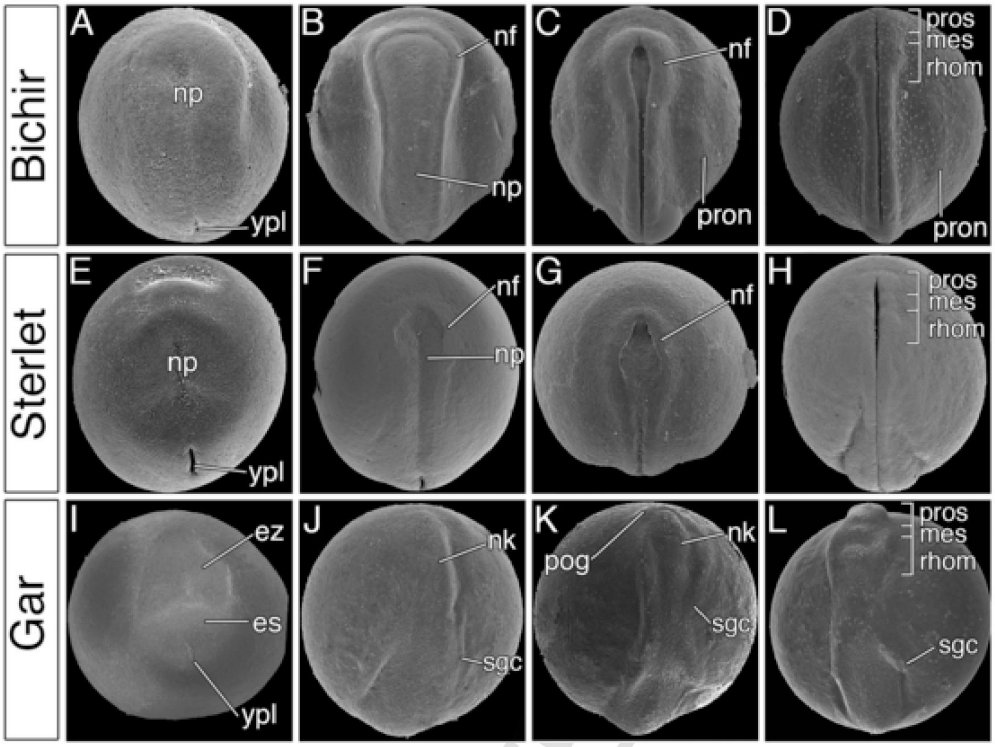

Fig. 1. *Transitional patterns in neurulation of non-teleost fishes.* (A–L) Whole mount dorsal view at neurulation in bichir (A–D), sterlet (E–H) and gar (I–L). es, embryonic shield; ez, evacuation zone; mes, mesencephalon; nf, neural fold; nk, neural keel; np, neural plate; pog, pre-oral gut; pron, pronephros; pros, prosencephalon; rhom, rhombencephalon; sgc, subgerminal cavity; ypl, yolk plug.

the neural plate border (Fig. 2P–R′). In pike, the first *Sox9* transcripts are detectable concomitantly in mandibular and hyoid CNC, but the expression is again more intense in the hyoid region (Fig. 2S). Transverse sections at this early stage show *Sox9* positive cells in the neuroepithelium of the neural plate border in the mandibular region, while sections of the hyoid region reveal strong expression in already migrating CNC cells (Fig. 2S-U′). At later stages of neurulation, CNC cells maintain strong *Sox9* expression particularly in the hyoid stream (Fig. 2V–X′).

This comparative analysis of spatiotemporal *Sox9* expression demonstrates that in bichir, gar, and pike, the hyoid CNC cells are uniquely accelerated in their migration compared to the mandibular CNC cells (cf. Fig. 2A-C'; P-R'; S–U′). In contrast, CNC cells in sterlet embryos follow the canonical sequential anteroposterior order in emigration (Fig. 2G-L′).

3.3. Cranial neural crest cells patterning and migration

Having established patterns of premigratory and migratory neural crest cells, we sought to examine spatiotemporal changes in the expression of Sox9 and other neural crest genes at multiple stages. To this end, we identified four critical stages of neural crest development: (i) specification, (ii) emigration, (iii) early phase and (iv) late phase of migration (Figs. 3–6). We examined the expression of several neural crest specifier genes: *Sox9*, *Sox10*, *FoxD3*, *Snail1/2* and *Twist1*, together with *Krox20*, a marker for rhombomeres 3 (r3) and 5 (r5) which separates individual neural crest streams (Figs. 3–6) (Wilkinson et al., 1989; Nieto et al., 1995; Sauka-Spengler and Bronner-Fraser, 2008; Simões-Costa and Bronner, 2015; Martik and Bronner, 2017). For better resolution, we also analyzed SOX9 protein expression in all examined species, from emigration through the late phase of migration (Fig. 7).

In bichir, *Sox9*, and *FoxD3* genes are the earliest neural crest specifier genes expressed in the presumptive mandibular and hyoid neural crest streams (Fig. 3I, Q) and their expressions persists through later stages (Fig. 3J-L, R). Although *Sox9* expression overlaps with that of *FoxD3* during early neurulation, the *FoxD3* signal is weaker than *Sox9* (cf. Fig. 3I and J and Fig. 3Q–R). During the emigration phase, in the mandibular region, Sox9 expression resolves into two distinct stripes corresponding to the presumptive subpopulations of the mandibular stream (Fig. 3J; Fig. 7A; Fig. S1). In more posterior regions of the developing head, *Sox9* is strongly expressed in the migrating cells of the hyoid CNC and is first seen in cells of the branchial streams (Fig. 3J; Fig. 7A). During the migratory phase, *Sox9* and *Snail1/2* expressions are predominantly located in the hyoid region (Fig. 3K, P). SOX9 immunostaining yielded similar results (Fig. 7B). A few *Snail1/2*-positive and SOX9-positive migratory mandibular CNC cells were also observed in close contact with the pre-oral gut (Fig. 3P; Fig. 7C), which represents the rostral-most endodermal head domain (Minarik et al., 2017).

In sterlet, we examined several neural crest genes such as *Sox9*, *Sox10*, *FoxD3*, and *Twist1* (Fig. 4). At the early neurula stage, while *Sox9* and *FoxD3* transcripts are detected in prospective mandibular and hyoid CNC cells, *Sox10* is detected only in mandibular CNC cells, and *Twist1* is not detected in CNC at this stage (Fig. 4I, M, Q, U). During emigration, *Sox9*/SOX9-positive and *FoxD3*-positive cells are observed in the emigrating CNC of the mandibular and hyoid streams (Fig. 4J, R; Fig. 7D), and expression can also be seen in newly emigrating branchial CNC posterior to r5 (cf. Fig. 4F and J, R). At this developmental stage, *Sox10* and *Twist1* transcripts are detectable only in the mandibular CNC (Fig. 4N, V). During early migration, mandibular CNC marked by *Sox9*, *Sox10*, *FoxD3*, *Twist1* and also by SOX9 antibody comprises the vast majority of neural crest cells in the developing head (Fig. 4K, O, S, W; Fig. 7E). Interestingly, our data show that the hy-

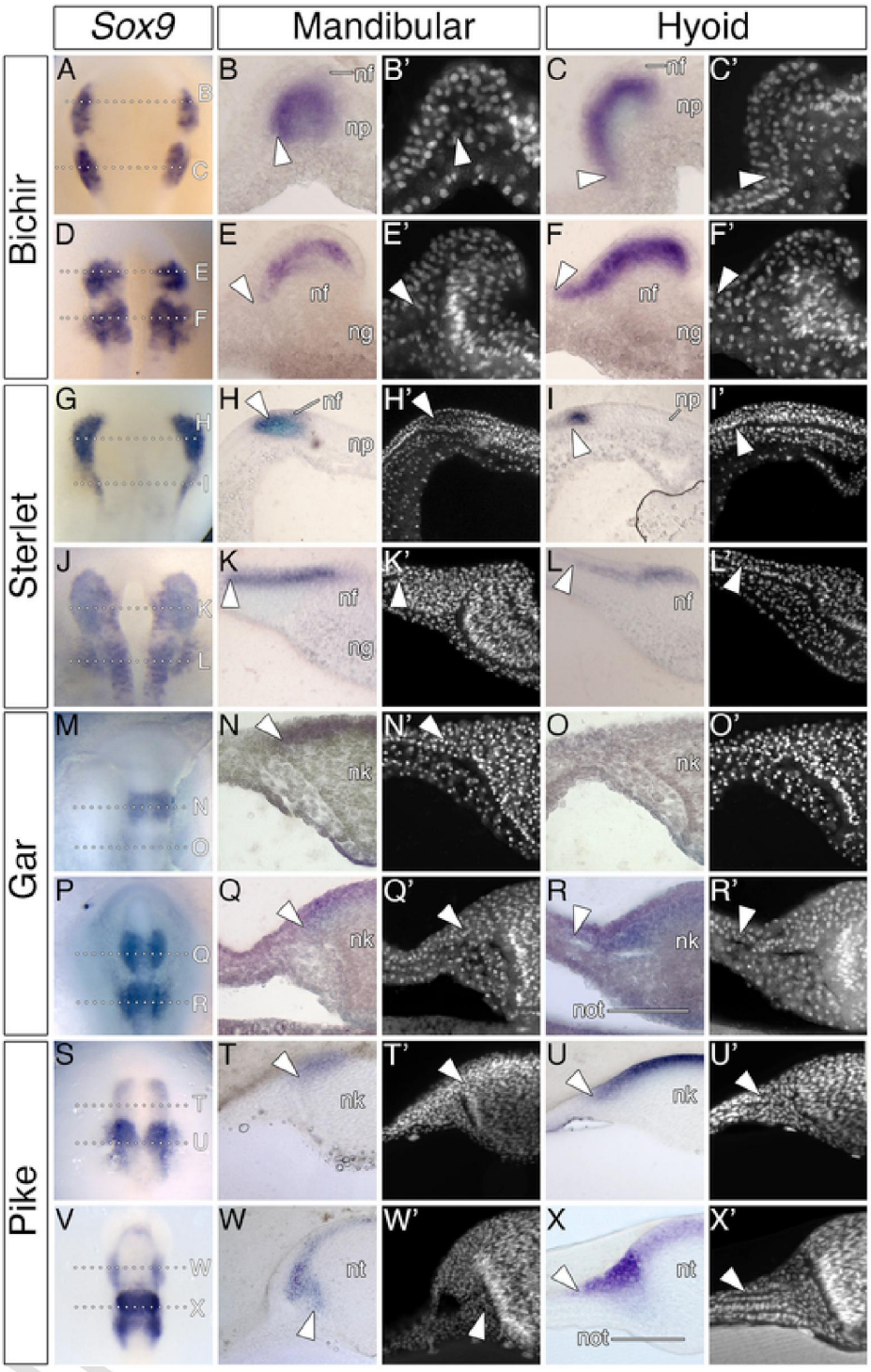

Fig. 2. *Accelerated emigration of CNC cells and heterochronic development of hyoid CNC cells. Sox9* expression demonstrates that in bichir (A–C), gar (P–R), and pike (S–U), the hyoid CNC cells are uniquely accelerated in their migration compared to the mandibular CNC cells. (A, D, G, J, M, P, S, V) Cranial expression of *Sox9* in CNC cells in bichir (A, D), sterlet (G, J), gar (M, P), and pike (S, V). White dotted lines indicate the section planes through the mandibular (B, E, H, K, N, Q, T, W) and hyoid domains (C, F, I, L, O, R, U, X), respectively. Identical sections stained with DAPI are marked by (′). White arrowheads mark the leading edge of the CNC streams. nf, neural fold; ng, neural groove; nk, neural keel; np, neural plate; not, notochord; nt, neural tube.

oid and branchial neural crest migrate as a single sheet of cells from the level of hindbrain into the presumptive pharyngeal region, thus forming a common 'hyobranchial sheet' (Fig. 4O, K, S; Fig. S2). We also observed distinct stripes of *Krox20* expression lateral to the neural tube at the level of r5, which co-localized with *Twist1* (Fig. 4G, W), corresponding to the cells of the cardiac neural crest (Odelin et al., 2018

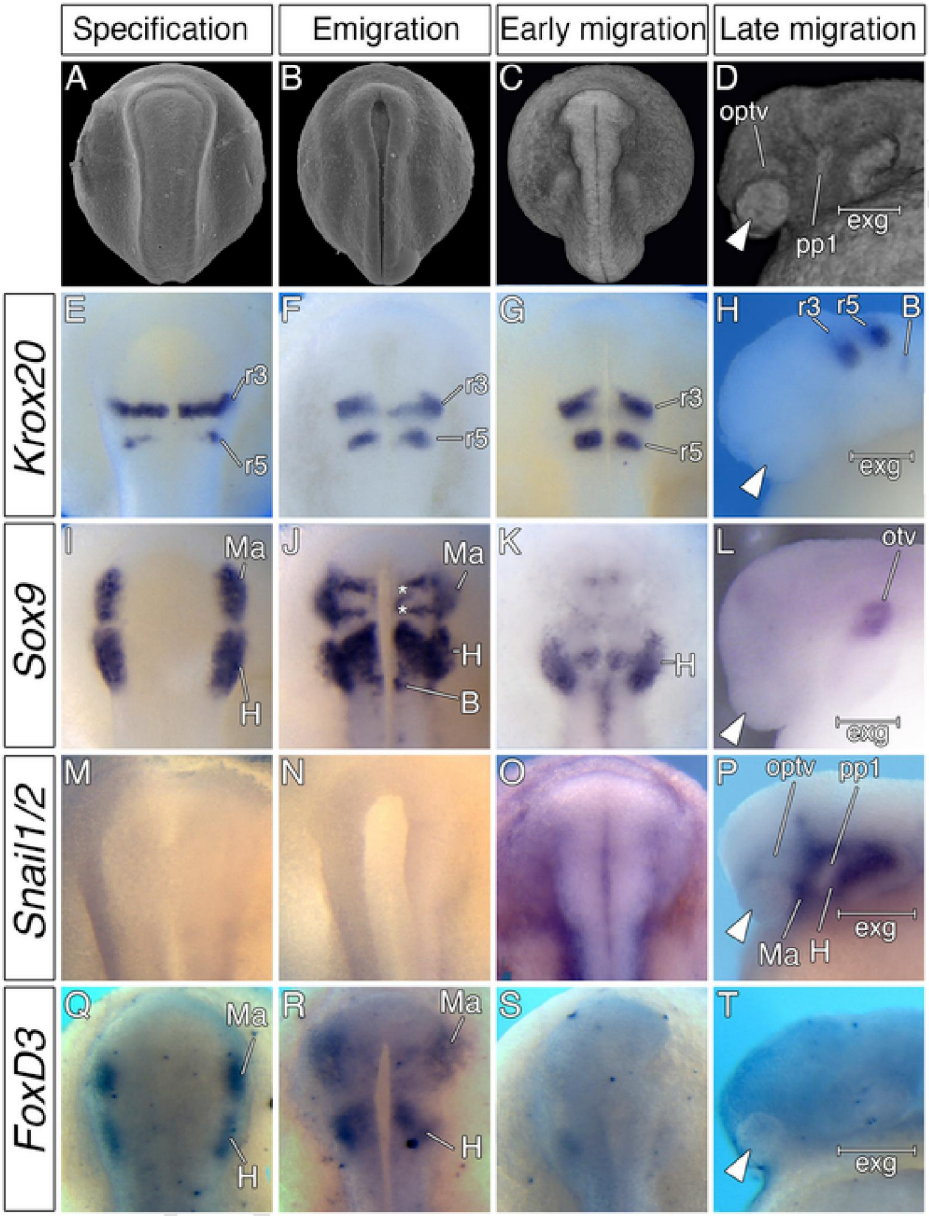

Fig. 3. *Expression summary of neural crest markers in CNC cells of the Senegal Bichir from the specification through the late phase of migration.* (A–D) SEM and micro-CT images showing dorsal (A–C) and lateral (D) views of CNC developmental stages. (E–H) *Krox20* expression showing position of rhombomere 3 and 5. Dorsal (I–K, M-O, Q-S) and lateral (L, P, T) views of embryos after in situ hybridization for cranial neural crest-specific transcription factors across developmental time-course. White arrowheads mark the pre-oral gut. Asterisks mark exit points of mandibular substreams. B, branchial NC stream; exg, external gill; H, hyoid NC stream; Ma, mandibular NC stream; optv, optic vesicle; otv, otic vesicle; pp1, spiraculum; r3, rhombomere 3; r5, rhombomere 5.

). Next, we examined the later phase of CNC cell migration. While *Sox9* and *Twist1* are expressed in the majority of CNC cells, *Sox10* and *FoxD3* transcripts are found in cells of the hyoid and branchial neural crest streams and in a small number of mandibular CNC cells (Fig. 4L, P, T, X). In the mandibular region, *Sox9* and *Twist1* were expressed in two distinct subpopulations, the mandibular and maxillary branches (Fig. 4L, X; Cerny et al., 2004a,b). Furthermore, our data show that cells of the mandibular neural crest stream migrate around the pre-oral gut, similar to that observed in bichir embryos (cf. Fig. 4K-L, O, W-X; Figs. 7F and 3P; Fig. 7C). At this stage, the hyobranchial sheet is completely divided into hyoid and branchial streams (cf. Fig. 4O, P and Fig. 7F).

At the beginning of gar neurulation, neural crest specifiers are first seen in cells of the prospective mandibular neural crest stream (Fig. 5I, M, Q). While *Sox9* is strongly expressed in CNC located in the dorsal and lateral part of the forming neural tube, *FoxD3* and *Sox10* are expressed in cells lateral to the neural tube (Fig. 5I, M, Q). In slightly older embryos during emigration, CNC cells marked by *Sox9*/SOX9, *FoxD3,* and *Sox10* can be seen in the mandibular and hyoid regions (Fig. 5J, N, R; Fig. 7G), but emerging CNC cells are detectable only in the hyoid region (see Fig. 2). During early migration, expression of *Sox9* and *Sox10* can be seen in freshly emigrating mandibular and migrating CNC cells (Fig. 5K, S). By immunostaining, we identified SOX9+ cells of the branchial neural crest stream (Fig. 7H). At late mi-

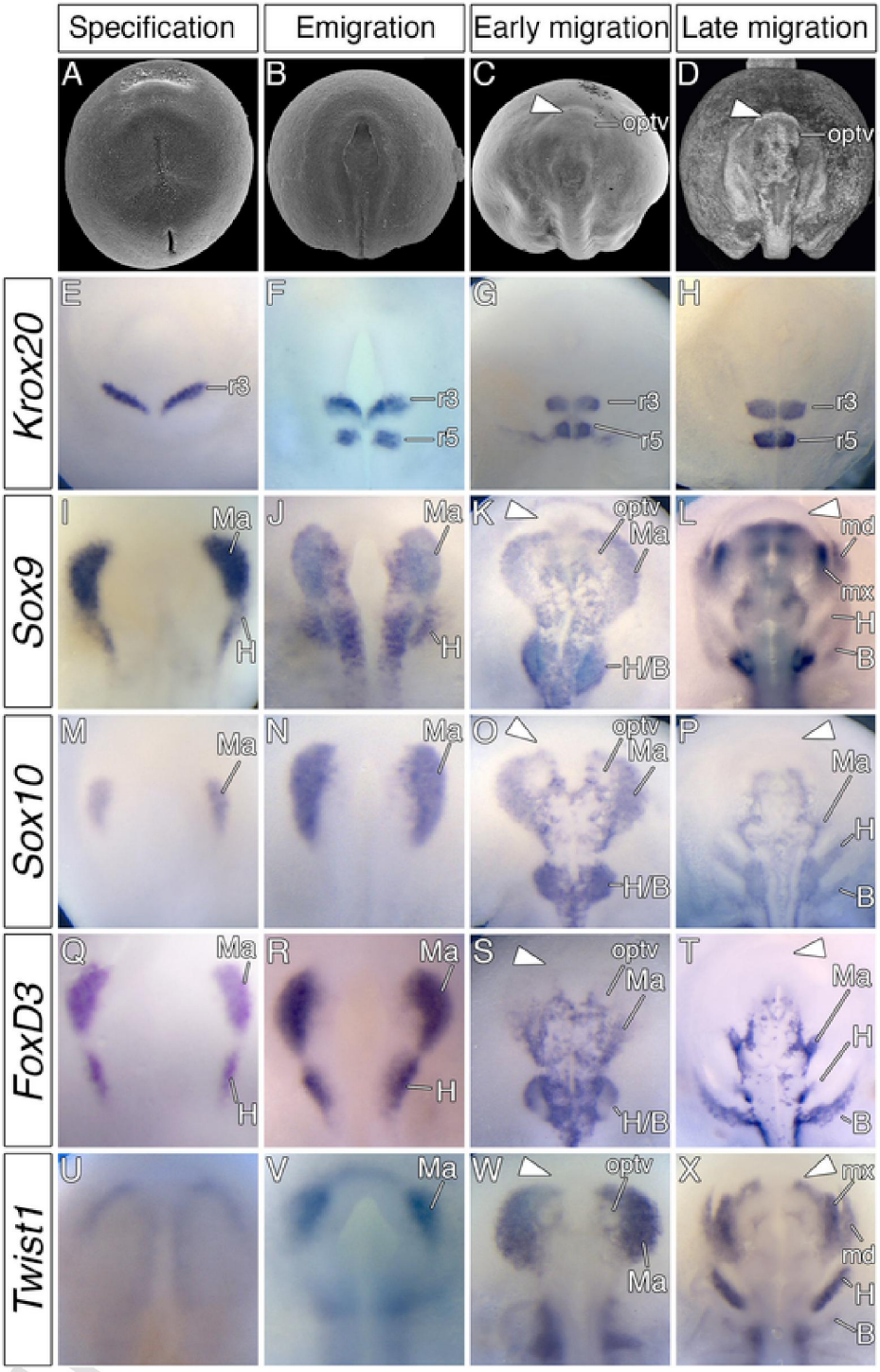

Fig. 4. *Expression summary of neural crest markers in CNC cells of the sterlet sturgeon from the specification through the late phase of migration.* (A–D) SEM and micro-CT images showing dorsal views (A–D) of CNC developmental stages. (E–H) *Krox20* expression showing position of rhombomere 3 and 5. (I–X) Dorsal views of embryos after in situ hybridization for cranial neural crest-specific transcription factors across developmental time-course. The morphology of the presented developmental stage precludes obtaining a clear lateral view. White arrowheads mark the pre-oral gut. B, branchial NC stream; H, hyoid NC stream; H/B, hyobranchial sheet; Ma, mandibular NC stream; md, mandibular substream of mandibular NC stream; mx, maxillary substream of mandibular NC stream; optv, optic vesicle; otv, otic vesicle; r3, rhombomere 3; r5, rhombomere 5.

gration, *Sox9* transcripts are detected throughout the otic vesicle (Fig. 5L), but the *FoxD3* signal is no longer detected at this stage (Fig. 5P). In gar, similar to sterlet embryos, *Krox20* expression is also detectable in cardiac neural crest cells (Fig. 5H). SOX9 immunostaining marks the whole CNC population at the late phase of migration, including two segregated branchial neural crest streams (Fig, 7I). Furthermore, *Sox10*

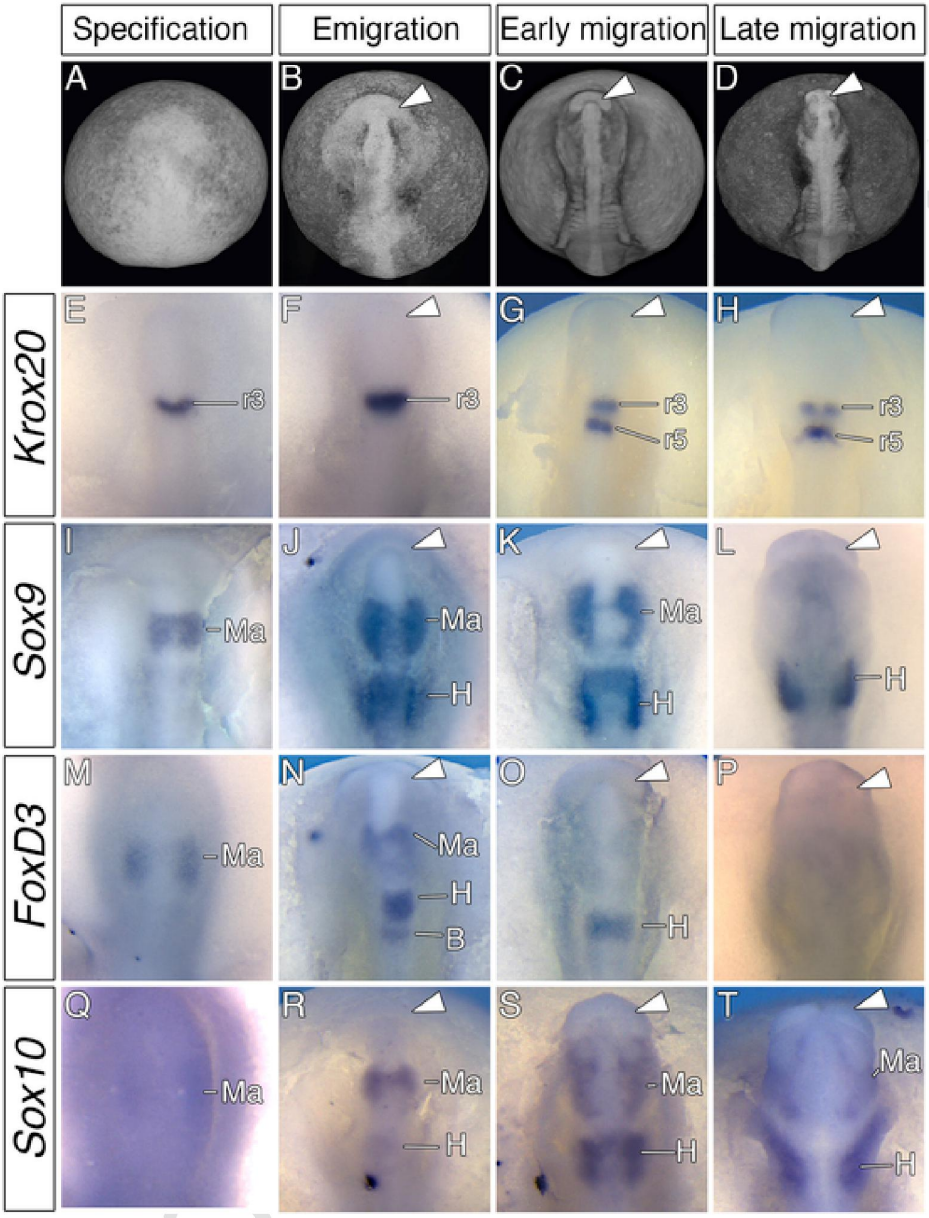

Fig. 5. *Expression summary of neural crest markers in CNC cells of the tropical gar from the specification through the late phase of migration.* (A–D) Micro-CT images showing dorsal views (A–D) of CNC developmental stages. (E–H) *Krox20* expression showing position of rhombomere 3 and 5. (I–T) Dorsal views of embryos after in situ hybridization for cranial neural crest-specific transcription factors across developmental time-course. White arrowheads mark the pre-oral gut. B, branchial NC stream; H, hyoid NC stream; Ma, mandibular NC stream; r3, rhombomere 3; r5, rhombomere 5.

expression is maintained in migrating mandibular and hyoid CNC cells (Fig. 5T). As in bichir and sterlet embryos, we also observed a similar migratory pattern of mandibular CNC cells migrating in close contact with the pre-oral gut in gar embryos (Fig. 5T; Fig. 7H and I).

Next, we characterized the expression of neural crest markers across developmental time-course in pike (Fig. 6A–D). During the specification stage, mandibular and hyoid CNC cells are marked by *Sox9* expression (Fig. 6I). A small number of *Sox9*-positive cells are located lateral to the forming neural tube, while a large number of *Sox9*/SOX9-positive cells are found in the dorsal neural tube spreading more into the hyoid region (Fig. 6I; Fig. 7J). At later developmental stages, *Sox9*/SOX9-positive cells are maintained in migratory mandibular and hyoid CNC cells and are detected for the first time in branchial neural crest (Fig. 6J; Fig. 7K). We also observed an overlap between *Sox10* and *FoxD3* expressions in CNC cells in the dorsal aspect of the neural tube (Fig. 6M, P). At the migratory phase, *Sox9, FoxD3,* and *Sox10* expression mark the maxillo-mandibular and preoptic subpopulation of the mandibular neural crest (Fig. 6K-L, N–O, Q-R). At this stage, distinct hyoid and branchial neural crest streams can be resolved (Fig. 6K-L, N–O, Q-R; Fig. 7L).

3.4. Accelerated hyoid neural crest stream is associated with different hyoid structures in different species

Previous observations reveal remarkably accelerated development of the hyoid neural crest in bichir, gar, and pike embryos (Fig. 8A–

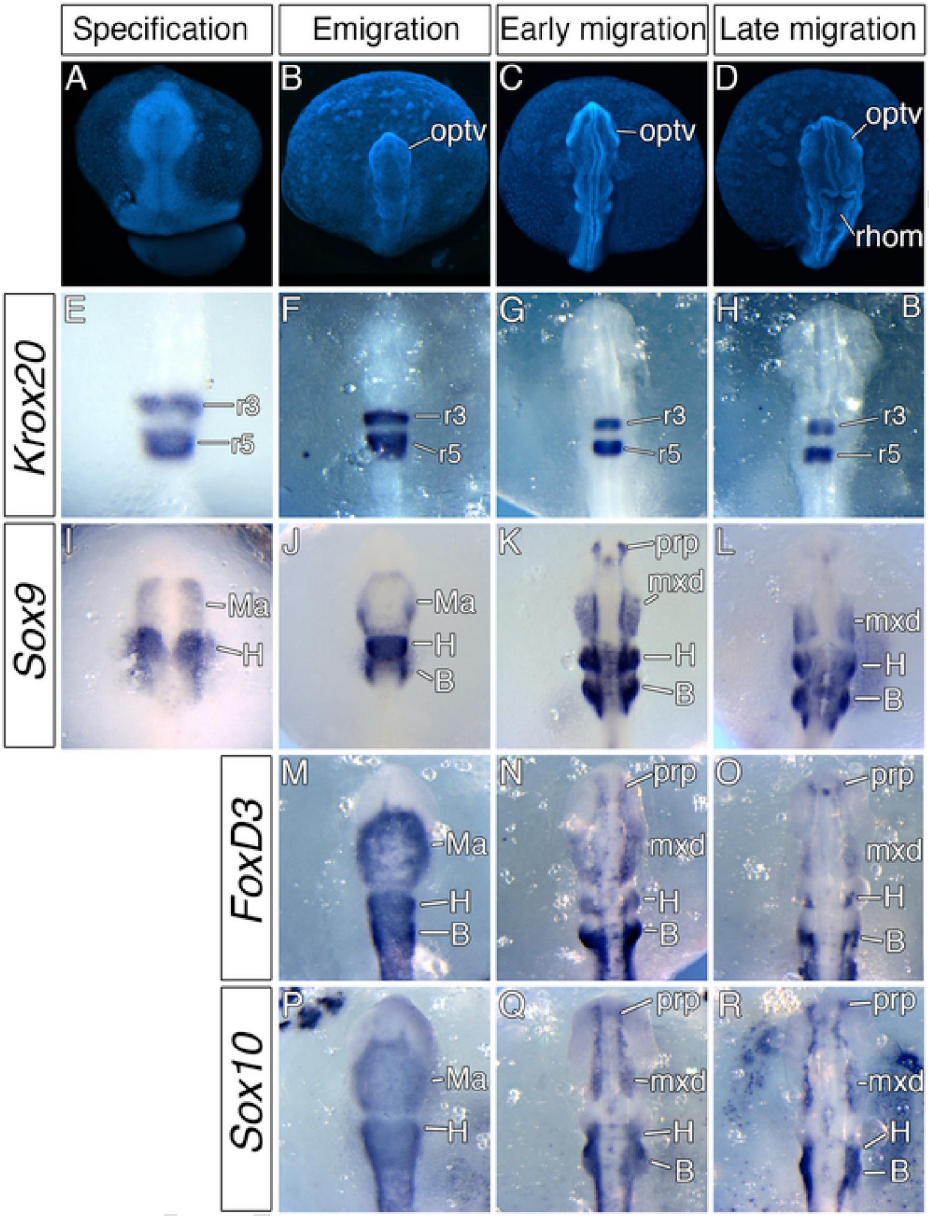

Fig. 6. *Expression summary of neural crest markers in CNC cells of the northern pike from the specification through the late phase of migration.* (A–D) DAPI staining showing dorsal views of CNC developmental stages. (E–H) *Krox20* expression showing position of rhombomere 3 and 5. (I–R) Dorsal views of embryos after in situ hybridization for cranial neural crest-specific transcription factors across developmental time-course. B, branchial NC stream; H, hyoid NC stream; Ma, mandibular NC stream; mxd, maxilo-mandibular subpopulation of mandibular NC stream; optv, optic vesicle; prp, pre-optic subpopulation of mandibular NC stream; r3, rhombomere 3; r5, rhombomere 5; rhom, rhombencephalon.

D, F–I, K–N). We thus asked if the accelerated formation of the hyoid neural crest is correlated with advanced morphogenesis of species-specific hyoid structures. To examine this possibility, we utilized *Hand2* expression, which marks the ventralmost CNC cells in the developing pharyngeal arches (Cerny et al., 2010; Compagnucci et al., 2013; Square et al., 2015) and thus reveals the first CNC cells populating the pharyngeal region. In bichir, the first *Hand2*-positive cells are observed in the developing hyoid external gills, which form prominent head larval structures (cf. Fig. 8D and E). Similarly, in gar embryos, *Hand2* expression is first detectable in the hyoid region (Fig. 8I), correlating with the early appearance of the opercular flap (cf. Fig. 8I and J). In pike, the first expression of *Hand2* can also be seen in the hyoid region (Fig. 8N); however, pike larvae do not develop any prominent hyoid structure similar to bichir and gar. We thus postulated that accelerated hyoid CNC development relates to precocious differentiation of neural crest-derived structures in pike larvae. Consistent with this, Alcian-blue staining revealed that the first detectable cartilaginous element in pike larvae is the hyosymplectic of the hyoid arch origin (Fig. 8O). Taken together, these data demonstrate that acceleration of the hyoid neural crest is associated with early formation of several key species-specific hyoid arch structures in bichir, gar, and pike embryos.

3.5. Sterlet cranial neural crest cells constitute a single hyobranchial sheet

In sterlet, our data revealed the presence of a common hyobranchial sheet of CNC cells (Fig. 4K, O, S; Fig. 7E and Fig. S2). In order

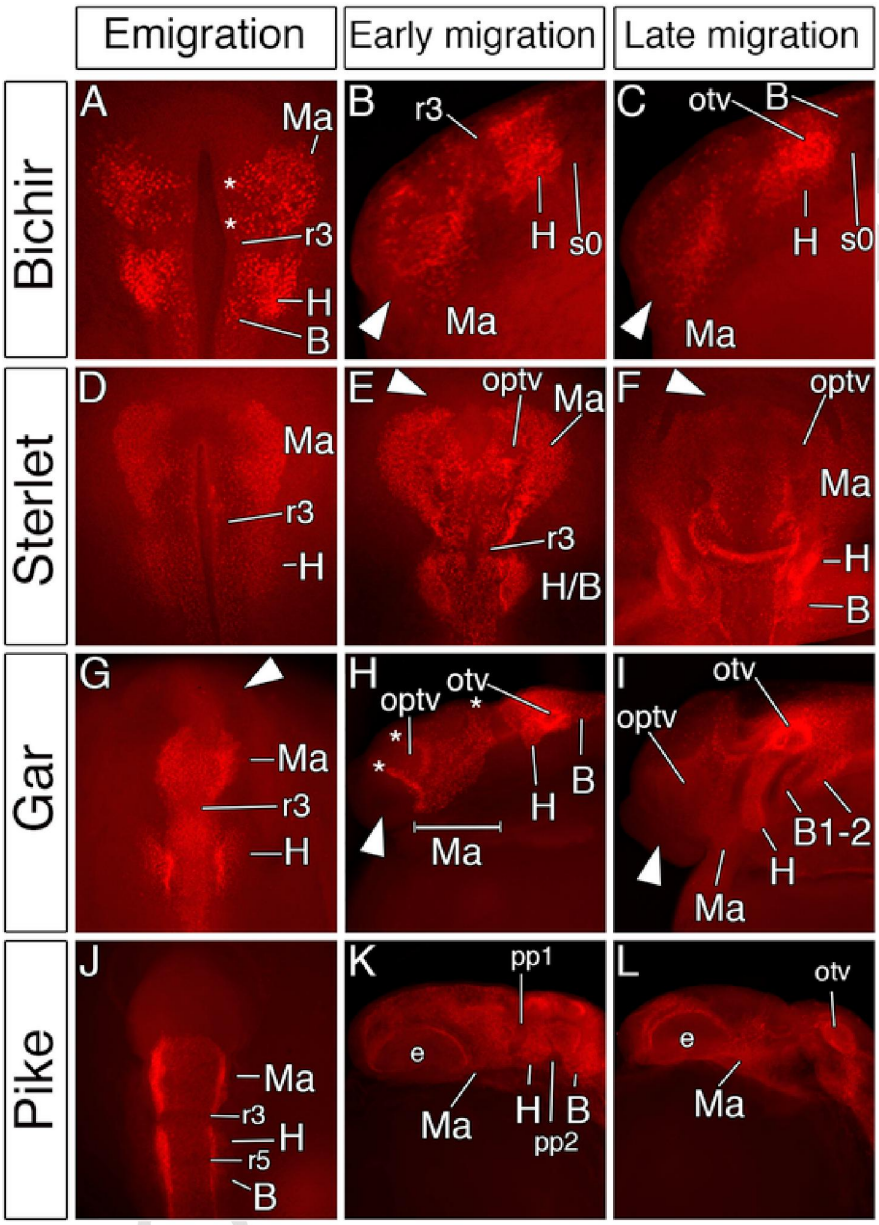

Fig. 7. *Comparison of SOX9 protein expression in CNC cells from the emigration through the late phase of migration.* Anti-SOX9 antibody visualizes individual neural crest cells of bichir (A–C), sterlet (D–F), gar (G–I), and pike (J–L). Dorsal (A, D-G, J) and lateral (B–C, H–I, K-L) views of cranial regions of examined embryos. White arrowheads mark the pre-oral gut and its derivatives. Asterisks mark exit points of mandibular substreams. B, branchial NC stream; e, eye primordium; H, hyoid NC stream; H/B, hyobranchial sheet; Ma, mandibular NC stream; optv, optic vesicle; otv, otic vesicle; pp1-2, pharyngeal pouch 1–2; r3, rhombomere 3; r5, rhombomere 5; s0, somite 0.

to complement our gene expression data with experimental lineage analysis, we took advantage of the accessibility of sterlet embryos and directly tested the exit points and migratory patterns of CNC streams using direct cell labeling with a lipophilic dye. To this end, we microinjected CM-DiI (Fig. 9) into the dorsal midline of the neural folds at selected levels along the anteroposterior axis (Fig. 9A; mandibular: 10/10, hyoid: 13/15). Sterlet embryos were then allowed to develop to stages when CNC cells begin to form migrating streams (Fig. 9A, E, I). We first performed focal microinjection of CM-DiI into the prospective mandibular CNC anterior to rhombomere 3 (cf. Figs. 9B and 4F); the results confirmed the migratory pattern we previously inferred using neural crest markers (cf. Figs. 9C and 4; Fig. 7; Fig. S2). At later developmental stages, CM-DiI-positive cells are detected throughout the anterior head and in the presumptive jaws (Fig. 9D and E). Next, we tested whether the hyobranchial sheet emerges from a single exit point. We performed CM-DiI microinjection into the presumptive hyobranchial neural crest population at the dorsal midline of the neural fold (cf. Fig. 9A, F and Fig, 4 F, J, R). Consistent with our previous gene expression analyses, the fate-mapping experiment corroborated the presence of a single hyobranchial sheet (Fig. 4K, O, S and Fig. 7E), with CM-DiI-positive cells later contributing to cells of both the hyoid and branchial streams (Fig. 9A, G-I). We next sought to determine the time point at which the hyobranchial sheet separates into the individual hyoid and branchial neural crest streams. Comparison of SOX9 antibody staining (Fig. 10A, D), micro-CT reconstruction of the endodermal epithelium (Fig. 10B, E) and transverse histological sections (

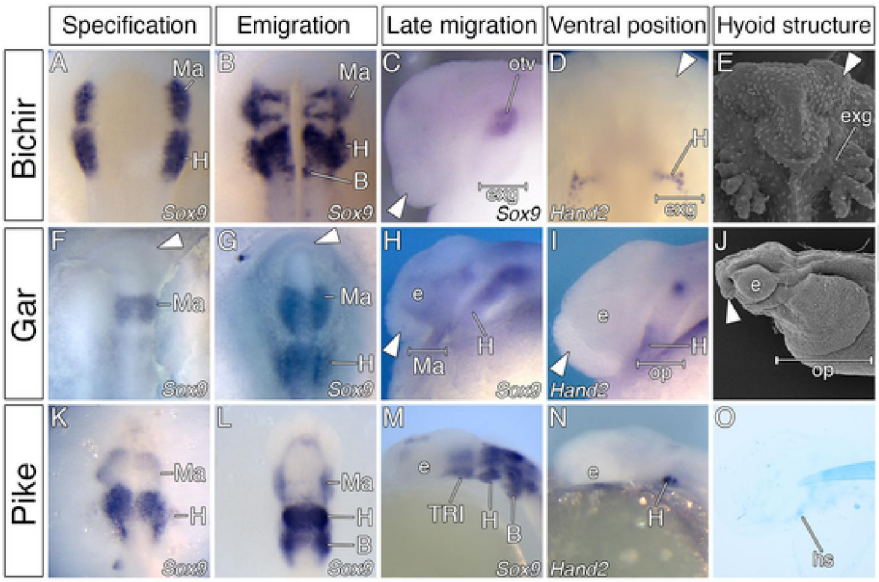

Fig. 8. *Accelerated hyoid neural crest stream is associated with development of hyoid species-specific structures. Sox9* (A-C, F-G, K-M) and *Sox10* (H) expressions in CNC cells reveal accelerated emigration of the hyoid NC stream in bichir (A), gar (F), and pike (K). Dorsal (A-B, F-G, K-L) and lateral (C, H, M) views of cranial region of examined embryos. (D, I, N) *Hand2* expression reveals first CNC cells populating the pharyngeal region. Dorsal (D) and lateral (I, N) views of cranial region of examined embryos. (E, J, O) Accelerated development of the hyoid stream of NC cells is associated with morphogenesis of key hyoid structure like external gills of bichir (E), large opercular flap of gar (J), and first forming cartilage in pike larvae (O). White arrowheads mark the pre-oral gut and its derivatives. B, branchial NC stream; e, eye primordium; exg, external gill; H, hyoid NC stream; hs, hyosymplectic; Ma, mandibular NC stream; op, opercular flap; otv, otic vesicle.

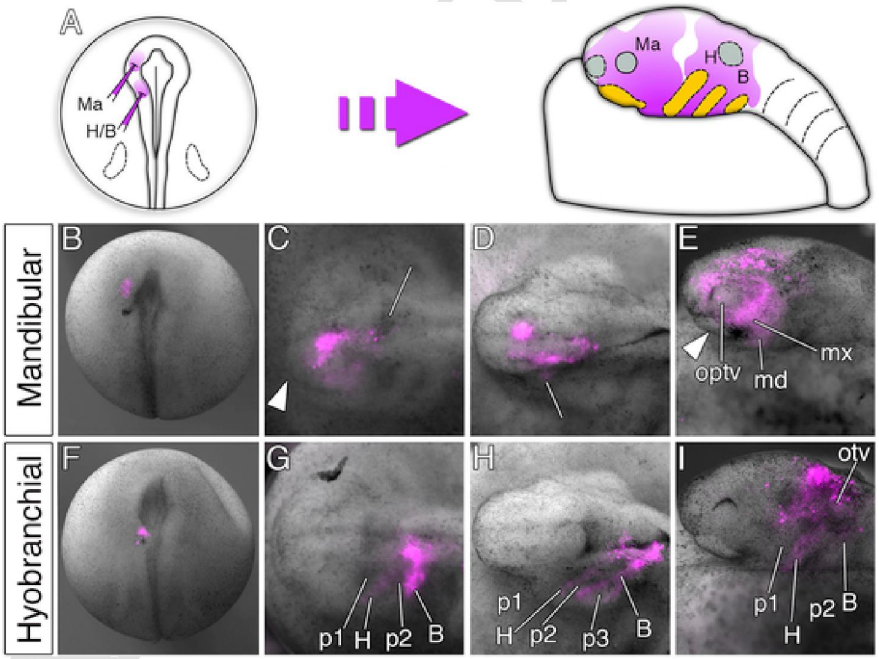

Fig. 9. *CM-DiI fate-mapping reveals contribution of hyobranchial sheet cells into hyoid and branchial streams in the sterlet sturgeon.* (A) Scheme of CM-DiI microinjection into mandibular (Ma) and hyobranchial (H/B) CNC exit points and contribution of each CNC subpopulation into the developing head. (B, F) Dorsal views of embryos at the time of injection. (C–E) Mandibular and hyobranchial (G–I) neural crest fate mapping (CM-DiI magenta). Superimposed fluorescent and dark-field images at successive stages of development. (C, D, G, H) Dorsal and lateral (E, I) views, anterior to the left. White arrowheads mark the pre-oral gut and its derivatives. B, branchial NC stream; H, hyoid NC stream; H/B, hyobranchial sheet; Ma, mandibular NC stream; mx + md, maxillo-mandibular subpopulation of mandibular NC stream; optv, optic vesicle; otv, otic vesicle; p1-3, pharyngeal pouch 1–3; IV., fourth brain cavity.

Fig. 10C, F) reveals that the separation of the hyobranchial sheet is tightly associated developmentally with morphogenesis of the second (hyo-branchial) pharyngeal pouch (Fig. 10B–C, E-F).

4. Discussion

In the present study, we analyzed the patterning and migration of cranial neural crest cells in the Senegal Bichir (Cladistia), the sterlet sturgeon (Chondrostei), the tropical gar (Holostei) and the north-

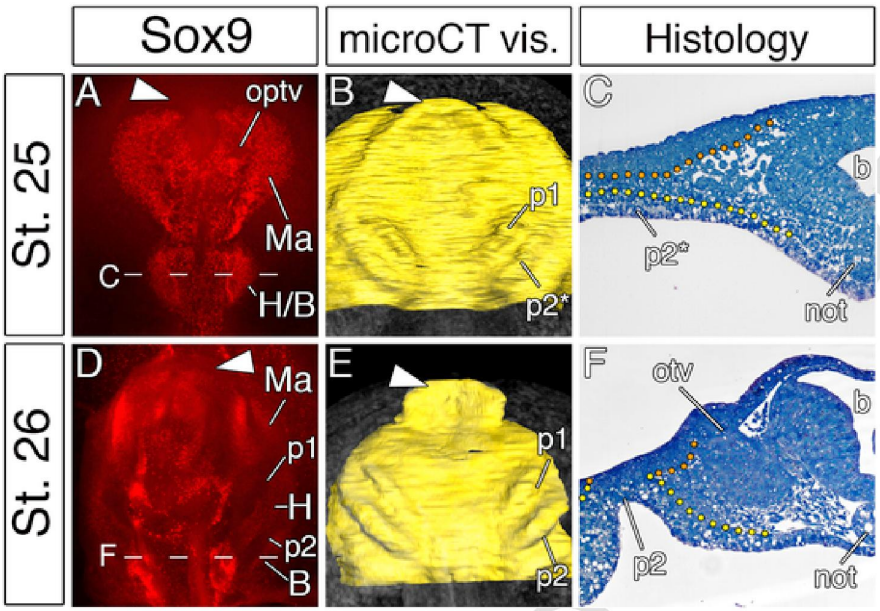

Fig. 10. *The separation of a single hyobranchial sheet in the sterlet sturgeon is associated with the formation of a second pharyngeal pouch.* (A, D) SOX9 protein expression in CNC cells of sterlet. Dashed lines indicate the plane of sections shown in panel C and F. (B, E) 3D reconstruction of pharyngeal endoderm (yellow). (C, F) Transverse section at the level of the hyobranchial sheet. Dotted lines mark the position of ectoderm (orange) and endoderm (yellow). White arrowheads mark the pre-oral gut. Asterisk marks a not well-developed second pharyngeal pouch. b, brain primordium; B, branchial NC stream; H, hyoid NC stream; H/B, hyobranchial sheet; Ma, mandibular NC stream; not, notochord; optv, optic vesicle; otv, vesicle; p1-2, pharyngeal pouch 1–2. (For interpretation of the references to colour in this figure legend, the reader is referred to the Web version of this article.)

ern pike (Teleostei). These species are representatives of all recent phylogenetic lineages of ray-finned fishes that together exemplify about half of extant vertebrates (Betancur-R et al., 2017; Hughes et al., 2018). While patterns of CNC migration are often assumed to be highly stereotypic across vertebrates (Minoux and Rijli, 2010; Theveneau and Mayor, 2012; Falck et al., 2002), our study reveals significant modifications in the canonical pattern of migration in ray-finned fishes (Fig. 11). This raises the interesting possibility that CNC migratory patterns may be much more variable than commonly assumed from studies of a small number of model organisms, further highlighting the importance of comparative analyses.

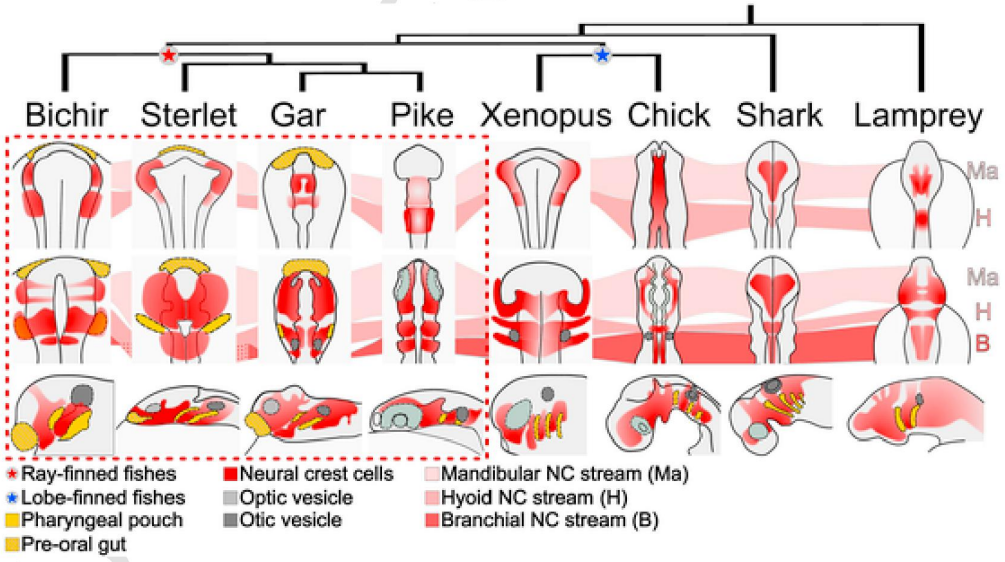

Fig. 11. *Ray-finned fishes reveal significant modification in the canonical pattern of CNC migration of vertebrates.* A cartoon of CNC migration and patterning (red) in representatives of all phylogenetic lineages of ray-finned fishes (bichir - Cladistia, sterlet - Chondrostei, gar - Holostei, and pike - Teleosts) (red star), in typical model systems of lobe-finned fishes (chick and xenopus) (blue star) and in shark and lamprey as outgroups. Notice that emigration of the hyoid CNC stream (H) is remarkably accelerated in bichir, gar and pike and further that sterlet CNC cells constitute a single hyobranchial sheet. The top two lines demonstrate the dorsal view and the bottom line the lateral view. The shades of red in the first two lines represent the individual mandibular (Ma; light red), hyoid (H; intermediate red), and branchial (B; dark red) NC streams. Yellow indicates the pharyngeal endoderm and its derivative, pre-oral gut (yellow-grey stripes). Light and dark grey indicates optic and otic vesicles. The dotted square defines the examined fish species. The drawings are adapted from several published studies (Ballard et al., 1993; Kuratani and Horigome, 2000; Theveneau and Mayor, 2012; Martik et al., 2019). (For interpretation of the references to colour in this figure legend, the reader is referred to the Web version of this article.)

4.1. Transitional patterns of neurulation

Our examined fish species provide powerful model systems for the study of evolution of neurulation in vertebrates as these embryos utilize modes of neurulation ranging from primary neurulation to neurulation via cavitation (Fig. 1), consistent with an evolutionary transition in this critical developmental process. Our data reveal that bichir embryos undergo primary neurulation when the entire morphogenetic process occurs above the yolk ball, which is apparently similar to the neurulation of salamanders and some frogs (cf. Fig. 1A–D and Schreckenberg and Jacobson, 1975; Eagleson, 1996; Del Pino et al., 2004; Mitgutsch et al., 2009). Therefore, the presence of primary neurulation in bichir may reflect another character shared with lobe-finned fishes. As in bichir, sterlet embryos undergo primary neurulation via rolling up of the neural folds (cf. Fig. 1A–D and Fig. 1E–H). However, the entire morphogenetic process in sterlet takes place within the yolk ball, apparently similar to the neurulation of direct-developing frogs (Olsson et al., 2002). In contrast, gar embryos undergo neurulation via formation of a neural keel, which is characteristic for all teleosts including pike (cf. Fig. 1I-L and Schmitz et al., 1993; Lowery and Sive, 2004; Pospisilova et al., 2019; Rocha et al., 2019). We next asked when CNC cells begin their migration. Our spatiotemporal analysis of neural crest markers reveals that CNC cells of all examined fish species initiate emigration during early neurulation (cf. Figs. 1 and 2), similar to that described in frogs (Mitgutsch et al., 2008) and mammals (Tan and Morriss-Kay, 1986; Smith, 2001) but contrasting with that of most vertebrates, which typically initiate migration after neural tube closure (Noden, 1988; Horigome et al., 1999; Falck et al., 2002; Diaz et al., 2019). Although neural crest development is tightly connected to morphogenesis of neurulation, our data suggest that the type of neurulation has little or no influence on CNC migratory patterns.

4.2. Accelerated hyoid neural crest stream is associated with different hyoid structures in different species

In all vertebrates, cranial neural crest cells migrate in three distinct streams, termed mandibular, hyoid and branchial, that emerge from consecutive positions along the anteroposterior axis (Minoux and Rijli, 2010; Theveneau and Mayor, 2012; Square et al., 2017). While this migratory pattern has been assumed to be stereotypic, our results clearly demonstrate heterochrony in the overall acceleration of the second, hyoid CNC stream. Specifically, in bichir, gar, and pike embryos, cells of the hyoid stream migrate before cells of the first, mandibular stream (Fig. 2A–C, P-R, S–U). In vertebrates, the hyoid stream is usually smaller in size and range compared to the mandibular stream, which occupies the entire rostral head (Couly et al., 1993; Creuzet et al., 2002; Santagati and Rijli, 2003; Piekarski et al., 2014). However, in bichir, our gene expression data suggest that the hyoid CNC constitutes the most prominent neural crest population in the developing head (Fig. 3J and K; Fig. 7A–C) and is the first to reach ventral-most positions in the developing pharyngeal region and the external gills, respectively (Fig. 8A–E). These data further corroborate our previous report (Stundl et al., 2019), showing that accelerated development of the entire hyoid arch segment also involves mesodermal and endodermal tissues, which together promote advanced morphogenesis of the external gills, forming a crucial structure of bichir embryos and larvae (Kerr, 1907, 1919).

Like bichir, gar embryos exhibit prominent heterochrony in the hyoid stream (Fig. 2P–R). While the gar hyoid stream initiates migration first, it does not form the dominant stream. Nevertheless, hyoid CNC cells are the first to reach ventral positions in the developing oropharynx and in the prominent opercular flap, respectively (Fig. 8I). The accelerated hyoid stream thus seems to be developmentally associated with the morphogenesis of large opercular flap (Fig. 8J), which forms a key supplemental respiratory organ in gar larvae (Agassiz, 1878; Balfour and Parker, 1882). We next asked whether, in gar embryos, the development of endoderm and mesoderm is accelerated similar as previously observed in bichir (Stundl et al., 2019). Interestingly, we found that the hyoid pharyngeal endoderm expands laterally, and later contributes to a massive opercular flap of gar embryos (Fig. S3; Minarik et al., 2017). Moreover, the hyoid mesoderm seems to be accelerated as well, as the hyomandibularis muscle is among the first cranial muscles forming in gar (Konstantidinis et al., 2015). Thus, in gar embryos similar to bichir, advanced development of the entire hyoid domain, comprising neural crest, mesoderm, and endoderm, is found to be the case. This apparently is associated with the morphogenesis of a large opercular flap constituting a key secondary breathing structure in gar (Fig. 8J). Interestingly, gar exhibits very similar embryogenesis to the bowfin, and both these representatives of the phylogenetic group Holostei also possess prominent opercular flap with probably the same key influence for their larvae (Dean, 1895; Ballard, 1986; Long and Ballard, 2001; Jaroszewska and Dabrowski, 2009). We thus speculate that bowfin may have a similar accelerated hyoid neural crest stream serving the same function as in gar embryos.

Pike belongs to teleost fishes that represent the vast majority of extant ray-finned fish species. Embryonic development of pike is very similar to other teleosts (Pospisilova et al., 2019), including model organisms like zebrafish or medaka (Kimmel et al., 1995; Iwamatsu, 2004). Despite the high similarity of the early development of pike and other teleosts, our data show that the hyoid CNC stream in pike embryos initiates migration much earlier than the mandibular neural crest stream (Fig. 2S-U) and is the first stream to reach the ventral part of the oropharyngeal region as in bichir and gar (Fig. 8N). We speculate that this advanced development of the hyoid CNC may be associated with a unique early chondrogenesis of the hyosymplectic cartilage in pike (Fig. 8O; Pospisilova et al., 2019) which forms an essential component of jaw attachment in ray-finned fishes (Richter and Underwood, 2018). Only in the whiting (*Merlangius merlangus* Linnaeus, 1758) has a similar process of advanced chondrogenesis been described (de Beer, 1937). Furthermore, gar seems to exhibit the same pattern as well (data not shown). However, this sequence of chondrogenesis might be more common among ray-finned fishes since most studies do not provide enough details on early chondrogenesis (Vandewalle et al., 1999; Borisov et al., 2012). Given that acceleration of the hyoid CNC was observed in representatives of two of three phylogenetic lineages of non-teleost fishes as well as in a representative of teleosts, it is tempting to speculate that such heterochrony in the hyoid CNC represents an ancient common character for all ray-finned fishes.

4.3. Sterlet cranial neural crest cells constitute a single hyobranchial sheet

In contrast to bichir, gar and pike, the hyoid neural crest of sterlet is not accelerated but does display unique morphogenesis in which the hyoid and branchial CNC cells are fused into a single 'hyobranchial sheet' (Fig. 4K, O, S; Fig. 7E and Fig. S2). This subpopulation becomes separated into individual streams only later in concert with second pharyngeal pouch morphogenesis (Fig. 10A–F), similar to the segregation of other migratory neural crest streams (Grevellec and Tucker, 2010). Whereas in most vertebrates, the otic capsule physically separates the hyoid and branchial neural crest streams, the formation of the otic capsule seems delayed in sterlet embryos (Fig. 10C, F). Therefore, the hyoid and branchial CNC of sterlet are initially unsegmented and migrate into the presumptive pharyngeal region in a sheet-like fashion, analogous to the common branchial stream of lamprey embryos (McCauley and Bronner-Fraser, 2003; Square et al., 2017). Possible evolutionary implications of this variation in the mi-

gratory pattern in sterlet are unclear, but it further supports the importance of pharyngeal endoderm morphogenesis for the segregation of CNC streams (Piotrowski and Nüsslein-Volhard, 2000; McCauley and Bronner-Fraser, 2003; Cerny et al., 2004a,b).

4.4. Unique pattern of cranial neural crest migration among vertebrates

While dogma has it that CNC migration patterns are highly conserved across vertebrates, our data show a clear departure from this concept. While there are clearly three topographically conserved streams among all vertebrates (Fig. 11; Falck et al., 2002; Cerny et al., 2004a,b; Square et al., 2017), we show that there is heterochrony of the hyoid CNC stream associated with early morphogenesis of key hyoid structures like external gills (bichir), large opercular flap (gar), or first forming cartilage (pike) essential for the hyostylic jaw suspension. However, this hyoid heterochrony has not yet been observed in fish model organisms such as zebrafish or medaka (Schilling and Kimmel, 1994; Stewart et al., 2006; Nagao et al., 2018; Rocha et al., 2019). This raises the question of what represents the ancestral state: do the observed heterochronic alterations in CNC migratory patterns represent an ancestral state of ray-finned fish development? or even an ancestral state of gnathostome development? One possibility is that this heterochrony exists in model fish but has been missed due to their rapid development. For example, twist1a expression is present in the premigratory CNC cells at the 2-somite stage of zebrafish, and the locations of twist1a-positive cells may well correspond to the hyoid region (Yeo et al., 2009) or may represent a posterior part of the mandibular CNC stream. Given the accelerated hyoid CNC stream found in all fish species in the present study (except the sterlet) and presumably in other teleost fishes, it seems likely that the heterochrony of hyoid CNC might represent an ancient plesiomorphic character of all ray-finned fishes (Fig. 11). Thus, the question is whether we can find similar heterochrony of the hyoid CNC associated with the development of specific hyoid structures in the other gnathostomes. Interestingly, the hyostylic jaw suspension is also characteristic for cartilaginous fishes. Based on published data, it appears that they do not possess heterochrony in hyoid CNC (Kuratani et al., 2000; Compagnucci et al., 2013; Johanson et al., 2015; Gillis et al., 2017; Martik et al., 2019). However, this may be due to little-studied embryonic development of different groups of cartilaginous fishes and a lack of focus on the details of CNC migration. Nevertheless, it is possible to reveal the developmental potential of the hyoid domain for the morphogenesis of the respiratory structure in the chimera, where gill filaments and especially opercular flap form on the outside of the hyoid arch (Didier et al., 1998; Barske et al., 2020) and thus could perform the same function as the gar opercular flap. This hyoid opercular flap remains in early embryogenesis of amniotes (Richardson et al., 2012), suggesting that it was present in the common ancestor. It remains to be determined whether these hyoid structures are also developmentally associated with the modifications of the hyoid CNC. In contrast, in sterlet, we identified the hyoid and branchial CNC are initially unsegmented and constitute a single hyobranchial sheet which migrates in a sheet-like fashion. This appears to be analogous to the migration of a common branchial CNC stream of lamprey emerging from a broad domain from 5th to 7th rhombomeres and part of the spinal cord (Kuratani et al., 1998; Square et al., 2017). These CNC sheets become segregated in concert with pharyngeal pouch morphogenesis in both sterlet and lamprey. The question arises as to whether a sister species of sturgeon, the paddlefish, has a similar pattern of CNC migration, which could indicate whether it is a common feature of Chondrosteans (Acipenseriformes) or not (Inoue et al., 2003; Near et al., 2012), but cannot be answered without a more in-depth analysis of CNC migration (Bemis and Grande, 1992). Interestingly, a similar constitution unsegmented hyoid and branchial CNC streams can be found in several species of frogs at early neurula stages (Olsson and Hanken, 1996; Del Pino and Medina, 1998; Mitgutsch et al., 2008, 2009) but the subsequent division of this CNC subpopulation does not appear to be influenced by the morphogenesis of hyo-branchial pharyngeal pouch as in sterlet. In the future work, it would be interesting to analyze receptor-ligand pairs (e.g., eph/ephrins or neuropillins/semaphorins) which may be important for the separating neural crest streams, and the establishment of intervening "neural crest free" zones.

5. Conclusions

In conclusion, we have performed a comparative analysis of cranial neural crest migration and patterning in representatives of all phylogenetic lineages of ray-finned fishes (bichir - Cladistia, sterlet - Chondrostei, gar - Holostei, and pike - Teleosts) (Fig. 11). Embryos of ray-finned fishes reveal several important variations in the migratory pattern of CNC cells that previously were assumed to be highly stereotypic and conserved in vertebrates. Accelerated development of the hyoid stream of neural crest cells was identified in bichir, gar and pike embryos, always associated with prominent morphogenesis of important species-specific structures of the hyoid arch origin. A single hyobranchial sheet of CNC cells was identified in sterlet embryos, where separate hyoid and branchial streams form only later following prospective morphogenesis of the hyo-branchial pharyngeal pouch. Together, our results reveal unexpected variability in the timing and sequence of CNC emergence and subsequent migratory patterns in several ray-finned species. Our findings thus suggest that vertebrate craniofacial diversity may be associated with heterochronic and heterotopic alterations in migratory patterns of CNC cells as a prime mode of producing varied craniofacial phenotypes.

Acknowledgements

We thank Vojtěch Miller and Karel Kodejš for the bichir colony care and logistic support; Roman Franěk, Michaela Fučíková, David Gela, Martin Kahanec and Marek Rodina for the sterlet spawns; Lenin Arias-Rodriguez and Adriana Osorio-Pérez for the gar spawns; Radek Holcman for the northern pike spawns; Peter Fabian, Martin Minařík and Brian D. Metscher for technical assistance; David Jandzik for the generous gift of primer sequences of Hand2_Ps; Vladimir Soukup and Jana Štundlová for critical reading of the manuscript. Special thanks are due to Radek Šanda for the support and continuous interest in our work. This study was supported by the European Union's Horizon 2020 research and innovation program under the Marie Skłodowska-Curie grant agreement No. 897949 (to JS), the Charles University grant GAUK 1448514 (to JS), NIH R35NS111564 (to MEB), the Czech Science Foundation GACR 19-18634S (to RC), and the Ministry of Education, Youth and Sports of the Czech Republic—project CENAKVA LM2018099 and Biodiversity CZ.02.1.01/0.0/0.0/16_025/0007370) (to MP).

Appendix A. Supplementary data

Supplementary data to this article can be found online at https://doi.org/10.1016/j.ydbio.2020.08.007.

Uncited reference

Konstantinidis et al., 2015.

References

Agassiz, A, 1878. The development of lepidosteus . Part I. Proc. Am. Acad. Arts Sci. 14, 65–76. doi:10.2307/25138527.

Baker, C V H, Bronner-Fraser, M, 1997. The origins of the neural crest. Part I: embryonic induction. Mech. Dev. 69, 3–11. doi:10.1016/S0925-4773(97)00132-9.
Balfour, F M, Parker, W N, 1882. VII. On the structure and development of Lepidosteus. Philos. Trans. R. Soc. B Biol. Sci. 173, 359–442. doi:10.1098/rstl.1882.0008.
Ballard, W W, 1986. Stages and rates of normal development in the holostean Fish, Amia calva. J. Exp. Zool. 238, 337–354. doi:10.1002/jez.1402380308.
Ballard, W W, Mellinger, J, Lechenault, H, 1993. A series of normal stages for development of Scyliorhinus canicula , the lesser spotted dogfish (chondrichthyes: scyliorhinidae). J. Exp. Zool. 267, 318–336. doi:10.1002/jez.1402670309.
Barske, L, Fabian, P, Hirschberger, C, Jandzik, D, Square, T, Xu, P, Nelson, N, Yu, H V, Medeiros, D M, Gillis, J A, Crump, J G, 2020. Evolution of vertebrate gill covers via shifts in an ancient Pou3f3 enhancer lindsey barske. bioRxiv 1–36. doi:10.1101/2020.01.27.918193.
Basch, M L, Bronner-Fraser, M, García-Castro, M I, 2006. Specification of the neural crest occurs during gastrulation and requires Pax 7. Nature 441, 1–5. doi:10.1038/nature04684.
Bemis, W E, Grande, L, 1992. Early development of the actinopterygian head. I. External development and staging of the paddlefish Polyodon spathula. J. Morphol. 213, 47–83. doi:10.1002/jmor.1052130106.
Betancur-R, R, Wiley, E O, Arratia, G, Acero, A, Bailly, N, Miya, M, Lecointre, G, Ortí, G, 2017. Phylogenetic classification of bony fishes. BMC Evol. Biol. 17, 1–40. doi:10.1186/s12862-017-0958-3.
Betters, E, Charney, R M, Garcia-Castro, M I, 2018. Early speci fi cation and development of rabbit neural crest cells. Dev. Biol. 444 (Suppl. 1), S181–S192. doi:10.1016/j.ydbio.2018.06.012.
Borisov, V B, Shkil, F N, Abdissa, B, Smirnov, S V, 2012. Development of the cranium in the large african hexaploid barb labeobarbus (=Barbus) intermedius (cyprinidae; teleostei). J. Ichthyol. 52, 838–860. doi:10.1134/S0032945212110021.
Bronner, M E, Ledouarin, N M, 2012. Development and evolution of the neural crest: an overview. Dev. Biol. 366, 2–9. doi:10.1016/j.ydbio.2011.12.042.
Carmona-Fontaine, C, Matthews, H K, Kuriyama, S, Moreno, M, Dunn, G, Parsons, M, Stern, C D, Mayor, R, 2008. Contact inhibition of locomotion in vivo controls neural crest directional migration. Nature 456, 957–961. doi:10.1038/nature07441.
Cerny, R, Cattell, M, Sauka-Spengler, T, Bronner-Fraser, M, Yu, F, Meulemans Medeiros, D, 2010. Evidence for the prepattern/cooption model of vertebrate jaw evolution. Proc. Natl. Acad. Sci. Unit. States Am. 107, 17262–17267. doi:10.1073/pnas.1009304107.
Cerny, R, Lwigale, P, Ericsson, R, Meulemans, D, Epperlein, H-H, Bronner-Fraser, M, 2004. Developmental origins and evolution of jaws: new interpretation of "maxillary" and "mandibular. Dev. Biol. 276, 225–236. doi:10.1016/j.ydbio.2004.08.046.
Cerny, R, Meulemans, D, Berger, J, Wilsch-Bräuninger, M, Kurth, T, Bronner-Fraser, M, Epperlein, H-H, 2004. Combined intrinsic and extrinsic influences pattern cranial neural crest migration and pharyngeal arch morphogenesis in axolotl. Dev. Biol. 266, 252–269. doi:10.1016/j.ydbio.2003.09.039.
Cheung, M, Briscoe, J, 2003. Neural crest development is regulated by the transcription factor. Development 130, 5681–5693. doi:10.1242/dev.00808.
Compagnucci, C, Debiais-Thibaud, M, Coolen, M, Fish, J, Griffin, J N, Bertocchini, F, Minoux, M, Rijli, F M, Borday-Birraux, V, Casane, D, Mazan, S, Depew, M J, 2013. Pattern and polarity in the development and evolution of the gnathostome jaw: both conservation and heterotopy in the branchial arches of the shark, Scyliorhinus canicula. Dev. Biol. 377, 428–448. doi:10.1016/j.ydbio.2013.02.022.
M.S. Cooper V.C. Virta Evolution of gastrulation in the ray-finned (actinopterygian) fishes 308B: 591–608https://doi.org/10.1002/jez.b.211422007
Couly, G F, Coltey, P M, Le Douarin, N M, 1993. The triple origin of skull in higher vertebrates: a study in quail-chick chimeras. Development 117, 409–429.
Creuzet, S, Couly, G, Vincent, C, Le Douarin, N M, 2002. Negative effect of Hox gene expression on the development of the neural crest-derived facial skeleton. Development 129, 4301–4313.
Crump, J G, Maves, L, Lawson, N D, Weinstein, B M, Kimmel, C B, 2004. An essential role for Fgfs in endodermal pouch formation influences later craniofacial skeletal patterning. Development 131, 5703–5716. doi:10.1242/dev.01444.
David, N B, Saint-Etienne, L, Tsang, M, Schilling, T F, Rosa, F M, 2002. Requirement for endoderm and FGF3 in ventral head skeleton formation. Development 129, 4457–4468.
de Beer, G R, 1937. The Development of the Vertebrate Skull. Oxford University Press, London.
Dean, B, 1895. The early development of Gar-pike and Sturgeon. J. Morphol. XI. doi:10.1002/jmor.1050110102.
Del Pino, E, Medina, A, 1998. Neural development in the marsupial frog Gastrotheca riobambae. Int. J. Dev. Biol. 42, 723–731.
Del Pino, E, Ávila, M-E, Pérez, O D, Benítez, M-S, Alarcón, I, Noboa, V, Moya, I M, 2004. Development of the dendrobatid frog Colostethus machalilla. Int. J. Dev. Biol. 48, 663–670. doi:10.1387/ijdb.041861ed.
Dettlaff, T A, Ginsburg, A S, Schmalhausen, O I, 1993. Sturgeon Fishes-Developmental Biology and Aquaculture. Springer.
Diaz, R E, Jr., Shylo, N A, Roellig, D, Bronner, M, Trainor, P A, 2019. Filling in the phylogenetic gaps: induction, migration, and differentiation of neural crest cells in a squamate reptile, the Veiled Chameleon (Chamaeleo calyptratus). Dev. Dynam. 248, 709–727. doi:10.1002/dvdy.38.
Didier, D A, LeClair, E E, Vanbuskirk, D R, 1998. Embryonic staging and external features of development of the chimaeroid fish , Callorhinchus milii (holocephali, callorhinchidae). J. Morphol. 236, 25–47. doi:10.1002/(SICI)1097-4687(199804)236:1<25::AID-JMOR2>3.0.CO;2-N.
Diedhiou, S, Bartsch, P, 2009. Staging of the early development of Polypterus (Cladistia: actinopterygii). In: Development of Non-teleost Fishes. pp. 104–169.
Donoghue, P C J, Keating, J N, 2014. Early vertebrate evolution. Palaeontology 57, 1–15. doi:10.1111/pala.12125.
Eagleson, G W, 1996. Developmental neurobiology of the anterior areas in amphibians: urodele perspectives. Int. J. Dev. Biol. 40, 735–743.
Falck, P, Hanken, J, Olsson, L, 2002. Cranial neural crest emergence and migration in the Mexican axolotl (Ambystoma mexicanum). Zoology 105, 195–202. doi:10.1078/0944-2006-00079.
Forey, P, Janvier, P, 1994. Evolution of the early vertebrates. Sci. Am. 82, 554–565.
Gans, C, Northcutt, R G, 1983. Neural crest and the origin of vertebrates: a new head. Science 220, 268–274. doi:10.1126/science.220.4594.268.
Gillis, J A, Alsema, E C, Criswell, K E, 2017. Trunk neural crest origin of dermal denticles in a cartilaginous fish. Proc. Natl. Acad. Sci. U S A. 18, 1–6. doi:10.1073/pnas.1713827114.
Gouignard, N, Andrieu, C, Theveneau, E, 2018. Neural crest delamination and migration: looking forward to the next 150 years. Genesis 56 e23107. doi:10.1002/dvg.23107.
Graham, A, 2008. Deconstructing the pharyngeal metamere. J. Exp. Zool. B Mol. Dev. Evol. 310B, 336–344. doi:10.1002/jez.b.21182.
Green, S A, Simoes-Costa, M, Bronner, M E, 2015. Evolution of vertebrates as viewed from the crest. Nature 520, 474–482. doi:10.1038/nature14436.
Grevellec, A, Tucker, A S, 2010. Seminars in Cell & Developmental Biology the pharyngeal pouches and clefts: development, evolution, structure and derivatives. Semin. Cell Dev. Biol. 21, 325–332. doi:10.1016/j.semcdb.2010.01.022.
Hall, B K, 2009. Neural crest derivatives. In: The Neural Crest and Neural Crest Cells in Vertebrate Development and Evolution. pp. 159–268.
Harrington, M J, Hong, E, Brewster, R, 2009. Comparative analysis of neurulation: first impressions do not count. Mol. Reprod. Dev. 76, 954–965. doi:10.1002/mrd.21085.
Hockman, D, Chong-Morrison, V, Green, S A, Gavriouchkina, D, Candido-Ferreira, I, Ling, I T C, Williams, R M, Amemiya, C T, Smith, J J, Bronner, M E, Sauka-Spengler, T, 2019. A genome-wide assessment of the ancestral neural crest gene regulatory network. Nat. Commun. 10, 1–15. doi:10.1038/s41467-019-12687-4.
Horigome, N, Myojin, M, Ueki, T, Hirano, S, Aizawa, S, Kuratani, S, 1999. Development of cephalic neural crest cells in embryos of Lampetra japonica, with special reference to the evolution of the jaw. Dev. Biol. 207, 287–308. doi:10.1006/dbio.1998.9175.
Hughes, L C, Ortí, G, Huang, Y, Sun, Y, Baldwin, C C, Thompson, A W, Arcila, D, Betancur, -R, R., Li, C, Becker, L, Bellora, N, Zhao, X, Li, X, Wang, M, Fang, C, Xie, B, Zhou, Z, Huang, H, Chen, S, Venkatesh, B, Shi, Q, 2018. Comprehensive phylogeny of ray-finned fishes (Actinopterygii) based on transcriptomic and genomic data. Proc. Natl. Acad. Sci. Unit. States Am. 115, 6249–6254. doi:10.1073/pnas.1719358115.
Inoue, J G, Miya, M, Tsukamoto, K, Nishida, M, 2003. Basal actinopterygian relationships : a mitogenomic perspective on the phylogeny of the " ancient fish". Mol. Phylogenet. Evol. 26, 110–120. doi:10.1016/S1055-7903(02)00331-7.
Iwamatsu, T, 2004. Stages of normal development in the medaka Oryzias latipes. Mech. Dev. 121, 605–618. doi:10.1016/j.mod.2004.03.012.
Jaroszewska, M, Dabrowski, K, 2009. Early ontogeny of semionotiformes and amiiformes (neopterygii: actinopterygii). In: Development of Non-teleost Fishes. pp. 230–274.
Johanson, Z, Boisvert, C, Maksimenko, A, Currie, P, Trinajstic, K, 2015. Development of the synarcual in the elephant sharks (holocephali; chondrichthyes): implications for vertebral formation and fusion. PloS One 10 (9), 1–19 e0135138. doi:10.1371/journal.pone.0135138.
Kerr, J G, 1907. The development of Polypterus senegalus Cuvier. In: The Work of John Samuel Budgett. Cambridge University Press.
Kerr, J G, 1919. Textbook of Embryology. Vol II. Vertebrata with the Exception of Mammalia. Macmillan and CO., London.
Kimmel, C B, Ballard, W W, Kimmel, S R, Ullmann, B, Schilling, T F, 1995. Stages of embryonic development of the zebrafish. Dev. Dynam. 203, 253–310. doi:10.1002/aja.1002030302.
Konstantinidis, P, Warth, P, Naumann, B, Metscher, B, Hilton, E J, Olsson, L, 2015. The developmental pattern of the musculature associated with the mandibular and hyoid arches in the longnose gar, Lepisosteus osseus (actinopterygii, ginglymodi, lepisosteiformes). Copeia 103, 920–932. doi:10.1643/OT-14-195.
Kulesa, P M, Bailey, C M, Kasemeier-Kulesa, J C, McLennan, R, 2010. Cranial neural crest migration: new rules for an old road. Dev. Biol. 344, 543–554. doi:10.1016/j.ydbio.2010.04.010.
Kunz, Y W, Luer, C A, Kapoor, B G, 2009. Development of Non-teleost Fishes. Science Publishers, Enfield.
Kuo, B R, Erickson, C A, 2010. Regional differences in neural crest morphogenesis Regional differences in neural crest morphogenesis. Cell Adhes. Migrat. 4, 567–585. doi:10.4161/cam.4.4.12890.
Kuratani, S, Horigome, N, Ueki, T, Aizawa, S, 1998. Stereotyped axonal bundle formation and neuromeric patterns in embryos of a cyclostome , Lampetra japonica. J. Comp. Neurol. 391, 99–114.
Kuratani, A, Kuratani, S, Horigome, N, 2000. Developmental morphology of branchiomeric nerves in a cat shark, Scyliorhinus torazame, with special reference to rhombomeres, cephalic mesoderm, and distribution patterns of cephalic crest cells. Zool. Sci. 17, 893–909. doi:10.2108/zsj.17.893.
Le Douarin, N M, Dupin, E, 2014. The neural crest, a fourth germ layer of the vertebrate embryo: significance in chordate evolution. In: Trainor, P A (Ed.), Neural Crest Cells. Elsevier, pp. 3–26.
Long, W L, Ballard, W W, 2001. Normal embryonic stages of the Longnose Gar, Lepisosteus osseus. BMC Dev. Biol. 1. doi:10.1186/1471-213X-1-6.
Lowery, L A, Sive, H, 2004. Strategies of vertebrate neurulation and a re-evaluation of teleost neural tube formation. Mech. Dev. 121, 1189–1197. doi:10.1016/j.mod.2004.04.022.
Martik, M L, Bronner, M E, 2017. Regulatory logic underlying diversification of the neural crest. Trends Genet. 33, 715–727. doi:10.1016/j.tig.2017.07.015.
Martik, M L, Gandhi, S, Uy, B R, Gillis, J A, Green, S A, Simoes-Costa, M, Bronner, M E, 2019. Evolution of the new head by gradual acquisition of neural crest regulatory circuits. Nature 574, 675–678. doi:10.1038/s41586-019-1691-4.
McCauley, D W, Bronner-Fraser, M, 2003. Neural crest contributions to the lamprey head. Development 130, 2317–2327. doi:10.1242/dev.00451.
Metscher, B D, 2009. MicroCT for developmental biology: a versatile tool for high-contrast 3D imaging at histological resolutions. Dev. Dynam. 238, 632–640. doi:10.1002/dvdy.21857.

VI. Soukup V, Tazaki A, Yamazaki Y, **Pospisilova A**, Epperlein H-H, Tanaka EM & Cerny R (in prep) Oral and palatal dentition of axolotl arises from a common tooth-competent zone and co-localizes with the ecto-endoderm boundary.

Oral and palatal dentition of axolotl arises from a common tooth-competent zone and co-localizes with the ecto-endoderm boundary

Vladimír Soukup[1]*, Akira Tazaki[2§], Yosuke Yamazaki[1#], Anna Pospisilova[1], Hans-Henning Epperlein[3], Elly M. Tanaka[2], Robert Cerny[1]

[1] Department of Zoology, Faculty of Science, Charles University, Vinicna 7, 12844 Prague, Czech Republic
[2] Max-Planck Institute for Molecular Cell Biology and Genetics, Pfotenhauerstraße 108, 01307 Dresden, Germany
[3] Department of Anatomy, Technische Universität Dresden, Fetscherstraße 74, 01307 Dresden, Germany

* Author of correspondence:
Vladimír Soukup
e-mail: soukup@natur.cuni.cz

[§] Current address:
Nagoya University Graduate School of Medicine, 65 Tsurumai-cho, Shouwa-ku, 466-8550 Nagoya, Japan

[#] Current address:
Department of Anatomy, Nihon University School of Dentistry, 1-8-13 Kanda-Surugadai, Chiyoda-ku, 101-8310 Tokyo, Japan

Keywords
tooth development, dental arcades, initiation, patterning, ectoderm, endoderm, axolotl

Abstract
Vertebrate dentitions have facilitated the evolutionary success of their owners and flourished into the astonishing diversity in form and function. This diversity stems from developmental events taking place at early ontogeny when the pattern and composition of the nascent dentition is laid down. Regrettably, the knowledge on how teeth are patterned during embryogenesis relies to a large extent on species that underwent dental modifications and reductions such as the mouse or zebrafish, thus biasing the search for developmental events underpinning the vertebrate dental diversity. Here we study development of the axolotl dentition, which consists of individual tooth fields arranged into the outer and inner dental arcades, a layout typical for tetrapods. By tracking the expression patterns of odontogenic genes, we show that teeth of both dental arcades originate from common tooth-competent zones, one present on the mouth roof and one on the mouth floor. Progressive compartmentalization of these zones and a simultaneous addition of new tooth germs distinct for each prospective tooth field subsequently control the final shape and composition of the axolotl dentition. Interestingly, by following the fate of the GFP-labeled oral ectoderm, we further show that first tooth germs develop in relation to the ecto-endoderm border. Our results thus indicate that a single tooth-competent zone gives rise to both of the dental arcades of a complex tetrapod dentition. Further, we propose that the ecto-endoderm boundary running through this zone should be accounted for as a potential source of instruction factors instigating the onset of the odontogenic program.

Introduction

One of the most important features of vertebrate dentitions is the patterned arrangement of their elemental units, the teeth. Each tooth has its defined position and a certain relation to other teeth of that dentition. In extant vertebrates, tooth development is restricted to the oropharyngeal region, where the locally thickened epithelium demarcates the prospective tooth-forming areas. This so-called odontogenic band usually invaginates into the underlying mesenchyme to form an epithelial strand, the dental lamina.

Shh and Pitx2 represent earliest markers of odontogenesis and factors responsible for tooth development in vertebrates. Absence of Shh or Pitx2 signaling results in the loss of tooth signaling centers, defects in tooth development and missing teeth (Dassule et al. 2000, Cobourne et al. 2004, Jackman et al. 2010, Lin et al. 1999, Yu et al. 2020) and a lack of co-expression of *Shh* and *Pitx2*, for example, is associated with toothlessness in cypriniforms (Jackman et al. 2010). Once *Shh* and *Pitx2* specify the positions of the nascent dentition, a sequence of events leading to the appearance of the first tooth controls addition of further tooth germs adjacent to this initiator-tooth (Gibert et al. 2019, Sadier et al. 2019, 2020). The way in which new tooth germs are sequentially added in the vicinity of this initiator-tooth then leads to the final appearance of the respective tooth field.

While the expression of *Shh* and *Pitx2* and the induction from the initiator-tooth may be among the earliest events of the developing dentition, it is not satisfactorily explained how the spatial distribution of this initial odontogenic potential within the oropharyngeal cavity is regulated (Balic 2019). Several cues have been proposed including (1) the polarization and regionalization of the mandibular arch along the proximo-distal axis (Sharpe 1995, Tucker and Sharpe 2004), (2) activator/inhibitor interactions specifying tooth-competent regions (Sarkar et al. 2000, Fraser et al. 2008, Zhang et al. 2009), (3) the progressive and reiterated partitioning of the initially established tooth-competent region (Jernvall and Thesleff 2000, Fraser et al. 2008) or (4) the influence of epithelial germ-layers contributing to different parts of the oropharyngeal cavity (Smith 2003, Ohazama et al. 2010).

Various roles have been assigned to the ectoderm and endoderm in triggering odontogenesis and patterning the teeth (Smith 2003, Huysseune et al. 2009, Ohazama et al. 2010). However, a definite distinction of these germ layers fails due to the lack of general germ layer-specific morphological markers. The germ layer specific expression of *Pitx2* (oral ectoderm) and *Shh* (endoderm) is present only until the rupture of the oral membrane (Helms et al. 1997, Schweickert et al. 2001, Eberhart et al. 2006). Thus, uncovering the roles of these epithelia in tooth development requires an experimental germ layer-specific labeling, which for now is to a large extent pending.

The Mexican axolotl is an extant amphibian with teeth assembled into dental arcades located in oral and palatal regions. The outer arcade composes of single-rowed premaxillary and dentary tooth fields and is tentatively homologous to the dental arcade in mammals, and the inner arcade composes of multi-rowed vomerine, palatine and coronoid (sometimes called splenial) tooth fields (Fig. 1). The composition of the axolotl dentition is typical for extant and extinct tetrapods (Matsumoto and Evans 2017). Yet, how this complex dental system becomes established developmentally has not been addressed.

The Mexican axolotl provides an opportunity to experimentally assess the germ-layer origin of oral epithelia (Soukup et al. 2008) and, in combination with the information on the developmental origin of the respective tooth fields thus represents an eligible developmental model for the understanding of the early events in the initiating dentition.

Results

The complex tetrapod dentition of axolotl arises by separation of initially compact tooth-competent zones

The outer and inner dental arcades of the axolotl dentition are composed of five pairs of tooth fields (Fig. 1). In order to understand how this complex dentition acquires such an arrangement, we studied the expression of the early odontogenic markers *Pitx2* and *Shh*. At early larval stages (st. 37-41), *Pitx2* is expressed over the extents of the jaws delineating tooth-competent zones. In contrast, *Shh* expression is focally restricted to initiating tooth germs and odontogenic bands, from where new germs will arise (Fig. 2). *Pitx2* expression becomes later downregulated at sites where new tooth germ are added, a situation reminiscent of other vertebrates (Keränen et al. 1999, Fraser et al. 2004, 2008). At stage 37,

Pitx2 expression is restricted into broad domains on the roof and floor of the mouth (Fig. 2A, C). The first tooth germs are initiated at this stage, as evidenced by the focal expression of *Shh*. They belong to the prospective vomerine, palatine and coronoid tooth fields, i.e. constituents of the inner dental arcade (Fig. 2B, D, small arrows). Additional strands of *Shh* expression are found on the roof and floor of the mouth labially from these first germs and represent odontogenic bands from where new germs will be generated (Fig. 2B, D, white arrowheads). During the course of development, the *Pitx2*-expressing tooth-competent zones progressively extend posteriorly on both the roof and floor of the mouth (Fig. 2A, C, E, G, I, K, parentheses) and concomitantly, the *Shh*-expressing odontogenic bands align to the labial limits of these zones (Fig. 2B, D, F, H, J, L). Based on the focal expression of *Shh* during subsequent stages, new tooth germs are added adjacent to the initiator-teeth, i.e. postero-medially in the palatine field (Fig. 2J, arrowheads) and both postero-laterally and postero-medially in the coronoid field (Fig. 2H, arrowheads). At stages 40 and 41, the splitting of the *Pitx2* expression pattern on the mouth floor suggests a separation of the tooth-competent zone into dentary and coronoid fields (Fig. 2K, O). Meanwhile, the first tooth germs of the dentary tooth field are initiated at the mandibular symphysis (Fig. 2L, small arrows). During subsequent stages, the *Shh* expression pattern labels newly initiated tooth germs that are added antero-medially in the vomerine tooth field (Fig. 2N, arrowheads), laterally along the lower jaw in the dentary tooth field (Fig. 2P, arrowheads) and postero-medially in the coronoid tooth field (Fig. 2L, P, arrowheads). Further analysis of expression patterns of other odontogenic factors, such as *Bmp2*, *Bmp7* or *Dlx5* confirms the addition of new tooth germs within individual tooth fields, which are delineated by the expression of *Dlx3* (Suppl. fig. 1). Moreover, focal expression of *Bmp2*, *Bmp7* and *Dlx5* labels the initiation of the first tooth germ of the premaxillary field at stage 41 (Suppl. fig. 1A, C, G, arrow). In order to further analyze the progressive compartmentalization of tooth-competent zones (Fig. 2), we performed an independent analysis using 3D reconstructions of the roof and floor epithelia of the axolotl mouth based on serial sections hybridized with the *Pitx2* probe (Suppl. fig. 2). Concordant with data from whole mounts, stage 38 shows a compact expression pattern in the basal epithelial layer of the roof and floor epithelia of the prospective mouth. At subsequent stages, the common *Pitx2* expression pattern becomes compartmentalized and eventually leads to discrete tooth fields. Thus, both the whole mount data and the 3D reconstructions show the separation of initially compact tooth-competent zones into distinct tooth fields. Therefore, the two dental arcades of the axolotl dentition originate from a single tooth competent zone.

Further differences among axolotl dental arcades arise by field-specific addition of tooth germs

The separation of tooth-competent zones into individual tooth fields is followed by a progressive and rapid addition of tooth germs within individual fields. Prior to hatching, the tooth germ-specific *Shh* expression becomes a challenge to be followed up. In contrast, *Pitx2* expression progressively changes from broadly delineating the tooth-competent zones into focal patterns that label individual tooth germs (compare the gradual change in *Pitx2* expression portrayed on figures 2M, O, 3A, B and 3C, D). Interestingly, this change in *Pitx2* expression takes place earlier on the mouth floor than on the mouth roof, i.e. stage 42 shows that *Pitx2* is expressed generally within premaxillary, vomerine and palatine fields (Fig. 3A) and focally within tooth germs of the dentary and coronoid fields (Fig. 3 B). This suggests that the development of tooth fields on the mouth floor is slightly advanced relative to that on the mouth roof.

Stages around hatching display a continuation of the addition of new tooth germs within individual tooth fields but also differences among their prospective single-rowed versus multi-rowed arrangements. Moreover, while new germs initially arise from the adjacent superficial epithelium (Fig. 4A-E), later tooth germs develop from the invaginated dental laminae, whose positions regulate the future arrangement of the respective tooth fields (Fig. 4F-J). For example, in the premaxillary field, new tooth germs are added laterally and medially to the initiator-teeth (Fig. 4A), while in the dentary field, new germs are added laterally from the pair of parasymphyseal initiator-teeth (Fig. 2L, P, 4D). Though formed differently, both fields eventually produce teeth assembled into a single row that runs along the jaw margins and is connected through continuous dental laminae at their labial sides (Fig. 4F, I). Likewise, the tooth fields on the mouth roof produce initial rows of tooth germs by antero-medial addition in vomerine fields and postero-medial addition in palatine fields (cf. Figs. 3C and 4B, C). The medial positions of dental laminae then result in the addition of new germs medially (Fig. 3E, 4G, H),

thus producing multi-rowed patches of teeth on the mouth roof. On the mouth floor, the coronoid tooth field is produced first by the sequential addition of tooth germs from the adjacent epithelium and then from the lingually positioned dental lamina (Fig. 4E, J). Thus, the pattern of the addition of tooth germs sets a basis for the arrangement of axolotl dentition into outer and inner dental arcades with different properties. During larval development, teeth of the outer dental arcade become arranged into a single functional row while teeth of the inner dental arcade become clustered into patches with many functional rows.

Axolotl dentition arises at the ecto-endoderm boundary

The distribution of the ectoderm and endoderm in the oropharynx has been hypothesized to play a key role in the initiation and patterning of teeth (Smith 2003, Ohazama et al. 2010), yet, a thorough knowledge on the distribution of these epithelia in extant vertebrates is largely unknown (reviewed in Soukup et al. 2013). We previously studied the distribution of these epithelia in the Mexican axolotl and showed that the labial portion of the nascent mouth epithelium consists of the ectodermal basal layer and the endodermal apical layer and that the lingual ectodermal border runs through the tooth fields (Soukup et al. 2008). We performed a new series of transplantations of the prospective oral ectoderm from a GFP-transgenic axolotl neurula into the white host (n=8). This experimental procedure resulted in an invariable labelling of ectodermal lining inside the oral cavity, thus allowing a detailed visualization of the ecto-endoderm border in the context of the developing dentition. On whole mounts, the GFP-labelled ectoderm reaches an anterior portion of the palate in front of and slightly behind inner nostrils (Fig. 5B) and the labial portion of the lower jaw (Fig. 5E). The ecto-endoderm border on the palate stereotypically displays an uneven, roughly bilaterally symmetrical shape with cells undergoing an intermingling, especially medially at the place of migration of the adenohypophyseal anlage (Fig. 5B, C). On the other hand, the ecto-endoderm border on the mouth floor displays a crescent-shaped arrangement running along the length of the lower jaw (Fig. 5E, F).

The ecto-endoderm border runs through the tooth fields so that individual tooth germs display a differential epithelial origin: ectodermal, endodermal or ecto-endodermal. Histological analysis shows that the dentary tooth fields are composed of ecto-endodermal germs developing close to the mandibular symphysis (Fig. 6E, yellow arrows). The other dentary teeth, on the other hand, develop from the ectodermal epithelium laterally along the jaw (Fig. 6E, white arrowheads). Interestingly, the parasymphyseal teeth represent the initiator-teeth from where new germs are added laterally, i.e. the dentary field is initiated directly at the ecto-endodermal border. Single ecto-endodermal tooth germs are also found antero-laterally in the coronoid and palatine tooth fields, while other teeth of these fields are of endodermal origin (Fig. 6A-D, yellow arrows). Combined with data from histology and *Shh* expression (Fig. 2F, J, 3E, 4C, H), we reason that the ecto-endodermal teeth represent the initiator-teeth of these fields and that other teeth are added lingually from endodermal regions. Similarly to the dentary field, the initiator-teeth of the coronoid and palatine fields are found at the ecto-endodermal border. The initiator-tooth and also the first added tooth germs of the vomerine field, on the other hand, develop anterior to the ecto-endodermal border, i.e. from the ectodermal epithelium (Fig. 6B, white arrow and white arrowheads). Yet, some teeth arising at later larval stages develop from ecto-endoderm due to the posteriorly positioned ecto-endodermal dental lamina (Fig. 6B, C, yellow arrowheads). In contrast to other tooth fields, the premaxillary field is composed solely of teeth of ectodermal origin (Fig. 5B, C).

The combination of data on the modes of the addition of new tooth germs within the tooth fields and their germ-layer derivation thus allows us to propose that the initiator-teeth in three tooth fields arise directly at the boundary between ectoderm and endoderm (Fig. 7A, E, G) and those of the other two are initiated in ectodermal regions. No initiator-tooth stereotypically develops from the endoderm. New tooth germs subsequently arise from ectoderm, endoderm or ecto-endoderm due to specific development of the respective tooth field.

Discussion

Axolotl tooth fields arise by separation of tooth-competent zones

The initial state of axolotl dentition is evidenced by two *Pitx2*-expressing tooth competent zones that are overlain by *Shh*-expressing odontogenic bands at their posterior portions (Fig. 7A, E). This initial co-expression of *Pitx2* and *Shh* corresponds well to the situation found on the mouth roof and floor of

other vertebrates such as shark, trout, cichlids, tetra, vole and mouse and it probably represents a blueprint of the developing oral dentitions in vertebrates (Keränen et al. 1999, Fraser et al. 2004, Stock et al. 2006, Fraser et al. 2008, Debiais-Thibaud et al. 2015, Rasch et al. 2016). Concordantly, the lack of co-expression of these two factors has been ascribed to the inability to form oral teeth in zebrafish or to initiate a third tooth row of the two-rowed dentition in the cichlid *Cynotilapia afra* (Stock et al. 2006, Fraser et al. 2008). In cichlids, the following reiterated focal expression of *Shh* within the solid *Pitx2*-expressing domain next defines positions of newly added tooth germs leading to the development of dentitions composed of many teeth (Fraser et al. 2008). Likewise, new foci of *Shh* expression within the *Pitx2*-expressing tooth-competent zones demark the newly added tooth germs also in axolotl (Fig. 7A, B, E, F). However, both the positioning of new tooth germs and the odontogenic bands occurs even prior to the complete separation of tooth competent zones.

The progressive compartmentalization of tooth competent zones leads to individual tooth fields whereas no tooth field is established *de novo*. This means that the entire axolotl dentition composed of five pairs of tooth fields and assembled into outer and inner dental arcades arises embryonically only from two *Pitx2*-expressing tooth-competent zones present on the mouth roof and floor. The progressive compartmentalization is reminiscent of the proposed sequential partitioning of tooth-competent zones during the establishment of the heterodont dentition in mammals, where a gene toolbox reiteratively functions in a nested fashion to progressively partition the previously defined regions into smaller compartments up to individual tooth cusps (Jernvall and Thesleff 2000). Under this scenario, a field of competence (odontogenic band) is first established, second, a tooth type area is specified (incisor, canine, premolar, molar), third, individual teeth are initiated, and finally, their cusps arise. By applying this scenario to homodont dentitions composed of many uniform teeth, such as those found in axolotl or e.g. ray-finned fishes, the initially defined tooth competent region would directly be compartmentalized into individual tooth germs (Streelman et al. 2003, Fraser et al. 2008). In axolotl, however, the tooth-competent zones give rise not only to the marginal teeth, for which the model of progressive partitioning was originally proposed, but to the entire tetrapod-type dentition composed of many tooth fields assembled into two dental arcades.

Interestingly, partitioning of the axolotl tooth-competent zones into prospective tooth fields also affects the odontogenic bands. The initiator-tooth germs of vomerine and palatine fields are among the first appearing teeth of axolotl dentition and these fields initially share a common odontogenic band (Fig. 7A, B). However, during the process of the partitioning of tooth-competent zones and the appearance of distinct vomerine and palatine fields, the single odontogenic band becomes divided into vomerine and palatine parts. Both parts produce replacement teeth of their respective field. In this respect, it is interesting to note that the early intimate relation between the vomerine and palatine odontogenic bands may explain the later association of vomerine and palatine dental laminae. Although probably not found in axolotl in the full extent (see Clemen and Greven 1977), the mature tooth-producing vomerine and palatine dental laminae of the fire salamander are joined by an unproductive epithelial band (Clemen 1978), thus reflecting the mature state of the once associated tooth fields.

Axolotl inner dental arcade is initiated prior to the outer dental arcade

The order of emergence of tooth fields in axolotl takes place in the sequence (1) vomerine + palatine + coronoid, (2) dentary, (3) premaxillary, i.e. teeth of the inner dental arcade are initiated prior to those of the outer arcade (Fig. 2). The initial sequence of appearance is reflected in the composition of the dentition at hatching (st. 44), when the tooth fields of the inner arcade show a multi-rowed arrangement, while those of the outer arcade still undergo the addition of new germs into a row. This developmental progression of the inner over the outer dental arcade is conspicuous. In general, the differentiation of body parts such as the pharyngeal region, rhombomeres or somites, usually progresses in an anterior-to-posterior fashion during embryonic and larval periods (Graham 2008, Schilling 2008, Dequéant and Pourquié 2008) and deviations to this law have been associated with the development of adaptive organs necessary for the embryonic or larval survival (Pospisilova et al. 2019, Stundl et al. 2019, Stundl et al. 2020). Salamander larvae, including the neotenic Mexican axolotl, are suction feeders. After being sucked in, the prey is firmly gripped in the oral cavity and then oriented through several cycles of releasing, reorienting and immediate re-gripping until swallowing (Deban and Wake 2000). This manipulation is facilitated by the presence of tooth patches at the rear of the mouth. Concordantly, the first odontogenic bands and dental laminae, from which subsequent tooth germs arise in axolotl,

develop in relation to vomerine, palatine and coronoid tooth fields, thus facilitating the early achievement of a multi-rowed arrangement of the inner dental arcade. The early establishment of tooth patches in the inner dental arcade assures that the newly hatched axolotl larva is equipped with a ready-to-use apparatus for prey capture and processing, whereas the outer arcade may developmentally be lagging and fully develop only at later larval stages.

The field-specific addition of teeth controls the final composition of the axolotl dentition

The pattern of the addition of tooth germs is disparate among individual axolotl tooth fields (Fig. 7). Generally, the final appearance of the respective tooth field depends on the shape of the *Pitx2*-expressing field and the position of the initiator-tooth. For example, the dentary field is narrow and strand-shaped, wherein tooth germs are sequentially added into a row and this situation reminds the developing mammalian dentition. The coronoid field, on the other hand, is wide and tooth germs are patterned into a cluster (Fig. 7G, H), i.e. a situation reminiscent of the multi-rowed dentition of cichlids (Fraser et al. 2008). The differences in tooth patterning at early stages of axolotl development are subsequently reflected in the final arrangement of teeth at larval stages.

Each prospective tooth field in axolotl starts its development with the appearance of the first tooth. In zebrafish, the first tooth acts as a signaling center for the initiation of two adjacent tooth germs and these three teeth then constitute the first row of the dentition (Gibert et al. 2019, Van der heyden and Huysseune 2000). In the mouse, the first tooth germ similarly initiates the whole molar row (Prochazka et al. 2010, Sadier et al. 2019). The first tooth thus acts as an initiator cue for the development of the whole tooth row or tooth patch (Sadier et al. 2020) while spacing between the teeth is mediated by the zone of inhibition surrounding each tooth germ (Osborn 1978, Huysseune and Witten 2006, Fraser et al. 2008). In axolotl, the position of the initiator-tooth is specific to each tooth field (Fig. 7) and these different positions next trigger disparate ways, how new germs are added (see Huysseune and Witten 2006). For example, among the narrow strand-shaped fields, the dentary tooth germs are added laterally from the parasymphyseally positioned initiator-tooth while the premaxillary tooth germs are added both laterally and medially to the mid-laterally positioned initiator-tooth (Fig. 7C, D, G, H). The addition of new germs within each tooth field progresses through redeployment of tooth-competent genes, such as *Shh*, *Bmp2* or *Bmp7*, until this region becomes fully filled up with tooth germs (Fig. 2, 3, suppl. fig. 2).

After filling up the initial extent of the tooth field with individual teeth, new tooth germs can only be added by further enlargement of this field. This may happen basically in two ways that can act simultaneously. First, the embryonic growth leads to the enlargement of the field by a medio-lateral prolongation, and so new tooth germs may be added sequentially along the jaw length. This is most notably visible in the case of the premaxillary or dentary tooth fields. Second, the dental lamina provides further space for the additional production of tooth germs behind the already formed tooth row(s). This is the case of vomerine or palatine tooth fields. In vertebrates, progressive enlargements of fields of competence have been associated with patterning of other, non-dental, iterative structures such as bird plumage, or shark denticles (Jung et al. 1998, Cooper et al. 2018) and the addition of new units into the existing row simultaneously with the addition of new rows thus seems to be a general phenomenon of dentitions composed of many teeth and tooth generations (Van der heyden and Huysseune 2000, Ellis et al. 2016). From this viewpoint, the addition of new tooth units simultaneously at the edges of the tooth fields and from the dental laminae in the axolotl is in good accord with that present in other vertebrates.

Some axolotl teeth develop stereotypically at the ecto-endoderm boundary

The border between ectoderm and endoderm in axolotl runs through individual tooth fields (Fig. 7). Except for the purely ectoderm-derived premaxillary tooth field that later expands laterally onto the maxillary bones (Clemen and Greven 1977), the remaining tooth fields are ecto-endodermal. In palatine, coronoid and dentary tooth fields, the relation between the ecto-endoderm border and the teeth is special in that the border stereotypically runs through the first-forming tooth germs, i.e. initiator-teeth of these fields. Thus, in axolotl, the initiator-tooth either develops from the ectoderm (premaxillary, vomerine), or directly at the ecto-endoderm boundary (palatine, coronoid, dentary, Fig. 7, orange circles). We found no purely endoderm-derived initiator-tooth. Interestingly, among the fields with the ecto-endodermal initiator tooth, the newly added tooth germs develop either from ectoderm (dentary

field), or from endoderm (palatine and coronoid fields). In the vomerine field, where the initiator-tooth is ectodermal, the subsequent germs are ectodermal or ecto-endodermal.

Concordantly, the ecto-endoderm boundary runs through the tooth fields in such a way that even the odontogenic bands of early larvae and the dental laminae that produce new tooth germs at later larval stages may be of double-germ layer origin. Besides the ectodermal dental lamina of the premaxillary field and the endodermal dental laminae of the palatine and coronoid fields, the dental lamina of the vomerine field is ecto-endodermal (Fig. 6B, C), and we propose its presence also in the case of the dentary field.

With spatial relations between the germ layer distribution and the initiator-tooth development, the axolotl constitutes a unique model among extant vertebrates. In mouse, the *Sox17*-reporter line shows the presence of the *Sox17*-positive endodermal epithelium at the back of the tongue and posterior to the developing dentition, meaning that all murine teeth are ectoderm-derived (Rothova et al. 2012). In zebrafish, the tooth-forming pharyngeal epithelium *per se* is endodermal, although teeth develop only in case the pharyngeal endoderm contacts the surface ectoderm via the pharyngeal cleft/pouch and only after an apical periderm-like layer on top of the odontogenic epithelium was formed (Oralová et al. 2020). In axolotl, mouth development progresses through a stomodeal collar, where the oral ectoderm involutes and eventually contributes, in the anteriormost oral regions, exclusively to the basal layer of the double-layered oral epithelium (Soukup et al. 2008, 2013). Given that initiator-teeth of individual axolotl tooth fields are either fully ectodermal or half ectodermal and half endodermal, this suggests that the ectoderm may be responsible for the factual initiation of axolotl dentition. In line with this assumption would be the argument, why the ectoderm progresses through such a complicated way if it does not exert a certain, perhaps tooth-instructive, role? Such an interpretation would, together with the data on the role of germ-layers during the initiation of teeth in zebrafish (Oralová et al. 2020), be mechanistically well in line with the modified outside-in hypothesis of tooth origin. This suggests that the tooth-forming potential evolved externally within the surface ectoderm and later became translocated into the oropharyngeal region in a way that teeth of extant vertebrates develop either from the ectoderm or from the endoderm, yet with a close-by presence of the tooth-instructive ectoderm (Huysseune et al. 2009, 2010). Conversely, in vitro experiments, in which different salamander embryonic tissues were combined and their differentiation potential was studied, corroborate that tooth germs are produced only when oral ectoderm, foregut endoderm and cranial neural crest are co-cultured (Wilde 1955, Graveson et al. 1997). No teeth form when either oral ectoderm or foregut endoderm alone are co-cultured with neural crest (Wilde 1955, Takata 1960). The combinatorial presence of ectoderm, endoderm and neural crest thus seems to be a necessary prerequisite for salamander tooth development.

This, together with our own data, leads us to reason that the boundary between the ectoderm and endoderm accounts for a potential source of instruction factors instigating the onset of the odontogenic program. Such an interaction system with a potential tooth-instructing role may be a widespread feature of the vertebrate oropharyngeal cavities especially at places, where the outer ectoderm comes into contact with the inner endoderm. For example, if the physical ecto-endodermal contact is compromised *in vivo* in zebrafish, the odontogenic program is not triggered (Oralová et al. 2020). Based on these data, we hypothesize that the combinatorial influence of the ectoderm and endoderm on tooth development, or the physical boundary of these epithelia *per se*, may be a much more widespread and perhaps ancient feature of vertebrate odontogenesis. In support for this suggestion, the basalmost stem osteichthyan *Lophosteus* shows initiation of dermal odontodes and teeth at the oral-dermal boundary running along the length of the lower jaw and sequential addition of new odontodes labially and teeth lingually from this boundary (Chen et al. bioRxiv preprint). This boundary presumably represents a generative interface of the outer and inner developmental environments from where new hard tissue elements (odontodes/teeth) develop in an ordered way. In this context and in the context of the current study, there is an apparent need for the broader use of detailed fate-mapping studies in the range of “model” and “non-model” vertebrates to visualize and evaluate the role of the ecto-endoderm boundary for the initiation of odontogenesis.

Conclusions

Vertebrates display a wide array of dentitions with patterned arrangements. Yet, how this pattern emerges during development and what are the initiation agents of tooth patterning are largely unanswered questions (Smith 2003, Huysseune and Witten 2006, Fraser et al. 2008, Balic 2019). Axolotl represents a suitable model for the study of patterning of teeth into a row versus a patch. Moreover, the colocalization of the initiator-teeth and the ecto-endodermal boundary in this animal points to the boundary as the potential source of initiation signals instigating odontogenesis. Be it directly at the boundary or in its proximity, vertebrate dentitions frequently develop at places of interactions of ectoderm and endoderm, such as the jaws, the palate or the branchial arches. Therefore, the role of the ecto-endodermal boundary on tooth initiation and development may be a vastly underestimated topic of vertebrate embryogenesis.

Material and methods

Axolotl embryos handling and GFP-oral ectoderm transplantation experiments

White strain and white GFP-transgenic (Sobkow et al. 2006) axolotl embryos were acquired from the axolotl colony at MPI-CBG Dresden, Germany. Eggs prepared for prospective oral ectoderm transplantations were rinsed in tap water and put into sterile Steinberg solution containing antibiotics. Early neurulae (st. 14, Bordzilovskaya et al. 1989) were placed into agarose-covered Petri dish, manually decapsulated and inserted firmly into beds cut into the agarose. Oral ectoderm was transplanted from white GFP-donors into white hosts at the early neurula stage (st. 14) as previously described (Soukup et al. 2008), and the larvae were fixed at hatching (st. 44) for whole mount analysis of the ectodermal extent in the oral cavity (n=8). Further oral ectoderm transplantation experiments were performed for histological analysis at stages of early tooth addition. Embryos and larvae were anaesthetized with MS-222 (Sigma) and fixed overnight in 4% paraformaldehyde in 0.1 M phosphate-buffered saline. Specimens prepared for in situ hybridization were dehydrated and stored in methanol at -20°C.

In situ hybridization

In situ hybridizations were performed on whole mounts using DIG-labelled RNA probes. Antisense probes for in situ hybridization were obtained by in vitro transcription using primers listed in the supplementary table 1. Rehydrated larvae were digested in 20 µg/ml proteinase K, fixed in 4% paraformaldehyde for 10 min, transferred into hybridization solution (50% formamide, 4× SSC, 0.1 mg/ml heparin, 1× Denhardt's, 0.1% CHAPS, 0.2 mg/ml yeast RNA, 10 mM EDTA, 0.1% Tween-20) and incubated overnight in hybridization solution containing probe (1:1000). Next day, the specimens were washed several times in post-hybridization solution (50% formamide, 4× SSC, 0.1% Tween-20) and transferred via MABT buffer (100 mM maleic acid, 150 mM NaCl, 0.1% Tween-20) into blocking solution (2% blocking reagent, 20% sheep serum, in MABT). Following blocking, the specimens were incubated overnight in the blocking solution containing alkaline phosphatase-conjugated antibody against DIG (Roche, 1:3000) at 4°C. The specimens were washed several times in MABT buffer, put into NTMT (0.1 M Tris, 0.1 M NaCl, 0.05 M $MgCl_2$, 0.1% Tween-20) and kept in BM Purple substrate (Roche) until the desired signal developed.

3D model of axolotl dentition development

Axolotl larvae at stages 38, 41 and 42 were sectioned sagittally using cryomicrotome at 10 µm thickness and processed through in situ hybridization with *Pitx2* probe. Serial sections were photographed and used for computer-assisted 3D reconstruction. Alignment, segmentation and surface rendering were carried out in Fiji using TrakEM2 plugin for ImageJ (Cardona et al. 2012, Schneider et al. 2012, Schindelin et al. 2012, Schindelin et al. 2015).

Alizarin red staining

Axolotl larvae were bleached in a solution containing 3% H_2O_2 and 0.5% KOH (1:4) with the help of cold light and stained by a saturated solution of Alizarin red (Fluka) plus 0.5% KOH (1:16) overnight. Stained larvae were washed thoroughly by 0.5% KOH to remove excess stain and transferred slowly through a graded series of 0.5% KOH and glycerol (4:1, 2:1, 1:1, 1:2, 1:4) into 100% glycerol.

Image acquisition and processing

Following in situ hybridization, larvae at stages 37-44 were dissected at the level of the jaw joint to enable whole mount visualization of teeth developing on the roof and floor of the mouth. Additionally, mouth roof epithelia of embryos hybridized with a *Shh* probe were excised and photographed as flat-mounts to prevent masking of the tooth-specific signal from the signal in the overlying neural tube. Whole mounts processed through in situ hybridization, skeletal stainings and transplantation of GFP-labelled oral ectoderm were photographed as Z-stacks using motorized dissection microscopes (Olympus SZX12, Zeiss SteREO Lumar.V12). The final deep-focus images were acquired by merging the Z-stacks using maximum projection function. Larvae processed through transplantation of GFP-labelled oral ectoderm were further sectioned using CM3050 cryomicrotome (Leica) and individual tooth germs were visualized using anti-calbindin antibody (Sigma) as described (Barlow et al. 1997, Soukup et al. 2008). Z-stacks of sections were taken on the Olympus Cell^{R} IX81 microscope and merged as maximum projection images.

Author contributions

VS and RC conceived and designed the experiments; VS, AT, YY, AP and RC performed the experiments and generated data; VS and RC analyzed the data; AT, HHE, EMT and RC provided technological support, RC administered the project, VS wrote the original draft of the manuscript. VS, HHE and RC reviewed and edited the final version of the manuscript. All authors read and approved the final version of the manuscript.

Conflict of interest

The authors declare no competing interests.

Acknowledgments

We thank Heino Andreas for dedicated axolotl care, Jan Stundl and Ann Huysseune for critically reading earlier versions of the manuscript and Martin Kralovic for technical assistance. This work was initially supported by the grant from the Czech Science Foundation (GACR 206/09/1007, awarded to Ivan Horacek). This work was further supported by the Charles University Research Centre program No. 204069, the German Academic Exchange Service, the Company of Biologists Development Travelling Fellowship (all to VS), the Czech Science Foundation GACR 18-04580S and the Charles University grant SVV 260571/2020 (to VS, AP and RC).

References

Balic AM (2019) Concise review: cellular and molecular mechanisms of regulation of tooth initiation. Stem Cells 37, 26-32.

Barlow LA and Northcutt RG (1997) Taste buds develop autonomously from endoderm without induction by cephalic neural crest or paraxial mesoderm. Development 124, 949-957.

Bordzilovskaya NP et al. (1989) Developmental-stage series of axolotl embryos. In: Developmental Biology of the Axolotl (eds Armstrong JB, Malacinski GM), Oxford: Oxford University Press, pp. 201-219.

Dassule HR et al. (2000) Sonic hedgehog regulates growth and morphogenesis of the tooth. Development 127, 4775-4785.

Cardona A et al. (2012) TrakEM software for neural circuit reconstruction. PLoS One 7, e38011.

Chen D et al. (preprint) Dental ontogeny in the most primitive bony fish *Lophosteus* reveals the developmental relationship between teeth and dermal odontodes. bioRxiv, doi: https://doi.org/10.1101/2020.07.14.202234

Clemen G and Greven H (1977) Morphologische Untersuchungen an der Mundhöhle von Urodelen III. Die Munddachbezahnung von *Ambystoma mexicanum* Cope (Ambystomatidae: Amphibia). Zool Jb Anat 98, 95-136.
Clemen G (1978) Aufbau und Veränderungen der Gaumenzahnleisten beim larvalen und metamorphosierenden *Salamandra salamandra* (L.) (Salamandridae: Amphibia). Zoomorphol 90, 135-150.
Cobourne MT et al. (2004) Restriction of sonic hedgehog signalling during early tooth development. Development 131, 2875-2885.
Cooper RL et al. (2018) An ancient Turing-like patterning mechanism regulates skin denticle development in sharks. Sci Adv 4, eaau5484.
Deban SM and Wake DB (2000) Feeding: Form, Function, and Evolution in Tetrapod Vertebrates (ed. Schwenk K), San Diego and London, Academic Press, p. 82-94.
Debiais-Thibaud M et al. (2015) Tooth and scale morphogenesis in shark: an alternative process to the mammalian enamel knot system. BMC Evol Biol 15, 292.
Dequéant ML and Pourquié O (2008) Segmental patterning of the vertebrate embryonic axis. Nat Rev Genet 9, 370-382.
Eberhart JK et al. (2006) Early Hedgehog signaling from neural to oral epithelium organizes anterior craniofacial development. Development 133, 1069-1077.
Ellis NA et al. (2016) Early development and replacement of the stickleback dentition. J Morphol 277, 1072-1083.
Fraser GJ et al. (2004) Conserved deployment of genes during odontogenesis across osteichthyans. Proc R Soc Lond B 271, 2311-2317.
Fraser GJ et al. (2008) A periodic pattern generator for dental diversity. BMC Biol 6, 32.
Fraser GJ et al. (2009) An ancient gene network is co-opted for teeth on old and new jaws. PLoS Biol 7, e100031.
Gibert Y et al. (2019) The first formed tooth serves as a signalling centre to induce the formation of the dental row in zebrafish. Proc R Soc B 286, 20190401.
Graham A (2008) Deconstructing the pharyngeal metamere. J Exp Zool B Mol Dev Evol 310, 336-344.
Graveson AC et al. (1997) Neural crest potential for tooth development in a urodele amphibian: Developmental and evolutionary significance. Dev Biol 188, 34-42.
Helms JA et al. (1997) *Sonic hedgehog* participates in craniofacial morphogenesis and is down-regulated by teratogenic doses of retinoic acid. Dev Biol 187, 25-35.
Huysseune A et al. (2009) Evolutionary and developmental origins of the vertebrate dentition. J Anat 214, 465-476.
Huysseune A et al. (2010) A revised hypothesis on the evolutionary origin of the vertebrate dentition. J Appl Ichthyol 26, 152-155.
Huysseune A and Witten PE (2006) Developmental mechanisms underlying tooth patterning in continuously replacing osteichthyan dentitions. J Exp Zool B Mol Dev Evol 306, 204-215.
Jackman WR et al. (2010) Hedgehog signaling is required at multiple stages of zebrafish tooth development. BMC Dev Biol 10, 119.
Jernvall J and Thesleff I (2000) Reiterative signaling and patterning during mammalian tooth morphogenesis. Mech Dev 92, 19-29.
Jung HS et al. (1998) Local inhibitory action of BMPs and their relationships with activators in feather formation: implication for periodic patterning. Dev Biol 196, 11-23.
Keränen SVE et al. (1999) Gene expression patterns associated with suppression of odontogenesis in mouse and vole diastema regions. Dev Genes Evol 209, 495-506.
Lin CR et al. (1999) Pitx2 regulates lung asymmetry, cardiac positioning and pituitary and tooth morphogenesis. Nature 401, 279-282.
Matsumoto R and Evans SE (2017) The palatal dentition of tetrapods and its functional significance. J Anat 230, 47-65.
Ohazama A et al. (2010) Ectoderm, endoderm, and the evolution of heterodont dentitions. Genesis 48, 382-389.
Oralová V et al. (2020) Multiple epithelia are required to develop teeth deep inside the pharynx. Proc Natl Acad Sci 117, 11503-11512.

Osborn JW (1978) Morphogenetic gradients: field versus clones. In: Development, Function and Evolution of Teeth (eds Butler PM, Joysey KA), London: Academic Press, pp. 171–201.
Pospisilova A et al. (2019) Embryonic and larval development of the northern pike: An emerging fish model system for evo-devo research. J Morph 280, 1118-1140.
Prochazka J et al. (2010) Patterning by heritage in mouse molar row development. Proc Natl Acad Sci 107, 15497-15502.
Rasch LJ et al. (2016) An ancient dental gene set governs development and continuous regeneration of teeth in sharks. Dev Biol 415, 347-370.
Rothova M et al. (2012) Lineage tracing of the endoderm during oral development. Dev Dyn 241, 1183-1191.
Sadier A et al. (2019) Modeling Edar expression reveals the hidden dynamics of tooth signaling center patterning. PLoS Biol 17, e3000064.
Sadier A et al. (2020) The vertebrate tooth row: is it initiated by a single organizing tooth? BioEssays 2020, 1900229.
Sarkar L et al. (2000) Wnt/Shh interactions regulate ectodermal boundary formation during mammalian tooth development. Proc Natl Acad Sci 97, 4520-4524.
Schilling TF (2008) Anterior-posterior patterning and segmentation of the vertebrate head. Comp Integr Biol 48, 658-667.
Schindelin J et al. (2012) Fiji: an open-source platform for biological-image analysis. Nat Methods 9, 676-682.
Schindelin J et al. (2015) The ImageJ ecosystem: An open platform for biomedical image analysis. Mol Repr Dev 82, 518-529.
Schneider CA et al. (2012) Image to ImageJ: 25 years of image analysis. Nat Methods 9, 671-675.
Schweickert A et al. (2001) Differential gene expression of *Xenopus Pitx1*, *Pitx2b* and *Pitx2c* during cement gland, stomodeum and pituitary development. Mech Dev 107, 191-194.
Sharpe PT (1995) Homeobox genes and orofacial development. Connect Tiss Res 32, 17-25.
Smith MM (2003) Vertebrate dentitions at the origin of jaws: when and how pattern evolved. Evol Dev 5, 394-413.
Sobkow L et al. (2006) A germline GFP transgenic axolotl and its use to track cell fate: Dual origin of the fin mesenchyme during development and the fate of blood cells during regeneration. Dev Biol 290, 386-397.
Soukup V et al. (2008) Dual epithelial origin of vertebrate oral teeth. Nature 455, 795-798.
Soukup V et al. (2013) Development and evolution of the vertebrate primary mouth. J Anat 222, 79-99.
Stock DW et al. (2006) Developmental genetic mechanisms of evolutionary tooth loss in cypriniform fishes. Development 133, 3127-3137.
Streelman JT et al. (2003) The cusp of evolution and development: a model of cichlid tooth shape diversity. Evol Dev 5, 600-608.
Stundl J et al. (2019) Bichir external gills arise via heterochronic shift that accelerates hyoid arch development. eLife 8, e43531.
Stundl J et al. (2020) Migratory patterns and evolutionary plasticity of cranial neural crest cells in ray-finned fishes. Dev Biol (forthcoming)
Takata C (1960) The differentiation *in vitro* of the isolated endoderm in the presence of the neural fold in *Triturus pyrrhogaster*. Embryologia 5, 194-205.
Tucker A and Sharpe P (2004) The cutting-edge of mammalian development; how the embryo makes teeth. Nat Rev Genet 5, 499-508.
Van der heyden C and Huysseune A (2000) Dynamics of tooth formation and replacement in the zebrafish (*Danio rerio*) (Teleostei, Cyprinidae). Dev Dyn 219, 486-496.
Wilde CE (1955) The urodele neuroepithelium I. The differentiation in vitro of the cranial neural crest. J Exp Zool 130, 573-591.
Yu W et al. (2020) Pitx2-Sox2-Lef-1 interactions specify progenitor oral/dental epithelial cell signaling centers. Development 147, doi: 10.1242/dev.186023
Zhang Z et al. (2009) Antagonistic actions of Msx1 and Osr2 pattern mammalian teeth into a single row. Science 323, 1232-1234.

Figure legends

Figure 1. Distribution and composition of axolotl tooth fields.

(A) Dentition of axolotl larva (TL 19 mm) is composed of several tooth fields assembled into outer (premaxillary, dentary) and inner dental arcades (vomerine, palatine, coronoid) showing various field-specific arrangements. Fields of the outer arcade initially form a single tooth row and those of the inner arcade constitute tooth patches. (B, C) Separation of the mouth roof from the floor shows presence of the oldest tooth (arrow) and the addition of new tooth germs (arrowheads) within each field. (B) In the premaxillary field (pmx), new germs are added laterally and medially as the field stretches along the upper jaw, and new germs are also added posteriorly. Vomerine (vom) and palatine (pal) fields develop by addition of new germs medially from the laterally located oldest teeth. (C) In the dentary field (den), the oldest tooth is present close to the mandibular symphysis and new germs are added laterally along the lower jaw, thus forming the tooth row. New germs are further initiated lingually. In the coronoid (cor) field, the oldest tooth is located labially and new germs are added lingually in a hand fan-shaped manner. Scale bar equals 1 mm.

Figure 2. Expression patterns of* Pitx2 *and* Shh *at early stages of axolotl odontogenesis.

Expression patterns of early odontogenic markers *Pitx2* and *Shh* on the mouth roof and floor whole mounts show initial stages of development of axolotl dentition (in case of *Shh* expression the epithelium of the mouth roof was dissected from whole mounts to circumvent masking of the tooth-restricted epithelial signal by the strong *Shh* signal from the adjacent neural tube). At stages 37-41, *Pitx2* labels tooth-competent regions while *Shh* is restricted to individual tooth germs and into postero-medially placed odontogenic bands (visualized as strands of *Shh* expression demarcated by white arrowheads). Positions of tooth germs are visible as regions of lower *Pitx2* expression. (A, E, I, M) Expression pattern of *Pitx2* on the mouth roof is initially restricted to its anterior part but becomes broader at later stages (parentheses). (B, F, J, K) Focal expression of *Shh* illustrates sequential addition of tooth germs starting from the initiator-teeth of vomerine (vom) and palatine (pal) teeth (B, F, arrows). New tooth germs are added postero-medially in the palatine tooth field (J, black arrowheads) and antero-medially in the vomerine tooth field (N, black arrowheads). (C, G, K, O) Expression pattern of *Pitx2* on the mouth floor enlarges posteriorly throughout development and, at stages 40-41, the pattern separates into the prospective dentary (den) and coronoid (cor) tooth fields (K, O, parentheses). (D, H, L, P) Focal *Shh* expression on the mouth floor marks positions of initiator-teeth of the coronoid (D, H, arrows) and dentary fields (L, P, arrows) and the addition of new tooth germs within both tooth fields (H, L, P, black arrowheads). New tooth germs are added lingually to the initiator tooth germ in the coronoid tooth field (H, L, P, black arrowheads) and laterally from the medially positioned initiator tooth in the dentary tooth field (P, arrowheads). b1, first branchial arch; cor, coronoid tooth field; den, dentary tooth field; h, hyoid arch; m, mandibular arch; pal, palatine tooth field; vom, vomerine tooth field. Scale bar equals 500 μm.

Figure 3. Expression pattern of* Pitx2 *at later stages of axolotl odontogenesis.

Pitx2 expression becomes gradually restricted to individual tooth germs (arrows mark initiator-tooth germs of respective tooth fields and arrowheads mark sequentially added tooth germs). (A, C, E) Within the mouth roof epithelium, the initial *Pitx2* expression delineating individual tooth fields (black broken lines in A) becomes focused into individual tooth germs, inter-germ regions and the forming dental laminae of vomerine (vom) and palatine (pal) tooth fields (C and E). *Pitx2* expression is further associated with the developing premaxillary tooth field (pmx), although individual tooth germs cannot be discerned. (B, D, F) Within the mouth floor epithelium, strong *Pitx2* expression is visible in the developing tooth germs of dentary (den) and coronoid (cor) tooth fields. cor, coronoid tooth field; den, dentary tooth field; pal, palatine tooth field; pmx, premaxillary tooth field; vom, vomerine tooth field. Scale bars equal 500 μm (scale bar in B is valid for A and B, scale bar in F is valid for C-F).

Figure 4. Histological analysis of tooth addition within axolotl tooth fields.

Horizontal sections (left sides shown, anterior to the top) through individual tooth fields show positions of the respective initiator-tooth (black arrows) and the newly added successive tooth germs (black arrowheads) at stages of early addition (A-E) and later morphogenesis (F-J), when dental laminae are clearly discernible (demarcated by white arrowheads). (A) Premaxillary tooth field at stage of opened

mouth (st. 43) contains three tooth germs (arrowheads) that are added laterally and medially to the initiator-tooth (arrow). (B, C) Vomerine (vom) and palatine (pal) tooth fields at stage 42 are composed of laterally positioned initiator-teeth (arrow) and two adjacent medially positioned tooth germs (arrowheads). (D) Dentary tooth fields are each initiated from the initiator-tooth (arrows) developing close to the mandibular symphysis (s) and new tooth germs (arrowheads) are added laterally along the Meckel's cartilage (Mc). (E) Coronoid tooth field is composed of a patch of tooth germs (arrowheads) with the initiator-tooth present antero-laterally (arrow). (F) Premaxillary tooth field of a 14 mm larva shows arrangement into a tooth row. New tooth germs are added lingually from the dental lamina and, as the upper jaw grows, the premaxillary field expands by further addition of tooth germs at lateral and medial edges of the dental lamina (white arrowheads). (G, H) Vomerine and palatine tooth fields containing several teeth arranged into a tooth patch with new germs arising from the postero-medially positioned dental laminae (white arrowheads). Slight difference in composition exists between these tooth fields that can be ascribed due to the addition of first teeth antero-medially to the initiator-tooth (black arrow) in the vomerine field (B) and postero-medially in the palatine field (C), and to the subsequent development of new tooth germs from the medially placed dental laminae (white arrowheads). (I) Dentary tooth field is arranged into the tooth row. New tooth germs are added from the lingually positioned dental lamina and laterally (white arrowhead) due to expansion of the growing Meckel's cartilage (Mc). (J) Coronoid tooth field at a slightly older stage than that of (E) develops from the postero-medial dental lamina (white arrowheads). Scale bars equal 100 μm.

Figure 5. Distribution and epithelial derivation of teeth in the axolotl oral cavity.
(A, D) Whole mount larvae at st. 44 dissected at the jaw joint and stained by alizarin red demonstrate developing teeth assembled into premaxillary (pmx), vomerine (vom) and palatine (pal) tooth fields on the mouth roof (A), and into dentary (den) and coronoid (cor) tooth fields on the mouth floor (D). (B, C, E, F) Epithelial origin of teeth and schematic interpretation of germ-layer distribution in the axolotl oral cavity (note that only the basal epithelial layer is depicted; the apical layer of the oral epithelium is derived from endoderm). Black dots in C and F represent individual teeth, positions of initiator-teeth of each tooth field are labelled with black arrows. Teeth developing at the ecto-endoderm border are found in vomerine, palatine, dentary and coronoid tooth fields. ad, adenohypophysis; ch, choana (inner nostril); den, dentary teeth; ECT, ectoderm; END, endoderm; pal, palatine teeth; pmx, premaxillary teeth; cor, coronoid teeth; vom, vomerine teeth. Scale bar equals 1 mm.

Figure 6. Histological analysis of the epithelial origin of the axolotl teeth.
Histological analysis shows details of epithelial origin and modes of addition of teeth (marked by anti-calbindin antibody) within the tooth fields. Arrows mark initiator-tooth germs in each tooth field, arrowheads mark sequentially added tooth germs, yellow arrow/arrowhead denotes tooth developing at the ecto-endoderm border, white arrow/arrowhead denotes tooth developing solely from either ectodermal or endodermal epithelium. (A) Sagittal section showing lateral-most palatine tooth developing at the ecto-endoderm border (yellow arrow) close to endoderm-derived coronoid tooth germs (white arrowheads). (B) Horizontal section through vomerine and palatine tooth fields. Two vomerine teeth develop in the ectodermal epithelium (white arrow and arrowhead) and one tooth germ is of ecto-endodermal origin (yellow arrowhead). Palatine tooth field is composed of one ecto-endodermal tooth germ laterally (yellow arrow) and two endodermal germs (white arrowheads) medially. Note the just-arising dental laminae (broken lines) that are of endodermal origin in case of the palatine field and ecto-endodermal origin in case of the vomerine field. (C) Horizontal section of later stage vomerine and palatine tooth fields showing ecto-endodermal germ in each vomerine and palatine fields (yellow arrow and arrowhead) next to other ectodermal vomerine teeth and endodermal palatine teeth (white arrowheads). Dental laminae (broken lines) are of ecto-endodermal origin in vomerine field and endodermal origin in palatine field. (D) Sagittal section medial to that shown in (A) depicting ecto-endodermal coronoid tooth (yellow arrow), which develops at the level of other tooth germs of vomerine, palatine and coronoid tooth fields (white arrow and arrowheads). (E) Horizontal section showing ecto-endodermal teeth developing medially in the dentary tooth field (yellow arrows) next to other ectodermal teeth of dentary and premaxillary fields and endodermal teeth of the coronoid field (white arrowheads). den, dentary teeth; pal, palatine teeth; pmx, premaxillary teeth; cor, coronoid teeth; s, symphysis; vom, vomerine teeth. Scale bar equals 50 μm.

Figure 7. Relations between the germ-layer distribution and patterning of the axolotl dentition.
During the course of the axolotl mouth development, oral ectoderm and endoderm do not form a sharp border, but instead the basal layer of oral ectoderm involutes to constitute the basal layer of the nascent oral epithelium while the solid endoderm forms the apical layer (A-D). As a result, the ecto-endodermal border within the basal layer of the mouth roof (black arrowhead) and floor (grey arrowhead) is different from that within the apical layer. The broken line in A-C shows the place of the future mouth cavity. Tooth-competent zones become established in the basal epithelial layer of the mouth roof and floor (blue regions in E, F, J, K) and later become separated into the prospective tooth fields (blue regions in G, H, L, M). Tooth germs arise progressively during the process of this separation. Orange circles mark the positions of the initiator-teeth of each prospective tooth field and yellow circles denote positions of successively added tooth germs. Yellow regions mark positions of odontogenic bands at earlier stages (E, F, J, K) and dental laminae at later stages (G, H, L, M). Green and magenta regions show the extent of oral ectoderm and endoderm, respectively. Only the basal epithelial layer, i.e. the tooth-forming layer of the double-layered epithelium is depicted (the black and grey arrowheads in E and J correspond to those in A-D). First tooth germs of vomerine (V), palatine (P) and coronoid (C) tooth fields appear prior to those of the premaxillary (Pm) and dentary (D) tooth fields. The initiator-teeth of palatine, coronoid and dentary tooth fields stereotypically arise at the boundary of ectoderm (green) and endoderm (magenta) (orange circles in F, K, L), while the initiator-teeth of the premaxillary and vomerine tooth fields arise from ectoderm (orange circles in E, G). The successive tooth germs arise from ectoderm in case of premaxillary and dentary tooth fields, from endoderm in case of palatine and coronoid tooth fields and from ectoderm or ecto-endoderm in case of vomerine tooth fields (F, G, H, K, L, M). These early events in oro- and odontogenesis lead to the salamander-specific distribution of teeth on the bones of the upper and lower jaws and on the palate (I, N). Orange teeth in I and N represent the initiator-teeth of each tooth field. Figures I and N are schematized Figures 1B and C, respectively. den, dentary; pal, palatine; pmx, premaxillary; cor, coronoid; vom, vomerine.

Supplementary figure 1. Expression of selected genes during axolotl odontogenesis
(A-D) Expression of *Bmp2* and *Bmp7* demarks positions of individual initiator-tooth germs of each nascent tooth field (arrows) and positions of successive tooth germs (arrowheads) in a pattern similar to that of *Shh* (see Fig. 2). (E, F) Expression of *Dlx3*, on the other hand, delineates positions of tooth fields (black broken lines) similarly to that of *Pitx2* (see Fig. 2). (G, H) *Dlx5* transcripts are restricted to the developing tooth germs besides their presence at other craniofacial regions. cor, coronoid field; den, dentary field; pal, palatine field; pmx, premaxillary field; vom, vomerine field. Scale bar equals 500 μm.

Supplementary figure 2. 3D models of the developing axolotl dentition based on serial sagittal sections hybridized with the* Pitx2 *probe.
The models visualize the shape and relationship of *Pitx2*-expressing areas aka tooth competent zones and tooth fields. During the course of embryonic development, the initially compact tooth-competent zones on the mouth roof and floor (st. 38) become compartmentalized into individual tooth fields. The models were reconstructed based on the complete series of sagittal sections hybridized with a *Pitx2* probe (left column, solid lines mark the basement membrane of the oropharyngeal epithelia, broken lines mark the place of future oropharyngeal opening). Mouth roof expression is in red color, mouth floor expression in blue color, basal epithelial layer of the oral epithelium in grey color and cyan dots demark positions of tooth germs. ad, adenohypophysis; cor, coronoid field; den, dentary field; n, nasal cavity; pal, palatine field; pmx, premaxillary field; vom, vomerine field. Scale bar equals 100 μm.

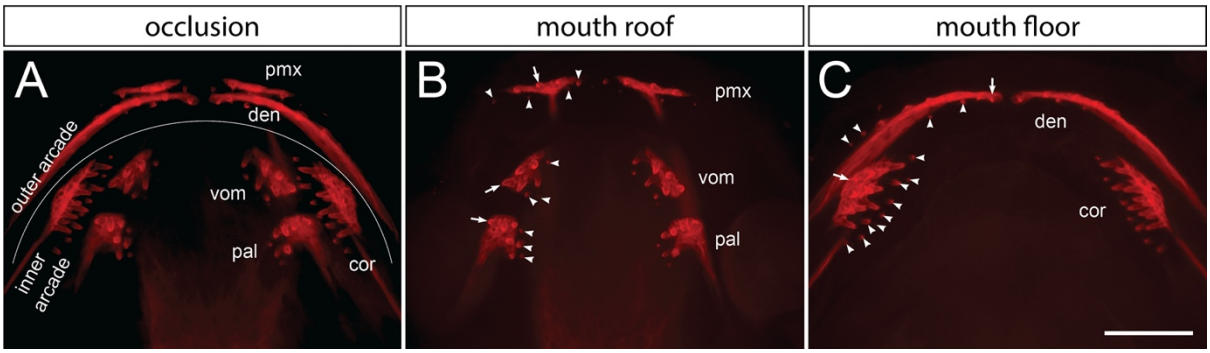
occlusion
mouth roof
mouth floor
A
pmx
den
outer arcade
vom
pal
cor
inner arcade
B
pmx
vom
pal
C
den
cor
Fig. 1

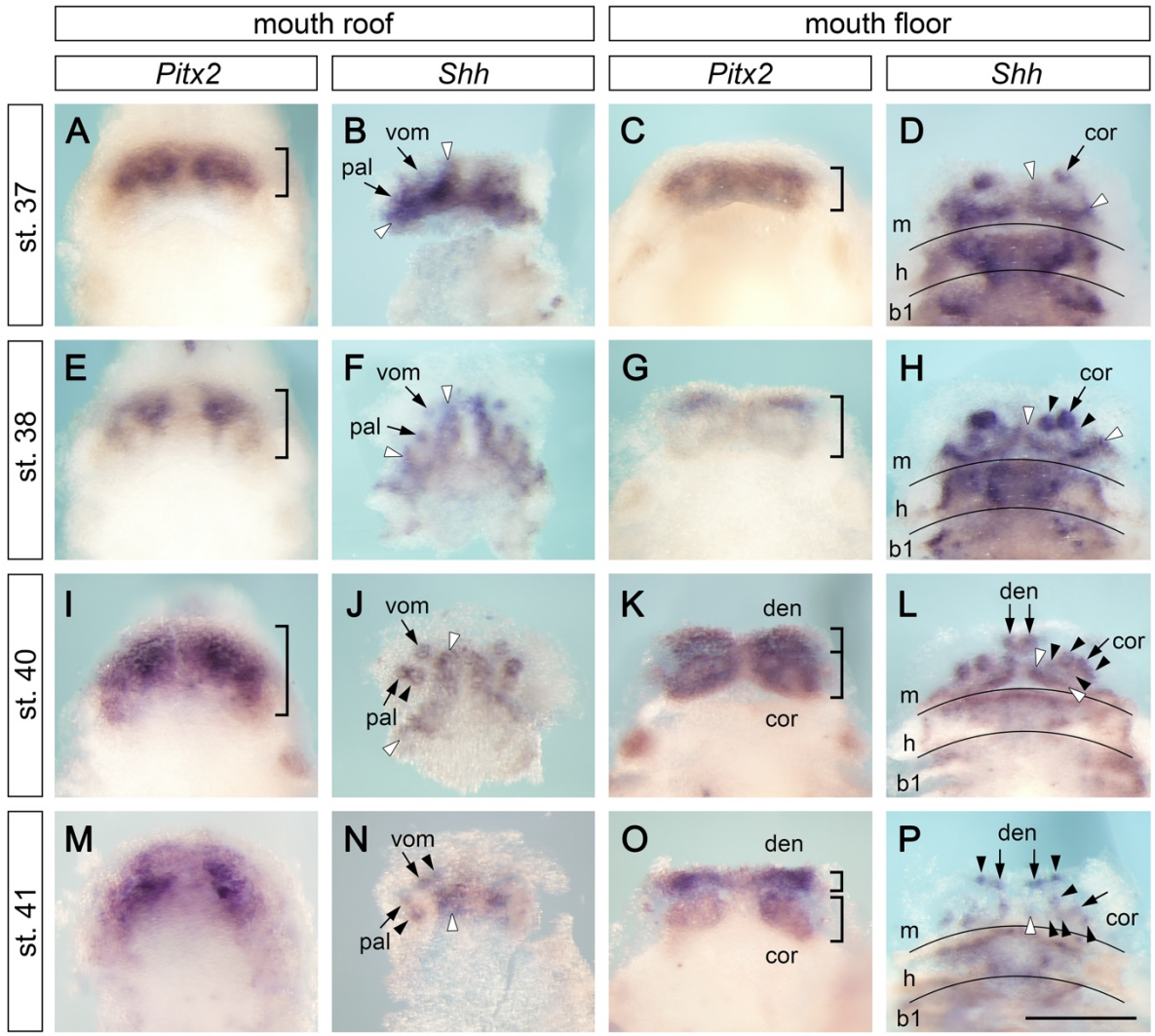
mouth roof
mouth floor
Pitx2
Shh
Pitx2
Shh
st. 37
st. 38
st. 40
st. 41
A
B
vom
pal
C
D
cor
m
h
b1
E
F
vom
pal
G
H
cor
m
h
b1
I
J
vom
pal
K
den
cor
L
den
cor
m
h
b1
M
N
vom
pal
O
den
cor
P
den
cor
m
h
b1

Fig. 2

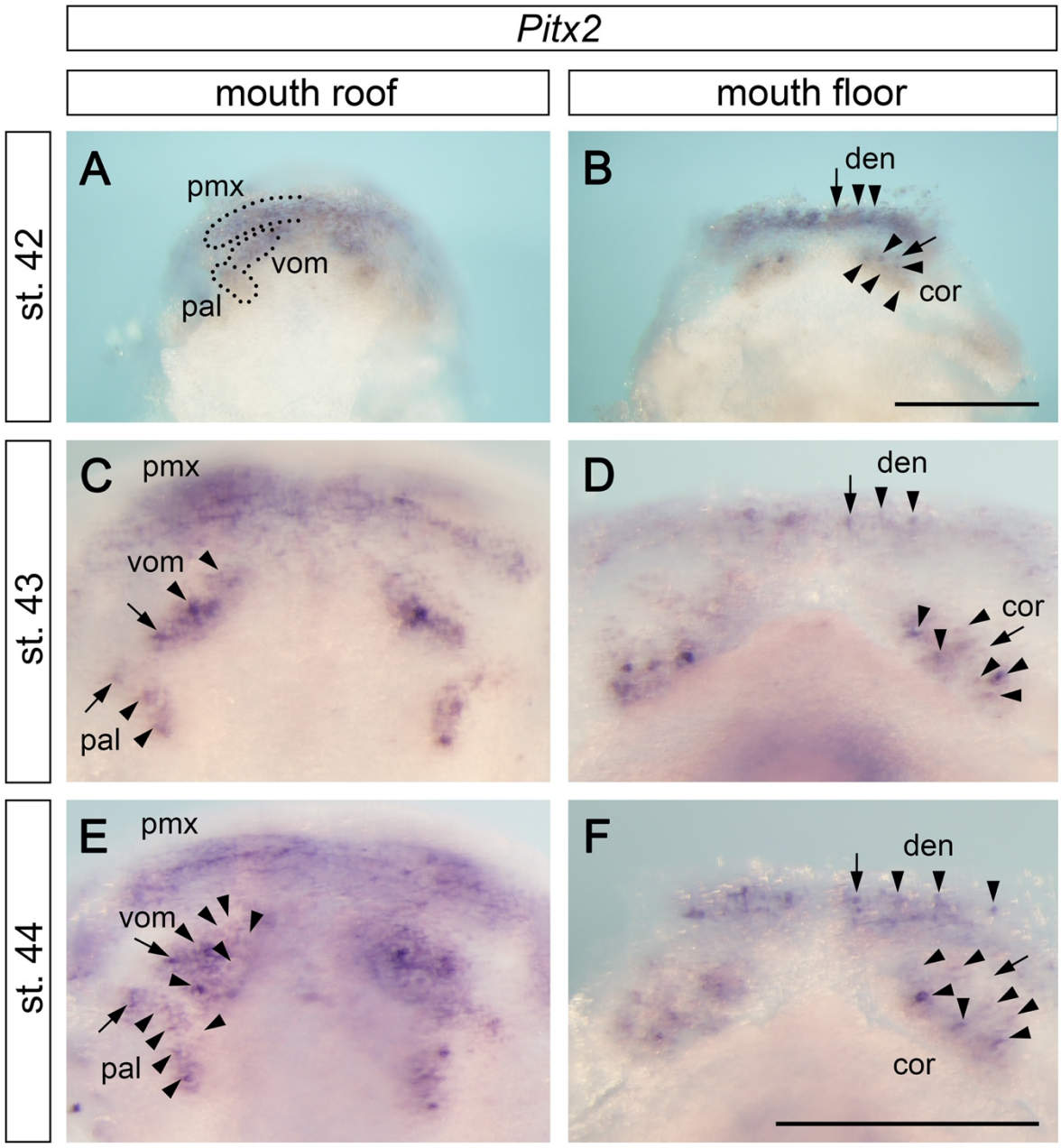
Pitx2
mouth roof
mouth floor
st. 42
st. 43
st. 44
A
pmx
vom
pal
B
den
cor
C
pmx
vom
pal
D
den
cor
E
pmx
vom
pal
F
den
cor

Fig. 3

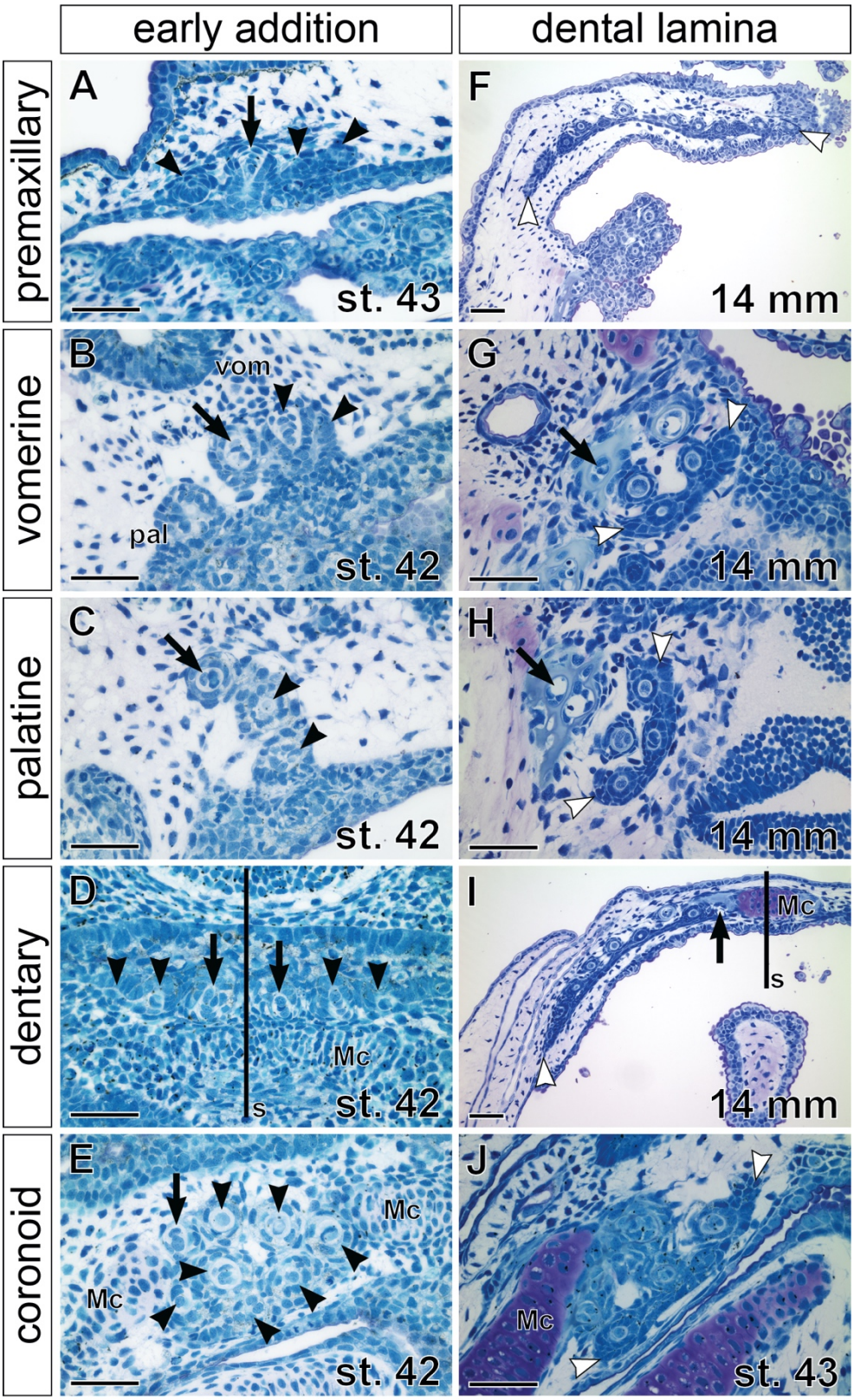
early addition
dental lamina
premaxillary
vomerine
palatine
dentary
coronoid
A
st. 43
F
14 mm
B
vom
pal
st. 42
G
14 mm
C
st. 42
H
14 mm
D
Mc
s
st. 42
I
Mc
s
14 mm
E
Mc
Mc
st. 42
J
Mc
st. 43

Fig. 4

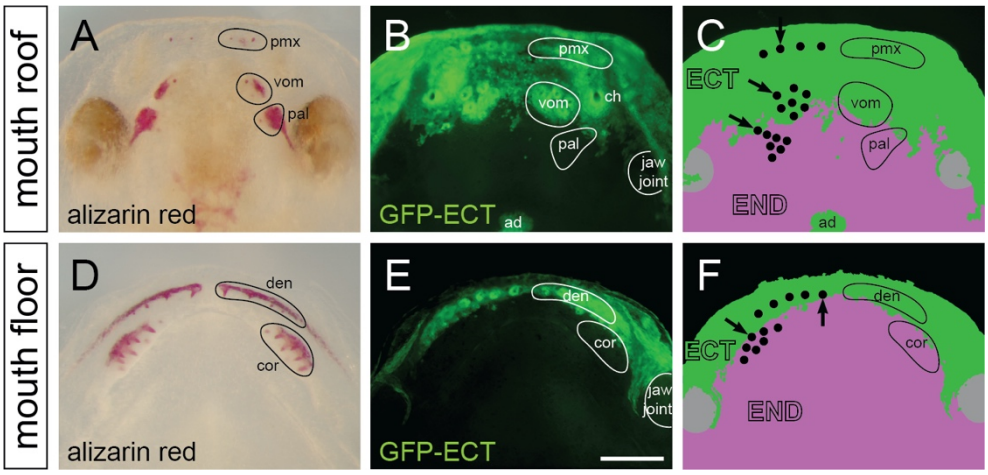
mouth roof
mouth floor
A
pmx
vom
pal
alizarin red
B
pmx
vom
ch
pal
jaw joint
GFP-ECT
ad
C
ECT
pmx
vom
pal
END
ad
D
den
cor
alizarin red
E
den
cor
jaw joint
GFP-ECT
F
ECT
den
cor
END
Fig. 5

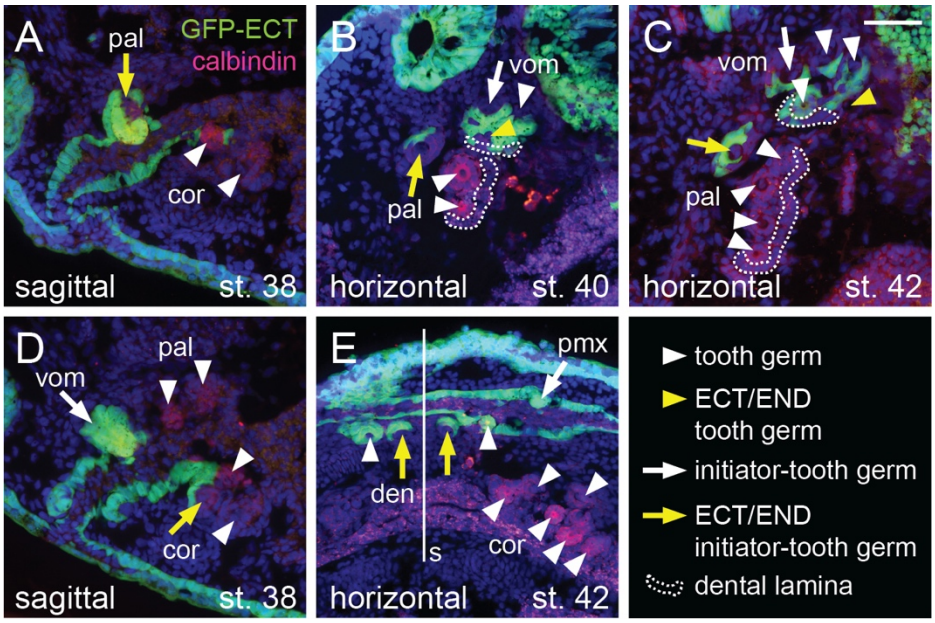
A
pal
GFP-ECT
calbindin
cor
sagittal
st. 38
B
vom
pal
horizontal
st. 40
C
vom
pal
horizontal
st. 42
D
vom
pal
cor
sagittal
st. 38
E
pmx
den
s
cor
horizontal
st. 42
tooth germ
ECT/END
tooth germ
initiator-tooth germ
ECT/END
initiator-tooth germ
dental lamina

Fig. 6

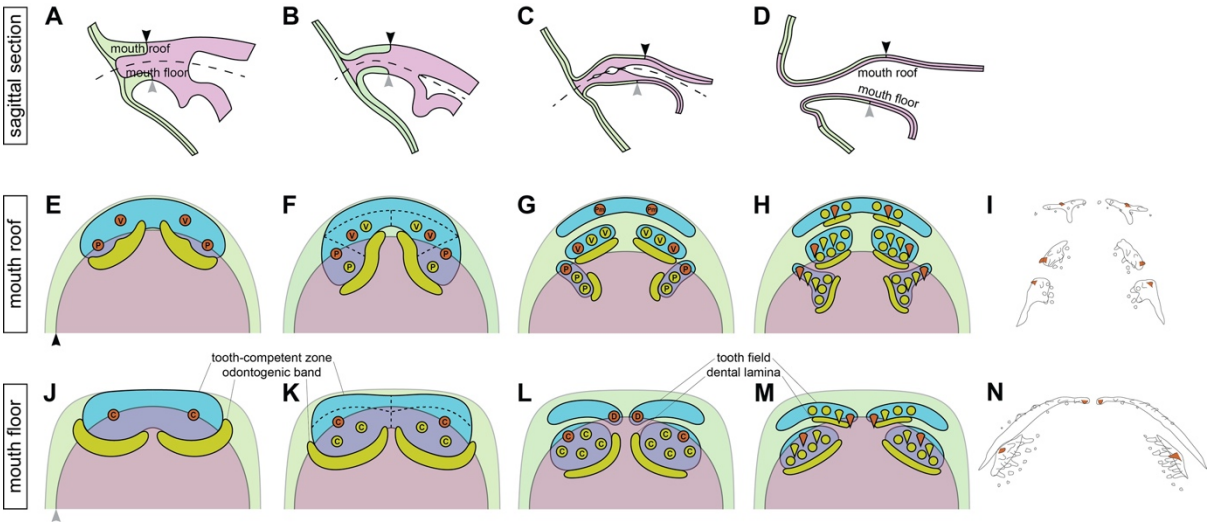
sagittal section
mouth roof
mouth floor
A
B
C
D
mouth roof
mouth floor
mouth roof
E
F
G
H
I
tooth-competent zone
odontogenic band
tooth field
dental lamina
mouth floor
J
K
L
M
N

Fig. 7

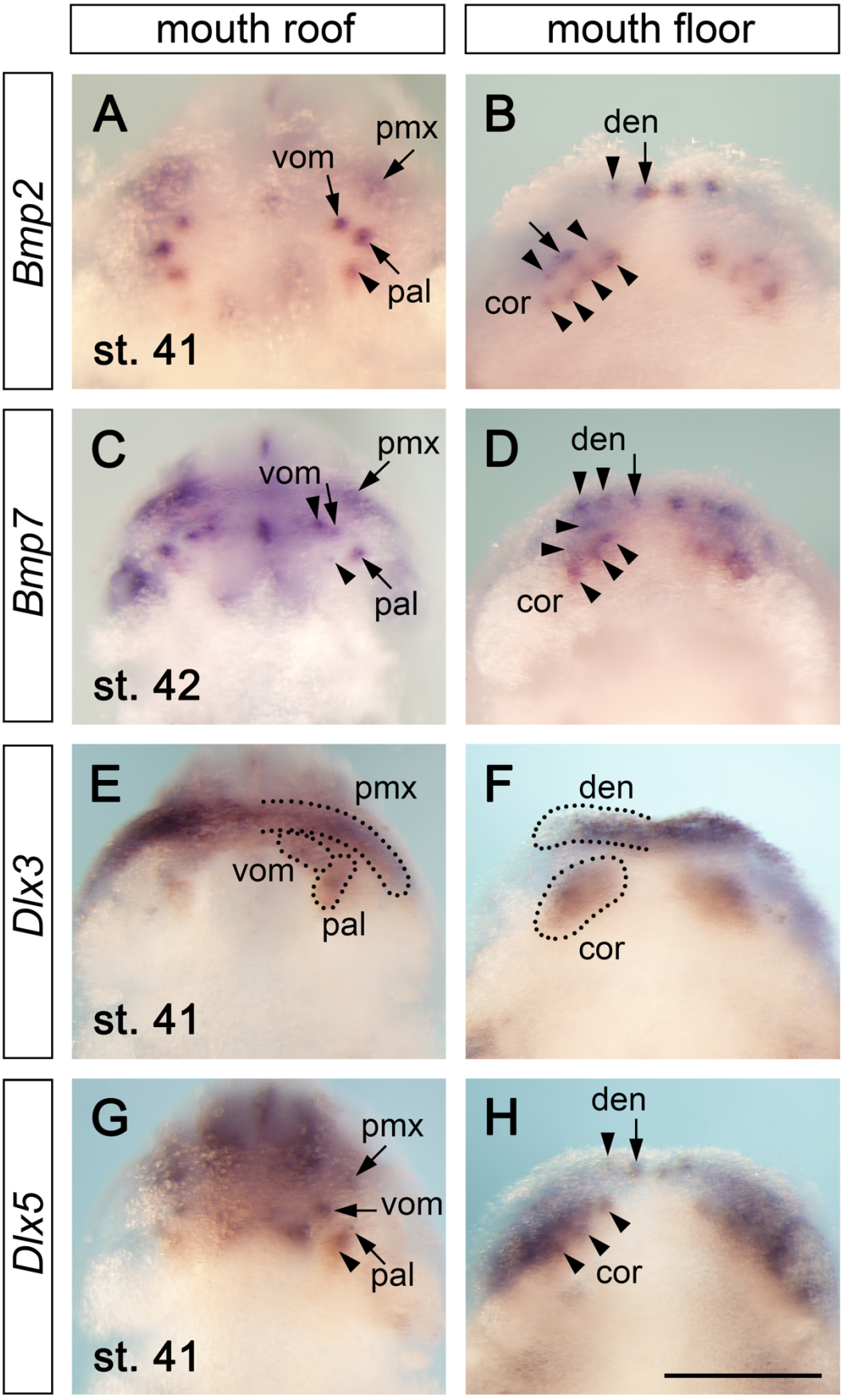
mouth roof
mouth floor
Bmp2
Bmp7
Dlx3
Dlx5
A
B
C
D
E
F
G
H
pmx
vom
pal
den
cor
st. 41
st. 42

Fig. S1

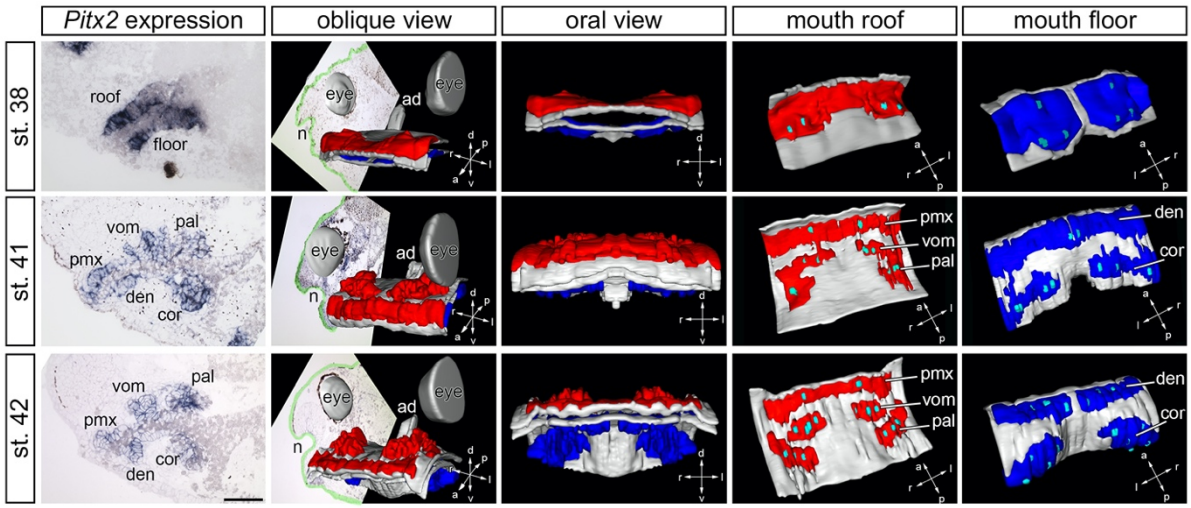
Pitx2 expression
oblique view
oral view
mouth roof
mouth floor
st. 38
st. 41
st. 42
roof
floor
vom
pal
pmx
den
cor
eye
ad
n
d
p
l
r
a
v
pmx
vom
pal
den
cor

Fig. S2

VII. **Pospisilova A**, Stundl J, Brejcha J, Metscher BD, Psenicka M, Cerny R & Soukup V (in prep) The dentition is a highly dynamic organ system during the sterlet sturgeon ontogeny (*Acipenser ruthenus*).

The dentition is a highly dynamic organ system during the sterlet sturgeon ontogeny (*Acipenser ruthenus*)

Anna Pospisilova[1], Jan Stundl[1,2], Jindrich Brejcha[3], Brian D. Metscher[4], Martin Psenicka[5], Robert Cerny[1], Vladimír Soukup[1]*

[1] Department of Zoology, Faculty of Science, Charles University, Prague, Czech Republic
[2] California Institute of Technology, Pasadena, California, USA
[3] Department of Philosophy and History of Science, Faculty of Science, Charles University, Prague, Czech Republic
[4] Department of Theoretical Biology, University of Vienna, Vienna, Austria
[5] South Bohemian Research Center of Aquaculture and Biodiversity of Hydrocenoses, Vodňany, Research Institute of Fish Culture and Hydrobiology, Faculty of Fisheries and Protection of Waters, University of South Bohemia, České Budějovice, Czech Republic

* Author of correspondence:
Vladimír Soukup
e-mail: soukup@natur.cuni.cz

Keywords
sterlet sturgeon, dentition, tooth development, initiation, patterning, loss

Abstract

Introduction

Teeth are among the key vertebrate innovations and, implicitly, evolutionary history of dentitions is a topic of longstanding discussions of paleontology and evo-devo research (Chen et al. 2015, Fraser et al. 2009, Qu et al. 2013 PLoS, Qu et al. 2015, Rücklin et al. 2014, Vaskaninova et al. 2020). Many dental features are proposed to have evolved at the stem and base of the gnathostome phylogeny comprising differences in tooth replacement between the two extant gnathostome lineages, the cartilaginous (chondrichthyans) and bony fishes (osteichthyans) (Chen et al. 2015). While cartilaginous fishes usually replace teeth embedded in oral mucosa through rapid exchange in a conveyor belt-like manner, those of bony fishes replace teeth through the resorption of tooth bases.

Among the bony fishes that represent the vast majority of extant vertebrates, several ray-finned fish species have become models of dental research, including the zebrafish *Danio rerio*, the medaka *Oryzias latipes*, the tetra *Astyanax mexicanus* or the stickleback *Gasterosteus oculatus* (e.g. Atukorala & Franz-Odendaal 2014, Ellis et al. 2016, Abduweli et al. 2014, Kague et al. 2018, Aigler et al. 2013). All these species represent derived teleosts with specialized dentitions and teeth allocated to oral and/or pharyngeal jaws. However, to address questions regarding various aspects of the evolutionary history of vertebrate dentitions, information from non-teleost ray-finned fish clades, such as polypteriforms (bichirs and reedfish), acipenseriforms (sturgeons and paddlefish) and holosteans (gars and bowfin), is indispensable. Despite the topicality, current knowledge on odontogenesis in these earliest-diverging extant ray-finned fish taxa is insufficiently limited to only a few reports.

Dentitions of many extant ray-finned fish species are characterized by tooth replacement with the absence of a deep epithelial invagination, the dental lamina. Instead, each new replacement tooth is initiated directly from the outer dental epithelium of the predecessor tooth. This type of tooth replacement occurs in bichir, paddlefish and salmon and seems to be an ancestral feature of ray-finned fish and teleost dentitions (Vandenplas et al. 2014, Vandenplas et al. 2016, Smith et al. 2015). Apart from this feature, dentitions of non-teleost ray-finned fish lineages display variable distribution of teeth throughout the oropharyngeal cavity. For example, bichir develops teeth in the mouth, on the palate and on every element of each branchial arch (Clemen et al. 1998, Wacker et al., 2001). This condition is

conserved also in other early diverging osteichthyans such as *Eusthenopteron* or *Latimeria* (Nelson 1969, Jarvik 1996), and is supposedly ancestral to all osteichthyans (Chen et al. 2015, Fraser et al. 2009, Smith & Coates 1998, Donoghue 2002). On the other hand, teeth of the acipenseriform sturgeon and paddlefish are restricted to oral margins, palate, and anterior pharyngeal regions (Smith et al. 2016, Warth et al. 2017, Jollie 1980). According to Nelson (1969), the distribution of tooth fields may invoke retainment of a certain phylogenetic information and traits that are present in individual lineages could bear information on the evolutionary translocation of the dentition within the oropharyngeal cavity. Given that the main prey-processing organ system in bichir is the oral apparatus (Clemen et al. 1998) and that, on the contrary, many teleosts process food on their pharyngeal jaws, sturgeons could, according to this premise, exhibit a transitory state. Acipenseriforms may thus be crucial for the understanding of the evolutionary translocation of the dental potential within the oropharynx from oral jaw-oriented prey-seizing fishes (such as bichirs) to pharyngeal jaw-oriented prey-processing fishes (such as modern teleosts).

The two acipenseriform orders, acipenserids and polyodontids, share many oral and dental features, comprising the specific placement of dental fields and the eventual tooth loss. In acipenserids, teeth are lost in a gradual manner throughout ontogeny (Bemis et al. 1997, Hilton et al. 2011), while teeth of polyodontids are, to a large extent, overgrown by the surrounding bone (Smith et al. 2015, Grande & Bemis 1991). In both orders, however, the eventually non-functional dentition is compensated for by the development of other structures within the oropharyngeal apparatus. The polyodontid paddlefish replaces the once functional dentition by prolonged gill rakers to establish efficient filtration apparatus (Imms 1904) and the acipenserids such as *Acipenser oxyrhynchus* or *Scaphirhynchus platorynchus* replace their dentition with evertible jaws and grinding ridges (Nelson 1969).

Prior to the eventual loss, however, the larval dentition of both polyodontids and acipenserids is composed of several tooth fields distributed over oral, palatal and anterior pharyngeal regions (Smith et al. 2015, Warth et al. 2017). In paddlefish, the dentary and dermopalatine tooth fields located at the jaw margins are initiated as single rows of tooth germs among which new germs are added (Smith et al. 2015). Similar alternate fashion of tooth addition and replacement is present also at palatopterygoid and first infrapharyngobranchial positions on the oropharyngeal roof, and on the first and second hypobranchial positions on the floor. In acipenserids, this arrangement seems to be preserved (Warth et al. 2017, Bemis & Grande 1997), although a thorough description of tooth composition throughout the sturgeon ontogeny is awaited.

To overcome the current lack of information on tooth addition and replacement at the base of the bony fish phylogeny, we present here the sterlet as an emerging system for the study of various aspects of odontogenesis, relevant for both the explanation of ancestral states of odontogenesis and specializations concerning allocation of tooth fields to certain oropharyngeal regions or mechanisms of tooth loss. We intend to provide a thorough description of odontogenesis throughout the ontogeny of the sterlet sturgeon (*Acipenser ruthenus*), from the earliest stages of initiation through replacement to loss of teeth, in order to provide a standpoint for direct comparison between acipenserid and polyodontid dentitions and for further studies dealing with various aspects of vertebrate odontogenesis.

Methods

Embryo collection and handling

The analyzed material includes a developmental series of the sterlet *Acipenser ruthenus* Linnaeus, 1758, obtained at the Research Institute of Fish Culture and Hydrobiology, Faculty of Fisheries and Protection of Waters of the University of South Bohemia in Ceske Budejovice, Czech Republic. Fertilized eggs were transported and reared at the Department of Zoology, Faculty of Science, Charles University, Prague, Czech Republic. The rearing procedures followed the guidelines of the institutional animal care and use committee of the Charles University in Prague. Embryos were transferred to well-oxygenated tanks and kept at 17 °C in the E2 Pen/Strep zebrafish embryo medium until the desired size was reached. Larval and juvenile specimens at appropriate stages were anesthetized by an overdose of MS-222 (Serva) and fixed in 4% PFA. Specimens for in situ hybridization were fixed in 4% PFA overnight and stored in 100% methanol at −20 °C until further processed. Individuals were staged according to total length (TL, measured after the fixation).

In situ hybridization
Partial sequences of candidate genes were amplified from cDNA using specific primers (*Pitx2* forward 5'-ATGCAGCCCTACGAAGACAT-3', reverse 5'-ATTTAGGTGACACTATAGTGGAGTTGCAAGTGTCCCTA-3', *Shh* forward 5'-GCBATYTCDGTRATGAACCA-3', reverse 5'-CARSRSSYTGGAGTACCAGT-3') and cloned into pGEM T-Easy vector (Promega) to synthesize probes for in situ hybridization. Whole-mount in situ hybridization was performed as previously described (Minarik et al. 2017). Whole-mount photomicrographs were taken as Z-stacks processed through maximum-projection function in the QuickPhoto Micro software using the Olympus SZX12 motorized dissecting microscope.

Alizarin red staining
Visualization of mineralized tissues of the majority of the presented specimens was performed using the bone staining protocol described in Rizzato et al. (2020). Besides these, the 286 mm TL specimen long-term fixed in formalin was washed by the tap water and prepared using dermestid beetles for two days under observation. Following preparation, the mineralized tissue was visualized by classical Alizarin red staining. Alizarin red brightfield or epifluorescent images (Connolly & Yelick 2010) were taken as Z-stacks using Zeiss SteREO Lumar.V12 dissecting microscope and processed through maximum-projection function in ZEN software.

Paraffin histology
Specimens were rinsed in distilled water and then placed in neutral 12.5% EDTA (ethylenediaminetetraacetic acid), pH 7.0 to soften the skeletal tissues before sectioning. Decalcification took place over 24 h for smaller fish and 4 days for larger fish. Subsequently, the specimens were rinsed in distilled water, dehydrated in a graded series of ethanol and cleared in xylene. Specimens were then embedded in paraffin and sectioned using a microtome (Leica RM2155) at the thickness of 10-12 μm. Sagittal sections were stained with Mayer's Hematoxylin & Eosin or against TRAP (see below).

Demonstration of hard tissue resorption
Hard tissue resorption was identified on whole-mount and sectioned samples using staining against TRAP (tartrate-resistant acid phosphatase) adapted from the published protocol (Witten & Villwock 1997). First, specimens were rehydrated and washed in distilled water. The specimens were then incubated at 37°C in the dark in a TRAP substrate detection solution composed of (i) 0.2 M acetate buffer (0.2 M acetic acid and 0.2 M sodium acetate) with 100 mM sodium tartrate dibasic dihydrate, (ii) 6% substrate solution (2 mM naphthol-AS-TR-phosphate in N,N-dimethylformamide) and (iii) Fast Red TR Salt (60 mg/100 ml). Incubation lasted one hour in case of sections and three hours in case of whole-mount specimens. After TRAP staining, the slides were washed in tap water and briefly counterstained with Mayer's Hematoxylin. The whole-mount specimens were washed in distilled water and subsequently bleached in 3% hydrogen peroxide in 0.5% KOH [1:4]. Samples were transferred into 100% glycerol and photographed.

MicroCT visualization
Selected larvae were mounted in 1% agar in 1000 μl pipette tip and scanned using MicroXCT (X-Radia) at the Department of Theoretical Biology, University of Vienna. Images were reconstructed in XMReconstructor (X-Radia) and analyzed in Amira (FEI Software).

Results

Sterlet dentition consists of several tooth fields distributed over the oropharyngeal cavity
Teeth of the sterlet dentition are allocated to several tooth fields distributed within the oropharyngeal cavity (Fig. 1A, B). At the jaw margins, teeth are present on the anterior portion of the dermopalatine bone dorsally and on the symphyseal portion of the dentary bone ventrally. Both dermopalatine and dentary tooth fields are composed of several teeth arranged into a single tooth row (monostichous arrangement, Fig. 1C, F). On the palate, a single tooth field is present on the antero-median portion (pars autopalatina) of the palatopterygoid bone and consists of several functional tooth rows

(polystichous arrangement, Fig. 1D). At anterior pharyngeal positions, tooth fields are associated with pharyngeal cartilages, namely first infrapharyngobranchial dorsally and first and second hypobranchials ventrally, and form polystichous patches of teeth interconnected with a bone of attachment (Fig. 1E, G). Individual tooth fields represent dynamic organ systems that pass through several developmental states. The teeth on the jaw margins become functional only for a limited time period and are not replaced after shedding. In contrast, other dentate fields undergo periods of initiation, addition of new tooth germs, active tooth cycling characterized by resorption and shedding of the oldest teeth and their simultaneous replacement, followed by the cessation of tooth replacement and the complete loss of the respective field. Replacement teeth at all positions develop from the superficial epithelium without the presence of the dental lamina (Fig. 1H-L). The newly formed tooth germ develops in the adjacent epithelium with the tooth cone lying parallel to the oropharyngeal epithelium (Fig. 1G, H, M, N, white arrowhead). Replacement occurs typically from behind, although in case of the palatopterygoid field, replacement teeth are added labially (Fig. 1J). To better understand aspects of development of the sterlet dentition, we divided the ontogeny of the tooth fields into several periods.

Expression of odontogenic genes denotes positions of tooth fields and initiating tooth germs

To describe the earliest events and the sequence of appearance of tooth fields during the sterlet odontogenesis, we followed expression of *pitx2* and *shh,* two genes generally expressed in the future dental epithelium and responsible for the differentiation of the oral epithelium towards a dental fate (Dassule et al. 2000, Cobourne et al. 2004, Jackman et al. 2010, Yu et al. 2020). Concordantly with the situation found in axolotl (Soukup et al. in prep), *pitx2* in the sterlet is expressed broadly at positions of future tooth fields and only later becomes expressed focally in the developing tooth germs. *shh*, on the other hand, shows focal tooth germ-specific expression at much earlier stages.

The first *pitx2* expression is present just before hatching (Fig. S1A) as diffuse bands surrounding the future mouth opening. These bands are allocated to the prospective upper and lower jaws from stage 35 to stage 37 and represent odontogenic bands of the dermopalatine and dentary tooth fields (Fig. S1B-D). Concordantly, the first *shh* expression is observed in the prospective mouth area in the form of bands running along the future jaw margins (Fig. S1E-G), and starting from stage 38 (TL 10 mm), *shh* becomes expressed focally in the developing dermopalatine and dentary tooth germs (Fig. S1H). After dissecting the embryonic heads at the level of the jaw joint, the *pitx2* expression associated with the prospective dermopalatine and dentary tooth fields at TL 10 mm (Fig. 2A, F) becomes supplemented with the *pitx2* expression domains of the palatopterygoid and hypobranchial 1 tooth fields at TL 11 mm (Fig. 2B, G) and the infrapharyngobranchial tooth field at TL 12 mm (Fig. 2C). During this time period, *shh* shows focal expression in individual tooth germs that co-localizes with the broader *pitx2* expression domains and no focal *shh* expression is present outside of the *pitx2* expression domains. Sometimes, focal loci of lower expression are found within the *pitx2* domains that correspond to the focal presence of *shh* transcripts and the positions of tooth germs. The order of appearance of individual tooth germs (determined by the focal *shh* expression) follows the order of appearance of the tooth field-related *pitx2* expression domains (Fig. 2K-M, P-R). Namely, individual tooth loci appear first in the dermopalatine and dentary fields at 10 mm (Fig. 2K, P), hypobranchial 1 at TL 11 mm (Fig. 2Q) and palatopterygoid and infrapharyngobranchial at 12 mm (Fig. 2M). New tooth germs are then added adjacent to the initiator-tooth in medial and lateral directions (Fig. 2K-T, black arrows and arrowheads) thus forming first tooth rows in each tooth field. At the same time, these initial tooth rows are surrounded by new *shh* expressing bands (Fig. 2N, S, asterisks) that become compartmentalized into foci of *shh* expression (Fig. 2O, T, asterisks). These foci will give rise to taste bud rows encircling each of the prospective tooth fields.

Skeletal preparations show establishment of the fully functional dentition

A series of skeletal preparations shows that the initial mineralization of the marginal teeth (dermopalatine and dentary teeth) commences at about TL 13 mm (Fig. 3A, A') and those of the more posterior teeth (palatopterygoid, infrapharyngobranchial and hypobranchial 1) slightly later at TL 14 mm (Fig. 3C, D). First teeth on hypobranchial 2 become visible even much later, no earlier than at TL 23 mm (Fig. 3H).

In the larvae, dermopalatine teeth are arranged into a single row that opposes the single-rowed teeth on the dentary (Fig. 3B). Typically, four to six teeth are present in each dentary and dermopalatine

element. The sequence of mineralization of teeth in the dentary field begins with the position 2 followed by positions 1 and 3 (Fig. 3A, arrow and arrowheads) and subsequent positions 4, 5 and 6 later on. At the same time, first signs of mineralization are visible also in the dermopalatine field (Fig. 3A, arrows). In a slightly older embryo, these tooth fields show further addition of tooth germs laterally to form tooth rows along the jaw length (Fig. 3A'). Interestingly, the sequence of tooth mineralization is rather random in the dermopalatine tooth field. At around TL 14 mm, the teeth become ankylosed to the ossifying dermopalatine and dentary bones (Fig. 3B-D). After setting up the definite number of teeth in these tooth fields, no further germs are added either at the ends of the tooth rows, or among individual teeth and, unlike in *Polyodon* (Smith et al. 2016), no replacement teeth are initiated.

The palatopterygoid bones become ossified at roughly the same time as the dermopalatine and dentary, and the first mineralization of tooth germs occurs also in the more posterior regions (palatopterygoid, infrapharyngobranchial and hypobranchial 1) (Fig. 3C, D). Three teeth are present in each of these posterior tooth fields. The first three mineralized teeth of the palatopterygoid field are arranged into a row (Fig. 3C). Soon after that, however, addition of new germs changes the arrangement from a tooth row into a tooth patch consisting of two to three functional tooth rows (polystichous arrangement) (Fig. 3E). The labial presence of mineralized tips with unmineralized bases shows that new tooth germs of the palatopterygoid field are added from the anterior (Fig. 3E, black arrowhead), unlike all the other tooth fields (see later).

At pharyngeal regions (infrapharyngobranchial, hypobranchial 1 and 2) the teeth are joined among each other with their bones of attachment and form patches with multiple functional tooth rows. At TL 14 mm, the infrapharyngobranchial and hypobranchial 1 fields are composed of three tooth germs arranged into a triangle with the most developmentally advanced tooth, i.e. the initiator-tooth of the tooth field, placed anteriorly (Fig. 3C, D). During further development, the sequential addition of new teeth from posterior leads to a multi-rowed arrangement of these fields (Fig. 3E-H). Namely, new tooth germs are added slightly posterior and in between the already formed teeth leading to the alternate arrangement of tooth rows of the resulting tooth patch (Fig. 3H). During the initial sequential tooth addition, the newly formed teeth can form their own bone of attachment that is initially isolated from, and not joined to the rest of, the mineralized patch (Fig. 3E) and that will become joined to the rest of the field at later stages.

Of the posterior tooth fields, the hypobranchial 2 is the last field to appear during the sterlet ontogeny. It emerges as a single mineralized tooth germ at the time when the infrapharyngobranchial and hypobranchial 1 fields already show a multi-rowed arrangement (TL 24 mm, Fig. 3H). Interestingly, the time of appearance of the hypobranchial 2 field further correlates with the time when the hypobranchial 1 initiator-tooth is already shed, i.e. this field undergoes tooth cycling (Fig. 3H, arrow), and when the functional dermopalatine and dentary teeth start being shed (see below). This means that a simultaneous presence of all tooth fields in the sterlet oropharyngeal cavity spans only a short time window.

Marginal dentition is lost through the resorption of tooth bases

The sterlet dentition is a system where, at a certain time point, some tooth fields are functional while others are not necessarily present. The fully formed tooth fields at the jaw margins are represented by a row of four to six teeth per jaw quadrant that, unlike the more posterior tooth fields, do not undergo active tooth cycling. Tooth shedding in the dermopalatine and dentary fields is visible from TL 24 mm (Fig. 4E black arrowhead and 4G white arrowhead) and the teeth are completely lost by TL 35 mm (compare Figs. 4G, K, Suppl. tab. 1).

To follow the process of marginal tooth loss in detail, we analyzed hard tissue remodelling and matrix resorption by tracking the odontoclast activity using staining for the activity of the tartrate-resistant acid phosphatase (TRAP). The earliest detected TRAP signal is located in the labial portions of the bases of the dermopalatine and dentary teeth at TL 23 mm (Fig. 5C) and becomes widespread throughout these tooth fields by TL 28 mm (Fig. 5G, H).

Further, microCT visualizations show that the tooth loss results from breaking off of the tooth tip (Fig. 5B, white arrow), followed by the demineralization of the tooth base and the eventual shedding of the tooth. Traces of tooth sockets on dermopalatine and dentary bones represent the only remnants of lost teeth and since then the jaw bone surfaces exhibit a wrinkled appearance (Fig. 4G, K and 5A, B).

Interestingly, the loss of the dermopalatine and dentary teeth is associated with the progressive appearance of the hypobranchial 2 field (from TL 23 mm). This concurrence likely reflects a posterior functional translocation of the dentition from the jaw margins to the anterior pharyngeal regions.

Posterior tooth fields undergo active tooth cycling

The palatopterygoid and all pharyngeal tooth fields show active tooth cycling via rapid replacement of the shed teeth. New teeth are added posteriorly in the infrapharyngobranchial, hypobranchial 1 and hypobranchial 2 fields (Fig. 4B, D, L white arrowheads) and anteriorly in the palatopterygoid field (Fig. 4A white arrowheads). The used teeth are shed on the opposite side of the respective field (Fig. 4, black arrowheads). Concordantly, the hard tissue resorption associated with tooth shedding (as estimated from the presence of the TRAP activity) occurs at the bases of the anterior teeth of the infrapharyngobranchial and hypobranchial 1 fields and posterior teeth of the palatopterygoid field (Fig. 5D-F). The TRAP activity is observed from TL 23 mm (Fig. 5C-F) but becomes widespread and pronounced within the tooth fields later on (Fig. 5G, H). The TRAP activity thus denotes remodelling of the tooth fields during the period of active tooth cycling.

In association with the tooth cycling period, the shape of the tooth fields changes over time. For example, within the palatopterygoid field, the addition of new tooth germs (Fig. 4I, white arrowhead) leads to a medially extended portion of this field (Fig. 6D, white arrowhead). Furthermore, the pharyngeal fields initially forming medio-laterally narrow tooth clusters transform into wide crescent-shaped tooth bands consisting of three to four tooth rows (cf. Fig. 4B, D with 4F, H and 4J, L). This shape change and the medio-lateral prolongation of these bands is generated by successive and continuous addition of new germs at the edges of the developing tooth fields that go hand-in-hand with the shedding of the old teeth (Fig 6B, C, E, E', F, F'). In case of the infrapharyngobranchial field, the continuous addition of new teeth in a medial direction eventually leads to the unification of the left and right tooth patches into a single band that spans the whole width of the roof of the pharyngeal cavity (Fig. 7B, B').

During tooth replacement, new teeth usually join the rest of the tooth patch by their bones of attachment, although, sometimes a single tooth or a cluster of fully developed teeth form apart from the rest of the tooth patch (Fig. 4J, L). These teeth are, however, joined later by further secretion of the bone of attachment of a newly added tooth in between the unjoined parts.

During active tooth cycling, tiny remnants of alizarin red-stained hard tissue appear anterior to the pharyngeal tooth fields. Most notably visible in the hypobranchial 1 field (Fig. 4L, 6C, 7C, 7E'', asterisks), these remnants likely represent leftovers of the non-resorbed hard tissue material after the extensive TRAP activity, which is associated with shedding of old teeth (Fig. 5G, H).

The situation of active tooth cycling in the hypobranchial 2 field is rather ambiguous. This field is the last appearing within the sterlet ontogeny (at TL 23-24 mm, Fig. 3H, white arrowhead) and tooth shedding starts soon after the very initiation of this field. Namely, the first tooth of this field is shed at the time when the field consists of only three mineralized teeth (Fig. 4H, black arrowhead). Throughout the ontogeny, the rapid shedding of the formed teeth continues in this field and impedes counting of the functional tooth rows and, further, the teeth of this field are often separated by the local lack of the bone of attachment (Fig. 4L, 6C, F, F'). At later stages, the median portion of this tooth field bends laterally and new tooth germs are thus added posteriorly, medially and anteriorly (Fig. 6F', white arrowheads).

Cessation of tooth replacement is followed by the loss of teeth

Teeth at all positions in the sterlet oropharyngeal cavity eventually become lost throughout the ontogeny, a feature associated with changes in lifestyle and emancipation of suction feeding. The marginal tooth fields become lost by TL 35 mm, whereas the palatopterygoid and pharyngeal tooth fields are lost at much later stages as a result of the cessation of tooth replacement. Cessation of tooth replacement of these tooth fields occurs when the addition of new teeth is considerably slowed down or completely stopped while, simultaneously, shedding of teeth continues. This feature then leads to the overall reduction and eventual loss of the tooth fields. We observed cessation of tooth replacement in the palatopterygoid and pharyngeal tooth fields roughly from TL 68 mm but the slowing down of tooth replacement occurs continuously already prior to this stage.

In the palatopterygoid field, the yet functional teeth show connection to the underlying bone, however, they are not joined among each other with their bones of attachment (Fig. 7A, arrowhead). At

places, where the teeth are shed, the degradation of the attachment material leaves holes and indentations in the palatopterygoid bone (Fig. 7A, A', arrowhead). The remnants of the palatopterygoid field are present also at juvenile stages, i.e. we could find a single tooth cluster on one palatopterygoid bone at TL 286 mm (Fig. 7D, D').

The reduction of pharyngeal fields is exhibited by the pronounced degradation of the bone of attachment in case of the infrapharyngobranchial field or by the progressive lack of its mineralization in case of the hypobranchial 1 and 2 fields. Here, remnants of mineralized bones of attachment are still present in the lateral parts of the fields, otherwise mineralization is present only in the tooth apices (Fig. 7C, C' arrowhead). These parts contain the highest number of functional tooth rows and thus the oldest teeth. Mineralization, at least partial, of tooth bases of the oldest teeth continues until TL 286 mm (Fig. 7 E, E', E''). Interestingly, TL 105 mm is the last examined stage to display presence of all multi-rowed tooth fields and, among them, only palatopterygoid and hypobranchial 1 fields are found in TL 286 mm stage (Fig. 7D, E).

Discussion

Conclusion

Acipenserid dentition encompasses various aspects of dental developmental biology including early initiation and addition of new teeth within a dentate field, together with later-occurring simultaneous resorption, and eventual loss of the whole dentition. These phenomena occur sequentially (or simultaneously) showing dynamic modifications of the dentition throughout the life cycle and making the sterlet an amenable model for various aspects of the dental research. Thanks to its phylogenetic position as a member of non-teleost ray-finned fishes, aspects of dental biology may have direct consequences for explaining the evolution of dental character states present in the teleosts. At the same time, non-teleost ray-finned fishes proved to be helpful in addressing various developmental questions across broad vertebrate phylogeny (Minarik et al. 2017, Stundl et al. 2019, Stundl et al. forthcoming), and in this sense, the sterlet may be informative also in case of general evolution of vertebrate dentitions.

Acknowledgments

We thank Ann Husseune for the discussions on the topic, Marie Landova-Sulcova and Marcela Buchtova for technical assistance with TRAP staining, lab members of Psenicka lab for their help with rearing the sterlet embryos, fry and juveniles and Radek Šanda for possibility to use motorized dissecting microscope. This project was supported by the Czech Science Foundation GACR 18-04580S (to V.S.), Charles University GAUK project 640616 (to A.P.) and BMWFW Österreich Aktion ICM-2016-03562 (to A.P.).

Conflict of interest

The authors declare no competing interests.

References

Abduweli D, Baba O, Tabata MJ, Higuchi K, Mitani H & Takano Y (2014) Tooth replacement and putative odontogenic stem cell niches in pharyngeal dentition of medaka (*Oryzias latipes*). *Microscopy* 63(2), 141–153.

Aigler SR, Jandzik D, Hatta K, Uesugi K & Stock DW (2014) Selection and constraint underlie irreversibility of tooth loss in cypriniform fishes. *Proceedings of the National Academy of Sciences* 111(21), 7707–7712.

Atukorala ADS & Franz-Odendaal TA (2014) Spatial and temporal events in tooth development of *Astyanax mexicanus*. *Mechanisms of Development* 134, 42–54.

Bemis WE, Findeis EK & Grande L (1997) An overview of Acipenseriformes. *Environmental Biology of Fishes* 48, 25–71.

Chen D, Blom H, Sanchez S, Tafforeau P & Ahlberg PE (2016) The stem osteichthyan Andreolepis and the origin of tooth replacement. *Nature* 539, 237–241.

Clemen G, Bartsch P & Wacker K (1998) Dentition and dentigerous bones in juveniles and adults of *Polypterus senegalus* (Cladistia, Actinopterygii). *Annals of Anatomy* 180, 211–221.

Connolly MH & Yelick PC (2010) High-throughput methods for visualizing the teleost skeleton: capturing autofluorescence of alizarin red. *Journal of Applied Ichthyology* 26, 274–277.

Donoghue PCJ (2002) Evolution of development of the vertebrate dermal and oral skeletons: unraveling concepts, regulatory theories, and homologies. *Paleobiology* 28, 474-507.

Ellis NA, Donde NN, Miller CT (2016) Early development and replacement of the stickleback dentition. *J Morphol* 277(8), 1072–1083.

Fraser GJ, Hulsey CD & Bloomquist RF, Uyesugi K, Manley NR & Streelman JT (2009) An Ancient Gene Network Is Co-opted for Teeth on Old and New Jaws. *PLOS Biology* 7(2): e1000031.

Grande L & Bemis WE (1991) Osteology and phylogenetic relationships of fossil and recent paddlefishes (Polyodontidae) with comments on the interrelationships of Acipenseriformes. *J. Vert. Paleo*. 11, 1–121.

Hilton EJ, Grande L & Bemis WE (2011). Skeletal Anatomy of the Shortnose Sturgeon, *Acipenser Brevirostrum* Lesueur, 1818, and the Systematics of Sturgeons (Acipenseriformes, Acipenseridae). *Fieldiana Life and Earth Sciences* 3, 1–168.

Imms AD (1904) 3. Notes on the Gill-rakers of the Spoonhill Sturgeon, *Polyodon spathula**. *Proceedings of the Zoological Society of London* 74, 22–35.

Jarvik E (1996) 1996. The Devonian tetrapod Ichthyostega. *Fossils and Strata* 40, 1–206.

Jollie M (1980) Development of Head and Pectoral Girdle Skeleton and Scales in Acipenser. *Copeia* 2, 226–249.

Kague E, Witten P, Soenens M, Campos, CL, Lubiana T, Fisher S, Hammond C, Robson Brown K, Passos-Bueno MR & Huysseune A (2018) Zebrafish sp7 mutants show tooth cycling independent of attachment, eruption and poor differentiation of teeth. *Developmental Biology* 435(2), 176–184.

Minarik M, Stundl J, Fabian P, Jandzik D, Metscher BD, Psenicka M, Gela D, Osorio-Pérez A, Arias-Rodriguez L, Horácek I & Cerny, R. (2017) Preoral gut contributes to facial structures in non-teleost fishes. *Nature*, 547, 209–212.

Nelson GJ (1969) Gill arches and the phylogeny of fishes, with notes on the classification of vertebrates. Bulletin of the American Museum of Natural History 141, 479–552.

Qu Q, Sanchez S, Blom H, Tafforeau P & Ahlberg PE (2013) Scales and Tooth Whorls of Ancient Fishes Challenge Distinction between External and Oral 'Teeth'. *PLoS ONE 8(8)*: e71890.

Qu Q, Haitina T, Zhu M & Ahlberg PE (2015) New Genomic and fossil data illuminate the origin of enamel. *Nature* 526(7571), 108–111.

Rizzato PP, Pospisilova A, Hilton EJ & Bockmann FA (2020) Ontogeny and homology of cranial bones associated with lateral-line canals of the Senegal Bichir, Polypterus senegalus (Actinopterygii: Cladistii: Polypteriformes), with a discussion on the formation of lateral-line canal bones in fishes. Journal of Anatomy 00, 1–29.

Rücklin M, Donoghue PCJ, Cunningham JA, Marone F & Stampanoni M (2014) Developmental paleobiology of the vertebrate skeleton. *Journal of Paleontology* 88(4), 676–683.

Smith MM & Coates MI (1998) Evolutionary origins of the vertebrate dentition: phylogenetic patterns and developmental evolution. *Eur. J. Oral Sci.* 106, 482–500.

Smith MM, Johanson Z, Butts T, Ericsson R, Modrell M, Tulenko FJ, Davis MC & Fraser GJ (2015) Making teeth to order: conserved genes reveal an ancient molecular pattern in paddlefish (Actinopterygii). *Proceedings of Royal Society B* 282: 20142700.

Soukup V, Tazaki A, Yamazaki Y, Pospisilova A, Epperlein H-H, Tanaka EM & Cerny R (in prep) Oral and palatal dentition of axolotl arises from a common tooth-competent zone and co-localizes with the ecto-endoderm boundary.

Stundl, J., Pospisilova, A., Matějková, T., Psenicka, M., Bronner, M. E. & Cerny, R. (2020) Migratory patterns and evolutionary plasticity of cranial neural crest cells in ray-finned fishes. *Developmental Biology* (forthcoming)

Štundl J (2019) *Migration and morphogenesis of neural crest cells in the context of craniofacial development of selected ray-finned fishes*. PhD. Prague: Charles University, pp. 78.

Vandenplas S, De Clercq A & Huysseune A (2014) Tooth replacement without a dental lamina: The search for epithelial stem cells in *Polypterus senegalus*. *Journal of Experimental Zoology Part B: Molecular and Developmental Evolution* 322(5), 281–293.

Vandenplas S, Willems M, Witten PE, Hansen T, Fjelldal PG & Huysseune A (2016) Epithelial Label-Retaining Cells Are Absent during Tooth Cycling in *Salmo salar* and *Polypterus senegalus*. *PLoS ONE* 11(4): e0152870.

Vaškaninová V, Chen D, Tafforeau P, Johanson Z, Ekrt B, Blom H & Ahlberg PE (2020) Marginal dentition and multiple dermal jawbones as the ancestral condition of jawed vertebrates. Science 369, 211–216.

Witten PE & Villwock W (1997) Growth requires bone resorption at particular skeletal elements in a teleost fish with acellular bone (*Oreochromis niloticus*, Teleostei: Cichlidae*). J. Appl. Ichthyol*. 13, 149–158.

Wacker K, Bartsch P & Clemen G (2001) The development of the tooth pattern and dentigerous bones in *Polypterus senegalus* (Cladistia, Actinopterygii). *Annals of Anatomy* 183, 37–52.

Warth P, Hilton EJ, Naumann B, Olsson L & Konstantinidis P (2017) Development of the skull and pectoral girdle in Siberian sturgeon, *Acipenser baerii*, and Russian sturgeon, *Acipenser gueldenstaedtii* (Acipenseriformes: Acipenseridae). *Journal of Morphology* 00:1–25.

Figure legends:

Fig. 1: Distribution and composition of the sterlet dentition.

(A, B) Schematic illustration of the sterlet oropharyngeal roof and floor with a depiction of individual tooth fields. (C-E) Alizarin red-stained tooth fields of the oropharyngeal roof, i. e. dermopalatine (C), palatopterygoid (D) and infrapharyngobranchial (E), and sagittal histological sections (anterior to the left) through these fields (F-H). (I-K) Alizarin red-stained tooth fields of the oropharyngeal floor, i. e. dentary (I), hypobranchial 1 (J), and hypobranchial 2 (K) and sagittal histological sections (anterior to the left) through these fields (F-H). White arrowheads mark positions of new tooth germs. den, dentary; dpl, dermopalatine; hb1, hypobranchial 1; hb2, hypobranchial 2; iph, infrapharyngobranchial; ppt, palatopterygoid.

Fig. 2: Expression patterns of* Pitx2 *and* Shh *at early stages of development of the sterlet dentition.

Expression patterns of early odontogenic markers *Pitx2* (A-J) and *Shh* (K-T) on the oropharyngeal roof (A-E; K-O) and floor (F-J; P-T) show initial stages of development of the sterlet dentition. (A-E) Expression pattern of *Pitx2* on the oropharyngeal roof labels tooth competent regions, which ontogenetically appear in the sequence dermopalatine, palatopterygoid and infrapharyngobranchial tooth fields. (F-J) On the oropharyngeal floor, the *Pitx2* expression is first present in the dentary and later in the hypobranchial 1 tooth fields. The *Pitx2* expression on both the roof and the floor initially labels broad tooth-competent regions and later becomes focally restricted to individual tooth germs (black arrows and arrowheads). (K-T) Focal expression of *Shh* marks positions of newly-forming tooth germs. (K-O) On the oropharyngeal roof, *Shh*-expressing teeth first appear in the dermopalatine field and next in the palatopterygoid and infrapharyngobranchial fields. (P-T) On the oropharyngeal floor, *Shh* transcripts are first detected in the dentary and next in the hypobranchial 1 tooth fields. Subsequent ontogenetic stages show addition of new *Shh*-expressing tooth germs (black arrowheads) in the vicinity of the first forming tooth germ, i.e. the initiator-tooth (black arrows), in each respective tooth field. Individual tooth fields are further surrounded by *Shh*-expressing bands that become progressively compartmentalized to give rise to rows of taste buds (asterisks). den, dentary; dpl, dermopalatine; hb1, hypobranchial 1; iph, infrapharyngobranchial; ppt, palatopterygoid.

Fig. 3. Establishment of the fully functional dentition.

(A) The first detectable mineralization of teeth is present in the dentary field at TL 13 mm (stage 41), where the tooth at position 2 shows the highest degree of matrix deposition (white arrow) and is followed by teeth at positions 1 and 3 (white arrowheads). (A', B) Newly mineralized teeth are added laterally (white arrowheads) and become attached to the ossifying dermopalatine and dentary bones (B; black arrowheads). (C, D) Distribution of tooth fields after separation of the oropharyngeal roof and floor shows spatial relations between the first three tooth germs arranged into a row in the palatopterygoid field and into a V-shape in the infrapharyngobranchial and hypobranchial 1 fields at 14 mm. (E, F) Later stage (TL 17 mm) shows a multi-rowed arrangement of the palatopterygoid, infrapharygobranchial and hypobranchial 1 fields. New teeth are added anteriorly in the palatopterygoid tooth field and posteriorly in the infrapharyngobranchial and hypobranchial tooth fields (white arrowheads). (G) Multi-rowed arrangement of the infrapharyngobranchial tooth field is present at the time of first mineralization of the parasphenoid bone (TL 18 mm). (H) The first mineralized hypobranchial 2 tooth is present at TL 24 mm juveniles (white arrowhead). Note the first evidence of tooth shedding in the hypobranchial 1 tooth field (black arrowhead). White arrows mark the first forming tooth, i.e. the initiator-tooth, and white arrowheads mark successional teeth in each tooth field. den, dentary; dpl, dermopalatine; ppt, palatopterygoid; iph, infrapharyngobranchial; hb1, hypobranchial 1; hb2, hypobranchial 2 tooth fields. Scale bars equal 500 μm.

Fig. 4: Full dentition and active tooth cycling.

(A-D) The sterlet dentition at TL 22 mm is characterized by the functional single-rowed dermopalatine and dentary tooth fields and multi-rowed palatopterygoid, infrapharyngobranchial and hypobranchial 1 tooth fields. In multi-rowed tooth fields, new teeth are added anteriorly in the palatopterygoid and posteriorly in the infrapharyngobranchial and hypobranchial 1 tooth fields (white arrowheads). (E-H) At TL 25 mm, the dermopalatine and dentary teeth start shedding (E, G, black arrowheads), while not being replaced; shedding of oldest teeth is observed also posteriorly in the palatopterygoid and

anteriorly in the infrapharyngobranchial, hypobranchial 1 and hypobranchial 2 tooth fields (E, F, H, black arrowheads). Note that in hypobranchial 2 field, the first tooth is shed at the time this tooth field consists of only three teeth (H, black arrowhead). (I-L) At TL 38 mm, the dermopalatine and dentary teeth are lost altogether (I, K, black arrowheads), while the palatopterygoid, infrapharyngobranchial, hypobranchial 1 and hypobranchial 2 fields renew their teeth through the simultaneous addition (white arrowheads) on one side and shedding on the opposite side (black arrowheads) of the respective field (I, J, L). Note the conspicuous resorption associated with tooth shedding in the palatopterygoid, hypobranchial 1 and hypobranchial 2 fields (J, black arrowheads) and the bony remnants resulting from this resorption (L, asterisks). den, dentary; dpl, dermopalatine; ppt, palatopterygoid; iph, infrapharyngobranchial; hb1, hypobranchial 1; hb2, hypobranchial 2 tooth fields. Note the posterior rotation of teeth before their shedding at the edge of the palatopterygoid (E, I, black arrows). Scale bars equal 500 μm.

Fig. 5: Sterlet teeth are lost through the resorption of tooth bases

(A, B) Oral jaws visualized by micro computed tomography showing fully developed dentition with teeth inserted in the bone sockets at TL 22 mm (A). Remnants of the sockets are preserved (B, black arrowhead) immediately after tooth shedding (white arrow marks the tooth base with a broken tooth apex). (C-F) TRAP staining on histological sections confirms initiation of hard tissue resorption associated with tooth shedding in all the up-to-now formed tooth fields at stage 23 mm TL (black arrowheads). (G, H) Whole-mount TRAP staining shows hard tissue resorption during tooth shedding in the whole dermopalatine and dentary fields, in the posterior portion of the palatopterygoid field and in the anterior portion of the infrapharyngobranchial, hypobranchial 1 and hypobranchial 2 fields. den, dentary; dpl, dermopalatine; ppt, palatopterygoid; iph, infrapharyngobranchial; hb1, hypobranchial 1; hb2, hypobranchial 2 tooth fields.

Fig. 6: Remodeling of the actively cycling tooth fields

The dentition of the TL 46 mm (A-C) and TL 68 mm (D-F') sterlet juveniles exhibits structural remodeling. In the palatopterygoid tooth field, local addition of new teeth (A, white arrowheads) leads to the antero-medial convergence of the left and right fields (D, black arrowhead). At these positions, the teeth are not joined among each other by their bones of attachment (D, black arrowhead). In the infrapharyngobranchial field, the continued addition of new tooth germs results in the medio-lateral prolongation and a strand-shaped appearance of this field (B, E, E'). At TL 46 mm, the hypobranchial 1 and hypobranchial 2 tooth fields become crescent-shaped (C) and at TL 68 mm, the medial portion of the hypobranchial 2 tooth field bends, so that new tooth germs are added not only posteriorly, but also medially and anteriorly (F, F', white arrowheads). Remnants of hard tissue resorption during tooth shedding are found anterior to the hypobranchial 1 field (C, asterisks). den, dentary; dpl, dermopalatine; ppt, palatopterygoid; iph, infrapharyngobranchial; hb1, hypobranchial 1; hb2, hypobranchial 2 tooth fields. Scale bars equal 500 μm.

Fig. 7: Cessation of tooth replacement and the loss of teeth

The number of teeth in the palatopterygoid field is substantially reduced at TL 105 mm (A), the teeth are not interconnected by their bones of attachment (A, black arrowhead) and the palatopterygoid itself is degraded leaving holes and indentations in the bone (A', black arrowhead). The median addition of new teeth causes unification of the left and right infrapharyngobranchial fields into a single band spanning the whole width of the oropharyngeal roof (B), despite the continued hard tissue resorption in this field (B'). The number of tooth rows in the hypobranchial 1 and hypobranchial 2 fields is reduced, the bone of attachment is degraded to a large extent (C), leaving only remnants of the bone of attachment in the lateral portions of these fields (C', black arrowhead). At TL 286 mm, the palatopterygoid field is reduced to only a small laterally placed isolated tooth patch (D, D'). Infrapharyngobranchial and hypobranchial 2 fields are absent. Teeth in the hypobranchial 2 field show reduced mineralization (E, E') and only the tooth cones and portions of the tooth bases are mineralized (E''). Remnants of hard tissue resorption during tooth shedding are found anterior to the hypobranchial 1 field (C, E'', asterisks). bb, basibranchial; cb, ceratobranchial; dpl, dermopalatine; hb, hypobranchial; hh, hypohyal; iph, infrapharyngobranchial tooth field; ppt, palatopterygoid. Scale bars equal 500 μm, unless otherwise specified.

Fig. 8: Summary of the sterlet dentition ontogeny
(A) Schematized cross section through the sterlet head depicting the positions of tooth fields. (B) Dermopalatine and dentary tooth fields show a single-rowed arrangement without tooth replacement. (C) Palatopterygoid, infrapharyngobranchial, hypobranchial 1 and hypobranchial 2 tooth fields show a multi-rowed arrangement with tooth replacement. Stages of tooth development schematized in the color circles (B, C) were characterized for each tooth field in selected specimens defined by their total length (TL). The source data for the graphs in (B) and (C) are from the supplementary table 1. den, dentary; dpl, dermopalatine; ppt, palatopterygoid; iph, infrapharyngobranchial; hb1, hypobranchial 1; hb2, hypobranchial 2 tooth fields.

Suppl. fig. 1: Expression of early odontogenic genes in the oral region of the sterlet larva
The early odontogenic markers *Pitx2* (A-D) and *Shh* (E-H) are expressed as diffuse bands in the oral region prior to and after hatching and represent the prospective places of the developing dermopalatine and dentary tooth fields (A, B, E-G, black arrowheads). The symphyseal regions are devoid of the presence of *Pitx2* and *Shh* transcripts (C, D, G, black arrows). At stage 38, the *Shh* expression pattern changes into focal spots representing individual tooth germs (H).

Suppl. table 1: Stages of tooth development in individual tooth fields during the sterlet ontogeny
Stages of tooth development across tooth fields and ontogenetic stages show dynamic composition of the sterlet dentition. Character states: 0 = no teeth (no mineralized teeth present), 1 = development (matrix deposition present in the developing teeth), 2 = eruption (teeth are erupted, replacement teeth may or may not be present, no signs of tooth shedding), 3 = shedding and addition (simultaneous presence of newly developing, functional and shedding teeth), 4 = shedding (presence of functional and shedding teeth, no newly developing teeth detected or significantly reduced), 5 = no teeth (teeth are lost altogether).

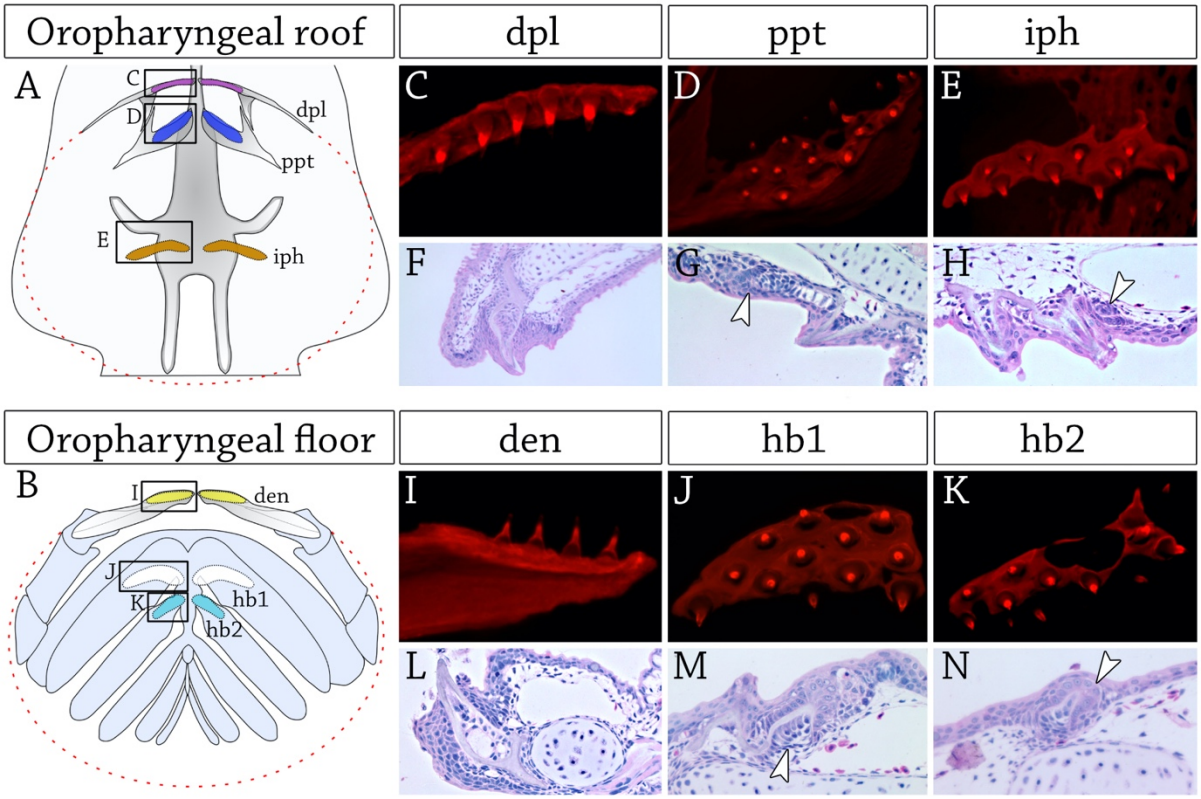
Oropharyngeal roof
dpl
ppt
iph
A
C
D
E
dpl
ppt
iph
C
D
E
F
G
H
Oropharyngeal floor
den
hb1
hb2
B
I
J
K
den
hb1
hb2
I
J
K
L
M
N

Fig. 1

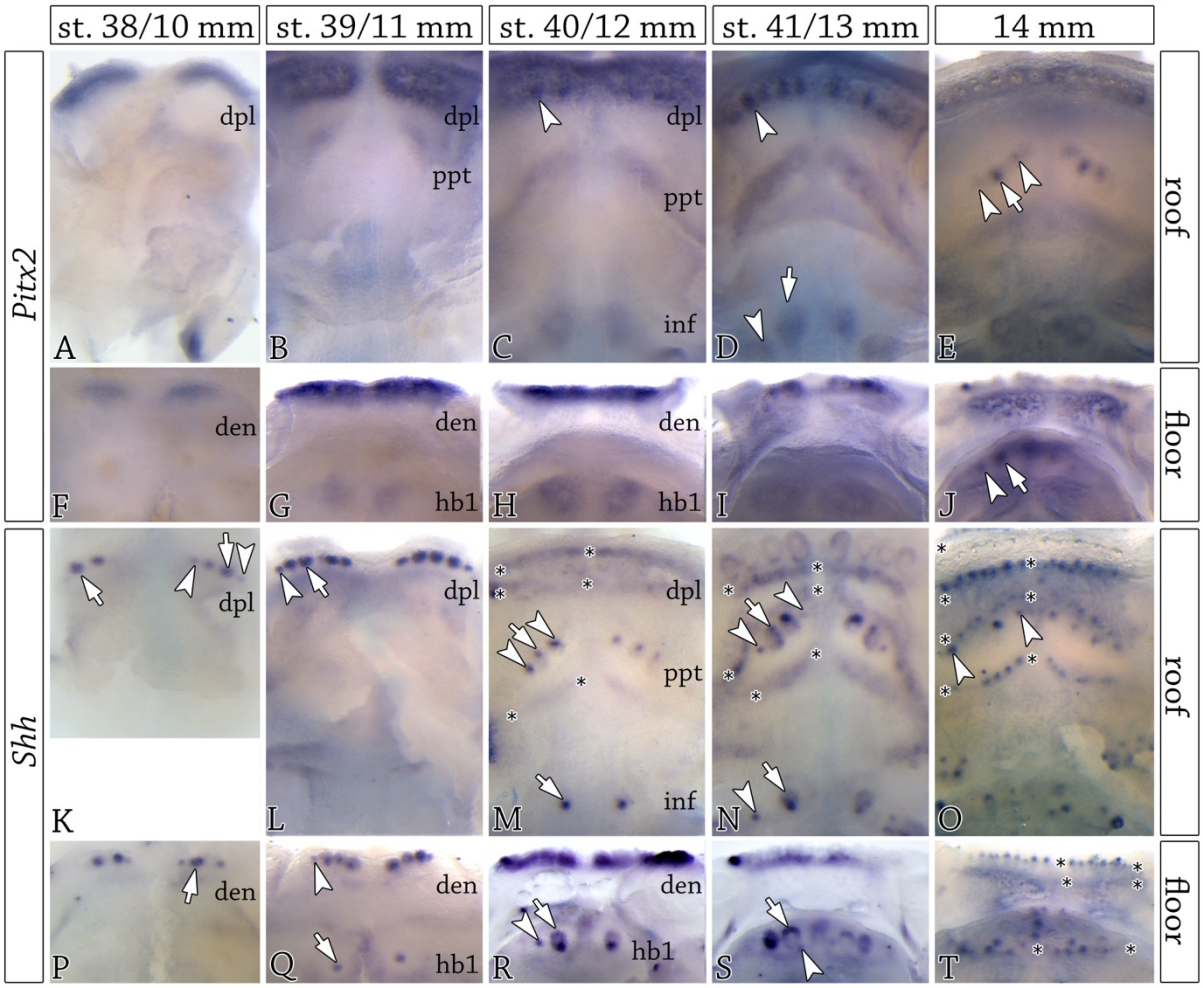
st. 38/10 mm
st. 39/11 mm
st. 40/12 mm
st. 41/13 mm
14 mm
Pitx2
Shh
roof
floor
A
B
C
D
E
F
G
H
I
J
K
L
M
N
O
P
Q
R
S
T
dpl
ppt
inf
den
hb1

Fig. 2

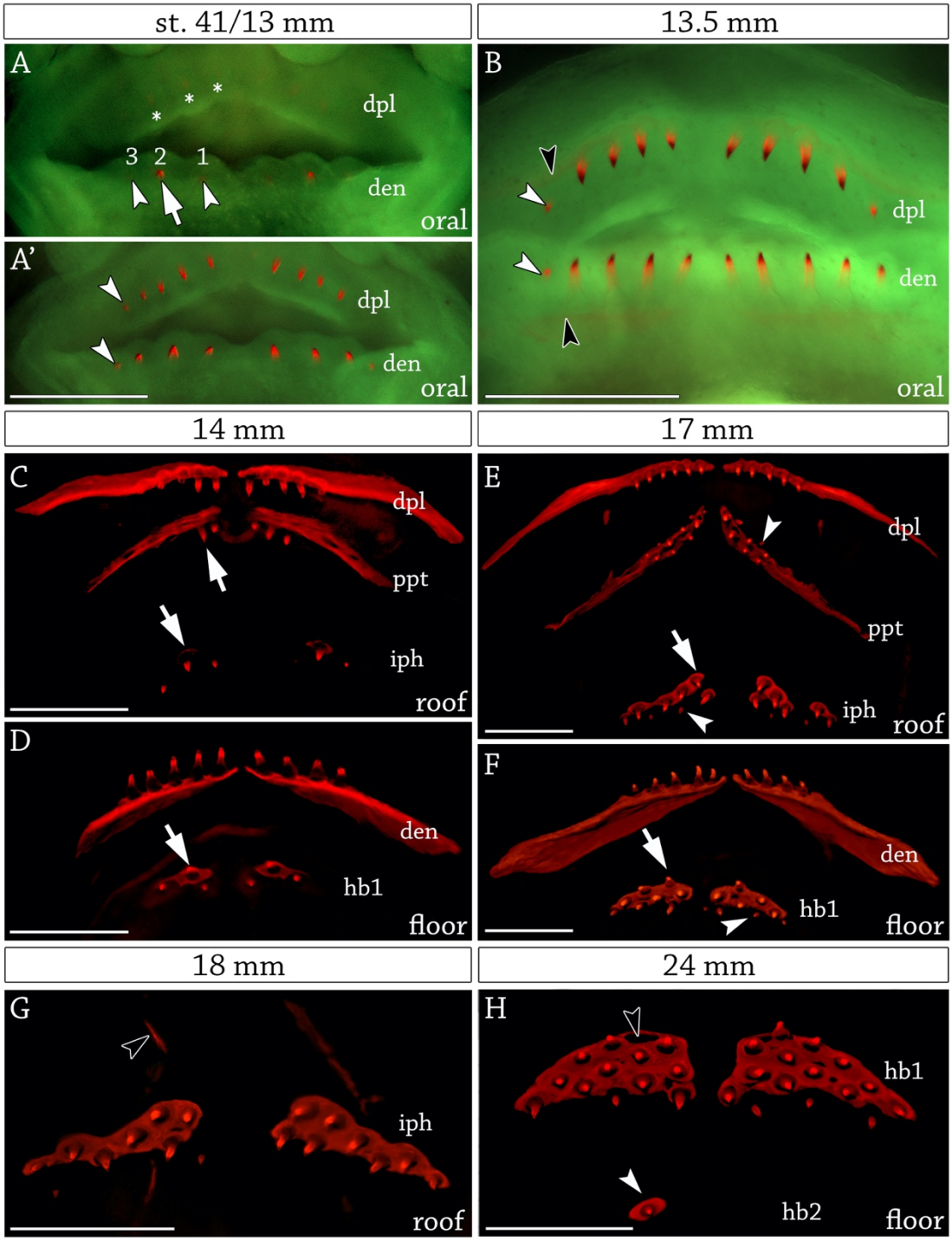
st. 41/13 mm
13.5 mm
A
dpl
3 2 1
den
oral
A'
dpl
den
oral
B
dpl
den
oral
14 mm
17 mm
C
dpl
ppt
iph
roof
D
den
hb1
floor
E
dpl
ppt
iph
roof
F
den
hb1
floor
18 mm
24 mm
G
iph
roof
H
hb1
hb2
floor

Fig. 3

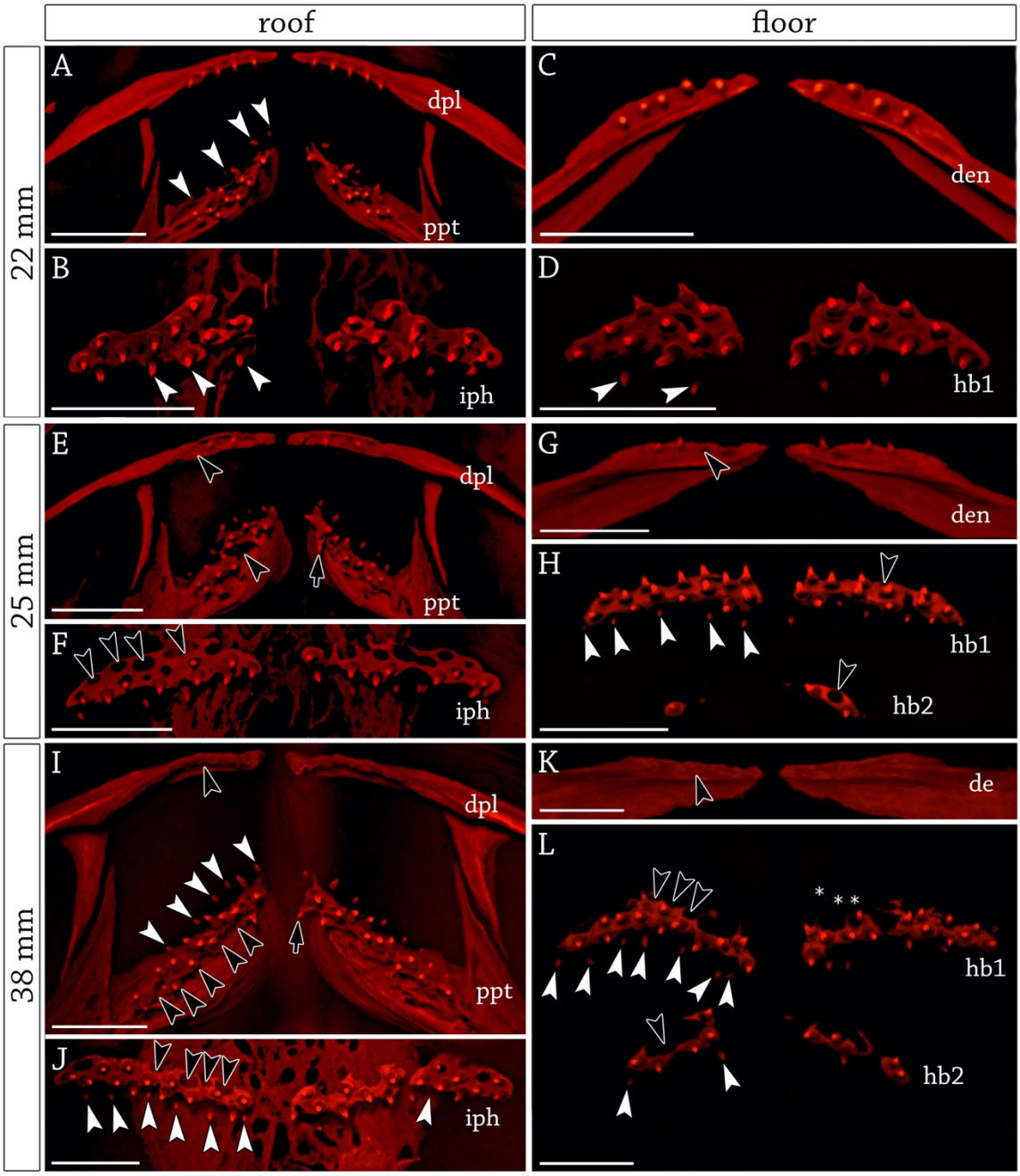
roof
floor
22 mm
25 mm
38 mm
A
dpl
ppt
B
iph
C
den
D
hb1
E
dpl
ppt
F
iph
G
den
H
hb1
hb2
I
dpl
ppt
J
iph
K
de
L
hb1
hb2
Fig. 4

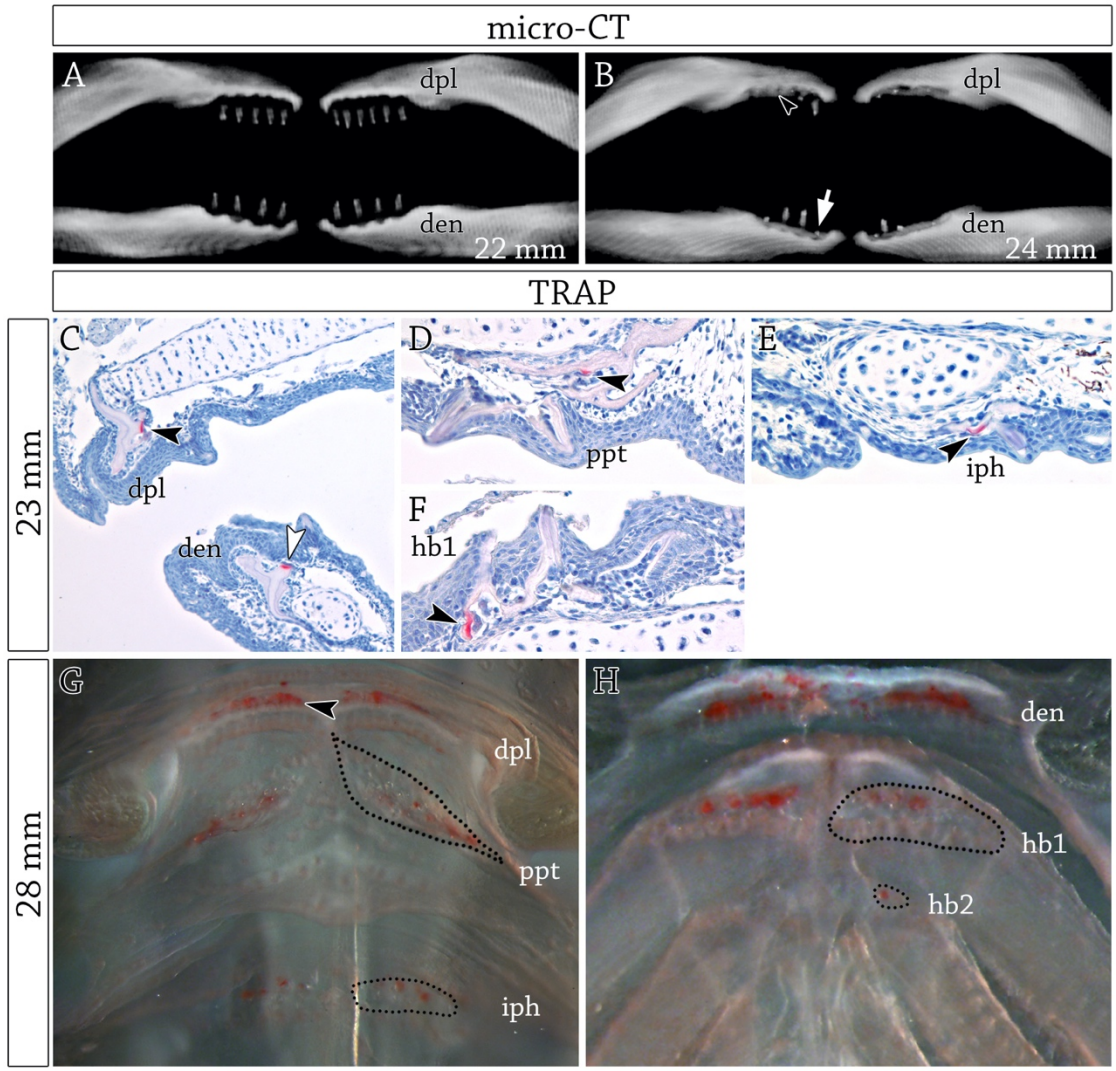
micro-CT
A
dpl
den
22 mm
B
dpl
den
24 mm
TRAP
23 mm
C
dpl
den
D
ppt
E
iph
F
hb1
28 mm
G
dpl
ppt
iph
H
den
hb1
hb2

Fig. 5

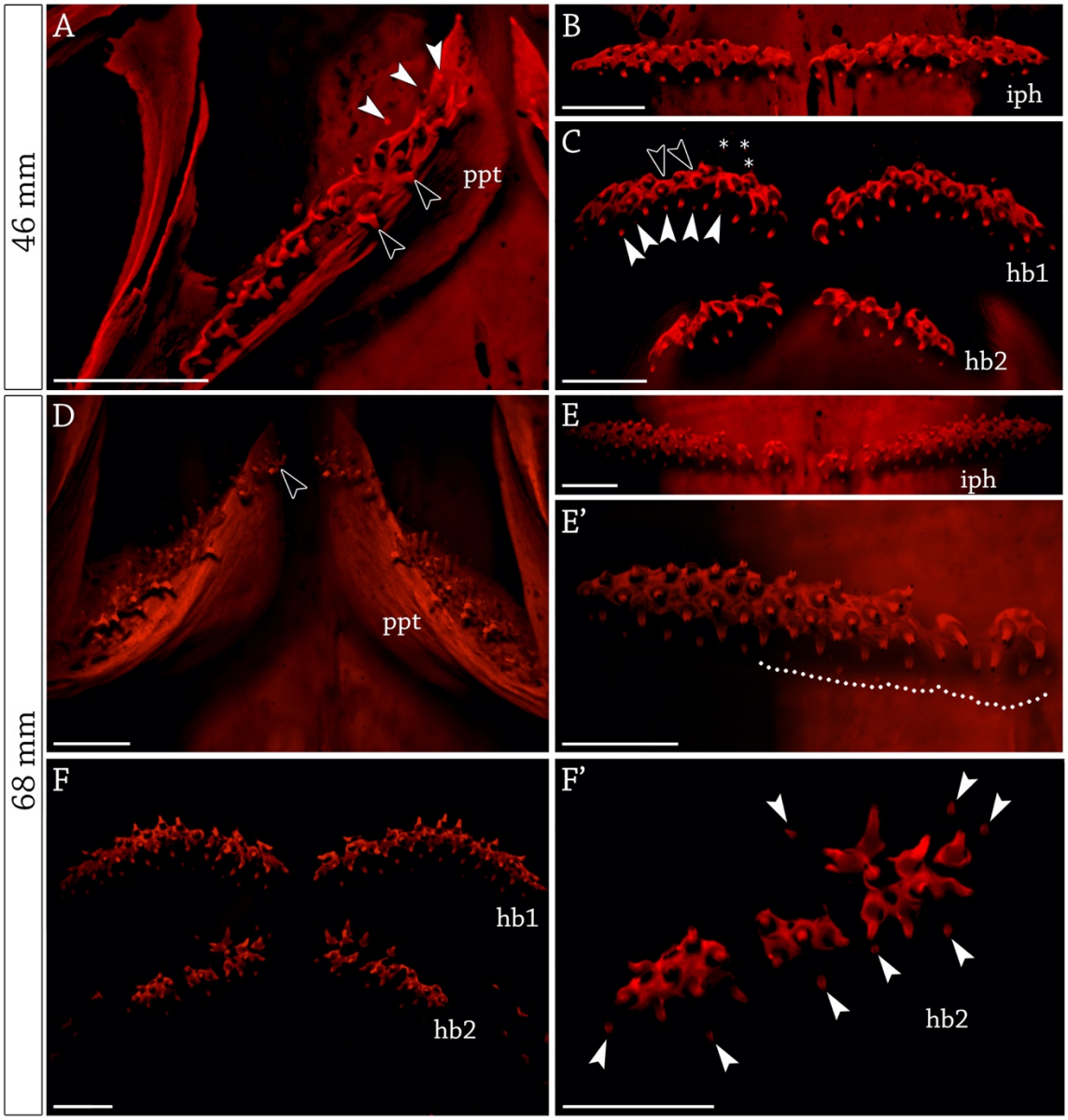

Fig. 6

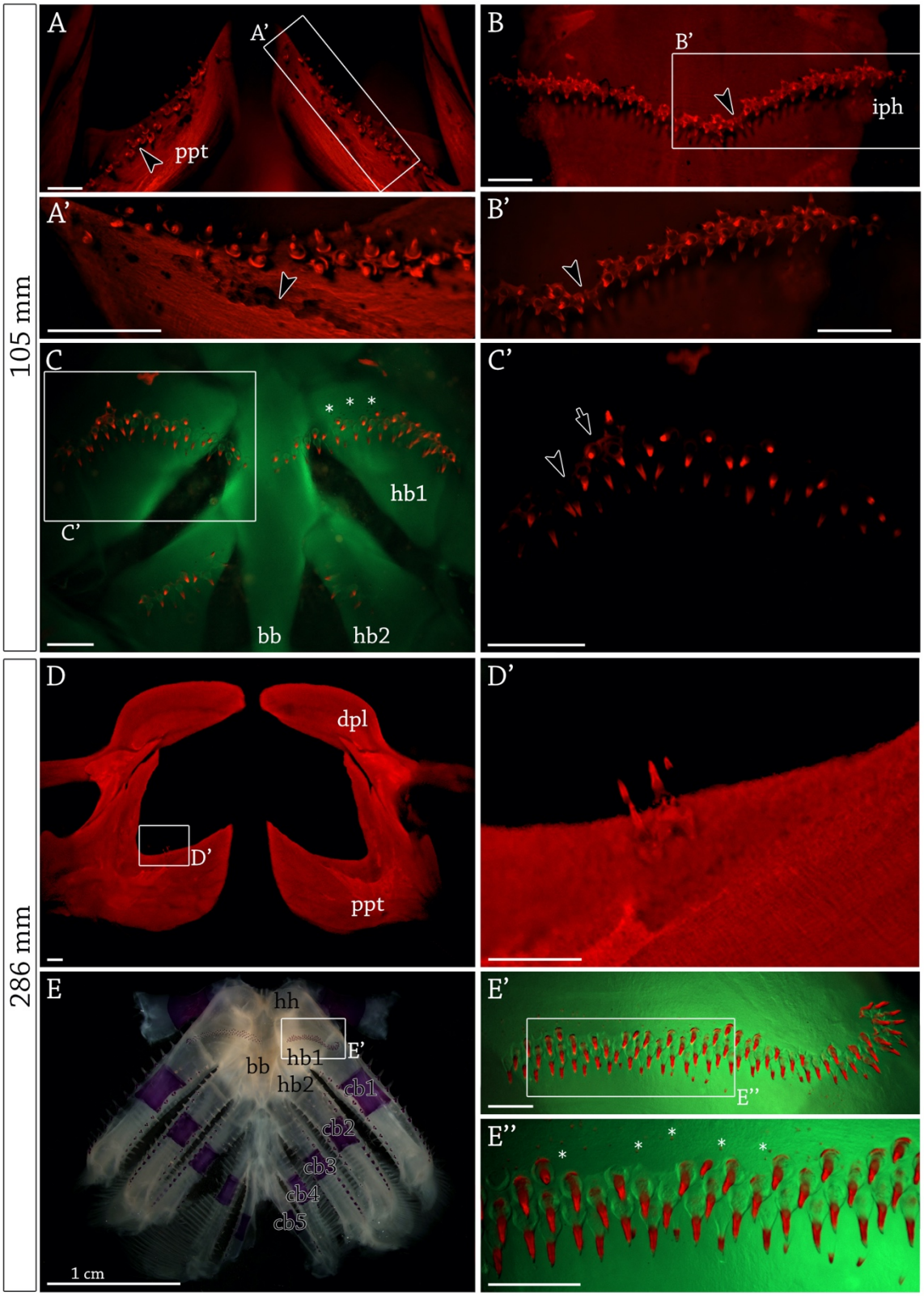
105 mm
286 mm
A
A'
ppt
B
B'
iph
A'
B'
C
C'
hb1
bb
hb2
C'
C'
D
dpl
D'
ppt
D'
E
hh
E'
bb
hb1
hb2
cb1
cb2
cb3
cb4
cb5
1 cm
E'
E''
E''

Fig. 7

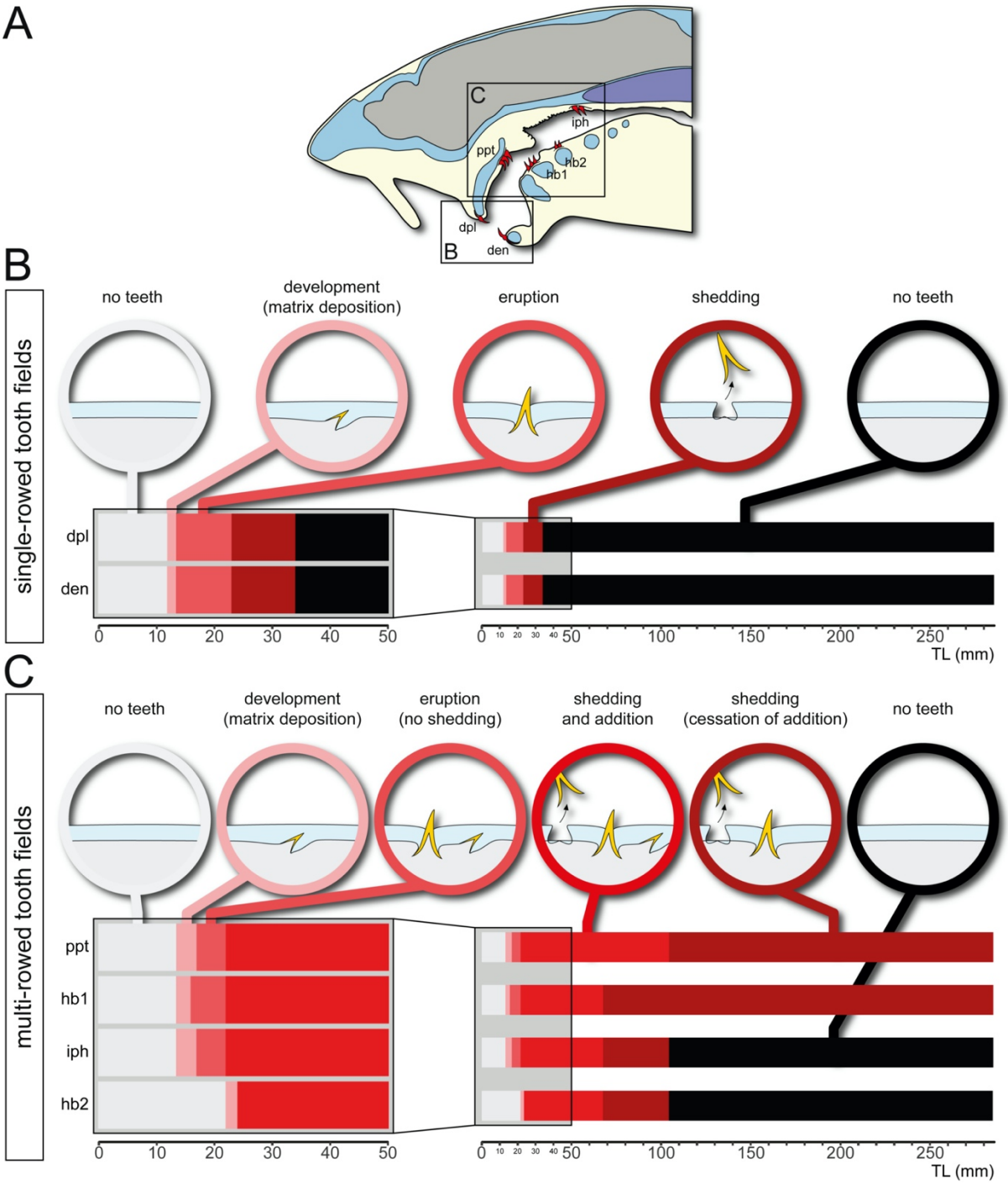
A
C
iph
ppt
hb2
hb1
dpl
B
den
B
single-rowed tooth fields
no teeth
development
(matrix deposition)
eruption
shedding
no teeth
dpl
den
0
10
20
30
40
50
100
150
200
250
TL (mm)
C
multi-rowed tooth fields
no teeth
development
(matrix deposition)
eruption
(no shedding)
shedding
and addition
shedding
(cessation of addition)
no teeth
ppt
hb1
iph
hb2
0
10
20
30
40
50
100
150
200
250
TL (mm)

Fig. 8

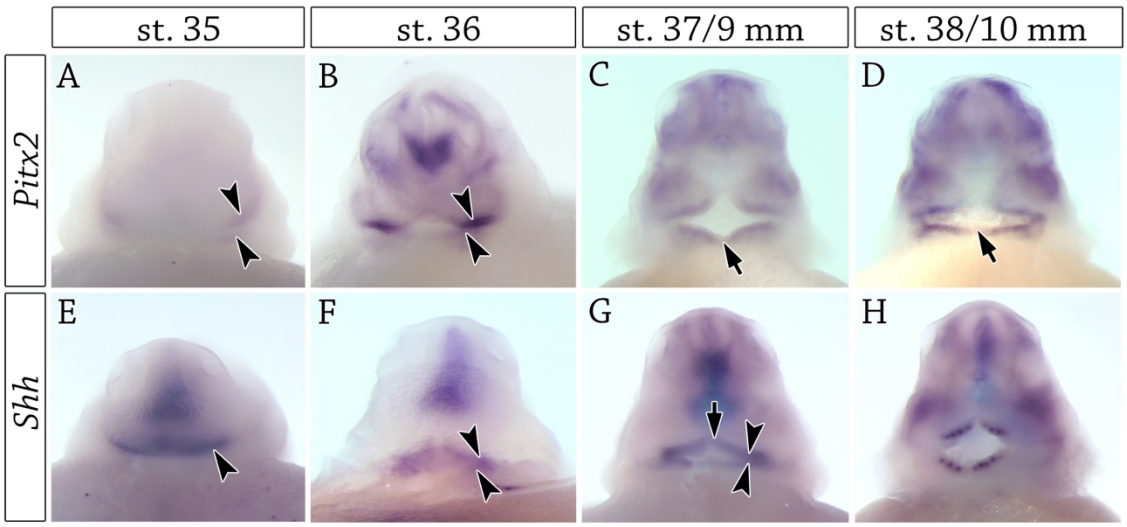

Fig. S1

stage [mm]	dpl	ppt	iph	den	hb1	hb2
11	0	0	0	0	0	0
12	0	0	0	0	0	0
13	1	0	0	1	0	0
13.5	1	0	0	1	0	0
14	2	1	1	2	1	0
15	2	1	1	2	1	0
16	2	1	1	2	1	0
17	2	1	1	2	2	0
18	2	2	2	2	2	0
19	2	2	2	2	2	0
20	2	2	2	2	2	0
21	2	2	2	2	2	0
22	2	2	2	2	2	0
23	2	3	3	2	3	1
24	4	3	3	4	3	1
25	4	3	3	4	3	3
26	4	3	3	4	3	3
27	4	3	3	4	3	3
28	4	3	3	4	3	3
29	4	3	3	4	3	3
30	4	3	3	4	3	3
31	4	3	3	4	3	3
32	4	3	3	4	3	3
33	4	3	3	4	3	3
34	4	3	3	4	3	3
35	5	3	3	5	3	3
37	5	3	3	5	3	3
38	5	3	3	5	3	3
43	5	3	3	5	3	3
46	5	3	3	5	3	3
68	5	3	3	5	3	3
105	5	3	4	5	4	4
286	5	4	5	5	4	5

0 =no teeth
1 =development
2 =eruption
3 =shedding and addition
4 =shedding
5 =no teeth

Tab. S1